UNIVERSIDAD DE MURCIA

ESCUELA INTERNACIONAL DE DOCTORADO

TESIS DOCTORAL

Biotechnological Synthesis and Molecular Encapsulation of Natural Stilbenes and Lipophilic Derivatives for Biomedical and Food Applications

Síntesis Biotecnológica y Encapsulación Molecular de Estilbenos Naturales y Derivados Lipófilos para su Aplicación en Biomedicina y Alimentación

D.ª Silvia Navarro Orcajada

2024

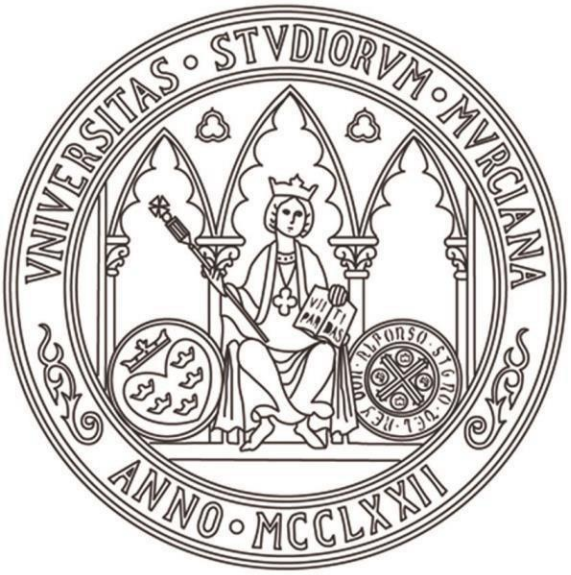

UNIVERSIDAD DE MURCIA

ESCUELA INTERNACIONAL DE DOCTORADO

TESIS DOCTORAL

Biotechnological Synthesis and Molecular Encapsulation of Natural Stilbenes and Lipophilic Derivatives for Biomedical and Food Applications

Síntesis Biotecnológica y Encapsulación Molecular de Estilbenos Naturales y Derivados Lipófilos para su Aplicación en Biomedicina y Alimentación

Autor: D.ª Silvia Navarro Orcajada

Director/es: D. José Manuel López Nicolás y

D. Adrián Matencio Durán

UNIVERSIDAD DE MURCIA

DECLARACIÓN DE AUTORÍA Y ORIGINALIDAD DE LA TESIS PRESENTADA PARA OBTENER EL TÍTULO DE DOCTOR

Aprobado por la Comisión General de Doctorado el 19-10-2022

D./Dña. Silvia Navarro Orcajada

doctorando del Programa de Doctorado en

Biología Molecular y Biotecnología

de la Escuela Internacional de Doctorado de la Universidad Murcia, como autor/a de la tesis presentada para la obtención del título de Doctor y titulada:

Biotechnological Synthesis and Molecular Encapsulation of Natural Stilbenes and Lipophilic Derivatives for Biomedical and Food Applications / Síntesis Biotecnológica y Encapsulación Molecular de Estilbenos Naturales y Derivados Lipófilos para su Aplicación en Biomedicina y Alimentación

y dirigida por,

D./Dña. José Manuel López Nicolás

D./Dña. Adrián Matencio Durán

DECLARO QUE:

La tesis es una obra original que no infringe los derechos de propiedad intelectual ni los derechos de propiedad industrial u otros, de acuerdo con el ordenamiento jurídico vigente, en particular, la Ley de Propiedad Intelectual (R.D. legislativo 1/1996, de 12 de abril, por el que se aprueba el texto refundido de la Ley de Propiedad Intelectual, modificado por la Ley 2/2019, de 1 de marzo, regularizando, aclarando y armonizando las disposiciones legales vigentes sobre la materia), en particular, las disposiciones referidas al derecho de cita, cuando se han utilizado sus resultados o publicaciones.

Si la tesis hubiera sido autorizada como tesis por compendio de publicaciones o incluyese 1 o 2 publicaciones (como prevé el artículo 29.8 del reglamento), declarar que cuenta con:

- *La aceptación por escrito de los coautores de las publicaciones de que el doctorando las presente como parte de la tesis.*
- *En su caso, la renuncia por escrito de los coautores no doctores de dichos trabajos a presentarlos como parte de otras tesis doctorales en la Universidad de Murcia o en cualquier otra universidad.*

Del mismo modo, asumo ante la Universidad cualquier responsabilidad que pudiera derivarse de la autoría o falta de originalidad del contenido de la tesis presentada, en caso de plagio, de conformidad con el ordenamiento jurídico vigente.

En Murcia, a 15 de mayo de 2024

Fdo.: Silvia Navarro Orcajada

Esta DECLARACIÓN DE AUTORÍA Y ORIGINALIDAD debe ser insertada en la primera página de la tesis presentada para la obtención del título de Doctor.

Información básica sobre protección de sus datos personales aportados	
Responsable:	Universidad de Murcia. Avenida teniente Flomesta, 5. Edificio de la Convalecencia. 30003; Murcia. Delegado de Protección de Datos: dpd@um.es
Legitimación:	La Universidad de Murcia se encuentra legitimada para el tratamiento de sus datos por ser necesario para el cumplimiento de una obligación legal aplicable al responsable del tratamiento. art. 6.1.c) del Reglamento General de Protección de Datos
Finalidad:	Gestionar su declaración de autoría y originalidad
Destinatarios:	No se prevén comunicaciones de datos
Derechos:	Los interesados pueden ejercer sus derechos de acceso, rectificación, cancelación, oposición, limitación del tratamiento, olvido y portabilidad a través del procedimiento establecido a tal efecto en el Registro Electrónico o mediante la presentación de la correspondiente solicitud en las Oficinas de Asistencia en Materia de Registro de la Universidad de Murcia

Firmante: SILVIA NAVARRO ORCAJADA; Fecha-hora: 17/06/2024 09:11:42; Emisor del certificado: CN=AC FNMT Usuarios,OU=Ceres,O=FNMT-RCM,C=ES;

@dministración electrónica

Código seguro de verificación: RUxFMnmi-DgvSZiKe-F8okhtO6-2HLob9LE

COPIA ELECTRÓNICA - Página 1 de 1

Esta es una copia auténtica imprimible de un documento administrativo electrónico archivado por la Universidad de Murcia, según el artículo 27.3 c) de la Ley 39/2015, de 1 de octubre. Su autenticidad puede ser contrastada a través de la siguiente dirección: https://sede.um.es/validador/

UNIVERSIDAD DE
MURCIA

D. José Manuel López Nicolás, Catedrático de Universidad del Área de Bioquímica y Biología Molecular en el Departamento de Bioquímica y Biología Molecular A, AUTORIZA:

La presentación de la Tesis Doctoral titulada "*Biotechnological Synthesis and Molecular Encapsulation of Natural Stilbenes and Lipophilic Derivatives for Biomedical and Food Applications / Síntesis Biotecnológica y Encapsulación Molecular de Estilbenos Naturales y Derivados Lipófilos para su Aplicación en Biomedicina y Alimentación*", realizada por Dª. Silvia Navarro Orcajada, bajo mi inmediata dirección y supervisión, y que presenta para la obtención del grado de Doctor por la Universidad de Murcia.

En Murcia, a 15 de junio de 2024

Firmante: JOSE MANUEL LOPEZ NICOLAS; Fecha-hora: 18/06/2024 20:53:56; Emisor del certificado: CN=AC FNMT Usuarios,OU=Ceres,O=FNMT-RCM,C=ES;

@dministración electrónica

Código seguro de verificación: RUxFMqzo-RgPVsXNi-5Gkablfz-XPTz5/Rd

COPIA ELECTRÓNICA - Página 1 de 1

Esta es una copia auténtica imprimible de un documento administrativo electrónico archivado por la Universidad de Murcia, según el artículo 27.3 c) de la Ley 39/2015, de 1 de octubre. Su autenticidad puede ser contrastada a través de la siguiente dirección: https://sede.um.es/validador/

UNIVERSIDAD DE
MURCIA

D. Adrián Matencio Durán, Doctor en el Dipartamento di Chimica de la Università di Torino, AUTORIZA:

La presentación de la Tesis Doctoral titulada "*Biotechnological Synthesis and Molecular Encapsulation of Natural Stilbenes and Lipophilic Derivatives for Biomedical and Food Applications / Síntesis Biotecnológica y Encapsulación Molecular de Estilbenos Naturales y Derivados Lipófilos para su Aplicación en Biomedicina y Alimentación*", realizada por Dª. Silvia Navarro Orcajada, bajo mi inmediata dirección y supervisión, y que presenta para la obtención del grado de Doctor por la Universidad de Murcia.

En Murcia, a 15 de junio de 2024

Firmante: ADRIAN MATENCIO DURAN; Fecha-hora: 17/06/2024 09:15:15; Emisor del certificado: CN=AC FNMT Usuarios,OU=Ceres,O=FNMT-RCM,C=ES;

Código seguro de verificación: RUxFMiLd-ZQgxaRYK-sZ1H0SPH-WuNHdpYh

COPIA ELECTRÓNICA - Página 1 de 1

Esta es una copia auténtica imprimible de un documento administrativo electrónico archivado por la Universidad de Murcia, según el artículo 27.3 c) de la Ley 39/2015, de 1 de octubre. Su autenticidad puede ser contrastada a través de la siguiente dirección: https://sede.um.es/validador/

Los trabajos de investigación realizados en la presente Tesis Doctoral han sido parcialmente subvencionados por los siguientes proyectos de investigación:

- "Fuentes, obtención, caracterización y modificación de nuevos pigmentos alimentarios con propiedades funcionales en modelos animales de envejecimiento saludable" (PID2021-122896NB-I00) (MCI/AEI/10.13039/501100011033/FEDER, UE) financiado por el Ministerio de Ciencia e Innovación.
- "Formulación y evaluación de nutraceúticos basados en la combinación de múltiples familias de compuestos bioactivos vegetales" (21660/PDC/21) financiado por la Fundación Séneca – Agencia de Ciencia y Tecnología de la Región de Murcia.
- "Protección frente a factores ambientales relacionados con el estrés oxidativo mediada por alimentos con componentes bioactivos hidrofílicos e hidrofóbicos en modelo *in vivo*" (AGL2017-86526-P) financiado por el Ministerio de Economía y Competitividad.
- "Biotechnological design of novel health-promoting compounds: enzymatic production, molecular stabilization and testing" (19893/GERM/15) financiado por el programa de Ayudas a Grupos de Excelencia de la Región de Murcia de la Fundación Séneca – Agencia de Ciencia y Tecnología de la Región de Murcia.

La autora de esta Tesis Doctoral ha disfrutado de un contrato predoctoral competitivo (21269/FPI/19) y opta a la Mención de Doctorado Internacional gracias a una ayuda para la realización de estancias externas destinada a investigadores predoctorales contratados (21678/EFPI/21), ambos financiados por la Fundación Séneca – Agencia de Ciencia y Tecnología de la Región de Murcia.

La presente Tesis Doctoral ha dado lugar a las siguientes publicaciones científicas:

1. **Navarro-Orcajada, S.**, Vidal-Sánchez, F. J., Conesa, I., Escribano-Naharro, F., Matencio, A., & López-Nicolás, J. M. (2023). Antiproliferative Effects in Colorectal Cancer and Stabilisation in Cyclodextrins of the Phytoalexin Isorhapontigenin. *Biomedicines*, *11*(11), 3023.

2. **Navarro-Orcajada, S.**, Conesa, I., Vidal-Sánchez, F. J., Matencio, A., Albaladejo-Maricó, L., García-Carmona, F., & López-Nicolás, J. M. (2023). Stilbenes: Characterization, bioactivity, encapsulation and structural modifications. A review of their current limitations and promising approaches. *Critical Reviews in Food Science and Nutrition*, *63*(25), 7269-7287.

3. **Navarro-Orcajada, S.**, Vidal-Sánchez, F. J., Conesa, I., Matencio, A., & López-Nicolás, J. M. (2023). Improvement of the Physicochemical Limitations of Rhapontigenin, a Cytotoxic Analogue of Resveratrol against Colon Cancer. *Biomolecules*, *13*(8), 1270.

4. **Navarro-Orcajada, S.**, Conesa, I., Matencio, A., Rodríguez-Bonilla, P., García-Carmona, F., & López-Nicolás, J. M. (2022). The use of cyclodextrins as solubility enhancers in the ORAC method may cause interference in the measurement of antioxidant activity. *Talanta*, *243*, 123336.

5. **Navarro-Orcajada, S.**, Conesa, I., Matencio, A., García-Carmona, F., & López-Nicolás, J. M. (2022). Molecular encapsulation and bioactivity of gnetol, a resveratrol analogue, for use in foods. *Journal of the Science of Food and Agriculture*, *102*(10), 4296-4303.

6. **Navarro-Orcajada, S.**, Matencio, A., Vicente-Herrero, C., Garcia-Carmona, F., & López-Nicolás, J. M. (2021). Study of the fluorescence and interaction between cyclodextrins and neochlorogenic acid, in comparison with chlorogenic acid. *Scientific Reports*, *11*(1), 3275.

7. Molinar, C., **Navarro-Orcajada, S.**, Ansari, I. A., Conesa, I., Hoti, G., Monfared, Y. K., Matencio, A., Scomparin, A., López-Nicolás, J. M., Cavalli, R., & Trotta, F. (2023). Cyclodextrins and Cyclodextrin-Based Nanosponges for Anti-Cancer Drug and Nutraceutical Delivery. In *Targeted Cancer Therapy in Biomedical Engineering* (pp. 597-629). Singapore: Springer Nature Singapore.

8. Guadarrama-Flores, B., Matencio, A., **Navarro-Orcajada, S.**, Martínez-Lede, I., Conesa, I., Vidal-Sánchez, F. J., García-Carmona, F., & López-Nicolás, J. M. (2022). Development if healthy milk and yogurt products for reducing metabolic diseases using cyclodextrin and omega-3 fatty acids from fish oil. *Food & Function*, *13*(10), 5528-5535.

9. Matencio, A., Rubin Pedrazzo, A., Difalco, A., **Navarro-Orcajada, S.**, Khazeai Monfared, Y., Conesa, I., Rezayat, A., López-Nicolás, J. M., & Trotta, F. (2021). Advances and classification of cyclodextrin-based polymers for food-related issues. *Polymers*, *13*(23), 4226.

10. Lucia Appleton, S., **Navarro-Orcajada, S.**, Martínez-Navarro, F. J., Caldera, F., López-Nicolás, J. M., Trotta, F., & Matencio, A. (2021). Cyclodextrins as anti-inflammatory agents: basis, drugs and perspectives. *Biomolecules*, *11*(9), 1384.

11. Matencio, A., **Navarro-Orcajada, S.**, García-Carmona, F., & López-Nicolás, J. M. (2021). Encapsulation of antimicrobial compounds. *Functionality of cyclodextrins in encapsulation for food applications*, 169-186.

12. Matencio, A., **Navarro-Orcajada, S.**, García-Carmona, F., & López-Nicolás, J. M. (2020). Applications of cyclodextrins in food science. A review. *Trends in food science & technology*, *104*, 132-143.

Antes de empezar la lectura de esta tesis doctoral, me gustaría dedicar unas merecidas palabras de sincero reconocimiento a aquellas personas que me han acompañado y ayudado de forma desinteresada durante esta etapa. Aquellas personas que, a nivel técnico o emocional, han supuesto un gran apoyo para superar los continuos retos del camino y para que hoy pueda leer el fruto de estos años de trabajo. ***GRACIAS****,*

Al Dr. José Manuel López Nicolás, por la inspiración y motivación que despertó en mí en esas clases de grado, por ver en mí la aptitud para conseguir esto y más, por la confianza que siempre ha tenido en mi criterio científico y por la ayuda que me ha brindado durante estos años.

Al Dr. Francisco García Carmona, por abrirme las puertas de su grupo de investigación y por su inmensa sabiduría que me ayudó cuando los problemas no me permitían ver la solución. Siempre fue un alivio y suerte poder contar con sus consejos.

Al Dr. Adrián Matencio, por hacerme sentir que todo era fácil, aunque no lo pareciera, por creer en mí y por darme ese impulso para que me fuese lo mejor posible.

Al resto de profesores del grupo de Bioquímica y Biotecnología Enzimática, Dr. Fernando Gandía Herrero, Dra. Manoli Pérez Gilabert, Dra. Mercedes Jiménez Atienzar, Dra. Pepa Escribano Cebrián, Dr. Álvaro Sánchez Ferrer y Dra. Juana Mercedes Cabanes Ros, por acogerme tan bien y por haber estado siempre dispuestos a ayudarme.

A mis compañeros y amigos de departamento, con los que siempre he podido contar cuando lo he necesitado y con quienes siempre se hizo más ameno el camino. Gracias a Paula, Samanta, Sandra y Román por vuestra ayuda y compañerismo. Y en especial gracias a los más cercanos, aquellos con los que compartí el día a día. A Karol que, pese a su ajetreada vida, siempre llegaba con una gran sonrisa que alegraba todo el laboratorio. A Pedro, un ejemplo de responsabilidad, honestidad y amistad; gracias a

él nunca se nos pasó ninguna fecha límite. A Irene, mi sucesora, mi cómplice, mi amiga, una bellísima persona a quien debo agradecer tanto, sobre todo gracias por esas risas y por formar tan buen equipo de investigación (para fines científicos y no tan científicos). A Fran, mi pupilo por excelencia, gracias por la confianza que depositó en mí, por todas las curiosidades e idiomas que he aprendido a su lado y, sobre todo, por tantos buenos momentos juntos. Gracias también a todos los alumnos internos y de TFG que me acompañaron en parte de esta tesis, han sido una gran alegría en mi camino y espero haberlos ayudado a lograr sus objetivos. Lorena, Patxi, Eva, Ángeles, Iván, Elena, Marta, Pedro… os deseo lo mejor en vuestro futuro.

A los profesionales y expertos de los servicios del ACTI que me ayudaron y aconsejaron durante el doctorado. A Toñi, Juana, María Jesús, Silvia, Pilar, Pepe y Vero del SCT, Alejandro de Biología Molecular, Pepe y María José de Instrumentación Científica y Diego y Mª del Mar de RMN, gracias por hacerme posible avanzar en los momentos de duda.

Al Dr. Nicholas Morton de The Queen's Medical Research Institute, por aceptarme como una más del equipo durante mi estancia internacional. A Shaden, Hongling y Angus por la ayuda que me brindaron durante esos meses.

A Antonio y Juan Carlos del CEBAS que altruistamente me acogieron y se preocuparon por formarme lo mejor posible. A Juan y Carlos, por su amabilidad y ayuda durante ese tiempo. Y en especial, a Ángela, mi gran ejemplo, a quien debo agradecer todo lo que me ha enseñado, y sobre todo aparecer en mi vida para quedarse en ella.

A los profesores que durante mis distintas etapas académicas me dieron la educación y las bases necesarias para estar aquí y se preocuparon de que fuese capaz de sacar lo mejor de mí.

A todos y cada uno de mis familiares, directos e indirectos, a los que están y a los que se fueron, gracias por quererme y desearme lo mejor en todo momento. Aunque fue difícil que comprendieran a lo que me dedicaba, siempre estuvieron orgullosos de mí.

A aquellos amigos a los que siento que dejé de ver con tanta frecuencia en algunos momentos críticos de la tesis, pero que el tiempo y la distancia no han podido alejarlos demasiado de mi vida.

A Rebeca, casi capaz de leerme la mente a veces, por tantos recuerdos juntas, por estar siempre disponible en caso de necesidad y por ser un gran apoyo para mí.

A Magda, tan soñadora y aventurera, por ser ese volcán de energía que anima a cualquiera y por ese optimismo innato que siempre ha sido esperanzador.

A Alex, por cultivar esa sincera amistad que tanto me ha ayudado a desconectar. A Pilar, por su bondad y gran corazón que la hacen ser tan maravillosa. A José Alberto, Eva, Alfonso y Elena, por los buenos ratos compartidos y los que quedan por venir.

A Noelia y Antonio, con quienes he compartido risas y riñas, pero con quienes siempre sé que podré contar. Gracias por vuestra confianza en mí.

A mis padres, que como buenos padres que son, siempre me dieron lo mejor para que llegará lejos y sé que hoy se sienten muy satisfechos y orgullosos con ese esfuerzo. Gracias por insistirme a que aspirase a lo más alto y no me rindiera jamás.

A Jose, por su infinita paciencia ante mi elección, por su apoyo incondicional, por su sabiduría y comprensión, por aportar perspectiva a mis problemas, por los momentos vividos y por tantas cosas que nunca tuvimos necesidad de compartir con nadie y que hoy no va a ser la excepción. Gracias por hacerme feliz.

Del salón en el ángulo oscuro,
de su dueña tal vez olvidada
silenciosa y cubierta de polvo
veíase el arpa.

¡Cuánta nota dormía en sus cuerdas
cómo el pájaro duerme en las ramas,
esperando la mano de nieve
que sabe arrancarlas!

¡Ay!, pensé; ¡cuántas veces el genio
así duerme en el fondo del alma,
y una voz como Lázaro espera
que le diga <<Levántate y anda>>!

G. A. Bécquer

List of Abbreviations

2,4-D: 2,4-Dichlorophenoxyacetic acid

A^-: Deprotonated form of an acid

AAPH: 2,2'-azobis(2-amidinopropane) dihydrochloride

Abs: Absorbance

ABTS: 2,2'-Azino-bis (3-ethylbenzothiazoline -6-sulfonic acid)

ACC: Acetyl-CoA carboxylase

Adipoq: Adiponectin (gene)

ALT: Alanine aminotransferase

APOL: Atomic polarizability

AST: Aspartate aminotransferase

AUC: Area Under the Curve

BUN: Blood urea nitrogen

c: Concentration

C: Cysteine

C/EBPα: CCAAT-enhancer-binding protein alpha

C4H: Cinnamate 4-hydroxylase

CD: Cyclodextrin

cDNA: Complementary DNA

CFU: Colony Forming Units

CHO: Cholesterol

CHS: Chalcone synthase

CL: 4-Coumarate CoA ligase

cm: Centimetre(s)

cm^2: Square Centimetre(s)

C_{max}: Maximum concentration

CMC: Critical Micelle Concentration

CoA: Coenzyme A

COX: Cyclooxygenase

CQA: Caffeoylquinic acid

CR: Creatinine

CS: Chorismate synthase

C_t: Cycle threshold

δ: Chemical shift

Da: Dalton

DAD: Diode Array Detector

DCC: N,N'-Dicyclohexylcarbodiimide

DHA: Docosahexaenoic acid

dL: Decilitre(s)

DMAP: 4-Dimethylaminopyridine

DMEM: Dulbecco's Modified Eagle Medium

DMF: N,N-Dimethylformamide

DMSO: Dimethyl sulfoxide

DNA: Deoxyribonucleic acid

DPPH: 2,2'-Diphenyl-1-picrylhydrazyl

ε: Absorptivity o extinction coefficient

EFSA: European Food Safety Agency

e.g.: *exempli gratia*

EIC: Extracted Ion Chromatogram

EMEM: Eagle's Minimum Essential Medium

ESI: Electrospray

EU: European Union

F: Phenylalanine

FAS: Fatty acid synthase

Fasn: Fatty acid synthase (gene)

FBS: Foetal Bovine Serum

FRAP: Ferric Reducing Antioxidant Power

GAPDH: Glyceraldehyde-3-phosphate dehydrogenase

Gapdh: Glyceraldehyde-3-phosphate dehydrogenase (gene)

GLUT4: Glucose transporter type 4

GPx: Glutathione peroxidase

GRAS: Generally Recognized As Safe

GST: Glutathione-S-transferase

h: Hour(s)

H: Histidine

HA: Protonated form of an acid

HAT: Hydrogen Atom Transfer

Hb: Haemoglobin

HBCD-Pol: Hyper-branched CD-based polymers

HBSS: Hank's Balanced Salt Solution

HDL: High Density Lipoprotein

HP-β-CD: 2-Hydroxypropyl-β-CD

HPLC: High Performance Liquid Chromatography

HRP: Horseradish peroxidase

IBMX: 3-Isobuthyl-1-methylxanthine

IC50: Half-maximal inhibitory concentration

i.e.: *id est*

IL: Interleukin

IPTG: Isopropyl β-D-1-thiogalactopyranoside

k: Capacity factor

kDa: Kilodalton

k_e: Apparent elimination constant

K_F: Formation or encapsulation constant

$K_{F\ ap}$: Apparent formation or encapsulation constant

kg: Kilogram(s)

λ: Wavelength

l: Optical path

L: Litre(s)

LB: Luria-Bertani o Lysogeny Broth

LC: Liquid Chromatography

LDL: Low Density Lipoprotein

λ_{em}: Fluorescence maximum emission wavelength

Lep: Leptin (gene)

λ_{ex}: Fluorescence maximum excitation wavelength

λ_{max}: Maximum absorbance wavelength

LogP: Lipophilicity index

LogS: Aqueous solubility index

LPL: Lipoprotein lipase

M: Molar

M-β-CD: Methyl-β-cyclodextrin

m/z: Mass-to-charge ratio

MDA: Malondialdehyde

Mfn2: Mitofusin 2 (gene)

µg: Microgram(s)

mg: Milligram(s)

min: Minute(s)

µL: Microlitre(s)

mL: Millilitre(s)

µm: Micrometre(s)

µM: Micromolar

mM: Millimolar

MR: Molar refractivity

mRNA: Messenger RNA

MS: Mass Spectrometry

MTT: 3-(4,5-Dimethylthiazol-2-yl)-2,5-diphenyltetrazolium bromide

MW: Molar weight

N: Asparagine

net AUC: Net Area Under the Curve

NF-kB: Nuclear Factor kappa B

ng: Nanogram(s)

NGM: Nematode Growth Medium

nM: Nanomolar

NMR-H: Proton Nuclear Magnetic Resonance

OD: Optical Density

OE: Oxyresveratrol stearate

OO: Oxyresveratrol oleate

OP: Oxyresveratrol palmitate

ORAC: Oxygen Radical Absorbance Capacity

ORO: Oil Red O

P: Proline

SDS-PAGE: Sodium Dodecyl Sulfate–PolyAcrylamide Gel Electrophoresis

PAL: Phenylalanine ammonia lyase

P_{ap}: Apparent permeability

PBS: Phosphate Buffered Saline

PDB: Protein Data Bank

pK_a: Acid dissociation constant

PKS: Polyketide synthase

PcE: Piceatannol stearate

PcO: Piceatannol oleate

PcP: Piceatannol palmitate

PCR: Polymerase Chain Reaction

PPARα: Peroxisome proliferator-activated receptor alpha

PPARγ: Peroxisome proliferator-activated receptor gamma

ppm: Parts per million

PtE: Pterostilbene stearate

PtO: Pterostilbene oleate

PtP: Pterostilbene palmitate

PUFA: Polyunsaturated fatty acids

R1, **R2**, **R3**…: Radical 1, Radical 2, Radical 3…

RE: Resveratrol stearate

RM-β-CD: Randomly methylated β-cyclodextrin

RMSE: Root Mean Square Error

RNA: Ribonucleic acid

RNS: Reactive Nitrogen Species

RO: Resveratrol oleate

ROS: Reactive Oxygen Species

RP: Resveratrol palmitate

rpm: Revolutions per minute

RT-qPCR: Real-Time quantitative PCR

s: Second(s)

SARS-CoV: Severe Acute Respiratory Syndrome Coronavirus

SDS: Sodium Dodecyl Sulphate

SEM: Standard Error of the Mean

SET: Single Electron Transfer

SIRT: Sirtuin

Sirt3: Sirtuin 3 (gene)

Slc2a4: Solute carrier family 2 member 4 (gene)

SOC: Super Optimal Broth

SOD: Superoxide dismutase

SREBP-1c: Sterol Regulatory Element-Binding Protein 1c

STS: Stilbene synthase

t: Time

$t_{1/2}$: Half-life

TAL: Tyrosine ammonia lyase

TAS: Total Antioxidant Status

TB: Terrific Broth

Tbp: TATA-binding protein (gene)

TEER: Transepithelial Electrical Resistance

TG: Triacylglycerides

TLC: Thin-Layer Chromatography

$\mathbf{t_{max}}$: Time to reach maximum concentration

TNF-α: Tumour Necrosis Factor alpha

TOF: Time Of Flight

TPSA: Topological Polar Surface Area

TPTZ: 2,4,6-Tri(2-pyridyl)-1,3,5-triazine

UCP: Uncoupling protein

Ucp1: Uncoupling protein 1 or thermogenin (gene)

UV: Ultraviolet

UV-Vis: Ultraviolet-Visible

v/v: Volume/volume ratio

Vis: Visible

vs: Versus

Ω: Ohm(s)

ω-3: Omega-3

WHO: World Health Organization

WOS: Web of Science

w/v: Weight/volume ratio

w/w: Weight/weight ratio

xg: Relative centrifugal force

INDEX

RESUMEN **2**

ABSTRACT **9**

CHAPTER I. GENERAL INTRODUCTION **16**

1. NUTRITION AND HUMAN HEALTH **16**

2. STILBENES **18**

2.1. SOURCES AND PRODUCTION 20
2.1.1. Dietary stilbenes *20*
2.1.2. Biosynthesis pathway *21*
2.1.3. Alternative sources *23*
2.2. PHYSICOCHEMICAL PROPERTIES 23
2.2.1. Solubility, lipophilicity and polarity *24*
2.2.2. Absorbance properties *25*
2.2.3. Fluorescence properties *26*
2.2.4. Acid dissociation constant *28*
2.2.5. Aggregation and critical concentration *28*
2.2.6. Stability and degradation *29*
2.3. HEALTH PROMOTING EFFECTS 30
2.3.1. Antimicrobial activity *31*
2.3.2. Antioxidant activity *32*
2.3.3. Anti-inflammatory activity *34*
2.3.4. Cardioprotective activity *36*
2.3.5. Anticarcinogenic activity *37*
2.3.6. Anti-obesity activity *39*
2.4. CHALLENGES AND CONSTRAINTS IN THE APPLICATIONS OF STILBENES 41
2.5. INNOVATIVE APPROACHES TO OVERCOME THE LIMITATIONS OF STILBENES 43
2.5.1. Molecular encapsulation *43*
2.5.1.1. Cyclodextrins 43
2.5.1.2. Polymeric nanoparticles 45
2.5.1.3. Liposomes 47
2.5.2. Structural modifications *47*
2.5.2.1 Hydroxylation 48
2.5.2.2. Glycosylation 49
2.5.2.3. Methoxylation 50
2.5.2.4. Halogenation 51
2.5.2.5. Acylation 52

CHAPTER II. OBJECTIVES **54**

CHAPTER III. MATERIALS AND METHODS **56**

1. MATERIALS **56**

2. ENZYMATIC SYNTHESIS OF PICEATANNOL **57**

2.1. SPECTROPHOTOMETRIC ANALYSIS 58
2.2. HPLC-UV/VIS ANALYSIS 58

3. PHYLOGENETIC ANALYSIS **59**

3.1. SEQUENCE SEARCH AND MULTIPLE ALIGNMENT 59
3.2. HIDDEN MARKOV MODEL 59
3.3. CONSTRUCTION OF PHYLOGENETIC TREES 60

4. DETERMINATION OF THERMOSTABILITY **61**

5. PRODUCTION OF A STS IN *ESCHERICHIA COLI* **61**

5.1. STRAINS, VECTOR, AND CULTIVATION CONDITIONS 61
5.2. BACTERIAL TRANSFORMATION BY ELECTROPORATION 62
5.3. PROTEIN EXPRESSION 62
5.4. PROTEIN PURIFICATION 63
5.5. PROTEIN QUANTIFICATION WITH BRADFORD 63
5.6. ELECTROPHORESIS SDS-PAGE 63

5.7. GEL STAINING WITH COOMASSIE BLUE 64

6. PHYSICOCHEMICAL CHARACTERISATION 64

6.1. NUCLEAR MAGNETIC RESONANCE 64
6.2. SPECTROPHOTOMETRY 65
6.3. FLUORESCENCE SPECTROSCOPY 65
6.4. HPLC-DAD ANALYSIS 66
6.5. DETERMINATION OF AQUEOUS SOLUBILITY 66
6.6. DETERMINATION OF STABILITY IN AQUEOUS SOLUTION 66
6.7. DETERMINATION OF ENZYMATIC OXIDATION 67
6.8. PREDICTION OF PHYSICOCHEMICAL PARAMETERS 67

7. MOLECULAR ENCAPSULATION 68

7.1. MOLECULAR ENCAPSULATION IN CDS 68
7.1.1. Molecular docking 69
7.1.2. Benesi-Hildebrand method 70
7.1.3. Competitive model for two binding sites in the guest molecule 72
7.1.4. Mohseni-Hurtubise method 74
7.2. MOLECULAR ENCAPSULATION IN HBCD-POL 76

8. SYNTHESIS AND PURIFICATION OF HYDROPHOBIC STILBENE DERIVATIVES 76

8.1. CHEMICAL SYNTHESIS 76
8.2. ENZYMATIC SYNTHESIS 77
8.3. PURIFICATION BY COLUMN CHROMATOGRAPHY AND TLC 78
8.4. PURIFICATION BY PREPARATIVE HPLC-DAD 79

9. PANCREATIC LIPASE ACTIVITY ASSAYS 79

9.1. DETERMINATION OF THE HYDROLYSIS DEGREE 80
9.2. PANCREATIC LIPASE ENZYMATIC INHIBITION ASSAYS 80
9.2.1. Spectrofluorometric enzymatic inhibition assays 81
9.2.2. Chromatographic enzymatic inhibition assays 81
9.3. PANCREATIC LIPASE ACTIVITY ASSAYS IN THE PRESENCE OF CDS 82

10. DETERMINATION OF ANTIOXIDANT ACTIVITY 82

10.1. ORAC METHOD 83
10.2. ABTS METHOD 84
10.3. DPPH METHOD 86
10.4. FRAP METHOD 86
10.5. ASSESSMENT OF CDS INTERFERENCE IN ANTIOXIDANT METHODS 87
10.5.1. Assessment of CDs interference in the ORAC method 87
10.5.2. Assessment of CDs interference in the ABTS method 88
10.5.3. Assessment of CDs interference in the DPPH method 89
10.5.4. Assessment of CDs interference in the FRAP method 90

11. HUMAN AND ANIMAL CELL CULTURE 90

11.1. CELL LINES AND CULTURE CONDITIONS 90
11.1.1. Caco-2 cell line 92
11.1.2. 3T3-L1 cell line 92
11.2. DETERMINATION OF CELL VIABILITY AND PROLIFERATION 93
11.2.1. MTT assay 93
11.2.2. Neutral Red assay 95
11.3. CELL PERMEABILITY AND METABOLISM 96
11.4. EXTRACTION OF CELLULAR MEDIA AND HPLC-DAD/ESI(-) ANALYSIS 98
11.5. CELL DIFFERENTIATION 99
11.6. ORO LIPID STAINING IN CELL CULTURES 100
11.7. MICROSCOPY IN CELL CULTURES 100
11.8. IMAGE ANALYSIS IN CELL CULTURES 101
11.9. GENE EXPRESSION DETERMINATION 101
11.9.1. RNA extraction 102

11.9.2. cDNA reverse transcription *102*
11.9.3. Real-Time qPCR *102*
11.9.4. Comparative quantification method ($2^{-\Delta\Delta Ct}$) *104*
11.10. EVALUATION OF LIPOLYSIS DEGREE 105

12. *CAENORHABDITIS ELEGANS* ANIMAL MODEL 105

12.1. STRAINS AND CULTIVATION CONDITIONS 106
12.2. CULTIVATION SYNCHRONIZATION 107
12.3. LIFESPAN ASSAYS 107
12.4. ORO LIPID STAINING IN ANIMAL MODELS 108
12.5. OXIDATIVE STRESS ASSAYS 109
12.6. MICROSCOPY IN ANIMAL MODELS 110
12.7. IMAGE ANALYSIS IN ANIMAL MODELS 110

13. *MUS MUSCULUS* ANIMAL MODEL 111

13.1. PHARMACOKINETIC ASSAYS 111
13.1.1. Experimental design *111*
13.1.2. Plasma extraction and HPLC-ESI(-) analysis *112*
13.1.3. Determination of pharmacokinetic parameters *113*
13.1.4. Determination of serum biological markers *114*
13.2. MELANOMA ASSAYS 115
13.2.1. Experimental design and tumour induction *115*
13.2.2. Histopathological examination *116*
13.2.3. Determination of tumour microvessel density *117*

14. DEVELOPMENT OF FUNCTIONAL FOOD MODELS 117

14.1. PREPARATION OF MILK AND JUICE FOOD MODELS 117
14.2. MONITORING OF INDUSTRIAL QUALITY PARAMETERS 118
14.3. DETERMINATION OF STILBENES IN FOOD MODELS 118
14.3.1. Spectrophotometric analysis of food models *119*
14.3.2. HPLC-UV/Vis analysis of food models *119*

15. DATA ANALYSIS 119

CHAPTER IV. RESULTS AND DISCUSSION 122

1. CURRENT AND FUTURE STRATEGIES TO INCREASE STILBENE PRODUCTION 122

1.1. CURRENT STRATEGY: TYROSINASE-CATALYSED PICEATANNOL SYNTHESIS 122
1.1.1. Spectrophotometric monitoring of piceatannol synthesis *123*
1.1.2. HPLC-UV/Vis monitoring of piceatannol synthesis *126*
1.2. FUTURE STRATEGY: PHYLOGENETIC ANALYSIS OF STS ENZYMES AND PRODUCTION OF A POTENTIAL BACTERIAL STS IN *E. COLI* 130
1.2.1. Study of the conservation and evolutionary origin of plant STS *130*
1.2.2. Study of the conservation of STS during evolution *136*
1.2.3. Search for STS in extremophilic microorganisms and thermostability of resveratrol *138*
1.2.4. Expression of STS from Meiothermus sp. Pnk-1 in E. coli *140*
1.2.5. Study of the evolutionary relationship between STS and CHS *142*
1.3. CONCLUSIONS ON STRATEGIES TO INCREASE STILBENE PRODUCTION 145

2. CHARACTERISATION AND MOLECULAR ENCAPSULATION OF NATURAL STILBENES 147

2.1. GNETOL 147
2.1.1. Optical properties of gnetol *148*
2.1.2. Physicochemical study of the gnetol inclusion complexes *148*
2.1.3. Molecular docking of gnetol in CDs *150*
2.1.4. Influence of pH and temperature on gnetol encapsulation *152*
2.1.5. Solubility and stability of free and encapsulated gnetol *154*
2.2. ISORHAPONTIGENIN 155
2.2.1. Optical properties of isorhapontigenin *156*

2.2.2. Physicochemical study of the inclusion complexes with isorhapontigenin 157
2.2.3. Molecular docking of isorhapontigenin in CDs 159
2.2.4. Influence of pH and temperature on isorhapontigenin encapsulation 160
2.2.5. Solubility and stability of free and encapsulated isorhapontigenin 161
2.3. RHAPONTIGENIN 163
2.3.1. Optical properties of rhapontigenin 163
2.3.2. Physicochemical study of rhapontigenin inclusion complexes 164
2.3.3. Molecular docking of rhapontigenin in CDs 166
2.3.4. Influence of pH and temperature on rhapontigenin encapsulation 167
2.3.5. Solubility and stability of free and encapsulated rhapontigenin 169
2.4. PINOSTILBENE 170
2.4.1. Optical properties of pinostilbene 171
2.4.2. Physicochemical study of the inclusion complexes with pinostilbene 172
2.4.3. Molecular docking of pinostilbene in CDs 173
2.4.4. Influence of pH on pinostilbene encapsulation 175
2.4.5. Solubility and stability of free and encapsulated pinostilbene 175
2.5. CONCLUSIONS ON THE CHARACTERISATION AND MOLECULAR ENCAPSULATION OF NATURAL STILBENES 177

3. SYNTHESIS, CHARACTERISATION AND MOLECULAR ENCAPSULATION OF HYDROPHOBIC STILBENE DERIVATIVES 179

3.1. SYNTHESIS AND PURIFICATION OF HYDROPHOBIC STILBENE DERIVATIVES 179
3.2. CHARACTERISATION OF HYDROPHOBIC STILBENE DERIVATIVES 184
3.2.1. Nuclear Magnetic Resonance 184
3.2.2. Chromatography 185
3.2.3. Spectrophotometry 188
3.2.4. Fluorescence spectroscopy 191
3.2.5. Other physicochemical parameters 194
3.3. MOLECULAR ENCAPSULATION OF HYDROPHOBIC STILBENE DERIVATIVES 197
3.3.1. Molecular docking of hydrophobic stilbene derivatives in CDs 197
3.3.2. Physicochemical study of the inclusion complexes with hydrophobic stilbene derivatives 201
3.4. CONCLUSIONS ON THE SYNTHESIS, CHARACTERISATION AND MOLECULAR ENCAPSULATION OF HYDROPHOBIC STILBENE DERIVATIVES 206

4. DIGESTION, ABSORPTION AND METABOLISM OF HYDROPHOBIC STILBENE DERIVATIVES 209

4.1. *IN VITRO* ASSAYS 210
4.1.1. Effect of pancreatic lipase on hydrophobic stilbene derivatives 210
4.1.1.1. Hydrolysis degree of hydrophobic stilbene derivatives 210
4.1.1.2. Inhibition of pancreatic lipase catalytic activity with free caffeoylquinic acids 212
4.1.1.2.1. Spectrofluorometric inhibition tests 212
4.1.1.2.2. Chromatographic inhibition tests 213
4.1.1.3. Molecular encapsulation of caffeoylquinic acids 215
4.1.1.3.1. Molecular docking of caffeoylquinic acids in CDs 216
4.1.1.3.2. Effect of complexation on solubility and enzymatic oxidation of neochlorogenic acid 218
4.1.1.3.3. Effect of complexation on the inhibitory activity of caffeoylquinic acids against pancreatic lipase 219
4.1.1.4. Influence of CDs on the catalytic activity of pancreatic lipase 221
4.1.2. Cytotoxicity of hydrophobic stilbene derivatives in intestinal cells 224
4.1.2.1. MTT cytotoxicity assays 224
4.1.2.2. Neutral red cytotoxicity assays 226
4.1.3. Apparent permeability of hydrophobic stilbene derivatives 229
4.1.4. Metabolism of hydrophobic stilbene derivatives 232
4.2. *IN VIVO* ASSAYS: *M. MUSCULUS* ANIMAL MODEL 236
4.2.1. Pharmacokinetics of resveratrol stearate in free form and encapsulated in CDs 236
4.2.2. Serum biomarker analysis 239
4.2.2.1. Lipid profile 239
4.2.2.2. Hepatic-renal profile 240
4.2.2.3. Oxidative profile 242
4.2.2.4. Inflammatory profile 243

4.3. CONCLUSIONS ON DIGESTION, ABSORPTION AND METABOLISM OF HYDROPHOBIC STILBENE DERIVATIVES 244

5. BIOACTIVITY OF HYDROPHOBIC STILBENE DERIVATIVES AND NATURAL STILBENES 248

5.1. *IN VITRO* BIOLOGICAL ACTIVITY 248
5.1.1. Antioxidant activity 248
5.1.1.1. Antioxidant activity of hydrophobic stilbene derivatives and their natural stilbenes 248
5.1.1.1.1. ORAC method 249
5.1.1.1.2. ABTS method 251
5.1.1.1.3. DPPH method 252
5.1.1.1.4. FRAP method 254
5.1.1.1.5. Comparison of the antioxidant activity of hydrophobic stilbene derivatives by different methods 256
5.1.1.2. Influence of CDs on antioxidant methods 260
5.1.1.2.1. Influence of CDs on the ORAC method 261
5.1.1.2.2. Influence of CDs on the ABTS method 266
5.1.1.2.3. Influence of CDs on the DPPH method 270
5.1.1.2.4. Influence of CDs on the FRAP method 275
5.1.1.2.5. Overall discussion on the influence of CDs on different antioxidant methods 278
5.1.2. Cytotoxicity of stilbene analogues of resveratrol 281
5.1.3. Anti-obesity activity of hydrophobic resveratrol derivatives 284
5.1.3.1. Effect on adipogenesis and lipid accumulation 284
5.1.3.2. Gene expression during adipogenesis 288
5.1.3.3. Effect on lipolysis in mature adipocytes 292
5.2. *IN VIVO* BIOLOGICAL ACTIVITY 293
5.2.1. C. elegans animal model 293
5.2.1.1. Survival assays 294
5.2.1.2. Oxidative stress assays 295
5.2.1.3. Lipid accumulation assays 297
5.2.2. M. musculus animal model for melanoma 299
5.2.2.1. Inhibition of tumour growth 299
5.2.2.2. Angiogenesis in tumours 300
5.2.2.3. Histopathological examination 301
5.2.2.3.1. Histopathological examination of tumours 301
5.2.2.3.2. Histopathological examination of liver 303
5.2.2.3.3. Histopathological examination of kidneys 305
5.2.2.4. Serum biomarker analysis 307
5.2.2.4.1. Hepatic-renal profile 307
5.2.2.4.2. Oxidative profile 308
5.2.2.4.3. Inflammatory profile 309
5.3. CONCLUSIONS ON THE *IN VITRO* AND *IN VIVO* BIOACTIVITY OF HYDROPHOBIC STILBENE DERIVATIVES AND NATURAL STILBENES 311

6. PRACTICAL APPLICATION OF HYDROPHOBIC STILBENE DERIVATIVES FOR THE FOOD INDUSTRY 316

6.1. THERMOSTABILITY IN FORTIFIED FOOD MODELS 316
6.2. MONITORING OF QUALITY PARAMETERS IN FORTIFIED FOOD MODELS 317
6.3. STABILITY OF THE HYDROPHOBIC STILBENE DERIVATIVE IN THE FOOD MATRIX DURING STORAGE 319
6.4. CONCLUSIONS ON THE USE OF HYDROPHOBIC DERIVATIVES OF STILBENES AS BIOACTIVE INGREDIENTS IN FUNCTIONAL FOODS 322

CHAPTER V. CONCLUSIONS 325

REFERENCES 329

APPENDICES 386

RESUMEN / ABSTRACT

RESUMEN

Los estilbenos son compuestos fenólicos con numerosas bioactividades que los hacen de interés para la salud humana, como su actividad antimicrobiana, antioxidante, anti-inflamatoria, cardioprotectora, anticancerígena o anti-obesidad, entre otras muchas. Se trata de metabolitos secundarios que son producidos por determinadas plantas en situaciones de estrés biótico o estrés abiótico, mediante la ruta de síntesis de fenilpropanoides, siendo la enzima estilbeno sintasa clave en el proceso de biosíntesis. Entre las fuentes principales de obtención de estilbenos a través de la dieta, se encuentran la uva, el vino tinto y los cacahuetes. Dentro de este grupo de compuestos bioactivos, destaca el resveratrol por ser el más investigado, sin embargo, existen otros estilbenos menos conocidos con mayor potencial terapéutico. No obstante, la limitada producción en planta, baja solubilidad en agua, facilidad para degradarse, así como baja biodisponibilidad de esta familia de compuestos bioactivos dificultan su correcta aplicación en la industria alimentaria, farmacéutica o cosmética. En esta tesis doctoral se han investigado varios planteamientos para hacer frente a estas limitaciones.

Con el fin de abordar los problemas en la obtención de estilbenos naturales, se han desarrollado estrategias presentes y futuras para aumentar su producción. En este contexto, se ha diseñado un método para incrementar la síntesis enzimática de piceatanol a partir de resveratrol utilizando tirosinasa como agente catalizador, logrando hasta un 56 % de conversión con la incorporación de agentes reductores en la reacción. Como estrategia futura, se ha optimizado la expresión de una estilbeno sintasa recombinante, encontrada mediante análisis filogenéticos de estas proteínas en microorganismos extremófilos, para próximas aplicaciones biotecnológicas en la síntesis de estilbenos. Estos estudios bioinformáticos también permitieron descubrir el origen y la evolución de las proteínas estilbeno sintasa en distintos reinos, pudiéndose observar una distribución

más amplia de la que se pensaba en un principio y una clara relación con las proteínas chalcona sintasa, habiendo evolucionado las proteínas estilbeno sintasa de estas otras proteínas en varias ocasiones, de manera independiente dentro de cada género.

Por otra parte, se caracterizaron y encapsularon algunos de los análogos del resveratrol más prometedores, como gnetol, isorapontigenina, rapontigenina y pinoestilbeno, logrando incrementar su solubilidad y estabilidad en disoluciones acuosas mediante la formación de complejos de inclusión con ciclodextrinas. Las propiedades espectrofotométricas y fluorescentes de estos estilbenos fueron analizadas y comparadas con las de otros estilbenos. La estequiometria y las constantes de formación con ciclodextrinas naturales y modificadas fueron determinadas mediante ensayos bioinformáticos y fisicoquímicos. Se pudo observar que la encapsulación molecular se regía por un modelo 1:1 en todos los complejos analizados, con una mayor afinidad por la ciclodextrina modificada hidroxipropil-β-ciclodextrina, reflejada por una constante de encapsulación superior y *score* del *docking molecular* inferior. Además, el estudio de los complejos de inclusión en distintas condiciones de pH y temperatura demostró que estos dos parámetros influyen notablemente en la encapsulación molecular y permitió determinar los parámetros termodinámicos.

Para hacer frente a la baja biodisponibilidad de los estilbenos, se sintetizaron nuevos derivados hidrofóbicos de estilbenos que podrían actuar como precursores de estos protegiéndolos de las reacciones de fase II que disminuyen su biodisponibilidad, como la sulfatación y glucuronidación, y facilitando su transporte hacia los adipocitos, tejido diana donde los estilbenos han demostrado tener efectos anti-obesidad. Estos derivados hidrofóbicos de estilbenos fueron caracterizados fisicoquímicamente y encapsulados en ciclodextrinas para después analizar sus propiedades biológicas *in vitro* e *in vivo*.

La síntesis de los derivados hidrofóbicos de estilbenos se llevó a cabo por vía química y por vía enzimática, alcanzando rendimientos de hasta el 78 % y 56 %, respectivamente, con una alta especificidad para la formación de monoésteres. Entre los métodos de síntesis optimizados, el químico alcanzó un mayor rendimiento en menor tiempo y sin necesidad de mantener temperaturas elevadas durante el proceso, por lo que fue el seleccionado para la obtención de la mayoría de los derivados. En algunas reacciones, se pudo observar una mezcla racémica estable de los distintos isómeros posibles según el grupo hidroxilo modificado. La derivatización modificó las propiedades ópticas, resonancia, polaridad y solubilidad de los estilbenos, de forma variable según el tipo de derivado sintetizado. Los derivados hidrofóbicos de estilbenos mostraron una mayor afinidad por hidroxipropil-β-ciclodextrina, formando complejos de estequiometria 1:1 con esta ciclodextrina en presencia de un 85 % de metanol.

Al investigar la digestión, absorción y metabolismo de estos derivados hidrofóbicos de estilbenos, se pudo observar que eran susceptibles de ser hidrolizados por lipasa pancreática *in vitro*, una enzima clave durante el proceso digestivo de este tipo de moléculas. El grado de hidrólisis varió según el tipo de derivado estilbenoide y pudo ser inhibido mediante el uso de ácidos cafeoilquínicos libres. Por el contrario, el uso de ciclodextrinas activó la actividad catalítica sobre aquellos isómeros con una mayor afinidad, probablemente debido a la disgregación de la conformación micelar de los derivados hidrofóbicos de estilbenos a partir de cierta concentración de ciclodextrina. El uso de ácidos cafeoilquínicos complejados también mostró este efecto por la presencia de ciclodextrinas. A pesar de ello, la encapsulación molecular de estos inhibidores mejoró su solubilidad acuosa y estabilidad frente a la oxidación enzimática. La encapsulación molecular de los ácidos cafeoilquínicos fue caracterizada mediante un modelo competitivo con dos posibles sitios de complejación en el ligando, estableciéndose dos

constantes de formación identificadas con ensayos computacionales, y observándose una mayor afinidad por α-ciclodextrina e hidroxipropil-β-ciclodextrina.

Los ensayos con células Caco-2 mostraron que los derivados hidrofóbicos de estilbenos eran menos sensibles a las reacciones de sulfatación y glucuronidación que disminuyen la biodisponibilidad de los estilbenos, siendo capaces de mantener su forma aglicona mejor que los estilbenos originales. Además, algunos de los derivados hidrofóbicos de estilbenos también mostraron una mejora en la permeabilidad aparente a través de células intestinales. A nivel preclínico, a pesar de observarse hidrólisis parcial, mejoraron los niveles de biomarcadores de transporte de lípidos, daño hepático, función renal, estrés oxidativo e inflamación tras la administración oral de derivados hidrofóbicos de estilbenos en *Mus musculus*, especialmente, si estos se administraban en su forma encapsulada. La biodisponibilidad relativa de estilbeno también mejoró aparentemente con el uso de estos agentes, a pesar de ser mayoritariamente en su forma hidrolizada.

En la evaluación de la actividad antioxidante *in vitro* de los derivados hidrofóbicos de estilbenos se pudo observar que estos nuevos estilbenos tenían una menor reactividad frente a los radicales libres y complejos metálicos en comparación con los estilbenos originales, probablemente debido a la desaparición de los grupos hidroxilo libres tras la esterificación. Esta menor reactividad podría sugerir una mayor estabilidad de los derivados hidrofóbicos de estilbenos en presencia de agentes oxidantes en el medio, pudiendo ser capaces de mantener más intacto al estilbeno en la matriz previo a su administración. Tras analizar la actividad antioxidante de los derivados hidrofóbicos de estilbenos, se investigó el efecto de las ciclodextrinas en estos métodos, puesto que la bibliografía muestra cierta discrepancia sobre su uso. Durante estos ensayos, se descubrió que las ciclodextrinas pueden interferir con los métodos de determinación de actividad antioxidante *in vitro,* dando lugar a variaciones en las medidas que podrían ser

malinterpretadas como una mayor o menor actividad antioxidante. Los estudios espectrales y bioinformáticos revelaron que esta interferencia podría deberse a la encapsulación de los reactivos implicados en las reacciones redox, sin tener prácticamente efecto la propia naturaleza glucídica de las ciclodextrinas. Esta desviación dependió del tipo y concentración de ciclodextrina, y varío según el método utilizado. Aunque hubo métodos en los que algunas concentraciones de ciclodextrina no mostraron una desviación significativa, dado que la interacción con ciclodextrinas es no covalente y no específica, no se descarta la interferencia al variar las condiciones de los ensayos.

Por otra parte, se evaluó la actividad citotóxica de algunos análogos del resveratrol en células de cáncer colorrectal con el fin de establecer relaciones estructura-actividad e identificar estilbenos con mayor actividad que el resveratrol. La viabilidad celular mostró una correlación positiva con el número de grupos hidroxilo en la molécula de estilbeno y negativa con el número de grupos metoxi. Así, estilbenos metoxilados como el pteroestilbeno o trimetoxiestilbeno lograron una mayor inhibición de la proliferación celular que el resveratrol, a diferencia de análogos hidroxilados, como el oxirresveratrol o gnetol.

Los estudios de bioactividad de los derivados hidrofóbicos de estilbenos en cultivos celulares y en el modelo animal *Caenorhabditis elegans* mostraron que la derivatización de los estilbenos afecta a su actividad anti-obesidad. En células, los derivados hidrofóbicos de estilbenos no mostraron beneficio sobre la acumulación de lípidos, ni sobre la lipólisis, sin embargo, su forma hidrolizada fue capaz de inhibir la adipogénesis en pre-adipocitos y activar la lipólisis en adipocitos maduros. A pesar de ello, durante la adipogénesis, algunos derivados hidrofóbicos de estilbenos mostraron sobreexpresión de genes relacionados con la sensibilización a la insulina, la movilización de grasas y la termogénesis, lo cual podría ser relevante en enfermedades como la diabetes

tipo 2 y la obesidad. A diferencia de los cultivos celulares, en el modelo *C. elegans*, se pudo observar una reducción significativa en la acumulación de lípidos tras el tratamiento con los derivados hidrofóbicos de estilbenos encapsulados en polímeros de ciclodextrina. Estos resultados en cultivos celulares y *C. elegans*, junto con los obtenidos previamente en *M. musculus*, sugieren que los efectos beneficiosos de los derivados hidrofóbicos de estilbenos sobre la obesidad podrían estar relacionados con una mejora en el transporte de lípidos, más allá de su propia actividad en el tejido adiposo.

El tratamiento de *C. elegans* con los derivados hidrofóbicos de estilbenos, en presencia de los polímeros de ciclodextrina, no alteró la vida media de los nematodos, sugiriendo que los derivados no presentan toxicidad para los individuos. Además, el mismo tratamiento sobre la cepa TJ375 no tuvo efecto sobre el estrés oxidativo, probablemente debido a la complejación de los derivados.

En modelos *in vivo* de melanoma, el tratamiento intratumoral con los derivados hidrofóbicos de estilbenos logró una mayor inhibición del crecimiento tumoral asociada con una menor angiogénesis, en comparación con el tratamiento con los estilbenos originales, libres o encapsulados. La administración de los derivados hidrofóbicos de estilbenos encapsulados fue la más efectiva, obteniendo los tumores más pequeños con menor vascularización, así como un mayor grado de necrosis y menor número de células mitóticas. Además, el examen histopatológico de los tejidos de este grupo reveló menos daños en hígado y riñones. Los niveles de biomarcadores séricos de inflamación y daño hepático-renal de estos individuos disminuyeron notablemente, aproximándose a los valores de los individuos sanos, mientras que los biomarcadores antioxidantes aumentaron por encima incluso que los niveles de los individuos sin tumor. En su conjunto, estos resultados respaldan las potenciales aplicaciones de los derivados hidrofóbicos de estilbenos frente al cáncer.

Finalmente, se desarrollaron modelos de alimentos funcionales enriquecidos con uno de los derivados hidrofóbicos de estilbenos, en su forma libre y encapsulada, monitorizando los parámetros de calidad y estabilidad del ingrediente bioactivo en distintas condiciones de almacenamiento, con el fin de evaluar la viabilidad de su aplicación en la industria alimentaria. Los resultados mostraron que el derivado hidrofóbico estilbenoide era más estable en los modelos de leche que en los modelos de zumo, donde se pudo observar una ligera degradación durante el tratamiento térmico y el almacenamiento. Los parámetros de calidad industrial permanecieron estables en el tiempo, a pesar de observarse un ligero incremento inicial de los sólidos solubles tras la suplementación con ciclodextrinas. La protección de la exposición a la luz durante el almacenamiento resultó ser crucial para la conservación del ingrediente bioactivo, más incluso que la temperatura, por lo que es recomendable el uso de envases opacos en las futuras aplicaciones industriales de derivados hidrofóbicos de estilbenos.

En general, los resultados de esta Tesis Doctoral presentan distintos enfoques para abordar la problemática actual que restringe el uso de estilbenos, consiguiendo aumentar su producción, caracterización, solubilidad, estabilidad y biodisponibilidad mediante diversas metodologías. Los derivados hidrofóbicos de estilbenos sintetizados pueden ser de interés en áreas como la alimentación y la biomedicina, por sí mismos o como precursores de estilbenos, por su actividad beneficiosa contra la obesidad y el cáncer, sin haberse observado efectos nocivos *in vivo* tras su administración, en forma libre o encapsulada en ciclodextrinas monoméricas o poliméricas.

ABSTRACT

Stilbenes are phenolic compounds whose many bioactivities make them of great interest for human health, such as antimicrobial, antioxidant, anti-inflammatory, cardioprotective, anti-cancer and anti-obesity activity, among others. They are secondary metabolites that are produced by certain plants under biotic stress or abiotic stress via the phenylpropanoid pathway, with the enzyme stilbene synthase being a key factor in the biosynthesis process. The main sources of dietary stilbenes include grapes, red wine and peanuts. Within this group, resveratrol is the most researched, but there are other lesser-known stilbenes with greater therapeutic potential. However, the reduced production in plant, low water solubility, ease of degradation and low bioavailability of this family of bioactive compounds hinder their successful application in the food, pharmaceutical and cosmetic industries. In this PhD thesis, several strategies have been investigated to overcome these limitations.

In order to address the challenges in obtaining natural stilbenes, current and future strategies to enhance the production of stilbenes have been developed. A method to increase the enzymatic synthesis of piceatannol from resveratrol catalysed by tyrosinase was developed, achieving up to 56 % of conversion by using reducing agents in the reaction. As a future approach, the expression of a novel recombinant stilbene synthase found by phylogenetic analyses of these proteins in extremophile microorganisms was optimised, encouraging the future biotechnological synthesis of stilbenes. These bioinformatic studies also led to the discovery of the origin and evolution of these relevant proteins in different kingdoms, finding a wider distribution than expected and a clear relation with chalcone synthase proteins, from which stilbene synthase may have developed in several times and independently within each genus.

In addition, some of the most promising resveratrol analogues, such as gnetol, isorhapontigenin, rhapontigenin and pinostilbene, were characterised and encapsulated, increasing their solubility and stability in aqueous solutions by means of inclusion complexes with cyclodextrins. Spectrophometric and spectrofluorimetric properties of these stilbenes were analysed and compared to other stilbenes. The stoichiometry and encapsulation constants with natural and modified cyclodextrins were determined by physicochemical and bioinformatics assays. A 1:1 stoichiometry was followed for all the inclusion complexes tested, giving hydroxypropyl-β-cyclodextrin the higher affinity, evidenced by a higher encapsulation constant and a lower molecular docking score. Moreover, the study of the inclusion complexes at different pH and temperature conditions showed that these two parameters have a significant influence on molecular encapsulation and enabled the thermodynamic parameters to be determined.

In order to address the low bioavailability of stilbenes, novel hydrophobic stilbene derivatives that could act as precursors to protect stilbenes from undesirable phase II reaction, such as sulphation and glucuronidation, and to better deliver stilbenes to adipocytes, the target tissue where stilbenes have demonstrated anti-obesity effects, were synthesised. These derivatives were physicochemically characterised, encapsulated in cyclodextrins, and their biological properties were analysed *in vitro* and *in vivo*.

A chemical and an enzymatic process were optimised for the synthesis of hydrophobic stilbene derivatives, obtaining yields up to 78 % and 56 %, respectively, with high specificity for monoester products. The chemical synthesis achieved a higher yield in much less time and without the need for high temperatures, so this was the procedure selected for the majority of the derivatives. In some of the reactions, a stable racemic mixture with the different isomers according to the modified hydroxyl group, was obtained. The derivatisation modified the optical properties, resonance, polarity and

solubility of the stilbenes, depending on the type of derivative synthesised. The hydrophobic stilbene derivatives showed higher affinity for hydroxypropyl-β-cyclodextrin, resulting in inclusion complexes with a 1:1 stoichiometry in the presence of 85 % methanol.

The digestion, absorption and metabolism of these hydrophobic stilbene derivatives were analysed. It was observed that these derivatives were susceptible to hydrolysis by pancreatic lipase *in vitro*, a key enzyme during digestion. The hydrolysis degree varied according to the type of stilbene derivative and could be inhibited by the use of free caffeoylquinic acids. In contrast, the use of cyclodextrins triggered catalytic activity on the isomers with a higher affinity, probably due to the disaggregation of the micellar conformation above certain concentration of cyclodextrin. The use of complexed caffeoylquinic acids also showed this effect due to the presence of cyclodextrins, although molecular encapsulation improved the aqueous solubility and stability against enzymatic oxidation of these acids. The molecular encapsulation of caffeoylquinic acids was characterised by means of a competitive model with two potential complexation sites in the ligand. This model establishes two encapsulation constants that were identified by computational assays. The higher affinity was obtained for the α-cyclodextrin and hydroxypropyl-β-cyclodextrin complexes.

In Caco-2 cell cultures, hydrophobic stilbene derivatives were found to be less sensitive to the sulphation and glucuronidation reactions that decrease the bioavailability of stilbenes, being able to better preserve the aglycone form compared to the original stilbenes. Moreover, some of the hydrophobic stilbene derivatives exhibited improved apparent permeability across intestinal cells. Preclinical assays, revealed an enhancement in the levels of serum biomarkers of lipid transport, hepatic damage, renal function, oxidative stress and inflammation after oral administration of hydrophobic stilbene

derivatives in *M. musculus*. In addition, administration of encapsulated hydrophobic stilbene derivatives further improved serum biomarker levels as well as the relative bioavailability of the stilbene, despite its partial hydrolysis.

Antioxidant studies *in vitro* revealed that the hydrophobic stilbene derivatives were less reactive to free radicals and metallic complexes compared to the original stilbenes, probably due to the removal of the free hydroxyl groups after esterification. This could indicate that hydrophobic stilbene derivatives may be less reactive in the presence of oxidising agents in the medium, thus keeping the stilbene molecule intact in the matrix prior to the administration. Besides that, the effect of cyclodextrins in these methods was also investigated, since the literature shows some discrepancy in their use. Cyclodextrins were found to interfere with *in vitro* methods for determining antioxidant activity *in vitro*, leading to deviations in the readings that could be misinterpreted as higher or lower antioxidant activity. Spectral and bioinformatic assays revealed that this interference could be due to the encapsulation of the reagents involved, with almost no effect due to the glucidic nature of cyclodextrins. This deviation in readings was dependent on the type and concentration of cyclodextrin, and varied according to the method used. Although there were methods where some cyclodextrin concentrations showed no significant variation, since the interaction with cyclodextrins is non-covalent and non-specific, interference cannot be discarded if test conditions change.

On the other hand, the cytotoxic activity of some resveratrol analogues was evaluated in colorectal cancer cells in order to establish structure-activity relationships and identify stilbenes with higher activity than resveratrol. Cell viability showed a positive correlation with the number of hydroxyl groups in the stilbene molecule and a negative correlation with the number of methoxy groups. Thus, methoxylated stilbenes such as pterostilbene or trimethoxystilbene achieved greater inhibition of cell

proliferation than resveratrol, in contrast to hydroxylated analogues, such as oxyresveratrol or gnetol.

Bioactivity studies of hydrophobic stilbene derivatives in cell cultures and in the animal model *C. elegans* showed that derivatization of stilbenes affects their anti-obesity activity. In cells, hydrophobic stilbene derivatives showed no beneficial effect on lipid accumulation or lipolysis. Still, the hydrolysed form of the derivatives inhibited adipogenesis in pre-adipocytes and activated lipolysis in mature adipocytes. Despite that, during adipogenesis, some hydrophobic stilbene derivatives showed overexpression of some genes related to sensibilisation to insulin, fat mobilisation and thermogenesis, which could be relevant in diseases such as type 2 diabetes and obesity. By contrast, in *C. elegans* model, a significant decrease in lipide accumulation was observed after the treatment with hydrophobic stilbene derivatives encapsulated in cyclodextrin polymers. These results in cell culture and *C. elegans*, together with those previously obtained in *M. musculus*, suggest that the beneficial effects of hydrophobic stilbene derivatives on obesity could be related to an enhancement in lipid transport beyond their inherent activity in adipose tissue.

The treatment of *C. elegans* with hydrophobic stilbene derivatives in the presence of cyclodextrin polymers, do not alter the lifespan of the nematodes, suggesting that the derivatives do not pose toxicity to individuals. Besides, the same treatment in TJ375 strain showed no effect on the oxidative stress, probably due to the complexation.

In melanoma models, intratumorally treatment with these derivatives achieved a greater inhibition of tumour growth associated with reduced angiogenesis, compared to the original stilbenes, in free form or encapsulated. The administration of encapsulated hydrophobic stilbene derivatives was the most effective, resulting in the smallest tumours with less vascularisation, as well as a higher degree of necrosis and fewer mitotic cells.

In addition, histopathological examination of tissues from this group revealed less damage to the liver and kidneys. The serum biomarkers levels of inflammation and hepatic-renal damage of these individuals decrease notably, approaching those of the healthy individuals, while the levels of antioxidant biomarkers increase above the levels of the individuals with no tumour. Overall, these results encourage the potential applications of hydrophobic stilbene derivatives against cancer.

Finally, functional food models fortified with a free and encapsulated hydrophobic stilbene derivative were developed, monitoring the quality parameters and stability of the bioactive ingredient under different storage conditions, in order to check the industrial application feasibility. The results revealed that the hydrophobic stilbene derivative was more stable in milk models than juice models, where a slightly degradation was appreciated during heat treatment and storage. The industrial quality parameters remained stable over time, despite the initial slight increase in soluble solids after cyclodextrin supplementation. Light protection during storage was found to be even more critical for preserving the bioactive ingredient than temperature, therefore, the use of opaque packaging is recommended for future industrial applications of hydrophobic stilbene derivatives.

Overall, the findings of this PhD Thesis present different approaches to address the current problem restricting the use of stilbenes by increasing their production, characterisation, solubility, stability and bioavailability by means of diverse methodologies. The hydrophobic stilbene derivatives synthesised may be of interest in areas such as food and biomedicine, on their own or as stilbene precursors, due to their beneficial activity against obesity and cancer, with no harmful effects observed *in vivo* after administration, in free form or encapsulated in monomeric or polymeric cyclodextrins.

CHAPTER I

GENERAL INTRODUCTION

CHAPTER I. GENERAL INTRODUCTION

1. Nutrition and human health

The importance of diet in the prevention of chronic diseases is undeniable. Fruit and vegetable consumption has been associated with reduced risk of diseases that are the leading causes of death in most developed countries, such as cardiovascular disease, cancer, diabetes, neurological diseases and obesity (Liu, 2003). Food Phytochemicals are the bioactive compounds responsible for these beneficial effects through multiple mechanisms of action such as the protection against oxidative stress, a common factor in the aetiology of many chronic diseases (Liu, 2003; Rodriguez-Casado, 2016). A wide variety of phytochemical have been identified (Figure 1) and research on them is growing due to their potential applications in various industries, such as food, cosmetics and pharmaceuticals (Dillard and German, 2000).

Within the food industry, the development of functional foods is the response to this research. Functional foods are foods that provide the consumer with a beneficial effect on human health in the amounts normally consumed in the diet, beyond the basic nutritional properties (EFSA, 2006). They can be designed by adding a bioactive compound (e.g. rice with β-carotene), removing an ingredient (e.g. lactose-free milk), replacing an ingredient with a more beneficial one (e.g. milk enriched in PUFA like ω-3) or increasing the concentration of a beneficial component (e.g. juices fortified with vitamins or minerals). At the moment, in the European Union (EU), functional foods are regulated by the European Food Safety Agency (EFSA) through Regulation 1924/2006 on nutrition and health claims made on foods (EFSA, 2006). This EU agency is responsible for authorising health claims for food ingredients that have a proven beneficial effect at a certain dose.

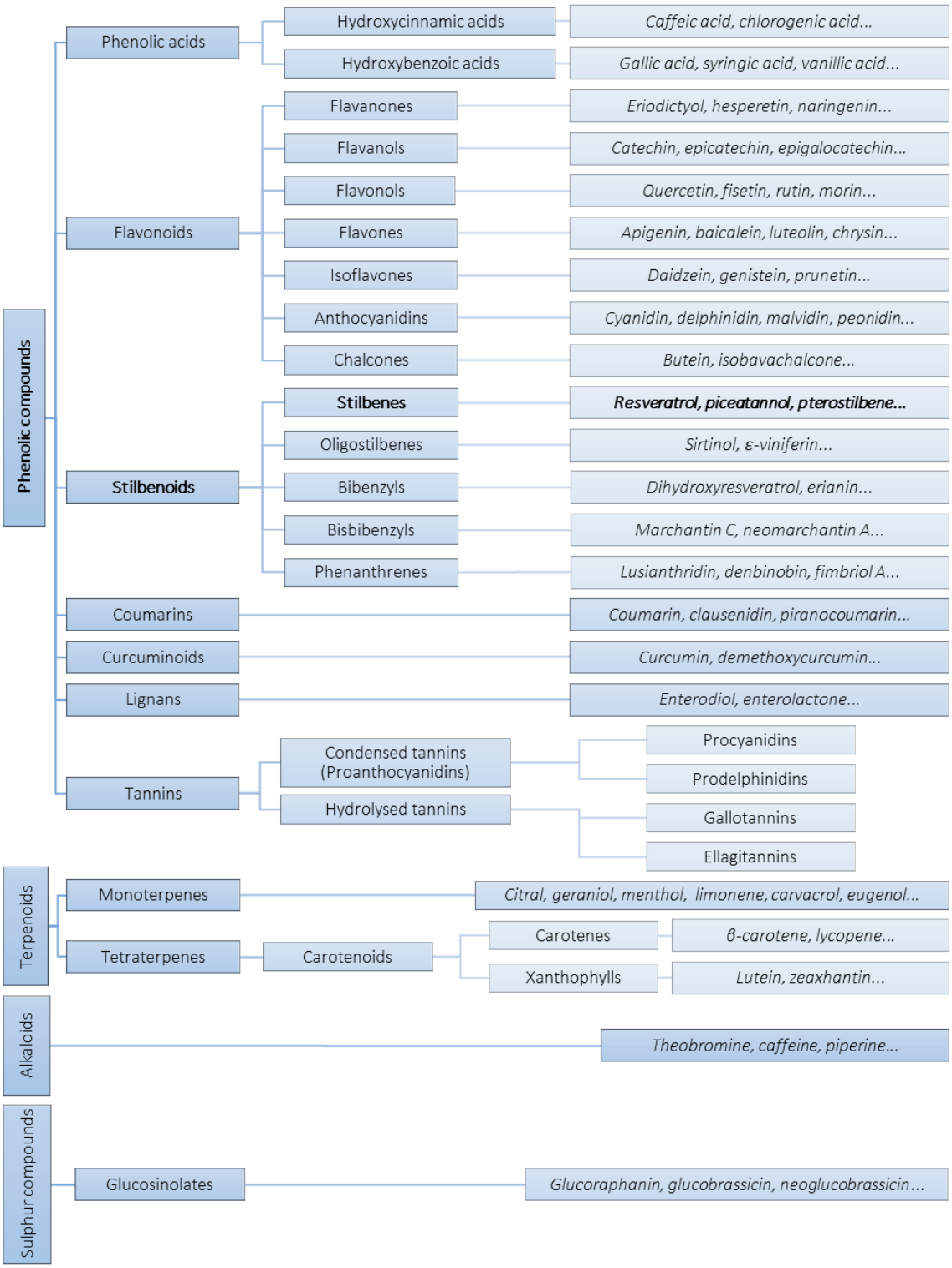

Figure 1. Classification of major food phytochemicals, according to (Gulcin, 2020; Rao, 2012; Shen et al., 2013; Xiao et al., 2008)

2. Stilbenes

Among the wide variety of phytochemicals available, stilbenes stand out. They are phenolic compounds constituting a major family of molecules along with the oligo-stilbenes, bibenzyls, bisbibenzyls and phenanthrenes: the stilbenoids. Despite those remaining members, stilbenes are the most investigated molecules within this family. A key feature is that they have a basic 1,2-diphenylethylene frame to which a variety of substituents are bond (Shen et al., 2013) (Figure 3).

Stilbenes are also phytoalexins, a product of the secondary metabolism of plants aimed to protect them from biotic stress (such as attack by pathogenic microorganisms or insects) and abiotic stress (such as exposure to UV radiation or physical damage). In natural sources, they can be found in their free form as aglycones (e.g. resveratrol, piceatannol...) or conjugated as glycosides (e.g. piceid, astringin...) (Figure 2). The beneficial effects that stilbenes have on human health are directly related to their structure, so the chemical form in which they are found influences their biological activity.

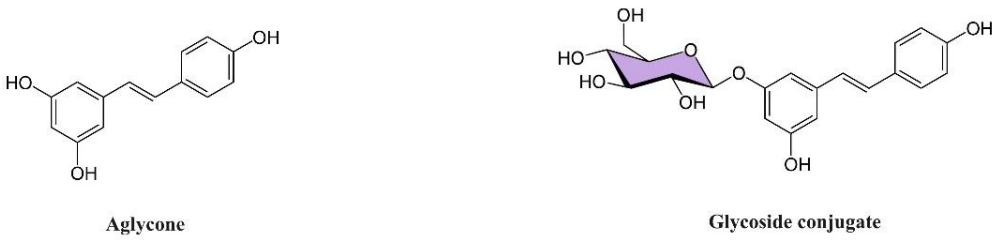

Figure 2. Structural forms of stilbene resveratrol in nature

Among them, resveratrol (*trans*-3,4',5-trihydroxystilbene) is the most highly studied and cited since the French paradox (Tian and Liu, 2020). It reaches 2404 publications in WOS only in 2022. So far away from the 123 publications for pterostilbene (*trans*-3,5-dimethoxy-4'-hydroxystilbene) or the 84 for piceatannol (*trans*-3,3',4',5-tetrahydroxystilbene). Nevertheless, researchers are discovering and studying

an enlarging figure of natural and synthesised stilbenes. In addition, despite the well retained popularity of resveratrol other lesser-known stilbenes are claiming the spotlight (de Vries et al., 2021; Likhitwitayawuid, 2021; Pecyna et al., 2020; Szekeres et al., 2010). However, studies on other stilbenes tend to be scarcer and limited to few aspects, like their sources, activity or pharmacokinetics (Akinwumi et al., 2018; El Khawand et al., 2018; Oh et al., 2021). Indeed, knowledge on the physicochemical characterisation or constraints of stilbenes other than resveratrol are very scarce, hindering major advances in the research of these molecules.

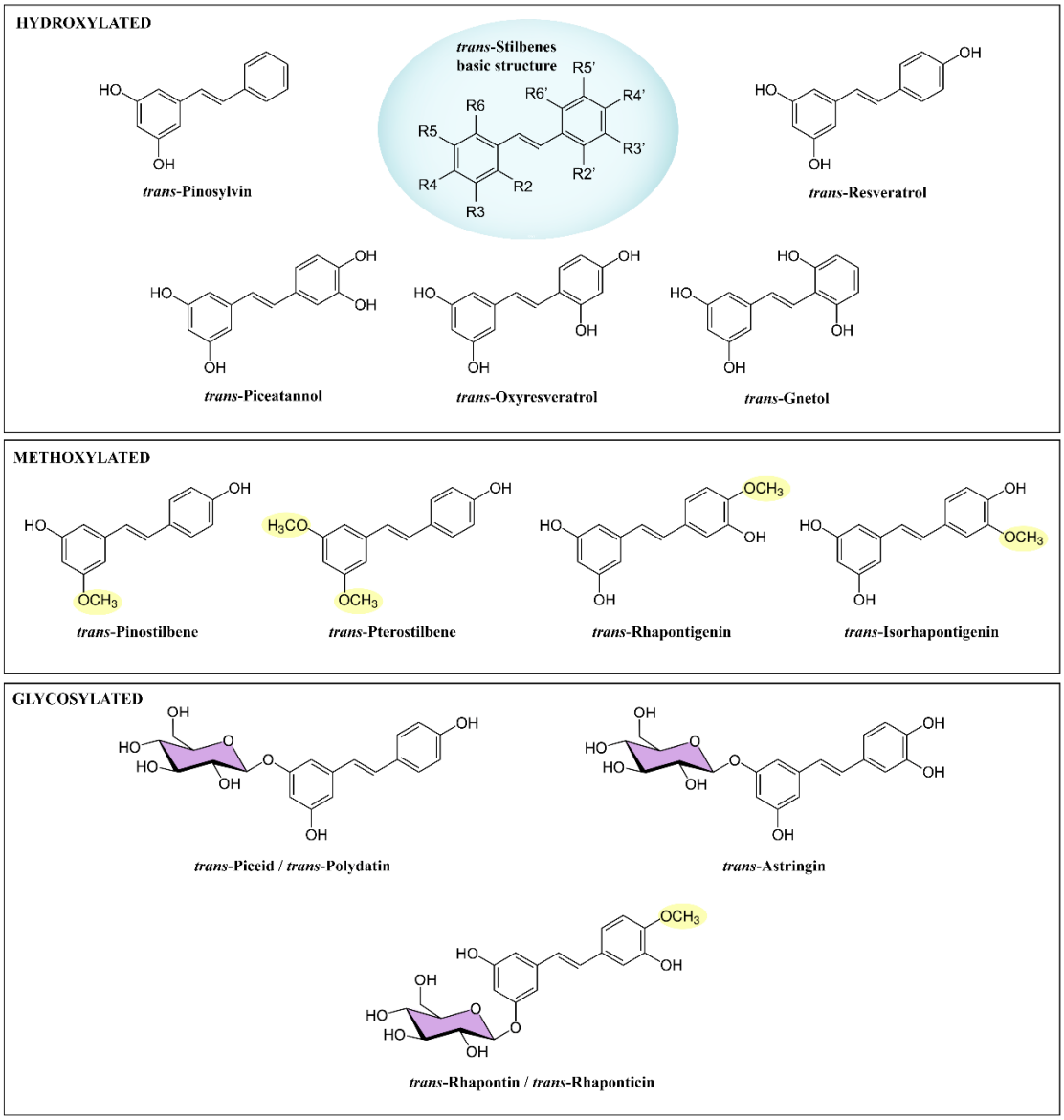

Figure 3. Examples of natural stilbenes and their chemical structure.

2.1. Sources and production

Stilbenes can be extracted from a limited variety of plant species across different botanical families, such as Vitaceae (grapes), Pinaceae (pine), Poaceae (sorghum), Ericaceae (blueberry) and Fabaceae (peanut). Typically, these compounds are predominantly located in the roots, rhizomes, leaves, and bark of the plants (Cassidy et al., 2000; Chong et al., 2009; Dubrovina and Kiselev, 2017).

The irregular taxonomic distribution of stilbenes in plants is largely due to the enzyme stilbene synthase (STS), because it is present only in certain taxa. This enzyme is crucial for stilbene biosynthesis, acting in the final step of the pathway (Figure 4). The occurrence of STS in various taxa might be attributed to convergent evolution of chemical processes (Grayer et al., 1999). Another explanation could be differential gene expression. Some species might have lost or deactivated the STS gene after having developed more effective defence mechanisms (Rivière et al., 2012).

2.1.1. Dietary stilbenes

In plants, phenolic compounds are produced in greater quantities than stilbenes specifically. While many plants are rich in stilbenes, these compounds are often found in non-edible tissues or in plants that are not typically consumed as food. For instance, *Polygonum cuspidatum* and *Veratrum formosanum*, both used in traditional Chinese medicine, contain high levels of stilbenes. However, these plants are not eaten as food, with *Veratrum formosanum* being a poisonous species (Cassidy et al., 2000).

It is important to note that the consumption of stilbenes varies across different countries and cultures. For instance, in Europe, the roots of *Polygonum cuspidatum* are processed to extract resveratrol for food supplements, whereas in Asia, they are utilized in traditional medicine. In Europe, the primary dietary sources of stilbenes include grapes,

red wine, and peanuts. Research has identified the presence of resveratrol and its glycoside, piceid, in a variety of fruits and vegetables such as plums, apples, pears, peaches, and blueberries (Dubrovina and Kiselev, 2017; Li et al., 2013). In fruits, stilbenes accumulate mostly in the skin, being practically absent in the pulp (Morales et al., 2000). It is for this reason that red wine is richer in stilbenes than white wine, as fermentation is carried out with the grape skin, whereas in white wine, fermentation occurs after the grape skin has been removed.

2.1.2. Biosynthesis pathway

Stilbenes are produced in plants through the phenylpropanoid pathway (Figure 4). This metabolic pathway begins with a molecule of cinnamic acid or *p*-coumaric acid, which are initially produced by the enzyme phenylalanine ammonia lyase (PAL, EC 4.3.1.24) or tyrosine ammonia lyase (TAL, EC 4.3.1.23) from L-phenylalanine or L-tyrosine from the shikimate pathway, respectively. In addition, the enzyme cinnamate 4-hydroxylase (C4H, EC 1.14.14.91) can oxidise the aromatic ring of cinnamic acid to *p*-coumaric acid. This is followed by the addition of a coenzyme A (CoA) molecule catalysed by the enzyme 4-coumarate-CoA lyase (CL, EC 6.2.1.12) to form cinnamoyl-CoA or *p*-coumaroyl-CoA, respectively. Next, the enzyme stilbene synthase (STS, EC 2.3.1.146 or EC 2.3.1.95) utilizes three units of malonyl-CoA and one unit of cinnamoyl-CoA or *p*-coumaroyl-CoA to generate a polyketide intermediate. The STS then catalyses the aldol condensation reaction on this intermediate, resulting in the production of stilbene-2-carboxylic acid. This compound serves as a decarboxylated template for synthesizing various stilbenoids, including *trans*-resveratrol. From this structure, stilbenes can undergo further modifications to form different stilbenes, such as glycosylation by glycosyltransferases, methylation by methyltransferases,

oligomerisation by peroxidases, or prenylation by prenyltransferases (Dubrovina and Kiselev, 2017; Rivière et al., 2012).

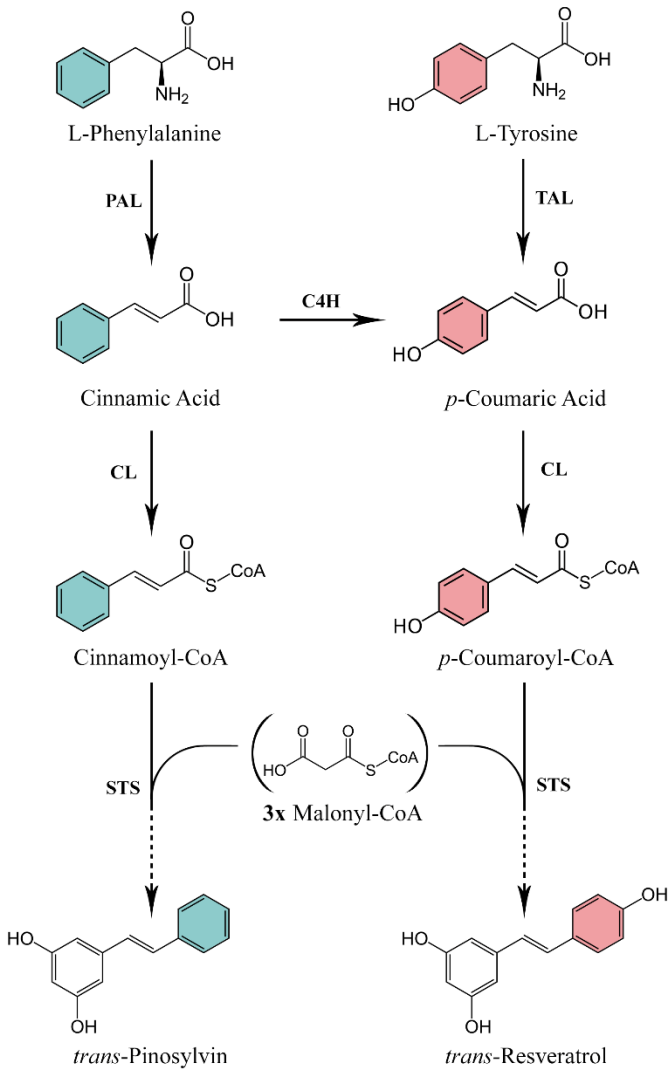

Figure 4. Stilbenes biosynthesis pathway in plants. PAL = Phenylalanine Ammonia Lyase, TAL = Tyrosine Ammonia Lyase, CL = 4-Coumarate-CoA Ligase, C4H = Cinnamate 4-Hydroxylase, STS = Stilbene Synthase

Furthermore, the CL enzyme can catalyse the formation of caffeoyl-CoA from caffeic acid. It is speculated that the STS enzyme might utilize the caffeoyl-CoA molecule to generate piceatannol (Dubrovina and Kiselev, 2017). The substrates of STS can alternatively be processed by the enzyme chalcone synthase (CHS, EC 2.3.1.74) to produce flavonoids rather than stilbenes. These enzymes exhibit significant similarity and

share a high degree of homology in their amino acid sequences. For instance, STS and CHS from *Arachis hypogea* differ by only 35 amino acid residues in their entire sequence while sharing up to 70 % (Jeandet et al., 2010; Shomura et al., 2005).

2.1.3. Alternative sources

Historically, stilbenes have been sourced from various plant components where they occur naturally. However, achieving a commercially viable yield poses challenges due to the multiple extraction and isolation procedures involved, as well as the dependency on seasonal variations (Thapa et al., 2019). Hence, numerous studies are underway to explore alternative production techniques. For instance, suspension cells and cultured roots, including those of *Vitis vinifera* treated with different elicitors such as cyclodextrins, methyl jasmonate, or UV light, are being investigated to enhance stilbene production (Cai et al., 2013; Hosseini et al., 2017; Laura et al., 2007; Sák et al., 2021). Other option would be the use of plants (Giovinazzo et al., 2005; Hain and Grimmig, 2000) or microorganism (Beekwilder et al., 2006; Kallscheuer et al., 2016; Lim et al., 2011; Shrestha et al., 2018) that underwent a genetical modification on genes involved in the stilbene biosynthesis pathway. Additionally, stilbenes can be chemically synthesized through Heck, Perkin, or Wittig reactions (Tian and Liu, 2020).

2.2. Physicochemical properties

Stilbenes occur in two natural isomeric forms: *trans*-stilbenes (E-stilbenes) and *cis*-stilbenes (Z-stilbenes). *Trans*-stilbenes are considered the more significant isoforms due to their recognised bioactivities, whereas *cis*-stilbenes are typically formed as degradation products following the photo-oxidation of *trans*-stilbenes (Tian and Liu, 2020). Typically, when no isomerization is specified for a stilbene, it usually refers to the *trans* form, given its prevalence as the most common isomer.

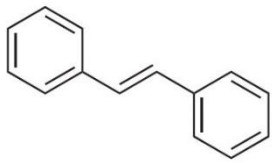

trans-stilbene

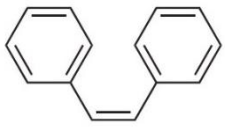

cis-stilbene

Figure 5. Isomeric forms of stilbenes

The stilbene molecule has the potential for having substituents at various positions such as hydroxyl, methoxy and/or glycoside groups. These functional groups cause stilbenes to have different physicochemical properties, and although much characterisation is still lacking, some of them are summarised in Table 1.

2.2.1. Solubility, lipophilicity and polarity

A significant challenge with stilbenes in formulations is their low water solubility, attributed to their highly hydrophobic nature. For instance, the aqueous solubility of resveratrol is typically within the range of 3 mg/100 mL(Kershaw and Kim, 2017), similar to pterostilbene with a water solubility of 2.1 mg/100 mL (Bethune et al., 2011). Stilbenes containing more hydroxyl groups exhibit increased solubility, like piceatannol (50 mg/100 mL) (Kershaw and Kim, 2017) and oxyresveratrol (75 mg/100 mL) (Suzuki et al., 2019). Those groups enhance interaction with water molecules through the formation of hydrogen bonds.

Despite the low water solubility, stilbenes can be solubilised in organic solvents, such as methanol, ethanol, and dimethyl sulfoxide (DMSO). Hence, the solubility of resveratrol reaches 50 g/L and 16 g/L in ethanol and DMSO, respectively (Kershaw and Kim, 2017). On the other hand, solubility of piceatannol is 10 g/L, both in ethanol and DMSO (Kershaw and Kim, 2017). Nevertheless, these solubility values are highly

influenced by environmental factors and may undergo significant variations under different temperature or pH (Zupančič et al., 2015).

Stilbenes lipophilicity (logP) exhibits an inverse relationship with the number of hydroxyl groups, and glycoside groups presence further reduces it (Table 1). Conversely, glycosylated stilbenes tend to have a higher topological polar surface area (TPSA), while the presence of more hydroxyl groups in the aglycones increases this value. However, the inclusion of methoxy groups has minimal impact on the TPSA.

2.2.2. Absorbance properties

trans-Stilbenes exhibit a maximum peak in the UV region at 300 – 330 nm (Table 1), while *cis*-stilbenes have it at shorter wavelengths. For instance, *trans*-resveratrol has its maximum absorbance wavelength (λ_{max}) at 304 – 308 nm, while *cis*-resveratrol has it at 286 nm (Trela and Waterhouse, 1996). *Trans*-piceid has a λ_{max} of 318.4 nm, unlike *cis*-piceid, which has a λ_{max} of 284.4 nm (Giorcelli et al., 2004). These spectrophotometric features enable isomer isolation by chromatographic techniques using UV-Vis detectors. Additionally, the ratio of cis- to *trans*-oxyresveratrol can be determined by comparing the absorbance ratio at 290 nm and 301 nm (secondary peaks in the spectrum), enabling the measurement of the degradation level in the molecule (Maafi and Al-Qarni, 2018).

The absorptivity or extinction coefficient (ε) of *trans*-stilbenes seems to be in the range of 30000 – 44000 $M^{-1}cm^{-1}$, depending on the substituents and solvent (Table 1). Previous studies reported that *trans*-resveratrol has an ε_{306nm} of 31800 $M^{-1}cm^{-1}$, while *cis*-resveratrol has an ε_{286nm} of 13100 $M^{-1}cm^{-1}$, both in aqueous solution with 10 % (v/v) ethanol (Trela and Waterhouse, 1996). Moreover, these values can change according to the excitation and protonation state of the molecule (Džeba et al., 2015). Piceatannol, with an extra hydroxyl group, has ε_{326nm} of 33100 M^{-1} cm^{-1} in pure ethanol, while ε_{304nm} of

26350 M^{-1} cm^{-1} at the shoulder on its spectrum (Rhayem et al., 2008). Meanwhile, the methoxylated analogue of piceatannol, rhapontigenin was reported a ε_{325nm} of 36824 M^{-1} cm^{-1} in 50 % (v/v) methanol. The glycoside of rhapontigenin, rhapontin, maintained rhapontigenin λ_{max} but showed a higher ε of 43894 M^{-1} cm^{-1} (Hui et al., 2011).

2.2.3. Fluorescence properties

The structure of stilbenes, featuring two aromatic rings connected by a methylene bridge, renders them fluorescent when exposed to UV light. The term "stilbene" originates from the Greek word *στίλβω*, meaning "shining." Most natural stilbenes exhibit fluorescence at a maximum emission wavelength (λ_{em}) around 370 – 400 nm (Table 1), For instance, *trans*-resveratrol has reported to emit fluorescence at 389 nm when excited at 300 – 330 nm, while *cis*-resveratrol emits at 400 nm following excitation at 260 nm (Vitrac et al., 2002). The amount and position of hydroxyl groups can change these values, as well as the solvent and conditions of the readings. Tetrahydroxylated stilbenes such as piceatannol and oxyresveratrol have recorded a λ_{em} of 400 nm upon excitation at 321 nm and 288 nm, respectively (Cai et al., 2019; He et al., 2017; Shi et al., 2020). In contrast, other stilbenes with fewer hydroxyl groups, such as pinosylvin and pterostilbene, have been reported to emit fluorescence at a lower wavelength of 374 nm (López-Nicolás et al., 2009a, 2009b).

Understanding these fluorescence properties, particularly emission wavelengths, is crucial for quantifying the stilbene concentration of a sample. Fluorescence spectroscopy offers greater sensitivity compared to absorbance spectroscopy, making it a valuable tool for stilbene research.

*Table 1. Physicochemical properties of natural trans-stilbenes. * PubChem database; [a] Measured in ethanol; [b] Measured in 10% ethanol (v/v); [c] Measured in 50% methanol (v/v); LogP = Lipophilicity index; TPSA = Topological Polar Surface Area; ε = Absorptivity; λ_{max} = Maximum absorbance wavelength; λ_{ex} = Fluorescence maximum excitation wavelength; λ_{em} = Fluorescence maximum emission wavelength;*

Stilbene	Aqueous solubility (mg/100mL)	pK_a	LogP*	TPSA* (Å^2)	ε (M^{-1}cm^{-1})	λ_{max} (nm)	λ_{ex} (nm)	λ_{em} (nm)	References
Pinosylvin 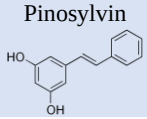	-	7,7 10,3	3,5	40,5	-	312	330	374	(López-Nicolás et al., 2009a; Stojanović and Brede, 2002)
Resveratrol 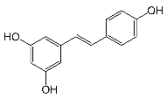	3	8,8 9,8 11,4	3,1	60,7	31800 [b]	306	334	389	(Kershaw and Kim, 2017; López-Nicolás and García-Carmona, 2008a; Trela and Waterhouse, 1996; Vitrac et al., 2002)
Piceatannol 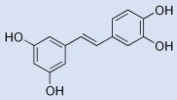	50	-	2,9	80,9	33100 [a]	323	321	402	(Cai et al., 2019; Kershaw and Kim, 2017; Rhayem et al., 2008; Shi et al., 2020)
Oxyresveratrol 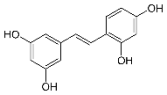	75	-	2,8	80,9	-	328	288	400	(He et al., 2017; Matencio et al., 2017a; Suzuki et al., 2019)
Gnetol 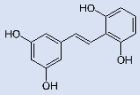	-	-	2,8	80,9	-	-	-	-	-
Pterostilbene 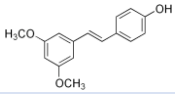	2.1	9,4	3,8	38,7	-	315	330	374	(Bethune et al., 2011; López-Nicolás et al., 2009b; Orgován et al., 2017)
Pinostilbene 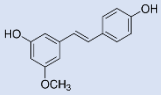	-	9,1 9,9	3,5	49,7	35481 [a]	307	-	-	(Orgován et al., 2017; Tyukavkina et al., 1972)
Rhapontigenin 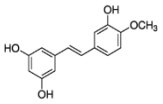	-	-	3,1	69,9	36824 [c]	324,5	-	-	(Hui et al., 2011)
Isorhapontigenin 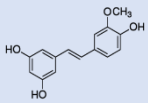	-	-	3,2	69,9	-	325	-	-	(Fernández-Marín et al., 2012)
Piceid 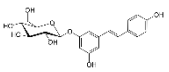	-	-	1,7	140	-	318,4	-	-	(Giorcelli et al., 2004)
Astringin 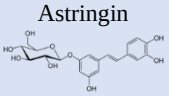	-	-	0,7	160	-	325	298	400	(Carando et al., 1999; Toscano Underwood and Pearce, 1991)
Rhapontin 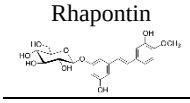	-	6,39	0,5	149	43894 [c]	325	355	390	(Hui et al., 2011; Liu et al., 2019)

2.2.4. Acid dissociation constant

The protonation state of stilbenes plays a pivotal role in their bioactivity, being an example its radical scavenging activity, which relies heavily on the ability to transfer hydrogen atoms. For instance, resveratrol, with its three hydroxyl groups, exhibits three distinct acid dissociation constants (pK_a) reported at pH 8.8, pH 9.8, and pH 11.4 (López-Nicolás and García-Carmona, 2008a)). The 4'-OH group is reported to be the most unstable, thus the first pK_a has been linked to the deprotonation at this position. However, there is ambiguity as to whether the second or third pK_a corresponds to deprotonation at 3-OH or 5-OH, as both are situated nearby (López-Nicolás and García-Carmona, 2008a). Others researchers have proposed that the protonation constants of the three phenolates overlap within a similar pH range (Orgován et al., 2017).

Stojanović and Brede (2002) determined that the protonation constants of pinosylvin, a resveratrol analogue lacking the 4'-OH group, were at pH 7.7 and 10.3 (Stojanović and Brede, 2002). Methoxylated stilbenes, like pinostilbene, a 3-methoxy analogue of resveratrol, have been documented to possess pK_a values at pH 9.1 and pH 9.9, whereas pterostilbene, a 3,5-dimethoxy analogue, exhibits it at pH 9.4 (Orgován et al., 2017). Furthermore, the pK_a of rhapontin, the glycoside of rhapontigenin, was documented to be at pH 6.39 (Liu et al., 2019). In contrast, the pK_a of some *cis*-stilbenes were reported to be slightly higher (Orgován et al., 2017).

2.2.5. Aggregation and critical concentration

The state of aggregation is significantly pH-dependent, thus the pK_a values of stilbenes also impact their critical concentration, i.e. the concentration at which the molecule aggregates (López-Nicolás and García-Carmona, 2008a). At acidic pH levels (5.5), the critical concentration of resveratrol was documented at 12.5 µM. Beyond this

concentration, fluorescence spectroscopy reveals a bathochromic shift in both excitation and emission wavelengths, with λ_{em} transitioning from 376 to 393 nm. Conversely, at a basic pH (10.5), the critical concentration of resveratrol notably rises to 37 μM. Above this concentration, resveratrol begins to form aggregates (López-Nicolás and García-Carmona, 2008a).

2.2.6. Stability and degradation

Stilbenes, especially *trans*-stilbenes, are highly light-sensitive, undergoing conversion from the *trans*- to the *cis*-isomer, which is less bioactive and can be considered a degradation product. Isomerization of resveratrol typically takes place after exposure for several hours to sunlight or under UV light irradiation. This photocatalytic degradation is more pronounced when *trans*-resveratrol is exposed to UV-Vis light compared to UV or just visible light (Francioso et al., 2014; Silva et al., 2013).

Trans-resveratrol exhibits greater stability compared to *cis*-resveratrol *in vitro*, while *cis*-resveratrol can lead to the formation of phenanthrenoids, including 4a,4b-dihydrophenanthrene and trihydroxydihydrophenanthrene due to photocatalytic degradation (Francioso et al., 2014).

Trans-piceatannol is similarly sensitive to light, and its degradation mechanism closely mirrors that of resveratrol. Upon irradiation with a λ_{ex} of 366 nm, *trans*-piceatannol undergoes isomerization to the *cis*-form. Afterwards, *cis*-piceatannol loses two hydrogens, leading to the formation of a phenanthrenoid ring (Latva-Mäenpää et al., 2021). The mechanism of degradation described was also applicable to analogues of stilbenes such as isorhapontigenin, isorhapontin, and astringin.

Although they share a similar degradation mechanism, there are discernible differences in the stability of each stilbene. Tang et al. (2017) investigated the half-life of

various *trans*-stilbenes *in vitro*, i.e. the time required for 50 % degradation (Tang et al., 2017). In their study they found that certain stilbenes exhibited high stability, such as pinosylvin or pterostilbene, with degradation times exceeding 180 minutes. Following these were resveratrol, gnetol, and oxyresveratrol, with half-life of 109.35, 66.51, and 65.43 minutes, respectively. Conversely, piceatannol or isorhapontigenin displayed much lower stability, with half-life of 14.38 and 27.89 minutes, respectively. Interestingly, the glycosides astringin and piceid demonstrated half-life of 42.05 minutes and over 180 minutes, respectively (Tang et al., 2017). Generally, glycosides like piceid, astringin, and rhapontin are more susceptible to light-induced degradation compared to their aglycone counterparts such as resveratrol, piceatannol, and rhapontigenin (Latva-Mäenpää et al., 2021).

Besides photosensitivity, various factors impact the stability of stilbenes, including pH and temperature. Resveratrol, for instance, exhibits maximum stability at low pH and temperature, remaining almost unaltered for months in low pH buffers. However, its stability diminishes as the pH exceeds 6.8. At pH 10, the half-life of *trans*-resveratrol is approximately 1.6 hours (Francioso et al., 2014). This phenomenon occurs because the alkaline pH triggers deprotonation of resveratrol at 4'-OH, leading to the formation of a quinonoid radical. At neutral pH, temperatures exceeding 25 °C can entirely degrade resveratrol within days, whereas storage at 4 °C or -22 °C can maintain its integrity for months (Zupančič et al., 2015). This information is important for experimenting at physiological conditions.

2.3. Health promoting effects

The structural characteristics of stilbenes confer upon them various biological properties, including antioxidant, antimicrobial, and anti-inflammatory effects. An

increasing number of research indicates that these molecules also offer protective effects against health conditions like cardiovascular diseases, cancer, and obesity, among others (Figure 6). This Section describes the diverse biological activities of stilbenes, aiming to establish structure-activity relationships wherever feasible.

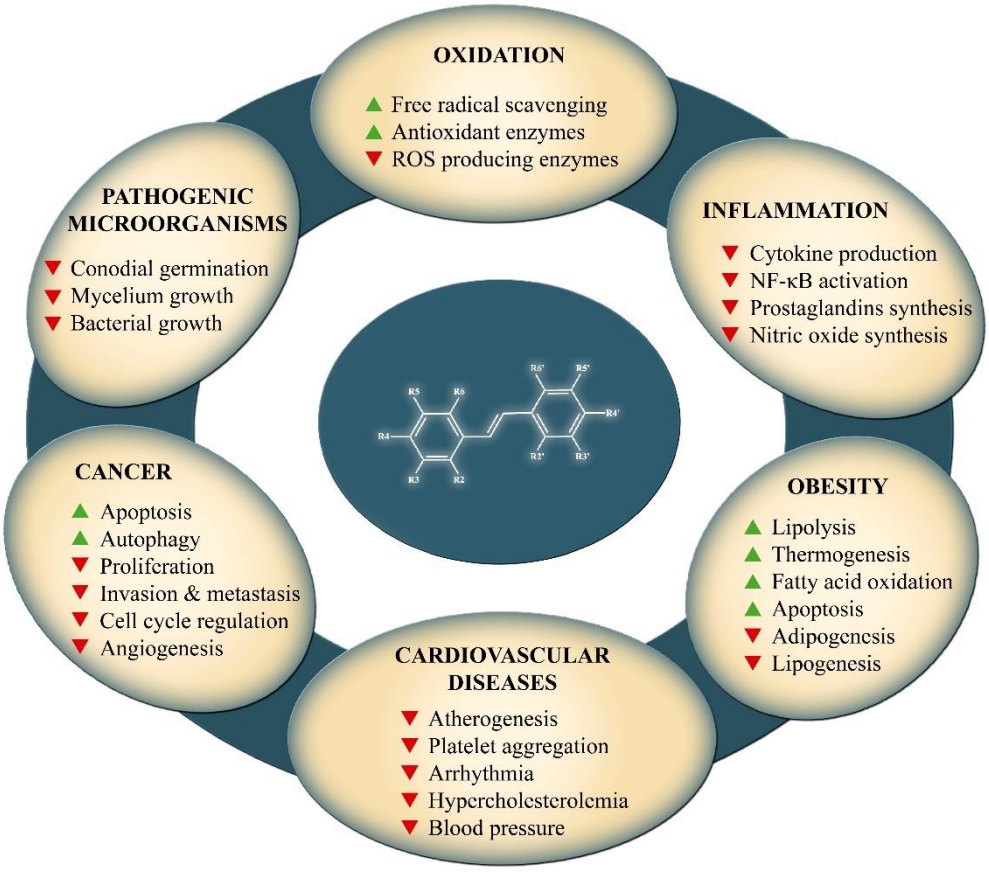

Figure 6. Summary of the biological activity of stilbenes against damaging biological processes, pathogens, and human diseases. Upward triangles denote activation or enhancement, while downward triangles indicate inhibition or decrease.

2.3.1. Antimicrobial activity

As phytoalexins, stilbenes have demonstrated activity against bacterial and fungal pathogens that threaten plants. An assessment of the antibacterial efficacy of various stilbenes indicated that pinosylvin exhibits the highest activity against gram-negative bacteria, followed by resveratrol. Piceatannol, oxyresveratrol, and pterostilbene demonstrated lower activity compared to resveratrol. However, pinosylvin and

pterostilbene exhibited greater activity against gram-positive bacteria than resveratrol (Singh et al., 2019). The observation that pterostilbene showed ineffectiveness against gram-negative bacteria but displayed the highest activity against gram-positive bacteria underscores the notion that distinct stilbene structures may produce varying effects depending on the bacterial type.

Furthermore, resveratrol, pterostilbene, pinosylvin, and piceatannol exhibited inhibitory activity against filamentous fungi. Pterostilbene demonstrated five times greater activity than resveratrol in inhibiting conidial germination and mycelial growth *in vitro*, suggesting that methylation of hydroxyl groups may enhance antifungal activity. Additionally, the higher hydrophobicity of pterostilbene has been proposed to facilitate its diffusion across the cytoplasmic membrane in comparison with resveratrol (Mattio et al., 2021).

2.3.2. Antioxidant activity

The balance between oxidants and antioxidants is crucial for maintaining optimal physiological conditions. The antioxidative properties of stilbenes have the potential to hinder the formation of reactive oxygen and nitrogen species (ROS and RNS), which are implicated in various diseases by causing damage to important biomolecules (proteins, DNA or lipids) (Liu, 2003; Rodriguez-Casado, 2016). As there is no official standardised method, it is recommended to assess the antioxidant activity under a variety of oxidative conditions and using different measurement methods.

Antioxidant activity assessed through ABTS and FRAP assays has indicated that oxyresveratrol exhibits greater activity compared to resveratrol, followed by pinosylvin, and finally, pterostilbene (Rodríguez-Bonilla et al., 2017). Similar trends were observed using the DPPH method when testing a broader range of stilbenes: piceatannol > gnetol

> oxyresveratrol > astringin > isorhapontigenin > resveratrol > pterostilbene > pinosylvin > pinostilbene > piceid (Tang et al., 2017). In the ORAC assay, resveratrol exhibited higher antioxidant activity than oxyresveratrol, followed by pterostilbene and pinosylvin. (Rodríguez-Bonilla et al., 2017); Meanwhile, glycosylated stilbenes showed reduced antioxidant activity (Uesugi et al., 2017).

In general, antioxidant activity is better if the molecule has more hydroxyl groups. Nonetheless, the positioning of these groups and the presence of other substituents on the aromatic rings can influence it. For instance, glycosylation or methylation of hydroxyl groups, particularly at the R4' position, diminishes the antioxidant activity of stilbenes. In addition, the abstraction of hydrogen from R4' in resveratrol during free radical scavenging is more advantageous than from R3 or R5 due to the formation of a stable semiquinone radical with electron delocalisation throughout the molecule, rather than being limited to a single ring (Figure 7) (Papuc et al., 2017). Moreover, the *ortho* position of the hydroxyl groups in piceatannol enhances its efficiency compared to resveratrol because hydrogen abstraction from R4' is easier, leading to a more stable semiquinone radical (Rossi et al., 2008). The pH of the medium also impacts this ability by modifying the protonation state of the molecule (Rodríguez-Bonilla et al., 2017).

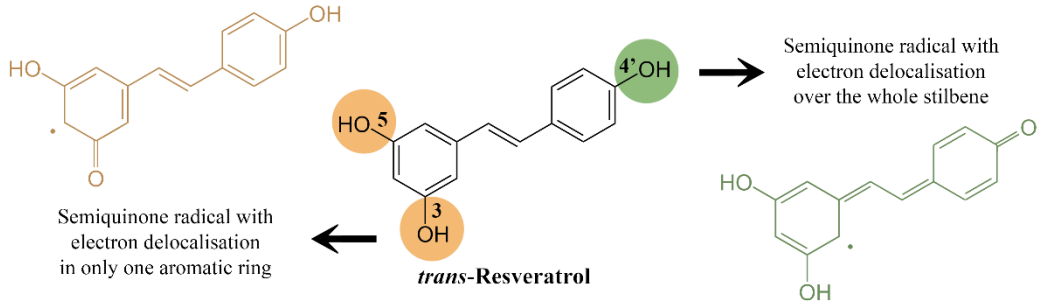

Figure 7. Summarised free radical scavenging mechanism of trans-resveratrol, whether hydrogen abstraction occurs at the 4'-OH group (green) or at the 3/5-OH group (orange), according to (Papuc et al., 2017)

Additionally, stilbenes have been found to modulate the expression of several endogenous enzymes possessing antioxidant properties, such as catalase, glutathione peroxidase (GPx), superoxide dismutase (SOD), glutathione-S-transferase (GST) and NADPH quinone oxidoreductase (Rubiolo et al., 2008). In fact, the antioxidant efficacy of stilbenes *in vivo* is primarily attributed to their ability to regulate gene expression rather than their inherent capacity for free radical scavenging (Xia et al., 2017). For instance, in the hearts of apolipoprotein E knockout mice, resveratrol was shown to up-regulate SOD1, SOD3, catalase and GPx1, while down-regulating NADPH oxidase 2 and NADPH oxidase 4 (Xia et al., 2010).

2.3.3. Anti-inflammatory activity

Inflammation occurs as a response to pathogens and tissue damage, with immune cells releasing several inflammatory mediators, such as cytokines, leukotrienes, nitric oxide, histamine or prostaglandins, alongside the production of ROS. When inflammation and oxidative stress persist, they can lead to chronic inflammation, which may cause diseases like inflammatory bowel diseases, arthritis, asthma, cardiovascular diseases, neurodegenerative disorders, liver fibrosis or cancer. Stilbenes have been traditionally used in folk medicine to treat certain inflammatory disorders (Dvorakova and Landa, 2017).

Stilbenes can intervene at various steps of the inflammatory process. For example, resveratrol has been proved to inhibit the prostaglandin-producing cyclooxygenase enzymes COX-1 and COX-2 (Dvorakova and Landa, 2017). *In vitro* studies have shown that resveratrol suppresses prostaglandin synthesis in a dose-dependent manner by inhibiting COX-2 gene expression and enzyme activity (Willenberg et al., 2015). Other stilbenes, such as piceatannol, pterostilbene, pinosylvin and rhapontigenin, have also been

found to inhibit COX-2 (Dvorakova and Landa, 2017; Tang et al., 2017; Teplova et al., 2018). Additionally, piceatannol and oxyresveratrol significantly reduced nitrite production and inducible nitric oxide synthase activity, as well as decreased prostaglandin synthesis (Lee et al., 2019; Wongwat et al., 2020). Pterostilbene and pinosylvin down-regulated iNOS gene and protein expression.

Resveratrol, oxyresveratrol, and piceatannol have been shown to inhibit the activation of NF-κB, a transcription factor that regulates genes involved in inflammation and various diseases (Dvorakova and Landa, 2017; Tang et al., 2017; Wongwat et al., 2020). Additionally, pterostilbene has been reported to prevent the nuclear translocation of NF-κB, thereby reducing the production of pro-inflammatory cytokines (Dvorakova and Landa, 2017).

In general, oxyresveratrol exhibited lower anti-inflammatory activity compared to resveratrol, potentially due to its inability to form a semiquinone radical (Dvorakova and Landa, 2017). In contrast, piceatannol proved more effective than resveratrol in inhibiting NF-κB activity, COX-2 activity and cytokine production (Dvorakova and Landa, 2017). Pinosylvin demonstrated approximately twice the potency of resveratrol in inhibiting COX-2 (Teplova et al., 2018). Additionally, rhapontigenin was less effective at inhibiting COX-1 and COX-2 compared to deoxyrhapontigenin, which lacks a 3'-OH group (Dvorakova and Landa, 2017).

In vivo, the administration of resveratrol at a dose of 20 mg/kg to mice with chronic inflammation of the colon induced the aforementioned biochemical changes but also alleviated clinical symptoms such as diarrhoea, body weight loss and rectal bleeding (Sánchez-Fidalgo et al., 2010). Additionally, in studies on fatty acid-related inflammation, resveratrol mitigated kidney damage in obese mice on a high-fat diet by reducing inflammation and oxidative stress (Cheng et al., 2019). In a clinical trial

involving 271 patients with Takayasu's arteritis, participants were randomly assigned to receive either 250 mg of resveratrol or a placebo for three months. The study measured disease activity using the Birmingham Vascular Activity Scale and parameters such as erythrocyte sedimentation rate, TNF-α and plasma levels of C-reactive protein. While parameters in the placebo group remained largely unchanged, the resveratrol group showed a consistent decline throughout the study, demonstrating a strong linear correlation with the assessed parameters (Shi et al., 2017).

2.3.4. Cardioprotective activity

The World Health Organization (WHO) reported that cardiovascular diseases are the leading cause of death globally, responsible for approximately 18 million deaths in 2019, which constitutes 32 % of all deaths worldwide. Key risk factors for cardiovascular diseases include age, lifestyle such as physical inactivity, diet, genetic predisposition, alcohol and smoking (WHO 2021). Stilbenes could play a role in the prevention and treatment of these diseases given their cardioprotective properties.

In human vascular endothelial cells, resveratrol helps maintain a balance between vasoconstrictors and vasodilators, preventing atherogenesis and providing resistance to thrombosis. It achieves this by decreasing the expression of the vasoconstrictor endothelin-1, and increasing the expression of endothelial nitric oxide synthase, which produces the vasodilator nitric oxide. Additionally, resveratrol inhibits platelet aggregation induced by epinephrine, collagen and thromboxane, and exerts antioxidant effects on cholesterol metabolism (Colica et al., 2018). *In vivo* studies have confirmed that resveratrol reduces blood pressure in a dose-dependent manner in animal models, and inhibits platelet aggregation in both animal and human research (Akinwumi et al., 2018).

Meanwhile, piceatannol may help prevent cardiovascular disease, such as cardiac arrhythmias and atherosclerosis, through mechanisms such as reducing platelet aggregation, plasma LDL cholesterol and inflammation. It also combats hypercholesterolaemia by activating PPAR-α receptors (D. Wang et al., 2019). Furthermore, piceatannol has demonstrated greater anti-arrhythmic efficacy than resveratrol in ischaemia-reperfusion rat hearts (Ellermann et al., 2017).

Pterostilbene has been shown to improve cardiac function in rat models of ischaemia-reperfusion, lower systolic and diastolic blood pressure in humans at high doses and protects vascular endothelial cells against autophagy. Similar to resveratrol, pterostilbene inhibits platelet aggregation, although it does not inhibit thrombin-induced aggregation (Otręba et al., 2020).

2.3.5. Anticarcinogenic activity

The WHO has identified cancer as a leading cause of death worldwide, accounting for almost 10 million of deaths in 2020 (WHO 2020). Factors contributing to cancer include exposure to chemical, physical and/or biological carcinogens, genetic predisposition, infections, lifestyle and poor dietary habits. Recent studies highlight that various human cancers can be influenced by bioactive compounds, with resveratrol being one of the most extensively researched (Rauf et al., 2018).

In vitro, resveratrol has shown potential therapeutic effects in different cancer types, including gastric, colorectal, breast, liver cancer, head and neck or oesophageal (Fulda, 2010; Rauf et al., 2018; Varoni et al., 2016). It achieves this by modulating various signalling pathways involved in cancer progression. Resveratrol can inhibit cell cycle regulation, angiogenesis and invasion/metastasis, while promoting apoptosis and autophagy through the regulation of cell cycle-associated proteins (Kim and Kim, 2018).

Despite that, only a few human clinical trials have reported beneficial effects in cancer treatment, with most showing neutral outcomes likely due to a poor bioavailability and fast metabolism (Ávila-Gálvez et al., 2020; Kim and Kim, 2018). Notable clinical trials include one by Patel et al. (2010), where a 5 % reduction in tumour cell proliferation was observed in colorectal cancer patient consuming 0.5 or 1 gram of resveratrol daily for eight days (n = 20) (Patel et al., 2010). Another study by Howells et al. (2011) reported increased levels of cleaved caspase-3, a marker of apoptosis, in patients with colorectal cancer and liver metastases after administering 5 grams of micronised resveratrol daily for 15 days (n = 9) (Howells et al., 2011). Additionally, there are promising studies on breast, prostate and colon cancers using plant extracts or formulations containing resveratrol, but the presence of other phenolic compounds makes it difficult to attribute the effects solely to resveratrol (Nguyen et al., 2009; Paller et al., 2015; Zhu et al., 2012).

Oxyresveratrol has shown cytotoxic effects against human gastric cancer cells and murine leukaemia cells, demonstrating selectivity for the latter. It also induces caspase-independent cell death and inhibits angiogenesis in highly chemotherapy-resistant breast cancer cell lines (Likhitwitayawuid, 2021). However, in head and neck squamous cell carcinoma, oxyresveratrol exhibited lower anti-angiogenic and anti-proliferative efficacy in comparison with resveratrol (Sintuyanon et al., 2017).

Piceatannol has been shown to induce apoptosis in an intrinsic manner and inhibit the proliferation of various tumour cells, including leukaemia, breast, lymphoma, prostate, melanoma and colon cancers (Seyed et al., 2016). Some studies suggest that piceatannol has stronger anticancer activity than resveratrol (Lee et al., 2019). Comparing the activity of resveratrol, oxyresveratrol and piceatannol, it seems that the addition of a hydroxyl group to resveratrol in the *ortho*-position enhances its activity compared to the *meta*-position.

Pinosylvin regulates apoptosis and growth inhibition in cancer cells by modulating the overexpression of nonsteroidal anti-inflammatory drug-activated gene. It also inhibits metastatic oral cancer cells by regulating metalloproteinase-2 expression and activity through the ERK pathway (Chen et al., 2019). In leukaemia cells, pinosylvin induces cell death via autophagy or apoptosis by down-regulating AMPKα1 (Song et al., 2018).

Pterostilbene can modulate the cell cycle, enhance autophagy and apoptosis, and inhibit angiogenesis, tumour invasion and metastasis by affecting multiple signalling pathways involved in cancer progression (Lin et al., 2020). Due to its higher lipophilicity, pterostilbene has shown more potent inhibitory effects on human colon cancer cells compared to resveratrol (Y. Zhang et al., 2021).

Another methoxylated stilbene, isorhapontigenin, has been shown to induce cell cycle arrest, cell death, oxidative stress and inhibit of cell proliferation in breast cancer. It demonstrated greater potency than resveratrol in inducing cell death and growth arrest through the activation of caspase-dependent cell death cascades (Subedi et al., 2019).

Meanwhile, piceid, the resveratrol glycoside, mainly affects tumour cell viability by causing cell cycle arrest, with minor effects on apoptosis. Its cytotoxicity was weaker than that of resveratrol, likely due to its lower cellular uptake (Su et al., 2013).

2.3.6. Anti-obesity activity

Obesity has become the epidemic of the 21st century, affecting 16 % of the adult population worldwide, while 43 % suffer from overweight (WHO 2022). Its prevalence has increased rapidly in recent years, especially in young people, with obesity doubling in adults but quadrupling in adolescents since 1990. This condition increases the risk of many other diseases such as cardiovascular disease and diabetes. However, since obesity

is caused by an imbalance of energy intake and energy expenditure, it is easily preventable through healthy dietary habits and physical activity. For this reason, some bioactive compounds, such as stilbenes, may be of interest in functional foods to target obesity.

Stilbenes have been reported to prevent obesity by modulating various metabolic pathways, including adipogenesis, lipogenesis, apoptosis, lipolysis, thermogenesis and fatty acid oxidation. Resveratrol, the most studied stilbene in this regard, has been shown to inhibit peroxisome proliferator-activated receptor gamma (PPARγ), CCAAT-binding protein (C/EBPα), sterol regulatory element protein (SREBP-1c), fatty acid synthase (FAS), acetyl-CoA carboxylase (ACC) and lipoprotein lipase (LPL) involved in adipogenesis and lipogenesis, as well as regulate uncoupling proteins (UCP) and sirtuin-1 (SIRT1) involved in thermogenesis and cellular homeostasis (Aguirre et al., 2014; Baile et al., 2011; Fernández-Quintela et al., 2017; Scapagnini et al., 2014).

Pterostilbene and piceatannol also influence adipogenesis, lipogenesis and fatty acid oxidation by regulating ACC, PPARγ, PPARα or SREBP1 (Carpéné et al., 2018; Kim et al., 2020; Yang et al., 2020). Notably, pterostilbene was found to be more effective than resveratrol *in vivo* at a dose of 15 mg/kg/day, likely due to its higher bioavailability (Gómez-Zorita et al., 2014). Moreover, molecular docking studies suggest that pterostilbene can form hydrogen bonds with three amino acids of PPARα, whereas resveratrol binds with only two (Kim et al., 2020).

By comparing the physicochemical and biological properties of the stilbenes described above, the following structure-activity relationships can be established: 1) Hydroxylated and glycosylated stilbenes seem to be more soluble in water, which would facilitate their incorporation into hydrophilic matrices, albeit at still modest

concentrations; 2) The greater lipophilicity of methoxylated stilbenes could enhance bioavailability, rendering them more promising for clinical investigation; 3) Glycosylated stilbenes are more easily isomerised than aglycones, requiring more effort to preserve them; 4) *Ortho*-hydroxylated stilbenes may exhibit superior antioxidant, anti-inflammatory and anticancer properties compared to methoxylated stilbenes, likely attributable to the formation of a stable semiquinone radical.

2.4. Challenges and constraints in the applications of stilbenes

As described above, obtaining stilbenes from their natural sources is restricted to certain plant species, which have a limited stilbene production capacity. Various techniques are currently being studied to improve production, such as elicitation of plant cultures, genetic modification of plants or chemical synthesis, but new ways of obtaining pure stilbenes in large quantities and at low cost are still needed.

Moreover, characterisation of these bioactive compounds is still scarce, with most studies focusing on a single stilbene, resveratrol. Nevertheless, it is known that the physicochemical properties of the natural stilbenes described above pose some issues that restrict their potential applications. For example, its low aqueous solubility may prevent their incorporation in hydrophilic matrices (such as functional foods) at effective concentrations. Furthermore, the stability of stilbenes can be compromised during industrial manufacturing and storage because they can easily degrade by external factors such as light, pH, oxygen or temperature (Zupančič et al., 2015).

Besides, there is a discrepancy between the biological activity of stilbenes reported *in vitro* and *in vivo* related to their low bioavailability and hormetic activity. Hormetic activity refers to a phenomenon where certain molecules exhibit beneficial effects within a specific dosage range. However, below or above this range may not yield

any significant benefit or could potentially lead to adverse effects (Scapagnini et al., 2014). Although preclinical and clinicals doses should be established considering the hormetic curve of stilbenes, it is often difficult to extrapolate cell or animal doses to humans, as well as to set the proper exposure times. In fact, many preclinical studies on stilbenes fail in this respect, either by employing too high concentrations or exposures of short duration, using non-physiological metabolites or concentrations (Tome-Carneiro et al., 2013).

Furthermore, despite their high oral absorption, 75 % for resveratrol, stilbenes undergo rapid metabolism in the liver or intestine, compromising the effective concentration that reaches target tissues. Stilbenes can suffer from phase II reactions, such as glucuronidation and sulphation, leading to the formation of more soluble derivatives that are readily excreted, primarily in the urine. In fact, some studies have indicated that the available concentration of resveratrol reaching target tissues in humans may be less than 1 % (Walle, 2011). In rats, oral bioavailability can vary widely, from 9.13 % for oxyresveratrol to 80% for pterostilbene (Akinwumi et al., 2018). This underscores the significance of the molecular structure in the bioactivity of stilbenes.

These circumstances led the EFSA to decline the health claim for resveratrol (EFSA, 2010), despite the acceptance of synthetic resveratrol as a safe novel food (EFSA, 2016). Nonetheless, dietary supplements containing resveratrol and bearing health claims are currently on the market and in use. However, these assertations are not related to resveratrol itself, but to other vitamins or minerals in the formulation that have approved health claims. While this marketing tactic is legally permissible, its ethical implications are questionable. A different research approach is necessary to achieve an EFSA-approved health claim for stilbenes, with essential emphasis on addressing their physicochemical challenges before considering their application.

Some approaches have been suggested to overcome the physicochemical and bioavailability challenges associated with stilbenes (de Vries et al., 2021; López-Nicolás et al., 2014). In this thesis, two different strategies that have demonstrated effectiveness in mitigating some of these issues are outlined: 1) the molecular encapsulation of stilbenes using various agents, and 2) the structural modification of stilbenes to create novel compounds with better properties.

2.5. Innovative approaches to overcome the limitations of stilbenes

2.5.1. Molecular encapsulation

Encapsulation takes places when the stilbene is embedded within a matrix, facilitating the delivery and safeguarding the molecule. This process involves a dynamic equilibrium that can shift to either form the complex or release the molecule, depending on factors like composition and temperature. There are several agents and mechanisms involved in molecular encapsulation, among which cyclodextrins, polymeric nanoparticles and liposomes are recognised for their versatility in accommodating small molecules, such as stilbenes.

2.5.1.1. Cyclodextrins

Cyclodextrins (CDs) are oligosaccharides with a torus-shaped structure, composed of α-(1,4)-linked glucose units. Natural CDs are obtained from starch degradation through the enzyme cyclodextrin glucosyltransferase (CGTAse), while modified CDs are obtained through derivatisation of natural CDs. The CD ring exhibits a conical cylinder shape with amphiphilic properties, featuring a hydrophilic outer layer compromised of hydroxyl groups and a slightly lipophilic cavity, which allows them to trap poorly soluble molecules inside forming inclusion complexes (Kurkov and Loftsson, 2013).

The most common CDs are natural α-CD, β-CD and γ-CD, which contain six, seven and eight glucose units, respectively, and are authorised for food use as additives, designated as E-457, E-459 and E-458, respectively (Figure 8). CD complexes can improve water solubility and protection against degradation or volatilisation of the molecules they encapsulate, as well as mask off-flavours (Astray et al., 2009; Del Valle, 2004). In addition, some CDs have intrinsic bioactivity to treat diseases, such as the modified hydroxypropyl-β-CD (HP-β-CD) that is use as a drug for Niemann-Pick type C disease (Matencio et al., 2020a, 2020e).

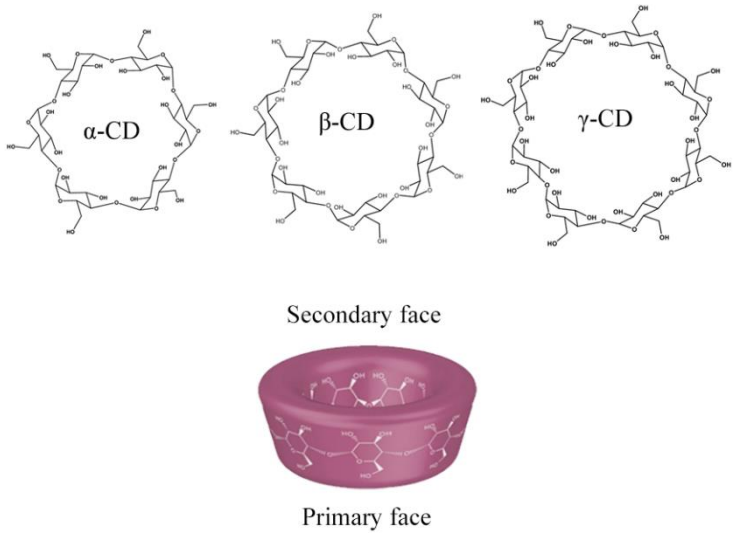

Figure 8. 2D and 3D structure of natural CDs indicating their faces according to the position of their primary and secondary hydroxyl groups

Some natural stilbenes have been encapsulated in CDs to order to enhance their solubility or stability, such as resveratrol (López-Nicolás et al., 2006; López-Nicolás and García-Carmona, 2010; Lucas-Abellán et al., 2007), pinosylvin (López-Nicolás et al., 2009a), pterostilbene (López-Nicolás et al., 2009b), *trans*-α-methylstilbene (Matencio et al., 2017b), piceatannol (Matencio et al., 2016; Messiad et al., 2013) or oxyresveratrol (He et al., 2017; Matencio et al., 2017a; Rodríguez-Bonilla et al., 2010). A recent publication comprehensively explores the significant applications of resveratrol and CDs,

from the physicochemical to the biomedical levels (Jeandet et al., 2021). Additionally, the diverse biological activities of stilbenes may be influenced by complexation due to the increased stability or concentration (Matencio et al., 2021). For example, complexation of oxyresveratrol with β-CD not only improved its stability in food models during storage but also the antimicrobial activity of the stilbene in these matrices (Matencio et al., 2020d). Resveratrol exhibited similar outcomes in anticancer, antimicrobial or antioxidant activity (Duarte et al., 2015; Hao et al., 2021; Lu et al., 2009), and pterostilbene showed enhanced anti-inflammatory and antimicrobial activity when encapsulated in HP-β-CD (Lim et al., 2020).

2.5.1.2. Polymeric nanoparticles

Polymeric nanoparticles consist on particles typically range in size 1 – 1000 nm that can encapsulate active molecules either within the polymeric core or through surface adsorption onto the nanoparticle (Figure 9). This type of encapsulation has demonstrated significant potential for targeted delivery of bioactive compounds in the treatment of various diseases (Zielińska et al., 2020).

Various authors have investigated the impact of different polymers on stilbenes. For instance, a polymer composed of polyethylene glycol-polylactide was utilized to supplement resveratrol, resulting in increased stability and improved release of the compound, leading to enhanced anticancer activity *in vitro* and similar efficacy *in vivo* (Jung et al., 2015). More recently, a polyethylene glycol-polylactic acid polymer was employed to transport resveratrol for age-related macular degeneration treatment. This formulation demonstrated good stability and compatibility, with cells effectively uptaking resveratrol, leading to a greater decrease in the expression of the vascular endothelial growth factor compared to free resveratrol (Bhatt et al., 2020). Chitosan nanoparticles

modified with biotin and avidin, and containing resveratrol, were prepared to target liver carcinoma, resulting in enhanced delivery (Bu et al., 2013).

Other stilbenes are also under investigation in this regard. For example, oxyresveratrol was embedded in polyethylene glycol-polylactic acid nanoparticles to inhibited inflammatory mediators released by human dendritic cells (Gaglio et al., 2021). Similarly, piceatannol in chitosan/polylactic acid nanoparticles demonstrated increased apoptotic activity *in vitro* in liver, breast and lung cancer cell lines (Dhanapal and Balaraman Ravindrran, 2018).

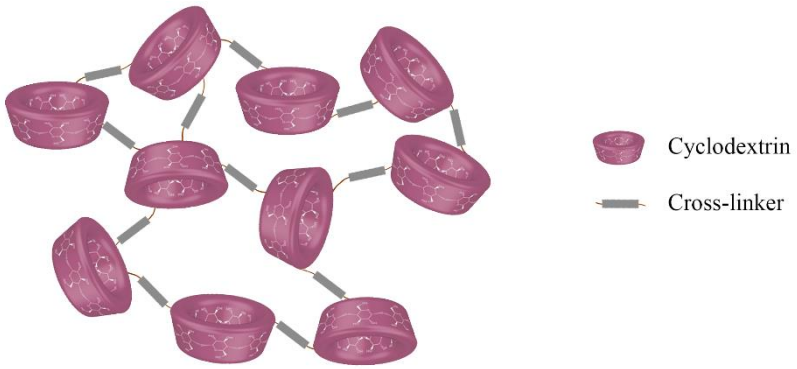

Figure 9. CD polymers capable of encapsulating molecules within the polymer core or by surface adsorption

Moreover, the above-described CDs can be polymerised using cross-linkers to improve their properties (Figure 9). CD polymers can be classified by their structure, according to differences in CD assembly (Matencio et al., 2021). Within CD polymers, insoluble nanosponges have emerged as an interesting alternative to monomeric CDs (Krabicová et al., 2020). Resveratrol and oxyresveratrol complexed with different nanosponges exhibited increased stability and anticancer activity (Dhakar et al., 2019; Matencio et al., 2020b) or enhanced anti-aging activity (Matencio et al., 2020c).

2.5.1.3. Liposomes

Liposomes typically consist of an aqueous core enclosed by a phospholipid bilayer, with additives like cholesterol often incorporated to enhance vesicle stability (Lee et al., 2005). These particles are effective for transporting hydrophilic drugs in the aqueous core and lipophilic drugs within the bilayer. For instance, liposomes significantly increased the chemical stability of *trans*-resveratrol, with 70 % remaining stable after 16 minutes of UV light exposure compared to just 10% of the free form (Coimbra et al., 2011). Additionally, the ratio of *cis*- and *trans*-resveratrol influence liposome stability, while *trans*-resveratrol does not affect bilayer stability, *cis*-resveratrol may cause destabilisation (Detoni et al., 2012). The structure of liposomes facilitates cellular uptake, enhancing drug efficacy, as demonstrated by the improved cytotoxicity of resveratrol against HeLa cervical carcinoma cells and Hep 2 hepatocellular carcinoma cells when complexed in polyPEG2000 or standard liposomes (Lu et al., 2012). In addition, the conjugation to liposomes can increase the targeting activity. For instance, an immunoliposome with resveratrol and curcumin, which was developed to target the human epidermal growth factor receptor type 2, enhanced the selectivity of the codelivery (Catania et al., 2013).

2.5.2. Structural modifications

Another approach to address the limitations and enhance the properties of stilbenes is the modification of their structure, by adding or changing their functional groups (Fulda, 2010). These structural modifications can change the physicochemical properties of stilbenes such as its solubility, as well as affect bioactivity by changing interactions with enzymes or other molecules.

This Section emphasises research that not only synthesises new stilbenes but also evaluates their efficacy, with Table 2 providing a summary of these effects. For clarity, these modifications have been classified into the following groups according to the radicals added to the basic stilbene structure, regardless the synthesis process: hydroxylation (-OH), methoxylation (-O-CH_3), glycosylation (-O-$C_6H_{11}O_5$), halogenation (-F, -Br...) and acylation (-CO-R).

Table 2. Summary of the effect of structural modification on the physicochemical and biological properties of stilbenes. The symbols ↑, ↓ and ~ means increase, decrease or similar activity compared to resveratrol; MR = molar refractivity; APOL = atom polarizability; TPSA = topological polar surface area; LogP = lipophilicity index

Modification	Physicochemical effect	Biological effect	References
Hydroxylation (-OH)	↑ MR ↑ APOL ↑ TPSA ↓ logP	↑ Anticancer ↑ Antioxidant ↑ Anti-inflammatory ↑ Antiviral	(Li et al., 2006; Szekeres et al., 2010)
Glycosylation (-O-$C_6H_{11}O_5$)	↑ Water solubility	↓ Antioxidant ↓ Enzymatic oxidation	(Lepak et al., 2015; Regev-Shoshani et al., 2003; Torres et al., 2011)
Methoxylation (-O-CH_3)	↑ MR ↑ APOL	↑↓ Anticancer ↑↓ Anti-inflammatory ↓ Inhibition of tyrosinase ↑ Antimicrobial	(Cardile et al., 2007; Hu et al., 2017; Likhitwitayawuid et al., 2006; Szekeres et al., 2010)
Halogenation (-F, -Br...)	-	Antimicrobial ↑↓ Anticancer	(Albert et al., 2011)
Acylation (-CO-R)	↑ logP ↓ Oxidative discoloration	↓~ Anticancer ↓ Antioxidant ↓ Anti-inflammatory ~Antimelanogenic	(Oh and Shahidi, 2018, 2017; Park et al., 2014)

2.5.2.1 Hydroxylation

As mentioned above, some natural hydroxylated analogues of resveratrol have improved aqueous solubility and free radical scavenging activity. Therefore, stilbene derivatives containing more hydroxyl substituents are expected to exhibit greater antioxidant activity. This aspect, alongside the influence of radical position, was examined on di-, tri-, tetra- and penta-hydroxylated stilbenes (Wang et al., 1999). Additionally, the presence of an *ortho*-dihydroxylated ring was noted to improve antioxidant capacity (Fulda, 2010). Moreover, the antiproliferative activity of *trans*-

stilbenes in cancer is believed to be closely related to the presence of 4-OH or 4'-OH groups, with *trans*-4,4'-dihydroxystilbene showing higher antioxidant and cytotoxic effects compared to resveratrol (Fulda, 2010).

Another research that evaluated tetra-, penta- and hexa-hydroxylated analogues of resveratrol with 4-OH, 3'-OH and/or 5'-OH groups, revealed that the presence of pyrogallol and catechol groups gave higher antioxidant and anticancer activity against leukaemia cells than those with resorcinol groups (Murias et al., 2005). Furthermore, these derivatives exhibited greater anti-inflammatory effects than resveratrol, through the inhibition of COX-2, and lower logP but higher TPSA, atomic polarizability (APOL) and molar refractivity (MR) (Murias et al., 2004). Among them, *trans*-3,3',4,4,4',5,5'-hexahydroxystilbene highlights due to its great activity against breast cancer, melanoma and colon tumour cells (Szekeres et al., 2010).

In addition, *trans*-2',3,5,5'-tetrahydroxystilbene was effective in inhibiting SARS-CoV-1 replication, as was the pyridine derivative *trans*-2',5,5',6-tetrahydroxystilbene-2-nitrogen (Li et al., 2006).

2.5.2.2. Glycosylation

As stated above, natural glycosylated stilbenes exhibit greater sensitivity to isomerisation compared to aglycones, but may have higher aqueous solubility. Glycosylated derivatives of resveratrol at R3 and/or R4' were at least 65 and 5 times more water soluble than natural resveratrol and piceid (Torres et al., 2011). However, this modification also resulted in a reduction in antioxidant capacity, more notably in 3-O-glucosyl-stilbenes. Another study that synthesised a resveratrol derivative glycosylated at R3 and R5 positions also observed a decrease in antioxidant activity compared to resveratrol or piceid, but an increase in solubility of approximately 1700 times more than

the activity of resveratrol (Lepak et al., 2015). Besides, the antioxidant activity of this derivative was better than that of resveratroloside, a natural stilbene glycosylated at R4'. Additionally, glycosylation of resveratrol completely inhibited its oxidation by the enzyme tyrosinase (Regev-Shoshani et al., 2003).

2.5.2.3. Methoxylation

Natural pterostilbene, which has two methoxy groups where resveratrol has hydroxyl groups, exhibited superior oral bioavailability due to its more lipophilic and metabolically stable structure (Pecyna et al., 2020). This is because unlike hydroxyl groups, methoxy groups cannot undergo sulphation and glucuronidation reactions that reduce oral bioavailability. Moreover, methoxylation of resveratrol has shown to protect it against oxidation by tyrosinase (Regev-Shoshani et al., 2003).

Tri-, tetra- and penta-methoxystilbenes exhibited higher inhibition of cell growth compared to resveratrol, with some demonstrating selectivity for transformed cells (Fulda, 2010). Some *trans*- and *cis*- analogues of resveratrol di- and tri-methoxylated at R3, R4, R5 or R4' showed greater cytotoxicity than resveratrol against cancer cell lines of prostate (androgen sensitive and non-responsive), melanoma and oral epidermoid carcinoma, highlighting the notable effect of *cis*-3,4',5-trimethoxystilbene (Cardile et al., 2007). Another study also found an enhancement in cytotoxicity against cervical carcinoma, lymphoma, and lung cancer cell lines with mono-, di- and tetra-methoxylated derivatives of oxyresveratrol compared to the natural stilbene (Likhitwitayawuid, 2021; Likhitwitayawuid et al., 2006). This effect depended on the number of methoxy groups and isomerisation, being the *cis*-isomer with four substituted radicals the most active. Consequently, a loss of tyrosinase inhibitory activity was observed after modification.

The presence of methoxy groups has also proved to enhance the antifungal activity of stilbenes against *Candida albicans* biofilms, with the *meta*-dimethoxy structure standing out from the trimethoxy structure (Hu et al., 2017).

However, stilbene methyl ethers at R2', R3, R5 and R5' gave lower SARS-CoV-1 inhibition than their corresponding hydroxylated stilbenes, as was observed for those modified at R2', R3, R6 and R5' with a pyridine ring instead of a benzene ring (Li et al., 2006). Furthermore, some tri-, tetra-, penta- and hexa-methoxylated stilbenes showed reduced anti-inflammatory activity compared to hydroxylated analogues, due to a low inhibition of COX enzymes and poor selectivity for COX-2 (Murias et al., 2004). Although hexa- and penta-methoxylstilbenes, as well as 3,3',4',5-tetramethoxylstilbene, exhibited a stronger inhibition of COX-2 than resveratrol. These methoxylated derivatives had higher MR and APOL than resveratrol.

The addition of methoxy groups in resveratrol at the R2', R4 and/or R5' positions enhanced its antioxidant activity while decreased its genotoxicity (Fukuhara et al., 2008). Moreover, the antioxidant and anticancer activity of resveratrol was also improved after methylation of all their radicals and hydroxylation at the R2 position (Basini et al., 2010).

2.5.2.4. Halogenation

Fluorinated resveratrol analogues have also demonstrated enhanced properties. For example, *trans*-3,5-difluoro-4'-acetoxystyloxystilbene showed greater activity than resveratrol against melanoma and lung cancer (Moran et al., 2009). In another study, some synthesised fluoro-hydroxystilbenes, with and without methoxy groups, were found to have greater cytotoxicity than resveratrol in the mouse embryonic fibroblast cells (Albert et al., 2011). Meanwhile, *trans*-6-fluoro-4-methoxy-2',3,5'-trihydroxystilbene and *trans*-3-hydroxy-3',4',5'-trifluorostilbene exhibited great antimicrobial activity against some

bacteria and fungi. In addition, the modification of resveratrol with mono-, di- and tri-bromoethyl radicals also improved its *in vitro* anticancer activity (Ruan et al., 2006).

2.5.2.5. Acylation

Similar to methoxylated stilbenes, acetylated stilbenes have demonstrated greater stability and bioavailability. For example, triacetyl resveratrol showed better resistant to oxidative discolouration compared to resveratrol while retaining its anticancer and antimelanogenic properties (Duan et al., 2016; Fu et al., 2019; Park et al., 2014). Within mono-, di- and tri-acetylated derivatives of resveratrol, the degree of substitution was found to decrease antioxidant activity, especially when modified at the R3 position rather than the R4' (Torres et al., 2010).

The acylation of resveratrol with short- and long-chain fatty acids also resulted in a decrease in antioxidant activity *in vitro* (Oh and Shahidi, 2017). However, some of these derivatives showed higher antioxidant capacity in ground beef, hydroxyl radical-induced DNA cleavage and inhibition against copper-induced LDL oxidation (Oh and Shahidi, 2018). Moreover, resveratrol monoesters with propionic acid or docosahexaenoic acid (DHA) did not exhibit clear enhancement in anti-inflammatory and anticancer activity in liver, colon, breast and gastric cancer cell lines compared to unmodified resveratrol (Oh et al., 2019). Nonetheless, the authors suggested potential benefits of these compounds for resveratrol applications in food and biological systems.

CHAPTER II

OBJECTIVES

CHAPTER II. OBJECTIVES

Bearing in mind the health promoting effects of stilbenes and the challenges that limit their potential applications in different industries, the main objective of this PhD thesis was to synthesise, characterise, encapsulate and analyse the biological activity of natural and novel stilbenes derivatives.

For this purpose, the following specific objectives were defined:

1. To seek and develop new approaches to increase the production of stilbenes in the present and in the future, using biotechnological, bioinformatics and biochemical techniques.
2. To determine and improve some physicochemical properties of natural stilbenes by molecular encapsulation in CDs, characterising the stoichiometry and formation constants with natural and modified CDs.
3. To synthesise chemically and enzymatically, characterise and encapsulate novel hydrophobic stilbenes derivatives.
4. To analyse the absorption and metabolism *in vitro* and *in vivo* of novel hydrophobic stilbenes derivatives, as well as their hydrolysis and different ways of inhibiting it *in vitro*.
5. To investigate and compare the bioactivity *in vitro* and *in vivo* of novel hydrophobic stilbenes derivatives and natural stilbenes against oxidative stress, cancer and obesity.
6. To fortify food models with novel hydrophobic stilbenes derivatives, assessing the industrial quality and shelf life under different storage conditions.

CHAPTER III

MATERIALS AND METHODS

CHAPTER III. MATERIALS AND METHODS

1. Materials

All *trans*-stilbenes used (resveratrol (>99%), piceatannol (>98%), oxyresveratrol (>98%), gnetol (>97%), pterostilbene (>98%), pinostilbene (>97%), isorhapontigenin (>96%), rhapontigenin (>98%), and 3,4',5-trimethoxystilbene (>98%)) and DCC were obtained from TCI (Zwijndrecht, Belgium). Modified CDs, HP-β-CD (DS = 5.0) and M-β-CD (DS = 5.4), were obtained from Carbosynth (Berkshire, United Kingdom). Natural CDs (α-CD, β-CD, γ-CD), fatty acids (stearic acid (>97%), palmitic acid (>98%), and oleic acid (>99%)), caffeic acid, chlorogenic acid, DMAP, vinyl stearate, Novozym 435 (≥5000 U/mg), porcine pancreas lipase (Type II, ≥125 U/mg), mushroom tyrosinase (≥1000 U/mg), horseradish peroxidase (HRP) (Type VI, 950-2000 U/mg), bovine serum albumin, ABTS, ammonium persulphate, fluorescein, AAPH, TPTZ, ferric chloride, ferrous sulphate, glucose, trolox, monobasic sodium phosphate dihydrate, boric acid, IPTG, kanamycin, chloramphenicol, Trizma base, glycerol, SDS, β-mercaptoethanol, bromophenol blue, Coomassie Brilliant Blue R-250, TEMED, molecular sieve, and LB agar culture medium were obtained from Sigma-Aldrich (Madrid, Spain). Soy lecithin, D-(-)-quinic acid, silica 60 Å, and culture media, Lysogeny Broth (LB) and Terrific Broth (TB), were obtained from Fisher Scientific (Geel, Belgium). DPPH was obtained from ThermoFisher (Madrid, Spain). Neochlorogenic acid was from Baoji Guokang Bio-Technology Co. (Baoji City, China). The Bradford reagent and acrylamide/bisacrylamide (30% / 0.8% (w/v)) were obtained from Bio-Rad Laboratories (Hercules, CA, USA).

The buffers used were prepared from their corresponding salts or acids by adjusting the pH in a Crison GLP 21+ pH meter (Barcelona, Spain) with acidic solutions (0.1 - 5 M hydrochloric acid) or basic solutions (0.1 - 5 M sodium hydroxide), previously

prepared with hydrochloric acid 37% (v/v) and sodium hydroxide from Sigma-Aldrich (Madrid, Spain).

Chloroform (>99%), methanol (HPLC grade), acetonitrile (HPLC grade), and water (HPLC grade) were obtained from Fisher Scientific (Loughborough, United Kingdom). DMSO (>99.9%) and DMF (>98%) were from Sigma-Aldrich (Madrid, Spain). Ethanol and glacial acetic acid were from PanReac AppliChem ITW Reagents (Barcelona, Spain). All solvents used for chromatography were HPLC grade, while for other experiments, they were reagent grade. The water used was deionised water, except in cell experiments, that water was obtained through a Merck Millipore Mili-Q Advantage A10 system (Darmstadt, Germany).

All reagents were stored under the temperature, humidity and lighting conditions indicated by the manufacturer.

2. Enzymatic synthesis of piceatannol

Several enzymatic reactions were carried out with tyrosinase to synthesise piceatannol from resveratrol, taking advantage of the cresolase activity of this enzyme (Figure 10). The progress of the reactions was monitored by two techniques: UV-Vis spectrophotometry and HPLC chromatography.

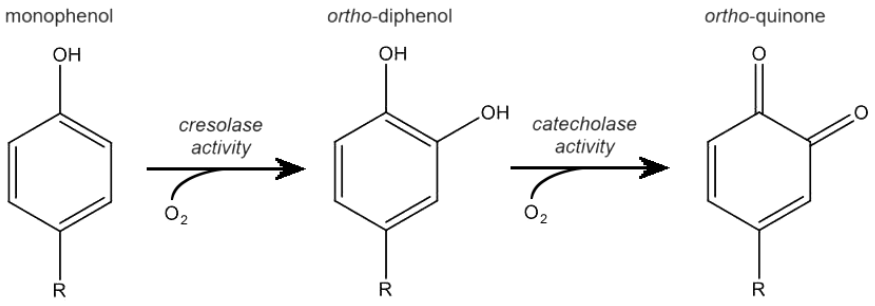

Figure 10. Enzymatic reaction catalysed by tyrosinase

2.1. Spectrophotometric analysis

Samples were prepared with 25 µM of resveratrol and 2 µg/mL of tyrosinase enzyme, in the presence or absence of 25 µM of catechol, 25 µM of ascorbic acid, or 1 mM of β-CD in 0.1 M sodium phosphate buffer pH 7. The samples were incubated at 30 °C in a Thermomixer Comfort (Eppendorf AG, Hamburg, Germany). Absorption spectra were recorded between 200 and 500 nm every 2 minutes for 30 minutes, after gentle agitation, using a Jasco V-630 spectrophotometer (Madrid, Spain) with Thorlabs CV10Q1400 cuvettes. A solution with buffer and methanol at the same final concentration as the samples was used as a blank.

2.2. HPLC-UV/Vis analysis

Samples were prepared with 12.5 µM of resveratrol and 100 µg/mL of tyrosinase enzyme, in the presence or absence of 25 µM catechol, 12.5, 25 or 100 µM ascorbic acid, or 1, 5 or 10 mM β-CD in 0.1 M sodium phosphate buffer pH 7. Additionally, samples with combined treatments of 100 µM ascorbic acid and 1 or 5 mM β-CD were prepared, maintaining the rest of the conditions. The reactions were incubated at 30 °C in the autosampler tray of a Shimadzu LC2010C HT HPLC system (Shimadzu, Kyoto, Japan) in reverse phase, with UV-Vis detector set at 310 nm, equipped with a Kromasil C18 column of 5 µm (150 × 4.6 mm) (Análisis Vínicos, Tomelloso, Spain). Aliquots were injected every 20 minutes for 4 hours at a flow rate of 1 mL/min at 25 °C and an isocratic method of acetonitrile and water (25:75 (v/v)). Calibration curves were performed for quantification, and conversion percentage was calculated using the equation below:

$$Conversion\ (\%) = \frac{[Piceatannol]_f}{[Resveratrol]_0} \quad (1)$$

where $[Piceatannol]_f$ is final concentration obtained of piceatannol and $[Resveratrol]_0$ is the initial concentration of resveratrol at time 0.

3. Phylogenetic analysis

Phylogenetic analyses were performed to investigate the evolution of STS proteins in cooperation with the Departamento de Informática y Sistemas (Universidad de Murcia, Murcia, Spain).

3.1. Sequence search and multiple alignment

UniProtKB database (UniProt KnowledgeBase, UniProt consortium, v2020) (The UniProt Consortium, 2023) was used to search for amino acid sequences of plant STS proteins. This database comprises the set of reviewed proteins in Swiss-Prot and the set of unreviewed proteins in TrEMBL. Both Sections of the database were used to obtain a greater number of sequences, carrying out an initial screening of predicted and homology-interfered sequences to retain only those sequences with experimental evidence at the transcript level, followed by a second screening to select sequences cited and used in scientific publications.

Multiple alignment of selected plant STS protein sequences was performed using the MUSCLE software (Edgar, 2004), which employs the Log-Expectation method for comparison. This software constructs a guide tree by counting short sequences (k-mers), then carries out progressive pair-wise alignment and refinement using tree-dependent restrained participation. MUSCLE represents residue conservation at each position with the following signs: (*) identical, (:) conservative substitutions, (.) semi-conservative substitutions, and ( ) if there is no match.

3.2. Hidden Markov Model

The Hidden Markov Model (HMM) is a statistical model that can be used in bioinformatics studies to identify remote homologous sequences with high sensitivity.

This model is based on a set of states and the possible transitions between states based on observations, i.e., the probability of a state occurring within another (emission) and the probability of transitioning from one state to another (transition).

In sequence family modelling, states are used for match, insertion, and deletion. When comparing sequences with HMM, a score called E-value is obtained, which represents the probability that the sequence is related to the created model. Thus, if a residue is well conserved at a position, it will give a higher E-value.

Using the default sequence pondering scheme based on the Henikoff position, an HMM was created with the sequences obtained from the multiple alignment of MUSCLE using the hmmbuild tool of the HMMER software (Henikoff and Henikoff, 1994). The most conserved protein parts of the sequences were studied with the positional HMM model obtained. Additionally, using the hmmsearch tool of the HMMER software, similar sequences were searched for in the UniProtKB (proteins) and Ensembl (genomes) databases.

3.3. Construction of phylogenetic trees

Phylogenetic trees represent the evolutionary relationships among various organisms or taxa through a series of nodes connected by branches. These nodes can be terminal or internal, depending on whether they refer to the analysed sequences or the ancestral sequences that gave rise to them, respectively.

The construction of STS phylogenetic trees was carried out using the Phylogeny.fr software (Dereeper et al., 2008) by selecting a customized workflow. From the multiple alignment in MUSCLE, the phylogenetic tree was constructed using the maximum likelihood model PhyML, omitting the Gblocks curation stage to retain less conserved

sequences. Finally, visualization of the phylogenetic tree was obtained in the TreeDyn format.

4. Determination of thermostability

Aqueous solutions containing 25 μM of resveratrol were prepared and incubated in a Thermomixer Comfort (Eppendorf AG, Hamburg, Germany) at 50 °C with agitation at 500 rpm for 5 days. Aliquots were taken at 0; 0.25; 0.5; 1; 2; 24, 48, and 120 hours to measure their absorption spectrum between 200 and 600 nm using a Jasco V-630 spectrophotometer (Madrid, Spain) with Thorlabs CV10Q1400 cuvettes. A solution with water and ethanol at the same final concentration as the samples was used as a blank.

5. Production of a STS in *Escherichia coli*

5.1. Strains, vector, and cultivation conditions

For the production of the STS obtained from the phylogenetic analysis, two strains of *Escherichia coli* were transformed: DH5α and Rosetta 2 (DE3), both obtained from Novagen (Merck KGaA, Darmstadt, Germany). *E. coli* DH5α was used for gene conservation, while *E. coli* Rosetta 2 (DE3) was used for protein expression due to its lower degree of recombinant protein degradation, lacking the ompT gene that encodes a membrane protease.

The gene of the selected bacterial STS was incorporated into the pET-28a(+) vector designed by GenScript Biotech (Leiden, Netherlands) with BamHI and XhoI restriction enzymes. This vector contains the kanamycin resistance gene and a histidine tag, facilitating the selection of transformed colonies and subsequent protein purification.

The *E. coli* strains were cultured in liquid LB medium, solid LB medium (with agar), or liquid TB medium. These media were supplemented with 34 mg/L of chloramphenicol for the Rosetta 2 (DE3) strain culture and 50 mg/L of kanamycin for strains transformed with the pET-28a(+) vector.

All procedures were carried out under sterile conditions using laminar flow hoods, sterile materials, and continuous disinfection with 70 % (v/v) ethanol. All materials and media were previously sterilised by autoclave. In the case of solutions, these were sterilised with 0.2 µm sterile filters.

5.2. Bacterial transformation by electroporation

Electrocompetent cells of *E. coli* DH5α and *E. coli* Rosetta 2 (DE3) were transformed with the vector using an electroporator. Controls were also prepared with water instead of the vector. Subsequently, the cells were incubated in SOC medium at 37 °C for 1 hour and plated on Petri dishes with solid LB medium supplemented with the necessary antibiotics according to the strain. After 48 hours of incubation at 37 °C, the transformation efficiency was determined by colony counting, and the transformed cells were transferred to liquid LB medium supplemented with the corresponding antibiotics to induce protein expression the next day.

5.3. Protein expression

The induction of expression of the recombinant protein in the transformed Rosetta 2 (DE3) strain was performed by adding IPTG when reaching an optical density (OD_{600nm}) of 4 in a culture in TB medium with the necessary antibiotics at 37 °C. Induction-expression tests were carried out using IPTG at concentrations between 0.2 and 2 mM and incubating at 15, 20, 30, and 37 °C. After 24 hours, the cells were centrifuged at 2500 xg for 5 minutes to discard the medium and lysed in 0.8 % (v/v) saline solution

using a Branson Digital Sonifier 450D sonicator (Branson Ultrasonics, Danbury, CT, USA) configured to apply 5 pulses of 10 seconds. Subsequently, they were centrifuged, and the supernatant and precipitate were saved for protein quantification and analysis by electrophoresis.

5.4. Protein purification

Protein purification was carried out with His GraviTrap TALON histidine columns (GE Healthcare, Freiburg, Germany). The samples were resuspended in 50 mM sodium phosphate buffer with 300 mM sodium chloride at pH 7.4 and introduced into the histidine columns. Then, they were washed with 50 mM sodium phosphate buffer containing 300 mM sodium chloride and 5 mM imidazole (pH 7.4), and eluted with 50 mM sodium phosphate buffer containing 300 mM sodium chloride and 150 mM imidazole (pH 7.4).

5.5. Protein quantification with Bradford

Prior to protein separation by electrophoresis, the total protein amount was quantified using the Bradford method (Kruger, 2009). This method is based on the ability of the hydrophobic dye Coomassie Blue to bind to proteins. Quantification was carried out by measuring the absorbance of the samples with the Bradford reagent (1:50 (v/v)) at 595 nm in a Jasco V-630 spectrophotometer (Madrid, Spain), using bovine serum albumin for the calibration curve.

5.6. Electrophoresis SDS-PAGE

The samples obtained from the expression were diluted in loading buffer, composed of 7.5 % (v/v) β-mercaptoethanol, 0.015 % (v/v) bromophenol blue, 3 % (w/v) SDS, and 15 % (v/v) glycerol in 100 mM tris-HCl buffer pH 6.8. Then, they were denatured at 100 °C for 4 minutes in a Thermomixer Comfort (Eppendorf AG, Hamburg,

Germany), and 5 µg of total protein per well was loaded onto polyacrylamide gels, consisting of a stacking gel with 4 % (w/v) acrylamide and a separating gel with 12 % (w/v) acrylamide. Electrophoresis was initiated by applying a constant voltage of 180 V to the gels immersed in running buffer, in a miniProtean II device (Bio-Rad Laboratories, Hercules, CA, USA). The Fisher BioReagents™ BP3603-500 protein marker was used to determine the size of the separated proteins.

5.7. Gel staining with Coomassie blue

After electrophoresis, the gels were stained with Coomassie Blue, using an aqueous staining solution with 0.1 % (w/v) Coomassie Blue, 10 % (v/v) glacial acetic acid, and 40 % (v/v) ethanol. The gels were kept in this solution at room temperature with gentle orbital shaking for 1.5 hours. Then, they were transferred to an aqueous destaining solution with 10 % (v/v) glacial acetic acid and 30 % (v/v) ethanol. The expression level of the protein was quantified by processing scanned gel images in Fiji (ImageJ version 1.53t) (NIH, USA) (Schindelin et al., 2012).

6. Physicochemical characterisation

6.1. Nuclear magnetic resonance

The chemical structure was analysed using proton nuclear magnetic resonance (NMR-H) on a Bruker Avance 600 MHz spectrometer (Bruker, Germany) at 25°C. Tubes of 3 mm containing 3 mg of pure compounds dissolved in 0.3 mL of deuterated chloroform, were used for the analysis. Chemical shifts (δ) were expressed in ppm, and the difference between natural and modified stilbenes was calculated.

6.2. Spectrophotometry

Serial dilutions were made at increasing concentrations of stilbenes, from 1.56 to 400 µM in ethanol from a stock solution at 1 mg/mL in ethanol. Then, their absorption spectra were recorded between 200 and 600 nm using a Jasco V-630 spectrophotometer (Madrid, Spain) with Thorlabs CV10Q1400 cuvettes, and the maximum absorption wavelength (λ_{max}) for each stilbene was determined. A solution with buffer and ethanol at the same final concentration as the samples was used as a blank. Using the absorbance value at the λ_{max}, the extinction coefficient or absorptivity was determined using Lambert-Beer's law:

$$Abs_{\lambda_{max}} = \varepsilon \cdot l \cdot c \quad (2)$$

where Abs is the absorbance at λ_{max}, ε is the extinction coefficient or absorptivity, l is the optical path length of the cuvette, and c is the concentration in the solution.

6.3. Fluorescence spectroscopy

Serial dilutions were made at increasing concentrations of stilbenes, from 1.56 to 400 µM in ethanol from a stock solution at 1 mg/mL in ethanol. Excitation spectra between 200 and 360 nm and emission spectra between 340 and 500 nm were recorded using a Shimadzu RF-6000 spectrofluorometer (Shimadzu, Kyoto, Japan) with thermostatically controlled cells, setting the excitation and emission bandwidth to 3 and 5 nm, respectively. The wavelength of maximum excitation (λ_{ex}) and emission (λ_{em}) for each analysed stilbene was determined, and it was used to measure their emission and excitation spectra, respectively.

6.4. HPLC-DAD analysis

Natural and modified stilbenes were injected into an Agilent 1100 series HPLC system (CA, USA) in reverse phase, equipped with a 5 µm Kromasil C18 column (150 × 4.6 mm) (Análisis Vínicos, Tomelloso, Spain) using a flow rate of 1 mL/min at 25°C. Detection was set at 310 nm in an Agilent 1200 series UV-Vis diode array module (CA, USA). An isocratic method with methanol and water in a ratio of 85:15 (v/v) was used for resveratrol, oxyresveratrol, and piceatannol derivatives, and in a ratio of 99:1 (v/v) for pterostilbene derivatives. Samples intercalated with methanol were injected following the same method in long sequences. Calibration curves were generated for the quantification.

6.5. Determination of aqueous solubility

To determine water solubility, saturated aqueous solutions of bioactive compounds were prepared at a concentration of 1 mg/mL. In the case of assays with CDs, these were added during preparation at concentrations between 1 and 10 mM. Samples were agitated using a vortex and incubated at 25°C in darkness for 10 minutes. Subsequently, they were centrifuged at 15600 xg for 1 minute, and the supernatant fraction containing the dissolved stilbenes was separated. The supernatants were diluted 1:100 in ethanol, and their absorbance at the previously established λ_{max} was measured using a Jasco V-630 spectrophotometer (Madrid, Spain) with Thorlabs CV10Q1400 cuvettes. A solution with ethanol and water at the same final concentration as the samples was used as a blank. The concentration of soluble bioactive compound was determined by Lambert-Beer's law with the previously calculated ε (Equation 2).

6.6. Determination of stability in aqueous solution

Solutions containing bioactive compounds at 25 µM in 0.1 M phosphate buffer pH 7 were prepared and stored at room temperature in darkness for a maximum of 3

months. In the case of assays with CDs, these were added during preparation at concentrations between 1 and 10 mM. The remaining percentage of bioactive compound was monitored every two weeks by measuring absorbance at the λ_{max} previously determined for each bioactive compound using a Jasco V-630 spectrophotometer (Madrid, Spain) with Thorlabs CV10Q1400 cuvettes. A solution with buffer and ethanol at the same final concentration as the samples was used as a blank. Results were expressed as the percentage remaining using the following formula:

$$Remaining\ (\%) = \frac{Abs_i}{Abs_0} \cdot 100 \quad (3)$$

where Abs_i is the absorbance at each time i, and Abs_0 is the absorbance at time 0.

6.7. Determination of enzymatic oxidation

Enzymatic oxidation of neochlorogenic acid was determined spectrophotometrically after 10 minutes of reaction with 10 µg/mL of neochlorogenic acid in the presence of increasing concentrations of α-CD or HP-β-CD, using 2 µg/mL of tyrosinase enzyme at 25°C pH 6.5 as a catalyst. The remaining percentage of bioactive compound was calculated by measuring absorbance at λ_{max} = 324 nm using a Jasco V-630 spectrophotometer (Madrid, Spain) with Thorlabs CV10Q1400 cuvettes and applying Equation (3). A solution with buffer at the same final concentration as the samples was used as a blank.

6.8. Prediction of physicochemical parameters

The prediction of physicochemical parameters was carried out from molecular structures in SMILES format, designing the molecules previously in ChemSketch (version 2020.1.2) (ACD/Labs, Canada).

The determination of lipophilicity parameters or octanol/water coefficient (logP) and aqueous solubility (logS) was performed using the ALOGPS software (version 2.1) (Tetko and Tanchuk, 2002). It is described that the prediction accuracy of logP with this software has a root mean square error (RMSE) of 0.35 and a standard error of the mean (SEM) of 0.26, while the prediction accuracy of logS has an RMSE of 0.49 and an SEM of 0.38.

The determination of topological polar surface area (TPSA) and molecular volume was carried out using the Molinspiration software (version 2018.10 and 2018.03) (Molinspiration Cheminformatics, Slovensky Grob, Slovakia).

7. Molecular encapsulation

7.1. Molecular encapsulation in CDs

To characterise the inclusion complexes formed between CDs (receptors or host molecules) and bioactive compounds (ligands or guest molecules), up to 4 different methodologies were employed, including both physicochemical methods (such as the Benesi-Hildebrand method, the Mohseni-Hurtubise method, and a competitive model created to consider two complexation sites in the ligand) and computational methods (such as molecular docking). Physicochemical methods allow the determination of the stoichiometry and encapsulation constants of the inclusion complexes, while computational methods enable the prediction of affinities and visualization of the three-dimensional conformation of molecular docking and possible atomic interactions, such as hydrogen bonds. In this doctoral thesis, both methodologies have been combined to obtain as much information as possible and to compare predictive results with experimental ones.

7.1.1. Molecular docking

Generally, the molecular structures of ligands were obtained from the PubChem database (NCBI, USA), except for ligands of new synthesis not characterised in this database. These new molecular structures were built in ChemSketch (version 2020.1.2) (ACD/Labs, Canada), and their three-dimensional geometry was optimized in Avogadro (version 1.2) (Hanwell et al., 2012). The molecular structures of natural CDs α-CD and β-CD were extracted from their crystal obtained in the Protein Data Bank (PDB ID: 2XFY and 1Z0N, respectively), while γ-CD was obtained from the London South Bank University website. Modified CDs HP-β-CD and M-β-CD were constructed by adding hydroxypropyl or methyl groups to the β-CD structure. The topology of the modified CDs was obtained using PRODRG with default parameters. For other molecules used, their default topology was maintained. AutoDock tools (version 1.5.6) with default parameters and charges were used to generate input files for molecular docking. Molecular docking was performed using AutoDock Vina (Trott and Olson, 2010) with default parameters, setting a seed of 5000 and considering flexible atoms in the structure of CDs.

The results of molecular docking provide 9 possible 3D configurations ordered by a score value, which is used to predict the binding strength between two molecules coupled by non-covalent interactions. Therefore, since the score is negative, the lower its value, the greater the interaction between guest and host molecules. The final representations were prepared using PyMOL (Molecular Graphics System, version 1.3, Schrödinger, LLC). To facilitate visualization, the ligand structure was displayed as sticks, while the receptor structure was displayed as lines, with hydrogens hidden. Flexible carbon atoms of CDs were coloured orange, while non-flexible carbon atoms of CDs were in blue. Carbon atoms of the ligand were coloured green, while aromatic rings

were automatically shown in white. Visualization of hydrogen bonds was obtained with default parameters, and were displayed as discontinuous yellow lines.

7.1.2. Benesi-Hildebrand method

The Benesi-Hildebrand method (Benesi and Hildebrand, 1949) characterise inclusion complexes based on their optical properties. In this method, the ligand concentration is fixed, and the relative variations of absorbance or fluorescence are analysed by increasing the CD concentration. In this doctoral thesis, this method has been used to characterise inclusion complexes formed with natural stilbenes, performing fluorometric measurements, given their greater sensitivity and selectivity compared to absorbance. Unless otherwise stated, the fixed concentration of bioactive compounds was 25 μM, and the concentration of α-CD, β-CD, γ-CD, HP-β-CD and M-βCD varied between 0 and 10 mM.

The pH was fixed in all assays using buffers previously prepared: pH 3 0.1 M sodium acetate buffer; pH 5 0.1 M sodium phosphate buffer; pH 7 0.1 M sodium phosphate buffer; pH 9 0.1 M sodium borate buffer; and pH 11 0.1 M sodium borate buffer. All samples were vortexed and incubated for 30 minutes in darkness before measuring their fluorescence intensity. Measurements were performed on a Kontron SFM-25 spectrofluorometer (Zurich, Switzerland) equipped with thermostatically controlled cells, a xenon light source, and 2 mm quartz cells. The excitation and emission bandwidths were set to 2 nm. The λ_{ex} and λ_{em} used were previously determined using a Shimadzu RF-6000 spectrofluorometer equipped with thermostatically controlled cells, setting the excitation and emission bandwidths to 5 nm. Fluorescence intensity values were recorded at 5, 15, 25, or 35°C to determine thermodynamic parameters.

The Benesi-Hildebrand method proposes two possible mathematical models depending on the stoichiometry of the complexes. A 1:1 model in which a single CD molecule binds to each molecule of the bioactive compound, and a 1:2 model in which two CD molecules bind to each molecule of the bioactive compound:

$$Bioactive\ compound + CD \rightleftharpoons Bioactive\ compound - CD \quad (4)$$

$$Bioactive\ compound + 2CD \rightleftharpoons CD - Bioactive\ compound - CD \quad (5)$$

Considering both models, the encapsulation or formation constant (K_F) is calculated using the following expression:

$$K_F = \frac{[Inclusion\ complex]}{[Bioactive\ compound] \cdot [CD]^x} \quad (6)$$

where [*Inclusion complex*], [*Bioactive compound*], and [*CD*] are the concentrations at equilibrium of the inclusion complex, ligand, and CD, respectively, and *x* is the stoichiometric coefficient (*x* = 1 for the 1:1 model ~*vs*~ *x* = 2 for the 1:2 model).

The encapsulation constant is a parameter of special interest for characterising the interaction between CDs and ligands. The higher its value, the greater the interaction between molecules, and therefore, the more stable the inclusion complex. This allows screening of CDs for the same bioactive compound.

Experimentally, the encapsulation constant was obtained with relative fluorescence measurements at increasing CD concentrations using the following equation:

$$\frac{1}{F - F_0} = \frac{1}{(F_\infty - F_0) \cdot K_F \cdot [CD]^x} + \frac{1}{F_\infty - F_0} \quad (7)$$

where F_0 is the basal fluorescence intensity of the bioactive compound in the absence of CDs, F_∞ is the fluorescence intensity when all molecules of the bioactive compound are encapsulated in CDs, *F* is the observed fluorescence intensity at each CD

concentration, K_F is the encapsulation constant, [CD] is the CD concentration, and x is the stoichiometric coefficient.

The linear representation of this expression for both models enables determining the stoichiometry of the encapsulation process and calculating the encapsulation constant by means of the slope and the intercept.

By performing the same procedure at different temperatures, the thermodynamic parameters (enthalpy, entropy, and Gibbs free energy) of the most stable inclusion complexes were determined with the following expressions:

$$ln\, K_F = \frac{-\Delta H°}{R \cdot T} + \frac{\Delta S°}{R} \quad (8)$$

$$\Delta G° = \Delta H° - T \cdot \Delta S° \quad (9)$$

where T is the temperature, R is the gas constant, $\Delta H°$ is the enthalpy, $\Delta S°$ is the entropy, and $\Delta G°$ is the Gibbs free energy.

7.1.3. Competitive model for two binding sites in the guest molecule

To determine the encapsulation constants of the inclusion complexes formed between different CDs and neochlorogenic or chlorogenic acids (caffeoylquinic acids, CQA), a new competitive model with two possible binding sites in the guest molecule was designed. One site is in the caffeic acid moiety of the molecule, and the other is in the D-(-)-quinic acid moiety. As a result, there are two encapsulation constants for each complexed region, K_{F1} and K_{F2}. This methodology was based on that described by (Álvarez-Parrilla et al., 2010) for chlorogenic acid and by (Matencio et al., 2018) for ellagic acid.

Considering this, two possible chemical equilibria are considered depending on the ligand region to which the CD binds:

$$(CD - CQA) \overset{K_{F1}}{\leftrightarrows} CQA + CD \overset{K_{F2}}{\rightleftharpoons} (CQA - CD) \quad (10)$$

where (*CD-CQA*) is the inclusion complex formed in the caffeic acid moiety and (*CQA-CD*) is the inclusion complex formed in the D-(-)-quinic acid moiety. The encapsulation constants of these complexes would be determined with the expression:

$$K_{F1} = \frac{[CD - CQA]}{[CQA] \cdot [CD]} \qquad K_{F2} = \frac{[CQA - CD]}{[CQA] \cdot [CD]} \quad (11)$$

where [*CQA*], [*CD*], [*CD-CQA*], and [*CQA-CD*] are the equilibrium concentrations of caffeoylquinic acid, CD, inclusion complex in the caffeic acid moiety, and inclusion complex in the D-(-)-quinic acid moiety, respectively.

Finally, the model used to analyse the interaction with CD was:

$$(F - F_0) = \frac{F_0 + (F_1 - F_0) \cdot K_{F1} \cdot [CD]}{1 + (K_{F2} + K_{F1}) \cdot [CD]} \quad (12)$$

where F is the experimentally observed fluorescence intensity, F_0 is the basal fluorescence intensity in the absence of CDs, F_1 is the fluorescence intensity of the fully complexed fluorophore, K_{F1} and K_{F2} are the encapsulation constants for complexes formed by the caffeic acid and D-(-)-quinic acid moieties, respectively, and [*CD*] is the CD concentration. Fluorescence in the absence of CD was normalized to 1 in the spectrofluorometer.

Sample preparation and measurement were carried out in the same way as described above for the Benesi-Hildebrand method, except that only pH 3, pH 5, and pH 9 buffers were used, with the latter prepared with 0.1 M tris-HCl, and measurements were only recorded at 25°C.

Equation 12 was solved in SigmaPlot (version 10.0.0.54) by inputting the normalized fluorescence values obtained for each CD concentration, including the

normalized basal fluorescence value when the CD concentration is zero. Iterations were set to 10000000, size to 100, and tolerance to 0.00001.

The identification of the encapsulation constants obtained for each region of the CQAs (K_{F1} and K_{F2}) was determined from the assumption that the molecular moiety with the lowest score in molecular docking should also have higher encapsulation constants, as both results are related to greater stability of the inclusion complexes.

7.1.4. Mohseni-Hurtubise method

The Mohseni-Hurtubise method (Mohseni and Hurtubise, 1990) characterise inclusion complexes by chromatographic techniques. Analogous to the Benesi-Hildebrand method, the ligand concentration is fixed, and variations in retention time are analysed by increasing the CD concentration. In this case, the CD concentration is regulated through the mobile phase. In this doctoral thesis, this method has been used to characterise inclusion complexes formed with hydrophobic derivatives of stilbenes. Unlike the previously described methods, this method allows the analysis of various isomers within the same sample.

The samples used were dissolved in methanol, water, and tetrahydrofuran (57:10:33 (v/v)) and injected into an Agilent 1100 series HPLC system (CA, USA) in reverse phase, equipped with a Kromasil C18 column of 5 µm (150 × 4.6 mm) (Análisis Vínicos, Tomelloso, Spain) using a flow rate of 1 mL/min of methanol and water (85:15 (v/v)) with concentrations of 0 to 50 mM of HP-β-CD at 25°C. Detection was at 310 nm in an Agilent 1200 series UV-Vis diode array module (CA, USA). Samples intercalated with methanol were injected following the same method in long sequences. Unlike the Benesi-Hildebrand method, this method yields apparent encapsulation constants ($K_{F\,ap}$)

because interactions of the CD with the methanol in the mobile phase result in the active CD concentration being lower than the theoretical one (Matsui and Mochida, 1979).

The Mohseni-Hurtubise method also proposes two possible mathematical models depending on the stoichiometry of the complexes. A 1:1 model in which a single CD molecule binds to each molecule of the bioactive compound, and a 1:2 model in which two CD molecules bind to each molecule of the bioactive compound:

$$Bioactive\ compound + CD \quad \rightleftharpoons \quad Bioactive\ compound - CD \qquad (13)$$

$$Bioactive\ compound + 2CD \quad \rightleftharpoons \quad CD - Bioactive\ compound - CD \qquad (14)$$

Considering both models, the apparent encapsulation constant can be determined from the capacity factor with the following equation:

$$\frac{1}{k} = \frac{1}{k_0} + \frac{K_{F\,ap}}{k_0} \cdot [CD]^x \qquad (15)$$

where k is the solute capacity factor, k_0 is the solute capacity factor without CD, $K_{F\,ap}$ is the apparent encapsulation constant, $[CD]$ is the CD concentration in the mobile phase, and x is the stoichiometric coefficient ($x = 1$ for the 1:1 model ~*vs*~ $x = 2$ for the 1:2 model).

The capacity factor was calculated from the following expression:

$$k = \frac{t_R - t_0}{t_0} \qquad (16)$$

where k is the capacity factor, t_R is the solute retention time, and t_0 is the void time of the column.

The linear representation of this expression for both models enables the determination of the stoichiometry of the encapsulation process and calculating the apparent encapsulation constant by means of the slope and the intercept. The higher the

value of the apparent encapsulation constant, the greater the interaction between the molecules, and therefore, the more stable the inclusion complex.

In this model, it is assumed that any interaction of the inclusion complexes with the stationary phase is insignificant.

7.2. Molecular encapsulation in HBCD-Pol

In addition to CDs, hyper-branched CD-based polymers (HBCD-Pol) have been used, formed by the crosslinking of pyromellitic dianhydride (PMDA) (Monfared et al., 2022). This crosslinking was carried out with anhydrous DMSO and triethylamine in glass scintillation vials, adding β-CD until complete dissolution. Then, the required amount of PMDA was added to obtain a CD and PMDA ratio of 1:12, and leave it react for 24 hours at room temperature. The resulting product was precipitated by adding ethyl acetate in excess. Subsequently, it was filtered with more ethyl acetate to remove impurities and dried. Then, it was dissolved in deionised water, lyophilized, and subjected to a Soxhlet extraction with acetone for 24 hours to completely remove residues and unreacted reagents. The total removal of residual DMSO was verified by elemental analysis. The resulting white powder was dried, ground with a mortar, and stored in darkness. The synthesis of these HBCD-Pol was carried out by the Materiali Polimerici research group at the Università di Torino (Turin, Italy).

8. Synthesis and purification of hydrophobic stilbene derivatives

8.1. Chemical synthesis

Hydrophobic stilbene derivatives were synthesised chemically via Steglich esterification in anhydrous chloroform and DMF (94:6 (v/v)) with molecular sieve. In a

three-neck flask equipped with a condenser, stilbenes (4.4 mM), fatty acids (4.4 mM), DCC (4.4 mM), and DMAP (44 µM) were added. The stilbenes used were resveratrol, oxyresveratrol, piceatannol, and pterostilbene, while the fatty acids were stearic acid (C18:0), oleic acid (C18:1), and palmitic acid (C16:0). The reaction was stirred gently at 25 °C in an inert atmosphere for 24 hours (Figure 11).

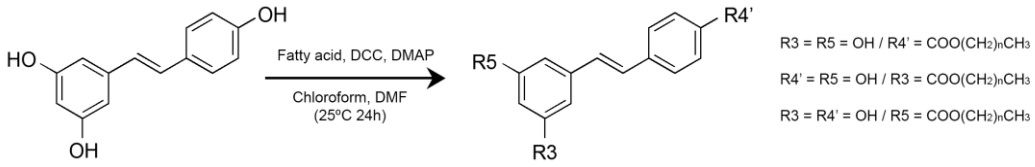

Figure 11. Basic scheme of chemical esterification of resveratrol with saturated fatty acids

The formation of products was monitored by thin-layer chromatography (TLC) on silica plates using chloroform and methanol (9:1 (v/v)) as the mobile phase and revealing with UV light lamp, and by direct injection LC-MS after dilution on an Agilent HPLC 1200 series equipped with a time-of-flight (TOF) 6220 detector (acquisition range 100-1100) in negative mode, using a mobile phase of 0.6 mL/min of methanol and water (60:40 (v/v)) with 20 mM ammonium acetate at 25 °C. EICs were obtained for the target *m/z*. The reaction yield was obtained by calibration with the initial concentration of natural stilbenes (resveratrol, oxyresveratrol, piceatannol, or pterostilbene). The reactions were stored at -20 °C in darkness. During their use, care was taken to protect them from direct exposure to light sources.

8.2. Enzymatic synthesis

The enzymatic synthesis of resveratrol stearate was carried out using the enzyme Novozym 435 (immobilized lipase from *Candida antarctica*), based on the method described by Nicolosi *et al.* (2002) for resveratrol acetate synthesis, with slight modifications (Nicolosi et al., 2002). Reactions conducted in a vial or flask with 2 – 10

mL of *tert*-amyl alcohol and molecular sieve, 0.1 g of resveratrol, 0.268 – 1.34 g of vinyl stearate, and 0.1 g of Novozym 435 were added and incubated in an inert atmosphere at 40 °C and 400 rpm for 90 hours (Figure 12). The enzyme was recovered by filtration, washed, and dried.

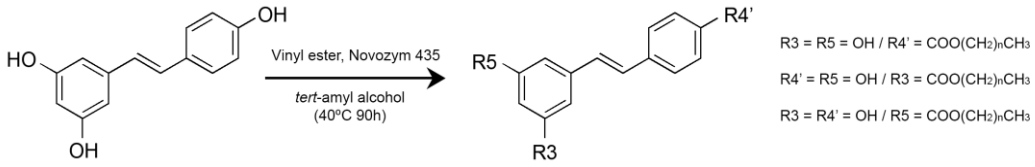

Figure 12. Basic scheme of enzymatic esterification of resveratrol with saturated fatty acids

The formation of products was monitored by thin-layer chromatography on silica plates using chloroform and methanol (9:1 (v/v)) as the mobile phase and revealing with UV light lamp, and by direct injection LC-MS after dilution on an Agilent HPLC 1200 series equipped with a TOF 6220 detector (acquisition range 100-1100) in negative mode, using a mobile phase of 0.6 mL/min of methanol and water (60:40 (v/v)) with 20 mM ammonium acetate at 25°C. EICs were obtained for the target *m/z*. The reaction yield was obtained by calibration with the initial concentration of resveratrol.

8.3. Purification by column chromatography and TLC

Purification was carried out by silica gel column chromatography using chloroform and methanol (9:1 (v/v)) as the mobile phase. Product elution was monitored by thin-layer chromatography on silica plates using chloroform and methanol (9:1 (v/v)) as the mobile phase and revealing with UV light lamp. Fractions containing the pure product were mixed and concentrated using a Heidolph VV2001 rotary evaporator (Heidolph Instruments GmbH & Co. KG, Schwabach, Germany) and Eppendorf Concentrator 5301 vacuum microtube concentrator (Eppendorf, Hamburg, Germany), avoiding exceeding 25 °C temperature in the sample.

Since fatty acids do not contain fluorophore groups that enable them to be detected under UV light, and do not ionise well, preventing their accurate quantification by LC-MS, their absence in the pure samples was confirmed with a colorimetric kit for quantification of free fatty acids at 570 nm (Sigma Aldrich, no. MAK044).

After purification, samples were stored in darkness at -20 °C in powder form or dissolved in organic solvent for further use. Care was always taken to protect them from direct exposure to light during their use.

8.4. Purification by preparative HPLC-DAD

Preparative HPLC purification was performed on a Shimadzu LC-20AP preparative HPLC system in reverse phase, equipped with a DAD SPD-M40 detector, FRC-10A fraction collector (Shimadzu, Kyoto, Japan), and Kinetex C18 column of 5 μm (250 × 21.2 mm) (Phenomenex, Torrance, CA, USA). Injected samples were previously concentrated and eluted on Solid Purple C18 500 mg 3 mL columns (Análisis Vínicos, Tomelloso, Spain) with water and methanol, retaining fractions with the desired isomers. A flow rate of 25 mL/min at 25 °C was set with the following aqueous acetonitrile gradient (v/v): 40 % from 0 to 2.5 min, 99 % from 5 to 20 min, and 40 % from 20.01 min. Detection and fraction collection were at 310 nm, setting the most suitable parameters for peak width, slope and level for each sample to collect the pure fractions.

9. Pancreatic lipase activity assays

The enzyme pancreatic lipase is a key enzyme in the digestion of lipids at the intestinal level, catalysing the hydrolysis of the ester bond of triacylglycerides to release monoacylglycerides and free fatty acids. In this doctoral thesis, porcine pancreatic lipase was used, which shares 86% homology with human pancreatic lipase (Narita et al., 2012).

9.1. Determination of the hydrolysis degree

Different reactions with pancreatic lipase enzyme were conducted to determine the degree of hydrolysis. The substrate concentration (stilbene derivatives) was fixed at 100 µM and the enzyme concentration at 0.05 mg/mL, using 0.1 M sodium phosphate buffer pH 7 as the reaction medium (Narita et al., 2012). Samples were incubated at 37°C with agitation at 850 rpm in a Thermomixer Comfort (Eppendorf AG, Hamburg, Germany), and the reaction was stopped with ice. Aliquots were collected at time 0 and every 0.5 hours up to 2 hours, to be injected into a Shimadzu LC2010C HT HPLC system (Shimadzu, Kyoto, Japan) in reverse phase, with UV-Vis detector set at 310 nm, equipped with a Kromasil C18 column of 5 µm (150 × 4.6 mm) (Análisis Vínicos, Tomelloso, Spain) and a flow rate of 1 mL/min at 25°C. For samples containing resveratrol, oxyresveratrol, and piceatannol derivatives, a gradient of aqueous methanol (v/v) was used: 30 % from 0 to 5 min, 40 % from 8 to 9.5 min, 50 % at 12 min, 99 % from 12.5 to 25 min, and 30 % from 25.01 to 30 min. For pterostilbene derivatives, due to their higher hydrophobicity, an isocratic method of 20 minutes with 99 % methanol (v/v) was used. Samples were injected intercalated with 50% (v/v) methanol following the same method in long sequences. Results were expressed as remaining percentage of stilbene using calibration curves for each stilbene derivative.

9.2. Pancreatic lipase enzymatic inhibition assays

Inhibition assays were performed with resveratrol stearate as substrate and chlorogenic and neochlorogenic acids as inhibitors (Narita et al., 2012). Reactions were analysed by two different techniques: fluorescence spectroscopy and chromatography.

9.2.1. Spectrofluorometric enzymatic inhibition assays

Different reactions were prepared with 20 μM resveratrol stearate and 0.05 mg/mL pancreatic lipase, in the presence and absence of 10, 20, and 50 μM chlorogenic or neochlorogenic acid, using 0.1 M sodium phosphate buffer pH 7 as the reaction medium. Samples were incubated at 37 °C with agitation at 850 rpm in a Thermomixer Comfort (Eppendorf AG, Hamburg, Germany), and the reaction was stopped with ice. Aliquots were collected at time 0 and every 10 minutes up to 80 minutes, to be analysed in a Shimadzu RF-6000 spectrofluorometer (Shimadzu, Kyoto, Japan) with thermostatically controlled cells, fixing the excitation and emission bandwidth at 3 and 5 nm, respectively. The emission spectrum of samples was recorded between 330 and 500 nm with the excitation wavelength fixed at 300 nm. Results were expressed as percentage of substrate remaining from the relative fluorescence intensity at the λ_{em} previously established.

9.2.2. Chromatographic enzymatic inhibition assays

Different reactions were prepared with 100 μM resveratrol stearate and 0.05 mg/mL pancreatic lipase, in the presence and absence of 100 and 150 μM chlorogenic or neochlorogenic acid, using 0.1 M sodium phosphate buffer pH 7 as the reaction medium. Samples were incubated at 37°C in the autosampler tray of an Agilent 1100 series HPLC system (CA, USA) in reverse phase, equipped with a Kromasil C18 column of 5 μm (150 × 4.6 mm) (Análisis Vínicos, Tomelloso, Spain). Aliquots were injected every 0.5 hour up to 2 hours with a flow rate of 1 mL/min at 25 °C and an isocratic method of methanol and water (97:3 (v/v)). Detection was set at 310 nm in an Agilent 1200 series UV-Vis diode array module (CA, USA). Samples were injected intercalated with 50% (v/v) methanol following the same method in long sequences. Results were expressed as remaining percentage of stilbene using calibration curves.

9.3. Pancreatic lipase activity assays in the presence of CDs

Following the previous methodology, different reactions were prepared with 100 μM resveratrol stearate and 0.05 mg/mL pancreatic lipase, in the presence and absence of various concentrations of HP-β-CD (0.1; 0.3; 0.5; and 1 mM), using 0.1 M sodium phosphate buffer pH 7 as the reaction medium. Samples were incubated at 37 °C in the autosample tray of an Agilent 1100 series HPLC system (CA, USA) in reverse phase, equipped with a Kromasil C18 column of 5 μm (150 × 4.6 mm) (Análisis Vínicos, Tomelloso, Spain). Aliquots were injected every 0.5 hour up to 2 hours with a flow rate of 1 mL/min at 25 °C and an isocratic method of methanol and water (97:3 (v/v)). Detection was set at 310 nm in an Agilent 1200 series UV-Vis diode array module (CA, USA). Samples were injected intercalated with 50% (v/v) methanol following the same method in long sequences. Results were expressed as remaining percentage of stilbene using calibration lines.

10. Determination of antioxidant activity

Since there is no standardised method for measuring antioxidant activity and different oxidation conditions can lead to different results, it is recommended that the evaluation of antioxidant activity be carried out using several techniques. For this reason, in this doctoral thesis, the antioxidant activity of stilbenes was determined with up to four different methods of *in vitro* determination of antioxidant activity. One of them is based on the hydrogen atom transfer reaction (HAT), in which there is a competition between the antioxidant and a substrate for free radicals (ORAC method), and the other three are based on electron transfer (SET), monitored through the colour change that occurs when the oxidant is reduced (ABTS, DPPH, and FRAP methods) (Gulcin, 2020). Unless otherwise indicated, the concentrations of stilbenes and trolox used will refer to the initial

concentrations before adding the other reagents of the method. In general, the samples to be analysed for stilbenes and trolox were previously dissolved in methanol, also preparing controls with the same concentration of organic solvent to verify that it did not affect the method, except in the assays to evaluate the effect of CDs, where stilbenes and trolox were dissolved in water, and the CDs in 0.1 M sodium phosphate buffer at pH 7.

10.1. ORAC method

The ORAC method (Oxygen Radical Absorbance Capacity) consists of a competitive reaction between a fluorescent probe (*FH*) and the antioxidants (*AH*) present in the sample by neutralizing the generated free radicals ($R^{\bullet}$), according to the following expression:

$$\begin{matrix} FH \\ F^{\bullet} \end{matrix} \overset{R^{\bullet}}{\underset{RH}{\curvearrowleft\curvearrowright}} \begin{matrix} AH \\ A^{\bullet} \end{matrix} \qquad (17)$$

This method was carried out with fluorescein as the fluorescent probe and AAPH as the free radical generator. Unless otherwise indicated, the initial concentrations used of hydrophobic derivatives of stilbenes were between 25 and 500 µM, natural stilbenes between 0.3 and 3.125 µM, and trolox between 1 and 200 µM. Blanks with methanol and water instead of the samples were also prepared.

Compounds to be analysed (70 µL) were pre-incubated at 37 °C with 100 µL of fluorescein at 60 nM in 75 mM sodium phosphate buffer pH 7.4. The reactions were carried out in the inner wells of 96-well polystyrene plates with black edges and transparent bottom, keeping the outer wells with water. After 30 minutes, 30 µL of freshly prepared 0.2 M AAPH was quickly added, and the fluorescence of the wells was recorded every 1.14 minutes for 180 minutes on a Synergy HT plate reader (Biotek Instrument, Winooski) equipped with a thermostat at 37 °C, setting the excitation wavelength at

485/20 nm and emission at 528/20 nm (Rodríguez-Bonilla et al., 2017). The plate was gently shaken before each fluorescence reading.

The results were expressed as the net area under the curve (net AUC), using the following expression to calculate the area under the curve (AUC) in each well:

$$AUC = 1 + \sum_{i=1,14}^{i=180} \frac{f_i}{f_0} \tag{18}$$

where f_0 is the initial fluorescence at time 0 and f_i is the fluorescence measured at time i. The net AUC value was obtained by subtracting the AUC of the blank from each AUC value obtained.

The method was previously validated by checking the fluorescent signal of fluorescein in the absence of AAPH.

10.2. ABTS Method

The ABTS method is based on the reduction of the absorbance of the $ABTS^{\bullet+}$ radical cation upon interaction with the antioxidants in the sample. This decrease in absorbance is reflected by the loss of its characteristic green colour. The $ABTS^{\bullet+}$ radical cation has a broad absorption spectrum, with the maximum absorbance wavelengths at 414 nm and 734 nm being the most commonly used to determine antioxidant activity.

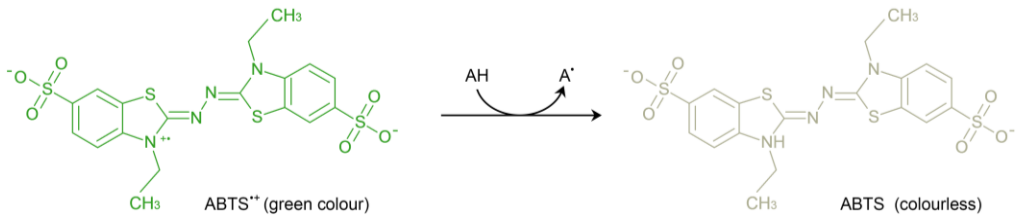

Figure 13. Scheme of $ABTS^{\bullet+}$ reaction in the presence of an antioxidant (AH)

There are two variants of the method depending on how the radical is generated: chemical or enzymatic. The chemical variant uses oxidizing agents to generate the radical,

while the enzymatic variant uses the enzyme peroxidase in the presence of hydrogen peroxide. In this thesis, the enzymatic variant was used to obtained the radical.

To generate the $ABTS^{\bullet+}$ radical enzymatically, 2 mM ABTS was reacted with 88 U/mL HRP type VI and 45 µM hydrogen peroxide in 0.2 M sodium acetate buffer pH 5. The resulting solution was incubated in darkness at room temperature for one hour, and then diluted with the same buffer to an absorbance of 0.3 mAU at 414 nm after dilution 1:10 (Rodríguez-Bonilla et al., 2017).

Samples of stilbenes and their derivatives were dissolved in methanol, and controls with the same concentration of this organic solvent were prepared. Unless otherwise indicated, the initial concentrations used of hydrophobic derivatives of stilbenes were between 12.5 and 500 µM, natural stilbenes between 12.5 and 200 µM, and trolox between 1 and 500 µM.

The compounds to be analysed were diluted with the solution containing the $ABTS^{\bullet+}$ radical and 0.2 M pH 7 sodium phosphate buffer in a 1:10:4 (v/v) ratio to a final volume of 300 µL. Inner wells of 96-well plates were used, leaving the outer wells filled with water. After 6 minutes and/or 24 hours of incubation at room temperature, the absorbance at 414 nm was read on a Synergy HT plate reader (Biotek Instrument, Winooski).

The results of the chemical and enzymatic ABTS method were expressed as trolox equivalents and as percentage inhibition of the free radical or remaining amount of free radical, according to the following equations:

$$Inhibition\ (\%) = \frac{Abs_{control} - Abs_{sample}}{Abs_{control}} \cdot 100 \quad (19)$$

$$Remaining\ (\%) = \frac{Abs_{sample}}{Abs_{control}} \cdot 100 \quad (20)$$

10.3. DPPH method

The principle of the DPPH method is similar to that of the ABTS method, as it is also based on the reduction of absorbance of a radical upon interaction with the antioxidants in the sample. However, the reaction occurs in an organic medium. The DPPH$^{\bullet}$ radical has a violet colour with a λ_{max} at 517 nm.

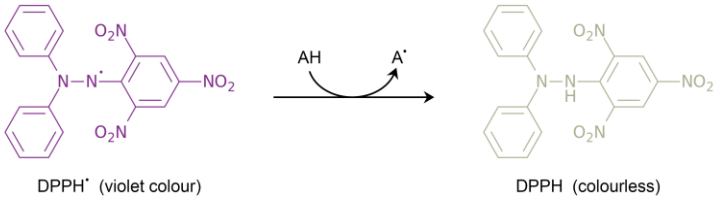

Figure 14. Scheme of DPPH$^{\bullet}$ reaction in the presence of an antioxidant (AH)

Unless otherwise indicated, the initial concentrations used of hydrophobic derivatives of stilbenes were between 25 and 500 µM, natural stilbenes between 25 and 200 µM, and trolox between 1 and 150 µM.

The DPPH$^{\bullet}$ radical was prepared at a concentration of 0.004 % (w/v) in methanol and mixed with the compounds to be analysed, also dissolved in methanol, in a 1:1 (v/v) ratio (Ebada et al., 2008). The reaction was incubated for 30 minutes or 24 hours in darkness at room temperature. Then, the absorbance at 517 nm was measured on a Synergy HT plate reader (Biotek Instrument, Winooski). The results were expressed as trolox equivalents and as percentage inhibition of the free radical or remaining amount of free radical according to Equations (19) and (20), respectively.

10.4. FRAP method

Unlike the methods previously described, the FRAP method is based on the reduction of iron present in the ferric tripyridyl triazine complex (Fe^{III}-TPTZ) from Fe^{III} to Fe^{II}, in the presence of the antioxidants of a sample at pH 3.6. While the initial complex

is colourless, the formation of the ferrous tripyridyl triazine complex (Fe^{II}-TPTZ) results in an intense blue colour with a maximum absorption wavelength at 593 nm (Figure 15).

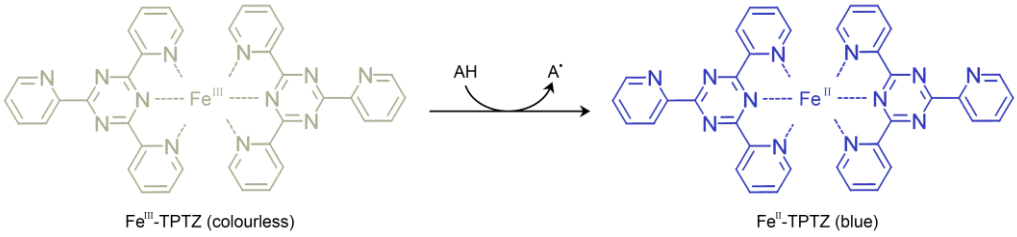

Figure 15. Scheme of Fe^{III}-TPTZ reaction in the presence of an antioxidant (AH)

Unless otherwise indicated, the initial concentrations used of hydrophobic derivatives of stilbenes were between 12.5 and 500 µM, natural stilbenes between 12.5 and 200 µM, ferrous sulphate between 1 and 500 µM, and trolox between 1 and 500 µM.

The preparation of the FRAP reagent was carried out with 10 mM TPTZ in 40 mM hydrochloric acid, 20 mM ferric chloride in water, and 0.3 M sodium acetate buffer at pH 3.6, mixed in a 1:1:10 (v/v) ratio (Rodríguez-Bonilla et al., 2017). In the inner wells of 96-well plates, 280 µL of the freshly prepared reagent was added with 30 µL of the compounds to be analysed, leaving the outer wells filled with water. After incubation for 2 hours or 24 hours, the absorbance at 593 nm was measured with a Synergy HT plate reader (Biotek Instrument, Winooski). The results were expressed as trolox equivalents and as Fe^{II} concentration using a calibration curve of ferrous sulphate.

10.5. Assessment of CDs interference in antioxidant methods

10.5.1. Assessment of CDs interference in the ORAC method

Solutions with concentrations between 0.5 and 9 mM of α-CD, γ-CD, HP-β-CD, and M-β-CD, and between 0.5 and 3 mM of β-CD, were prepared, both in the presence and absence of 2 µM oxyresveratrol in 0.1 M pH 7 sodium phosphate buffer. Solutions of

trolox between 1 and 20 μM were also prepared. Samples were processed and measured as described in Section 10.1.

Interference due to the glucidic nature was assessed by preparing glucose solutions at final concentrations between 1 and 50 mM, corresponding to equivalent concentrations of α-CD between 0.17 and 8.33 mM, β-CDs between 0.14 and 7.14 mM, and γ-CD between 0.13 and 6.25 mM. The samples were processed and measured as described in Section 10.1.

Interference due to the complexing capacity of the CDs on fluorescein was evaluated by preparing solutions with 30 nM fluorescein and concentrations between 0.5 and 9 mM of α-CD, γ-CD, HP-β-CD, and M-β-CD, and between 0.5 and 3 mM of β-CD, in the absence of the antioxidant and peroxyl radical generator. After two hours, fluorescence was measured on a Synergy HT plate reader (Biotek Instrument, Winooski) equipped with a thermostat at 37 °C, setting the excitation wavelength at 485/20 nm and emission at 528/20 nm.

Interference due to the complexing capacity of the CDs on AAPH was evaluated by preparing solutions with 30 mM AAPH and β-CD concentrations between 0.5 and 8 mM. After 30 minutes of incubation, absorbance was measured between 250 and 500 nm on a Jasco V-630 spectrophotometer (Madrid, Spain) with Thorlabs CV10Q1400 cuvettes.

10.5.2. Assessment of CDs interference in the ABTS method

Solutions with concentrations between 0.2 and 1.5 mM of α-CD, γ-CD, HP-β-CD, and M-β-CD, and between 0.05 and 0.5 mM of β-CD, were prepared, both in the presence and absence of 1 μM oxyresveratrol in 0.1 M pH 7 sodium phosphate buffer. Samples were processed and measured as described in Section 10.2.

Interference due to the glucidic nature was assessed by preparing glucose solutions at final concentrations between 0.2 and 12 mM, corresponding to equivalent concentrations of α-CD between 0.03 and 2 mM, β-CDs between 0.03 and 1.7 mM, and γ-CD between 0.03 and 1.5 mM. The samples were processed and measured as described in Section 10.2.

Interference due to the complexing capacity of the CDs on $ABTS^{\bullet+}$ was evaluated by preparing solutions with the $ABTS^{\bullet+}$ radical and β-CD concentrations between 0.05 and 0.5 mM, maintaining the same volume proportions used previously, and incubating for 24 hours in darkness at room temperature. Subsequently, absorbance was measured between 380 and 900 nm on a Jasco V-630 spectrophotometer (Madrid, Spain) with plastic cuvettes.

10.5.3. Assessment of CDs interference in the DPPH method

Solutions with concentrations between 0.5 and 10 mM of α-CD, γ-CD, HP-β-CD, and M-β-CD, and between 0.5 and 4.4 mM of β-CD, were prepared, both in the presence and absence of 1 μM oxyresveratrol in 0.1 M pH 7 sodium phosphate buffer. Samples were processed and measured as described in Section 10.3.

Interference due to the glucidic nature was assessed by preparing glucose solutions at final concentrations between 2 and 80 mM, corresponding to equivalent concentrations of α-CD between 0.33 and 13.33 mM, β-CDs between 0.29 and 11.43 mM, and γ-CD between 0.25 and 10 mM. The samples were processed and measured as described in Section 10.3.

Interference due to the complexing capacity of the CDs on $DPPH^{\bullet}$ was evaluated by preparing solutions with the $DPPH^{\bullet}$ radical and β-CD concentrations between 0.5 and 4.4 mM, maintaining the same volume proportions used previously, and incubating for

24 hours in darkness at room temperature. Subsequently, absorbance was measured between 400 and 650 nm on a Jasco V-630 spectrophotometer (Madrid, Spain) with plastic cuvettes.

10.5.4. Assessment of CDs interference in the FRAP method

Solutions with concentrations between 0.25 and 4 mM of α-CD, γ-CD, HP-β-CD, and M-β-CD, and between 0.25 and 2 mM of β-CD, were prepared, both in the presence and absence of 25 μM oxyresveratrol in 0.1 M pH 7 sodium phosphate buffer. Samples were processed and measured as described in Section 10.4.

Interference due to the glucidic nature was assessed by preparing glucose solutions at final concentrations between 1.5 and 30 mM, corresponding to equivalent concentrations of α-CD between 0.25 and 5 mM, β-CDs between 0.21 and 4.29 mM, and γ-CD between 0.19 and 3.75 mM. The samples were processed and measured as described in Section 10.4.

Interference due to the complexing capacity of the CDs on the iron tripyridyl triazine complex was evaluated by preparing solutions with the FRAP reagent and β-CD concentrations between 0.25 and 2 mM, maintaining the same volume proportions used previously, and incubating for 24 hours in darkness at room temperature. Subsequently, absorbance was measured between 450 and 700 nm on a Jasco V-630 spectrophotometer (Madrid, Spain) with plastic cuvettes.

11. Human and animal cell culture

11.1. Cell lines and culture conditions

In this doctoral thesis, two cell lines were used: Caco-2 (ATCC HTB-37), a human colorectal cancer cell line, and 3T3-L1 (ATCC CL-173), a mouse preadipocyte cell line.

Both cell lines were obtained from the ATCC (American Type Culture Collection) (ATCC, Rockville, USA), and the supplier's recommendations for use were followed.

The cell lines were maintained in an incubator at 37 °C with 5 % carbon dioxide and 85% relative humidity. They were cultured in ventilated adherent culture flasks of 25 or 75 cm^2. The culture medium was changed every 2 or 3 days, and cells were subcultured when they reached 80 % confluence.

All procedures were carried out under sterile conditions using type II biological safety cabinets, sterile material, and continuous disinfection with 70 % (v/v) ethanol. The assays with Caco-2 cell line were performed at the Servicio de Cultivo de Tejidos – ACTI (Universidad de Murcia, Murcia, Spain), while the assays with 3T3-L1 cell line were carried out at the Centre for Cardiovascular Science – The Queen's Medical Research Institute (The University of Edinburgh, Edinburgh, United Kingdom).

During subculture, the cells were washed with PBS and trypsinised at 37 °C with 2 mL of a solution containing 0.25 % (w/v) Trypsin and 0.53 mM EDTA. Once detached from the flask, the triple volume of culture medium was added to stop trypsinization, thanks to the α1-antitrypsin content of fetal bovine serum (FBS). Subsequently, they were centrifuged at 125 xg for 5 minutes to discard the trypsin-containing medium. Then, they were resuspended in culture medium, and the percentage of viability and the number of total and viable cells were analysed after a 1:1 dilution with trypan blue, an exclusion dye capable of staining dead cells but not viable cells. This count was performed using a TC10™ automated cell counter (BioRad, Madrid, Spain), which also allows visualization of cell images and the count histogram. Finally, the cells were transferred to a new culture flask or culture plates at the density recommended by the ATCC for each cell line.

11.1.1. Caco-2 cell line

The human colorectal cancer cell line Caco-2 originates from a colorectal adenocarcinoma in a 72-year-old man. They are adherent cells that grow in culture with epithelial morphology, forming a monolayer (Figure 16). They are commonly used for cytotoxicity assays and to predict the intestinal absorption of drugs.

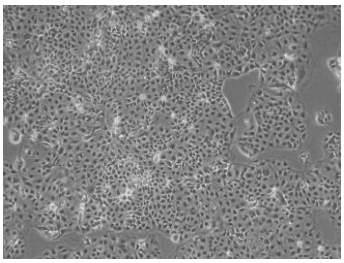

Figure 16. Caco-2 cell morphology at high density. Magnification 5x

These cells were cultured in complete EMEM medium without phenol red, with 10 % (v/v) FBS, 2 mM L-glutamine, and 1 % (v/v) penicillin/streptomycin. Subcultures were performed by seeding 10000 viable cells/cm^2. Unless otherwise stated, experiments were performed with passages 25 – 40, using the later passages for cell permeability assays. Cell freezing was performed by adding 5 % (v/v) DMSO to their usual medium and storing the vials in liquid nitrogen with controlled temperature reduction.

11.1.2. 3T3-L1 cell line

The 3T3-L1 preadipocyte cell line originates from mouse embryonic tissue. They are adherent cells that, when undifferentiated, grow with fibroblast morphology. Differentiation of these cells causes them to begin accumulating lipids, appearing larger and rounder (Figure 17). They are commonly used to study mechanisms associated with metabolic diseases such as obesity.

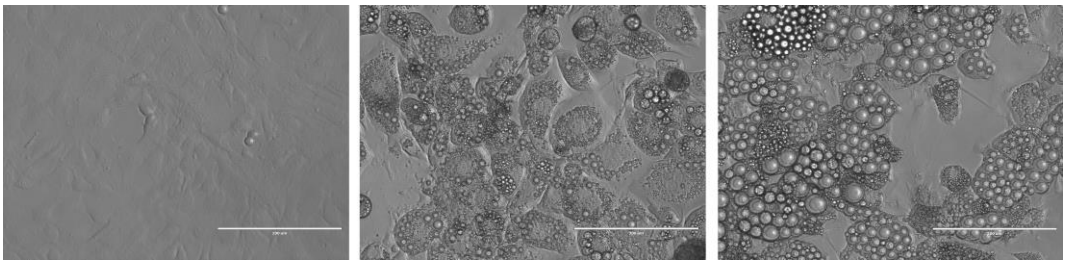

Figure 17. 3T3-L1 cell morphology during differentiation. From left to right, images at day 0, 7 and 14 after the start of cell differentiation. Magnification 20x

Cells were cultured in growth medium, differentiation medium, or post-differentiation medium as appropriate. The growth medium was prepared with complete DMEM medium with high glucose and L-glutamine, supplemented with 10 % (v/v) FBS, 1 % (v/v) penicillin/streptomycin, and 33 µM biotin. Unless otherwise stated, this medium contained phenol red. The differentiation medium was prepared with growth medium adding 0.5 mM IBMX, 1 µM dexamethasone, and 10 µg/mL insulin. Finally, the post-differentiation medium was prepared with growth medium adding 10 µg/mL insulin. Subcultures were performed by seeding 2000 – 3000 viable cells/cm^2. Unless otherwise stated, experiments were performed with passages 4 – 10. Cell freezing was performed by adding 5 % (v/v) DMSO to their usual medium and storing the vials in liquid nitrogen with controlled temperature reduction.

11.2. Determination of cell viability and proliferation

11.2.1. MTT assay

The MTT assay is a colorimetric method to measure the metabolic activity of cells in an active proliferation phase. It is one of the most widely used methods for measuring cell cytotoxicity and is based on the ability of mitochondrial dehydrogenases, specifically succinate dehydrogenase in metabolically active cells, to reduce in the presence of NADH, the tetrazolium salt MTT, a yellow, water-soluble substrate, into formazan

crystals, a purplish-coloured, water-insoluble product that is retained inside the cells (Figure 18). These crystals can be solubilised with organic solvent, allowing their quantification by spectrophotometry. The amount of MTT formazan produced is directly proportional to the number of metabolically active cells (González-Sarrías et al., 2015; Hansen and Bross, 2010).

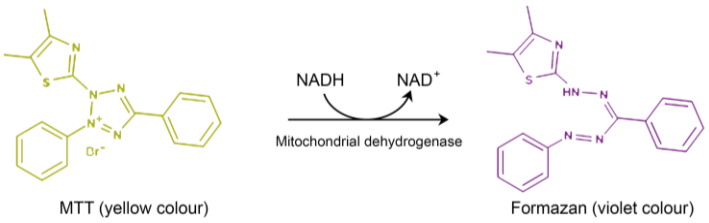

Figure 18. Scheme of MTT reaction catalysed by mitochondrial dehydrogenase in the presence of NADH

To perform this assay, cells were seeded at a density of 10 000 viable cells/cm^2 in the inner wells of 96-well plates, with outer wells filled with sterile water. After 48 hours of incubation, the culture medium was renewed by adding the compounds to be analysed at concentrations between 0 and 300 µM in 200 µL. Controls with water, DMSO (≤ 1% (v/v)), and sucrose (≤300 µM) instead of the compounds, as well as blanks without cells, were also prepared. All treatments and additional controls were previously sterilised with 0.2 µm sterile filters.

After 48 hours of incubation with the compounds, the medium was removed from the cells and replaced with fresh medium containing MTT at a final concentration of 1 mg/mL from a filtered stock solution at 5 mg/mL. The cells were then incubated in darkness for 4 hours under controlled temperature, gas, and humidity conditions. After this time, the medium was removed, and 100 µL of DMSO was added to solubilise the formazan crystals formed. The plates were gently shaken for 5 minutes on an orbital shaker before measuring the absorbance at 560 nm (MTT formazan) and 690 nm (background signal) using a FLUOstar Omega plate reader (BMG Labtech, Ortenberg,

Germany). The final results were expressed as a percentage of cell viability calculated by subtracting the absorbance of the blank and applying the following equation:

$$Cell\ viability\ (\%) = \frac{Abs_{560-690}\ (treated\ cells)}{Abs_{560-690}(control\ cells)} \cdot 100 \qquad (21)$$

11.2.2. Neutral Red assay

The neutral red assay is a colorimetric method based on the ability of viable cells to incorporate the vital dye neutral red into their lysosomes. This weakly cationic dye penetrates cell membranes by passive diffusion and binds to anionic groups and/or phosphates in the lysosomal matrix through electrostatic hydrophobic bonds. It can then be extracted using an acidified ethanol solution, allowing quantification by spectrophotometry. The uptake of neutral red by cells depends on their ability to maintain pH gradients through ATP production. The amount of neutral red retained by cells is directly proportional to the number of viable cells (Repetto et al., 2008). It is an inexpensive and sensitive method that also avoids the interference that compounds with antioxidant activity can cause in the MTT reaction (Chiba et al., 1998).

To perform this assay, cells were seeded at a density of 10000 viable cells/cm^2 in the inner wells of 96-well plates, with outer wells filled with sterile water. After 48 hours of incubation, the culture medium was renewed by adding the compounds to be analysed at concentrations between 0 and 300 µM in 200 µL. Controls with water, DMSO (≤ 1% (v/v)), and sucrose (≤300 µM) instead of the compounds, as well as blanks without cells, were also prepared. All treatments and additional controls were previously sterilised with 0.2 µm sterile filters.

The neutral red solution to be used was prepared by a 1:100 dilution in culture medium of another concentrated solution of neutral red at 4 mg/mL in PBS. After 48 hours

of incubation with the compounds, the cells were washed with PBS, and the neutral red solution was added at 40 µg/mL. The cells were then incubated in darkness for 2 hours under controlled temperature, gas, and humidity conditions. After this time, they were washed again with PBS, dried, and 150 µL of a solution of ethanol, water, and acetic acid in a 1:1:0.02 (v/v) ratio was added. The plates were gently shaken for 10 minutes on an orbital shaker before measuring the absorbance at 540 nm (neutral red) and 690 nm (background signal) using a FLUOstar Omega plate reader (BMG Labtech, Ortenberg, Germany). The final results were expressed as a percentage of cell viability calculated by subtracting the absorbance of the blank and applying the following equation:

$$Cell\ viability\ (\%) = \frac{Abs_{540-690}\ (treated\ cells)}{Abs_{540-690}(control\ cells)} \cdot 100 \qquad (22)$$

11.3. Cell permeability and metabolism

The ability of the Caco-2 intestinal cell line to grow as a monolayer allows for assays that predict *in vitro* the absorption of orally administered bioactive compounds. The Caco-2 cell monolayer has a differentiated phenotype that shares many functions of the epithelium of the small intestine villi (Hubatsch et al., 2007). Additionally, these cells express several functional enzymes related to phase II metabolism such as glucuronosyltransferases, glutathione-S-transferases, and sulfotransferases (Li et al., 2003), enabling *in vitro* studies of bioavailability and metabolism of bioactive compounds.

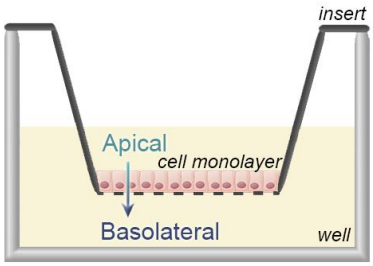

Figure 19. Schematic representation of the permeability assay with Caco-2 cells in transwell plates

The Caco-2 cell monolayer was formed by seeding 260000 viable cells/cm^2 onto 3 µm polycarbonate inserts incorporated into 24-well Costar Transwell plates from Corning (Corning, NY, USA). The apical chamber (insert) was filled with medium up to 140 µL, and the basolateral chamber (well) up to 860 µL. Cells were grown under usual culture conditions, with the integrity of the monolayer checked periodically by measuring its transepithelial electrical resistance (TEER) using a Millicell®ERS-2 voltmeter (Srinivasan et al., 2015). Once reaching a value equal to or greater than 300 Ω·cm^2 considering the inherent resistance of the insert membrane, the cell permeability assay was initiated. Experiments were conducted with an apical → basolateral flow, so treatments were added to the insert chamber, and aliquots were collected from the well chamber. Sink conditions were maintained, meaning that the concentration in the basolateral chamber did not exceed 10 % of the concentration in the apical chamber.

On the day of the assay, the medium was removed from the cells, and they were pre-incubated under usual culture conditions with complete HBSS (with 25 mM HEPES) for 15 minutes with gentle orbital agitation. After this time, the medium was removed, and 600 µL of complete HBSS was added to the basolateral chamber, and 100 µL of complete HBSS supplemented with the compounds of interest was added to the apical chamber. The concentration of stilbenes was 300 µM, and HBCD-Pol were at 100 ppm. The concentration of DMSO applied with the treatments did not exceed 1.3 % (v/v) of

the final volume. All treatments were previously sterilised using 0.2 µm sterile filters or UV light (for HBCD-Pol). Cell-free blanks were used to confirmed that the compounds passed through the insert filter.

Aliquots of 300 µL were collected from the basolateral chamber at 0, 0.5, 1, 1.5, 2, 4, 6, and/or 24 hours, with this volume replaced with the medium used during the experiment. Additionally, aliquots were collected from the apical chamber at the beginning and end of the experiment. Monolayer integrity was verified at the end of the assay by measuring TEER using a Millicell®ERS-2 voltmeter. All collected samples were stored at -20 °C and processed as soon as possible. For cellular metabolism studies, the total content of sulphate and glucuronide metabolites in the apical and basolateral regions was analysed after 24 hours.

11.4. Extraction of cellular media and HPLC-DAD/ESI(-) analysis

The extraction of the compounds of interest from cellular media was carried out by mixing with acetonitrile in a 1:1 (v/v) ratio. This mixture was then vortexed and centrifuged at 13000 rpm for 10 minutes. The supernatants containing the compounds of interest were recovered and evaporated using an Eppendorf Concentrator 5301 vacuum microtube concentrator (Eppendorf, Hamburg, Germany), ensuring that the sample temperature did not exceed 25 °C. Finally, the evaporated samples were resuspended in methanol and injected into an HPLC system, along with the corresponding calibration curve for each compound to be analysed, except for sulphate and glucuronide metabolites, which were identified by their *m*/*z* ratio as no standard was available.

An Agilent HPLC series 1200 equipped with a TOF 6220 detector (acquisition range 100-1100) in negative mode was used, with a Kromasil C18 column of 5 µm (150 × 4.6 mm) (Phenomenex, Torrance, CA, USA) and a flow rate of 0.8 mL/min at 25°C.

The method used was an aqueous gradient of methanol (with 20 mM ammonium acetate) (v/v): 30 % from 0 to 5 min, 40 % from 8 to 9.5 min, 50 % at 12 min, 99 % from 12.5 to 25 min, and 30 % from 25.01 to 30 min. EICs were obtained for the target *m/z*.

The apparent permeability coefficient (P_{ap}) was determined from the concentration *versus* time data using the following equation:

$$P_{ap}(^{cm}/_{s}) = \frac{dc}{dt} \cdot \frac{V}{A \cdot c_0} \quad (23)$$

where (dc/dt) is the steady-state flux (μM/s), V is the volume in the basolateral chamber (mL), A is the area of the insert membrane (cm^2), and c_0 is the initial concentration in the apical chamber (μM).

11.5. Cell differentiation

3T3-L1 preadipocytes were induced to initiate the adipogenesis process by differentiating into mature adipocytes capable of lipid accumulation. Unless otherwise stated, cells were seeded at 2700 viable cells/cm^2 in 6-well culture plates previously coated with 5 μg/cm^2 of collagen. Cells were incubated under standard culture conditions until reaching confluence (approximately 10 days). At that point, the medium was changed to differentiation medium (day 0) and maintained for an additional 48 hours. After this period, cells were changed to post-differentiation medium and kept in this medium until the end of the assay. Stilbenes were added to the differentiation medium at final concentrations of 50, 100, and 150 μM. Controls with water and DMSO (0.5% (v/v)) instead of the compounds were also prepared. All treatments and controls were previously sterilised using 0.2 μm sterile filters.

11.6. ORO lipid staining in cell cultures

On day 10 after cellular differentiation, staining of accumulated lipids by cells was performed using Oil Red O (ORO) dye. This dye is a lysochrome capable of staining the most hydrophobic and neutral lipids (such as triacylglycerides, diacylglycerides, and cholesterol esters), but not polar lipids (such as phospholipids, sphingolipids, and ceramides) (Mehlem et al., 2013). Therefore, in mature adipocytes, the ORO dye binds to the lipids accumulated inside the cell, while the cell membranes are not stained. During application, a partially aqueous solution is used, so that the dye can be released from the solvent and associate with the lipids inside the cells.

For the assay, cells were washed with PBS and fixed for one hour with a 4 % (v/v) formaldehyde solution in PBS. Subsequently, cells were washed again with PBS and with a 60 % (v/v) aqueous solution of isopropanol, and allowed to air dry. They were then stained for one hour with a filtered solution of 0.3 % (w/v) ORO dye in 60 % (v/v) isopropanol. Finally, stained cells were washed with water and allowed to air dry.

Lipid quantification after staining was performed in two ways: 1) by processing images of the stained cells taken by microscopy, and 2) by elution and spectrophotometric determination of the ORO dye in the dried wells. Elution of the dye was carried out with isopropanol and the absorbance at 540 nm (ORO) was measured on an OPTImax plate reader (Molecular Devices, Sunnyvale, CA) using pre-shaken 96-well plates.

11.7. Microscopy in cell cultures

Twenty-five images from different fields within each well were collected using a Zeiss Axiovert 200 M inverted microscope (Carl Zeiss, Gottingen, Germany) equipped with an Axiocam 305 colour camera and Zen version 2.6 software (blue edition). Grayscale images were collected on days 0, 3, 7, and 10 of cellular differentiation using

a 20x objective and adjusting the exposure to 2.0 to visualize lipid accumulation evolution. On day 10 after cellular differentiation, colour images of cells stained with ORO were taken using a 5x objective with exposure adjusted to 0.5. Additionally, images of cell-free wells were taken under the same conditions for image processing.

11.8. Image analysis in cell cultures

Images collected by microscopy were processed using Fiji (ImageJ 1.53t version) (NIH, USA) (Schindelin et al., 2012). Firstly, the image scale was adjusted to the appropriate pixels/µm according to the objective used and the dimensions of the image exported from the microscope. Then, the images were processed differently depending on whether they were taken in grayscale or in colour.

For grayscale images of adipogenesis evolution, a uniform threshold was set to obtain lipid droplets in white and the rest of the image in black, and the mean was measured. This procedure was also performed in a cell-free well, with this mean subtracted from each of the means of the wells with cells.

For colour images obtained after ORO staining, an H AEC colour deconvolution was performed, and channel 2 (red) was processed. Using this image, a uniform threshold was set to obtain cells stained with ORO in black and the rest of the image in white, and the mean was measured. This procedure was also performed in a cell-free well, with this mean subtracted from each of the means of the wells with cells.

11.9. Gene expression determination

On days 0, 3, 7, and 10 after the cellular differentiation of 3T3-L1 preadipocytes into mature adipocytes, the expression analysis of certain genes related to obesity was performed by RNA extraction, cDNA synthesis, and Real-Time qPCR. Stilbenes were

added to the differentiation medium at a final concentration of 150 µM. Controls with DMSO (0.5% (v/v)) instead of the compounds were also prepared. All treatments and controls were previously sterilised using 0.2 µm sterile filters.

11.9.1. RNA extraction

RNA extraction and purification from cells were carried out on ice with QIAzol (Qiagen GmbH, Hilden, Germany), using the commercial kit Direct-zol RNA Miniprep (Zymo Research Corporation, no. R2072), following the manufacturer's instructions and treated with DNase I enzyme to eliminate possible genomic DNA contaminations. The quantity and quality of extracted RNA were analysed using a NanoDrop ND-1000 spectrophotometer (NanoDrop Technologies, Wilmington, DE, USA). Samples were stored at -80 °C and processed as soon as possible.

11.9.2. cDNA reverse transcription

From 1 µg of extracted RNA, complementary DNA (cDNA) was synthesised using the commercial kit High-Capacity cDNA Reverse Transcription Kit (Applied Biosystems, no. 4368814), following the manufacturer's instructions. Reactions were carried out in RNAase-free 96-well conical-bottom plates. A negative control without the reverse transcriptase enzyme was prepared. The plate was sealed, centrifuged at 1200 xg for 1 minute, then incubated at 25 °C for 10 minutes, 37 °C for 120 minutes, and finally at 85 °C for 5 minutes in a Veriti 96-well thermocycler (Applied Biosystems, Singapore). Samples were stored at -20 °C and processed as soon as possible.

11.9.3. Real-Time qPCR

cDNA samples were diluted 1:10 with RNAase-free water and amplified using the commercial reagent TaqMan Universal PCR Master Mix (Applied Biosystems, no.

4326708) containing Taq DNA polymerase and nucleotides. The manufacturer's instructions were followed, using the following commercial mouse primer-probe sets from Applied Biosystems:

- Mm99999915_g1 – *Gapdh* (Glyceraldehyde-3-phosphate dehydrogenase)
- Mm01277042_m1 – *Tbp* (TATA-binding protein)
- Mm00662319_m1 – *Fasn* (Fatty acid synthase)
- Mm00436615_m1 – *Slc2a4* (Glucose transporter type 4)
- Mm00500120_m1 – *Mfn2* (Mitofusin 2)
- Mm04933656_m1 – *Adipoq* (Adiponectin)
- Mm00452131_m1 – *Sirt3* (Sirtuin 3)
- Mm01244861_m1 – *Ucp1* (Uncoupling protein 1)
- Mm00434759_m1 – *Lep* (Leptin)

Reactions were performed in 384-well plates, mixing 5 µL of TaqMan Universal PCR Master Mix, 0.5 µL of primers-probes, and 1.5 µL of diluted cDNA. The volume was completed with RNAase-free water to a final volume of 10 µL. Additionally, a standard curve was prepared for each gene by serial dilutions from a representative cDNA sample, obtained by mixing an equal volume of cDNA samples to be analysed.

The plate was sealed, centrifuged at 1200 xg for 1 minute, and subjected to 50 cycles of amplification at 95 °C for 10 seconds and 60 °C for 30 seconds, following pre-incubation at 95 °C for 5 minutes, using a LightCycler 480 II instrument (Roche Diagnostics, West Sussex, UK).

11.9.4. Comparative quantification method ($2^{-\Delta\Delta Ct}$)

The results obtained from Real-Time qPCR were analysed using the $2^{-\Delta\Delta Ct}$ comparative quantification method (Livak and Schmittgen, 2001), using *Tbp* and *Gapdh* as reference genes (housekeeping) to normalize the results. From the amplification curves of each sample and using the standard curves for each gene, the threshold cycle value (C_t) was obtained, which is the point at which the amplification reaction begins, as the fluorescent signal exceeds the baseline fluorescence or threshold line.

This method assumes that the amplification efficiency of the target gene and the reference gene are equal, so it was previously validated by calculating the reaction efficiency for each gene, plotting the cycle threshold against the logarithm of the concentration, and applying the following equation considering the slope of the linear fit:

$$Efficiency = 10^{\left(\frac{-1}{slope}\right)} \quad (24)$$

The reaction efficiency was considered valid when efficiency was equal to 2.

Subsequently, the results were normalized with respect to the reference genes by calculating the difference between both cycle thresholds:

$$\Delta C_t = C_t(target\ gene) - C_t(reference\ gene) \quad (25)$$

As this was a kinetic assay, with RNA samples obtained at different times of cell differentiation, the results were also normalised with respect to the initial conditions or time 0, subtracting this value from each time *i*:

$$\Delta\Delta C_t = \Delta C_t(i) - \Delta C_t(0) \quad (26)$$

The final results were expressed with the following equation:

$$Mean\ fold\ change = 2^{-\Delta\Delta C_t} \quad (27)$$

A gene expression value above the control indicates overexpression of the target gene, while a value below the control indicates underexpression of the target gene.

11.10. Evaluation of lipolysis degree

During lipolysis, triacylglycerides are hydrolysed by the action of three enzymes: adipose triglyceride lipase (ATGL), hormone-sensitive lipase (HSL), and monoacylglycerol lipase (MGL), releasing free fatty acids and glycerol. In this doctoral thesis, the quantification of the degree of lipolysis was carried out by quantifying the released glycerol after this process.

Mature adipocytes (day 9 after differentiation) were treated, without phenol red, with the stilbenes at a final concentration of 150 μM with and without CL316,243 at 1 and 10 nM. CL316,243 is a β3 adrenergic agonist used as a lipolysis inducer (Morton et al., 2016). Controls with water and DMSO (0.5 % (v/v)) instead of the stilbenes, with and without CL316,243 at 1 and 10 nM, were also conducted. All treatments and additional controls were previously sterilised using 0.2 μm sterile filters. After 24 hours of incubation under standard conditions, treatments were removed, and glycerol release by cells was quantified using a colorimetric glycerol analysis kit at 570 nm (Sigma Aldrich, no. MAK117).

12. *Caenorhabditis elegans* animal model

C. elegans is a small nematode of approximately 1 mm in length, with a rapid life cycle of just 3 days at 25°C, and mainly hermaphroditic, although males can be found at a frequency of less than 0.2 % (Figure 20). This nematode share many of the metabolic pathways related to human diseases, making it suitable as an animal model for studies of aging, oxidative stress, obesity, or cancer, among many others. Its transparency allows working with fluorescently labelled molecules, expanding the possibilities of studies in this model. Additionally, it does not have the working restrictions imposed for other more

developed models, and its cultivation is relatively easy, as it can be grown on Petri plates with *E. coli* as a food source, obtaining a large number of specimens in a small space.

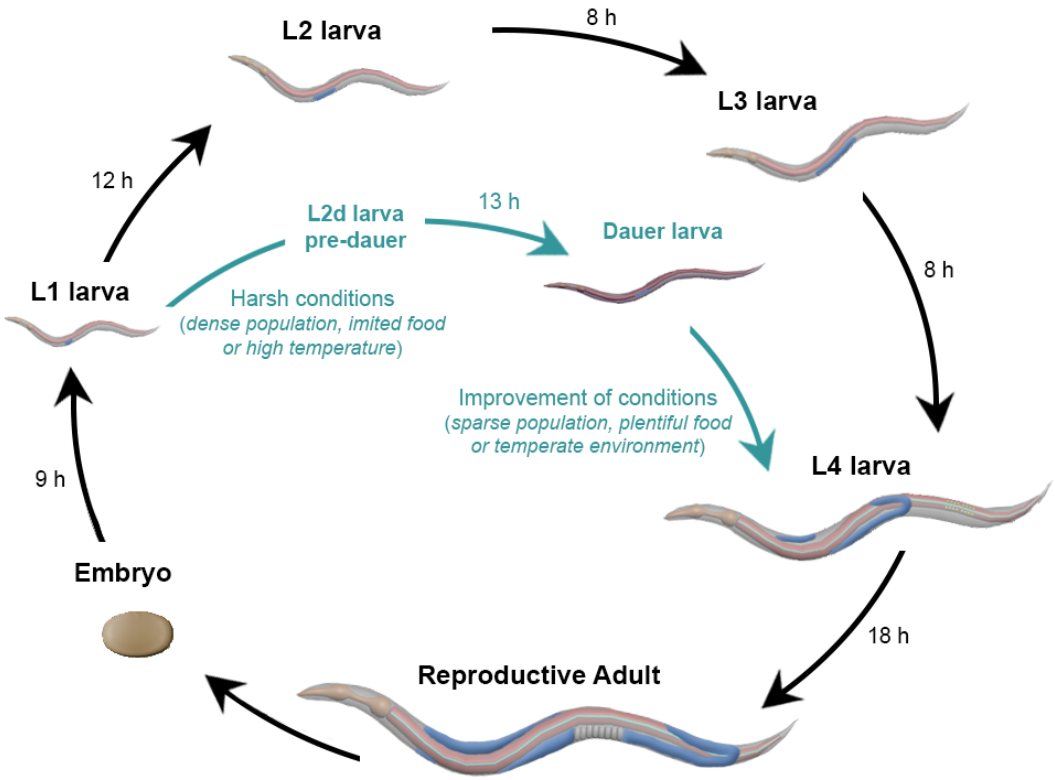

Figure 20. Life cycle of C. elegans at 20°C. The blue lines indicate the alternative route leading to dauer larva, which can resist up to 4 months under harsh conditions

12.1. Strains and cultivation conditions

In this doctoral thesis, the N2 (wild-type) and TJ375 (*hsp-16.2p*::GFP) strains of *C. elegans* were used, both obtained from the Caenorhabditis Genetic Center (CGC, St Paul, MN, USA), funded by the NIH Office of Research Infrastructure Programs (P40 OD010440). Unless otherwise indicated, strain maintenance was performed on solid nematode growth medium (NGM), while experiments were conducted in liquid medium S (Stiernagle, 2006), incubating at 20 °C. Nematodes were fed with the OP50 strain of *E. coli*, which was grown the day before in LB medium at 37 °C, then concentrated ten-fold in M9 medium and heat-inactivated (65°C for 30 minutes) before use. Additionally,

during experiments, 2'-deoxy-5-fluorouridine was used to prevent progeny. All materials and media were previously sterilised by autoclave. In the case of solutions, these were sterilised with 0.2 µm sterile filters or UV light (for HBCD-Pol).

12.2. Cultivation synchronization

C. elegans experiments were conducted with worms that were in the same stage of the life cycle. To achieve this, cultivation synchronization was performed, eliminating adult and larval stage nematodes to maintain only the eggs.

This procedure was carried out by collecting 3-day-old adults in 3.5 mL of M9 medium and adding 1.5 mL of freshly prepared 5 M sodium hydroxide bleach in a 2:1 (v/v) ratio. After 10 minutes at room temperature with vortex agitation every 2 minutes, the samples were centrifuged at 7500 xg to discard the supernatant. The pellet, containing the *C. elegans* eggs, was washed twice and incubated with 10 mL of M9 medium at 20°C on an orbital shaker until the next day.

12.3. Lifespan assays

Synchronized *C. elegans* N2 (wild-type) nematodes were treated with stilbenes at a final concentration of 50 µM and HBCD-Pol at 0.2 g/L in flasks with S medium. Controls with DMSO (0.33% (v/v)) instead of stilbenes, with and without HBCD-Pol at 0.2 g/L, were also conducted. All treatments and controls were previously sterilised using 0.2 µm sterile filters or UV light (for HBCD-Pol).

After 48 hours of incubation at 20°C, nematodes were centrifuged at 2000 xg and washed with M9 medium, then transferred (40 – 50 individuals) to 35 mm plates with 8 mL of NGM medium (with agar) supplemented with 30 µg/mL nystatin, 100 µM ampicillin, and 10 µg/mL 2'-deoxy-5-fluorouridine (Alvarez-Illera et al., 2017; García-

Casas et al., 2019), as well as 100 µL of heat-inactivated *E. coli* OP50. Closed plates were pre-incubated at 20°C for 20 minutes, then placed in the Lifespan Machine, designed for automatic control of *C. elegans* mobility. The temperature inside the scanners was set to 25°C for the entire 25-day assay using external temperature probes (USB Reference Thermometers, Thermoworks, Utah, USA). This control is essential as the *C. elegans* life cycle is very sensitive to temperature variations.

The assay results were analysed using the online survival analysis software OASIS 2 (Han et al., 2016), with Kaplan-Meier estimator, Boschloo test, Kolmogorov-Smirnov test, and log-rank test.

12.4. ORO lipid staining in animal models

Lipid accumulation in *C. elegans* was determined using ORO staining similarly to the procedure performed in cell cultures (Section 11.6), but with an additional permeabilization step allowing the dye to penetrate the whole organisms.

Synchronized *C. elegans* N2 (wild-type) nematodes were treated with stilbenes at a final concentration of 50 µM and HBCD-Pol at 0.2 g/L in flasks with S medium. Controls with DMSO (0.33% (v/v)) instead of stilbenes, with and without HBCD-Pol at 0.2 g/L, were also conducted. All treatments and controls were previously sterilised using 0.2 µm sterile filters or UV light (for HBCD-Pol).

After 48 hours of incubation at 20 °C, nematodes were centrifuged at 2000 xg and washed with M9 medium, then fixed for 72 hours with a 4 % formaldehyde solution in PBS. Subsequently, they were washed again with M9 medium containing 1 % (v/v) Triton-100 and permeabilized at 37 °C and 300 rpm for 24 hours with a solution of 5 % (v/v) β-mercaptoethanol and 1 % (v/v) Triton-100 in tris-HCl buffer pH 7.4. Then, they were washed with M9 medium containing 1 % (v/v) Triton-100 and stained for 5 minutes

with a filtered solution of 0.3 % (w/v) ORO dye in 60 % (v/v) isopropanol. The stained nematodes were washed with M9 medium containing 1 % (v/v) Triton-100, centrifuged at 3000 xg for 1 minute, and resuspended in the same medium. Finally, 20 µL were transferred to a microscope slide with a coverslip, and lipid content was quantified by processing images taken by microscopy of the stained nematodes (Sections 12.6 y 12.7).

12.5. Oxidative stress assays

The level of oxidative stress in *C. elegans* was measured using the TJ375 strain (*hsp-16.2p*::GFP). This strain has the green fluorescent protein (GFP) marker attached to the *hsp-16.2* gene, which is expressed in the nematode pharynx in response to a stimulus that generates oxidative stress. Therefore, when this strain is subjected to oxidative stress, fluorescence emission can be observed and quantified in the pharyngeal cells of the nematode.

Synchronized *C. elegans* TJ375 (*hsp-16.2p*::GFP) nematodes were treated with stilbenes at a final concentration of 50 µM and HBCD-Pol at 0.2 g/L in flasks with S medium. Controls with DMSO (0.33% (v/v)) instead of stilbenes, with and without HBCD-Pol at 0.2 g/L, were also conducted. All treatments and controls were previously sterilised using 0.2 µm sterile filters or UV light (for HBCD-Pol).

After 48 hours of incubation at 20°C, nematodes were centrifuged at 2000 xg and washed with M9 medium, then transferred to flasks with S medium supplemented with 20 µM juglone naphthoquinone to induce oxidative stress. A negative control without the stressful agent was also included. After 24 hours of incubation at 20 °C, they were washed with M9 medium and incubated with the same medium for 1 hour at 20 °C. Finally, 20 µL of nematodes with 10 mM sodium azide (anaesthetic) were transferred to a microscope slide with a coverslip, and oxidative stress was quantified by processing images taken by

fluorescence microscopy of the fluorescence emitted in the nematode pharynx (Sections 12.6 y 12.7).

12.6. Microscopy in animal models

Images were collected at a fixed exposure with a 40x objective from a minimum of 25 individuals per treatment on a Leica DM 2500 LED microscope equipped with a Leica DFC550 camera (Leica Microsystems, Wetzlar, Germany) with incident light beam and Las version 4.8 software. Images of nematodes stained with ORO were taken in bright-field colour, while images of fluorescence from the pharyngeal region of nematodes induced with oxidative stress were taken using an L3 filter (Leica, excitation range 450 – 490 nm).

12.7. Image analysis in animal models

Images collected by microscopy were processed in Fiji (ImageJ 1.53t version) (NIH, USA) (Schindelin et al., 2012). First, the image scale was adjusted to the appropriate pixels/µm according to the objective used and the dimensions of the image exported from the microscope. Next, the images were processed differently depending on the experiment. For images obtained after ORO staining, a H AEC colour deconvolution was performed, and channel 2 (red) was processed. On this image, a single threshold was set to obtain ORO-stained cells in black and the rest of the image in white, and the mean was measured. For fluorescence images, an RGB channel separation was performed, and the green channel was processed. On this image, a single threshold was set to obtain fluorescence in black and the rest of the image in white, and the mean was measured.

13. *Mus musculus* animal model

The mouse (*M. musculus*) is one of the classic and most common animal models for the study of human diseases due to the large number of shared metabolic pathways. It is a widely accepted model for drug bioavailability assays and *in vivo* bioactivity studies. Additionally, it can undergo genetic modifications to obtain mutants or transgenics according to the objective. In this doctoral thesis, the albino BALB/c strain was used for pharmacokinetic assays, and the C57BL6/J dark-furred strain was used for anticancer activity assays on melanoma, due to its low susceptibility to tumours.

The BALB/c mice used were males, approximately 21-23 grams, obtained from the Tabriz University of Medical Sciences – Animal Centre (Tabriz, Iran), while the C57BL6/J mice were females, 6 to 8 weeks old, approximately 22 grams, obtained from Pasteur Institution (Tehran, Iran). The animals were maintained in the facilities of the Department of Pharmacy at Tabriz University of Medical Sciences (Tabriz, Iran) and handled by accredited personnel according to the Tabriz University of Medical Science Ethical Committee (Tabriz, Iran). They were fed a standard diet for laboratory mice, with free access to water, under pathogen-free conditions, and controlled environmental conditions (22 ± 3 °C, 50 ± 5 % relative humidity, and 12-hour light/dark cycle).

13.1. Pharmacokinetic assays

13.1.1. Experimental design

For the experiment, BALB/c mice were randomly divided into six groups, with a population of at least 6 individuals per group:

- Group 1: Control | PBS (untreated individuals)
- Group 2: CD | HP-β-CD

- Group 3: R | Resveratrol
- Group 4: R + CD | Resveratrol + HP-β-CD
- Group 5: RE | Resveratrol stearate
- Group 6: RE + CD | Resveratrol stearate + HP-β-CD

The animals were fasted overnight before the experiment. Each group received treatments or placebo orally in a single dose via gastric tube. A dose of stilbenes of 50 mg/kg/day was used, with or without HP-β-CD in a 1:5 (w/w) ratio. After euthanasia, blood samples were taken by cardiac puncture at times 0, 12.5, 25, 45, 60, 90, 120, 240, and 360 minutes after compound administration to analyse the concentration of stilbenes in the blood. At the end of the assay, blood samples were taken to analyse biological markers of interest.

13.1.2. Plasma extraction and HPLC-ESI(-) analysis

Blood samples were immediately centrifuged after collection to separate plasma from blood cells and stored at -80 °C. Extraction of the compounds from plasma samples was performed by mixing with acetonitrile in a 1:1 (v/v) ratio. This mixture was then vortexed and centrifuged at 13000 rpm for 10 minutes. The supernatants containing the compounds were recovered and evaporated in a vacuum microtube concentrator, avoiding exceeding a temperature of 25 °C in the sample. Finally, the evaporated samples were resuspended in methanol and injected into an HPLC system, along with the corresponding calibration curve for each compound to be analysed. The samples were analysed by direct injection in negative mode on an HPLC system with an Alliance 2795 separation module (Waters, Milford, MA, USA) coupled to a triple quadrupole LC-MS/MS Quattro Micro API (Waters, Micromass, Manchester, UK).

13.1.3. Determination of pharmacokinetic parameters

From the pharmacokinetic curve obtained with the concentration of stilbene in plasma *versus* time, various pharmacokinetic parameters were determined according to Tillement & Tremblay (2007) and Turfus *et al.* (2017) (Tillement and Tremblay, 2007; Turfus et al., 2017). The maximum concentration (C_{max}) and the time to reach that maximum concentration (t_{max}) were obtained directly from the pharmacokinetic curve.

Assuming that absorption and distribution are nearly complete and have no significant influence on metabolism and excretion at the end of the pharmacokinetic curve, it can be fitted to the following monoexponential equation:

$$C = C_0 \cdot e^{-k_e \cdot t} \tag{28}$$

where C is the concentration at a given time t, C_0 is the concentration extrapolated to the origin, and k_e is the apparent elimination constant.

By using natural logarithms, this curve can be transformed into a linear equation to determine C_0 and k_e by linear regression, with the equation as follows:

$$ln\, C = ln\, C_0 - k_e \cdot t \tag{29}$$

To determine the area under the curve extrapolated to infinity ($AUC_{0-\infty}$), first, the area under the curve in the analysed time interval (AUC_{0-6h}) was determined using the following equation:

$$AUC_{0-6h} = \frac{1}{2}\sum (C_n + C_{n-1}) \cdot (t_n - t_{n-1}) \tag{30}$$

where C_n is each of the obtained concentrations and t_n is its corresponding time.

Then, with AUC_{0-6h}, k_e, and the last concentration (C_{6h}), the results were extrapolated to infinity with the following formula:

$$AUC_{0-\infty} = AUC_{0-6h} + AUC_{6h-\infty} = AUC_{0-6h} + \frac{C_{6h}}{k_e} \quad (31)$$

Finally, half-life ($t_{1/2}$) can be calculated with k_e, as $t_{1/2}$ is constant during elimination:

$$t_{1/2} = \frac{ln\,2}{k_e} \quad (32)$$

13.1.4. Determination of serum biological markers

Plasma samples from the different groups obtained at 6 hours post-oral administration were analysed to identify the following biomarkers:

- Oxidative stress: TAS (total antioxidant status), SOD (superoxide dismutase), GPx (glutathione peroxidase), and MDA (malondialdehyde)
- Inflammation: TNF-α (tumour necrosis factor alpha), IL-6 (interleukin 6), and COX-2 (cyclooxygenase 2)
- Obesity: TG (triglycerides), CHO (cholesterol), HDL (high-density lipoproteins), and LDL (low-density lipoproteins)
- Renal function: BUN (blood urea nitrogen) and CR (creatinine)
- Hepatic function: AST (aspartate aminotransferase) and ALT (alanine aminotransferase)

Diagnostic kits from Randox Laboratories (Crumlin, County Antrim, UK) were used to determine TAS (Miller et al., 1993), SOD (Arthur and Boyne, 1985), and GPx (Paglia and Valentine, 1967), and the Yoshika method was used for MDA marker (Yoshioka et al., 1979). To determine AST, ALT, BUN, CR, TG, CHO, HDL, and LDL markers, a fully automated clinical chemistry spectrophotometer SPECORD M40 (Carl

Zeiss, Jena, Germany) was used. Inflammatory markers TNF-α, IL-6, and COX-2 were determined using DueSet® ELISA kits (R&D Systems, Minneapolis, MN, USA).

13.2. Melanoma assays

13.2.1. Experimental design and tumour induction

The induction of melanoma tumours in mice was performed by subcutaneous injection of B16-F10 cells at a density of 1 000 000 cells per mL. For the experiment, the animals were randomly divided into seven groups, with a population of at least 6 individuals per group:

- Group 1: Healthy | PBS (untreated individuals without melanoma)
- Group 2: Control | PBS (untreated individuals with melanoma)
- Group 3: CD | HP-β-CD
- Group 4: R | Resveratrol
- Group 5: R + CD | Resveratrol + HP-β-CD
- Group 6: RE | Resveratrol stearate
- Group 7: RE + CD | Resveratrol stearate + HP-β-CD

When the tumours were palpable, treatments or controls were administered intratumorally at a volume of 0.1 mL daily for one week. A dose of stilbenes of 50 mg/kg/day was used, with or without HP-β-CD in a 1:5 (w/w) ratio.

Every two days, tumour size was analysed in two dimensions using a calliper. At the end of the treatment, the animals were anaesthetised to collect blood samples from the heart for analysis of biomarkers, and tumours were measured with a calliper to determine their volume (length × width^2 × 0.52) (Cai et al., 2016). Biological markers of oxidative stress, inflammation, renal function and hepatic function were quantified as

described in Section 13.1.4. Subsequently, they were euthanised by cervical dislocation, and the melanoma, liver and kidneys were excised for histopathological examination after fixation. Tumours were also weighed before histological examination.

13.2.2. Histopathological examination

Tumours, adjacent tissues, livers, and kidneys from euthanised animals in each group were dissected and processed for histopathological examination. They were fixed with 10 % formaldehyde (v/v) for 24 hours, dehydrated with ethanol at 30, 50, 70, 90, and 100 % (v/v), cleaned with benzene, and embedded with low melting point paraffin. Subsequently, tissue sections of 5 µm thickness were cut using a mechanical microtome, stained on slides, and stained with hematoxylin-eosin for evaluation under a Leica DM 3000 microscope (Leica, Shanghai, China).

In tumours, the mitotic and angiogenesis rates were determined by counting cells in mitosis and the number of vessels in 15 different random fields with a 400x objective on a Nikon Eclipse E200 optical microscope (Nikon Instruments, Amstelveen, Netherlands). Necrosis was also determined and classified as: grade I absent to mild necrosis, grade II moderate necrosis with multiple foci of necrotic tumour cells, and grade III advanced necrosis with confluent necrotic cells (Souza et al., 2021).

In livers and kidneys, the degree of tissue lesions was semi-quantitatively evaluated using the method described by Jamshidzadeh *et al*. (2008) (Jamshidzadeh et al., 2008), in a minimum of 10 fields, using a Nikon Eclipse E200 optical microscope (Nikon Instruments, Amstelveen, Netherlands). Histological changes were blindly evaluated by a pathologist in non-consecutive histological fields chosen randomly. The observed damages were scored as: 0 absent, + slight, ++ mild, +++ moderate, and ++++ severe.

13.2.3. Determination of tumour microvessel density

Tumour microvessel density (TMD) was determined by immunohistochemical staining of the CD31 antibody (Santa Cruz Biotechnology, no. sc-376764 AF488), followed by counting individual microvessels in 3 fields of each tumour section in areas of the most intense staining, using an Olympus BX50 microscope equipped with an Olympus DP72 digital camera (Olympus Optical, Tokyo, Japan) (Gigliotti et al., 2016; Passaro et al., 2015). Both groups and individual stained endothelial cells were considered. Images collected by microscopy were processed in Fiji (ImageJ 1.52n version) (NIH, USA) (Schindelin et al., 2012).

14. Development of functional food models

14.1. Preparation of milk and juice food models

Milk and juice food models were prepared to assess the feasibility of industrial development of functional foods enriched in hydrophobic stilbene derivatives. For the milk food model a 0.1 M sodium citrate buffer pH 6.51 was used, while for the juice food model a 0.1 M sodium citrate buffer pH 3.73 was used (Babazadeh et al., 2016). Each of these food models was supplemented with 200 μM resveratrol palmitate, free or encapsulated in 5 mM γ-CD, using 0.05 mg/mL soy lecithin as an emulsifying agent to promote solubilisation. In addition, controls were prepared for each model without supplementation, supplementing only with soy lecithin, and supplementing with soy lecithin and γ-CD, at the same concentrations used.

After preparation, the fortified food models were subjected to heat treatment at 121 °C for 15 minutes using an autoclave, with aliquots taken before and after heat treatment to assess the degree of degradation by HPLC.

The fortified models were aliquoted into microtubes under sterile conditions to obtain disposable samples for analysing parameters in time, avoiding possible microbial contaminations. Subsequently, they were stored simulating typical storage and commercialization conditions of such products: refrigerated or non-refrigerated and with opaque or transparent packaging. Refrigerated food models were stored at a temperature of 4 °C, while non-refrigerated ones at room temperature (approximately 25 °C). Food models with opaque packaging were stored protected from light, while models with transparent packaging were stored without light protection.

Weekly, for a total of 10 weeks, industrial quality parameters were evaluated, and the remaining percentage of stilbenes in the fortified models stored under different conditions was quantified spectrophotometrically every two days and chromatographically, at the beginning and end of the experiment.

14.2. Monitoring of industrial quality parameters

In the food industry, monitoring parameters such as pH and ºBrix in different manufacturing batches is common for ensuring the quality and safety of final products. The pH allows quantifying the acidity of food products, and variations in this parameter can indicate the presence of microbial contamination or degradation of certain components. The ºBrix measured the soluble solid content are an important parameter in sugary products, to quantify and correct the sweetness of the final product. pH was measured using a Crison GLP 21+ pH meter (Barcelona, Spain), and ºBrix using an Atago PAL-3 refractometer (Tokyo, Japan) with water as reference.

14.3. Determination of stilbenes in food models

The quantification of the remaining concentration of stilbenes in food models was performed by two techniques: spectrophotometry and HPLC.

14.3.1. Spectrophotometric analysis of food models

Samples of the fortified food models were diluted 1:3 in methanol, and their absorption spectrum was recorded between 200 and 600 nm using a Jasco V-630 spectrophotometer (Madrid, Spain) with Thorlabs CV10Q1400 cuvettes. A solution with the corresponding buffer and methanol at the same final concentration as the samples was used as a blank. The results were expressed as the remaining percentage of stilbene using the Lambert-Beer Law (Equation 2) and the previously calculated absorptivity.

14.3.2. HPLC-UV/Vis analysis of food models

Aliquots of the fortified food model samples were injected into a Shimadzu LC2010C HT HPLC system (Kyoto, Japan) in reverse phase, with UV-Vis detector set at 310 nm, equipped with a Kromasil C18 column of 5 µm (150 × 4.6 mm) (Análisis Vínicos, Tomelloso, Spain), and a flow rate of 1 mL/min at 25 °C. The method used was an aqueous acetonitrile gradient (v/v): 40 % from 0 to 2.5 min, 99 % from 3 to 13.5 min, and 40 % from 13.5 to 18.5 min. The results were expressed as the remaining percentage of stilbene using a calibration curve.

15. Data analysis

All experiments were conducted at least in triplicate, increasing the replicates per assay in the case of *in cellulo* and *in vivo* experiments. Unless otherwise indicated, the final results are the mean ± standard deviation of the replicates performed. Linear regressions and graphical representations were performed using SigmaPlot (version 10.0.0.54), GraphPad Prism (version 9.0.0) or Excel 2021 (version 2309), except for molecular docking which was performed using the software mentioned in Section 7.1.1. Unless otherwise indicated, the results were statistically analysed setting a significance

value of $p < 0.05$, using one-way analysis of variance ANOVA for independent measures and Tukey's post hoc test with the SocSciStatistics software (version 2018) or SPSS-21 (version 17.0), or using the T-test with Rstudio software (version 0.99.878) or Excel 2021 (version 2309). The results of survival assays in the *C. elegans* animal model were analysed as described in Section 12.

CHAPTER IV

RESULTS AND DISCUSSION

CHAPTER IV. RESULTS AND DISCUSSION

1. CURRENT AND FUTURE STRATEGIES TO INCREASE STILBENE PRODUCTION

As previously explained in the introduction, one of the limitations of stilbenes is their low production in plants and the limited number of species capable of biosynthesising them. Therefore, research into new ways of obtaining stilbenes and increasing their production is of great interest to boost their application in industry. In this doctoral thesis, two different strategies for obtaining stilbenes have been evaluated: the synthesis of piceatannol catalysed by the enzyme tyrosinase, and the identification, through phylogenetic analysis, and recombinant expression of a potential stilbene synthase protein (STS) from extremophilic bacteria.

1.1. Current strategy: Tyrosinase-catalysed piceatannol synthesis

Taking advantage of the cresolase activity of the enzyme tyrosinase (Figure 10), which in the presence of oxygen catalyses the hydroxylation of monophenols into *ortho*-diphenols, reactions were carried out to synthesise piceatannol (*ortho*-diphenol) from resveratrol (monophenol). For that purpose, several compounds that could stop the catecholase activity of the enzyme, which would oxidise the piceatannol into its corresponding *ortho*-quinone and then continue to generate other oxidation products, were used. These compounds added were: catechol, which has a structure analogous to that of piceatannol and could be oxidised by tyrosinase instead (Lee et al., 2012), ascorbic acid or vitamin C, as a reducing agent capable of reducing *ortho*-quinone upon oxidation (Ros et al., 1993), and β-CD, capable of encapsulating piceatannol and protecting it from

oxidation (Matencio et al., 2016). The reactions were monitored spectrophotometrically and chromatographically to complement the information obtained by both methodologies.

1.1.1. Spectrophotometric monitoring of piceatannol synthesis

The absorption spectra of resveratrol showed a remarkable variation after the addition of the enzyme tyrosinase, decreasing the absorbance at 300 - 320 nm, i.e. in the region of the λ_{max} of resveratrol (306 nm), and increasing the absorbance at 360 - 440 and 440 - 550 nm, i.e. the regions of the λ_{max} of oxidised products, such as *ortho*-quinone that other authors have identified at 485 nm (Ito et al., 2019) (Figure 21A). The absorbance evolution was slow during the first minutes, giving the highest conversion between approximately 6 and 16 minutes after enzyme addition (Figure 22). After 30 minutes of reaction, the absorbance at 306 nm had decreased by 62 %, i.e. a drop of 0.48 mAU.

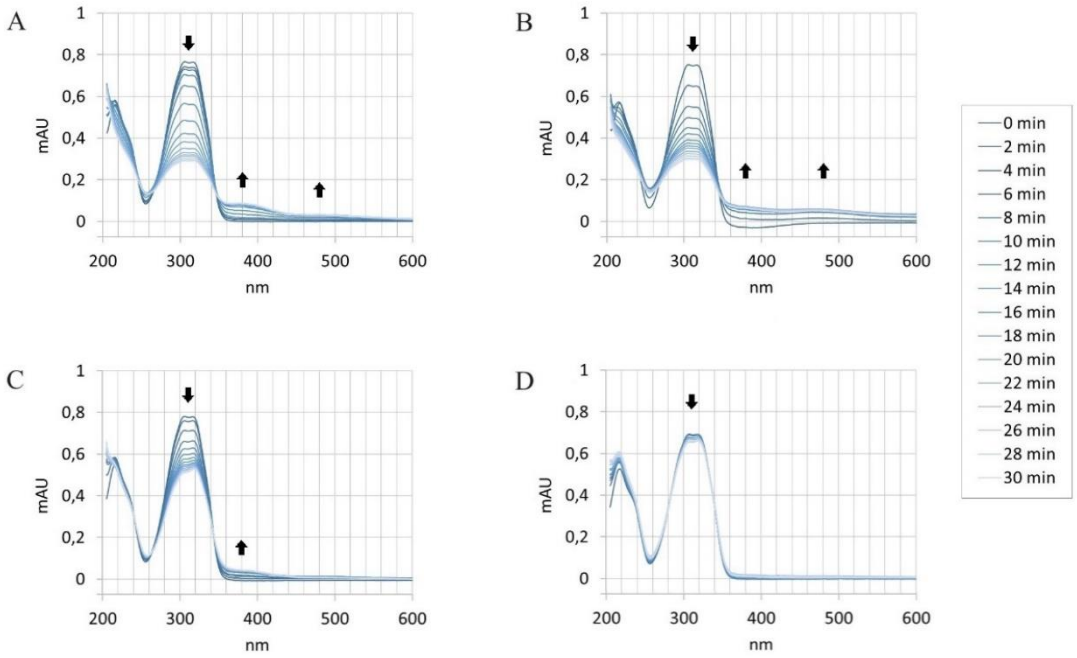

Figure 21. Absorption spectra during the resveratrol (25 µM) oxidation reaction catalysed by tyrosinase (2 µg/mL), in A) absence and presence of B) catechol 25 µM, C) ascorbic acid 25 µM or D) β-CD 1 mM (30 °C pH 7)

When the reaction was carried out in the presence of catechol, the latter absorption spectra were very similar to those of the control reaction, although they were obtained in

less time (Figure 21B). These spectra showed large variations in absorbance at 306 nm in the first 15 minutes (Figure 22A), with the initial absorbance dropping by 60 % after 30 minutes. In addition, absorbance values at 377 nm and 485 nm reached plateau in just 6 minutes, compared to 16 minutes for the control (Figure 22B-C), which might suggest that the addition of catechol accelerates tyrosinase activity rather than inhibiting it.

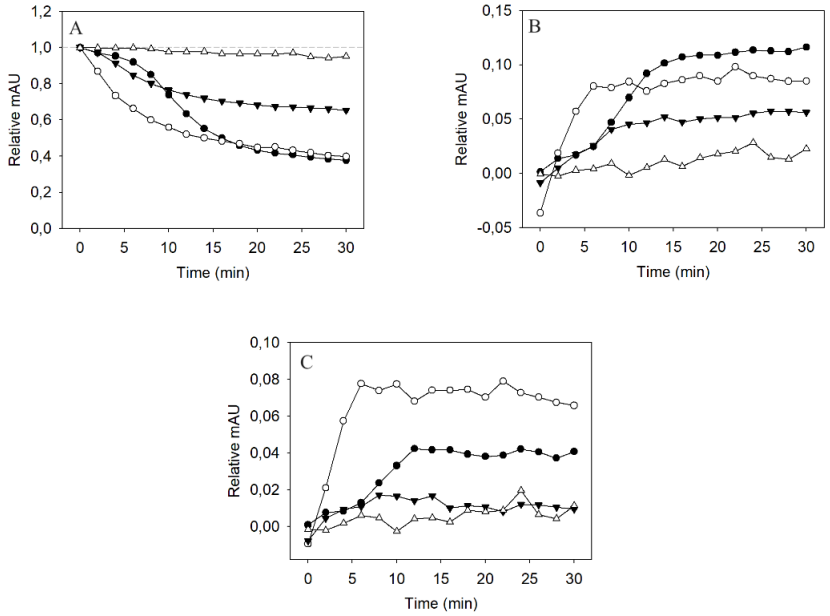

Figure 22. A) Evolution of the relative absorbance at 306 nm, B) 377 nm and C) 485 nm of resveratrol (25 µM) oxidation reaction catalysed by tyrosinase (2 µg/mL) in the (●) absence and presence of (○) catechol (25 µM), (▼) ascorbic acid (25 µM) or (△) β-CD (1 mM) (30 °C pH 7)

On the other hand, in the spectra obtained in the reactions with ascorbic acid, although a slightly higher conversion rate was observed in the first 10 minutes than in the control (Figure 22A), the decrease in absorbance in the 300 - 320 nm region at the end of the assay was lower (Figure 21C). In particular, at 306 nm, the absorbance decreased by 35 % compared to the absorbance at the beginning of the reaction. Furthermore, although monitoring the transformation of resveratrol to piceatannol by spectrophotometry is limited due to the similarity of their spectra and proximity of their λ_{max}, it could be seen that the shape of the final spectra resembled that of piceatannol, with the decrease at 306 nm being more intense than at 322 nm (Figure 21C). Meanwhile, in the two distinguished

λ_{max} regions of the oxidised products, differences were only observed around 377 nm, detecting a smaller increase in absorbance than the control (Figure 22B). In contrast, the variation at 485 nm was negligible (Figure 22C), possibly indicating that the inhibition of catecholase activity had been effective, and the reaction was redirected towards *ortho*-diphenol or piceatannol formation, decreasing the synthesis of the downstream products.

Finally, the use of CDs in the enzymatic reaction resulted in less absorbance variation in the spectra compared to the control (Figure 21D). After 30 minutes of reaction, the absorbance at 306 nm had only decreased by 5 % compared to 62 % for the control, with even less variation at 377 and 485 nm (Figure 22). Despite this, the shape of the final spectra resembled that of the piceatannol spectrum, showing higher absorbance at 322 nm than at 306 nm (Figure 23). This could mean that, as was observed in the reactions with ascorbic acid, the addition of β-CD could be inhibiting the tyrosinase enzyme reaction, favouring the production of piceatannol. Since CDs can modify the optical properties of the molecules they encapsulate, it would not be correct to make an assessment comparing these results with those of the other reactions only on the basis of the variation of their spectra. For this reason, chromatographic assays were also performed to accurately determine the variation in concentration of both stilbenes.

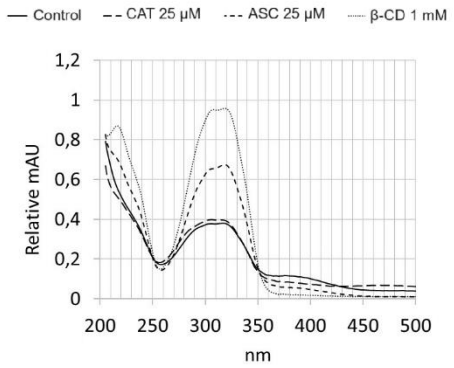

Figure 23. Absorption spectra after 30 minutes of resveratrol (25 µM) oxidation reaction catalysed by tyrosinase (2 µg/mL), in the absence and presence of catechol (CAT), ascorbic acid (ASC) or β-CD (30 °C pH 7)

1.1.2. HPLC-UV/Vis monitoring of piceatannol synthesis

In contrast to the monitoring of the reactions with absorption spectra, HPLC monitoring make it possible to distinguish precisely between the kinetics of resveratrol disappearance and piceatannol appearance. The reagent concentrations and reaction time were adjusted to obtain a good conversion to complement the previous results.

In the reactions with catechol, although the variation in resveratrol concentration was slightly lower than that of the control (Figure 24A), the formation of piceatannol was minimal (Figure 24B). Therefore, as observed by spectrophotometry and HPLC, catechol could be forming other more oxidised products from piceatannol, not being effective in increasing piceatannol synthesis.

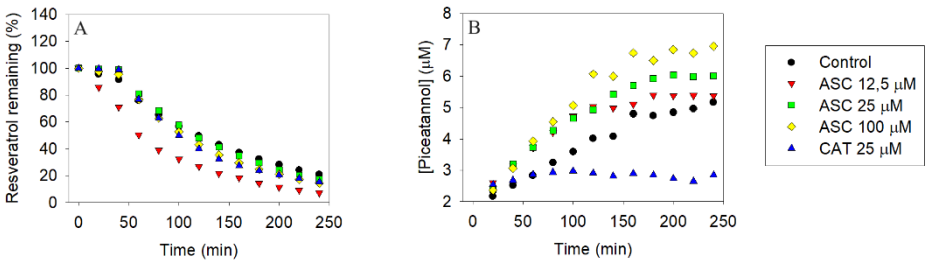

Figure 24. Evolution of the concentration of A) resveratrol and B) piceatannol during the resveratrol (12.5 µM) oxidation reaction catalysed by tyrosinase (100 µg/mL), in the absence and presence of catechol (CAT) or ascorbic acid (ASC), determination by HPLC-UV/Vis (30 °C pH 7)

In contrast, the addition of ascorbic acid showed a clear increase in piceatannol production over time, which was directly proportional to the concentration used (Figure 24B). At the lowest concentration of 12.5 µM, both resveratrol disappearance and piceatannol formation were faster than in the control, but there was no significant difference in the final piceatannol concentration at 4 hours (Figure 24). However, with 25 µM or 100 µM ascorbic acid, although the rate of resveratrol disappearance was similar to the control, the appearance of piceatannol was accelerated, also resulting in a higher piceatannol concentration at the end of the assay, especially at the higher concentration

(Figure 24). A stable piceatannol concentration was reached after 2.5 – 3 hours of reaction with all concentrations of ascorbic acid. Although the resveratrol remaining at the end of the assay was similar between the different ascorbic acid concentrations, the lower piceatannol concentration obtained with a low ascorbic acid concentration could be due to the formation of other oxidised products.

The use of encapsulating agents also affected the reaction significantly, but in a different way than ascorbic acid. While the disappearance of resveratrol slowed with increasing concentration of β-CD in the medium (Figure 25A), the formation of piceatannol was faster at the intermediate concentration of 5 mM (Figure 25B), also giving a higher concentration of piceatannol at the end of the assay at this concentration of CD. Unlike ascorbic acid, the piceatannol formation curves with β-CD did not appear to reach a plateau at the end of the assay and piceatannol was not detected in the first 60 minutes of reaction (Figure 25B). These results seem to indicate that the CDs may be forming inclusion complexes with both piceatannol and resveratrol, protecting them from the action of the tyrosinase enzyme, leading to slower conversion.

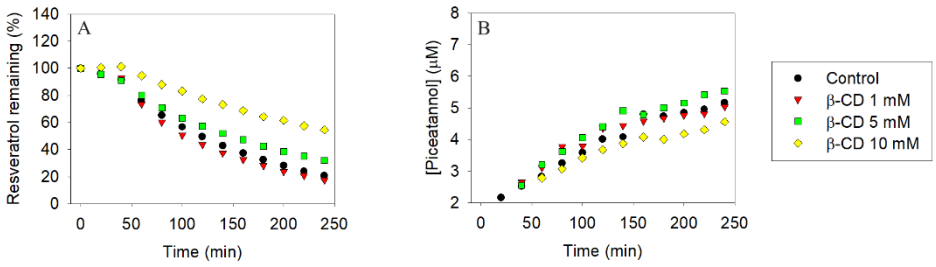

Figure 25. Evolution of the concentration of A) resveratrol and B) piceatannol during the resveratrol (12.5 µM) oxidation reaction catalysed by tyrosinase (100 µg/mL), in the absence and presence of β-CD, determination by HPLC-UV/Vis (30 °C pH 7).

The combined effect of ascorbic acid and β-CD showed no advantage over the use of ascorbic acid alone (Figure 26). The combination of 100 µM ascorbic acid with 1 mM β-CD decelerated the rate of resveratrol disappearance (Figure 26A), while 5 mM β-CD

showed no difference with the control curve. And although 1 mM β-CD significantly increased piceatannol, the use of ascorbic acid only achieved a higher concentration at the end of the assay (Figure 26B).

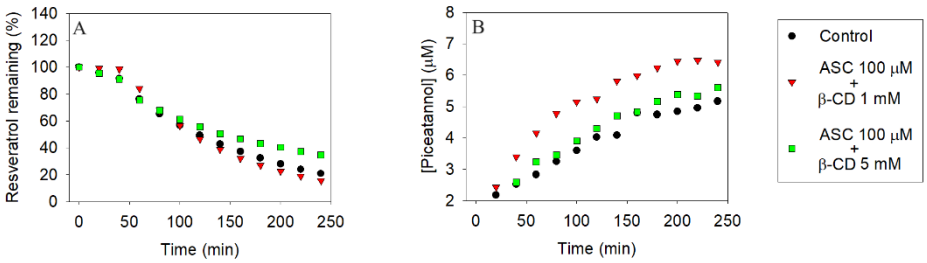

Figure 26. Evolution of the concentration of A) resveratrol and B) piceatannol during the resveratrol (12.5 μM) oxidation reaction catalysed by tyrosinase (100 μg/mL), in the absence and presence of ascorbic acid (ASC) and β-CD, determination by HPLC-UV/Vis (30 °C pH 7)

Therefore, of all the compounds and concentrations tested, the use of ascorbic acid at 100 μM was the most effective in the synthesis of piceatannol, with a conversion of 56 % compared to 41 % for the control (Figure 27). This result was followed by that obtained with ascorbic acid and β-CD at 1 mM, which gave a conversion of 51 %, and ascorbic acid at 25 μM with a conversion of 48 %. In contrast, 25 μM catechol decreased basal piceatannol production by almost half that of the control, being the worst of the compounds tested (Figure 27). On the other hand, the incorporation of 10 mM β-CD in the reactions also slightly reduced the conversion rate, which could be due to the fact that a high concentration of CD interacts with the hydrophobic amino acids of the enzyme. However, the use of 1 or 5 mM β-CD, 12.5 μM ascorbic acid or the combination of 5 mM β-CD and 100 μM ascorbic acid did not give significant differences in the percentage conversion compared to the control.

Overall, although the assay conditions were not the same, the results obtained from the HPLC study of piceatannol synthesis complement and explain the variations observed in the absorption spectra during the reactions.

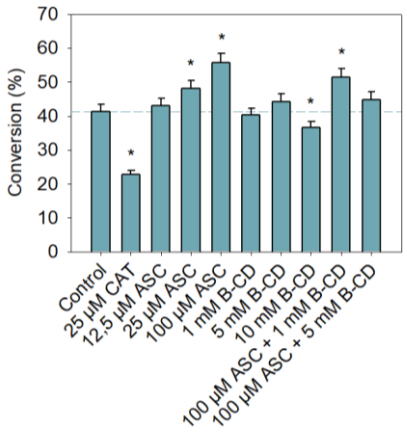

Figure 27. Conversion of resveratrol to piceatannol after 4 hours resveratrol oxidation reaction (12,5 µM) catalysed by tyrosinase (100 µg/mL), in the absence and presence of catechol (CAT), ascorbic acid (ASC) and/or β-CD (B-CD), determination by HPLC-UV/Vis (30 °C pH 7)

The direct *in vitro* production of piceatannol from resveratrol using the enzyme tyrosinase has not been investigated before, however, previous studies have examined this activity in cells expressing the enzyme. For example, Lee *et al*. (2012) used whole *Streptomyces avermitilis* MA4680 cells that secrete MelC2 tyrosinase (Lee et al., 2012). Contrary to what was observed in this doctoral thesis, these authors obtained an increase in piceatannol production with catechol, even higher than that obtained with ascorbic acid. However, it should be considered that when using whole cells it is likely that other compounds and mechanisms are involved that could be favouring the inhibitory activity of catechol. Furuya *et al*. (2018) analysed the effect of natural CDs on this enzymatic activity using *E. coli* cells expressing HpaBC monooxygenase, and concluded that β-CD managed to produce more piceatannol, probably due to its higher encapsulation constant for the inclusion complex with piceatannol (Furuya et al., 2018). Ito *et al*. (2019) investigated the adducts formed from *ortho*-quinone generated by the oxidation of piceatannol catalysed by the mushroom tyrosinase enzyme for their involvement in melanocyte toxicity (Ito et al., 2019). Although their study did not focus on piceatannol production, their assays also observed a rapid transformation of resveratrol to piceatannol after the addition of ascorbic acid.

1.2. Future strategy: Phylogenetic analysis of STS enzymes and production of a potential bacterial STS in *E. coli*

The STS enzyme is a key protein in the biosynthesis of stilbenes, and as mentioned above, its presence has only been described in a few higher plant species, notably grapevine and peanut, where stilbene production is generally low. Although the evolutionary origin of the STS enzymes is unclear, there is evidence to suggest that their ancestor may be a chalcone synthase (CHS), with all STS having evolved from this protein at various times and independently (Tropf et al., 1994). However, it is still unknown whether other STS exist in non-plant kingdoms, e.g. in extremophilic bacteria, whose recombinant proteins are usually more stable and suitable for industrial biotechnological applications (Coker, 2016; Fujiwara, 2002). For this reason, the evolution of plant STS, identifying sequences of this enzyme in other kingdoms, and the expression of a recombinant protein from one of these sequences in *E. coli* was investigated.

1.2.1. Study of the conservation and evolutionary origin of plant STS

Following the criteria described in materials and methods, a screening of STS sequences from plants was carried out, obtaining a total of 19 sequences (Table 3). A multiple alignment with MUSCLE was carried out to assess the degree of conservation of the enzyme in the plant kingdom. In general, the alignment (Appendix 1) revealed a good conservation of the amino acid residues of plant STS. At most positions, the amino acids were identical in all sequences, and the main changes were conservative or semi-conservative substitutions. Most of the gaps were located at the beginning or end of the sequences due to variations in length, although there were also some gaps in specific areas of the sequences.

Table 3. STS sequences of plants selected for multiple alignment

UniProtKB code	Protein name	Plant
P28343	Stilbene synthase 1	*Vitis vinifera*
P51070	Stilbene synthase 2	*Vitis vinífera*
P51071	Stilbene synthase 3	*Vitis vinífera*
A5AEM3	Stilbene synthase 4	*Vitis vinífera*
A5C9M2	Stilbene synthase 5	*Vitis vinífera*
A2ICC6	Stilbene synthase 6	*Vitis vinífera*
P20178	Stilbene synthase 1	*Arachis hypogaea*
P51069	Stilbene synthase 3	*Arachis hypogaea*
Q84Q58	Stilbene synthase	*Rheum tataricum*
A0A140KXU0	Stilbene synthase STS1a	*Picea jezoensis*
G5CUA3	Stilbene synthase	*Picea glauca*
G5CU92	Stilbene synthase	*Picea sitchensis*
Q8LPP4	Stilbene synthase	*Parthenocissus henryana*
Q8LPP2	Stilbene synthase	*Parthenocissus quinquefolia*
Q8LPP3	Stilbene synthase	*Cissus rhombifolia*
Q9FEK7	Stilbene synthase	*Vitis labrusca*
Q9SLX8	Stilbene synthase	*Psilotum nudum*
Q1G0Y3	Stilbene synthase	*Phanera variegata*
B2MWQ8	Stilbene synthase	*Polygonum cuspidatum*

A Hidden Markov Model (HMM) was constructed with this multiple alignment using HMMER, to better analyse the conservation of amino acids in the sequences and, thus, to search for new sequences related to the STS family. In the complete model, that can be seen in Appendix 2, numerous positions with highly conserved residues and/or a single amino acid were observed. These residues matched those previously identified as relevant for the enzyme's cyclisation reactions (D. Y. Suh et al., 2000). For example, the histidine (H), asparagine (N) and proline (P) residues at positions 303, 336 and 375, respectively, largely define the active centre of the enzyme, while the proline at position 375 is part of a GFGPG loop, which extends from position 372 to 376, and contributes to the sidewall structure of the STS active site, influencing the outcome of cyclisation.

Next, a UniProtKB search was performed with the HMM to identify new sequences related to the STS family. The first results showed a total of 10000 eukaryotic

and 12650 bacterial sequences related to the analysed matrix, with the eukaryotic sequences being the most similar due to their lower E-value. Most of these sequences corresponded to STS proteins, to highly related CHS proteins or to yet uncharacterised proteins that could be related to the family, possibly STS not classified so far.

In order to analyse the origin and evolution of STS enzymes, the search was narrowed down to sequences from more distant organisms that could be precursors of those found in plants, i.e. bacterial or archaeal sequences. In the results, no known archaeal sequences were found that were related to the STS family, while the bacterial sequences that gave the highest similarity were CHS and type III polyketide synthases (Figure 28). Since STS, CHS and type III polyketide synthase proteins belong to the same PKS superfamily (Izumikawa et al., 2003), it is logical that they share domains and sequence similarities. In addition, uncharacterised proteins and STS from other bacteria such as *Paenibacillaceae bacterium*, *Paenibacillus* and *Bacillus* were also found among the related sequences.

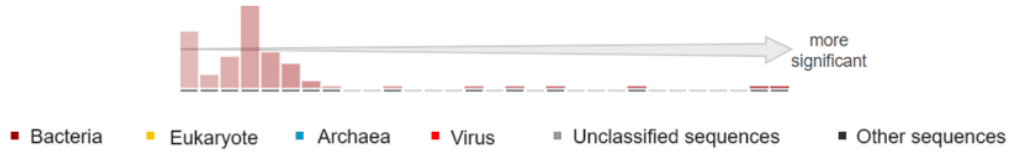

Figure 28. Distribution of bacterial sequences related to the designed HMM

To identify possible ancestral sequences of plant STS not collected in UniProtKB, the HMM obtained was compared with all genomes deposited in Ensembl. Although a first search yielded mainly eukaryotic transcripts, limiting the search to bacterial genomes yielded 9094 possible transcripts with similarity to the HMM. Most of these transcripts corresponded to CHS sequences, although some STS were also observed, especially predicted sequences in bacteria of the genus *Paenibacillus*. A similar search was launched

in the fungal genomes of Ensembl, obtaining mainly hypothetical proteins not yet studied and a small proportion of CHS and STS.

The phylogenetic tree was created with selected bacterial and fungal STS sequences obtained after HMM comparison, as well as the previously used plant sequences (Table 4). The selected fungal sequences were all those classified as STS obtained after submitting the HMM to the Ensembl fungal genome database. Meanwhile, the selected bacterial sequences were those classified as STS with lower E-value obtained by comparing the HMM to the Ensembl bacterial genome database. Subsequently, the redundancy of the *Paenibacillus* genus was removed from the bacterial sequences, keeping only a representative sample of the genus. In addition, the sequence of serpin B10 from *Homo sapiens* was included as a control for the creation of the phylogenetic tree as it was not related to STS.

Although some of these sequences are predicted, they suggest a wider distribution of STS than previously thought, being present in a wide variety of organisms, including bacteria of diverse environments and characteristics (marine, terrestrial, phototrophic, chemotrophic or halotolerant). Moreover, the bacterial genus found include diverse species used to promote plant growth, bioremediation processes and/or production of compounds of industrial interest (Daane et al., 2002; Dai et al., 2015; Gu and Dou, 2016; Lee et al., 2014; Luo et al., 2012; Msaddak et al., 2017; Park et al., 2009; Rodríguez-Díaz et al., 2005; Tanyildizi et al., 2005; White et al., 1996). Thus, the diversity of bacteria could be exploited in biotechnological applications to obtain enzymes with specific properties.

Table 4. STS sequences of plants, fungi and bacteria selected for STS phylogenetic tree

	UniProtKB code	Protein name	Organism
Plants	P28343	Stilbene synthase 1	*Vitis vinifera*
	P51070	Stilbene synthase 2	*Vitis vinifera*
	P20178	Stilbene synthase 1	*Arachis hypogaea*
	P51069	Stilbene synthase 3	*Arachis hypogaea*
	Q84Q58	Stilbene synthase	*Rheum tataricum*
	A0A140KXU0	Stilbene synthase STS1a	*Picea jezoensis*
	G5CUA3	Stilbene synthase	*Picea glauca*
	G5CU92	Stilbene synthase	*Picea sitchensis*
	Q8LPP4	Stilbene synthase	*Parthenocissus henryana*
	Q8LPP2	Stilbene synthase	*Parthenocissus quinquefolia*
	Q8LPP3	Stilbene synthase	*Cissus rhombifolia*
	Q9FEK7	Stilbene synthase	*Vitis labrusca*
	Q9SLX8	Stilbene synthase	*Psilotum nudum*
	Q1G0Y3	Stilbene synthase	*Phanera variegata*
	B2MWQ8	Stilbene synthase	*Polygonum cuspidatum*
Fungi	A0A0N0DHY2	Stilbene synthase 3	*Fusarium langsethiae*
	N4U208	Stilbene synthase 3	*Fusarium oxysporum*
	A0A0I9XL45	Stilbene synthase 2	*Gibberella fujikuroi*
Bacteria	A0A098M3J0	Stilbene synthase	*Paenibacillus wynnii*
	A0A1C1A4G7	Stilbene synthase	*Paenibacillus pectinilyticus*
	A0A0U2WE93	Stilbene synthase	*Phaenibacillus naphtalenovorans*
	A0A1B8VTV0	Stilbene synthase	*Bacillus sp.* FJAT-26390
	A0A0Q6GDM5	Stilbene synthase	*Rhodococcus sp.* Leaf7
	A0A0Q6JYE2	Stilbene synthase	*Rhodococcus sp.* Leaf258
	A0A1A7QMH1	Stilbene synthase	*Erythrobacter sp.* QSSC1-22B
	A0A0H0XQ51	Stilbene synthase	*Erythrobacter marinus*
	A0A1A5RNY4	Stilbene synthase	*Mesorhizobium sp.* WSM3873
	X6DPU4	Stilbene synthase	*Mesorhizobium sp.* LNHC252B00
	A0A086MHU8	Stilbene synthase	*Microvirga sp.* BSC39
	A0A1B2EAG2	Stilbene synthase	*Microvirga ossetica*
	A0A0Q5PA12	Stilbene synthase	*Sphingomonas sp.* Leaf343
	A0A147HVU9	Stilbene synthase	*Sphingomonas endophytica*
	A0A0B1ZM91	Stilbene synthase	*Novosphingobium malaysiense*
	A0A147ELF3	Stilbene synthase	*Novosphingobium barchaimii*
	A0A0T2QE93	Stilbene synthase	*Altererythrobacter sp.* Root672
	W9H2F6	Stilbene synthase	*Skermanella stibiiresistens* SB22

The phylogenetic tree was configured without curation to retain less conserved sequences, as it was the option that provided the most plausible results within the different possible configurations. The resulting tree showed a grouping of the sequences according

to their kingdom of origin, with bacterial, plant and fungal STS evolving from a common ancestor (Figure 29). The fungal sequences are classified together in a group, while the bacterial STS are divided into two groups, one close to the plant STS and one further away.

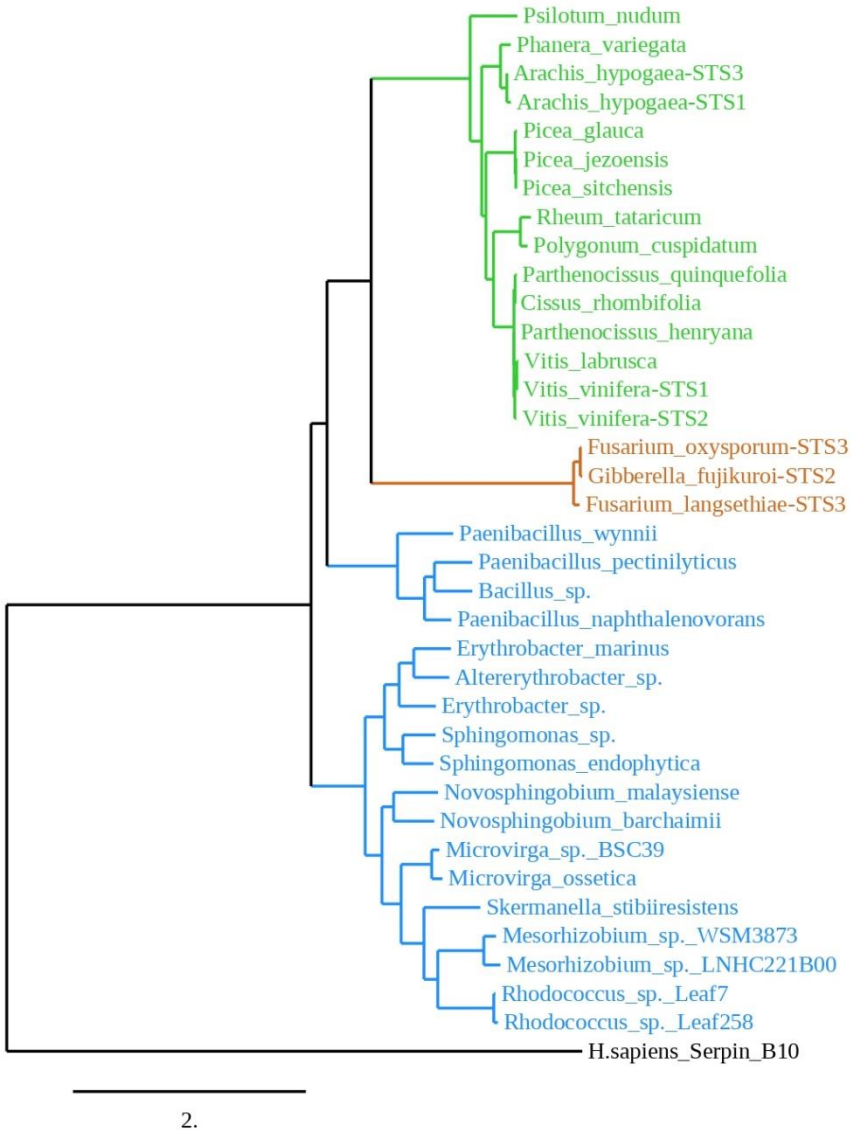

Figure 29. Phylogenetic tree from Table 4 sequences of plants (green), fungi (orange) and bacteria (blue)

Despite the paucity of STS sequences found in fungi, these were grouped as a distinct set (Figure 29), indicating that the analysis was not biased due to their lower representation. In addition, fungal STS were shown to be genetically closer to those of

plants, suggesting that both plant and fungal STS evolved from a common ancestor. On the other hand, the bacterial STS sequences were divided into two groups: one that included the sequences of the genus *Paenibacillus* and *Bacillus*, which appeared to be more similar to those of plants; and another group comprising the rest of the bacterial STS, forming a more distant phylogenetic branch (Figure 29). In the plant STS sequences, the fern, *Psilotum nudum*, was shown to be more distantly related than the other angiosperm and gymnosperm plants (Figure 29). These findings are consistent with evolutionary theories, which suggest that bacteria and their enzymes appeared first in evolution, followed by fungi and plants at later stages. Within the plant kingdom, evolution progressed from algae and mosses through ferns to angiosperms and gymnosperms, which would explain the clusters observed in this kingdom.

1.2.2. Study of the conservation of STS during evolution

A multiple alignment was performed in MUSCLE with the sequences selected in Table 4 to analyse the degree of conservation of the residues in the different kingdoms. Previously, all the sequences studied were checked to ensure that they shared the STS-specific N-terminal and C-terminal domains with the Pfam database (El-Gebali et al., 2019). In Appendix 3, it can be seen that the conservation of STS sequences was lower than that observed in plant STS (Appendix 1), probably due to the divergence of the sequences and the changes they may have undergone during the evolutionary process. Despite this, the amino acids that constitute the active centre of the enzyme appeared to be conserved in all sequences studied, such as cysteine (C) 164 and histidine (H) 303, which are involved in the condensation of *p*-coumaroyl-CoA with three molecules of malonyl-CoA (D.-Y. Suh et al., 2000), and asparagine (N) 336, which together with the GFGPG loop at positions 372 - 376, forms part of the sidewall of the enzyme active site (D. Y. Suh et al., 2000) (Appendix 3).

HMMs were then created with the sequences from each of the kingdoms studied and compared with each other in order to identify the most conserved regions, using the PRC software (Brandt and Heringa, 2009). The results of this analysis are shown below, coded with the letters (M) for matches, (D) for insertions or (I) for deletions, or with the symbol (~) indicating a placeholder that generally aligns with a deletion state.

Global alignment of plant (green) and bacterial (blue) HMM profiles:

```
MMMMMMMMMMMMMMMMMMMMMMMMMMMMMMMMMMMMMMMMMMMMMMMMMMMMMMMMMMMMMMMMMMMMMM
MMMMMMMMMMMIIMMMMMMMMMMMMMMMMMMMMMMMMMMMMMMMMMMMMMMMMMMMMMMMMMMMMMMMMM
MMMMMMMMMMMMMMMMMMMMMMMMMMMMMMMMMMMMMMMMMMMMMMMMMMMMMMMMMMMMMMMMMMMMMM
MMMMMMMMMMMMMMMMMMMMMMMMMMMMMMMMMMMMMMMMMMMMMMMMMMMMMMMMMMMMMMMMMMMMMM
MMMMMMMMMMMMMMMMMMMMMMMMMMMMMMMMMMMMMMMMMMMMMMMMMMMMMMMMMMMMMMMMMMMMMM
MMMMMMMMMMMMMMMMMMMMMMMMMMMMMMMMMMMMMMMMMMM
```

```
MMMMIIIIIIIIIMMMMMMMMMMMMMMMMMMMIMMMMMMMMMMIIIMMMMMMMMMMMMMMMMMMMMMMMM
MMMMMMMMMMMMMMMMMMMMMMMMMMMMMMMMMMMMMMMMMMMMMIIMMMMMMMMMMMMMMMMMMMMMMM
MMMMMMMMMMMMMMMMMMMMMMMMMMMMMMMMMMMMMMMMMMMMMMMMMMMMMMMMMMMMMIIMMMMMMM
MMMMMMMMMMMMMMMMMMMMMMIIIIIIMMMMMMMMMMMMMMMMMMMMMMMMMMMMMMMMMMMMMMMMMM
MMMMMMMMMMMMIMMMMMMMMMMMMMMMMMMMMMMMMMMMMMMMMMMMMMMMMMMMMMMMMMMMMMMMMM
MMMMMMMMMIIIIIIIIIMMMMMMMMMMMMMMMMMMMIIIMMM
```

Global alignment of plant (green) and fungal (orange) HMM profiles:

```
MMMMMMMMMMMMMMMMMMMMMMMMMMMMMMMMMMMMMMMMMMMMMMMMMMMMMMMMMMMMMMMMMMMMMM
MMMMMMMMMMMMMMMMMMMMMMMMMMMMMMMMMMMMMMMMMMMMMMMMMMMMMMMMMMMMMMMMMMMMMM
MMMMMMMMMMMMMMMMMMMMMMMMMMMMMMMMMMMMMMMMMMIIIMMMMMMMMMMMMMMMMMMMMMIII
MMMMMMMMMMMMMMMMMMMMMMMMMMMMMMMMMMMMMMMMMMMMMMMMMMMMMMMMMMMMMMMMMMMMMM
MMMMMMMMMMMMMMMMMIIIIIMMMMMMMMMMMMMMMMMMMMMMMMMMMMMMMMMMMMMMMMMMMMMMMM
MMMMMMMMMMMMMMMMMMMMMMMMMMMMMMMMMMMMMMMMMMMMMMMIIIIIIIIIIIIIIIIIIIIIII
IIIIIIIIIIIIIIIIIMIIIIIIIIIIIMMIMIIIIIIIIIIIMM
```

```
MMMMMMMMMMIIIIIMMMMMMMMMMMMMMMMMMMMMMMMMMMMIIIMMMMMMMMMMMMMMMMMMMMMMMM
MIIIIMMMMMMMMMMMMMMMMMMMMMMMMMMMMMMMMMMMMMMMMMMMMMMMMMMMMMMMMMMMMMMMMM
MMMMMMMMMMMMMMMMMMMMMMMMMMMMMMMMMMMMMMMMMMMMMMMMMMMMMMMMMMMMMMMMMMMMMM
MMMMMMMMMMMMMMMMMMMMMIMMMMMMMMMMMMMMMMMMMMMMMMMMMMMMMMMMMMMMMMMMMMMMMM
MMMMMMMMMMMMMMMMMMMMMMMMMMMMMMMMMMMMMMMMMMMMMMMMMMMMMMMMMMMMMMMMMMMMMM
MMMMMMMMMMMMMMMMMMMIMMMMMMMMMMMMMMMMMMMMMMMMMMMMMMMMMMMMMMMMMMMMMMMMMM
MMMMMMMMMMMMMMMMMIMMMMMMMMMMMIIMIMMMMMMMMMMMMM
```

Global alignment of fungal (orange) and bacterial (blue) HMM profiles:

```
MMMMMMMMMMMMMMMMMMMMMMMMMMMMMMMMMMMMMMMMMMMMMMMMMMMMMMMMMMMMMMMMMMM~~~
~~IMMMMMMMMMMMMMMMMMMMMMMMMMMMMMMMMMMMMMMMMMMMMMMMMMMMMMMMMMMMMMMMMMMM
MMMMMMMMMMMMMMMMMMMMMMMMMMMMMMMMMMMMMMMMMMMMMMMMMMMMMMMMMMMMMMMMMMMMMM
MMMMMMMMMMMMMMMMMMMMMMMMMMMMMMMMMMMMMMMMMMMMMMMMMMMMMMMMMMMMMMMMMMMMMM
MMMMMMMMMMMMMMMMMMMMMMMMMMMMMMMMMMMMMMMMMMMMMMMMMMMMMMMMMMMMMMMMMMMMMM
MMMMMMMMMMMMMMMMMMMMMMMMMMMMMMMMMMMMMMMMMMMMMMMMMMMMMMMMMMMMMMMMMMMMMM
MMMMMMMMMMMMMMMMMMMMMMMMMMMMMMMMMM

MMMMMMMIIIIMMMMMMMMMMMMMMMMMMMMMIMMMMMMMMMMMMMMMMMMMMMMMMMMMMMMMMMMDDD
DDMMMMMMMMMMMMMMMMMMMMMMMMMMMMMMMMMMMIIMMMMMMMMMMMMMMMMMMMMMMMMMMMMMMM
MMMMMMMMMMMMMMMMMMMMMMMMMMMMMMMMMMMIIIIMMMMMMMMMMMMMMMMMMMMMMIIIIIMMMM
MMMMMMMMMMMMMMMMMMMMMIIIIIMMMMMMMMMMMMMMMMMMMMMMMMMMMMMMMMMMMMMMMMMMMM
MMMMMMIIIIIIMMMMMMMMMMMMMMMMMMMMMMMMMMMMMMMMMMMMMMMMMMMMMMMMMMMMMMMMMM
MMMMMMMMMMMMIIIIIIIIIIIIIIIIIIIIIIIIIIIIIIIIIIIIIIIIIIIIIIIIIIIIIIIIII
IIIIIIIIIIIIMMMMMMMMMMMMMMMMMMMMMM
```

The three alignments showed a high degree of conservation as most positions were represented by an (M), indicating coincidence. Since the fungal STS sequences were longer than those of plants or bacteria, there was a higher number of insertions (I) in the comparisons of the fungal HMM with the HMMs of the other two kingdoms. Something similar was observed when comparing the HMM of plants with that of bacteria, due to the greater length of the plant sequences. Furthermore, only in the comparison between fungi and bacteria were deletions aligned with placeholders, suggesting a greater similarity between the STS of fungi and plants, which corroborates the distribution of these kingdoms in the phylogenetic tree created (Figure 29).

1.2.3. Search for STS in extremophilic microorganisms and thermostability of resveratrol

Since proteins from extremophilic bacteria are usually more resistant and suitable for biotechnological applications (Coker, 2016; Fujiwara, 2002), the previous HMM of STS was compared with the protein sequences of extremophilic bacteria deposited in

UniProtKB, specifically with the genus *Leptospirillum*, *Acidithiobacillus*, *Acremonium*, *Acrostalagmus*, *Halomonas*, *Thermotoga*, *Albidovulum*, *Thermococcus*, *Deinococcus*, *Microterricola* and *Cytophaga*, in the class Halobacteria and in the order Thermales. Possible STS were only found in *Meiothermus silvanus* (A0A4Q4KZ93) and *Meiothermus sp* (A0A323U6F3 and A0A370K1W9) of the order Thermales, which are thermophilic bacteria that inhabit natural thermal waters or artificial thermal environments, withstanding temperatures of over 45 °C. In addition, *M. silvanus* has known applications in the paper industry due to its ability to generate coloured biofilms (Sikorski et al., 2010).

Although these bacterial STS sequences were predicted, if the studied microorganisms show the STS activity and are able to produce resveratrol, the production of the recombinant enzyme could open new lines of research towards potential more heat-resistant STS. For this, it would be essential that the resveratrol is able to withstand high temperatures during the reaction time. For this reason, the thermostability of resveratrol in aqueous solution was evaluated by analysing the possible variation in its absorption spectrum at high temperature over time. The maximum incubation time was 5 days, based on similar reactions performed by other authors previously (Dai et al., 2022; Katsuyama et al., 2007; Thapa et al., 2019). The results revealed that this stilbene is able to withstand a temperature of 50°C for at least 5 days, with only a non-significant decrease of 0.075 mAU in its absorption spectrum (Figure 30). Therefore, it is likely that the resveratrol obtained after synthesis reactions with *Meiothermus* STS proteins remains stable under the possible optimal conditions of the enzyme, enabling its biotechnological application.

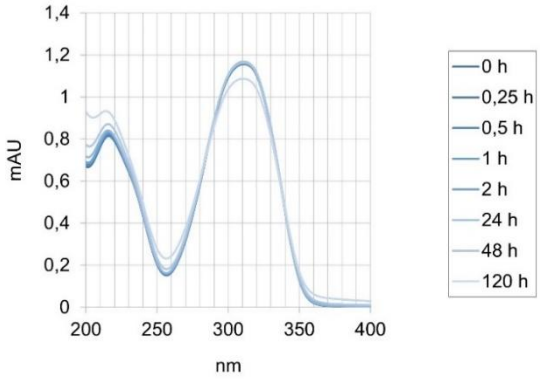

Figure 30. Absorption spectra of resveratrol in water during 5 days incubation at 50°C

1.2.4. Expression of STS from *Meiothermus sp*. Pnk-1 in *E. coli*

Following phylogenetic analysis of the bacterial STS family, the sequence of the STS found in the extremophile bacterium *Meiothermus sp*. Pnk-1 was selected to transform *E. coli* strains DH5α and Rosetta 2, using a pET-28a(+) vector. The resulting protein consisted of a total of 367 amino acids, giving a molecular mass of 39.12 kDa. The transformation efficiency of the DH5α strain was very low, only 2.5×10^2 CFU/µg DNA, while the transformation of Rosetta 2 reached 9.8×10^3 CFU/µg DNA.

Transformed colonies isolated from *E. coli* Rosetta 2 were induced to express the protein under different temperature conditions. Although a large part of the protein was observed to remain in the precipitated fraction, upon induction at 15, 20 and 30°C some of it was obtained in the soluble fraction, easily visualised as the most intense band between the 34 and 43 kDa markers of the gel (Figure 31). In general, soluble protein expression was highest at 20°C, followed by expression at 30°C and finally at 15°C. The concentration of the inducing agent had a variable effect depending on temperature, while at 30°C the lowest concentrations were the most productive, at 20°C, induction with 1.5 or 2 mM IPTG achieved the highest protein expression, with little difference between the two concentrations.

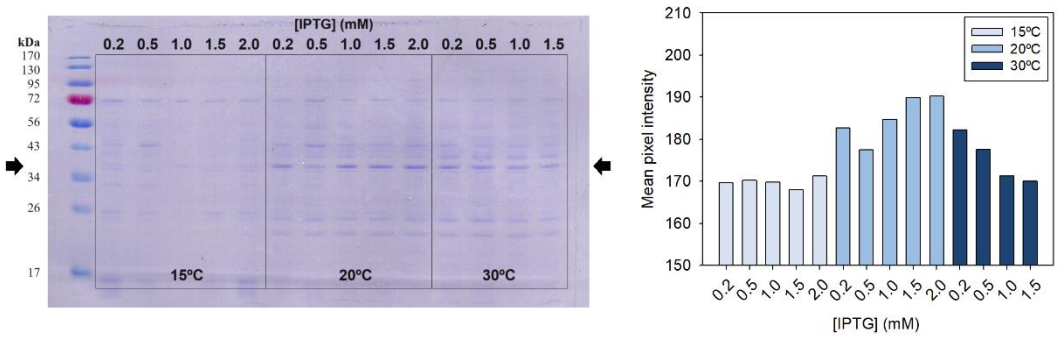

Figure 31. SDS-PAGE gel electrophoresis and quantification by image analysis of intracellular soluble recombinant protein (39.12 kDa) after induction of expression at various temperatures and IPTG concentrations

In addition, the culture media in which the cells were incubated during induction were analysed to find out whether any of the conditions studied led to secretion of the protein into the medium. Secreted proteins are easier to purify, which also facilitates their industrial scale-up. Although the amount of protein was very low, a light band around 39.12 kDa could be clearly detected when induction was carried out at 15°C, especially in the presence of 1.5 mM IPTG (Figure 32). Moreover, this band did not appear in culture media of untransformed *E. coli* Rosetta 2 cells incubated under the same conditions (Figure 33), suggesting that cells with the vector can excrete the recombinant protein into the extracellular medium when induced with 1.5 mM IPTG at 15°C.

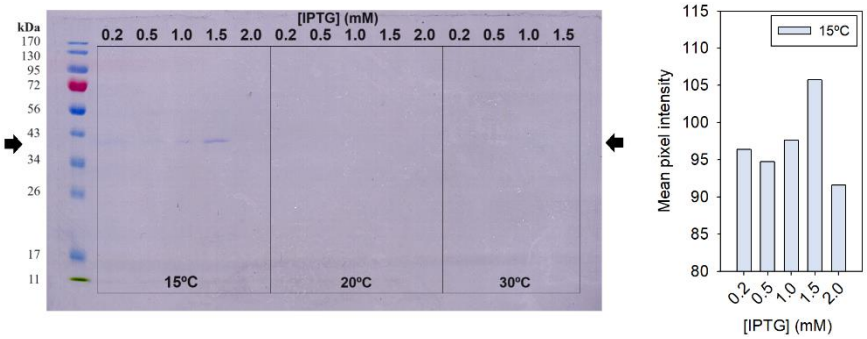

Figure 32. SDS-PAGE gel electrophoresis and quantification by image analysis of the recombinant protein (39.12 kDa) secreted into the extracellular medium after induction of expression at various temperatures and IPTG concentrations

Then, the intracellular recombinant protein was expressed on a larger scale so that it could be purified. Moreover, it was found that the recombinant protein band did not appear in untransformed *E. coli* Rosetta 2 cell culture media incubated under the same conditions (Figure 33). The unpurified expression samples showed a large amount of protein and cell debris because the volume used for resuspension of the cells was maintained during scale-up to optimise solvent expenditure. Although purification on histidine columns removed many of the non-specific proteins, it was not sufficient to obtain pure protein, as other bands, especially of higher molecular weight, were also observed (Figure 33). Therefore, further purification steps would be necessary to obtain a pure recombinant protein from cells that could be used to evaluate its possible enzymatic activity as an STS capable of synthesising stilbenes.

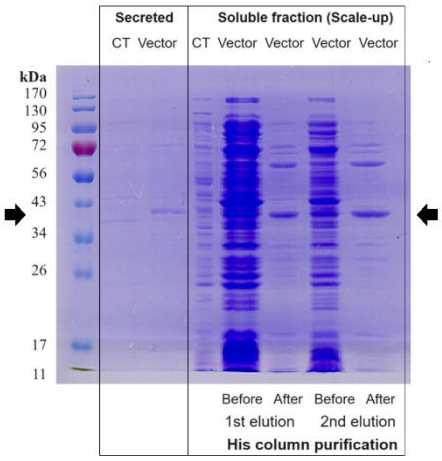

Figure 33. SDS-PAGE gel electrophoresis of expression samples with 1.5 mM IPTG at 15°C (Secreted) or 20°C (Soluble fraction), in transformed (Vector) or non-transformed (CT) cells, before or after purification with histidine columns

1.2.5. Study of the evolutionary relationship between STS and CHS

As mentioned above, research suggests that STS have evolved from CHS in multiple times and independently (Tropf *et al*., 1994). Thus, to better understand the phylogenetic origin of STS, it is crucial to study CHS, as they share a common ancestor.

To this end, a phylogenetic tree was constructed using the maximum likelihood method in TreeDyn format. This tree included both the bacterial STS described above and the CHS of those same strains or others of the same species or genus in case the studied strains did not have CHS (Table 5). In addition, bacterial sequences of chorismate synthase (CS) enzyme were added to obtain a tree with STS and CHS together in the same group.

Table 5. STS, CHS and CS sequences of bacteria selected for the phylogenetic tree

UniProtKB code			Microorganism
STS	**CHS**	**CS**	
A0A098M3J0	-	-	*Paenibacillus wynnii*
A0A1C1A4G7	-	-	*Paenibacillus pectinilyticus*
A0A098M3J0	-	-	*Paenibacillus pectinilyticus*
-	A0A3N6CKY0	A0A1L5LT27	*Paenibacillus xylanexedens*
A0A1B8VTV0	-	-	*Bacillus sp.* FJAT-26390
-	A0A0M4GE71	A0A0M5JIC6	*Bacillus sp.* FJAT-22090
A0A0Q6GDM5	-	-	*Rhodococcus sp.* Leaf7
A0A0Q6JYE2	-	-	*Rhodococcus sp.* Leaf258
-	N1MHL3	N1MD46	*Rhodococcus sp.* EsD8
A0A1A7QMH1	-	-	*Erythrobacter sp.* QSSC1-22B
A0A0H0XQ51	-	-	*Erythrobacter marinus*
-	A0A0G9MPL8	A0A0G9MK93	*Erythrobacter gangjinensis*
A0A1A5RNY4	-	-	*Mesorhizobium sp.* WSM3873
X6DPU4	-	-	*Mesorhizobium sp.* LNHC252B00
-	A0A1I5J7T6	A0A1I5LZL7	*Mesorhizobium sp.* NFR06
A0A086MHU8	-	-	*Microvirga sp.* BSC39
A0A1B2EAG2	-	-	*Microvirga ossetica*
-	I4YY57	I4YQ87	*Microvirga lotononidis*
A0A0Q5PA12	-	-	*Sphingomonas sp.* Leaf343
A0A147HVU9	-	-	*Sphingomonas endophytica*
-	J8VUC8	J8VVN7	*Sphingomonas sp.* LH128
A0A0B1ZM91	-	-	*Novosphingobium malaysiense*
A0A147ELF3	A0A561HGI2	A0A0J7XQM9	*Novosphingobium barchaimii*
A0A0T2QE93	-	-	*Altererythrobacter sp.* Root672
-	A0A369Q853	A0A369Q7D2	*Altererythrobacter sp.* HME9302
W9H2F6	-	-	*Skermanella stibiiresistens* SB22
-	A0A512DVH4	A0A512DKI7	*Skermanella aerolata*
A0A4Q4KZ93	-	-	*Meiothermus silvanus*
A0A323U6F3	-	-	*Meiothermus sp.* Pnk-1
A0A370K1W9	-	-	*Meiothermus sp.* QL-1
-	A0A511R5J9	A0A511R6N7	*Meiothermus hypogaeus* NBRC 106114

Unlike CS, STS and CHS did not form isolated clusters in the phylogenetic tree by the type of enzyme they encoded, and were shown grouped according to the bacterial genus of origin (Figure 34). This suggests that the similarity between STS and CHS from the same genus is higher than the similarity between STS from different genus or CHS from different genus. These results are consistent with previous observations by other authors in plant STSs, where STS cluster with CHS from the same or related plants (Tropf et al., 1994). Taken together, these results support the hypothesis that STS have evolved from CHS at various times and independently.

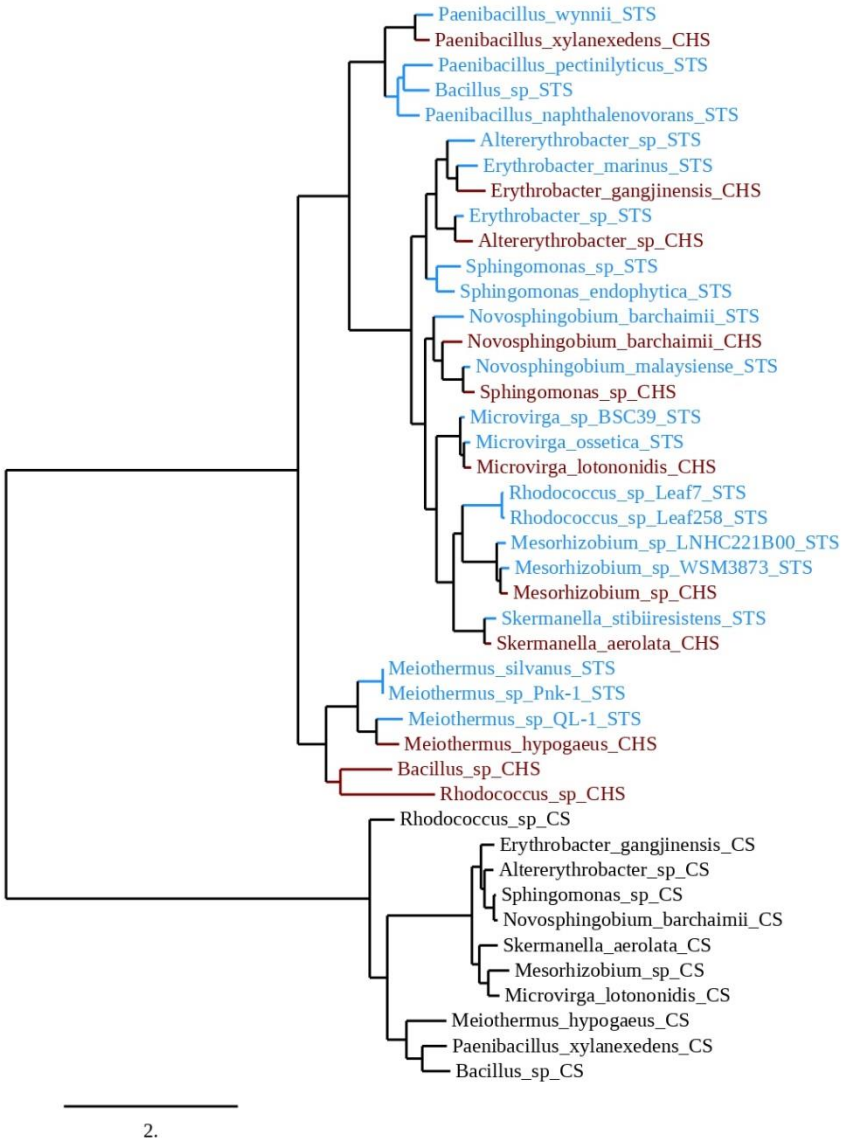

Figure 34. Phylogenetic tree from sequences in Table 5 of STS (blue), CHS (red) and CS (black) of bacteria

1.3. Conclusions on strategies to increase stilbene production

Since stilbenes are produced in low amounts in only a few higher plant species, two different strategies have been developed that could help to create new lines to increase stilbene production. On the one hand, a method for the synthesis of piceatannol from resveratrol was achieved using the enzyme tyrosinase as a catalyst. The use of ascorbic acid during this reaction achieved the highest production of piceatannol, especially when administered at a concentration of 100 μM, where the conversion rate reached 56 %. The addition of catechol caused the opposite effect by accelerating the reaction, leading to the formation of other more oxidised products. Finally, the use of β-CD delayed the oxidation of resveratrol, but did not significantly increase the production of piceatannol, unless it was administered together with ascorbic acid.

Furthermore, bioinformatic studies on the evolutionary origin of plant STS, key enzymes in the biosynthesis of stilbenes, revealed that these proteins may also be present in other kingdoms, such as fungi and bacteria, maintaining a higher degree of conservation with the former than with the latter, in line with evolutionary theories. Furthermore, phylogenetic analyses supported the theory that bacterial STS could have developed from CHS independently within each bacterial genus. Finally, some STS sequences were found in extremophilic microorganisms of the genus *Meiothermus*, and recombinant protein expression of the *Meiothermus sp*. Pnk-1 strain was optimised in *E. coli*. The highest concentration of soluble protein in the cells was reached upon induction of expression with 1.5 mM IPTG at 20°C, while secreted protein was detected in the extracellular medium upon induction at 15°C. Overall, these results could help in the development of new STS enzymes for the production of stilbenes, which may be more stable than the current ones from plants as they are derived from thermophilic bacteria.

2. CHARACTERISATION AND MOLECULAR ENCAPSULATION OF NATURAL STILBENES

As described in the introduction, there are stilbenes that have shown better properties than resveratrol, but their low solubility and ease of degradation, as well as the lack of physicochemical characterisation, hinder scientific progress with these stilbenes. In this Section, the molecular encapsulation in natural and modified CDs of the resveratrol analogues gnetol, isorhapontigenin, rhapontigenin and pinostilbene was evaluated using the Benesi-Hildebrand method and molecular docking, in order to determine the stoichiometry of the inclusion complexes and the encapsulation constants, as well as to visualise the complexes and their possible interactions. Before, the optical properties of these stilbenes were studied, determining their absorptivity. Moreover, since the pH of the medium can alter the protonation state of stilbenes and the temperature can affect the hydrogen bonds that stabilise the inclusion complexes, these two parameters were also considered in the determination of the encapsulation constants of the different complexes. Finally, the water solubility and stability of the free and complexed stilbenes were evaluated to find whether molecular encapsulation was able to improve these properties, thus allowing the development of stable formulations for human administration.

2.1. Gnetol

Gnetol (*trans*-2',3,5,6'-tetrahydroxystilbene) is a hydroxylated stilbene from plants of the genus *Gnetum*. Although many of the studies on its bioactivity have been conducted with plant extracts rather than the isolated compound, it has been reported to have anti-inflammatory, antithrombotic, cardioprotective and anticancer activity, due to its ability to inhibit COX-1, tyrosinase, acetylcholinesterase, histone deacetylase, CYP2C9 and CYP3A4 (Barua et al., 2015; Cahyana and Ardiansah, 2016; Dvorakova

and Landa, 2017; Jinadatta et al., 2019). In addition, in rats, it has been shown to be less bioavailable than resveratrol but has a longer half-life after oral administration (Akinwumi et al., 2018).

2.1.1. Optical properties of gnetol

The absorption spectrum of gnetol showed a similar shape to that of resveratrol, differing in a bathochromic shift of 4 nm at its λ_{max} and a distinct shoulder near 337 nm (Figure 35A). Concentrations of gnetol between 1 and 50 μM gave a high linearity with the absorbance at 310 nm ($R^2 > 0.999$), establishing a molar absorptivity value of 40003 $M^{-1}cm^{-1}$. In contrast, the emission spectrum of gnetol showed a peak with λ_{em} at 503 nm and a secondary peak of lower intensity near 390 nm (Figure 35B), reaching an emission wavelength considerably further away from that of resveratrol (Table 1). It seems that the 2',6'-hydroxyl substitution makes stilbenes emit fluorescent at higher wavelengths.

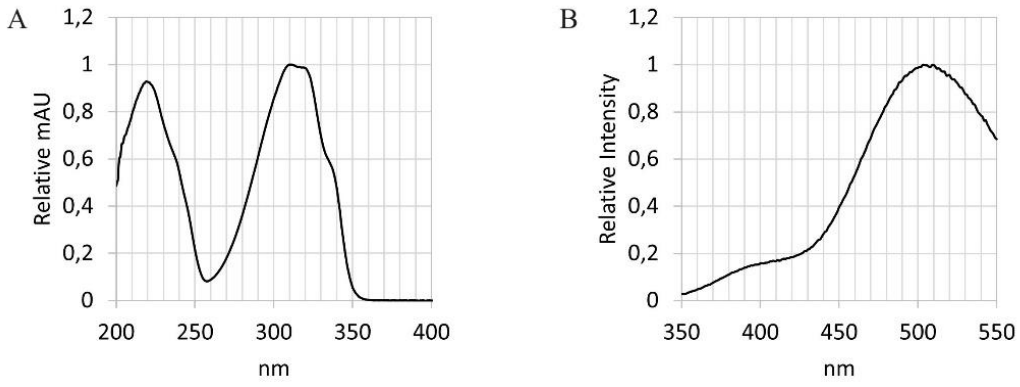

Figure 35. A) Absorption and B) emission spectra (λ_{ex} =290 nm) of gnetol in ethanol and 0.1 M phosphate buffer pH 7, respectively

2.1.2. Physicochemical study of the gnetol inclusion complexes

The molecular encapsulation of gnetol was monitored by determining its relative fluorescence upon addition of CDs. Complexation curves with β-CD and its modified CDs showed a rapid increase in fluorescence intensity, reaching an almost stable value at

4 mM β-CD and 2 mM HP-β-CD or M-β-CD (Figure 36A). However, α-CD and γ-CD were not as efficient in increasing the fluorescence signal of gnetol, which was reflected in their lower encapsulation constants (Table 6).

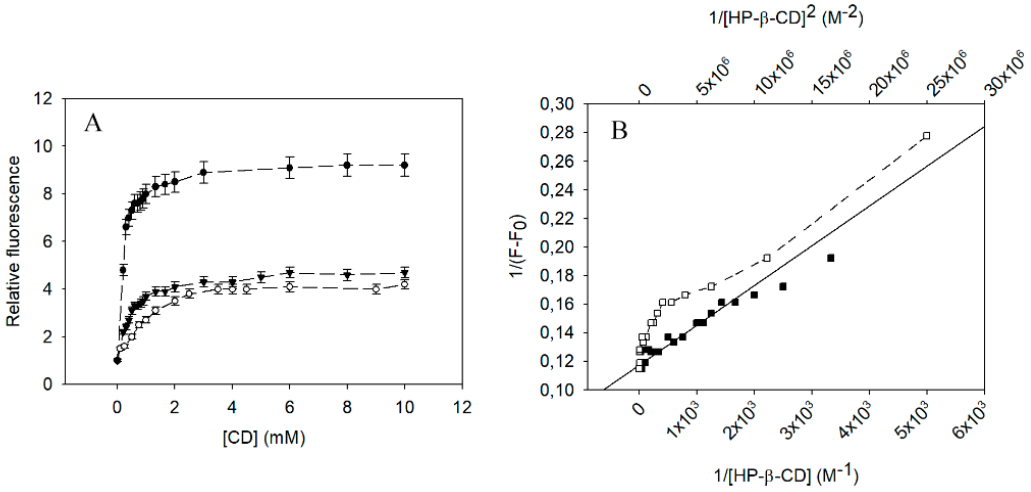

Figure 36. A) Complexation curves of gnetol in (○) β-CD, (●) HP-β-CD and (▼) M-β-CD. B) Stoichiometric fitting of gnetol inclusion complexes with HP-β-CD to a (■) 1:1 and (□) 1:2 model by the Benesi-Hildebrand method (25 °C pH 7)

All CDs showed a lower linear correlation when a 1:2 model was assumed with the Equation (7), indicating that the stoichiometry of the inclusion complexes was 1:1 (Table 6 and Figure 36B). This means that one CD molecule interacts with only one gnetol molecule (Equation 4). This stoichiometry matches that of other stilbenes (López-Nicolás et al., 2009a, 2009b; Matencio et al., 2016).

Table 6. Encapsulation constants and correlation coefficients obtained by the Benesi-Hildebrand method (Equation 7) and molecular docking score of the gnetol inclusion complexes with different CDs (25 °C pH 7)

CD	K_F (M^{-1})	R^2		Score
		1:1 model	1:2 model	
α-CD	161.35 ± 8.07	0.988	0.874	-7.3
β-CD	597.93 ± 29.90	0.996	0.959	-9.6
γ-CD	60.29 ± 3.01	0.983	0.956	-6.8
HP-β-CD	4542.90 ± 227.15	0.951	0.938	-11.1
M-β-CD	2756.92 ± 137.85	0.976	0.790	-9.7

By determining the encapsulation constants for each complex, it could be found that the modified CDs formed the best inclusion complexes with gnetol, with K_F of

4542.90 ± 227.15 M^{-1} and 2756.92 ± 137.85 M^{-1}, using HP-β-CD and M-β-CD, respectively (Table 6). Among the natural CDs, β-CD formed the most stable complexes with K_F of 597.93 ± 29.90 M^{-1}, while α-CD and γ-CD were the least efficient CDs to complex gnetol, with $K_F < 200$ M^{-1}.

2.1.3. Molecular docking of gnetol in CDs

The score values obtained from the molecular docking of gnetol with each CD studied correlated well with the experimental results (Table 6). The score is proportional to the binding strength between two molecules coupled with non-covalent interactions. The higher the bond strength between the molecules, the lower the score.

As expected from the fluorometric assays, the complex with HP-β-CD gave the lowest score (score = -11.1), followed by M-β-CD and β-CD which gave similar results (score = -9.7 and -9.6, respectively), and finally α-CD (score = -7.3) and γ-CD (score = -6.8). Therefore, it seems that the CD structure with 7 glucose rings is the most suitable for gnetol encapsulation.

Three-dimensional modelling of the complexes showed that β-CD (Figure 37B), γ-CD (Figure 37C), HP-β-CD (Figure 37D) and M-β-CD (Figure 37E) mainly trapped gnetol by the 2',6'-hydroxyl ring and part of the methylene bridge (except M-β-CD), while α-CD (Figure 37A) interacted mainly with the 3,5-hydroxyl ring and the methylene bridge. It highlights that the orientation of the guest molecule in the cavity of natural and modified β-CDs differs from α-CD and γ-CD. Gnetol enters β-CD, HP-β-CD and M-β-CD with the 2',6'-hydroxyl ring oriented downward from the secondary face (wider) to the primary face (narrower) of the CD, i.e. from the part of the CD where the secondary hydroxyl groups are positioned to the part of the CD where the primary hydroxyl groups are positioned (Figure 37B, D and E). Meanwhile, in the complexes with α-CD and γ-

CD, the 3,5-hydroxyl ring of gnetol is oriented downward from the secondary face to the primary face of the CD (Figure 37A and C). These variations in the interaction between host and guest molecules could explain the different affinity and K_F values obtained by fluorescence spectroscopy.

On the other hand, the formation of hydrogen bonds in the coupling of gnetol with HP-β-CD and β-CD is noteworthy. These weak interactions help to stabilise the inclusion complexes and their presence is corroborated by the higher encapsulation constants obtained for natural and modified β-CDs (Table 6).

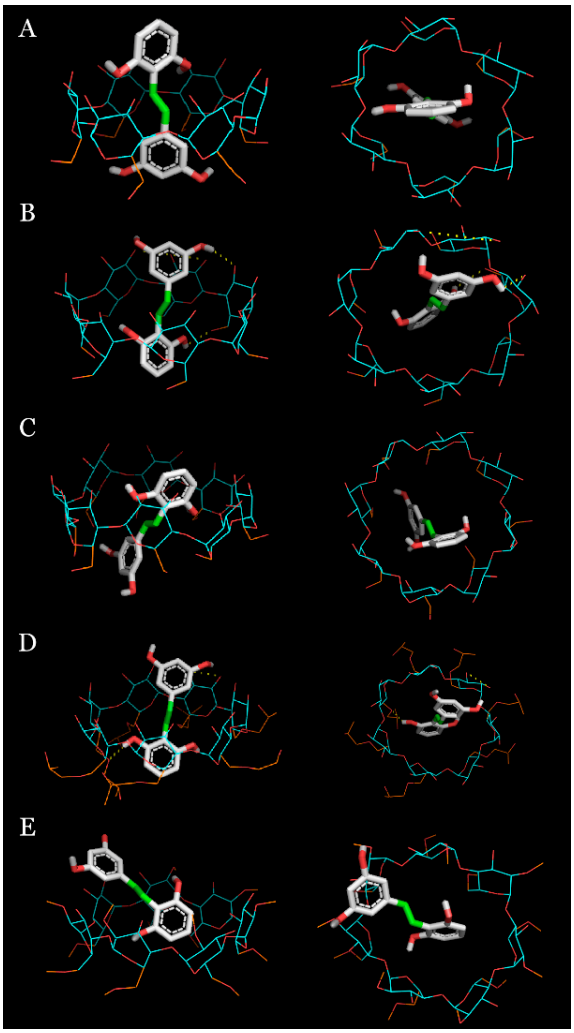

Figure 37. 3D molecular docking of gnetol in A) α-CD, B) β-CD, C) γ-CD, D) HP-β-CD and E) M-β-CD. The flexible atoms of the CD are displayed in orange, while the non-flexible atoms are displayed in blue. Possible hydrogen bonds are shown as yellow dotted lines

2.1.4. Influence of pH and temperature on gnetol encapsulation

As mentioned above, variations in pH or temperature, which can occur during industrial processes and the shelf life of a product fortified with stilbenes, can affect the stability of the inclusion complexes by altering the protonation state and interactions between molecules. For this reason, the encapsulation constants were determined at different pH and temperature conditions with the best tested CDs.

The encapsulation constants decreased with increasing pH, indicating that the inclusion complexes were more stable at lower pH values (Figure 38A). While the HP-β-CD and M-β-CD constants showed a slight decrease from acidic to neutral pH and a pronounced decrease from neutral to alkaline pH, the βCD constant decreased steadily to alkaline pH. The overall change of encapsulation constants from acidic to basic pH was highest for HP-β-CD (75 %), followed by M-β-CD (68 %) and β-CD (55 %). This behaviour was similar to that of other stilbenes such as resveratrol (López-Nicolás and García-Carmona, 2008b) and piceatannol (Matencio et al., 2016), where the marked decrease in constants from pH 9 onwards was associated with the dissociation constant of the stilbene, at which its hydroxyl groups deprotonate. It is possible that the dissociation constants of gnetol are similar to those of its analogues, and that CDs have a higher affinity for the protonated form of gnetol than the deprotonated form.

Similarly, the encapsulation constants showed a decreasing trend with increasing temperature (Figure 38B), as has been described for other stilbenes such as resveratrol (López-Nicolás and García-Carmona, 2008b), oxyresveratrol (Rodríguez-Bonilla et al., 2010) and piceatannol (Matencio et al., 2016). With HP-β-CD, the encapsulation constant decreased by 23 % when the temperature increased from 15 °C to 25 °C, and by 61 % when the temperature reached 35 °C. Meanwhile, the M-β-CD constant hardly changed

at low temperatures and decreased by 47 % from 25 °C to 35 °C. On the other hand, the β-CD constant decreased by 59 % from 15 °C to 25 °C and remained stable up to 35 °C (Figure 38B).

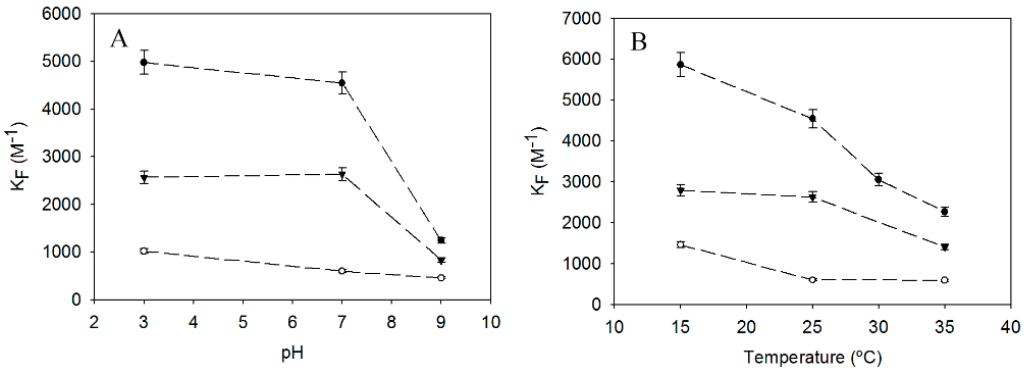

Figure 38. Effect of A) pH and B) temperature on the encapsulation constants of gnetol inclusion complexes with (○) β-CD, (●) HP-β-CD and (▼) M-β-CD

The gnetol complex with HP-β-CD was selected to determine the thermodynamic parameters with the encapsulation constants at 15, 25, 30 and 35 °C using Equations (8) and (9). The negative value obtained for the enthalpy changes (ΔH° = -34.93 ± 1.75 kJ/mol) revealed that the encapsulation process was exothermic, more so than the encapsulation of other stilbenes such as oxyresveratrol (ΔH° = -32. 61 ± 1 kJ/mol), piceatannol (ΔH° = -24.6 ± 1.2 kJ/mol) or resveratrol (ΔH° = -22.56 kJ/mol) (López-Nicolás and García-Carmona, 2008b; Matencio et al., 2016; Rodríguez-Bonilla et al., 2010). These results have previously been associated with hydrophobic interactions due to the displacement of water molecules from the internal cavity of the CD, increased Van der Waals interactions between molecules and hydrogen bond formation, among other interactions. The entropy changes were also negative (ΔS° = -48.52 ± 2.43 J/mol), indicating that complexation leads to a more ordered system, probably due to the decreased translational and rotational degrees of freedom of the complexed gnetol compared to the free gnetol. Previous studies with other stilbene analogues showed that

complexation of oxyresveratrol gave a lower entropy than that of gnetol (ΔS° = -56.13 ± 2 J/mol), while complexation of resveratrol and piceatannol gave a higher value (ΔS° = -12.30 and -3.7 ± 0.2 J/mol, respectively) (López-Nicolás and García-Carmona, 2008b; Matencio et al., 2016; Rodríguez-Bonilla et al., 2010). The process was spontaneous because the Gibbs free energy change was negative (ΔG° = -33.72 ± 1.69 kJ/mol at 25 °C). Compared to other stilbenes, the encapsulation of gnetol was more spontaneous than the encapsulation of piceatannol (ΔG° = -23.5 ± 1.2 kJ/mol at 25 °C), resveratrol (ΔG° = -18.89 kJ/mol at 25 °C) and oxyresveratrol (ΔG° = -15.88 ± 1 kJ/mol at 25 °C) (López-Nicolás and García-Carmona, 2008b; Matencio et al., 2016; Rodríguez-Bonilla et al., 2010).

2.1.5. Solubility and stability of free and encapsulated gnetol

It was also tested whether molecular encapsulation of gnetol in HP-β-CD (the most optimal CD for its encapsulation) was able to improve some of its limitations in terms of water solubility and stability in aqueous solution.

In the absence of CDs, the water solubility of gnetol was 0.31 mg/mL, which was slightly lower than the solubility of other hydroxylated stilbenes, such as piceatannol (0.50 mg/mL (Kershaw and Kim, 2017)) or oxyresveratrol (0.75 mg/mL (Suzuki et al., 2019)). However, the highest concentration of HP-β-CD was able to solubilise 0.82 mg of gnetol in one millilitre of water, i.e. almost three times the basal solubility (Figure 39A). Lower concentrations of CD also gave significant differences, achieving a 62 % increase in the aqueous solubility of this stilbene when supplemented with only 1 mM HP-β-CD.

The shelf life of gnetol after 7 days storage also improved with the presence of CDs (Figure 39B). While 25 % and 44 % of the initial gnetol was degraded in free form

at 4 °C and 25 °C storage, respectively, inclusion complexes with more than 1 mM HP-β-CD retained the initial amount of stilbene. One day storage made no differences.

Temperature proved to be a relevant factor in the preservation of this bioactive compound when it was in free or partially complexed form (1 mM HP-β-CD), giving a higher degradation when stored at room temperature (Figure 39B). In contrast, fully complexed gnetol was very stable at both temperatures, and advantage for storage, distribution and marketing of fortified products. It appears that encapsulation in CDs is an effective technique to better preserve gnetol, even more than refrigerated storage alone.

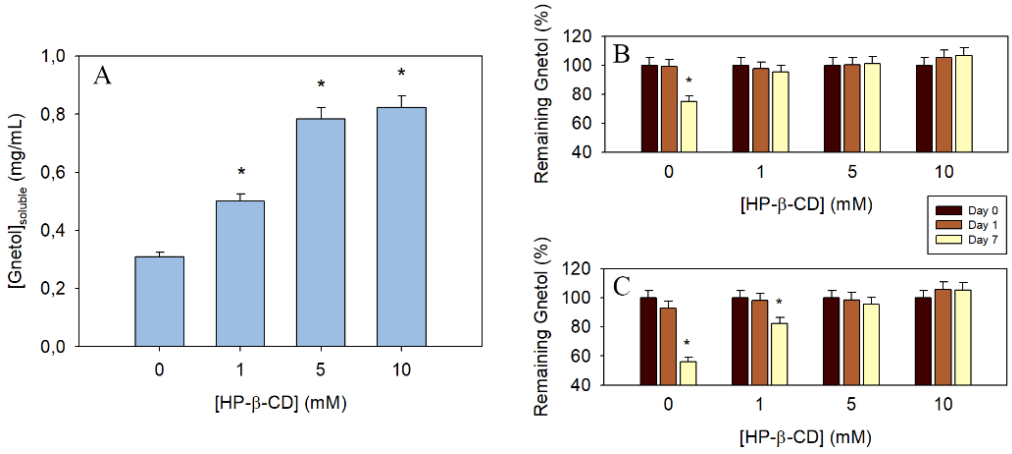

*Figure 39. A) Aqueous solubility of gnetol in the absence and presence of different concentrations of HP-β-CD (25 °C). Stability of free and encapsulated gnetol in HP-β-CD after storage at B) refrigeration (4 °C pH 7) and C) room temperature (25 °C pH 7). * Significance p-value < 0.05*

2.2. Isorhapontigenin

Isorhapontigenin (*trans*-3,4′,5-trihydroxy-3'-methoxystilbene) is a methoxylated stilbene found in Asian medicinal plants such as *Gnetum cleistostachyum* and in grapes (Fernández-Marín et al., 2012). It has a similar structure to resveratrol and piceatannol, but with a methoxy group on the R3' radical. This slight difference in structure makes it more bioavailable than resveratrol and therefore a better candidate for oral administration (Dai et al., 2018). However, the methoxy group may also negatively affect the water

solubility of this stilbene. Furthermore, isorhapontigenin is an active metabolite of piceatannol, the biotransformation of which is mediated by the enzyme catechol-O-methyl transferase (COMT) and is capable of transforming 17.70 % of intravenously administered piceatannol into isorhapontigenin in rats (Dai et al., 2020). Although further comparative studies on the biological activity of this stilbene and its analogues are still needed, a recent review has described it as a successor to resveratrol (Pecyna et al., 2020), for its antioxidant (Lu et al., 2017, 2015), anti-inflammatory (Ma et al., 2019), antimicrobial (Zakova et al., 2018), cardioprotective (Abbas, 2016; Ravishankar et al., 2019), anticarcinogenic (Fang et al., 2013, 2012; Luo et al., 2020; Subedi et al., 2019; N. Zhang et al., 2021; Zhu et al., 2018), anti-diabetic (Chu et al., 2020) and neuroprotective (Sun and Cui, 2020; Xue et al., 2021) activity (Abbas, 2016; Chu et al., 2020; Fang et al., 2013, 2012; Lu et al., 2017, 2015; Luo et al., 2020; Ma et al., 2019; Ravishankar et al., 2019; Subedi et al., 2019; Sun and Cui, 2020; Xue et al., 2021; Zakova et al., 2018; N. Zhang et al., 2021; Zhu et al., 2018).

2.2.1. Optical properties of isorhapontigenin

The absorption spectrum of isorhapontigenin showed a similar shape to that of its hydroxylated analogue piceatannol, with λ_{max} at 326 nm and a small shoulder near 305 nm (Figure 40A). Fernández-Marín *et al*. (2012) obtained a similar λ_{max} value of 325 nm for isorhapontigenin (Fernández-Marín et al., 2012). Concentrations of this stilbene between 1 and 50 μM gave a high linearity with the absorbance at 326 nm ($R^2 > 0.999$), establishing a molar absorptivity value of 39769 $M^{-1}cm^{-1}$. On the other hand, the emission spectrum of isorhapontigenin showed a single peak with λ_{em} at 410 nm after being excited at 290 nm (Figure 40B).

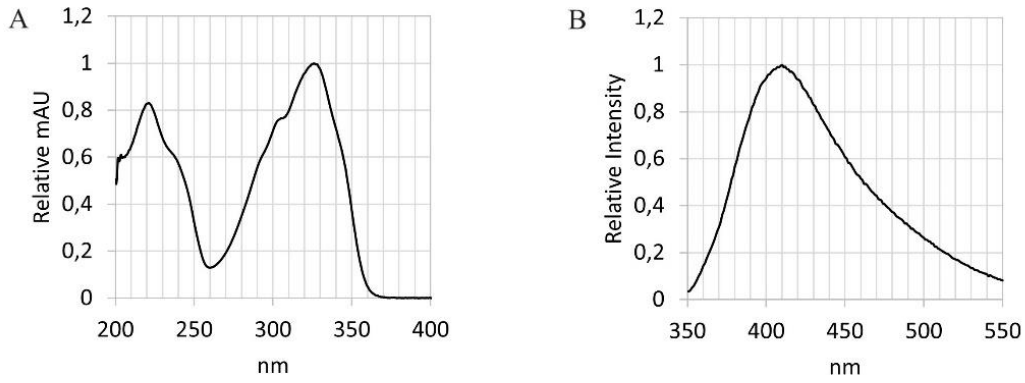

Figure 40. A) absorption and B) emission spectra (λ_{ex} = 290 nm) of isorhapontigenin in ethanol and 0.1 M phosphate buffer pH 7, respectively

2.2.2. Physicochemical study of the inclusion complexes with isorhapontigenin

As gnetol encapsulation (Section 2.1.2.), the fluorescence of isorhapontigenin increased when CDs were added to the solutions in a concentration-dependent manner, probably due to increased molecular rigidity (López-Nicolás and García-Carmona, 2010) (Figure 41A). Except for γ-CD, all CDs were able to increase the fluorescence signal sufficiently to determine the stoichiometry and the encapsulation constant of the inclusion complex (Table 7).

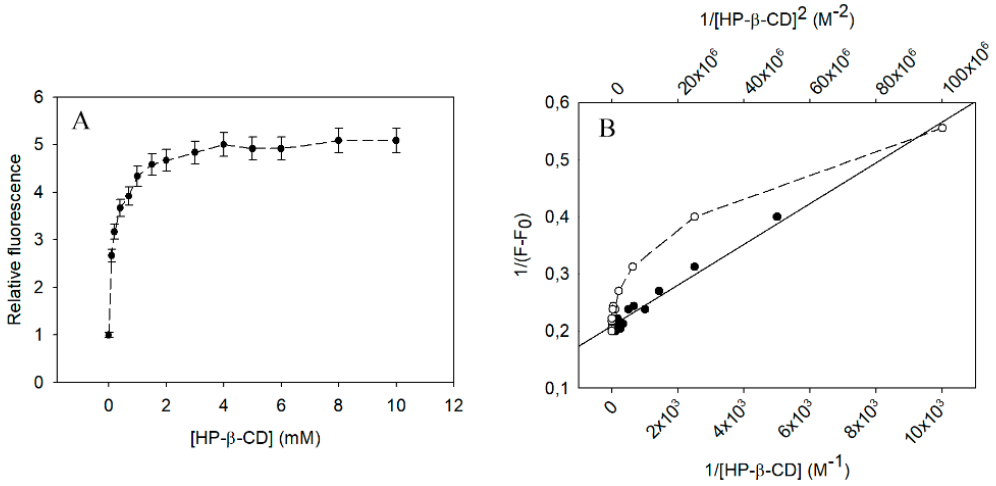

Figure 41. A) Complexation curve of isorhapontigenin in HP-β-CD. B) Stoichiometric fitting of isorhapontigenin inclusion complexes with HP-β-CD to a (●) 1:1 and (○) 1:2 model by the Benesi-Hildebrand method (25 °C pH 7)

By linear fitting of the Benesi-Hildebrand method it could be observed that the complexation model was a 1:1 (Figure 41B), i.e. one CD molecule interacts with one isorhapontigenin molecule. This stoichiometry matches that previously observed when encapsulating other stilbenes in CDs (López-Nicolás et al., 2009a, 2009b; Matencio et al., 2016).

Among the natural CDs (Table 7), the complex with β-CD (K_F = 3518.86 ± 175.94 M^{-1}) was more stable than the complex with α-CD (K_F = 1265.55 ± 63.28 M^{-1}) and γ-CD (K_F not determined). On the other hand, the modified CDs improved the efficiency of isorhapontigenin encapsulation, reaching higher encapsulation constants than with natural CDs. Specifically, the complex with HP-β-CD achieved the best constant (K_F = 6295.78 ± 314.79 M^{-1}), while that with M-β-CD (K_F = 3823.47 ± 191.17 M^{-1}) was similar to that obtained with β-CD.

Table 7. Encapsulation constants and correlation coefficients obtained by the Benesi-Hildebrand method (Equation 7) and molecular docking score of isorhapontigenin inclusion complexes with different CDs (25 °C pH 7)

CD	K_F (M^{-1})	R^2		Score
		1:1 model	1:2 model	
α-CD	1265.55 ± 63.28	0.932	0.719	-6.9
β-CD	3518.86 ± 175.94	0.709	0.467	-9.3
γ-CD	-	-	-	-6.6
HP-β-CD	6295.78 ± 314.79	0.992	0.925	-10.2
M-β-CD	3823.47 ± 191.17	0.942	0.744	-8.9

This CD preference order was similar to that obtained with the analogue piceatannol (K_F = 14048 ± 702 M^{-1}) in a previous study (Matencio et al., 2016), although the encapsulation constants with isorhapontigenin were lower, probably because the hydroxyl group lost in isorhapontigenin decreases the interaction with CD, forming fewer hydrogen bonds, one of the most important interactions in this type of complexation. As with piceatannol, the best CD to encapsulate isorhapontigenin was HP-β-CD, which

reached a plateau in the fluorescence signal at 3 mM (Figure 41A), indicating that above that concentration all molecules are forming a complex with the CDs.

2.2.3. Molecular docking of isorhapontigenin in CDs

The computational results of isorhapontigenin complexation were in agreement with the experimental results. The lowest score was obtained with HP-β-CD (score = -10.2) (Table 7), indicating that the encapsulation of isorhapontigenin on this CD was more efficient than with the other CDs. In order of score, encapsulation with HP-β-CD, was followed by that with β-CD (score = -9.3), M-β-CD (score = -8.9), α-CD (score = -6.9) and finally γ-CD (score = -6.6).

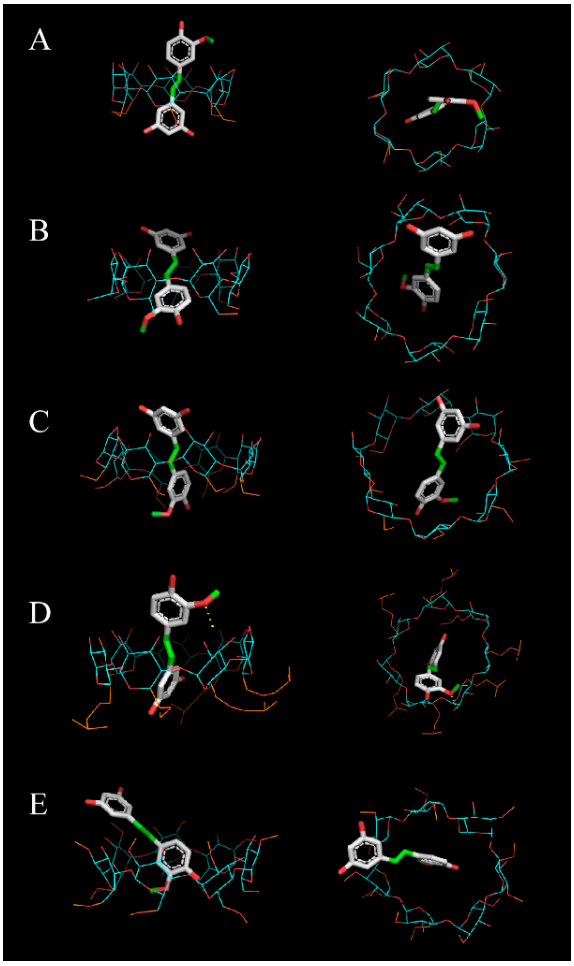

Figure 42. 3D molecular docking of isorhapontigenin in A) α-CD, B) β-CD, C) γ-CD, D) HP-β-CD and E) M-β-CD. The flexible atoms of CD are displayed in orange, while the non-flexible atoms are displayed in blue. Possible hydrogen bonds are shown as yellow dotted lines

In addition, the three-dimensional configurations of each inclusion complex (Figure 42) showed the formation of hydrogen bonds between the oxygen of the methoxy group of isorhapontigenin and a hydrogen of the secondary face of HP-β-CD, which could explain the better results obtained with this CD.

2.2.4. Influence of pH and temperature on isorhapontigenin encapsulation

The pH of the medium proved to be able to alter the encapsulation constants of inclusion complexes with the best tested CD, HP-β-CD. At acidic and neutral pH, the variation of the constant did not exceed 10 %, maintaining a K_F value > 6000 M^{-1} (Figure 43A). However, above pH 7, the constants decreased drastically, especially at pH 11, where K_F = 2306.30 ± 115.31 M^{-1}, i.e. a 63 % decrease with respect to neutral pH. As described in the previous Section on the molecular encapsulation of gnetol, this behaviour has previously been associated with the pH region where the protonation state of the molecule changes. It appears that the fully protonated form of isorhapontigenin forms the most stable complexes with CDs, probably due to the formation of hydrogen bonds.

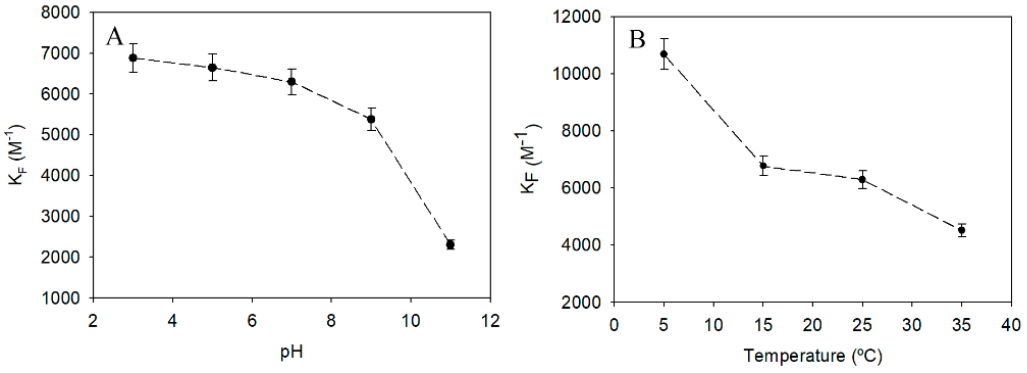

Figure 43. Effect of A) pH and B) temperature on the encapsulation constants of isorhapontigenin inclusion complexes with HP-β-CD

The study of the molecular encapsulation of isorhapontigenin at different temperatures revealed that the most stable inclusion complexes were formed at lower temperatures (Figure 43B), reaching a K_F = 10686.72 ± 534.34 M^{-1} under cooling conditions (5 °C). At 15 °C, 25 °C and 35 °C, the encapsulation constant decreased by 37 %, 41 % and 58 %, respectively, reaching a K_F = 4520.16 ± 226.00 M^{-1} at the highest temperature analysed.

The thermodynamic parameters were calculated using Equations (8) and (9). The encapsulation reaction was found to be exothermic with an enthalpy ΔH° = -18.95 ± 0.95 kJ/mol, probably due to the displacement of the water molecules from the CD cavity to accommodate the guest molecule. In contrast, the entropy value was positive (ΔS° = 8.53 ± 0.43 J/mol), which differs from previous results with other stilbenes, such as piceatannol, gnetol or oxyresveratrol ((Matencio et al., 2017a, 2016) and Section 2.1.4.). However, in the complexation of other phenolic compounds, such as rosmarinic acid in HP-β-CD, positive entropy values have also been observed, justified by the less polar nature of the guest molecule (D'Aria et al., 2021). Since isorhapontigenin is also less polar than other hydroxylated analogues, the release of structured hydration water in the bulk could explain the favourable entropy. Finally, the process was spontaneous, as the Gibbs free energy was negative (ΔG° = -21.49 ± 1.07 kJ/mol at 25 °C), similar to that of its analogue piceatannol (ΔG° = -23.5 ± 1.2 kJ/mol 25 °C (Matencio et al., 2016)).

2.2.5. Solubility and stability of free and encapsulated isorhapontigenin

The basal water solubility of isorhapontigenin was 0.32 mg/mL, lower than that of its hydroxylated analogue piceatannol (0.50 mg/mL (Kershaw and Kim, 2017)), but similar to that of gnetol (0.31 mg/mL Section 2.1.5.). Although the addition of a low concentration of HP-β-CD did not cause a significant change in this value, the addition

of 5 mM achieved a 73 % increase in its solubility (Figure 44A). Furthermore, the highest concentration of 10 mM HP-β-CD managed to double the basal solubility of isorhapontigenin, achieving a higher solubility than the basal solubility of piceatannol. Therefore, complexation with CDs could overcome possible solubilisation problems of this bioactive compound.

The results of the 3-month storage of the inclusion complexes at room temperature showed that CDs have a beneficial role for the application of isorhapontigenin in industry (Figure 44B). In the first 6 weeks, free isorhapontigenin was rapidly lost at a rate of approximately 10 % of the initial amount per week. After 12 weeks, the remaining isorhapontigenin without CDs was 15 %, while the use of a medium or high concentration of CD preserved more than 78 % of the stilbene, and the lower concentration of 1 mM more than 65 %. The difference between 5 mM and 10 mM HP-β-CD was not significant, so the use of 5 mM HP-β-CD could be enough to improve the stability of isorhapontigenin in formulations intended to be stored at room temperature.

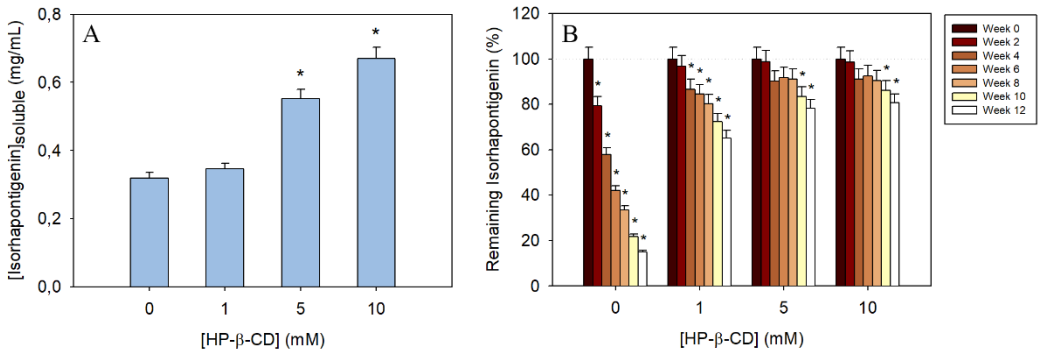

*Figure 44. A) Aqueous solubility of isorhapontigenin in the absence and presence of different concentrations of HP-β-CD (25 °C). B) Stability of isorhapontigenin free and encapsulated in HP-β-CD after storage at room temperature (25 °C pH 7). * Significance p-value < 0,05*

2.3. Rhapontigenin

Rhapontigenin (*trans*-3,3′,5-trihydroxy-4'-methoxystilbene) is a methoxylated stilbene biosynthesised by certain plant species such as *Rheum undulatum* and the family Polygonaceae. It has been found to possess numerous bioactivities of interest to human health, such as antioxidant (Zhang et al., 2007), antihyperlipidaemic (Jo et al., 2014), antimicrobial (Li et al., 2022), anticancer (Jung et al., 2011), cardioprotective (Fan, 2019) and neuroprotective (Ai et al., 2022) properties. Similarly to its isomer isorhapontigenin, with which it hardly varies in the position of its methoxy group, the more hydrophobic structure of rhapontigenin could be of great interest for the bioavailability of the molecule. However, it could also have a negative effect on aqueous solubility, which could pose a challenge in the development of fortified products. Therefore, its molecular encapsulation was investigated.

2.3.1. Optical properties of rhapontigenin

The absorption spectrum of rhapontigenin showed a similar shape to that of its isomer isorhapontigenin and its hydroxylated analogue piceatannol, sharing with the former λ_{max} at 326 nm and a small shoulder near 305 nm (Figure 45A). Concentrations between 1 and 100 µM gave a high linearity with the absorbance at 326 nm ($R^2 > 0.999$), determining a molar absorptivity value of 30094 $M^{-1}cm^{-1}$. Hui *et al*. (2011) previously determined the λ_{max} of rhapontigenin at 324.5 nm, with an absorptivity of 36824 $M^{-1}cm^{-1}$ in 50 % (v/v) methanol solution (Hui et al., 2011), a value slightly higher than that obtained in this thesis with 100 % (v/v) ethanol. On the other hand, the emission spectrum of rhapontigenin showed a single peak with λ_{em} at 400 nm after being excited at 290 nm (Figure 45B).

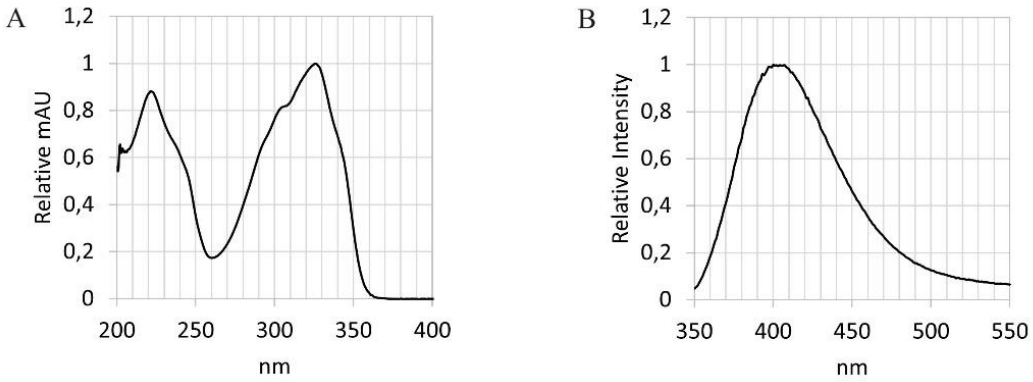

Figure 45. A) absorption and B) emission spectra (λ_{ex} = 290 nm) of rhapontigenin in ethanol and 0.1 M phosphate buffer pH 7, respectively

2.3.2. Physicochemical study of rhapontigenin inclusion complexes

The molecular encapsulation of rhapontigenin in CDs was characterised by determining the stoichiometry and encapsulation constants after obtaining the complexation curves (Figure 46A). Except for γ-CD, which could not fit any model, all CDs gave correlation coefficients $R^2 > 0.942$ for the 1:1 model, and $R^2 < 0.896$ for the 1:2 model (Table 8). The higher correlation coefficients in the first model reveal that the complexation follows a 1:1 stoichiometry, where one rhapontigenin molecule interacts with one CD molecule, as was the case for the encapsulation of other stilbene analogues such as piceatannol, resveratrol, oxyresveratrol (Matencio et al., 2017a, 2016), gnetol and isorhapontigenin (Section 2.1.2. and 2.2.2.).

Using Equation (7), rhapontigenin encapsulation constants for each CD were determined (Table 8). The modified HP-β-CD gave the highest value (K_F = 10308.89 ± 515.44 M^{-1}), which means that the cavity of this CD was the best to accommodate this stilbene. Figure 46 shows the complexation curve and the Benesi-Hildebrand fit of the rhapontigenin complexes with this CD. Apart from a better correlation with the 1:1

stoichiometry, it can be observed that the fluorescence signal reaches an almost stable value from a very low concentration of only 0.5 mM CD.

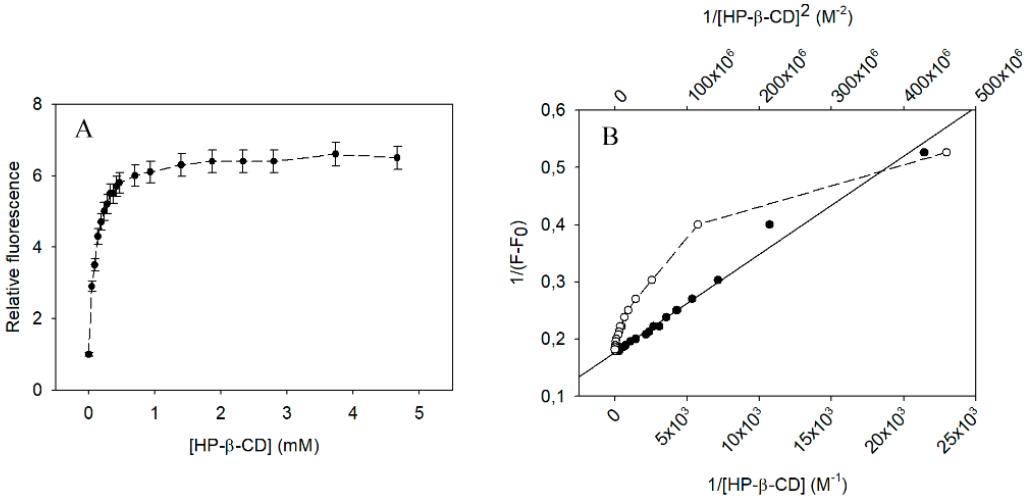

Figure 46. A) Complexation curve of rhapontigenin in HP-β-CD. B) Stoichiometric fitting of rhapontigenin inclusion complexes with HP-β-CD to a (●) 1:1 and (○) 1:2 model by the Benesi-Hildebrand method (25 °C pH 7)

Among the rest of CDs, M-β-CD (K_F = 5189.11 ± 259.45 M^{-1}) gave a encapsulation constant half that of HP-β-CD, while the constants of β-CD (K_F = 2990.11 ± 149.51 M^{-1}) and α-CD (K_F = 520.32 ± 26.02 M^{-1}) were more than three times and almost twenty times lower than those of HP-β-CD, respectively (Table 8). The encapsulation constant with γ-CD, as with isorhapontigenin, could not be determined due to the small increase in fluorescence signal after CD addition. These values are in the range of those previously obtained with its analogue piceatannol (Matencio et al., 2016), although the order of CD preference changes slightly (HP-β-CD > β-CD > M-β-CD > γ-CD > α-CD). With respect to its isomer isorhapontigenin, the encapsulation constants obtained with rhapontigenin were higher (except β-CD), keeping the same CD order, but with significant differences between M-β-CD and β-CD.

Table 8. Encapsulation constants and correlation coefficients obtained by the Benesi-Hildebrand method (Equation 7) and molecular docking score of the rhapontigenin inclusion complexes with different CDs (25 °C pH 7)

CD	K_F (M^{-1})	R^2		Score
		1:1 model	1:2 model	
α-CD	520.32 ± 26.02	0.993	0.881	-7.1
β-CD	2990.11 ± 149.51	0.942	0.844	-9.2
γ-CD	-	-	-	-6.5
HP-β-CD	10308.89 ± 515.44	0.995	0.895	-10.2
M-β-CD	5189.11 ± 259.46	0.994	0.891	-9.2

2.3.3. Molecular docking of rhapontigenin in CDs

The results of the bioinformatic modelling of each inclusion complex supported the experimental results described above. The HP-β-CD score was the lowest (score = -10.2), meaning that this CD was the most suitable for rhapontigenin encapsulation among the CDs studied (Table 8). Notably, this HP-β-CD docking was the only one in which rhapontigenin entered the internal cavity with the methoxy group on the secondary face of the CD (Figure 47D). This might suggest that the orientation of the guest molecule in the cavity of the host molecule plays a relevant role in the affinity of the complex, and that this arrangement with the methoxy ring close to the secondary face of the CD is the most favourable. Furthermore, this molecular docking showed hydrogen bonding between rhapontigenin and HP-β-CD, which improves the stability of the complex.

Although the score values of M-β-CD and β-CD were equal (score = -9.2) (Table 8), 3D modelling of the latter showed hydrogen bonds (Figure 47B). As in the fluorometric results, α-CD (score = -7.1) and γ-CD (score = -6.5) show the worst results, and although a score has been defined, it has previously been shown experimentally that γ-CD does not have sufficient affinity for this stilbene.

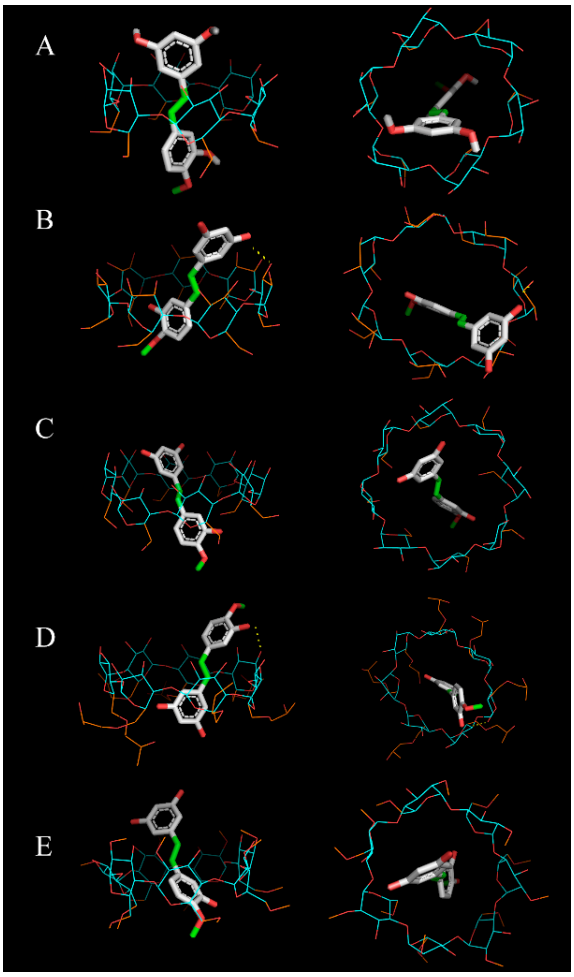

Figure 47. 3D molecular docking of rhapontigenin in A) α-CD, B) β-CD, C) γ-CD, D) HP-β-CD and E) M-β-CD. The flexible atoms of the CD are displayed in orange, while the non-flexible atoms are displayed in blue. Possible hydrogen bonds are shown as yellow dotted lines

2.3.4. Influence of pH and temperature on rhapontigenin encapsulation

The encapsulation constants of the complexes with rhapontigenin and HP-β-CD changed with pH (Figure 48A), showing a higher stability at neutral pH, reflected by a higher encapsulation constant. While variation at acidic pH caused a small loss of stability (from 8 % at pH 5 to 28 % at pH 3), variation at basic pH caused a sharp decrease in the encapsulation constant, reaching a K_F = 1305.68 ± 65.28 M^{-1} at pH 11, i.e. a decrease of 87 % compared to the K_F at pH 7. Therefore, for the development of a stable formulation

with encapsulated rhapontigenin it would be advisable to use a neutral pH, avoiding basic pH where it could deprotonate (Matencio et al., 2016).

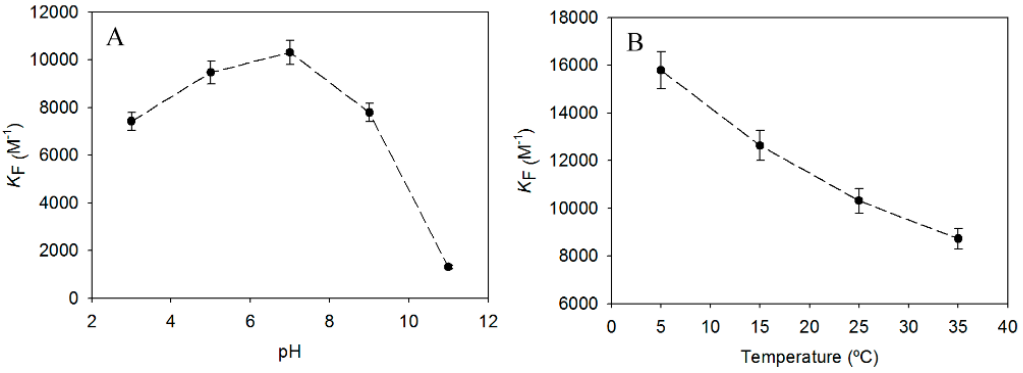

Figure 48. Effect of A) pH and B) temperature on the encapsulation constants of rhapontigenin inclusion complexes with HP-β-CD

The encapsulation constants of these inclusion complexes were inversely related to the temperature, giving a correlation coefficient $R^2 = 0.98$ (Figure 48B). The highest constant was obtained at 5 °C (K_F = 15785.24 ± 789.26 M^{-1}), indicating a stronger interaction between the molecules under cooling conditions. This interaction strength decreases with increasing temperature from 5 °C to 35 °C, by a reduction of 15 – 20 % in the encapsulation constant every 10 °C (approximately a decrease of 1.8 % per °C).

The determination of the thermodynamic parameters with Equations (8) and (9) revealed that the process was exothermic due to the negative enthalpy value (ΔH° = -14.12 ± 0.71 kJ/mol), which is common in this type of encapsulation due to the displacement of water molecules from the internal cavity to accommodate the stilbene. In contrast, the entropy value was positive (ΔS° = 29.51 ± 1.48 J/mol), which is not in agreement with previous results with hydroxylated analogues such as piceatannol, oxyresveratrol (López-Nicolás and García-Carmona, 2008b; Matencio et al., 2017a) or gnetol (Section 2.1.4.), where the entropy was unfavourable, but with the methoxylated analogue isorhapontigenin (Section 2.2.4.) where it was also favourable, although to a

lesser extent ($\Delta S° = 8.53 \pm 0.43$ J/mol (Section 2.2.4.)). Finally, the negative Gibbs free energy value ($\Delta G° = -22.92 \pm 1.15$ kJ/mol at 25 °C) indicated that the reaction was spontaneous and was similar to that of the analogue piceatannol ($\Delta G° = -23.5 \pm 1.2$ kJ/mol at 25 °C (López-Nicolás and García-Carmona, 2008b)) and isomer isorhapontigenin ($\Delta G° = -21.49 \pm 1.07$ kJ/mol at 25 °C (Section 2.2.4.)).

2.3.5. Solubility and stability of free and encapsulated rhapontigenin

After determination of the water solubility of free and encapsulated rhapontigenin, it could be observed that the basal solubility of 0.11 mg/mL (Figure 49A), could increase more than fourfold and sevenfold after the addition of 5 mM and 10 mM HP-β-CD to the formulation, respectively. In fact, similar to what was observed with isorhapontigenin (Section 2.2.5.), using concentrations above 5 mM HP-β-CD achieve an aqueous solubility similar to or higher than the basal solubility of piceatannol (0.50 mg/mL (Kershaw and Kim, 2017)). In contrast to what was observed in isorhapontigenin complexes, in rhapontigenin complexes even the lowest concentration of 1 mM CD was able to significantly increase solubility by 71 %. Despite the structural similarity, it is noteworthy that the basal solubility of rhapontigenin was lower than that of isorhapontigenin (0.32 mg/mL Section 2.2.5.), suggesting that the presence of a methoxy group at the R4' radical affects the solubility of stilbenes more negatively than at the R3' position.

The stability study after storage at room temperature showed that in the absence of encapsulating agents, rhapontigenin degraded in a fairly linear manner ($R^2 > 0.98$) with a negative slope of almost -5 units (Figure 49B). By the tenth week, half of the stilbene had already been degraded and, at the end of the assay, only 42 % of the initial amount of rhapontigenin remained, compromising the long-term viability of an enriched product. In

contrast, in the presence of CDs, the average slope decreased to approximately -2 units ($R^2 > 0.97$), keeping more than 73 % of rhapontigenin remaining after 12 weeks of storage. Furthermore, there was no significant difference between the concentrations tested, so the HP-β-CD concentration of 1 mM seems to be sufficient to improve the stability of the molecule.

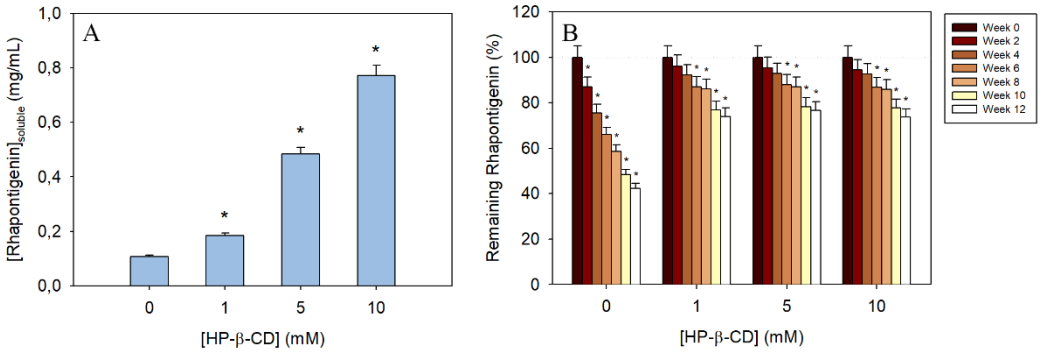

*Figure 49. A) Aqueous solubility of rhapontigenin in the absence and presence of different concentrations of HP-β-CD (25 °C). B) Stability of free and encapsulated rhapontigenin in HP-β-CD after storage at room temperature (25 °C pH 7). * Significance p-value < 0,05*

2.4. Pinostilbene

Pinostilbene (*trans*-3,4'-dihydroxy-5-methoxystilbene) is a methoxylated stilbene naturally present in *Pinus sibirica* (Shin et al., 2023), although it is usually synthesised from resveratrol in cultures modified with O-methyltransferases enzymes such as those of *V. vinifera* (Herrera et al., 2021), *V. riparia* or *Sorghum bicolor* (Jeong et al., 2014) or directly in plant cultures of *Phytolacca americana* (Shimoda et al., 2019). In mice, pinostilbene has been found to be the main metabolite of pterostilbene (Sun et al., 2016). The interest in this stilbene lies in its bioactivity as an antimicrobial (Zakova et al., 2018), anti-inflammatory (Leláková et al., 2019), anticarcinogenic (Mikstacka et al., 2007; Sun et al., 2016), neuroprotective (Chao et al., 2010) and anti-obesity (Chung and Hyun, 2021) compound. Furthermore, in colonic fermentation assays, it proved to be more stable as it was not metabolised to new products, unlike other stilbenes such as resveratrol,

oxyresveratrol and piceatannol (Jarosova et al., 2019). Like other methoxylated stilbenes, its structure may play a beneficial role in the bioavailability of the molecule, but may also limit its aqueous solubility.

2.4.1. Optical properties of pinostilbene

The absorption spectrum of pinostilbene showed a similar shape to that of its hydroxylated analogue resveratrol, with only a 2 nm bathochromic shift at its λ_{max}, which moved to 308 nm (Figure 50A). Concentrations of pinostilbene between 1 and 50 µM gave a high linearity with absorbance at its λ_{max} ($R^2 > 0.999$), establishing a molar absorptivity value of 32060 $M^{-1}cm^{-1}$. Tyukavkina *et al*. (1972) previously determined a log ε = 4.55 at a λ_{max} of 307 nm for pinostilbene in ethanol, which would be equivalent to 35481 $M^{-1}cm^{-1}$ (Tyukavkina et al., 1972), slightly higher than that obtained. The emission spectrum of this stilbene was also similar to that of resveratrol with a peak with λ_{em} at 397 nm after being excited at 290 nm (Figure 50B).

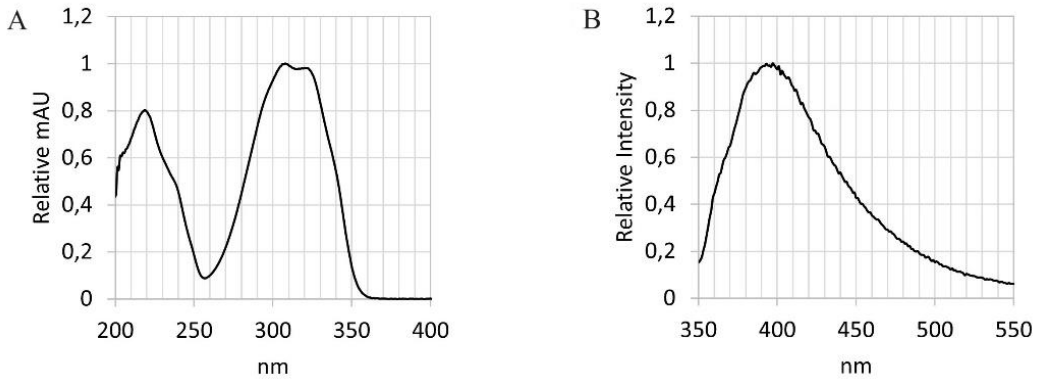

Figure 50. A) absorption and B) emission spectra (λ_{ex} = 290 nm) of pinostilbene in ethanol and 0.1 M phosphate buffer pH 7, respectively

2.4.2. Physicochemical study of the inclusion complexes with pinostilbene

Molecular encapsulation of pinostilbene in CDs (Figure 51A) showed a complexation curve similar to that previously observed with other stilbenes. Except for γ-CD, all CDs increased the basal fluorescence of pinostilbene as a function of the concentration used. By means of the linear Benesi-Hildebrand fit (Figure 51B) it could be observed that the complexation was governed by a 1:1 stoichiometry in which one CD molecule interacts with one molecule of pinostilbene. This type of interaction agrees with that previously observed in the molecular encapsulation of other stilbenes such as isorhapontigenin (Section 2.2.2.), rhapontigenin (Section 2.3.2.), gnetol (Section 2.1.2.), resveratrol (López-Nicolás and García-Carmona, 2008b), pterostilbene (López-Nicolás et al., 2009b), piceatannol (Matencio et al., 2016), oxyresveratrol (Matencio et al., 2017a).

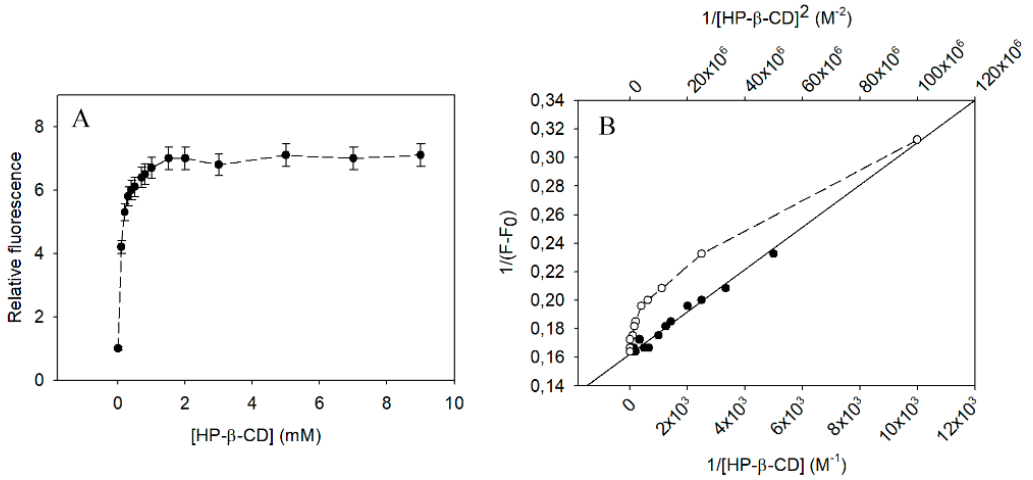

Figure 51. A) Complexation curve of pinostilbene in HP-β-CD. B) Stoichiometric fitting of pinostilbene inclusion complexes with HP-β-CD to a (●) 1:1 and (○) 1:2 model by the Benesi-Hildebrand method (25 °C pH 7)

The encapsulation constants of the pinostilbene complexes with the different CDs were determined using Equation (7) adjusted for the 1:1 model (Table 9). The results show that HP-β-CD was the most suitable CD for the molecular encapsulation of

pinostilbene given its higher encapsulation constant (K_F = 10074.45 ± 503.72 M^{-1}), followed by M-β-CD (K_F = 4870, 24 ± 243.51 M^{-1}), β-CD (K_F = 3503.62 ± 175.18 M^{-1}), α-CD (K_F = 633.62 ± 31.68 M^{-1}), and finally, γ-CD for which a linear fit could not be obtained to determine the encapsulation constant.

In previous similar studies with other stilbenes (Section 2.2.2., Section 2.3.2., Section 2.1.2. and (Matencio et al., 2016)), it was also observed that β-CDs were the CDs that formed the most stable inclusion complexes with each of the stilbenes studied, especially HP-β-CD.

Table 9. Encapsulation constants and correlation coefficients obtained by the Benesi-Hildebrand method (Equation 7) and molecular docking score of the inclusion complexes of pinostilbene with different CDs (25 °C pH 7)

CD	K_F (M^{-1})	R^2		Score
		1:1 model	1:2 model	
α-CD	633.62 ± 31.68	0.972	0.821	-6.8
β-CD	3503.62 ± 175.18	0.949	0.734	-9.1
γ-CD	-	-	-	-6.2
HP-β-CD	10074.45 ± 503.72	0.976	0.868	-10.1
M-β-CD	4870.24 ± 243.51	0.955	0.782	-9.2

2.4.3. Molecular docking of pinostilbene in CDs

The computational results showed a good correlation with the experimental results regarding the order of preference of CDs for the encapsulation of pinostilbene (Table 9). The highest score was given by the complex with HP-β-CD (score = -10.1), followed by the complex with M-β-CD (score = -9.2), β-CD (score = -9.1), α-CD (score = -6.8) and lastly, γ-CD (score = -6.2).

In the most likely configurations (Figure 52B and D), hydrogen bonds were observed between pinostilbene and two of the best scoring CDs, β-CD and HP-β-CD. It is possible that in the complex with M-β-CD (Figure 52E), where no hydrogen bonds are observed, but a similar score to β-CD was obtained, other types of weak interactions are

formed that stabilise the inclusion complex, such as hydrophobic or Van der Waals interactions. The lower affinity molecular dockings, i.e. with α-CD and γ-CD (Figure 52A and C), revealed that the pinostilbene was in a more centred position, leaving free spaces in the CD cavity. This suggests that these complexes may have fewer interactions that stabilise ligand-receptor coupling.

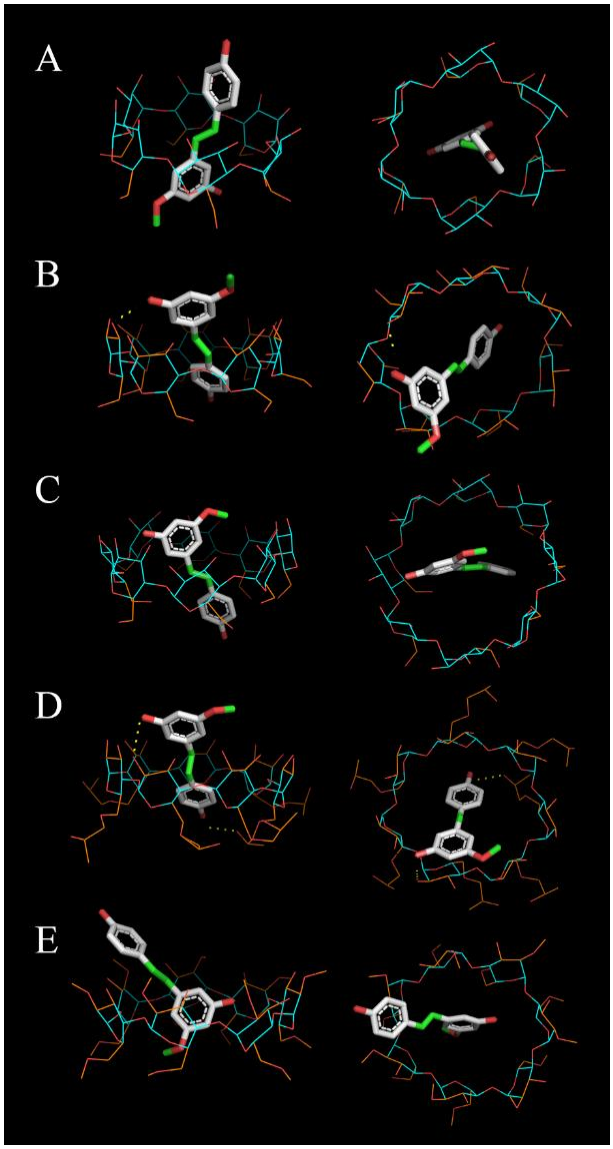

Figure 52. 3D molecular docking of pinostilbene in A) α-CD, B) β-CD, C) γ-CD, D) HP-β-CD and E) M-β-CD. The flexible atoms of CD are displayed in orange, while the non-flexible atoms are displayed in blue. Possible hydrogen bonds are shown as yellow dotted lines

2.4.4. Influence of pH on pinostilbene encapsulation

The encapsulation constants of the pinostilbene complexes with the best CD obtained by the Benesi-Hildebrand method and the molecular docking, HP-β-CD, were inversely related to the pH of the medium. At higher acidity in the medium, the inclusion complexes gave higher encapsulation constants reaching up to K_F = 12322.75 ± 616.14 M^{-1} at pH 5 (Figure 53). On the contrary, when the pH of the medium became more basic these values dropped, reaching the minimum value of K_F = 5105.60 ± 255.28 M^{-1} at pH 10. From pH 5 to pH 9, the decrease in the K_F value was constant (R^2 > 0.99), but from pH 9 onwards it intensifies, doubling the negative slope (Figure 53). As described above (Section 2.1.4.), this intensified decrease has been associated with the pH region where the pK_a of the stilbene is located.

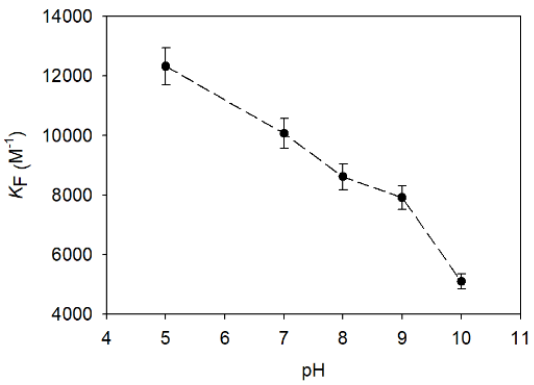

Figure 53. Effect of pH on the encapsulation constants of the HP-β-CD-pinostilbene inclusion complexes

2.4.5. Solubility and stability of free and encapsulated pinostilbene

Solubility studies of free and complexed pinostilbene highlighted that molecular encapsulation was able to increase the aqueous solubility of this stilbene significantly (Figure 54A). While in free form pinostilbene solubility in water was 0.06 mg/mL, the addition of 1 mM HP-β-CD tripled this value. The use of higher concentrations of CD

also made significant differences, achieving up to 7 and 10 times more soluble stilbene with 5 mM and 10 mM HP-β-CD, respectively (Figure 54A).

The solubility of pinostilbene was closer to that of pterostilbene (0.021 mg/mL (Bethune et al., 2011)) and resveratrol (0.03 mg/mL (Kershaw and Kim, 2017)) with which it shared the positions of its radicals, but was lower than that of other stilbenes with substitutions in other groups, such as oxyresveratrol (0.75 mg/mL (Suzuki et al., 2019)), piceatannol (0.50 mg/mL (Kershaw and Kim, 2017)), gnetol (0.31 mg/mL Section 2.1.5.), isorhapontigenin (0.32 mg/mL Section 2.2.5.) and rhapontigenin (0.11 mg/mL Section 2.3.5.).

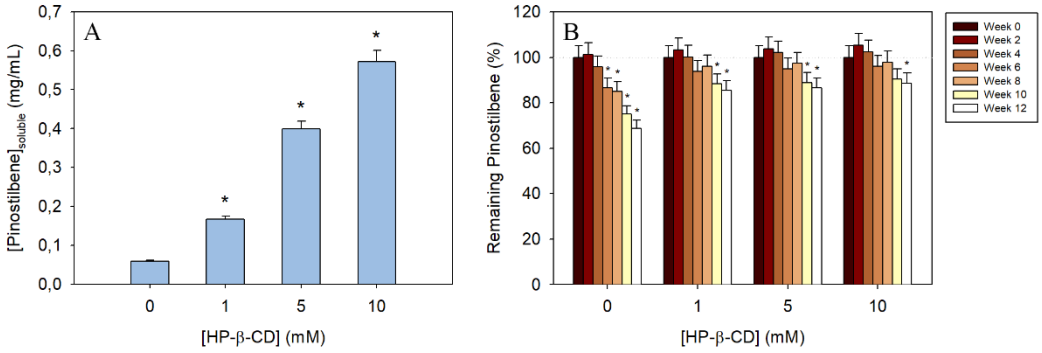

*Figure 54. A) Aqueous solubility of pinostilbene in the absence and presence of different concentrations of HP-β-CD. B) Stability of free and encapsulated pinostilbene in HP-β-CD after storage at room temperature (25 °C). * Significance p-value < 0.05*

On the other hand, the room temperature stability of pinostilbene also improved after molecular encapsulation (Figure 54B). The degradation of pinostilbene after storage in free form was milder compared to that observed for other stilbenes (Section 2.2.5. and 2.3.5.). From week 6 onwards, this decrease in pinostilbene concentration was already significant compared to the initial concentration. After 12 weeks of storage, the solutions without CDs had lost as much as 31 % of the initial pinostilbene, whereas in the presence of HP-β-CD this loss did not exceed 15% of the initial pinostilbene concentration, with more than 88 % of the initial amount preserved using a concentration of CD of 10 mM.

2.5. Conclusions on the characterisation and molecular encapsulation of natural stilbenes

The spectrophotometric and spectrofluorometric properties of the stilbenes gnetol, isorhapontigenin, rhapontigenin and pinostilbene were determined, as well as their solubility and stability in aqueous solutions. In general, their absorption and fluorescence spectra and parameters were similar to those of other analogues according to their substituted groups. It highlights the large bathochromic shift in the λ_{em} of gnetol compared to other stilbenes, despite sharing a similar absorption spectrum with them. Solubility was clearly influenced by the number, position and type of functional groups in the stilbene structure. Pinostilbene had the lowest water solubility among the stilbenes tested, but similar to that previously reported for resveratrol or pterostilbene, suggesting that the tri-substituted structure of stilbene is less soluble than the tetra-substituted structure. However, pinostilbene was more stable than rhapontigenin or isorhapontigenin after 3 months of storage. Furthermore, since the solubility of rhapontigenin was lower than that of isorhapontigenin, it seems that the presence of a 4'-methoxy group in the tetra-substituted stilbenes decreases water solubility more than the presence of a 3'-methoxy.

Molecular encapsulation of these four stilbenes in CDs proved to be able to improve their water solubility and stability in solution, which could enable a more effective application of these stilbenes in aqueous formulations. All inclusion complexes showed a 1:1 stoichiometry, i.e. one CD molecule encapsulated one stilbene molecule. Among the CDs tested, HP-β-CD formed the most stable complexes due to its higher encapsulation constant and lower molecular docking score. The encapsulation constants with this CD were higher at lower pH and temperature. This suggests that these inclusion complexes will be more stable in acidic formulations stored under refrigeration, for example citrus functional foods.

3. SYNTHESIS, CHARACTERISATION AND MOLECULAR ENCAPSULATION OF HYDROPHOBIC STILBENE DERIVATIVES

The low bioavailability of stilbenes is a limiting factor for the *in vivo* bioactivity of this family of bioactive compounds (Asensi et al., 2002). This low bioavailability has been associated with their rapid absorption and phase II metabolism, generating more soluble conjugates that are easily eliminated in the urine (Walle et al., 2004). Previous studies have shown that derivatisation of bioactive compounds can help avoid phase II reactions, improving bioavailability (Agrawal and Jaiswal, 2022; Biasutto et al., 2007). These derivatives can act as precursors of the original molecules, making their transport to target tissues easier (Crauste et al., 2014; Pokorski et al., 2003). In addition, lipophilic derivatisations can by-pass hepatic metabolism by transporting molecules through the lymphatic system (Charman and Porter, 1996; Han et al., 2021; Yan et al., 2023).

For all these reasons, the synthesis and characterisation of novel hydrophobic stilbene derivatives was studied in order to avoid their biotransformation after oral ingestion and facilitate their transport to adipocytes, a target tissue where stilbenes have demonstrated anti-obesity effects (Aguirre et al., 2014). Furthermore, given that this structural modification would negatively affect the solubility of the stilbene, the molecular encapsulation of these precursors in CDs was also evaluated to ensure their incorporation into aqueous formulations.

3.1. Synthesis and purification of hydrophobic stilbene derivatives

After optimisation of the chemical synthesis procedure, stearates (-E), oleates (-O) and palmitates (-P) of the stilbenes resveratrol (R-), oxyresveratrol (O-), piceatannol (Pc-) and pterostilbene (Pt-), were obtained (Figure 55). To facilitate data visualisation, in the

following figures or tables these products are shown abbreviated with the letters mentioned for stilbene followed by the letter mentioned for the fatty acid.

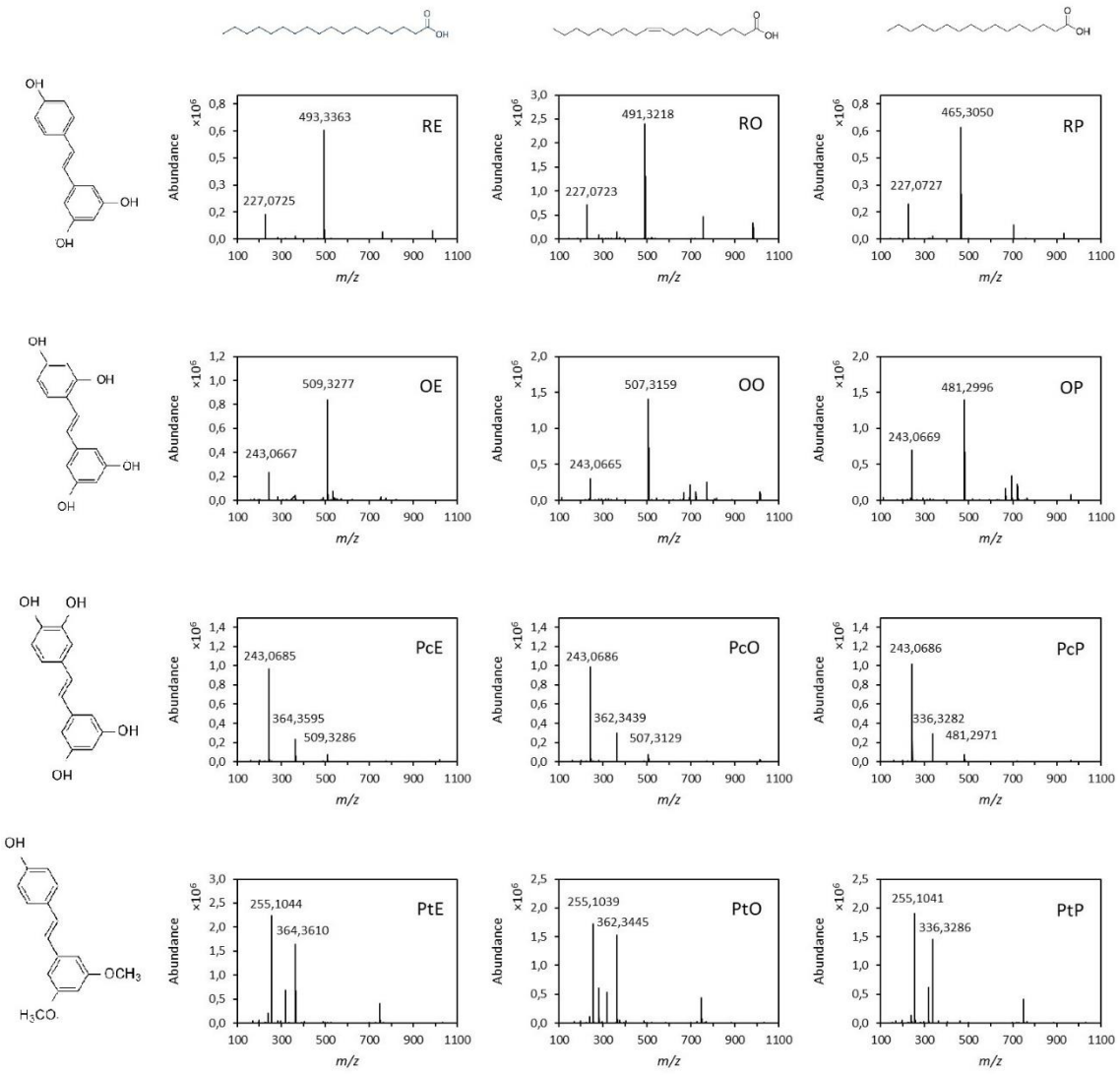

Figure 55. Mass spectra ESI(-) of chemical synthesis reactions of hydrophobic stilbene derivatives. For each reaction, the structures of the substrates used are displayed above and to the right.

From the 12 different chemical synthesis reactions, a total of 21 monoester products detectable by liquid chromatography were obtained, including some positional isomers. Unlike other synthesis procedures using chlorinated fatty acid derivatives (Oh and Shahidi, 2017), this process was much more specific in the formation of stilbene monoesters, with minimal diester formation.

The yields of the reactions with resveratrol and oxyresveratrol determined by mass spectrometry were 61 – 76 % and 49 – 78 %, respectively (Table 10). Yields could not be determined for the reactions with piceatannol and pterostilbene due to their difficulty to ionise, and in the case of the piceatannol products, ease of degradation by breaking the ester bond. Despite this, these reactions proved to be less efficient as the formation of a secondary product was observed, which was subsequently identified as a DCC derivative with the fatty acids used (m/z^- 364 with stearic acid, m/z^- 362 with oleic acid and m/z^- 336 with palmitic acid) (Figure 55).

Table 10. Results of chemical synthesis reactions of hydrophobic stilbene derivatives

Product	Isomer	Formula	MW	m/z^-	Yield (%) HPLC-ESI(-)	Isomer ratio (%) HPLC-DAD
RE	RE i1 RE i2	$C_{32}H_{46}O_4$	494.7052	493.3363	72	28 72
RO	RO i1 RO i2	$C_{32}H_{44}O_4$	492.6894	491.3218	76	32 68
RP	RP i1 RP i2	$C_{30}H_{42}O_4$	466.6521	465.3050	61	32 68
OE	OE i3 OE i1 OE i2	$C_{32}H_{46}O_5$	510.7046	509.3277	74	80 8 12
OO	OO i3 OO i1 OO i2	$C_{32}H_{44}O_5$	508.6888	507.3159	78	77 10 12
OP	OP i3 OP i1 OP i2	$C_{30}H_{42}O_5$	482.6515	481.2996	49	75 13 12
PcE	-	$C_{32}H_{46}O_5$	510.7046	509.3286	-	100
PcO	-	$C_{32}H_{44}O_5$	508.6888	507.3129	-	100
PcP	-	$C_{30}H_{42}O_5$	482.6515	481.2971	-	100
PtE	-	$C_{34}H_{50}O_4$	522.7584	-	-	100
PtO	-	$C_{34}H_{48}O_4$	520.7425	-	-	100
PtP	-	$C_{32}H_{46}O_4$	494.7052	-	-	100

The synthesised monoesters were purified by column chromatography with silica gel (Figure 56A), yielding a racemic mixture of stable ratio in resveratrol and oxyresveratrol derivatives (Table 10). By HPLC, 2 isomers in the resveratrol derivatives (named as i1 and i2) and 3 isomers in the oxyresveratrol derivatives (named as i3, i1 and i2) could be separated (Figure 56B). However, due to the low solubility and low

chromatographic resolution of these products, large amounts of pure isomers were not obtained, using the racemic mixture in most of the assays.

The purified products had a white powder appearance, except for the stilbene oleates, which were more viscous and slightly yellowish in appearance.

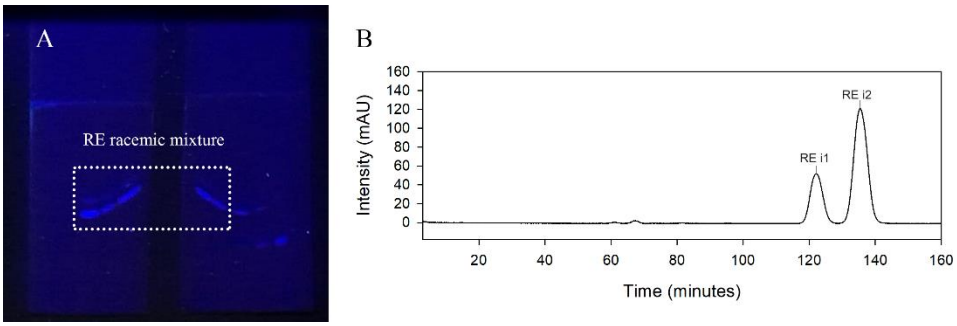

Figure 56. A) TLC with selected aliquots from the purification of resveratrol stearate by column chromatography. B) Chromatogram at 310 nm of the purified racemic mixture obtained from the resveratrol stearate synthesis reaction. The chromatograms of the other stilbene derivatives are shown in Section 3.2.2.

On the other hand, the enzymatic synthesis of resveratrol stearate achieved a maximum yield of 56 % after 90 hours of incubation with the Novozym 435 enzyme (Figure 57). At the end of the reaction, vinyl stearate had been transformed into stearic acid and there was still a considerable amount of unreacted vinyl stearate and resveratrol.

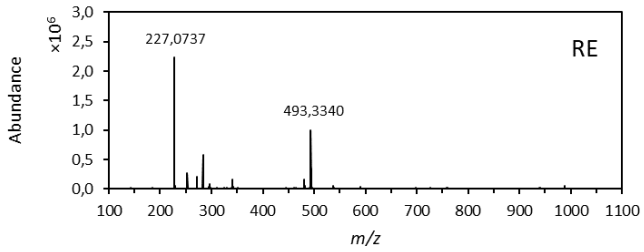

Figure 57. Mass spectrum ESI(-) of the enzymatic synthesis reaction of resveratrol stearate

Since the chemical synthesis gave a higher yield (72 %) in much less time (24 hours) and without the need for high temperatures, it was decided not to use this enzymatic synthesis procedure with the other hydrophobic stilbene derivatives. In a previous study in which resveratrol dodecanoate is synthesised chemically and

enzymatically (Peng and Shahidi, 2022), the authors also obtained higher yields with the chemical method (25 – 40 %) compared to the enzymatic method (9 – 15 %). The authors justify the use of the enzymatic method for the production of monoesters only, since the chemical method they use produces diesters and triesters.

The yields obtained in this PhD thesis show that the chemical synthesis and enzymatic synthesis developed are quite efficient and selective in the formation of monoesters, in comparison with previous literature on similar esterification reactions, although with other substrates and/or catalysts.

Regarding chemical synthesis, Tain *et al*. (2020) obtained a similar yield of 73 % in the synthesis of resveratrol butyrate with a Steglich esterification using N-ethyl-N'-(3-dimethylaminopropyl)-carbodiimide (EDC) instead of DCC and THF as solvent (Tain et al., 2020). Oh & Shahidi (2017) synthesised several hydrophobic resveratrol derivatives using chlorinated fatty acid derivatives as substrates. With this process they achieved yields of 37.7 % resveratrol docosahexanoate and 74 % resveratrol caprylate, but also obtained higher amounts of diesters and triesters than the procedure optimised in this PhD thesis (Oh and Shahidi, 2017). Pany *et al*. (2012) obtained similar yields to those of this thesis for the synthesis of resveratrol oleate (77 %), resveratrol linoleate (70 %) and resveratrol linolenate (68 %) (Pany et al., 2012). The process achieved a single isomer modified at the 4'-OH group, but was also more complex as it pre-methylated the 3'-OH and 5'-OH groups before to achieve this regioselectivity. Wong *et al*. (2020) achieved yields of 23 – 78 % by conjugating the stilbene combretastatin A4 and some isomers with stearic, oleic, linoleic and linolenic acid (Wong et al., 2020).

In relation to enzyme synthesis, Torres *et al*. (2010) obtained a maximum yield of 35 % of resveratrol stearate after 160 hours of reaction, using a higher proportion of enzyme and vinyl stearate than the one optimised in this doctoral thesis (Torres et al.,

2010). The same authors carried out a similar reaction using vinyl acetate as a substrate, and achieved a much higher yield (80 %) of resveratrol acetate after 50 h. Nicolosi *et al*. (2002) and Teng *et al*. (2005) also synthesised resveratrol acetate with Novozym 435 using different substrate ratios, but achieved lower yields of 40 % after 90 h and 45 % after 72 h, respectively (Nicolosi et al., 2002; Teng et al., 2005). All these authors emphasise that the process was very selective, yielding a single monoester product modified at the 4'-OH group, so it is likely that the resveratrol stearate synthesised in this PhD thesis also shows such regioselectivity.

3.2. Characterisation of hydrophobic stilbene derivatives

3.2.1. Nuclear Magnetic Resonance

The pterostilbene stearate and pterostilbene palmitate derivatives were analysed by H-NMR together with the original pterostilbene to confirm the formation of the product, as it was not ionisable and could not be visualised by mass spectrometry. The viscosity of the pterostilbene oleate prevented it from being analysed by this technique.

Table 11. Chemical shifts of pterostilbene and its hydrophobic derivatives by H-NMR

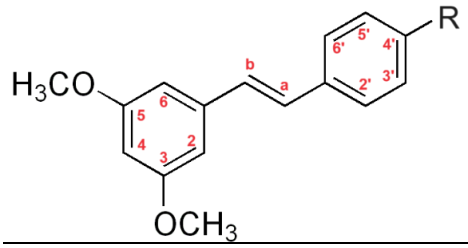

Pterostilbene: R = OH
PtE: R = $COO(CH_2)_{16}CH_3$
PtP: R = $COO(CH_2)_{14}CH_3$

H position	Chemical shift (ppm)		
	Pterostilbene	**PtE**	**PtP**
3, 5	3.813	3.812	3.813
4	6.366	6.380	6.380
2, 6	6.632	6.640	6.641
a	6.878	6.961	6.962
b	7.006	7.027	7.048
3', 5'	6.808	7.054	7.059
2', 6'	7.383	7.482	7.482

Pterostilbene has blocked for structural modification two of its radicals with methoxy groups, so the only group available for esterification is 4'-OH. Therefore, by modifying this group, the adjacent hydrogens are expected to undergo a chemical shift in their resonance. The results confirmed this by showing a notable increase of approximately 0.250 ppm in the closest hydrogens at the 3' and 5' positions, a moderate increase of 0.099 ppm in the next hydrogens at the 2' and 6' positions, and a minor increase of 0.060 ppm in the hydrogens at the methylene bridge between the two aromatic rings (Table 11). In contrast, the hydrogens of the unmodified ring (positions 4, 2, 6, 3 and 5) showed very low or even zero variation in chemical shifts. These results were quite consistent with both derivatives despite the fatty acid used in the derivatisation.

3.2.2. Chromatography

The products of the chemical synthesis were injected into an HPLC-DAD system with a mobile phase containing 85 % (v/v) methanol or 99 % (v/v) methanol in the case of the pterostilbene derivatives. This high percentage of organic solvent gave high retention times and good resolution between eluted peaks of the hydrophobic derivatives (Figure 58). By using a reversed phase column, a relative comparison of the polarity of the different stilbene derivatives synthesised could be made according to their retention time.

As with the natural stilbenes (Table 1), the pterostilbene derivatives were less polar than those of resveratrol and these, in turn, were less polar than those of oxyresveratrol and piceatannol. On the other hand, modification with stearic acid increased the retention time (Table 12), and therefore the apolarity of the stilbenes the most, followed by modification with oleic acid or palmitic acid, with less differences. In fact, the retention time of pterostilbene oleate and pterostilbene palmitate barely differed

by 3.24 seconds (Table 12). In general, the palmitates gave the highest polarity, except for the pterostilbene derivatives where oleate was the most polar. In the derivatives with isomers, it could be observed that the resolution between peaks followed the following order: stearates >> oleates > palmitates. It seems that the modification with stearic acid not only increases the apolarity of the stilbenes but also improves the chromatographic separation of their different isomers in the tested conditions.

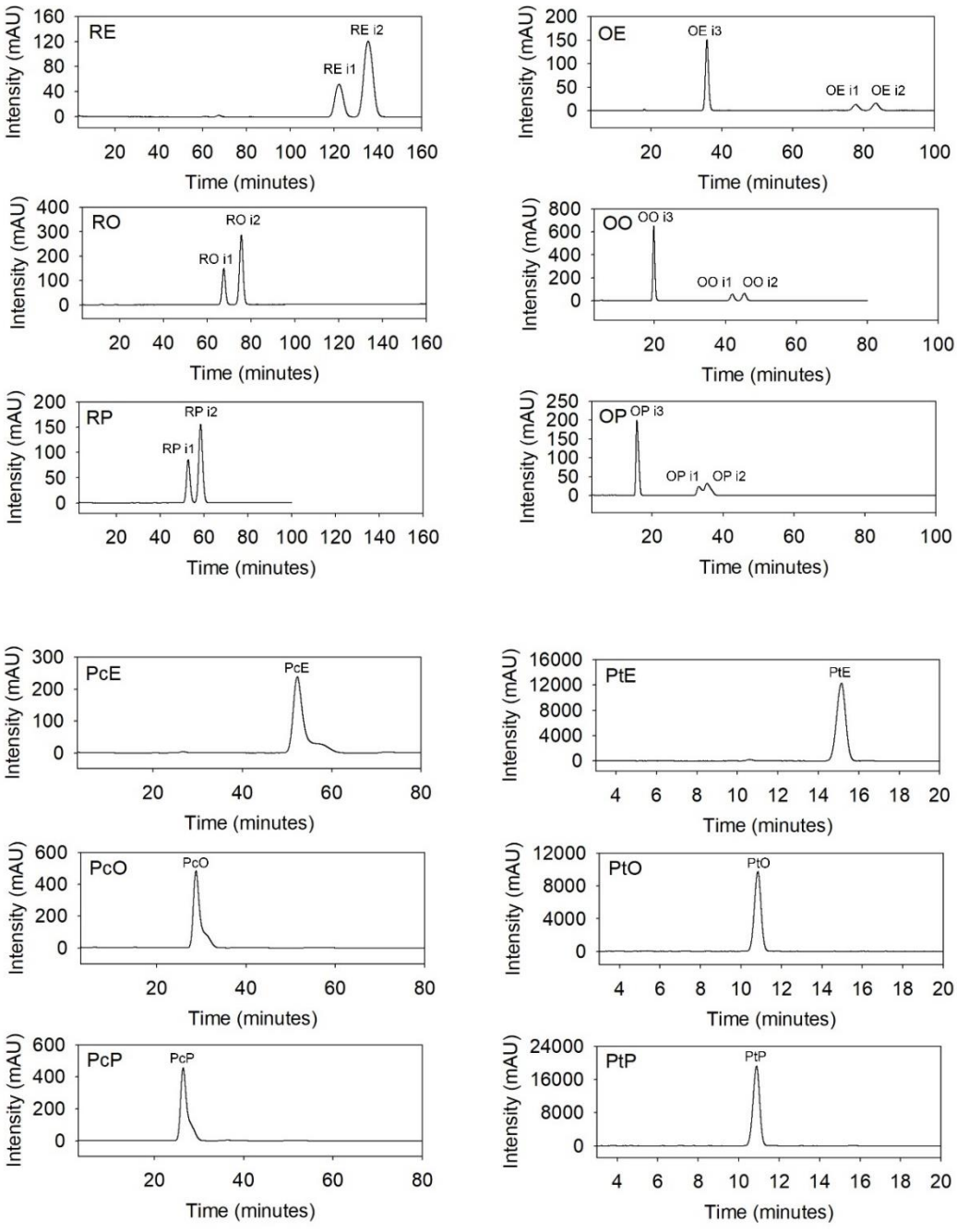

Figure 58. Chromatograms at 310 nm of the hydrophobic stilbene derivatives

Table 12. Retention times of hydrophobic stilbene derivatives

Product	Isomer	Methanol (%)	Retention time (min)
RE	RE i1	85	122.149
	RE i2		135.423
RO	RO i1	85	67.501
	RO i2		75.548
RP	RP i1	85	52.793
	RP i2		58.466
OE	OE i3	85	35.798
	OE i1		77.751
	OE i2		83.278
OO	OO i3	85	19.833
	OO i1		41.939
	OO i2		45.353
OP	OP i3	85	15.709
	OP i1		33.136
	OP i2		35.429
PcE	-	85	52.286
PcO	-	85	28.796
PcP	-	85	26.445
PtE	-	99	15.14
PtO	-	99	10.833
PtP	-	99	10.887

In the resveratrol derivatives, the majority isomer i2 was less polar than the minority isomer i1, with a separation of 5 – 13 minutes depending on the fatty acid used in the synthesis (Table 12). On the other hand, in the oxyresveratrol derivatives, the majority isomer i3 was the most polar of all and showed a large separation from the isomers i1 (17 – 42 minutes) and i2 (20 – 47 minutes). Between the i1 and i2 isomers of the oxyresveratrol derivatives there was only a difference of 2 – 6 minutes depending on the fatty acid used.

The piceatannol derivatives showed a tail at the end of the chromatographic peak, especially piceatannol stearate (Figure 58). Although this could indicate the presence of another isomer, a second peak could not be separated by varying the method, nor was a variation in the absorption spectrum between the peak and the tail of the peak observed.

3.2.3. Spectrophotometry

The derivatisation of the stilbenes with the fatty acids caused a modification in their absorption spectra which varied according to the hydroxyl group that was modified. The differences in both the shape of the absorption spectra and the λ_{max} of derivatives of the same stilbene with different fatty acids were minimal, with the type of stilbene and modified group being the determining factors in the spectrophotometric properties of the derivative (Figure 59).

Regarding the shape of the absorption spectra, in general, the derivatives showed a very similar pattern to the original stilbenes with varying λ_{max}. The major isomer of the oxyresveratrol derivatives (i3), showed the most changes in shape, losing the secondary peaks that the absorption spectrum of oxyresveratrol has at 301 and 290 nm (Figure 59). Similarly, the piceatannol derivatives also lost the shoulder prior to the main piceatannol peak at 305 nm.

The λ_{max} were determined for the isomers separately and for the racemic mixture obtained, determining the molar absorptivity value for the racemic mixture of the hydrophobic derivatives (Table 13).

Regarding the λ_{max} of the individual isomers, the minority isomer i1 showed a bathochromic shift of 14 nm in the resveratrol derivatives and 2 – 4 nm in the oxyresveratrol derivatives compared to the original stilbenes (Table 13). In contrast, the i2 isomer showed a hypsochromic shift of 4 nm in resveratrol derivatives (in which it is the predominant isomer), and 4 – 6 nm in oxyresveratrol derivatives. Finally, the i3 isomer (the majority of the oxyresveratrol derivatives), showed the most pronounced hypsochromic shift of 22 nm. In general, the λ_{max} determined in the racemic mixtures of these derivatives were also lower, possibly because the majority isomers were those

showing hypsochromic shifts. On the other hand, the hydrophobic derivatives of piceatannol and pterostilbene gave hypsochromic shifts of 14 – 16 nm and 5 nm, respectively. Overall, the fatty acid used in the esterification did not lead to significant differences in the λ_{max} observed for each stilbene.

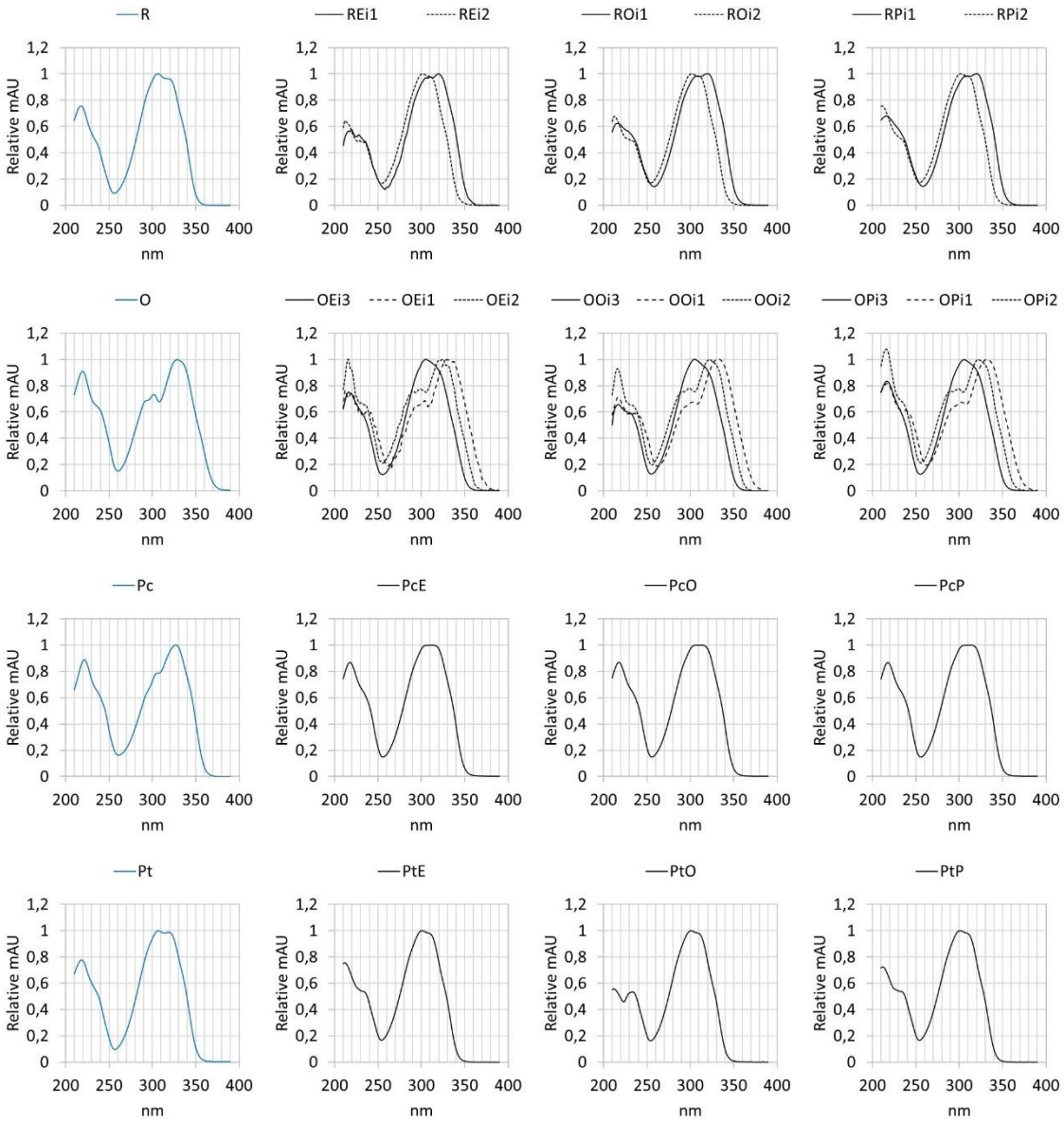

Figure 59. Relative absorption spectra of the hydrophobic stilbene derivatives (black) and their original stilbenes (blue). R: resveratrol, O: oxyresveratrol, Pc: piceatannol, Pt: pterostilbene

All hydrophobic derivatives of the synthesised stilbenes decreased significantly in molar absorptivity compared to the original stilbenes (Table 13). For resveratrol

derivatives the decrease was 35 – 80 %, for oxyresveratrol 85 – 98 % and for pterostilbene 80 – 93 %. The type of fatty acid had different effects depending on the stilbene. Resveratrol and oxyresveratrol oleates gave higher absorptivity than their corresponding palmitates and stearates, while pterostilbene oleate gave the opposite effect, showing a lower coefficient compared to its stearate and palmitate derivatives. Furthermore, the ranges of linear concentrations were extended with derivatisation, reaching up to 400 µM of hydrophobic stilbene derivatives (except with resveratrol oleate which was 200 µM), whereas with the original stilbenes only 50 - 100 µM was reached.

Table 13. Spectrophotometric and spectrofluorimetric characterisation of hydrophobic stilbene derivatives and their original stilbenes. R: resveratrol, O: oxyresveratrol, Pc: piceatannol, Pt: pterostilbene. [a] Measured in methanol; [b] Measured in 85 % methanol (v/v)

Product	Isomer	λ_{max} (nm) HPLC-DAD	λ_{max} [a] (nm) UV/Vis	ε [a] ($M^{-1}cm^{-1}$)	λ_{ex} [a] (nm)	λ_{em} [a] (nm)
R	-	-	306	30 257	304	377
RE	RE i1	320 [b]	304	5 948	301	408
	RE i2	302 [b]				
RO	RO i1	320 [b]	304	19 620	301	407
	RO i2	302 [b]				
RP	RP i1	320 [b]	304	9 006	301	408
	RP i2	302 [b]				
O	-	-	328	27 044	327	393
OE	OE i3	306 [b]	320	605	322	384
	OE i1	330 [b]				
	OE i2	324 [b]				
OO	OO i3	306 [b]	320	3 931	320	384
	OO i1	332 [b]				
	OO i2	322 [b]				
OP	OP i3	306 [b]	307	1 064	301	405
	OP i1	332 [b]				
	OP i2	322 [b]				
Pc	-	-	326	32 956	-	-
PcE	-	314 [b]	-	-	-	-
PcO	-	312 [b]	-	-	-	-
PcP	-	312 [b]	-	-	-	-
Pt	-	-	307	44 991	305	377
PtE	-	302 [a]	302	8 149	300	385
PtO	-	302 [a]	302	3 220	299	385
PtP	-	302 [a]	302	8 929	299	385

These results seem to indicate that the addition of a hydrocarbon chain interacts with the ability of stilbenes to absorb electromagnetic radiation, resulting in lower absorptivity values, probably due to a breakdown of the resonance of the aromatic rings.

Although the range of linear concentrations increases, these changes generate a greater difficulty for the spectrophotometric quantification of these compounds.

3.2.4. Fluorescence spectroscopy

Fluorescence spectra were determined for the racemic mixtures of isomers by spectrofluorometer. Hydrophobic piceatannol derivatives could not be characterised because of their ease of degradation, breaking the ester bond and releasing piceatannol.

In general, the shape of the fluorescence excitation and emission spectra were quite similar for the stilbenes before and after structural modification.

In the excitation spectra (Figure 60), the greatest difference in shape was in the oxyresveratrol derivatives, showing a less pronounced valley between the main and secondary peak, which completely disappeared in oxyresveratrol palmitate. Although the fluorescence of the individual isomers could not be determined, this could be related to the loss of the peaks at 301 and 290 nm in the absorption spectra of the major isomer i3.

In the emission spectra (Figure 61), all derivatives maintained the rise in fluorescent intensity sharper than the decay, although the resveratrol derivatives softened this decay with respect to resveratrol. In addition, oxyresveratrol stearate and oleate showed a shoulder in this decay, around 405 – 410 nm.

The λ_{ex} did not show much differences compared to the λ_{max} observed by spectrophotometry (Table 13). The λ_{em} increased by 31 – 32 nm for resveratrol derivatives, 15 nm for oxyresveratrol palmitate and 8 nm for pterostilbene derivatives, compared to their original stilbenes. In contrast, oxyresveratrol stearate and oleate decreased the λ_{em} of oxyresveratrol by 9 nm. The type of fatty acid used in the esterification had almost no effect on the observed λ_{em}.

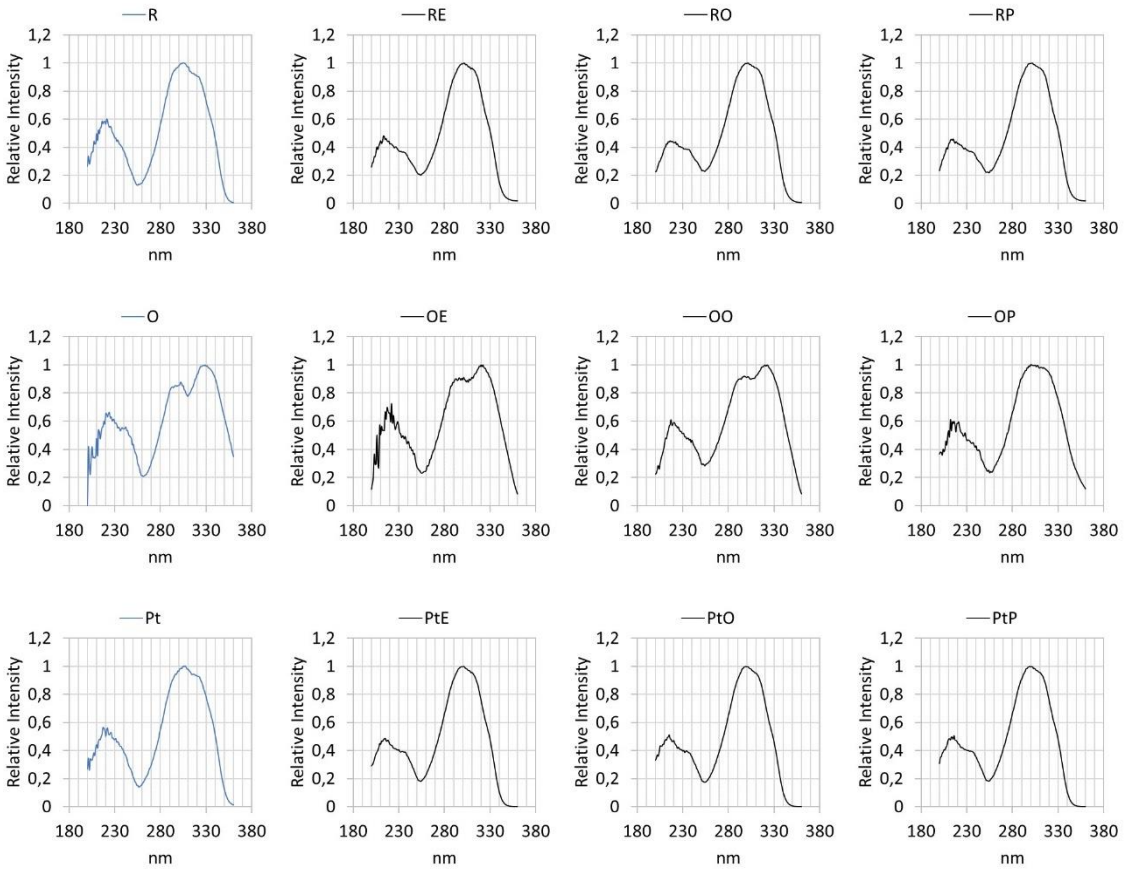

Figure 60. Relative fluorescence excitation spectra of the hydrophobic derivatives of stilbenes and their stilbenes (black) and their original stilbenes (blue). R: resveratrol, O: oxyresveratrol, Pt: pterostilbene

The fluorescence emission intensity was also markedly affected in most of the derivatives (Figure 62). While oxyresveratrol derivatives maintained (OO) or decreased (OE, OP) the intensity, resveratrol and pterostilbene derivatives significantly increased it. The type of fatty acid had an effect analogous to that observed with molar absorptivity. Resveratrol and oxyresveratrol oleates gave higher emission intensity than their corresponding palmitates and stearates, while pterostilbene oleate gave the opposite effect, showing lower intensity with respect to its stearate and palmitate derivatives.

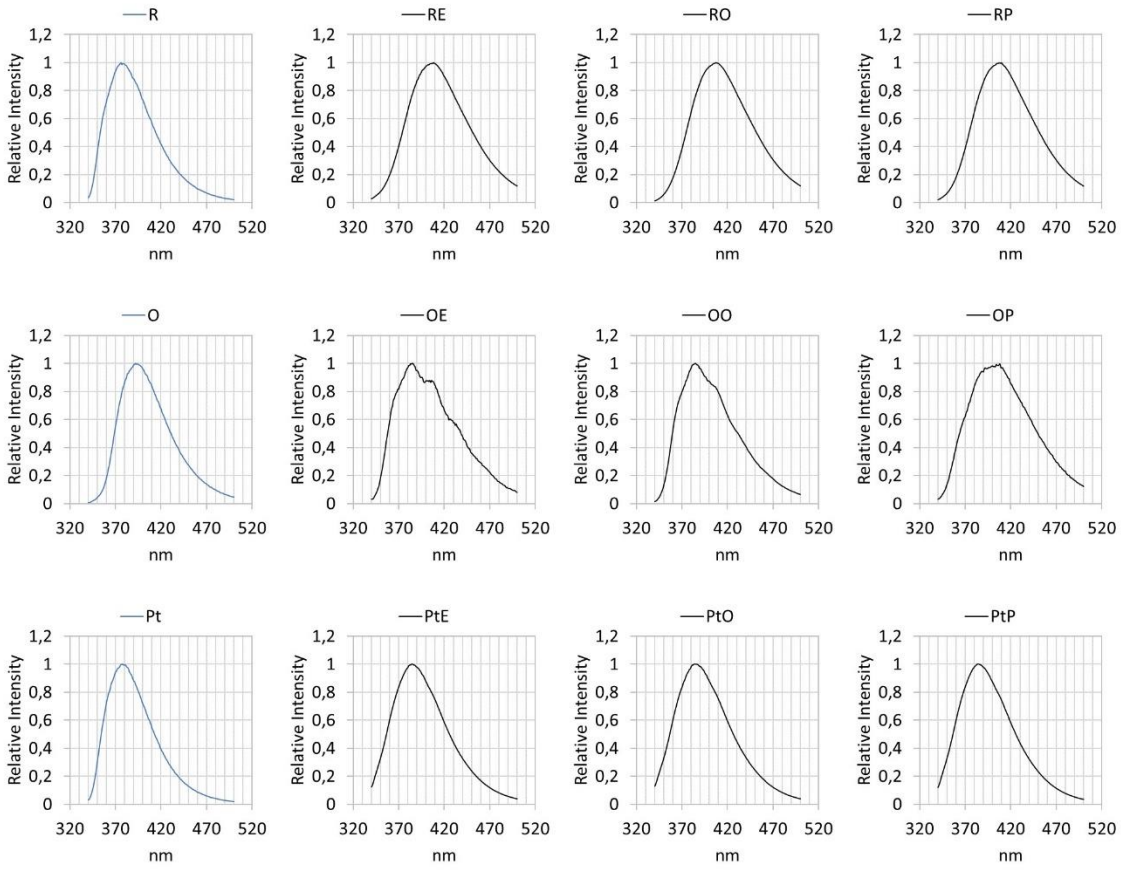

Figure 61. Relative fluorescence emission spectra of the hydrophobic stilbene derivatives (black) and their original stilbenes (blue). R: resveratrol, O: oxyresveratrol, Pt: pterostilbene

Similar to the absorbance, the ranges of linear concentrations in the fluorescent emission were extended with derivatisation and could reach up to 400 µM of hydrophobic stilbene derivatives (except with resveratrol oleate which was 200 µM), whereas with the original stilbenes only 100 µM was reached.

In contrast to absorbance, derivatisation with fatty acids seems to be able to enhance the fluorescent signal, facilitating spectrofluorometric quantification of stilbenes such as resveratrol and pterostilbene, but not oxyresveratrol. Therefore, the presence of a hydrocarbon chain in the 4', 3 or 5 position, keeping the other two groups hydroxylated or methoxylated, can increase the fluorescence of stilbenes and help their fluorometric detection.

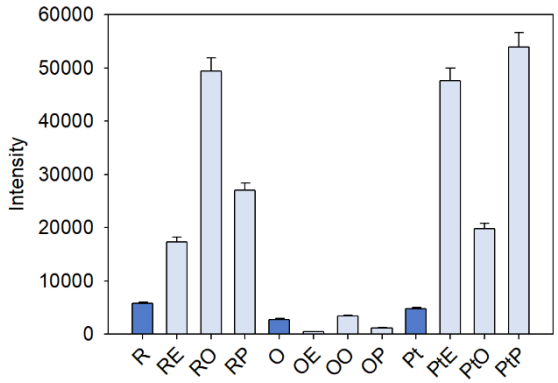

Figure 62. Fluorescence emission intensity of hydrophobic stilbene derivatives (light colour) and their original stilbenes (dark colour) at 100 µM. R: resveratrol, O: oxyresveratrol, Pt: pterostilbene

3.2.5. Other physicochemical parameters

Other parameters such as lipophilicity (logP), solubility (logS), topological polar surface area (TPSA) and molecular volume were computationally determined, with the chemical structures of the hydrophobic derivatives and their natural stilbenes (Table 14).

As expected, the structural modification of stilbenes led to an increase in their lipophilicity, accompanied by a decrease in their aqueous solubility. In general, all stilbenes halved their logS value after derivatisation, while the logP value tripled for the more lipophilic stilbenes, resveratrol and pterostilbene, and quadrupled for the less lipophilic stilbenes, oxyresveratrol and piceatannol (Table 14).

The lipophilicity results for stilbene derivatives showed a high correlation with the chromatograms obtained in Section 3.2.2. Stilbenes modified with stearic acid gave the highest lipophilicity, followed by those modified with oleic or palmitic acid. In general, palmitates were the least lipophilic, except for the pterostilbene derivatives where oleate was the least lipophilic. The shorter length and unsaturation degree of the hydrocarbon chain decreases lipophilicity. In the case of unsaturation, this is probably

because a negative charge density is created by the accumulation of electrons in the area of the π-type double bond which increases polarity.

Table 14. Physicochemical parameters of hydrophobic stilbene derivatives and their natural stilbenes. R: resveratrol, O: oxyresveratrol, Pc: piceatannol, Pt: pterostilbene

Product	Modified radical	-O-	-OH	logP	logS	TPSA (Å^2)	Molecular volume (Å^3)	MW
R	-	3	3	2.57	-3.52	60.68	206.92	228.2433
RE	R3 o R5	4	2	9.30	-7.04	66.76	512.26	494.7052
	R4’	4	2	9.34	-7.04	66.76	512.26	494.7052
RO	R3 o R5	4	2	9.07	-6.89	66.76	506.08	492.6894
	R4’	4	2	9.13	-6.90	66.76	506.08	492.6894
RP	R3 o R5	4	2	8.72	-6.75	66.76	478.66	466.6521
	R4’	4	2	8.80	-6.76	66.76	478.66	466.6521
O	-	4	4	2.06	-3.38	80.91	214.94	244.2427
OE	R2’	5	3	8.69	-6.43	86.99	520.28	510.7046
	R3 o R5	5	3	8.70	-6.43	86.99	520.28	510.7046
	R4’	5	3	8.72	-6.43	86.99	520.28	510.7046
OO	R2’	5	3	8.63	-6.39	86.99	514.09	508.6888
	R3 o R5	5	3	8.64	-6.39	86.99	514.09	508.6888
	R4’	5	3	8.66	-6.39	86.99	514.09	508.6888
OP	R2’	5	3	8.16	-6.15	86.99	486.68	482.6515
	R3 o R5	5	3	8.18	-6.15	86.99	486.68	482.6515
	R4’	5	3	8.19	-6.15	86.99	486.68	482.6515
Pc	-	4	4	2.12	-3.40	80.91	214.94	244.2427
PcE	R3’	5	3	8.70	-6.44	86.99	520.28	510.7046
	R4’	5	3	8.71	-6.43	86.99	520.28	510.7046
	R3 o R5	5	3	8.74	-6.45	86.99	520.28	510.7046
PcO	R3’	5	3	8.63	-6.39	86.99	514.09	508.6888
	R4’	5	3	8.64	-6.39	86.99	514.09	508.6888
	R3 o R5	5	3	8.69	-6.41	86.99	514.09	508.6888
PcP	R3’	5	3	8.18	-6.15	86.99	486.68	482.6515
	R4’	5	3	8.19	-6.16	86.99	486.68	482.6515
	R3 o R5	5	3	8.21	-6.17	86.99	486.68	482.6515
Pt	-	3	1	3.48	-4.37	38.70	241.98	256.2964
PtE	R4’	4	0	10.37	-8.11	44.77	547.32	522.7584
PtO	R4’	4	0	9.97	-8.18	44.77	541.13	520.7425
PtP	R4’	4	0	10.10	-8.15	44.77	513.72	494.7052

The modified isomers at the R3 and R5 radicals are shown together because no differences were observed between them in any of the parameters analysed (Table 14). Due to the symmetrical position of these radicals, their physicochemical properties were identical, and therefore, it is very likely that in chromatographic assays they elute as a single chromatographic peak. In general, structural modification at this R3 or R5 position generated less lipophilic stilbene derivatives than those modified at the R4' position. The presence of an additional hydroxyl group in the *meta* position, i.e. R2’ in oxyresveratrol

derivatives, did not modify this fact. However, in piceatannol, the presence of a hydroxyl group in the *ortho* position, i.e. R3', made the modification at R3 or R5 more lipophilic than the modification at R4'. On the other hand, modification at the R2' or R3' positions, i.e. at the additional hydroxyl groups present on oxyresveratrol or piceatannol, respectively, resulted in the least lipophilic isomers of all.

Based on the logP results obtained, the identification of the isomeric products synthesised could be deduced, with the isomers named i1 being those modified in the R3 or R5 position, i2 those modified in the R4' position, and i3 those modified in the R2' position. However, since there is no experimental evidence to confirm this, the designation of the isomers i1, i2 and i3 will be maintained throughout the doctoral thesis, without reference to the possible modified functional group.

On the other hand, structural modification with fatty acids increased the TPSA by almost 16 % in pterostilbene, 10 % in resveratrol, and almost 8 % in oxyresveratrol and piceatannol, regardless of the fatty acid used and the modified functional group (Table 14). The TPSA is defined as the sum of the surfaces of the polar atoms of a molecule, such as -OH or -NH_2, and is a parameter of interest for the prediction of the absorption of bioactive compounds. Some studies have demonstrated that there is a negative correlation between TPSA and the apparent permeability in cell cultures *in vitro* (Hou et al., 2004; Palm et al., 1998, 1996). Since this parameter takes into account the polar atoms of the molecule, the type of stilbene was the key factor, with the stilbene derivatives ordered according to their TPSA as follows: pterostilbene < resveratrol < oxyresveratrol = piceatannol. Therefore, the high TPSA of the oxyresveratrol and piceatannol derivatives could be an impediment to their intestinal absorption, with the resveratrol and pterostilbene derivatives being more interesting for oral applications.

Molecular volume, like TPSA, is used to predict intestinal transport of molecules, but it is a three-dimensional parameter. In general, all synthesised derivatives doubled their molecular volume, regardless of the modified functional group (Table 14). This parameter is directly related to the molecular mass, so the type of stilbene and fatty acid used in the modification were key factors in the molecular volume of the stilbene derivative. Therefore, the order of the derivatives by molecular volume according to the type of stilbene was: resveratrol < oxyresveratrol = piceatannol < pterostilbene, while according to the type of fatty acid was: palmitic acid < oleic acid < stearic acid.

3.3. Molecular encapsulation of hydrophobic stilbene derivatives

3.3.1. Molecular docking of hydrophobic stilbene derivatives in CDs

Molecular encapsulation of hydrophobic stilbene derivatives in natural and modified CDs was evaluated by means of computational molecular docking studies. The software used evaluates 1:1 ligand-receptor interactions. The assays were performed with one of the possible isomers of the synthesised derivatives. In the case of the resveratrol and oxyresveratrol derivatives, this isomer was the one that could be the majority according to the lipophilicity results previously described, and in piceatannol it was the isomer modified at the R3' position.

The score values obtained from molecular docking were similar among the different derivatives (Table 15). In general, molecular encapsulation in HP-β-CD showed the best results with an average score among all derivatives of -8.1, followed by β-CD with an average score of -7.6 and M-β-CD with an average score of -7.2. Finally, the CDs that gave the worst affinities were γ-CD and α-CD, with average scores of -5.3 and -4.9, respectively. Pterostilbene stearate was the only derivative studied that did not score best

with HP-β-CD, but ahead of this CD was M-β-CD. On the other hand, piceatannol palmitate showed the same affinity for HP-β-CD and β-CD.

It seems that the cavity with 7 glucose units is the most suitable to form inclusion complexes with these hydrophobic stilbene derivatives, especially if the glucose units are modified with hydroxypropyl groups. In contrast, other CD sizes with 6 or 8 glucose units may form less stable complexes with these stilbene derivatives. Previous studies with the natural stilbenes resveratrol (López-Nicolás and García-Carmona, 2008b), oxyresveratrol (Matencio et al., 2017a), piceatannol (Matencio et al., 2016) and pterostilbene (López-Nicolás et al., 2009b) also showed similar findings, so it seems that modification of stilbenes with fatty acids does not alter the type of CD with which to form the most stable complexes.

Table 15. Molecular docking score of hydrophobic stilbene derivatives with natural and modified CDs

Product	Modified radical	Score				
		α-CD	β-CD	γ-CD	HP-β-CD	M-β-CD
RE	R4'	-5.2	-7.6	-5.3	**-8.7**	-7.3
RO	R4'	-5.0	-7.6	-5.4	**-7.7**	-7.5
RP	R4'	-5.5	-7.4	-5.4	**-8.3**	-7.3
OE	R2'	-4.2	-7.6	-5.3	**-7.9**	-6.8
OO	R2'	-4.5	-7.8	-5.4	**-8.2**	-6.9
OP	R2'	-4.4	-8.3	-5.5	**-8.6**	-7.0
PcE	R3'	-4.8	-7.6	-5.2	**-8.3**	-7.1
PcO	R3'	-4.8	-7.1	-5.5	**-8.2**	-7.5
PcP	R3'	-5.3	**-8.0**	-5.1	**-8.0**	-7.0
PtE	R4'	-4.7	-7.0	-4.3	-7.1	**-7.3**
PtO	R4'	-5.1	-7.6	-5.2	**-8.0**	-7.0
PtP	R4'	-5.1	-7.3	-5.6	**-8.2**	-7.3

The 3D representation of the most likely molecular docking of these derivatives with HP-β-CD showed different conformations (Figure 63 and Figure 64). In general, the ligands folded over the ester bond, most of them penetrating the CD cavity through this junction. Hydrogen bonds were only observed in some of the more polar derivatives, so it is possible that given the high lipophilicity of these molecules, hydrophobic interactions also play a relevant role in stabilising the inclusion complexes with CDs.

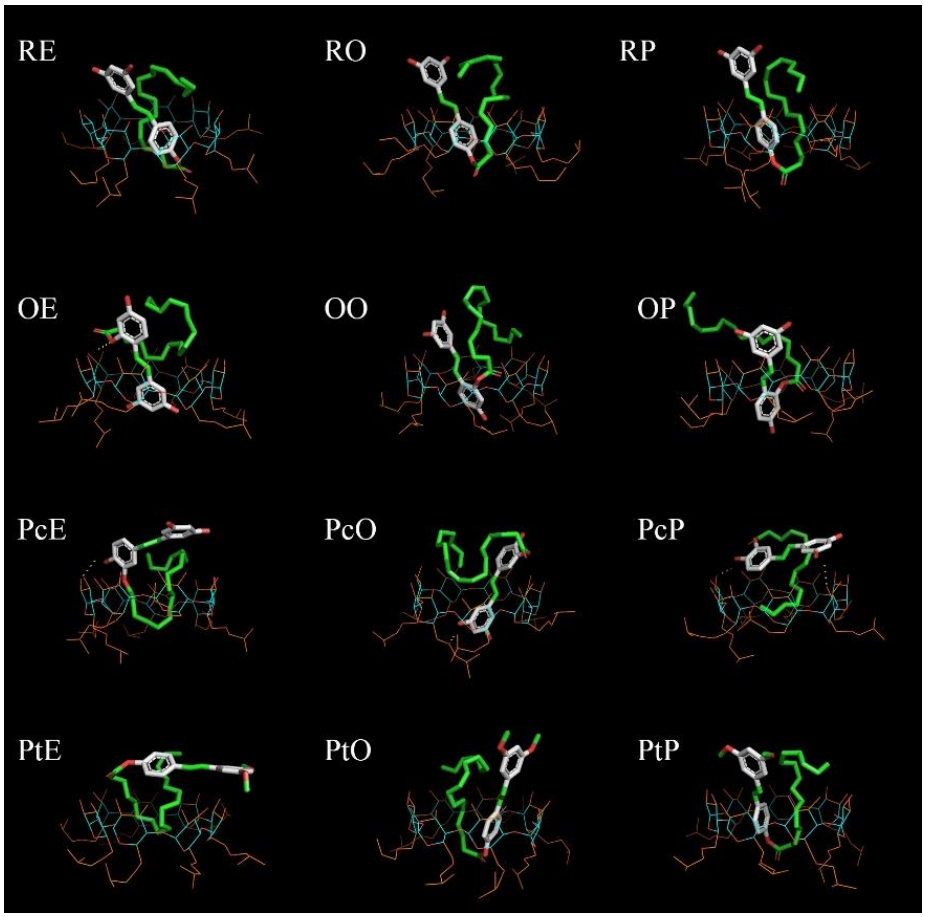

Figure 63. Front view of the 3D molecular docking of hydrophobic stilbene derivatives (isomers mentioned in Table 15) on HP-β-CD. The flexible atoms of the CD are visualised in orange, while the non-flexible atoms are visualised in blue. Hydrogen bonds are shown as yellow dashed lines

In the resveratrol derivatives, the fatty acid folded parallel to the stilbene, orienting the ester bond towards the primary face of the CD, where its hydroxypropyl groups are located. The unmodified ring and the end of the hydrocarbon chain of the resveratrol derivatives were outside the CD, towards its secondary face. Something similar could be observed for oxyresveratrol and pterostilbene derivatives with oleic and palmitic acids. However, stearate derivatives showed a different interaction with the CD. Oxyresveratrol stearate also kept the end of its hydrocarbon chain oriented towards the secondary face of the CD, but the unmodified ring was oriented towards the primary face, leaving the ester bond on the same side as the chain. In addition, stabilisation of the complex was observed

through the formation of a hydrogen bond between one of the secondary hydrogens of the CD and the oxygen of the ester bond.

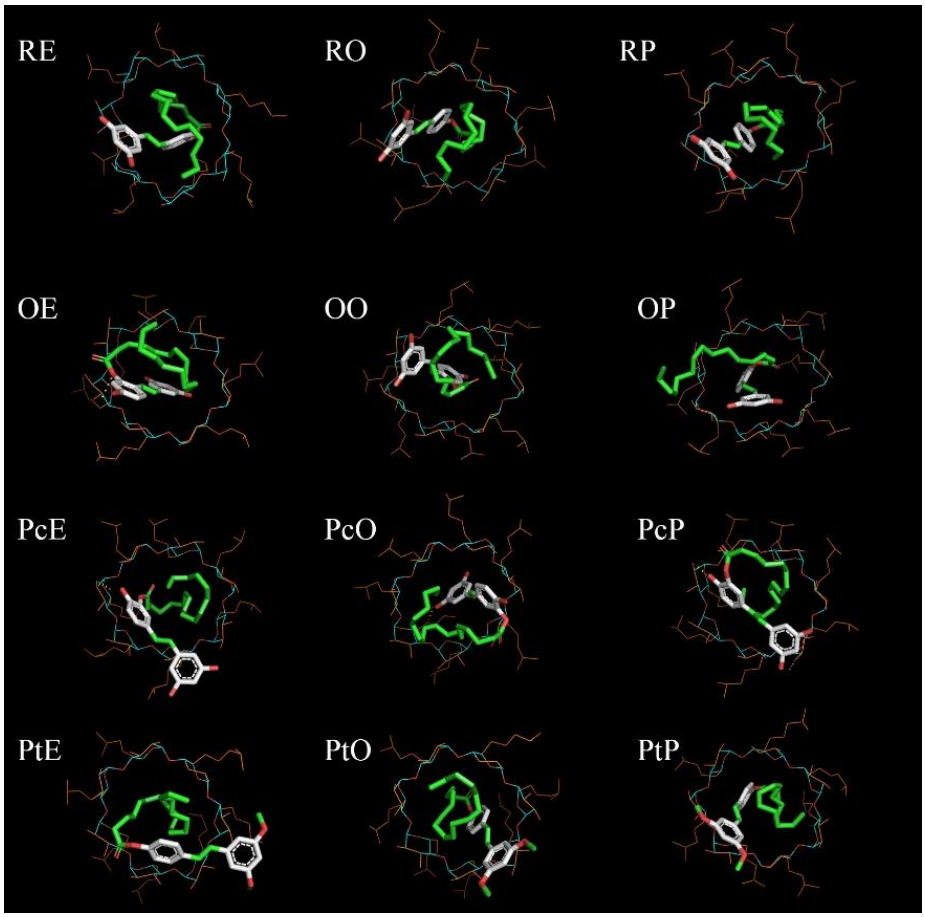

Figure 64. Top view of the 3D molecular docking of hydrophobic stilbene derivatives (isomers mentioned in Table 15) on HP-β-CD. The flexible atoms of the CD are visualised in orange, while the non-flexible atoms are visualised in blue. Hydrogen bonds are shown as yellow dashed lines

Pterostilbene stearate showed a more complex conformation, with only the hydrocarbon chain entering the CD cavity, leaving the rest of the molecule protruding from the secondary face. Piceatannol stearate and palmitate also showed this type of three-dimensional conformation in which the fatty acid was the main part of the molecule entering the CD cavity, but not piceatannol oleate. Piceatannol oleate interaction with the CD was more similar to that of oxyresveratrol stearate, with the unmodified ring entering the cavity towards the primary face of the CD and orienting the hydrocarbon chain and

ester bond towards the secondary face. In addition, in all piceatannol derivatives, hydrogen bonds were observed between the CD and the free hydroxyl groups of the stilbene. In piceatannol stearate and palmitate these hydrogen bonds were on the secondary face of the CD, while in piceatannol oleate were on the primary face.

3.3.2. Physicochemical study of the inclusion complexes with hydrophobic stilbene derivatives

The molecular encapsulation of the synthesised derivatives was performed by reversed-phase liquid chromatography with the CD that gave the best overall affinity results in molecular docking studies, HP-β-CD.

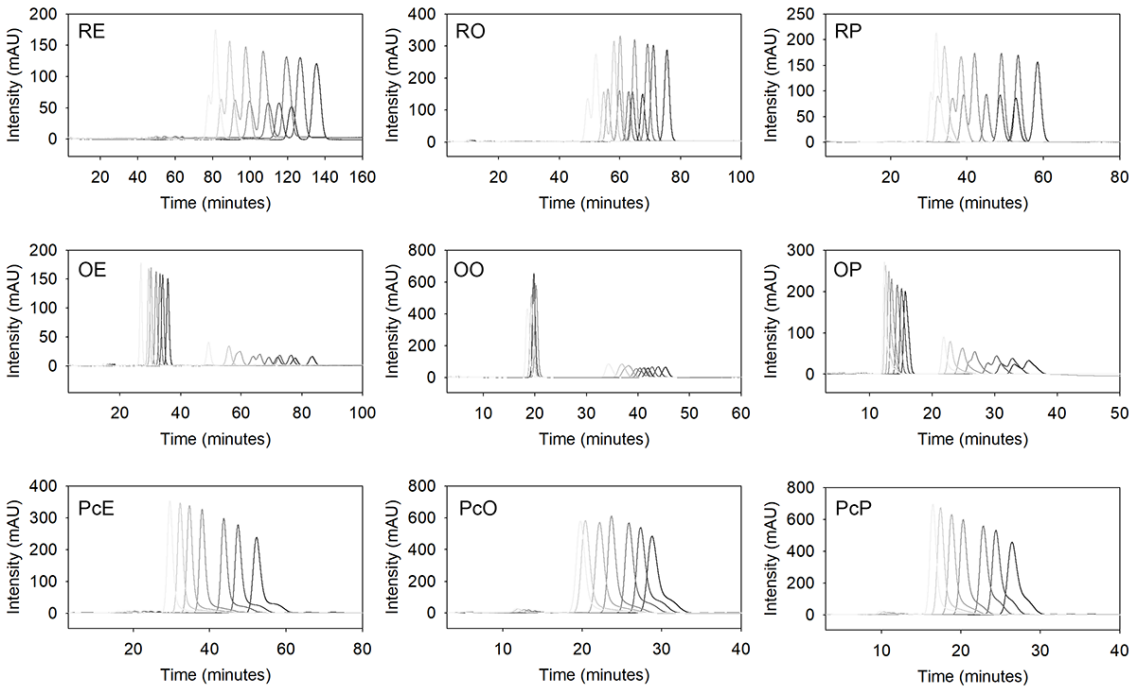

Figure 65. Chromatograms at 310 nm of the hydrophobic stilbene derivatives in the presence of HP-β-CD at 0 (higher grey intensity), 5, 10, 20, 30, 40 and 50 (lower grey intensity) mM (25 °C, 85 % (v/v) methanol)

The assays were carried out with an aqueous mobile phase containing 85 % (v/v) methanol with or without increasing concentrations of HP-β-CD. After optimisation, this percentage of methanol was the minimum concentration of organic solvent necessary to

ensure that the chromatographic peaks of the more hydrophobic derivatives did not elute at times longer than 150 min. This test could not be performed with the pterostilbene derivatives, as they required higher concentrations of organic solvent to elute from the chromatographic column.

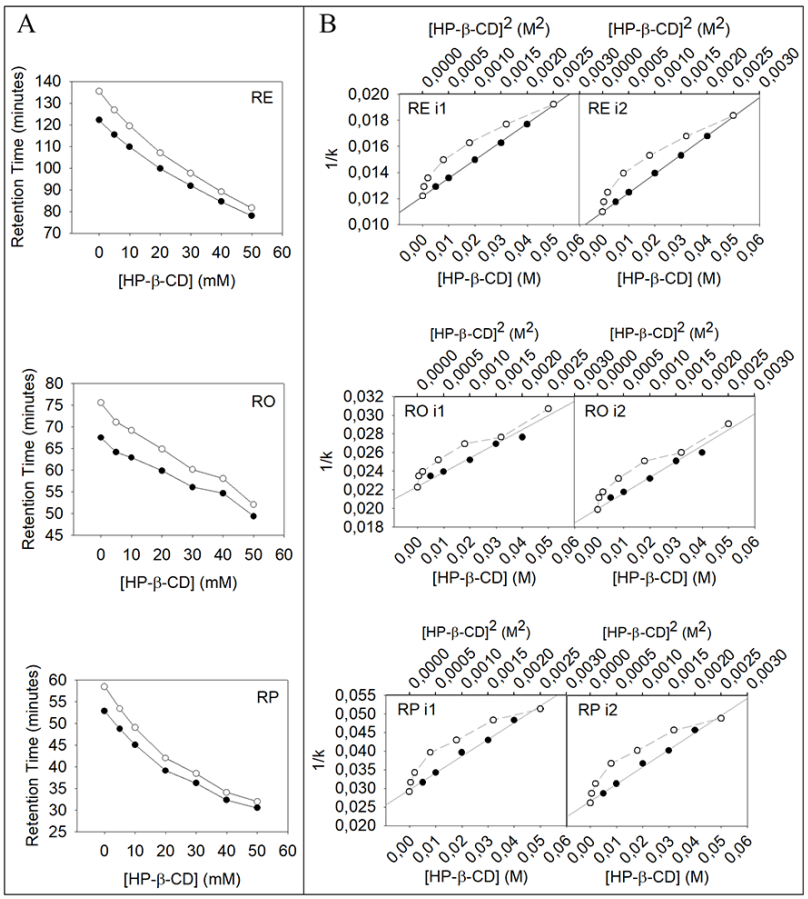

Figure 66. A) Effect of increasing HP-β-CD concentration on the retention time of the isomers (●) i1 and (○) i2 of resveratrol derivatives. B) Mohseni-Hurtubise fitting of the HP-β-CD complexes with the different isomers of resveratrol derivatives to a (●) 1:1 and (○) 1:2 model (25 °C, 85 % (v/v) methanol)

The chromatograms showed that increasing the concentration of CD in the mobile phase caused a decrease in the retention time of the chromatographic peaks associated with an increase in the aqueous solubility of the derivatives when encapsulated (Figure 65). This fact made it possible to characterise the inclusion complexes with the Mohseni-Hurtubise method (Figure 66A, Figure 67A and Figure 68A). In addition, narrowing and

co-elution of the closest isomers could also be observed above a certain concentration of CD (Figure 65).

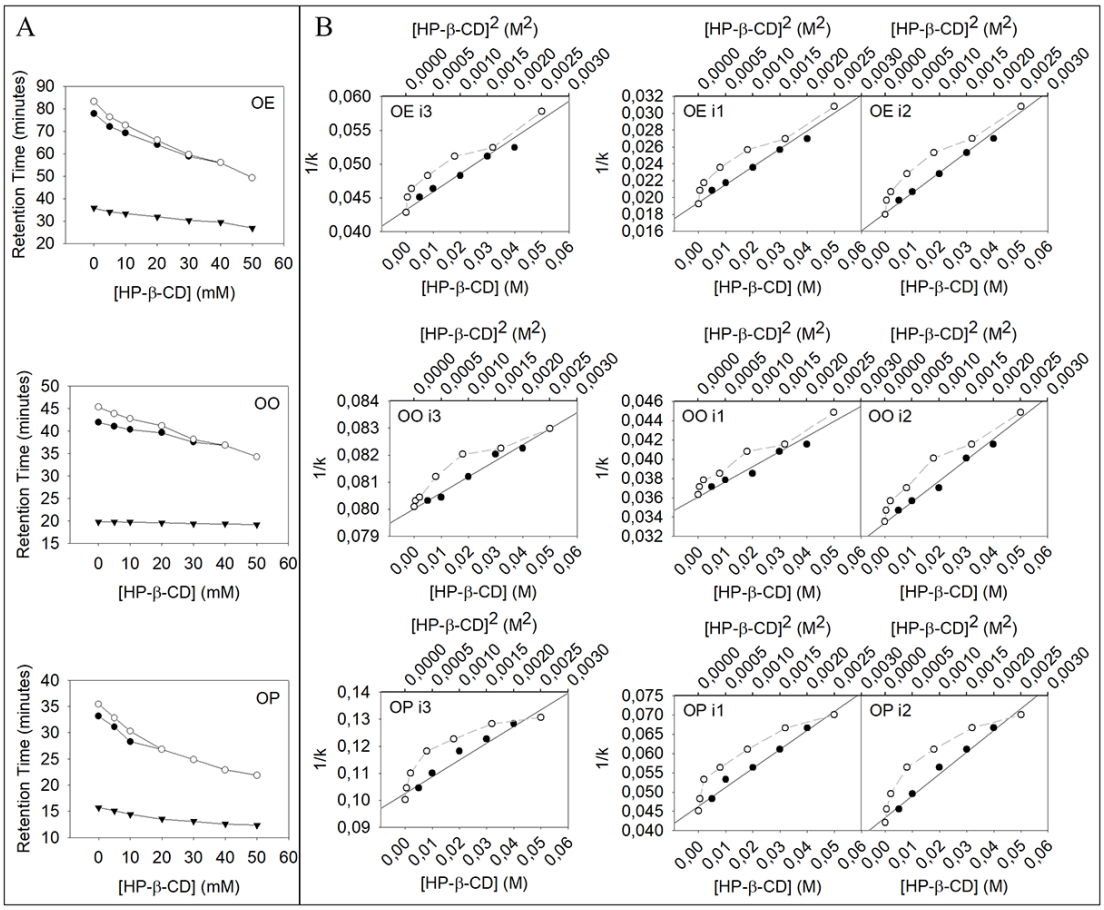

Figure 67. A) Effect of increasing HP-β-CD concentration on the retention time of the isomers (●) i1, (○) i2 and (▼) i3 of oxyresveratrol derivatives. B) Mohseni-Hurtubise fitting of the HP-β-CD complexes with the different isomers of oxyresveratrol derivatives to a (●) 1:1 and (○) 1:2 model (25 °C, 85 % (v/v) methanol)

After applying the Mohseni-Hurtubise fitting, it was observed that, under the conditions studied, the molecular encapsulation of hydrophobic stilbene derivatives in HP-β-CD was governed by a 1:1 stoichiometry, in which one molecule of the stilbene derivative interacted with a single molecule of CD (Figure 66B, Figure 67B and Figure 68B). Unlike the Benesi-Hildebrand method, this method allows the determination of the stoichiometry and apparent formation constants of the individual isomers without prior isolation.

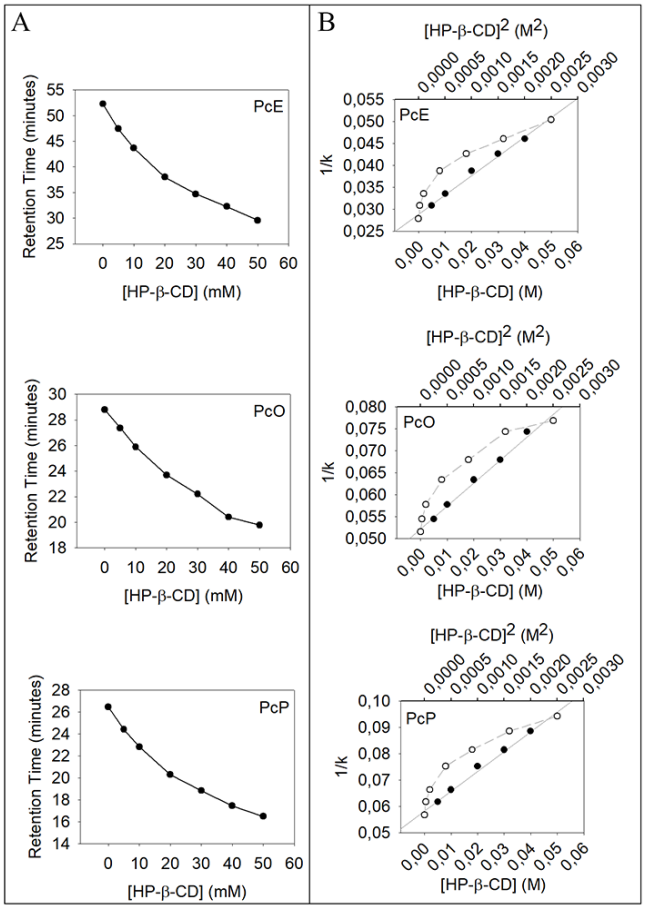

Figure 68. A) Effect of increasing HP-β-CD concentration on the retention time of piceatannol derivatives. B) Mohseni-Hurtubise fitting of the HP-β-CD complexes with piceatannol derivatives to a (●) 1:1 and (○) 1:2 model (25 °C, 85 % (v/v) methanol)

The apparent formation constants of the inclusion complexes with each of the isomers were determined using Equation (15) (Table 16). In general, these constants correlated positively with the apolarity and lipophilicity of the stilbene derivatives (Table 14 and Table 12). The derivatives that encapsulated best in CD were resveratrol palmitate and piceatannol stearate ($K_{F\,ap} > 15\ M^{-1}$), and those that formed the worst complexes were oxyresveratrol oleates ($K_{F\,ap} < 7\ M^{-1}$) (Table 16).

The less polar isomers gave higher apparent formation constants with HP-β-CD, i.e. K_{ap} i2 > K_{ap} i1 > K_{ap} i3 (Table 16). Therefore, the majority isomer obtained in the

resveratrol derivatisation (i2) was the most compatible with the CD cavity, whereas in the oxyresveratrol derivatives, the majority isomer obtained (i3) was the least compatible.

Within the isomers that gave the best constants, the type of stilbene had a variable influence on encapsulation depending on the fatty acid. While for stearates and oleate derivatives piceatannol gave higher constants, for palmitates it was resveratrol (Table 16).

Table 16. Apparent formation constants and correlation coefficients of hydrophobic derivatives of stilbenes with HP-β-CD, obtained by the Mohseni-Hurtubise method (25 °C, 85 % (v/v) methanol)

Product	Isomer	$K_{F\ ap}$ (M^{-1})	R^2	
			1:1 model	1:2 model
RE	RE i1	11.44 ± 0.57	1.000	0.937
	RE i2	13.30 ± 0.67	1.000	0.935
RO	RO i1	6.84 ± 0.34	0.972	0.963
	RO i2	8.50 ± 0.43	0.982	0.943
RP	RP i1	15.29 ± 0.76	0.994	0.895
	RP i2	17.32 ± 0.87	0.995	0.898
OE	OE i3	6.21 ± 0.31	0.972	0.938
	OE i1	10.89 ± 0.54	0.983	0.943
	OE i2	13.27 ± 0.66	0.990	0.942
OO	OO i3	0.74 ± 0.04	0.974	0.917
	OO i1	3.63 ± 0.18	0.976	0.913
	OO i2	6.55 ± 0.33	0.988	0.954
OP	OP i3	6.04 ± 0.30	0.963	0.804
	OP i1	10.58 ± 0.53	0.986	0.881
	OP i2	13.05 ± 0.65	0.987	0.863
PcE	-	15.31 ± 0.77	0.993	0.885
PcO	-	9.99 ± 0.50	0.992	0.886
PcP	-	12.83 ± 0.64	0.992	0.879

Depending on the lipid fraction of the stilbene derivative, the molecular encapsulation of derivatives with saturated chains was more efficient than the encapsulation of derivatives with unsaturated chains, regardless of the type of starting stilbene. The length of the hydrocarbon chain showed different results depending on the stilbene derivative. The length of the hydrocarbon chain showed different results depending on the stilbene derivative. In the resveratrol derivatives, the 16-carbon chain gave better apparent formation constants than the 18-carbon chain, while in the

oxyresveratrol derivatives there were no significant differences. The opposite was true for the piceatannol derivatives, with the derivatives with the longer chain encapsulating better in HP-β-CD.

3.4. Conclusions on the synthesis, characterisation and molecular encapsulation of hydrophobic stilbene derivatives

Hydrophobic derivatives of resveratrol, oxyresveratrol, piceatannol and pterostilbene were synthesised by esterification of their free hydroxyl groups with stearic acid, oleic acid and palmitic acid. The optimised chemical method achieved yields of 49 – 78 % and high specificity in the formation of monoester products. Two and three HPLC-identifiable isomers were obtained for resveratrol and oxyresveratrol derivatives, respectively. Enzymatic synthesis of resveratrol stearate proved not to be as effective as chemical synthesis, yielding 56 % in 90 hours.

The structural modification of the stilbenes led to changes in their physicochemical properties, with chemical shifts observed by H-NMR and bathochromic or hypsochromic shifts depending on the derivative by spectroscopy. As expected, the synthesised derivatives were less polar, more lipophilic and less soluble than their original stilbenes. In general, the spectra varied according to the type of stilbene and isomer rather than the type of fatty acid used in the esterification. In addition, although all derivatives showed lower molar absorptivity, the resveratrol and pterostilbene derivatives were more fluorescent than their parent stilbenes, indicating that these new compounds might be more easily detectable by fluorometric than photometric techniques. The resveratrol and pterostilbene derivatives also gave lower topological polar surface area values, which might suggest a higher permeability across biological membranes.

Overall, the molecular docking results showed that HP-β-CD formed the most stable inclusion complexes with the hydrophobic stilbene derivatives, just like natural stilbenes. In most of the 3D docking, the ligand was folded by the ester bond in order to enter the CD cavity. Moreover, only the more polar derivatives showed hydrogen bonds between guest and host molecules, so it is likely that hydrophobic interactions also play a role in the stabilisation of the inclusion complexes. Characterisation of the complexes by the Mohseni-Hurtubise method using 85 % (v/v) methanol showed a 1:1 stoichiometry in which one molecule of HP-β-CD interacted with one molecule of hydrophobic stilbene derivative. Apparent encapsulation constants were determined with this model and were correlated with the lipophilicity of the ligands. Stearates and palmitates showed the highest constants, suggesting a higher affinity for CDs.

4. DIGESTION, ABSORPTION AND METABOLISM OF HYDROPHOBIC STILBENE DERIVATIVES

The intestinal absorption, digestion and metabolism of the synthesised hydrophobic stilbene derivatives and their parent stilbenes were evaluated by different techniques. First, the effect of the key enzyme in the digestive process of this type of compounds, the pancreatic lipase enzyme, was analysed *in vitro*, investigating also possible inhibitors, as well as the effect of the administration of the compounds free or encapsulated in CDs. The selection of this type of enzyme was based on previous studies that evaluated the *in vitro* gastrointestinal digestion of monoesters, diesters and triesters of a resveratrol derivative with caprylic acid (Hu et al., 2019). The researchers observed that there was no hydrolysis reaction at the oral and gastric level, but there was a hydrolysis reaction at the intestinal level, especially in the case of the monoesters. This hydrolysis was due to the effect of the enzyme pancreatic lipase, while the enzyme phospholipase A2 showed no activity under the conditions studied.

Next, the intestinal permeability and metabolism of hydrophobic stilbene derivatives and their natural stilbenes were evaluated in cultured human colorectal Caco-2 cells, after studying their *in vitro* cytotoxicity. This cell line is widely used to predict the uptake of bioactive compounds after oral administration (Hubatsch et al., 2007). In addition, these cells are capable of expressing enzymes responsible for phase II reactions that decrease the bioavailability of stilbenes, such as sulfotransferases and glucuronosyltransferases (Li et al., 2003). For this reason, the potential metabolisation of the administered compounds was also assessed. Finally, these assays were complemented by *in vivo* studies in the animal model *M. musculus*, evaluating the pharmacokinetics of

one of the hydrophobic stilbene derivatives and its natural stilbene, in free form and encapsulated in HP-β-CD.

4.1. *In vitro* assays

4.1.1. Effect of pancreatic lipase on hydrophobic stilbene derivatives

4.1.1.1. Hydrolysis degree of hydrophobic stilbene derivatives

Hydrolysis of the ester bond of hydrophobic stilbene derivatives at the intestinal level could compromise the purpose of the structural modification by releasing the stilbene before it reaches the target tissue. For this reason, the degree of hydrolysis of the resveratrol, oxyresveratrol and pterostilbene derivatives was analysed. These tests were performed with the racemic mixture of the isomers obtained in the ratio described in Section 3.1.

The results revealed that, in the presence of pancreatic lipase, the hydrophobic stilbene derivatives were partially hydrolysed depending on the stilbene and the type of fatty acid used in the esterification (Figure 69).

For resveratrol and oxyresveratrol derivatives, the lowest degree of end-time hydrolysis was observed for palmitates (20 – 26 %), followed by oleates (29 – 40 %) and finally stearates (49 – 65 %). In the pterostilbene derivatives, both palmitate and stearate gave the lowest degree of hydrolysis (48 – 53 %), while pterostilbene oleate underwent rapid degradation in the first half hour, but thereafter remained almost stable until the end of the reaction (37 %). Prior to this, it was checked that, in the absence of the enzyme, the amount of stilbene did not change.

Oxyresveratrol stearate was the derivative most sensitive to the effect of the enzyme. Despite retaining more than half of the stilbene at 90 minutes, this derivative

decreased its remaining amount to below 36 % in the last half hour of the test. Except for oxyresveratrol stearate and pterostilbene palmitate, all other stilbene derivatives retained more than half of the initial amount after the two-hour test.

Resveratrol palmitate was shown to be the least sensitive hydrophobic derivative to the catalytic activity of the enzyme under the conditions tested, followed by oxyresveratrol palmitate and resveratrol oleate. These three stilbene derivatives were able to preserve more than 70 % of the initial amount at the end of the experiment.

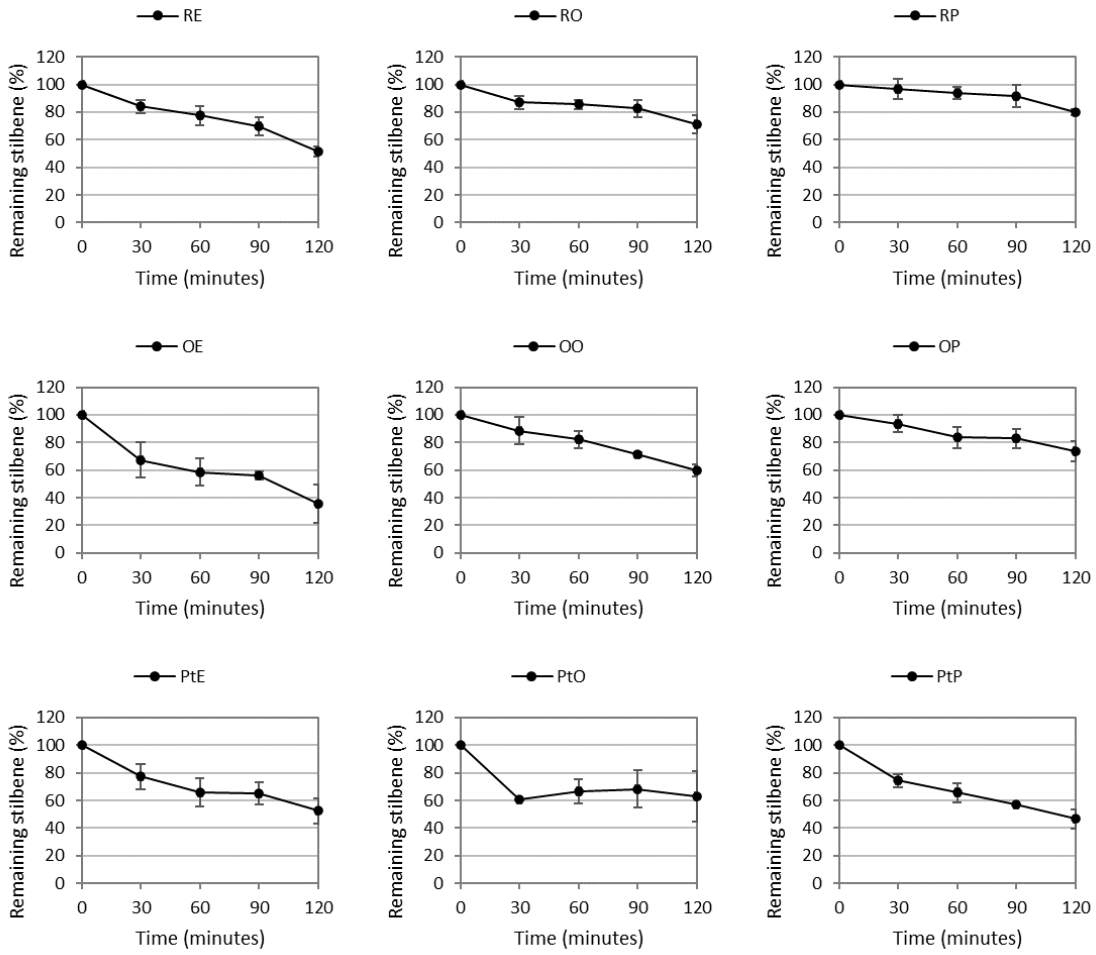

Figure 69. Hydrolysis of hydrophobic stilbene derivatives in the presence of pancreatic lipase, determined by HPLC-UV/Vis (37 °C pH 7)

4.1.1.2. Inhibition of pancreatic lipase catalytic activity with free caffeoylquinic acids

Pancreatic lipase enzyme activity can be inhibited by various compounds, including several phenolic compounds. In fact, some natural stilbenes are also capable of inhibiting its activity (Lee et al., 2013), so it is possible that hydrolysis of hydrophobic stilbene derivatives could lead to product inhibition above a certain concentration. However, to further protect hydrophobic stilbene derivatives, their inhibition by another type of phenolic compounds was studied. These compounds were chlorogenic acid (5-O-caffeoylquinic acid) and neochlorogenic acid (3-O-caffeoylquinic acid), both isomers found in green coffee beans and consisting of a caffeic acid linked by an ester bond to a D-(-)-quinic acid. These caffeoylquinic acids have been shown to have inhibitory activity against pancreatic lipase in emulsions with triolein as a substrate (Narita et al., 2012). In this PhD thesis, inhibition assays were performed by fluorometric and chromatographic techniques, using resveratrol stearate as substrate.

4.1.1.2.1. Spectrofluorometric inhibition tests

After 80 minutes of reaction with pancreatic lipase, resveratrol stearate underwent 40 % hydrolysis compared to the initial concentration in the absence of caffeoylquinic acids (Figure 70). The addition of neochlorogenic acid at low concentrations showed no significant difference in this value. However, neochlorogenic acid at 50 µM caused a significant decrease in the catalytic activity of pancreatic lipase, consuming less than 27 % of the resveratrol stearate.

On the other hand, chlorogenic acid was able to inhibit pancreatic lipase activity on resveratrol stearate significantly at lower concentrations than neochlorogenic acid. Chlorogenic acid at just 10 µM gave a degree of hydrolysis of 25 %, similar to that obtained with the highest concentration of its isomer. In general, under the conditions

studied, chlorogenic acid gave a higher inhibitory activity, reaching at the highest concentration of 50 µM a hydrolysis of only 17 %.

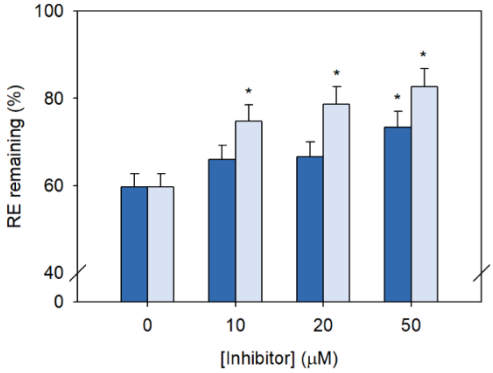

*Figure 70. Hydrolysis of resveratrol stearate (RE) in the presence of pancreatic lipase and different concentrations of neochlorogenic acid (dark colour) or chlorogenic acid (light colour), determined by fluorescence spectroscopy (37 °C pH 7 80 minutes) * Significance p-value < 0.05*

4.1.1.2.2. Chromatographic inhibition tests

Inhibition assays were also performed by HPLC and compared with those obtained by fluorescence spectroscopy. Previously, the concentrations and the time were optimised to obtain a quantifiable chromatographic peak throughout the reaction. Although the concentrations varied, a similar substrate-to-inhibitor ratio was maintained (fluorescence: 1:0.5 | 1:1 | 1:2.5 ~vs~ HPLC: 1:1 | 1:1.5).

Under these conditions, although the degree of basal hydrolysis of resveratrol stearate by HPLC was slightly higher (50 %) than that observed by fluorescence spectroscopy (40 %), higher levels of inhibition were achieved, reaching a complete inhibition of the enzyme activity with the use of neochlorogenic acid at 150 µM (Figure 71). Furthermore, a concentration of 100 µM (1:1 substrate-to-inhibitor ratio) of both inhibitors showed a significant effect on enzyme activity, in contrast to what was observed by fluorescence spectroscopy with neochlorogenic acid at 20 µM (1:1 substrate-to-inhibitor ratio). Despite this slight difference, the results by both techniques correlate

well, showing a concentration-dependent inhibition of the activity by neochlorogenic acid and chlorogenic acid.

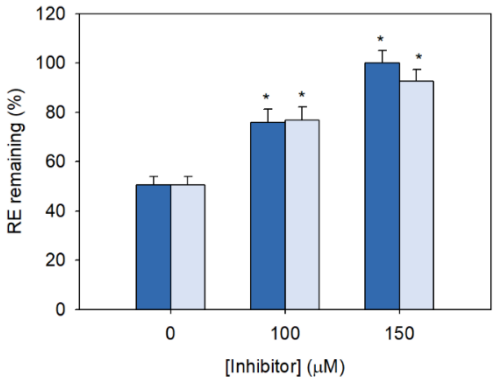

*Figure 71. Hydrolysis of resveratrol stearate (RE) in the presence of pancreatic lipase and different concentrations of neochlorogenic acid (dark colour) or chlorogenic acid (light colour), determined by HPLC-UV/Vis (37 °C pH 7 120 minutes) * Significance p-value < 0.05*

As this chromatographic technique allows to distinguish between isomers, it was also investigated whether the inhibitory activity affected equally or differently on the different resveratrol stearate isomers. In this respect, no significant differences were observed between the isomers, regardless of the concentration and type of inhibitor (Figure 72). Therefore, neochlorogenic acid and chlorogenic acid may be inhibitors of the catalytic activity of pancreatic lipase on hydrophobic stilbene derivatives, which could help to protect these newly synthesised stilbenes in future *in vivo* applications.

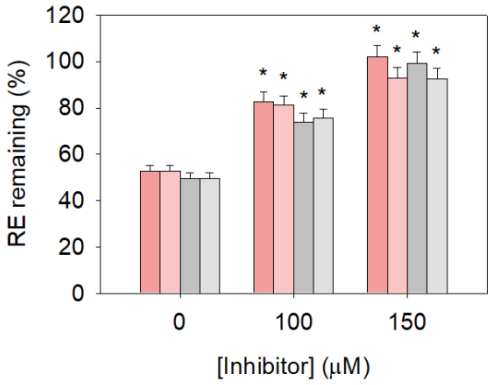

*Figure 72. Hydrolysis of the resveratrol stearate isomers RE i1 (pink) and RE i2 (grey) in the presence of pancreatic lipase and different concentrations of neochlorogenic acid (dark colour) or chlorogenic acid (light colour), determined by HPLC-UV/Vis (37 °C pH 7 120 minutes) * Significance p-value < 0.05*

4.1.1.3. Molecular encapsulation of caffeoylquinic acids

The complexation of these caffeoylquinic acids with CDs was then characterised in order to analyse whether the additional use of these encapsulating agents affected their inhibitory activity. As mentioned in Materials and Methods Section, a competitive model was used with two possible complexation sites in the guest molecule, i.e. one in the caffeic acid moiety (*CD-CQA* complex, with encapsulation constant K_{F1}) and the other in the D-(-)-quinic acid moiety (*CQA-CD* complex, with encapsulation constant K_{F2}).

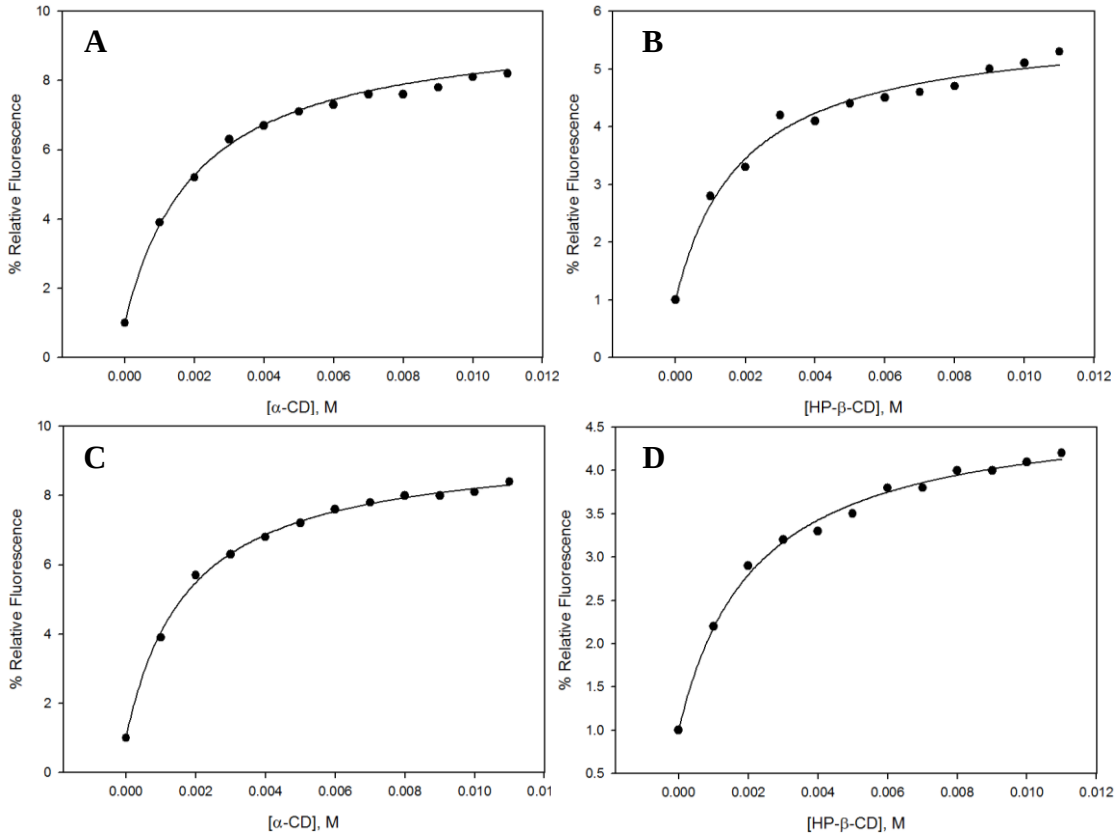

Figure 73. Complexation curve fit of neochlorogenic acid (A and B) and chlorogenic acid (C and D) with α-CD (A and C) and HP-β-CD (B and D) to the competitive model with two complexation sites according to Equation 12 (25 °C pH 5)

The complexation results showed a good fit to the selected model, giving correlation coefficients $R^2 > 0.98$ for all inclusion complexes studied (Figure 73). Despite

the structural similarity of these caffeoylquinic acids, their encapsulation constants with the different CDs analysed varied slightly (Table 17).

Table 17. Encapsulation constants and correlation coefficients of the inclusion complexes of caffeoylquinic acids with different CDs, obtained with the competitive model with two complexation sites (Equation 12) (25 °C pH 5)

CD	Neochlorogenic acid			Chlorogenic acid		
	K_{F1} (M^{-1})	K_{F2} (M^{-1})	R^2	K_{F1} (M^{-1})	K_{F2} (M^{-1})	R^2
α-CD	457.56 ± 22.88	30.64 ± 1.53	0.996	530.06 ± 26.50	32.63 ± 1.63	0.997
β-CD	159.77 ± 7.99	12.71 ± 0.64	0.985	311.75 ± 15.59	14.56 ± 0.73	0.975
γ-CD	22.42 ± 1.12	6.56 ± 0.33	0.981	0.58 ± 0.03	-	0.972
HP-β-CD	503.74 ± 25.19	24.93 ± 1.25	0.992	439.52 ± 21.98	21.20 ± 1.06	0.997
M-β-CD	314.94 ± 15.75	14.31 ± 0.72	0.991	381.87 ± 19.09	20.27 ± 1.01	0.987

The order of preference of CDs according to their encapsulation constant was quite similar in both isomers. HP-β-CD and α-CD were the best CDs to encapsulate these caffeoylquinic acids with $K_{F1} > 430$ M^{-1} and $K_{F2} > 21$ M^{-1}, followed by M-β-CD, β-CD, and lastly, γ-CD which gave the lowest values of $K_{F1} < 23$ M^{-1} and $K_{F2} < 2$ M^{-1} (Table 17). Chlorogenic acid gave higher encapsulation constants than those obtained with neochlorogenic acid in the inclusion complexes with α-CD, β-CD and M-β-CD, while in the complexes with HP-β-CD and γ-CD they were lower, in fact, the value of the encapsulation constant with the latter CD was negligible.

4.1.1.3.1. Molecular docking of caffeoylquinic acids in CDs

The molecular coupling of neochlorogenic acid and chlorogenic acid with the two best CDs obtained in the previous tests showed better score values with α-CD than with HP-β-CD (Table 18). However, in the three-dimensional modelling, the formation of several hydrogen bonds in the inclusion complexes with HP-β-CD could be appreciated, interacting mainly with the hydroxypropyl groups of this modified CD (Figure 74B and D). In general, the score values obtained with neochlorogenic acid were better than those

obtained with chlorogenic acid, indicating a possible higher affinity of this isomer for these encapsulating agents.

Table 18. Molecular docking score of caffeoylquinic acids with α-CD and HP-β-CD, classified by the encapsulated moiety of the ligand

CD	Neochlorogenic acid		Chlorogenic acid	
	Score CD-CQA (*caffeic moiety*)	**Score CQA-CD** (*quinic moiety*)	**Score CD-CQA** (*caffeic moiety*)	**Score CQA-CD** (*quinic moiety*)
α-CD	-7.4	-6.1	-7.0	-6.0
HP-β-CD	-6.7	-6.4	-6.3	-5.8

The inclusion complexes formed in the caffeic acid moiety of both caffeoylquinic acids gave better scores than the complexes in the D-(-)-quinic acid moiety, so it was assumed that the values of the higher encapsulation constants obtained in the previous Section corresponded to K_{F1}, i.e. the encapsulation by the caffeic acid moiety.

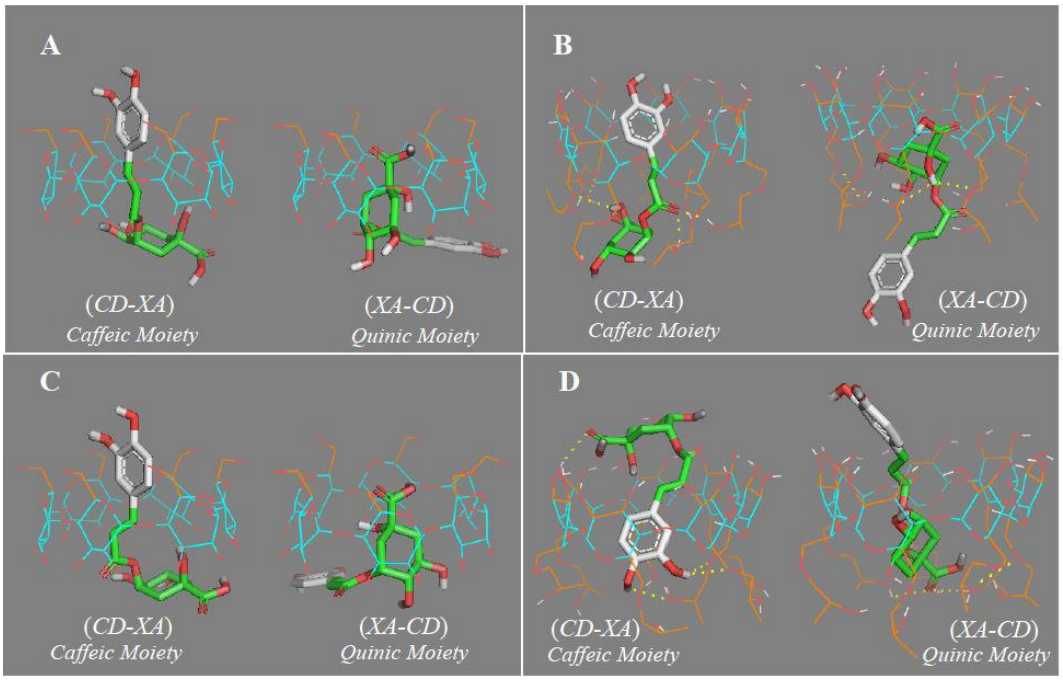

Figure 74. 3D molecular docking of neochlorogenic acid (A and B) and chlorogenic acid (C and D) with α-CD (A and C) and HP-β-CD (B and D), by the two possible moieties (caffeic or quinic). The flexible atoms of the CD are shown in orange, while the non-flexible ones are shown in blue. Possible hydrogen bonds are shown as yellow dotted lines

4.1.1.3.2. Effect of complexation on solubility and enzymatic oxidation of neochlorogenic acid

The aqueous solubility of neochlorogenic acid in the presence of α-CD and HP-β-CD was significantly improved, increasing by up to 17 % and 26 %, respectively, at the highest concentration of 10 mM compared to free neochlorogenic acid (Figure 75A). The differences between the control without CD and the other concentrations of both CDs were also significant. Although HP-β-CD achieved a higher concentration of soluble neochlorogenic acid, α-CD was more effective at the lowest concentration tested (1 mM).

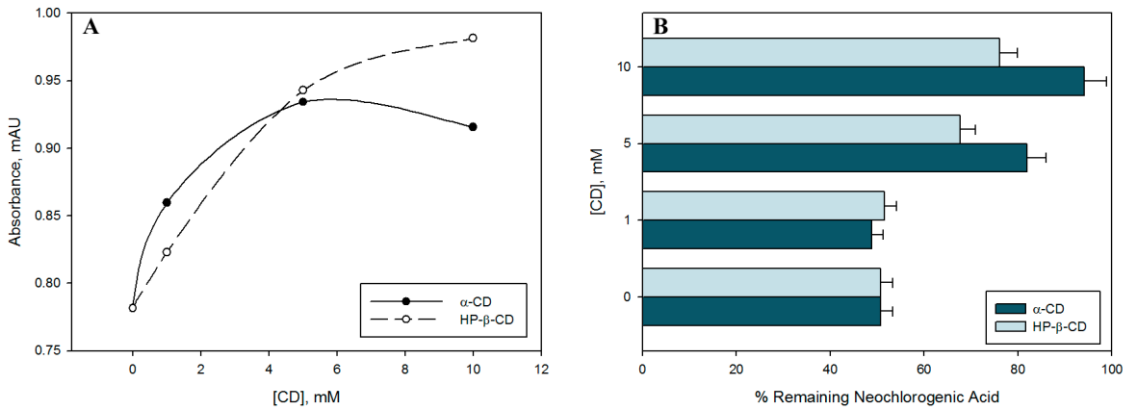

*Figure 75. A) Aqueous solubility of neochlorogenic acid in the absence and presence of different concentrations of α-CD and HP-β-CD (λ_{max} = 324 nm) (25 °C). B) Enzymatic oxidation of free and encapsulated neochlorogenic acid in α-CD and HP-β-CD catalysed by tyrosinase (25 °C pH 6.5). * Significance p-value < 0,05*

On the other hand, the ability of these two CDs to protect neochlorogenic acid from being oxidised by the enzyme tyrosinase was also evaluated. After 10 minutes of reaction in the absence of CDs, almost 50 % of the free neochlorogenic acid was oxidised, while complexation with the highest concentration (10 mM) of HP-β-CD or α-CD reduced this percentage to 24 % and less than 6 %, respectively (Figure 75B). The differences between the control without CDs and the treatments at 5 mM and 10 mM of both CDs were significant. Contrary to what was observed in aqueous solubility, α-CD was better than HP-β-CD in protecting neochlorogenic acid from enzymatic oxidation. It

seems that the inclusion complex formed with the smaller cavity CD provides better coverage to the neochlorogenic acid, preventing its contact with the active centre of the enzyme. The lower concentration of 1 mM showed no difference compared to the control without CD, so this protective effect is dependent on the concentration of the encapsulating agent. Something similar was also observed previously for inclusion complexes of chlorogenic acid with β-CD (Billaud et al., 1995).

4.1.1.3.3. Effect of complexation on the inhibitory activity of caffeoylquinic acids against pancreatic lipase

To assess whether CD complexation affected the ability of neochlorogenic acid or chlorogenic acid to inhibit the pancreatic lipase enzyme, the inhibition assays were repeated by setting the inhibitor concentration at 100 µM and adding increasing concentrations of HP-β-CD (one of the best CDs to encapsulate these caffeoylquinic acids). In this case, only chromatographic assays were performed, to avoid possible interferences in the fluorescent signal due to the presence of CDs.

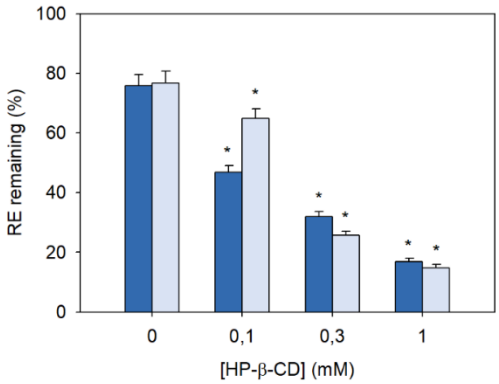

*Figure 76. Hydrolysis of resveratrol stearate (RE) in the presence of pancreatic lipase, different concentrations of HP-β-CD and 100 µM neochlorogenic acid (dark colour) or chlorogenic acid (light colour), determined by HPLC-UV/Vis (37 °C pH 7 120 minutes) * Significance p-value < 0.05*

The results showed that not only was the inhibitory effect no longer present when CD was added, but also that the hydrolysis of resveratrol stearate was significantly increased even with the lowest concentrations of HP-β-CD, regardless of the type of caffeoylquinic acid (Figure 76). While in the absence of CD, neochlorogenic and chlorogenic acids hydrolysed only 23 – 24 % of the resveratrol stearate, the presence of 1 mM HP-β-CD tripled the degree of hydrolysis, consuming more than 83 – 85 % of the initial resveratrol stearate.

Contrary to what was observed in Section 4.1.1.2.2, this effect was very different for each of the resveratrol stearate isomers, both with neochlorogenic acid and chlorogenic acid (Figure 77). While the major isomer of the racemic mixture of resveratrol stearate, RE i2, was significantly consumed from just 0.1 mM HP-β-CD, the minor isomer RE i1 remained almost the same as control at low HP-β-CD concentrations and was able to maintain more than 63 – 67 % at the highest concentration of 1 mM HP-β-CD, compared to 2 – 3 % of RE i2 at this same CD concentration.

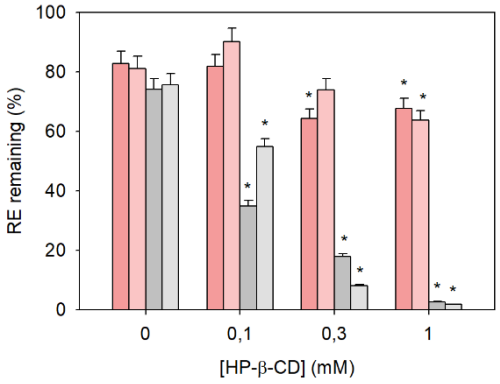

*Figure 77. Hydrolysis of resveratrol stearate isomers RE i1 (pink) and RE i2 (grey) in the presence of pancreatic lipase, different concentrations of HP-β-CD and 100 µM of neochlorogenic acid (dark colour) or chlorogenic acid (light colour), determined by HPLC-UV/Vis (37 °C pH 7 120 minutes) * Significance p-value < 0.05*

Since inclusion complexes with CDs are formed by non-covalent bonds, it is possible that in the enzymatic reaction these agents are encapsulating both the inhibitors

and the substrate. Therefore, due to the marked effect of CDs on the ability of neochlorogenic and chlorogenic acids to inhibit pancreatic lipase activity on resveratrol stearate, especially the RE i2 isomer, the effect of these encapsulating agents alone was also studied, thus considering the possible effect of substrate encapsulation on the course of the reaction.

4.1.1.4. Influence of CDs on the catalytic activity of pancreatic lipase

The use of HP-β-CD, in the absence of caffeoylquinic acids, also showed an increase in the hydrolysis of resveratrol stearate from a concentration of 0.5 mM HP-β-CD, despite a slight decrease at 0.25 mM compared to the control without CD (Figure 78). In this case, the 0.1 mM concentration of HP-β-CD did not generate a significant variation in the degree of hydrolysis, remaining at almost 50 %. In contrast, at the highest concentration of 1 mM HP-β-CD, up to 79 % of the total resveratrol stearate was hydrolysed.

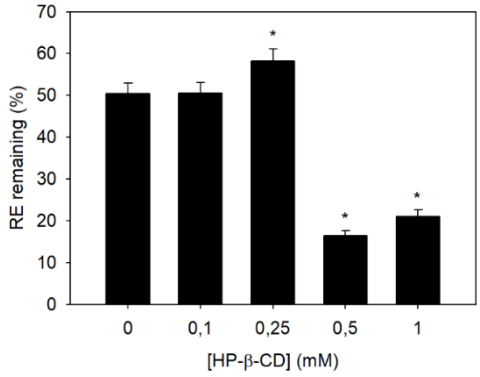

*Figure 78. Hydrolysis of resveratrol stearate (RE) in the presence of pancreatic lipase and different concentrations of HP-β-CD, determined by HPLC-UV/Vis (37 °C pH 7 120 minutes) * Significance p-value < 0.05*

Analysing these results by resveratrol stearate isomers, a similar behaviour to that observed in the presence of caffeoylquinic acids could be seen (Section 4.1.1.3.3.), although at 0.25 mM HP-β-CD both isomers seemed to slightly increase their remaining amount compared to the control (Figure 79). However, from 0.5 mM HP-β-CD onwards,

there was a very noticeable degradation of the major isomer RE i2, which went from retaining more than 56 % of its initial amount with 0.25 mM HP-β-CD, to 3 % or even less when the reaction was carried out in the presence of 0.5 mM or 1 mM HP-β-CD, respectively (Figure 79). In contrast, the minor isomer RE i1 did not decrease its remaining amount compared to the control, but in fact increased it by more than 75 % at a concentration of 1 mM HP-β-CD.

It seems that the presence of HP-β-CD promotes the activity of pancreatic lipase on the major isomer of resveratrol stearate RE i2, with little alteration of the hydrolysis of the minor isomer RE i1.

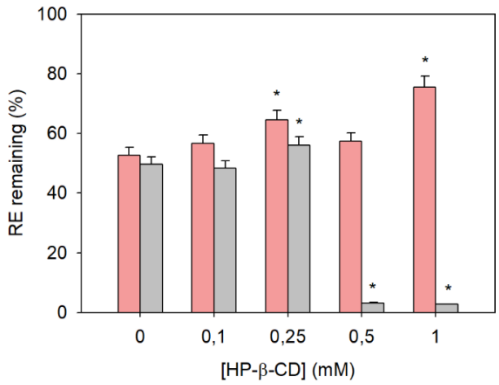

*Figure 79. Hydrolysis of the resveratrol stearate isomers RE i1 (pink) and RE i2 (grey) in the presence of pancreatic lipase and different concentrations of HP-β-CD, determined by HPLC-UV/Vis (37 °C pH 7 120 minutes) * Significance p-value < 0.05*

Due to the lipid nature of the hydrophobic stilbene derivatives synthesised, it is very likely that from a certain concentration, i.e. critical micelle concentration (CMC), they change from a monomeric to an aggregate or micellar conformation, the latter being a conformation that is difficult for the pancreatic lipase enzyme to access (Ávila-González et al., 2005). It is possible that, the concentrations used in this Section are above the CMC, thus the predominant conformation is the micellar one, and in the presence of CDs, a breakdown of the micelle occurs, allowing the entry of the monomers of the hydrophobic

stilbene derivatives into the internal cavity of the CD (López-Nicolás et al., 1995). By breaking down the aggregate conformation, the CDs could be making the hydrophobic stilbene derivatives more accessible to the pancreatic lipase enzyme, thus explaining the increased catalytic activity observed in the presence of these encapsulating agents.

The differences in the catalytic activity of the pancreatic lipase enzyme on the different isomers of the hydrophobic stilbene derivative in the presence of CDs could be explained by differences in the affinity for the CD, and thus the stability of the inclusion complexes. In Section 3.2.2., it was found that the major isomer RE i2 gave a higher encapsulation constant with HP-β-CD than the minor isomer RE i1. This result could explain what was observed in the enzymatic reactions in this Section. The higher affinity of CD for the RE i2 isomer could be modifying its micellar conformation, facilitating the access of the enzyme to the monomers so that they can be almost completely hydrolysed. On the contrary, the lower affinity of CD for the RE i1 isomer would allow it to maintain its aggregated conformation, which would partially protect it from enzymatic attack, allowing it to maintain a concentration similar or higher than that observed in the absence of CDs.

These results, apart from their interest in future *in vivo* applications of hydrophobic stilbene derivatives, are also relevant for their application in the purification of the isomers obtained from these hydrophobic stilbene derivatives. The combination of pancreatic lipase enzyme and HP-β-CD demonstrated a selective effect on the catalytic activity on the hydrophobic stilbene derivative, degrading almost completely the isomer with higher affinity for the CD cavity and retaining more of the isomer with lower affinity. Optimisation of the reaction concentrations and conditions could improve the results obtained by allowing a complete purification of the isomer with a lower affinity for the CD.

4.1.2. Cytotoxicity of hydrophobic stilbene derivatives in intestinal cells

Prior to the evaluation of the cell permeability of the hydrophobic stilbene derivatives in the human cell line Caco-2, the possible cytotoxicity of the compounds on these intestinal cells was analysed to ensure the integrity of the cell monolayer after administration of the different treatments. This was assessed using two different techniques, the MTT assay and the neutral red assay. Although the MTT assay is one of the most common tests, it has been reported that antioxidant molecules can cause interference (Chiba et al., 1998), so that cell viability was assessed using both methods.

4.1.2.1. MTT cytotoxicity assays

The results of cell viability determined by the MTT method showed that the hydrophobic stilbene derivatives were less cytotoxic to the cells than their natural stilbenes (Figure 80). Whereas resveratrol and oxyresveratrol significantly reduced cell viability from the lowest concentration, reaching up to 43 – 46 % viability at the highest concentration of 300 μM (Figure 80 R and O), their corresponding hydrophobic derivatives generally maintained viability above 70 %. In fact, many of the derivative concentrations gave the same or even higher viability than the solvent control (Figure 80 RE, RO, RP, OE, OO, OP), counteracting the cytotoxicity of the solvent used (DMSO).

Within the hydrophobic stilbene derivatives, both resveratrol stearate and palmitate got lower viability than the water control, but similar or slightly lower than the solvent control. Meanwhile, resveratrol oleate above 75 μM counteracted the loss of viability by solvent and showed similar viability to the water control. At low concentrations, oxyresveratrol stearate showed similar viability to the solvent control, and at 300 μM similar to the water control. Oxyresveratrol palmitate showed similar viability to oxyresveratrol stearate, however, at 300 μM its cytotoxicity increased. Finally,

oxyresveratrol oleate was the most effective derivative in counteracting solvent cytotoxicity from the lowest concentration tested, achieving the highest percentages of cell viability. Overall, all the hydrophobic stilbene derivatives studied maintained higher cell viability values than their natural stilbenes at all concentrations tested.

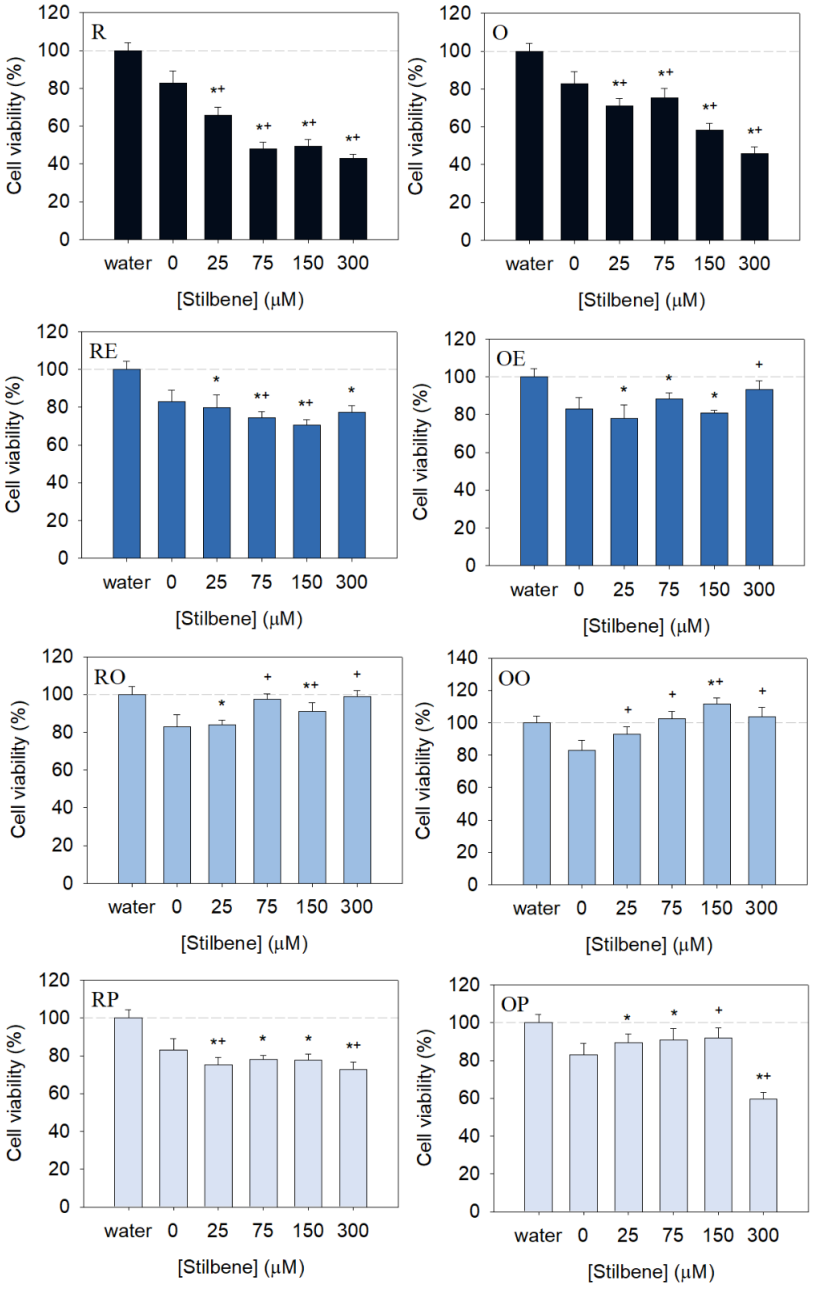

Figure 80. Viability of Caco-2 cells after 48 h of incubation with the hydrophobic stilbene derivatives and their natural stilbenes, determined by MTT. Significance p-value < 0.05 (*) compared to the water control and (⁺) compared to the DMSO control (0 μM)

4.1.2.2. Neutral red cytotoxicity assays

The results of cell viability determined by the neutral red method also showed that the hydrophobic stilbene derivatives were less cytotoxic to cells than their natural stilbenes (Figure 81).

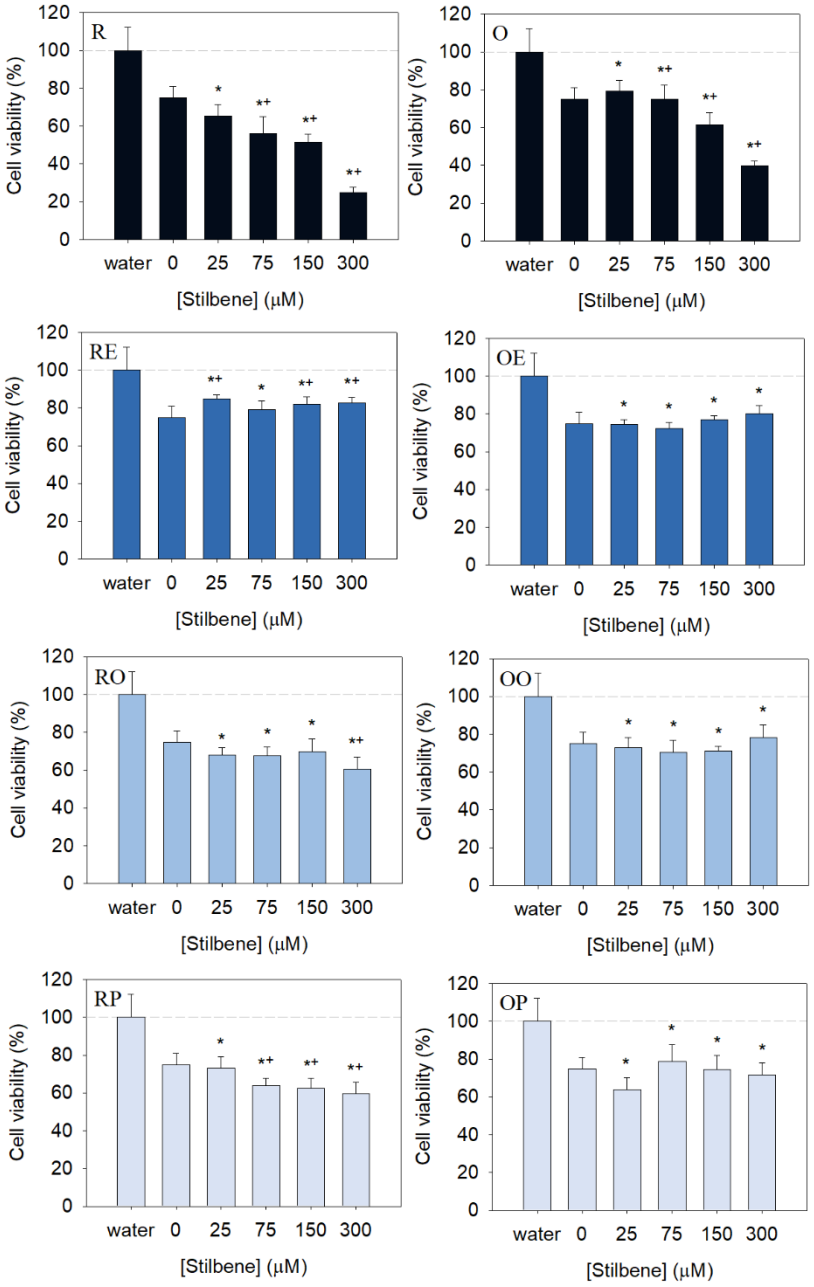

Figure 81. Viability of Caco-2 cells after 48 h of incubation with the hydrophobic stilbene derivatives and their natural stilbenes, determined with neutral red. Significance p-value < 0.05 (*) compared to the water control and (+) compared to the DMSO control (0 μM)

As was observed in the MTT assays, resveratrol significantly reduced cell viability from the lowest concentration, but in this case, oxyresveratrol did so from 150 μM onwards. At the highest concentration of 300 μM, these two natural stilbenes reached the lowest cell viability values of 25 – 40 % (Figure 81 R and O), while the hydrophobic derivatives generally maintained a viability of over 60 % at the concentrations tested, which in many cases was almost the same viability as the solvent control (Figure 81 RE, RO, RP, OE, OO, OP). Contrary to what was observed in the MTT assays, in the neutral red assays, cell viability never reached values close to the viability of the water control despite exceeding that of the solvent control. Moreover, with this method, the solvent showed a slightly higher cytotoxicity of 25 % compared to 17 % in the MTT assay.

Within the hydrophobic stilbene derivatives, resveratrol stearate showed the highest cell viability, exceeding that of the solvent control at some of the concentrations tested. Meanwhile, resveratrol oleate and resveratrol palmitate maintained similar viability to the solvent control until a concentration of 300 μM and 75 μM was reached, respectively, after which viability decreased significantly. None of the oxyresveratrol derivatives showed significant differences from the solvent control at any of the concentrations used. Overall, all hydrophobic stilbene derivatives tested exhibited higher cell viability values than their natural stilbenes at almost all concentrations tested, especially at the higher concentrations.

Finally, the neutral red assay was also used to test whether the HBCD-Pols had any cytotoxic effect on this cell line. The results showed no significant differences at any of the concentrations tested (Figure 82), so that HBCD-Pols could be used at concentrations up to 400 ppm without negatively affecting cell viability.

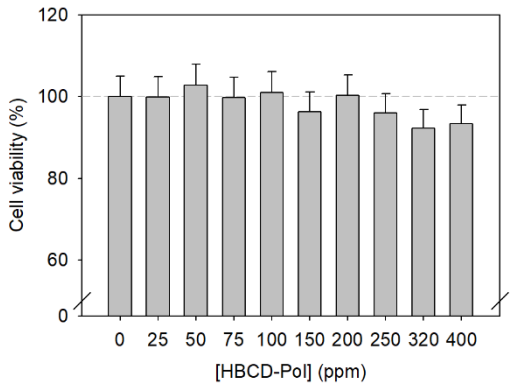

Figure 82. Viability of Caco-2 cells after 48 h of incubation with HBCD-Pols, determined with neutral red

Therefore, the results of cell viability by both methods showed that structural modification of stilbenes with fatty acids decreases the cytotoxicity of these compounds on intestinal Caco-2 cells, which would enable their use at higher concentrations in cell permeability assays without risking the integrity of the cell monolayer. Moreover, these results may suggest that high concentrations of hydrophobic stilbene derivatives are safer for intestinal cells than high concentrations of their natural stilbene.

However, previous studies analysing the viability of A549 (lung carcinoma), BxPC3 (pancreatic ductal adenocarcinoma), HT29 (colorectal adenocarcinoma) and BJ (human fibroblasts) cells treated with monoesters diesters and triesters of resveratrol with palmitic and oleic acid, as well as resveratrol with conjugated linoleic acid, also observed lower cytotoxicity with most derivatives compared to resveratrol, but higher cytotoxicity with resveratrol oleate, associated with an induction of apoptosis (Szczepańska et al., 2023). This slight discrepancy could be due to differences in the isomer ratio of the racemic mixture of hydrophobic stilbene derivatives used by these authors and in this PhD thesis. Therefore, it is likely that the esterified group has a significant influence on the cytotoxic activity of the hydrophobic stilbene derivatives.

4.1.3. Apparent permeability of hydrophobic stilbene derivatives

In order to investigate the uptake of the synthesised hydrophobic stilbene derivatives, their permeability *in vitro* through a monolayer of Caco-2 cells was studied. Due to the difficulty of quantifying these derivatives by the analytical techniques described in Section 3.2.3., a high concentration of these derivatives was used, in addition to HBCD-Pols. The integrity of the cell monolayer was checked by transepithelial electrical resistance measurements at both the beginning and the end of the experiments.

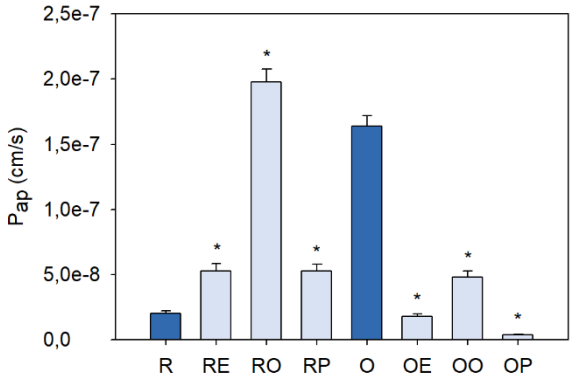

*Figure 83. Apparent permeability of hydrophobic stilbene derivatives (light colour) and their natural stilbenes (dark colour) in the presence of HBCD-Pols in the Caco-2 cell line, calculated from Equation 23. * Significance p-value < 0.05 compared to the original stilbene*

The results showed that hydrophobic resveratrol derivatives improved the apparent permeability of resveratrol, while hydrophobic oxyresveratrol derivatives worsened the apparent permeability of oxyresveratrol (Figure 83). Apart from the type of stilbene, the fatty acid used in the esterification also significantly influenced the ability of the derivative to cross the cell monolayer, with oleates showing the highest permeability, followed by stearates and palmitates. Within the hydrophobic stilbene derivatives, resveratrol oleate gave the best results, even exceeding the apparent permeability of oxyresveratrol. In contrast, oxyresveratrol palmitate was the derivative that exhibited the worst apparent permeability. Resveratrol stearate, resveratrol palmitate

and oxyresveratrol oleate gave similar permeability, with no significant differences between them. These three derivatives exceeded the apparent permeability of resveratrol.

The differences in apparent permeability between hydrophobic stilbene derivatives and their natural stilbenes could be partially related to the Lipinski's rule, also known as the rule of 5 (Lipinski et al., 1997; Pollastri, 2010). This rule is used in drug development to assess their suitability according to their physicochemical properties. According to this principle, bioactive compounds that give good oral bioavailability should not fail to meet more than one of the following conditions: 1) have no more than 5 hydrogen bond donors, 2) have no more than 10 hydrogen bond acceptors, 3) have a molecular mass less than 500 Da, and 4) have a partition coefficient (logP) less than 5. While in resveratrol derivatives only the partition coefficient condition is not fulfilled (logP > 5), in some of the oxyresveratrol derivatives, in addition to the partition coefficient, the molecular mass requirement is not satisfied (molecular mass > 500 Da), which could explain their lower permeability. However, this non-compliance with Lipinski's rule would not justify the very low apparent permeability of oxyresveratrol palmitate.

There are no studies on the apparent permeability of hydrophobic stilbene derivatives similar to those studied in this thesis. However, Thaweesest *et al*. (2022) analysed other smaller derivatives, such as tetra-acetate, tetra-propionate and tetra-butyrate of oxyresveratrol, observing an increase in their apparent permeability compared to oxyresveratrol (Thaweesest et al., 2022). The apparent permeability of resveratrol and oxyresveratrol has been previously determined, although under different conditions and without the presence of HBCD-Pols (Henry et al., 2005; Kaldas et al., 2003; Li et al., 2003; Maier-Salamon et al., 2006; Rastogi and Jana, 2016; Thaweesest et al., 2022). In general, these studies obtained orders of magnitude of 10^{-5} to 10^{-7} using initial

concentrations between 5 and 250 μM and incubation times between 1 and 16 hours, for apical → basolateral transport. In this PhD thesis, a lower apparent permeability with an order of magnitude of 10^{-8} was obtained using an initial concentration of 300 μM in the presence of 200 ppm HBCD-Pols and incubation time of 24 hours, for apical → basolateral transport. The lower permeability obtained could be due to the presence of the HBCD-Pols that cause a controlled release of stilbenes, delaying its passage through the cell monolayer and thus reducing its apparent permeability (Volkova et al., 2021).

Moreover, although the apparent permeability of the individual isomers could not be determined, it could be observed that the hydrophobic oxyresveratrol derivatives varied significantly in their isomer ratio between the beginning and the end of the experiments, whereas the resveratrol derivatives remained almost the same (Table 19).

Table 19. Isomer ratio at the beginning (0 h) and at the end (24 h, apical and basolateral average) of the permeability assays in Caco-2 cells, determined by HPLC-ESI(-)

Product	Isomer	Isomer ratio (%)	
		0 h	24 h
RE	RE i1	22	22
	RE i2	78	78
RO	RO i1	28	23
	RO i2	72	77
RP	RP i1	27	28
	RP i2	73	72
OE	OE i3	50	18
	OE i1	25	46
	OE i2	25	36
OO	OO i3	56	1
	OO i1	20	19
	OO i2	24	80
OP	OP i3	67	1
	OP i1	11	35
	OP i2	22	64

In comparison with the isomer ratio previously obtained by DAD detector (Section 3.1.), the isomer ratio obtained by TOF detector varied slightly (Table 19), especially for the hydrophobic oxyresveratrol derivatives. This could be due to a higher sensitivity of the mass spectrometer to detect the minor isomers of these derivatives.

Despite this, the order of the isomers according to their proportion in the racemic mixture remained stable between the two detectors.

In all hydrophobic oxyresveratrol derivatives studied, the major isomer i3 became the minor isomer after 24 hours of incubation with the intestinal cells, leaving at the end of the assay, the i2 isomer as the major isomer in oxyresveratrol oleate and palmitate, and the i1 isomer in oxyresveratrol stearate (Table 19). These changes could be due to an increase degradation or metabolisation of the i3 isomer compared to the other isomers in the oxyresveratrol derivatives. To rule out a possible degradation due to the medium used or the test conditions, the ratio of oxyresveratrol stearate isomers was analysed in the absence of the cells. These results showed smaller differences than those observed in the presence of cells (Table 20), so it is likely that this variation is due to a greater interaction of the i3 isomer with the intestinal cells.

Table 20. Oxyresveratrol stearate isomer ratio at the beginning (0 h) and at the end (24 h, apical and basolateral average) of the permeability assays in the absence and in the presence of Caco-2 cells, determined by HPLC-ESI(-)

Isomer	Isomer ratio (%)		
	0 h	24 h without cells	24 h with cells
OE i3	50	45	18
OE i1	25	28	46
OE i2	25	27	36

4.1.4. Metabolism of hydrophobic stilbene derivatives

Due to previous evidence that Caco-2 intestinal cells were able to interact with hydrophobic stilbene derivatives, the formation of metabolites typical of phase II reactions from hydrophobic stilbene derivatives and their natural stilbenes was investigated in the same cell line. Since no conjugated metabolites of the esterified stilbenes were found, the formation of the following conjugated metabolites of resveratrol and oxyresveratrol was analysed (Table 21):

Table 21. Metabolites in the extracellular media of Caco-2 cells after 24 hours (apical + basolateral), determined by HPLC-ESI(-)

	Metabolite	Formula	MW	*m/z*⁻	Retention time (min)
MR1	Resveratrol-O-glucuronide	$C_{20}H_{20}O_9$	404.1098	403.1025	6.998
MR2	Resveratrol sulphate	$C_{14}H_{12}O_6S$	308.0356	307.0284	9.634
MR3					10.896
MO1	Oxyresveratrol-O-glucuronide	$C_{20}H_{20}O_{10}$	420.1047	419.0974	4.314
MO2					6.659
MO3	Oxyresveratrol sulphate	$C_{14}H_{12}O_7S$	324.0303	323.0231	7.846
MO4					8.713

After 24 hours of incubation, the media with hydrophobic resveratrol and oxyresveratrol derivatives showed less formation of total sulphate (Figure 84A) and glucuronide (Figure 84B) metabolites than the media with the original stilbenes, except for the media with oxyresveratrol oleate, in which sulphate synthesis was higher than in the media with oxyresveratrol (Figure 84A). In particular, sulphate formation decreased between 2-fond and 5-fold in the derivatives compared to natural stilbenes, with the exception of oxyresveratrol oleate (Figure 84A), while glucuronide formation decreased 5-fold in oxyresveratrol oleate and more than 20-fold in the other derivatives, especially in resveratrol palmitate or resveratrol stearate (Figure 84B).

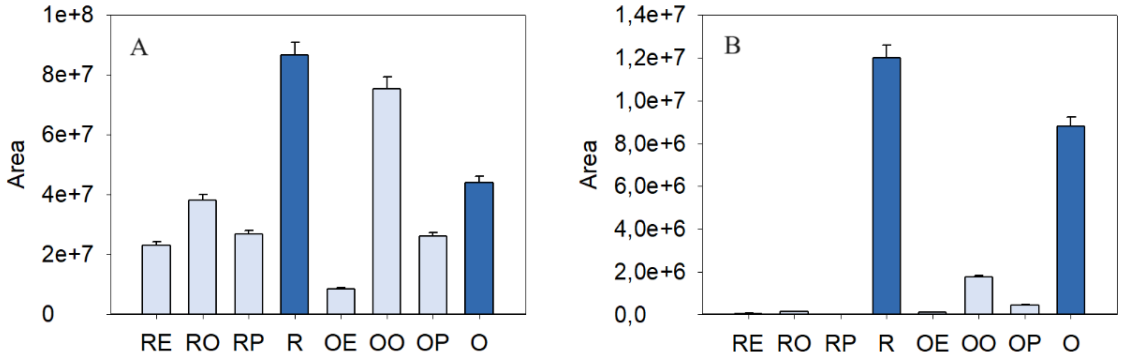

Figure 84. Formation of A) sulphate and B) glucuronide metabolites of resveratrol or oxyresveratrol by Caco-2 cells after 24 hours incubation (apical + basolateral) with hydrophobic stilbene derivatives (light colour) and their natural stilbenes (dark colour), determined by HPLC-ESI(-)

Although in the media with resveratrol the formation of conjugated metabolites was higher than in the media with oxyresveratrol, in general, the opposite occurred in the

media with hydrophobic derivatives, with the hydrophobic resveratrol derivatives giving a lower formation of these metabolites compared to the hydrophobic oxyresveratrol derivatives (Figure 84). The oleates of both stilbenes were also found to be the derivatives with the highest production of the conjugated metabolites compared to the palmitates and stearates (Figure 84).

Different unidentified isomers of some of these metabolites could be detected with a variable ratio depending on the stilbene added to the medium. For resveratrol derivatives and resveratrol itself, the sulphate conjugate isomer eluting after 10 minutes of analysis, MR3, was the major, with a proportion of 89 % (resveratrol) and 95 % or higher (hydrophobic resveratrol derivatives) compared to the isomer with the shortest retention time, MR2. (Table 22).

Table 22. Isomer ratio of resveratrol conjugated metabolites analysed in extracellular media of Caco-2 cells after 24 hours (apical + basolateral)

	Metabolite	Retention time (min)	Isomer ratio (%) HPLC-ESI(-)			
			RE	RO	RP	R
MR2	Resveratrol sulphate	9.634	5	5	3	11
MR3		10.896	95	95	97	89

A minimal part of the isomer of the oxyresveratrol sulphate conjugate with the shortest retention time, MO3, was produced, accounting for only 1 % or less of the total (Table 23). However, in the glucuronide conjugates of oxyresveratrol, the proportion of the isomeric metabolites varied markedly between the derivatives and oxyresveratrol. While in the derivatives, the glucuronide isomer MO2 was the major with a ratio of 79 – 95 % to the MO1 isomer, in oxyresveratrol this MO2 isomer with the longest retention time was the minor, accounting for 31 % of the total (Table 23).

Table 23. Isomeric ratio of oxyresveratrol conjugated metabolites analysed in the extracellular media of Caco-2 cells after 24 hours (apical + basolateral)

	Metabolite	Retention time (min)	Isomer ratio (%) HPLC-ESI(-)			
			OE	OO	OP	O
MO1	Oxyresveratrol-O-glucuronide	4.314	5	15	21	69
MO2		6.659	95	85	79	31
MO3	Oxyresveratrol sulphate	7.846	1	0	1	1
MO4		8.713	99	100	99	99

Previous studies on the intestinal metabolism of these natural stilbenes identified conjugates of resveratrol in the 3-OH or 4'-OH groups (Jarosova et al., 2020) and of oxyresveratrol mainly in the 2-OH group (Likhitwitayawuid, 2021).

The hydrophobic derivatives of resveratrol and oxyresveratrol also showed some degree of hydrolysis in the extracellular media, with concentrations of less than 1.5 µM of the original stilbenes. Oxyresveratrol oleate was the derivative with the highest degree of hydrolysis, followed by oxyresveratrol palmitate and resveratrol oleate (Figure 85). In contrast, resveratrol palmitate showed the lowest degree of hydrolysis forming only 90 nM resveratrol (Figure 85).

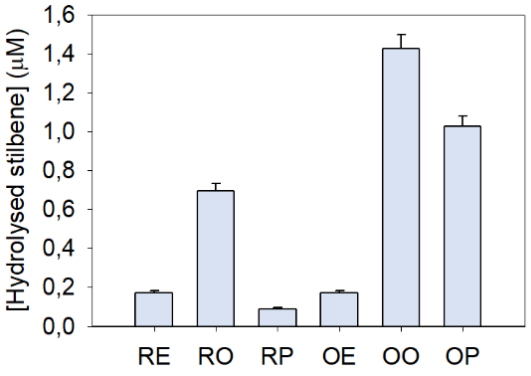

Figure 85. Hydrolysis of hydrophobic stilbene derivatives by Caco-2 cells after 24 hours, determined by HPLC-ESI(-)

The conjugation of stilbenes during metabolism after oral administration is responsible for the low bioavailability of these bioactive compounds (Walle, 2011). The results of this research show that, despite the slight level of hydrolysis observed,

hydrophobic stilbene derivatives seem to have a greater ability to maintain the aglycone form than natural stilbenes. Therefore, the use of hydrophobic stilbene derivatives as stilbene precursors could help to avoid such metabolisation reactions that negatively affect the bioavailability of stilbenes.

Previous studies with other molecules (Biasutto et al., 2007; Han et al., 2021; Pokorski et al., 2003), also showed that the use of a more hydrophobic derivative can modify interactions with metabolic enzymes and aid the distribution of the molecule, even though slight hydrolysis may occur during this process.

4.2. *In vivo* assays: *M. musculus* animal model

After evaluation of the digestion, absorption and metabolism of the hydrophobic stilbene derivatives *in vitro*, the *in vivo* pharmacokinetics and serum levels of some biomarkers of one of them was studied in BALB/c mice. Based on previous results, the derivative selected for these trials was resveratrol stearate. Furthermore, since CDs have influence on the hydrolysis of resveratrol stearate catalysed by pancreatic lipase (Section 4.1.1.4.), have demonstrated to improve the bioavailability of some bioactive compounds (Sarabia-Vallejo et al., 2023), this derivative was administered in free form and encapsulated in HP-β-CD.

4.2.1. Pharmacokinetics of resveratrol stearate in free form and encapsulated in CDs

Plasma samples from mice treated with 50 mg/kg of resveratrol stearate, free or encapsulated, showed a low concentration of the hydrophobic derivative in its original form, especially in the absence of CDs (Figure 86B). However, a higher amount was

detected in its hydrolysed form, i.e. as resveratrol (Figure 86A). Since the pharmacokinetic curve of the hydrolysed form showed a rising phase at the beginning, associated with the absorption phase, it is likely that this is due to the cleavage of the ester bond of resveratrol stearate by the enzyme pancreatic lipase during digestion (Section 4.1.1.) or by intestinal cells during absorption (Section 4.1.4.), as previously observed in *in vitro* results with this hydrophobic stilbene derivative.

Overall, the pharmacokinetic curves obtained showed a rapid rise in concentration and decline from 1 – 1.5 hours after oral administration (Figure 86). The presence of HP-β-CD was able to significantly increase the concentration of resveratrol stearate and resveratrol in plasma. Although *in vitro* it was observed that the presence of CDs above a certain concentration increased the hydrolysis of resveratrol stearate by the enzyme pancreatic lipase (Section 4.1.1.4.), in mice it was observed that the use of these agents in a 1:5 (w:w) ratio resulted in a higher concentration of stilbene, both in esterified and hydrolysed form, the latter being predominant. It seems that CDs, despite being able to increase catalysis by the pancreatic lipase enzyme *in vitro*, may also be protecting stilbene from degradation during digestion and absorption *in vivo*. This could be because the presence of other molecules in the gastric secretion prevents the chemical equilibrium from moving towards the hydrolysis.

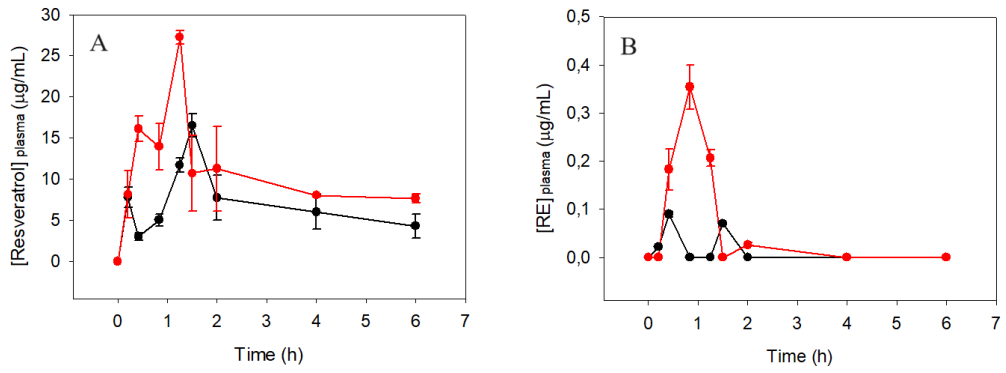

Figure 86. Quantification of A) resveratrol and B) resveratrol stearate in plasma of BALB/c mice after oral administration of 50 mg/kg resveratrol stearate free (black) and encapsulated in HP-β-CD 1:5 (red) (n=6)

Since, resveratrol stearate in its original form was not detected at some times, pharmacokinetic parameters were determined for the hydrolysed form, i.e. as resveratrol (Table 24). The results revealed that the presence of HP-β-CD achieved higher values of maximum concentration (C_{max}) of resveratrol in less time (t_{max}), as well as a higher area under the curve ($AUC_{0-\infty}$), with no significant differences in half-life ($t_{1/2}$). In fact, molecular encapsulation increased the maximum concentration by 65 % and doubled the area under the resveratrol curve detected after oral administration of resveratrol stearate at a dose of 50 mg/kg.

Table 24. Pharmacokinetic parameters of resveratrol in plasma of BALB/c mice after oral administration of 50 mg/kg resveratrol stearate (RE), in free form or encapsulated in HP-β-CD 1:5 (+ CD) (n=6)

Treatment	C_{max} (mg/L)	t_{max} (h)	$t_{1/2}$ (h)	$AUC_{0-\infty}$ (mg·h/L)
RE	16.52 ± 1.97	1.50 ± 0.00	2.92 ± 0.74	60.55 ± 18.85
RE + CD	27.26 ± 1.14	1.25 ± 0.00	5.29 ± 2.44	123.59 ± 20.93

Although the absolute bioavailability of resveratrol stearate could not be determined from the available data, a relative comparison between the two treatments could be made from their area under the curve. The $AUC_{0-\infty}$ is a parameter directly proportional to bioavailability if the treatments are administered at the same dose of the same compound, and assuming that the clearance (volume of plasma from which stilbene is eliminated per time unit) is constant (Tillement and Tremblay, 2007). Since CDs doubled the $AUC_{0-\infty}$, these results suggest that molecular encapsulation in HP-β-CD could improve the oral bioavailability of this stilbene, achieving higher concentrations in plasma of BALB/c mice, especially in its hydrolysed form.

4.2.2. Serum biomarker analysis

Blood samples from mice treated with 50 mg/kg of resveratrol stearate or resveratrol, free and encapsulated in HP-β-CD 1:5 (w:w), taken 6 hours after oral administration, were analysed for quantitative markers of lipid transport such as triacylglycerides (TG), cholesterol (CHO), high-density lipoproteins (HDL) and low-density lipoproteins (LDL), markers of liver damage such as aspartate aminotransferase (AST) and alanine aminotransferase (ALT), markers of renal function such as blood urea nitrogen (BUN) and creatinine (CR), markers of oxidative stress such as superoxide dismutase (SOD), glutathione peroxidase (GPx), total antioxidant status (TAS) and malondialdehyde (MDA), and markers of inflammation such as tumour necrosis factor-alpha (TNF-α), interleukin-6 (IL-6) and cycloxygenase-2 (COX-2).

4.2.2.1. Lipid profile

All treatments were able to improve the serum lipid profile of the mice by reducing triacylglycerides, cholesterol and LDL lipoproteins significantly compared to controls (Figure 87). In the case of HDL lipoproteins, only mice treated with the hydrophobic stilbene derivative showed a significant improvement by increasing their concentration, regardless of the use of CDs.

In the case of cholesterol and LDL lipoproteins, mice treated with the hydrophobic stilbene derivative showed significantly lower values of these markers compared to those treated with the natural stilbene (Figure 87). Furthermore, these values decreased further when both stilbenes were administered with CDs. A significant decrease could also be observed with the administration of free HP-β-CD, probably due to the ability of CDs to trap lipophilic molecules (H. Wang et al., 2019). Nevertheless, biomarkers of the inclusion complexes showed significant differences compared to biomarkers of the CD

control. Taken together, these changes in lipid transport markers after treatments may suggest a beneficial effect on obesity (Borato et al., 2016; Mika and Sledzinski, 2017).

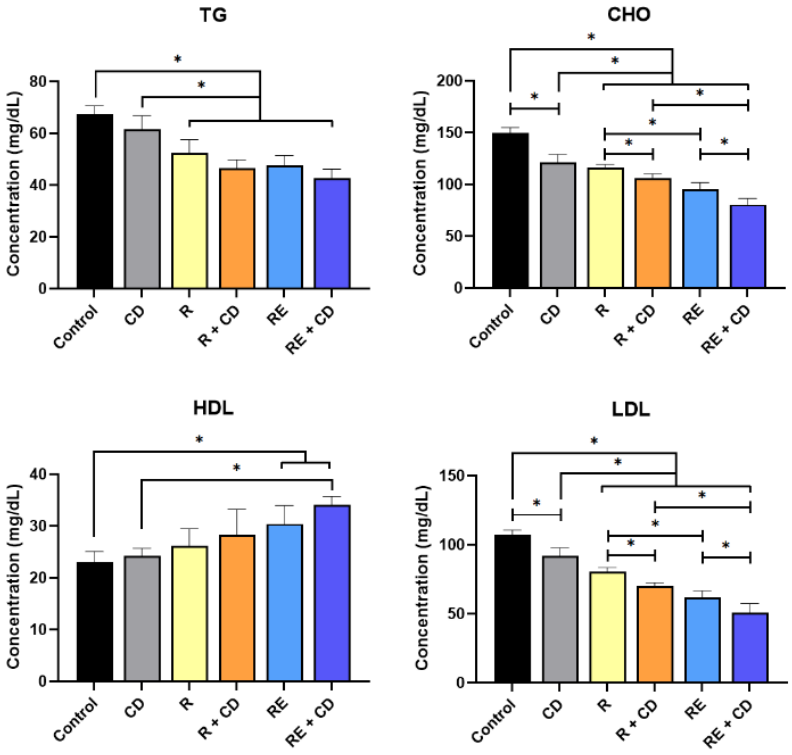

*Figure 87. Quantification of lipid transport markers in plasma of BALB/c mice after oral administration of 50 mg/kg resveratrol (R) or 50 mg/kg resveratrol stearate (RE), in free form or encapsulated in HP-β-CD 1:5 (+ CD). (n=6) * Significance p-value < 0.05*

4.2.2.2. Hepatic-renal profile

The determination of markers of liver damage and renal function enables the estimation of potential toxicity in individuals by the compounds administered. None of the treatments caused a significant increase in the concentration of the liver enzymes and renal markers analysed, suggesting that, at the selected dose, resveratrol stearate and resveratrol do not cause damage in mice at the hepatic-renal level, regardless of the use of CDs (Figure 88).

In fact, some of the treatments were able to decrease the concentration of these markers with respect to the control (Figure 88). In particular, resveratrol stearate, free or

complexed, showed significant differences in all four markers, except for the liver marker AST when administered in free form. Resveratrol only showed significant differences from the control in AST and BUN concentration, but the latter only when administered in encapsulated form. Moreover, free CDs also showed a significant decrease in AST and BUN biomarkers.

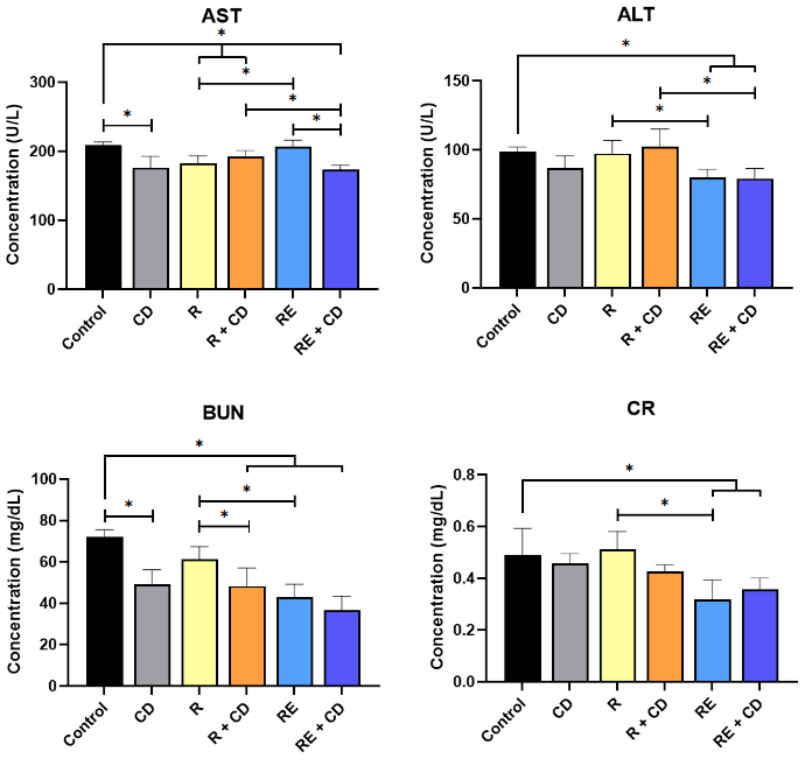

*Figure 88. Quantification of markers of liver damage and kidney function in plasma of BALB/c mice after oral administration of 50 mg/kg resveratrol (R) or 50 mg/kg resveratrol stearate (RE), in free form or encapsulated in HP-β-CD 1:5 (+ CD). (n=6) * Significance p-value < 0.05*

In addition, free resveratrol stearate showed significant differences from free resveratrol in all four markers, while HP-β-CD encapsulated resveratrol stearate only showed differences from encapsulated resveratrol in markers of liver damage. Significant differences between encapsulated and free form of resveratrol stearate were only observed in the marker AST, while between encapsulated and free form of resveratrol in the marker BUN.

4.2.2.3. Oxidative profile

All treatments helped to decrease blood oxidative stress levels in mice by increasing total antioxidant status and production of endogenous antioxidant enzymes (SOD and GPx), as well as decreasing malondialdehyde, a product of lipid peroxidation (Figure 89).

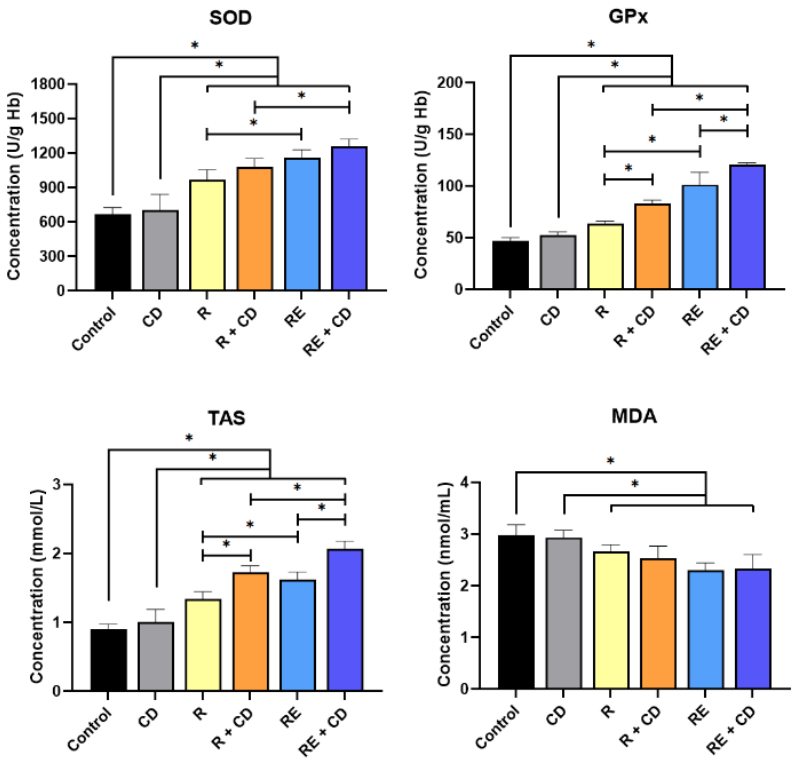

*Figure 89. Quantification of oxidative stress markers in plasma of BALB/c mice after oral administration of 50 mg/kg resveratrol (R) or 50 mg/kg resveratrol stearate (RE), in free form or encapsulated in HP-β-CD 1:5 (+ CD). (n=6) * Significance p-value < 0.05*

Resveratrol stearate, free or encapsulated, caused a significant increase in TAS and in serum SOD and GPx enzymes compared to resveratrol, free or encapsulated (Figure 89), indicating that this hydrophobic stilbene derivative may have greater endogenous antioxidant activity than its natural stilbene. Furthermore, administration of these stilbenes in inclusion complexes with HP-β-CD resulted in a significant improvement in TAS and GPx levels compared to administration in free form. In contrast,

although all four treatments showed a significant decrease in MDA levels compared to the control, no significant differences were observed between treatments, suggesting similar lipid peroxidation.

Previous studies have also reported that resveratrol administration is able to improve serum antioxidant biomarkers in animal models and humans, preventing oxidative stress and metabolic diseases (Franco et al., 2013; Omidian et al., 2020).

4.2.2.4. Inflammatory profile

Similar to what was observed for oxidative stress levels, all treatments improved the anti-inflammatory profile in the plasma of mice by decreasing TNF-α, IL-6 and COX-2 levels significantly compared to controls (Figure 90).

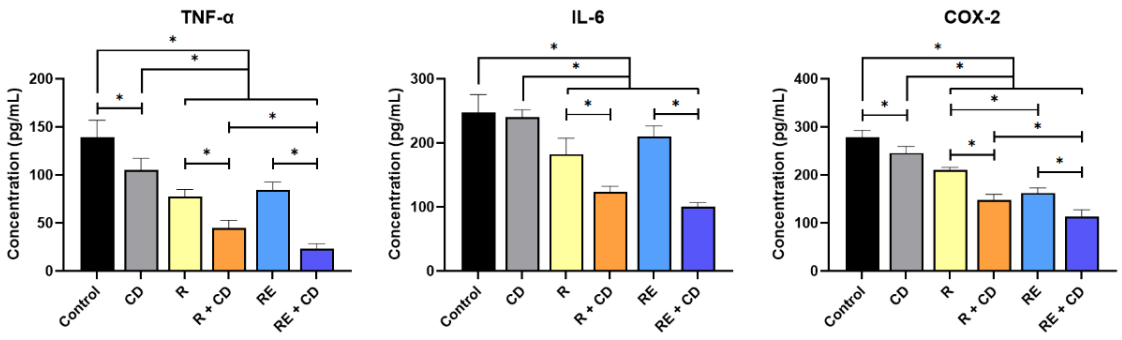

*Figure 90. Quantification of inflammation markers in plasma of BALB/c mice after oral administration of 50 mg/kg resveratrol (R) or 50 mg/kg resveratrol stearate (RE), in free form or encapsulated in HP-β-CD 1:5 (+ CD). (n=6) * Significance p-value < 0.05*

Among the different treatments, it could be observed that, in free form, resveratrol stearate only showed significant differences compared to resveratrol in the concentration of COX-2. Meanwhile, this hydrophobic resveratrol derivative encapsulated in CDs significantly reduced the concentration of COX-2 and TNF-α compared to resveratrol, free or encapsulated, and of IL-6 compared to free resveratrol (Figure 90). For all three markers tested, the effect of encapsulated stilbenes was significantly better than the effect

of free stilbenes. And although HP-β-CD also showed an effect on TNF-α and COX-2 markers by itself, the use of the inclusion complexes decreased the levels of both markers significantly compared to the use of the CD alone (Figure 90).

This decrease in pro-inflammatory markers following resveratrol treatment has previously been observed in other preclinical and clinical studies, in healthy individuals and individuals with obesity or non-alcoholic fatty liver disease (Koushki et al., 2018; Omraninava et al., 2021; Tung et al., 2015). Furthermore, some of these studies have associated this effect with an increase in antioxidant markers, as observed in this doctoral thesis.

4.3. Conclusions on digestion, absorption and metabolism of hydrophobic stilbene derivatives

Hydrophobic derivatives of resveratrol, oxyresveratrol and pterostilbene have proved to be susceptible to pancreatic lipase activity, a key enzyme in the digestive process of these types of molecules. The degree of hydrolysis varied according to the type of derivative and could be inhibited by the use of caffeoylquinic acids, such as chlorogenic acid or neochlorogenic acid.

Molecular encapsulation of these caffeoylquinic acids showed better encapsulation constants with the modified CD, HP-β-CD, and the natural CD, α-CD. Bioinformatic assays showed that the caffeic acid moiety of these caffeoylquinic acids has a higher affinity for the CD cavity than the D-(-)-quinic acid moiety. Complexation of neochlorogenic acid helped to improve its aqueous solubility and protect it from enzymatic oxidation, however, it also caused the caffeoylquinic acids to lose their inhibitory effect on the pancreatic lipase enzyme.

This suppression of inhibitory activity was due to the inherent effect of CDs on the hydrolysis of hydrophobic stilbene derivatives. Above a specific concentration of HP-β-CD, the catalytic activity of pancreatic lipase was found to increase, hydrolysing most of the major isomer of resveratrol stearate and keeping the minor isomer with a similar degree of hydrolysis to that observed without CDs. The increased catalytic activity was associated with the ability of the CDs to disaggregate the micelles into monomers readily accessible to the pancreatic lipase enzyme. Whereas the isomer selectivity in the hydrolysis was associated with the higher affinity of the CDs for the major isomer of resveratrol stearate, allowing the aggregated conformation of the minor isomer to protect it from the enzyme. These results also suggested that during hydrolysis of hydrophobic stilbene derivatives, HP-β-CD and pancreatic lipase could be used to purify the isomer with lower affinity for the CD cavity.

Studies in intestinal cells *in vitro* revealed that the hydrophobic derivatives of resveratrol and oxyresveratrol have lower or even no cytotoxicity compared to their natural stilbenes. In addition, structural modification of stilbenes with fatty acids was shown to increase the apparent permeability of resveratrol, but decrease that of oxyresveratrol. It was also observed that the major isomer of oxyresveratrol derivatives was more readily metabolised by cells than its minor isomers. In contrast, the isomers of the resveratrol derivatives did not show this effect. In general, the hydrophobic derivatives of resveratrol and oxyresveratrol were more capable of retaining their aglycone form compared to their natural stilbenes, by forming fewer sulphate and glucuronide conjugated metabolites. This greater resistance to metabolism may be an advantage in avoiding phase II reactions that decrease the bioavailability of stilbenes, with the hydrophobic stilbene derivatives acting as precursors of their corresponding stilbenes.

Finally, *in vivo* studies with one of the hydrophobic stilbene derivatives demonstrated its ability to reach the circulatory system in mice, albeit mostly in its hydrolysed form. The use of CDs helped to increase the maximum concentration in plasma and improve the relative oral bioavailability. Moreover, mice showed improvements in the levels of biomarkers of lipid transport, liver damage, kidney function, oxidative stress and inflammation following oral administration of resveratrol stearate and resveratrol, in free or encapsulated form. In fact, the use of resveratrol stearate, especially with CDs, showed significant differences from resveratrol in many of the biomarkers tested. Thus, although resveratrol stearate seems to be partially hydrolysed at blood level, the effects observed on the various markers show a beneficial effect compared to the direct administration of the hydrolysed form, i.e. resveratrol. These results could be due to an improvement in the oral bioavailability of hydrophobic stilbene derivatives compared to natural stilbenes, although further pharmacokinetic studies are needed to confirm this.

5. BIOACTIVITY OF HYDROPHOBIC STILBENE DERIVATIVES AND NATURAL STILBENES

5.1. *In vitro* biological activity

5.1.1. Antioxidant activity

As mentioned in Materials and Methods, the determination of antioxidant activity *in vitro* with different techniques is advisable as the redox reactions vary between them. For this reason, the antioxidant activity in this PhD thesis has been determined by hydrogen atom transfer (HAT) methods, such as ORAC, and electron transfer methods (SET), such as ABTS, DPPH and FRAP. While the former consists of a kinetic reaction, the ABTS, DPPH and FRAP methods used are end-point methods, with a time of 24 hours being selected for these three methods in the studies with the hydrophobic stilbene derivatives. Finally, the effect of CDs in these methods was also investigated, because of the large number of publications using these agents in antioxidant activity studies and the discrepancy between authors on their use in this type of experiments.

5.1.1.1. Antioxidant activity of hydrophobic stilbene derivatives and their natural stilbenes

The determination of the antioxidant activity of hydrophobic stilbene derivatives provides information on whether these compounds will be able to maintain their form or will be oxidised in the presence of other oxidising agents in the medium. Molecules with a high antioxidant capacity react rapidly in the presence of free radicals, changing to their oxidised form. Therefore, high antioxidant activity may not be desirable in the case of precursors of bioactive compounds, such as hydrophobic stilbene derivatives, since the objective would be to keep the molecule as intact as possible for its correct delivery. For

this reason, the *in vitro* antioxidant activity of hydrophobic derivatives of resveratrol, oxyresveratrol and pterostilbene was analysed by ORAC, ABTS, DPPH and FRAP methods.

5.1.1.1.1. ORAC method

Fluorescein decay curves in the presence of AAPH showed a delay with increasing stilbene concentration (Figure 91), due to competition for neutralising free radicals. From these curves, the net AUC values of the hydrophobic stilbene derivatives and their natural stilbenes were obtained.

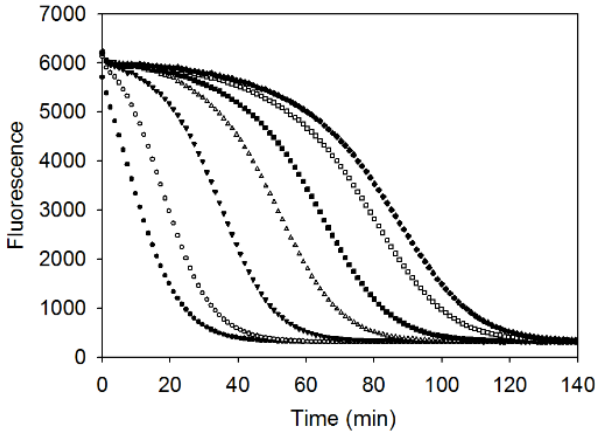

Figure 91. Fluorescein decay curve with AAPH in the presence of (●) 0, (○) 0.25, (▼) 1, (△) 2, (■) 3, (□) 4 and (◆) 5 µM oxyresveratrol

The antioxidant capacity observed by the ORAC method showed that the hydrophobic stilbene derivatives had lower activity than the original stilbenes, requiring higher concentrations to achieve similar effects (Figure 92).

Comparing the hydrophobic stilbene derivatives with their respective natural stilbenes at the highest tested concentration of 500 µM, the pterostilbene derivatives gave activity equivalent to that observed at concentrations below 1.7 µM pterostilbene, the resveratrol derivatives, equivalent to concentrations of 0.8 – 2.8 µM resveratrol, and the

oxyresveratrol derivatives, equivalent to concentrations above 3.125 µM oxyresveratrol (Figure 92).

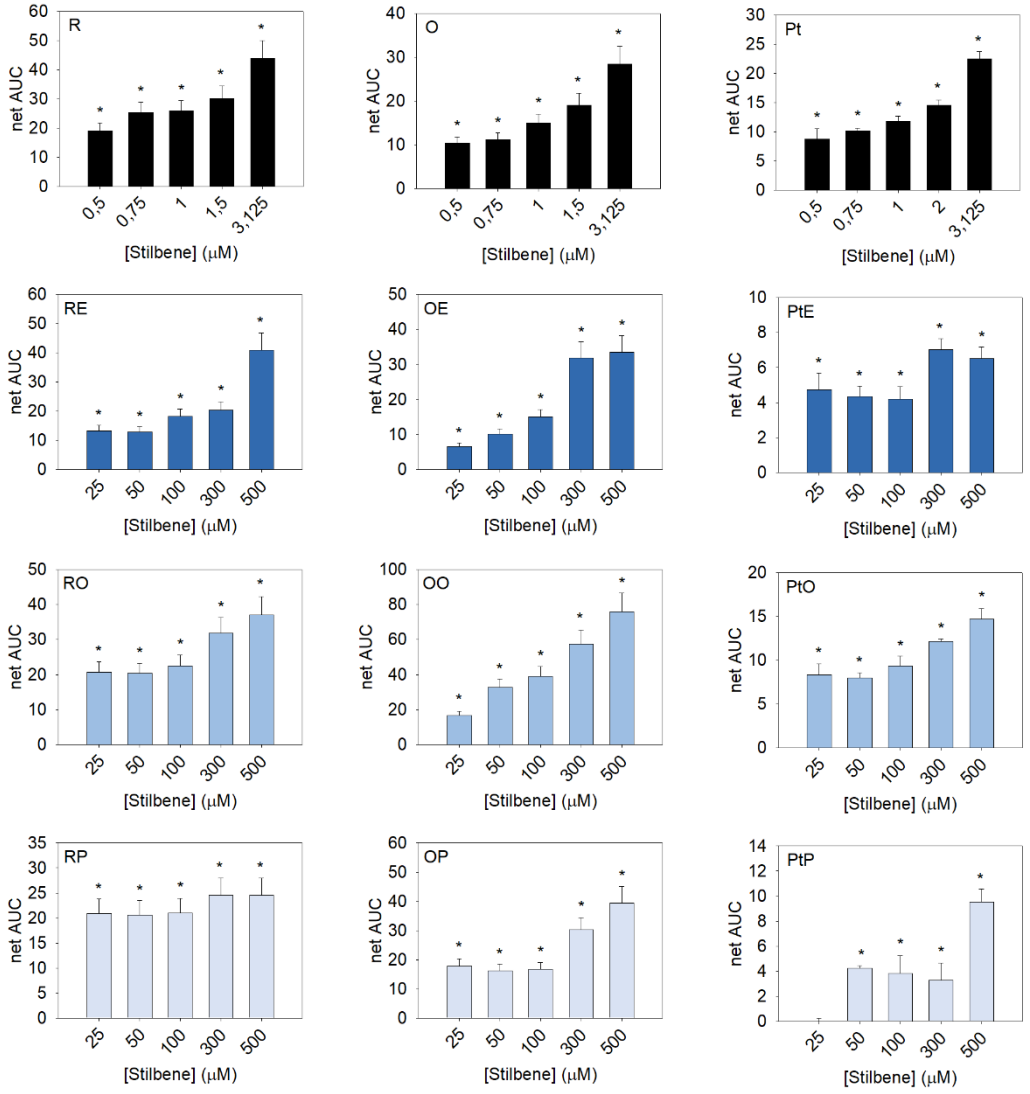

*Figure 92. Antioxidant activity of hydrophobic derivatives of stilbenes and their natural stilbenes, determined by the ORAC method. * Significance p-value < 0.05*

Within hydrophobic stilbene derivatives, oxyresveratrol derivatives achieved the highest antioxidant activity values, followed by those of resveratrol, and finally, pterostilbene (Figure 92). In relation to the type of fatty acid, oleates showed the highest antioxidant activity. In particular, oxyresveratrol oleate was the most reactive derivative,

exceeding a net AUC value of 75 at 500 μM, while pterostilbene stearate and palmitate showed the lowest activity, failing to exceed a net AUC value of 10.

All the AUC obtained were significant compared to the blanks, except for pterostilbene palmitate at 25 μM which gave no detectable activity by this method.

5.1.1.1.2. ABTS method

In general, the hydrophobic stilbene derivatives showed very low or no ability to neutralise the $ABTS^{\bullet+}$ free radical compared to their natural stilbenes (Figure 93).

For most of the hydrophobic resveratrol and oxyresveratrol derivatives, only the highest concentration showed significant differences in antioxidant activity against $ABTS^{\bullet+}$ radicals, while the other concentrations hardly changed the readings (Figure 93). At 500 μM, resveratrol derivatives gave activity equivalent to that observed at concentrations of 5 – 13 μM resveratrol, and oxyresveratrol derivatives equivalent to concentrations of 4 – 12 μM oxyresveratrol.

Meanwhile, resveratrol and oxyresveratrol above 50 - 100 μM had almost reached the maximum detectable activity under the conditions tested (Figure 93). In fact, the 100 μM concentration was outside the linear range of activity for both stilbenes. Furthermore, at 50 μM, the average remaining amount of $ABTS^{\bullet+}$ in the hydrophobic resveratrol derivatives was 3.5-fold higher than that of resveratrol, and in the oxyresveratrol derivatives 9.5-fold higher than that of oxyresveratrol.

The hydrophobic pterostilbene derivatives completely suppressed the low antioxidant activity of pterostilbene against this cation radical, showing no significant differences even at the highest concentration of 500 μM (Figure 93).

Within all the hydrophobic derivatives studied, oxyresveratrol oleate showed the highest reactivity against $ABTS^{\bullet+}$ radicals, followed by resveratrol stearate. Still the activity of these derivatives did not exceed 26 % inhibition (Figure 93).

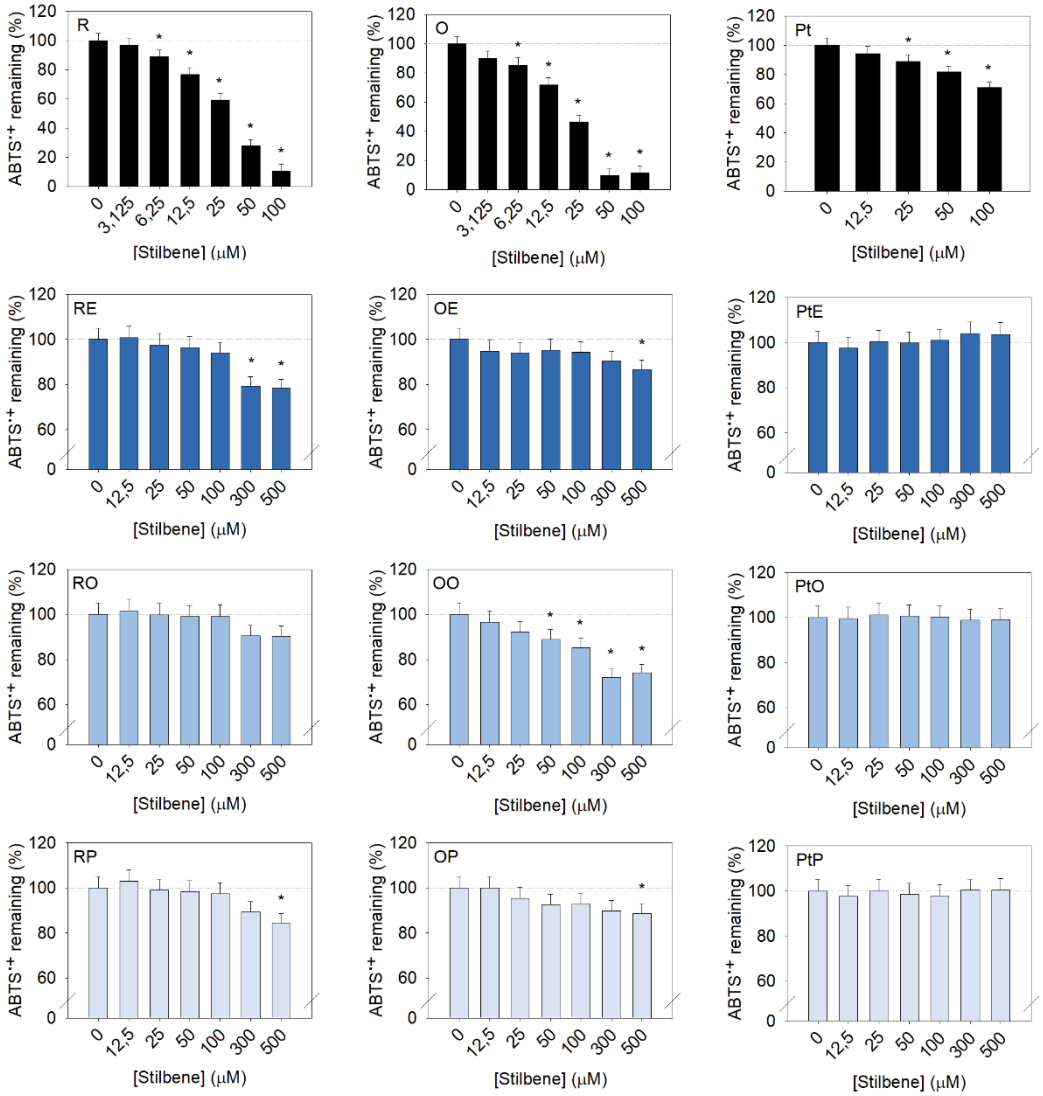

*Figure 93. Antioxidant activity of hydrophobic stilbene derivatives and their natural stilbenes, determined by the ABTS method after 24 hours. * Significance p-value < 0.05*

5.1.1.1.3. DPPH method

In contrast to the previous Section, the hydrophobic stilbene derivatives showed, in general, higher antioxidant activity against the $DPPH^{\bullet}$ free radical (Figure 94) than against $ABTS^{\bullet+}$ (Figure 93). This is probably because the reaction with the $DPPH^{\bullet}$ radical

takes place in an organic medium as opposed to the aqueous medium used in the reaction with $ABTS^{\bullet+}$. Thus, it seems that the reaction medium is a relevant factor in the antioxidant activity of these derivatives.

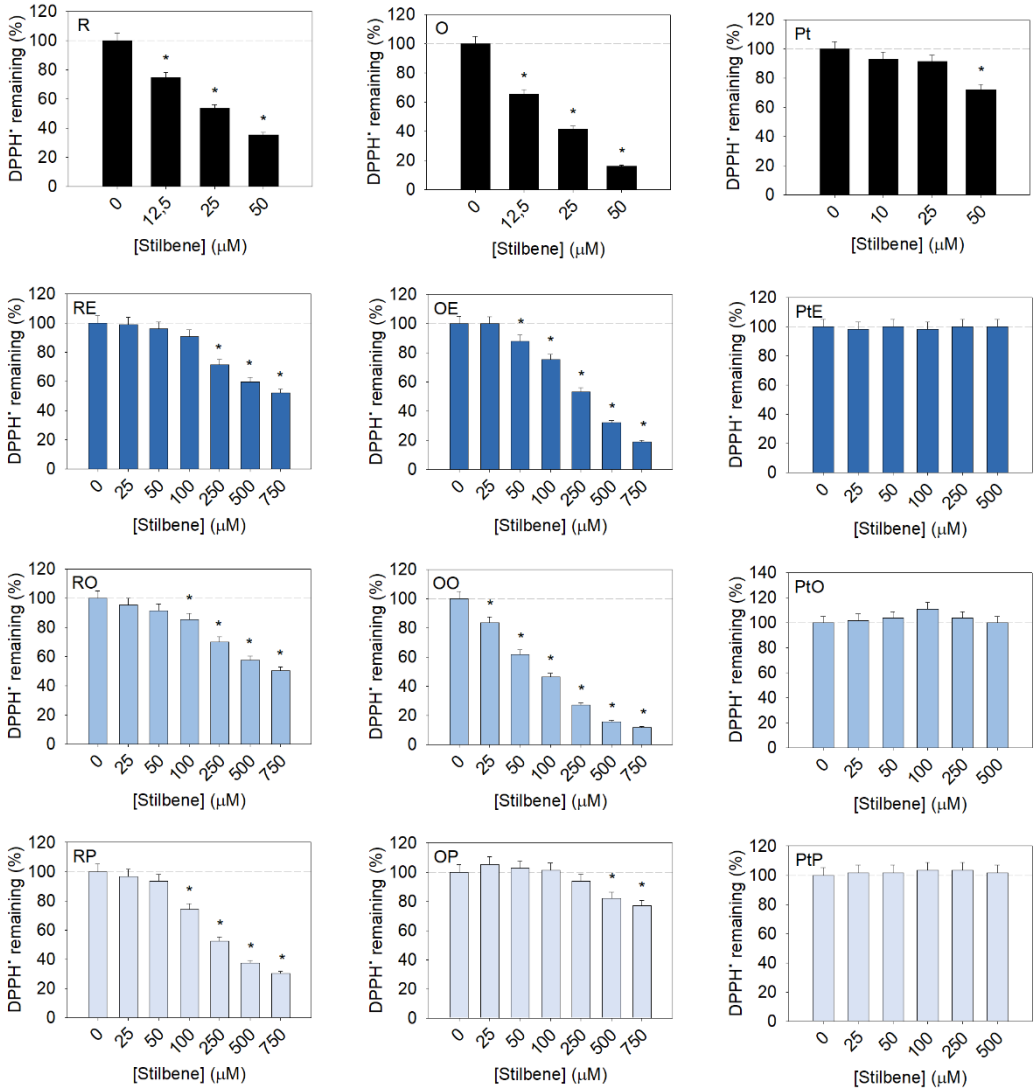

*Figure 94. Antioxidant activity of hydrophobic stilbene derivatives and their natural stilbenes, determined by the DPPH method after 24 hours. * Significance p-value < 0.05*

Resveratrol derivatives showed significant activity against the DPPH• radical from 100 – 250 μM and oxyresveratrol derivatives from 25 – 50 μM, except for oxyresveratrol palmitate which required to reach a concentration of 500 μM (Figure 94). At the highest concentration of 750 μM, resveratrol derivatives showed activity equivalent to

concentrations of 32 – 49 μM resveratrol, while oxyresveratrol stearate and oleate to concentrations of 43 – 48 μM oxyresveratrol, and finally, oxyresveratrol palmitate to a concentration below 12.5 μM oxyresveratrol. Meanwhile, at 50 μM, the average remaining amount of DPPH$^{\bullet}$ in the hydrophobic resveratrol derivatives was 2.6-fold higher than that of resveratrol, while in the oxyresveratrol derivatives it was about 5.2-fold higher than that of oxyresveratrol.

Consistent with the ABTS method, the hydrophobic pterostilbene derivatives showed no significant differences in their activity against the DPPH$^{\bullet}$ radical at any of the concentrations studied. In fact, natural pterostilbene only showed significant differences at 50 μM (Figure 94).

Among all the derivatives tested, oxyresveratrol oleate was the hydrophobic derivative with the highest capacity to neutralise DPPH$^{\bullet}$ radicals, followed by oxyresveratrol stearate. Both derivatives achieved inhibition percentages of 80 – 88 % by this method (Figure 94).

5.1.1.1.4. FRAP method

All hydrophobic stilbene derivatives studied, except pterostilbene stearate, were able to reduce the ferric complex of the FRAP reagent, although less than their parent stilbenes (Figure 95).

All oxyresveratrol derivatives exhibited significant differences in activity from a concentration of 12.5 μM, while resveratrol derivatives did so from 50 μM and pterostilbene oleate and palmitate from 300 μM. At the highest concentration tested, resveratrol derivatives showed activity equivalent to concentrations of 8 – 14 μM resveratrol, oxyresveratrol derivatives to concentrations of less than 17 μM oxyresveratrol and pterostilbene derivatives to concentrations of less than 22 μM

pterostilbene (Figure 95). Meanwhile, at 100 µM, the resveratrol derivatives gave an average Fe^{II} concentration 24.4-fold lower than that of resveratrol, the oxyresveratrol derivatives 14.6-fold lower than that of oxyresveratrol, pterostilbene oleate and palmitate derivatives 59.6-fold lower than that of pterostilbene and pterostilbene stearate 250.5-fold lower than that of pterostilbene (Figure 95).

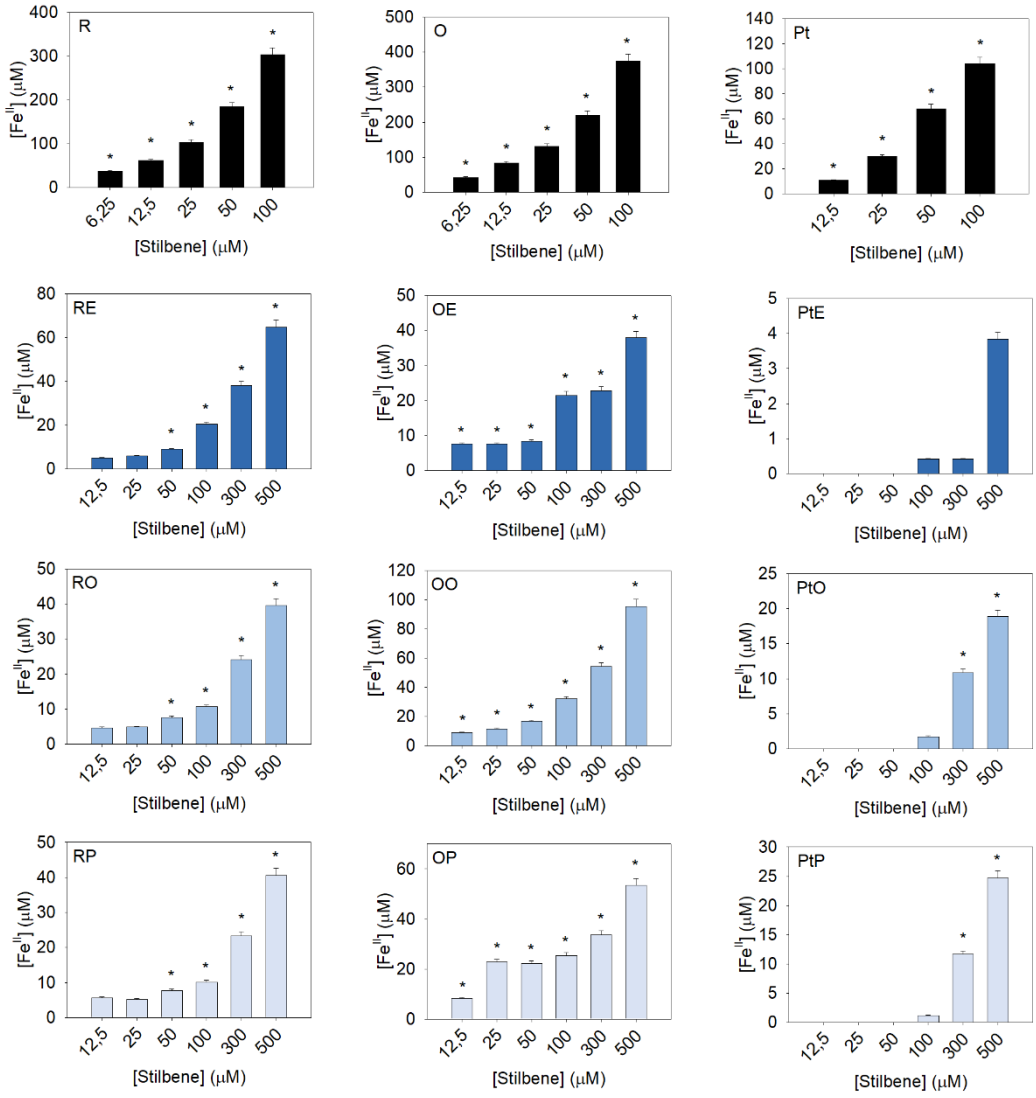

*Figure 95. Antioxidant activity of hydrophobic stilbene derivatives and their natural stilbenes, determined by the FRAP method after 24 hours. * Significance p-value < 0.05*

Oxyresveratrol oleate was the hydrophobic derivative that showed the highest reducing capacity against the ferric complex, followed by resveratrol stearate, reaching

Fe^{II} concentrations above 95 and 64 μM, respectively (Figure 95). These findings could be related to a chelating activity of the resorcinol groups within the molecule (Gulcin, 2020), which would justify oxyresveratrol or its derivatives (2x resorcinol) having more activity than resveratrol or its derivatives (1x resorcinol) and pterostilbene or its derivatives (0x resorcinol).

5.1.1.1.5. Comparison of the antioxidant activity of hydrophobic stilbene derivatives by different methods

Considering all the antioxidant methods tested, it was evident that the structural modification of stilbenes with fatty acids causes a considerable decrease in their antioxidant activity *in vitro*, becoming undetectable in pterostilbene derivatives when tested for their ability to neutralise $ABTS^{\bullet+}$ and $DPPH^{\bullet}$ free radicals (Figure 96A). Since free hydroxyl groups are the main interacting groups in this type of redox reaction, it is reasonable that their removal from the molecule by esterification with fatty acids will affect the antioxidant activity. In fact, it has been observed that, in general, the derivatives with the highest antioxidant activity were those with the highest number of free hydroxyl groups, while the derivatives with the lowest antioxidant activity were those with no free hydroxyl groups.

FRAP, ORAC and DPPH methods gave the highest antioxidant activity signals, intensifying the differences between the hydrophobic stilbene derivatives, including those of pterostilbene in FRAP and ORAC (Figure 96A). Within free radical neutralisation methods, DPPH was found to be more sensitive than ABTS, as well as the method that narrowed the differences between the antioxidant activity of the hydrophobic stilbene derivatives and their natural stilbenes (Figure 96B). This could be due to the higher solubility of the hydrophobic derivatives in the organic reaction medium of DPPH, as opposed to the aqueous medium of the other methods. In the case of pterostilbene

derivatives, the FRAP method narrowed the differences between these derivatives and pterostilbene compared to the ORAC method. Thus, it is possible that the acidic pH of the FRAP reaction medium also has some positive influence on the antioxidant activity of the derivatives without free hydroxyl groups. In a previous study that evaluated the ability of resveratrol stearate, and other derivatives with shorter hydrocarbon chains, to neutralise $ABTS^{\bullet+}$ radicals in aqueous and organic media (Peng and Shahidi, 2022), it was observed that in aqueous media, the differences between the antioxidant activity of resveratrol derivatives and resveratrol itself enlarged, and the negative correlation between antioxidant activity and hydrocarbon chain length intensified. This fact could justify the differences observed between the DPPH (organic medium) and ABTS (aqueous medium) methods, and in general, the low antioxidant activity of hydrophobic stilbene derivatives synthesised with long-chain fatty acids.

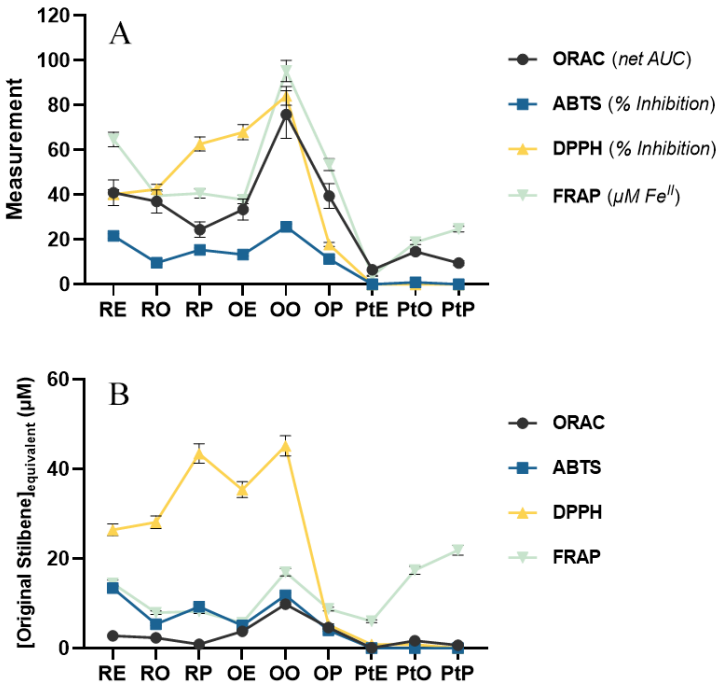

Figure 96. Comparison of the results obtained with the methods for determining the antioxidant activity of hydrophobic stilbene derivatives at 500 µM. Data expressed A) in the common units for the method and B) as the equivalent concentration of the corresponding natural stilbene

Comparing the antioxidant activity obtained among the hydrophobic stilbene derivatives by the different methods, it could be observed that oxyresveratrol oleate was the hydrophobic derivative that showed the highest capacity to neutralise free radicals and reduce iron, followed by resveratrol stearate. By contrast, pterostilbene derivatives, and in particular, pterostilbene stearate, proved to be the least reactive among all the derivatives studied. Figure 97 displays the three-dimensional representation of the antioxidant activity of all hydrophobic stilbene derivatives studied by electron transfer methods at a fixed concentration. In this figure, the order of the derivatives according to their level of antioxidant activity can be visualised in a simple way, with oxyresveratrol oleate (yellow dot) at the most reactive end and pterostilbene stearate (fuchsia dot) at the least reactive end (Figure 97).

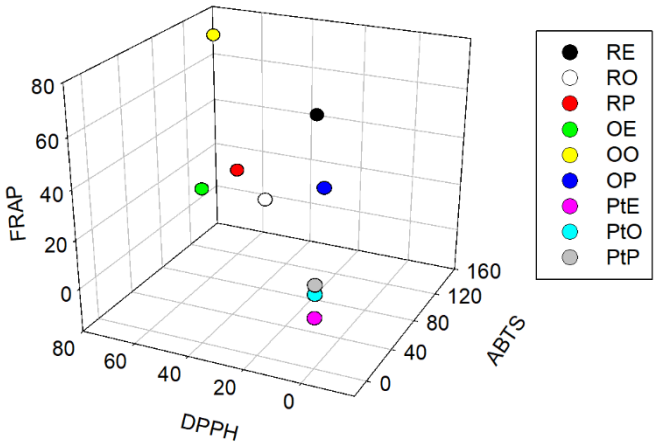

Figure 97. Comparison of the antioxidant activity of several hydrophobic stilbene derivatives at 500 µM, in trolox equivalents (µM), determined by electron transfer methods (SET) after 24 hours

The *in vitro* antioxidant activity of hydrophobic resveratrol derivatives, such as resveratrol stearate, oleate and palmitate, has been determined in previous studies (Oh and Shahidi, 2017; Peng and Shahidi, 2022). However, these studies have been carried out at a fixed antioxidant concentration, only with short incubation times and using variations of some of the methods described in this PhD thesis, such as chemical ABTS, DPPH or FRAP. The results of these authors show a decrease in the antioxidant activity

of the resveratrol derivatives compared to the original resveratrol, especially in the long-chain derivatives and in the diester or triester derivatives. In general, the results obtained in this PhD thesis on the antioxidant activity of hydrophobic resveratrol derivatives correlate with those obtained by these authors (Oh and Shahidi, 2017; Peng and Shahidi, 2022), with both studies showing lower antioxidant activity of hydrophobic resveratrol derivatives compared to resveratrol.

In another research (Oh and Shahidi, 2018), the antioxidant activity of hydrophobic resveratrol derivatives in different lipid matrices was analysed. The authors observed that some derivatives, such as resveratrol stearate and palmitate, were better than resveratrol at preventing oxidation in corn oil after 6 days of storage. They concluded that in order to obtain the greatest antioxidant potential from these derivatives, they should be used in lipid matrices.

Although the results obtained *in vitro* in this Section show a lower antioxidant activity of the hydrophobic stilbene derivatives compared to natural stilbenes, it should be considered that *in vivo* (Section 4.2.2.3.), the opposite was observed, with the hydrophobic stilbene derivative being able to trigger a greater antioxidant response in mice blood compared to its original stilbene. Thus, as the hydrophobic stilbene derivatives are capable of keeping the antioxidant activity in the whole organism, the lower activity observed *in vitro* against free radicals and metal complexes could be an advantage for the development and storage of aqueous formulations enriched in these hydrophobic stilbene derivatives. Hydrophobic stilbene derivatives may be less reactive to the presence of oxidising agents in the aqueous medium containing them compared to natural stilbenes, thus keeping the stilbene derivative intact in the matrix prior to administration.

5.1.1.2. Influence of CDs on antioxidant methods

Following the evaluation of the antioxidant activity of hydrophobic stilbene derivatives, it was investigated the effect of CDs on these methods of antioxidant activity determination. There are many publications using this type of agents being part of an inclusion complex with the antioxidant (Jo et al., 2021; Kfoury et al., 2019; Lu et al., 2009; Żyżelewicz et al., 2018) or being added to improve aqueous solubility and achieve higher concentrations of lipophilic antioxidants during the assay (Bangalore et al., 2005; Costa et al., 2015; Huang et al., 2002; Prior et al., 2003; Zhong et al., 2012).

In most of these studies, changes in antioxidant activity in the presence of CDs are observed, generally increases, which are often justified as a higher antioxidant activity of inclusion complexes compared to free molecules, due to the increased solubility when CDs are added (Alvarez-Parrilla et al., 2005; Aree and Jongrungruangchok, 2018; Ferreira et al., 2013; Jo et al., 2021; Jullian et al., 2008; Kfoury et al., 2019; Li et al., 2021; Lu et al., 2009; Savic et al., 2019; Zhong et al., 2012). However, there are also studies showing decreases in antioxidant activity in the presence of CDs, which are usually justified by the encapsulation of the antioxidant in the region of the hydroxyl group responsible for the interaction with the free radicals of the method (Bangalore et al., 2005; Folch-Cano et al., 2010; Sueishi et al., 2013; Żyżelewicz et al., 2018).

Some authors defend the use of these agents in methods such as ORAC and justify the enhancement in activity with the fact that CDs could act as a reservoir that protects the antioxidant from rapid oxidation (Gabaldón et al., 2010; Huang et al., 2002; Lucas-Abellán et al., 2011, 2008; Prior et al., 2003). However, it has also been suggested that CDs could participate in the ORAC reaction by interfering with the neutralisation of free radicals by antioxidants (García-Padial et al., 2013; Sueishi et al., 2013). In view of this

discrepancy between authors, there is a need to investigate the effect of CDs on the methods for determining antioxidant activity.

Since CD encapsulation is non-specific, non-covalent and can modify the UV-Vis signal of the guest molecules, it was investigated whether these changes in activity could be due to a possible interference of CDs in these methods of antioxidant activity determination. For this purpose, the effect of different types and concentrations of CD in the presence and absence of the antioxidant oxyresveratrol was analysed in each of the methods used above, setting the antioxidant concentration according to the linearity of the method. It was considered that, if CDs were interfering with the measurement, this could be due to the glucidic nature of the CD molecule itself or to its complexing capacity. To discern which of these might be involved, tests were performed with glucose concentrations equivalent to those of CD used to assess the effect of the CD molecule itself, and the absorption spectra and molecular docking of the main reagents involved in CD reactions were analysed to assess the effect of CD complexation.

5.1.1.2.1. Influence of CDs on the ORAC method

In the presence of oxyresveratrol, the net AUC value increased with the concentration of CD, depending on the type of CD (Figure 98). This effect was most marked with β-CD (Figure 98B), being able to increase the net AUC value of oxyresveratrol without CDs by 28 % with just 0.5 mM and doubling it at the highest concentration tested of 3 mM. This could be misinterpreted as an activity equivalent to that obtained with 4 μM of this stilbene.

The other CDs at 3 mM showed an increase in net AUC value ranging from 13 % with α-CD (Figure 98A) to 35 % with γ-CD (Figure 98C). Higher concentrations of α-CD (Figure 98A) or M-β-CD (Figure 98E), gave a slight gradual increase in net AUC up to 45 % at the highest concentration of 9 mM. In contrast, γ-CD (Figure 98C) or HP-β-

CD (Figure 98D) gave a more pronounced gradual increase, doubling the net AUC of oxyresveratrol without CDs at 9 mM.

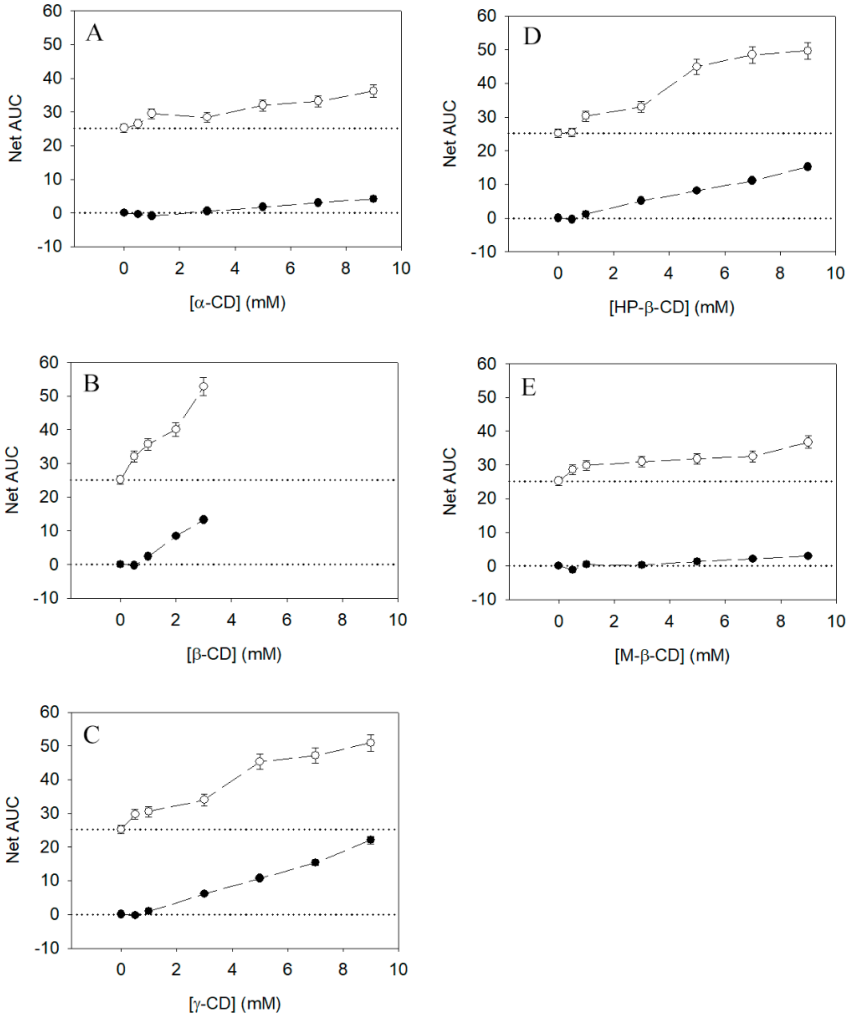

Figure 98. Effect of increasing concentrations of A) α-CD, B) β-CD, C) γ-CD, D) HP-β-CD and E) M-β-CD on the ORAC method, (●) in the absence and (○) in the presence of 2 μM oxyresveratrol

In the absence of the antioxidant, CDs still caused this variation in measurement in a dose-dependent manner (Figure 98). At concentrations below 0.5 mM β-CD (Figure 98B), 1 mM α-CD (Figure 98A), γ-CD (Figure 98C) or HP-β-CD (Figure 98D), and 5 mM M-β-CD (Figure 98E), no changes were observed, whereas above these concentrations a linear increase ($R^2 > 0.99$) in the net AUC value was observed, giving β-CD the steepest slope, followed by γ-CD, HP-β-CD, α-CD and finally, M-β-CD. In fact,

at a concentration of 3 mM CD in the absence of oxyresveratrol, β-CD gave a net AUC of 13.26, γ-CD of 6.05, HP-β-CD of 5.14, α-CD of 0.52 and M-β-CD of 0.17. Although the last two CDs caused a smaller deviation in the measurement, their effect with the antioxidant was larger and should not be underestimated.

These results suggest that the CDs could interfere with the ORAC method, leading to a deviation in the net AUC measurement, whereas the subtraction of the CD signal (without antioxidant) does not seem sufficient to obtain a reliable value of antioxidant activity.

To rule out possible interference due to the glucidic nature of the CDs, the effect of increasing concentrations of glucose (equivalent to those used with CDs previously) was evaluated under the same conditions. The results show a slight variation in the net AUC measurement of ± 5 (Figure 99). However, this deviation was not sufficient to justify the changes observed with CDs in the ORAC method. In fact, the use of CD concentrations higher than 1 mM in the presence of oxyresveratrol generated a variation of net AUC higher than this value (Figure 98). In the absence of oxyresveratrol, a higher variation than the effect of glucose was also obtained with β-CD, HP-β-CD and γ-CD (Figure 98B – D).

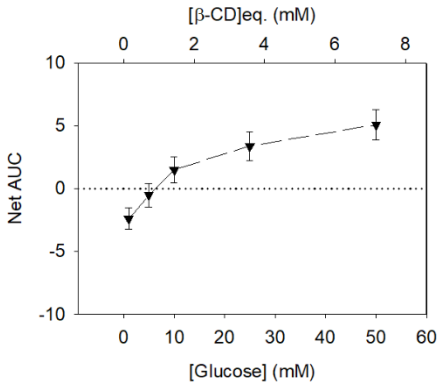

Figure 99. Effect of increasing concentrations of glucose on the ORAC method

Therefore, the interference in the measurement cannot only be associated with the glucidic nature of the CDs, and the effect of the encapsulation of other substances present in the reaction medium, such as fluorescein or AAPH, must be considered. For this purpose, the possible variation in the spectrophotometric and spectrofluorometric properties of these two molecules in the presence of increasing concentrations of CDs was first analysed.

In the presence of CDs, the initial fluorescence intensity of fluorescein also showed changes depending on the type of CD. At the highest concentration of 9 mM, there was a decrease in fluorescence ranging from 3 % in the presence of the modified CDs to 7 % in the presence of α-CD (Figure 100A). In contrast, with the highest concentration of β-CD and γ-CD, the fluorescent signal was similar to that obtained in the samples without CD. The decay in the fluorescence of fluorescein during the reaction in the ORAC method is what allows the determination of the net AUC value, therefore, a decrease in fluorescence intensity prior to the reaction could lead to erroneous values of antioxidant activity.

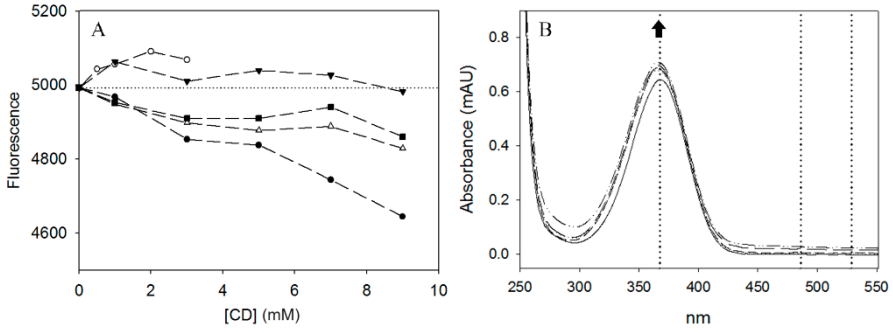

Figure 100. A) Initial fluorescence of fluorescein in the presence of (●) α-CD, (○) β-CD, (▼) γ-CD, (△) HP-β-CD and (■) M-β-CD. B) Absorption spectra of AAPH with increasing concentrations of β-CD (0, 2, 4, 6 and 8 mM). The dotted vertical lines represent the λ_{max} of AAPH and the λ_{exc} and λ_{em} selected in the ORAC method

On the other hand, in the presence of CD, the absorbance of AAPH increased by 6 – 8 % at its wavelength of maximum absorption (λ_{max} = 367 nm), depending on the

concentration of CD (Figure 100B). In fact, the absorbance was not only higher in the λ_{max} region, but also at the excitation (λ_{exc} = 485 nm) and emission (λ_{em} = 528 nm) wavelengths set in the ORAC method, reaching up to 40 – 46 % at λ = 295 nm, the wavelength where the absorbance was minimum (Figure 100B).

It appears that CDs can modify the optical properties of fluorescein and AAPH, suggesting that both molecules could be encapsulated during the reaction, in addition to the antioxidant. For this reason, a bioinformatics study was carried out on the inclusion complexes formed with β-CD, the CD that gave the highest interference in the net AUC value (Figure 98), in addition to having high affinity for oxyresveratrol (Rodríguez-Bonilla et al., 2010).

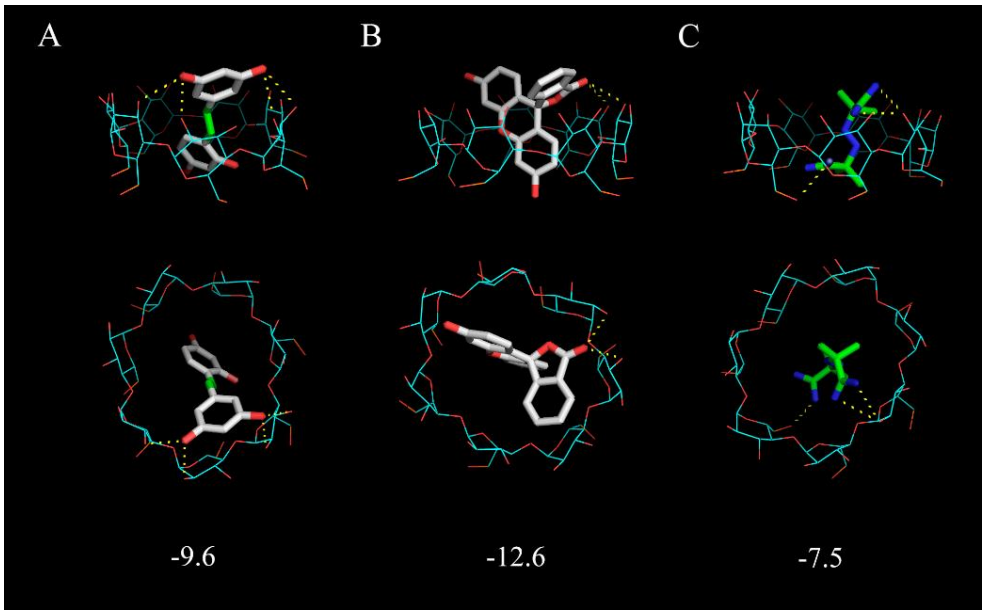

Figure 101. 3D molecular docking and scores of β-CD complexes with A) oxyresveratrol, B) fluorescein and C) AAPH. Hydrogen bonds are displayed as yellow dotted lines

The 3D molecular modelling results showed that β-CD could not only encapsulate oxyresveratrol but also the reagents involved in the ORAC reaction (Figure 101). In fact, it is noteworthy that the score obtained for the complex with oxyresveratrol (Figure 101A) was higher than the score obtained for the complex with fluorescein (Figure 101B),

indicating that the binding strength of β-CD with fluorescein was higher than with oxyresveratrol. In contrast, the complex with AAPH showed the worst score value (Figure 101C), suggesting that the affinity of CD for this reagent was lower than that of the antioxidant or fluorescein. In all the inclusion complexes analysed, hydrogen bond stabilisation could be observed.

These results correlate with those obtained by Sueishi *et al*. (2013) and by Garcia-Padial *et al*. (2013), in which the role of CDs in the ORAC method is also questioned. While Sueishi *et al*. (2013) claimed that complexes with CDs prevented the interaction of the antioxidant with free radicals, García-Padial *et al*. (2013) suggested that fluorescein might be encapsulated in the cavity of natural CDs. The results of this PhD thesis demonstrate experimentally and computationally, using a wide range of concentrations of natural and modified CDs, that both fluorescein and AAPH could interact with CDs leading to a deviation in the net AUC measurement, contrary to the conclusions obtained by Lucas-Abellán *et al*. (2011). Therefore, the determination of antioxidant activity by the ORAC method in the presence of CDs could lead to erroneous values if the influence of the other reagents in the medium is not taken into account.

5.1.1.2.2. Influence of CDs on the ABTS method

Since CDs do not have direct antioxidant activity, it would be expected that the measurement of the percentage of remaining $ABTS^{\bullet+}$ remain stable with increasing concentration. However, the results of the antioxidant activity of oxyresveratrol determined by this method showed the opposite. After 24 hours, the increase in CD concentration caused a gradual reduction in absorbance at 414 nm leading to a reduction in the percentage of free radical remaining (Figure 102B – E), except with α-CD (Figure 102A). This CD did not show any change in measurement until the highest concentration was reached, above which it showed slightly lower inhibition values than the control

without CD. In contrast, the use of just 0.4 mM β-CD significantly decreased the remaining cation radical (Figure 102B), while the other CDs needed to reach a concentration of 0.8 – 1 mM to have a significant variation in the measurement (Figure 102C – E). Above these concentrations, the percentage of remaining radical with β-CD showed a large negative slope, which was followed by the slope obtained with HP-β-CD, γ-CD and finally, M-β-CD, resulting in a 22 – 31 % decrease in remanent $ABTS^{\bullet+}$ at the highest analysed concentration of these CDs (γ-CD, HP-β-CD and M-β-CD: 1.5 mM / β-CD: 0.5 mM).

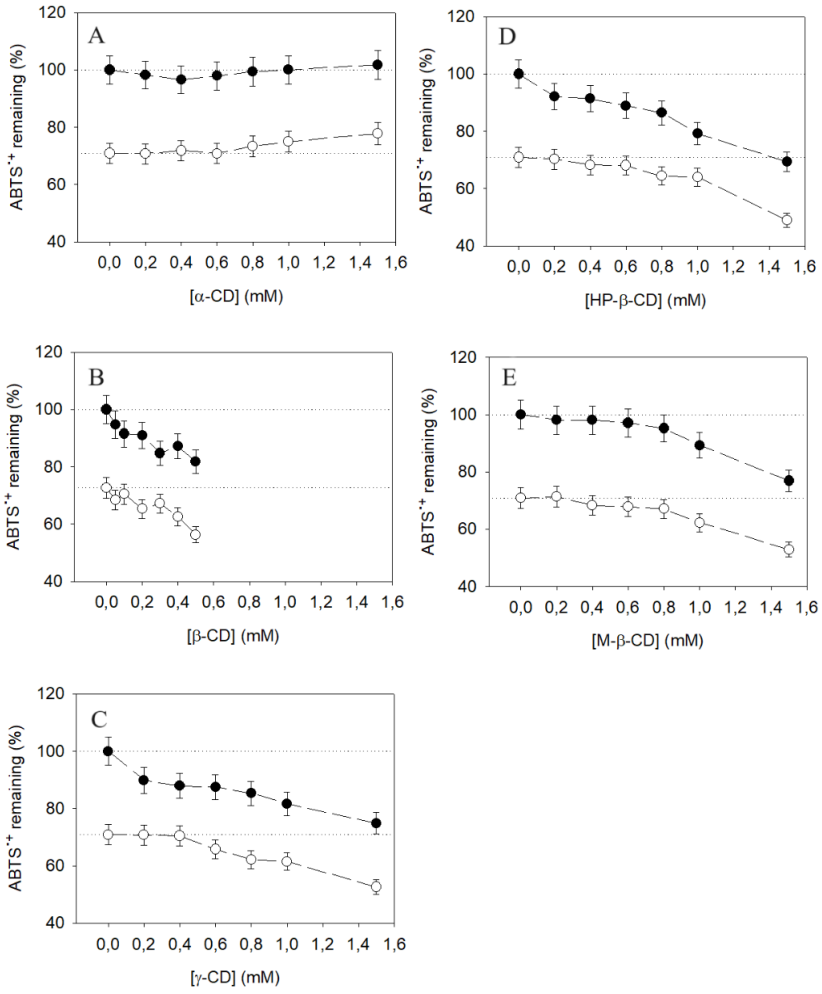

Figure 102. Effect of increasing concentrations of A) α-CD, B) β-CD, C) γ-CD, D) HP-β-CD and E) M-β-CD on the ABTS method, (●) in the absence and (○) in the presence of 1 μM oxyresveratrol, after 24 hours

When the antioxidant was not present in the redox reaction, it could also still be observed that the presence of CDs altered the measure of antioxidant activity. Indeed, β-CD, γ-CD and HP-β-CD, in the absence of oxyresveratrol, resulted in significant variations in the percentages of $ABTS^{\bullet+}$ remaining at a lower concentration than in the presence of oxyresveratrol (Figure 102B – D). This effect suggests an interference of CDs in the method, which could not be mitigated a posteriori by subtracting the measurement without antioxidant from the measurement with antioxidant. The observed decrease in the percentage of $ABTS^{\bullet+}$ remaining due to the presence of CDs in the absence of antioxidant would be equivalent to the level of activity obtained with approximately 1 µM oxyresveratrol (Figure 102B – E). In contrast, the use of α-CD hardly modified the readings, giving a similar effect in the presence and absence of oxyresveratrol at most of the concentrations tested (Figure 102A).

Following the methodology used to investigate the interference of CDs in the ORAC method, the effect of increasing concentrations of glucose equivalent to those of CDs used, was evaluated. The results of this study showed that glucose did not cause a significant change in the activity readings, and therefore, the glucidic nature of the CDs did not seem to be the reason for the interference (Figure 103).

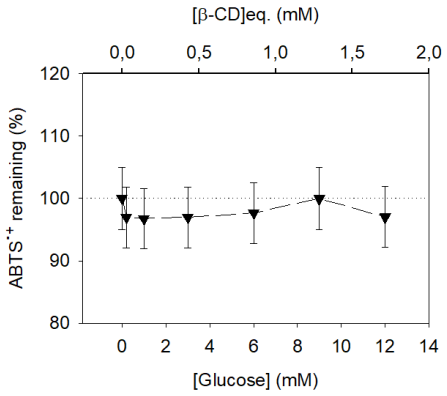

Figure 103. Effect of increasing concentrations of glucose on the ABTS method, after 24 hours

Therefore, the possible encapsulation of the radical was analysed by recording its absorption spectrum in the presence of increasing concentrations of β-CD and molecular docking of potential inclusion complexes.

The absorption spectra of $ABTS^{\bullet+}$ revealed that the presence of β-CD was able to decrease the absorbance at the wavelength selected in the method, i.e. 414 nm (Figure 104), which would justify the observed decrease in the remaining $ABTS^{\bullet+}$ in the ABTS method assays (Figure 102B). Additionally, the absorbance at the other λ_{max} of the cation radical, i.e. 734 nm, was also affected by the presence of the CD, resulting in a further reduction in absorbance compared to 414 nm. In fact, at the highest concentration of 0.5 mM, the absorbance at 734 nm decreased by 9 % compared to the control without CD, while at 414 nm this decrease was 6 % (Figure 104). These signal variations could suggest the formation of an inclusion complex between the CDs and the cation radical, with optical properties different from those of the radical itself.

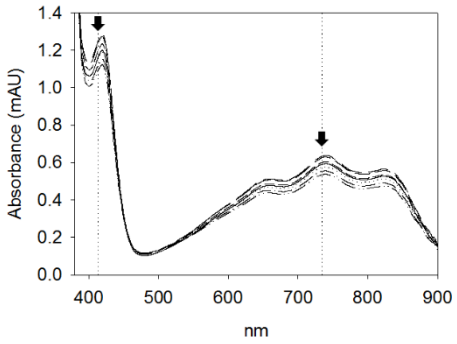

Figure 104. Absorption spectra of $ABTS^{\bullet+}$ with increasing concentrations of β-CD (0; 0.05; 0.1; 0.2; 0.3; 0.4; 0.5 mM), after 24 hours. The dotted vertical lines represent the λ_{max} of $ABTS^{\bullet+}$ (414 and 734 nm)

Computational assays with β-CD revealed that the inclusion complex formed with the $ABTS^{\bullet+}$ radical (Figure 105B) had a better score than the inclusion complex formed with oxyresveratrol (Figure 105A), indicating that the binding strength between the two molecules was higher in the case of CD interaction with the radical than with the

antioxidant. In addition, both three-dimensional modelling showed hydrogen bond formation between ligand and receptor.

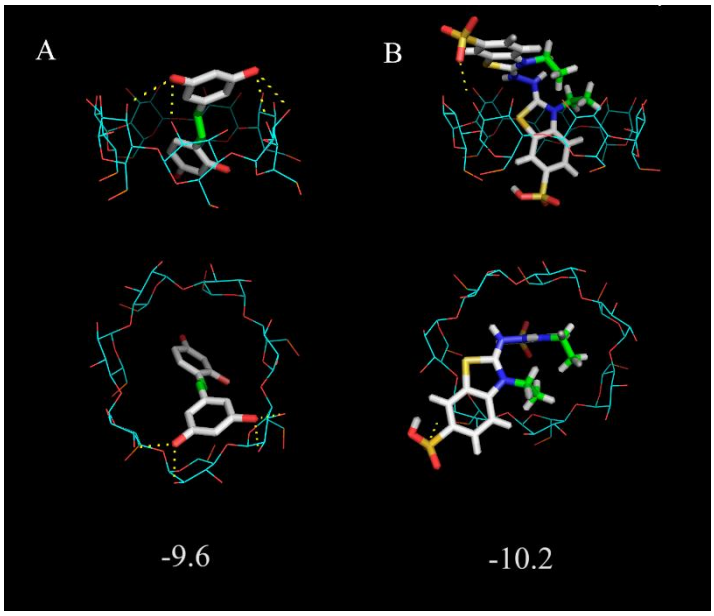

Figure 105. 3D molecular docking and scores of β-CD complexes with A) oxyresveratrol and B) ABTS$^{\bullet+}$. Hydrogen bonds are displayed as yellow dotted lines

Taken together, these results are consistent with those obtained previously by Lucas-Abellán *et al*. (2011), where it was observed that the use of HP-β-CD increased the measure of antioxidant activity in the chemical ABTS method after 30 minutes of incubation with the ABTS$^{\bullet+}$ radical, suggesting that the effect could be caused by the complexation of the cation radical. The results obtained in this PhD thesis demonstrate this possible encapsulation of ABTS$^{\bullet+}$, as well as the effect of other CDs at different concentrations.

5.1.1.2.3. Influence of CDs on the DPPH method

In contrast to the previous methods, the reaction with the DPPH$^{\bullet}$ radical takes place in a completely or partially organic medium, which, taking into account the hydrophobic cavity of the CDs, could affect the inclusion complexes (Lucas-Abellán et

al., 2011). In this case, the CD assays were performed with 50 % (v/v) methanol, which could allow complexes to still be formed during the method (Ferreira et al., 2013).

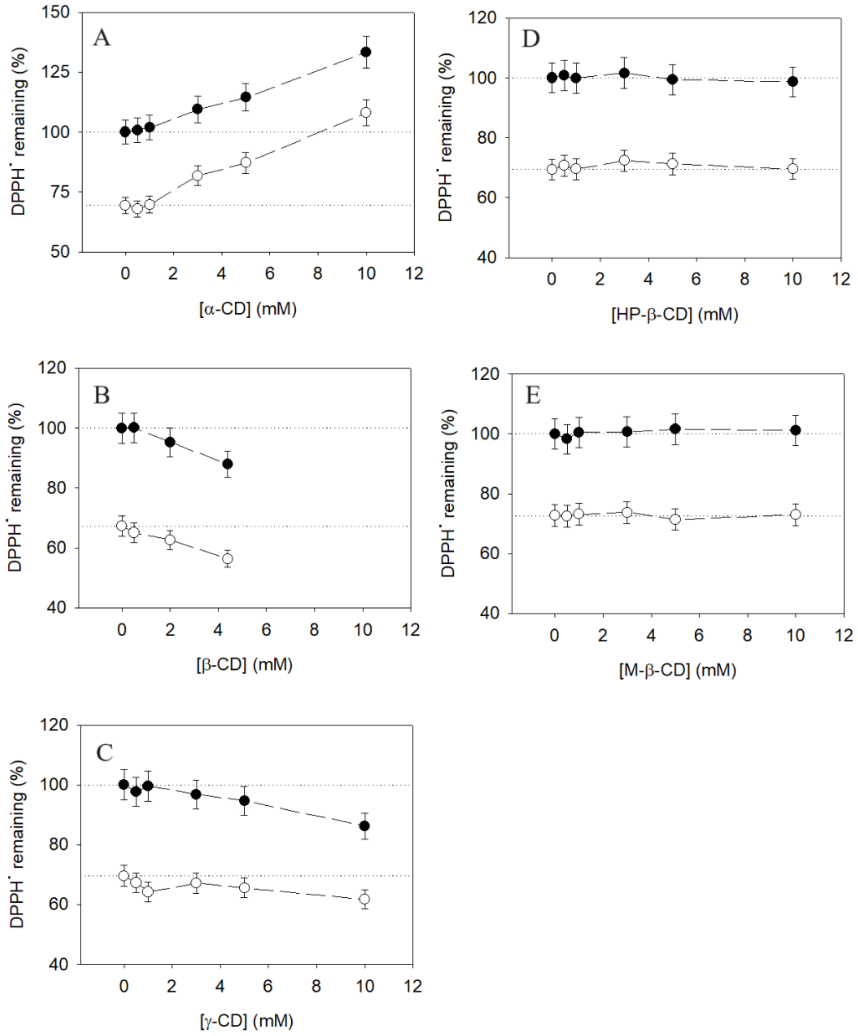

Figure 106. Effect of increasing concentrations of A) α-CD, B) β-CD, C) γ-CD, D) HP-β-CD and E) M-β-CD on the DPPH method, (●) in the absence and (○) in the presence of 5 μM oxyresveratrol, after 30 min

The results of the ability of oxyresveratrol to neutralise DPPH• radicals showed a deviation of the measured in the presence of natural CDs (Figure 106A-C), whereas modified CDs apparently did not alter the remaining amount of the radical under the conditions studied (Figure 106D – E). At the highest concentration tested, β-CD and γ-CD caused a significant decrease of 16 % and 11 % in the measurement, respectively

(Figure 106B – C), while α-CD caused a putative increase of up to 56 % compared to the control without CDs (Figure 106A).

In the absence of oxyresveratrol, natural CDs also showed this variation in the remaining percentage of DPPH• with increasing concentration, with α-CD maintaining the largest deviation from the control without CDs (Figure 106). At the highest concentration, β-CD and γ-CD gave a 12 % and 14 % decrease, respectively (Figure 106B – C), while α-CD gave a 33 % increase (Figure 106A). The modified CDs still showed no change in measurement when the antioxidant was removed from the reaction (Figure 106D – E). In contrast to the previous methods, the subtraction of the measurement without antioxidant from the measurement with antioxidant practically neutralises the variation by the concentration of CDs. However, it should be noted that this may not occur with other types of antioxidants.

The use of glucose concentrations equivalent to the CD concentrations selected in the method did not show significant variations in the remaining radical (Figure 107), suggesting that the glucidic nature of the CD molecule may not be responsible for the interference observed in the DPPH method.

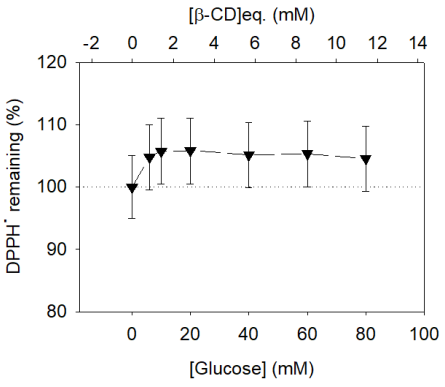

Figure 107. Effect of increasing concentrations of glucose on the DPPH method, after 30 min

In contrast, the use of increasing concentrations of β-CD modified the signal in the DPPH• absorption spectrum (Figure 108), suggesting a possible encapsulation of the radical during the assay. At the λ_{max} selected, a β-CD concentration of 4.4 mM caused a decrease in absorbance of 13 % (Figure 108), which would account for the observed increase in the remaining amount of the radical (Figure 106B). Furthermore, in the regions of the spectrum where the absorbance was minimum, the presence of CDs caused the opposite effect to that observed at the maximum, increasing the signal by up to 35 % at 282 nm and 44 % at 406 nm (Figure 108).

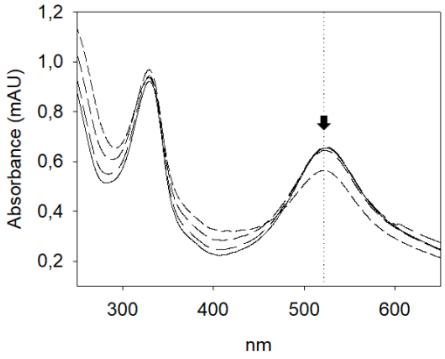

Figure 108. Absorption spectrum of DPPH• with increasing concentrations of β-CD (0; 0.5; 2; 4.4 mM), after 30 min. The dotted vertical line represents the λ_{max} of DPPH• (517 nm)

Using computational assays, the formation of the inclusion complex between β-CD and the DPPH• radical could also be observed (Figure 109B). This complex obtained better score than the complex between β-CD and oxyresveratrol (Figure 109A). These results suggest that during the DPPH method, the CDs could be encapsulating both the antioxidant and the free radical, causing an interference in this method of antioxidant activity determination.

The variations obtained in this method by the CDs correlate with those previously published by Ferreira *et al*. (2013), in which it was observed that mangiferin complexes with β-CD gave higher antioxidant activity than the free compound, and Lucas-Abellán

et al. (2011), in which it was observed that HP-β-CD did not alter the antioxidant measure with resveratrol. However, in the work of Lu *et al*. (2009), the opposite was observed with HP-β-CD when using a higher concentration of resveratrol and lower concentration of free radical than that used by Lucas-Abellán *et al*. (2011). Thus, these findings do not discard the possibility that under different conditions this CD may also interfere with the method. In the study performed by Lucas-Abellán *et al*. (2011), they conclude that the 100 % methanol medium prevents complexation, making the method not suitable for studying the antioxidant activity of inclusion complexes. The results of this PhD thesis, in a 50 % (v/v) methanol medium, show that some CDs can produce variations in the measurement, suggesting the formation of inclusion complexes, probably due to the aqueous percentage of the medium. However, these inclusion complexes might not be formed exclusively by the antioxidant, but the CDs might also be interacting with the DPPH$^{\bullet}$ radical.

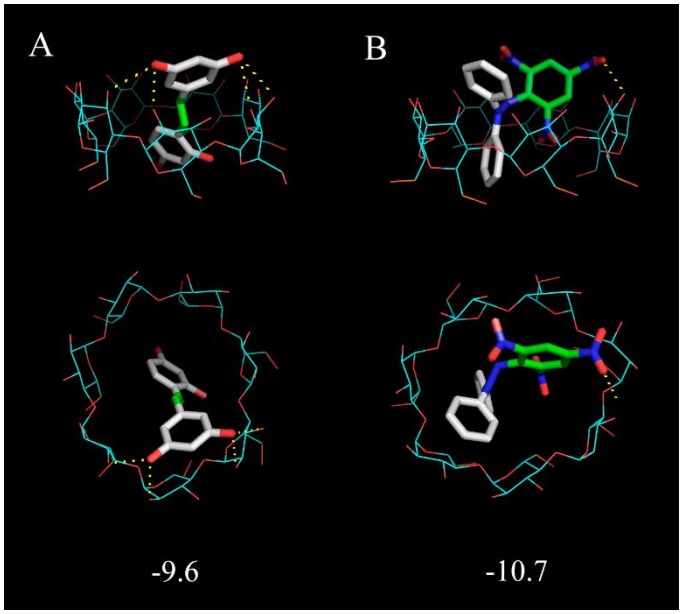

Figure 109. 3D molecular docking and scores of β-CD complexes with A) oxyresveratrol and B) DPPH$^{\bullet}$. Hydrogen bonds are displayed as yellow dotted lines

5.1.1.2.4. Influence of CDs on the FRAP method

In the FRAP method, only a few CDs gave significant variations in the measurement, depending on the type and concentration of CD (Figure 110).

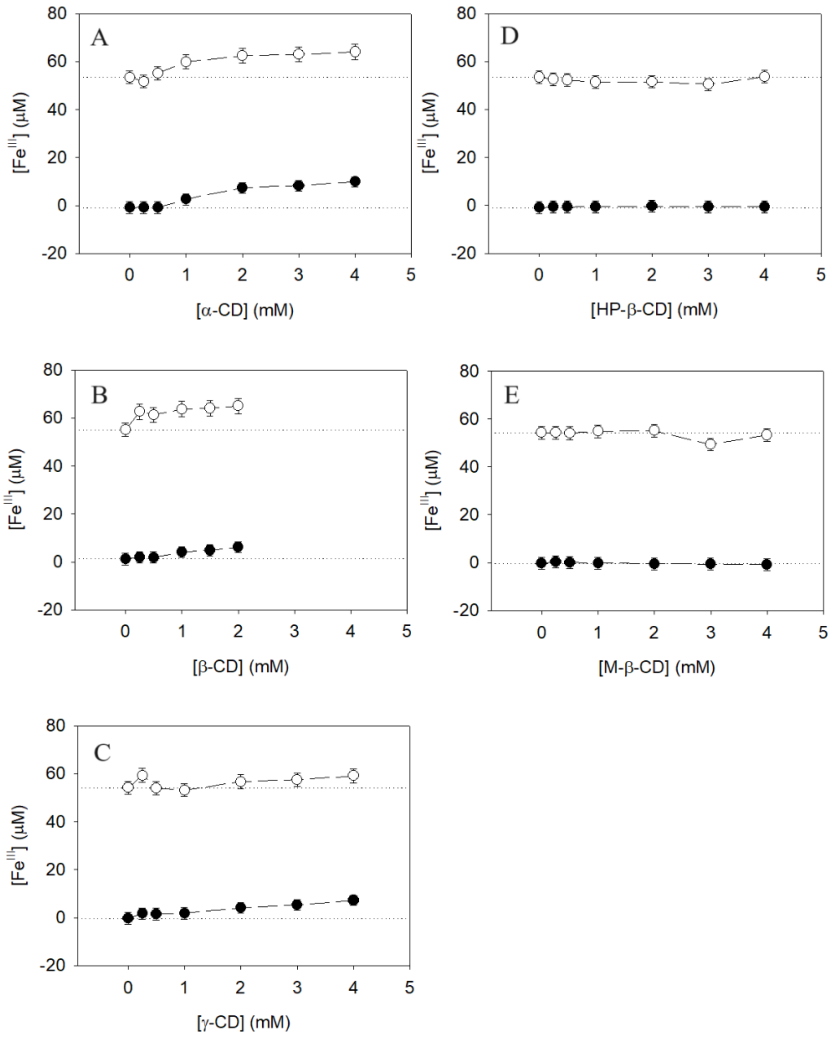

Figure 110. Effect of increasing concentrations of A) α-CD, B) β-CD, C) γ-CD, D) HP-β-CD and E) M-β-CD on the FRAP method, (●) in the absence and (○) in the presence of 25 μM oxyresveratrol, after 2 hours

As in the DPPH method (Figure 106D – E), none of the modified CDs showed changes in activity, regardless of the presence of the antioxidant oxyresveratrol (Figure 110D – E). In contrast, in the presence of oxyresveratrol, the natural α-CD and β-CD gave significantly higher values of the Fe^{II}-TPTZ complex from just 1 mM and 0.25 mM, respectively (Figure 110A – B). At the highest concentration, this increase in the

formation of the ferrous complex was 20 % with α-CD and 18 % with β-CD compared to the control without CDs.

However, in the absence of oxyresveratrol, the variation with β-CD was no longer significant at the concentrations tested and only α-CD and γ-CD, from 2 mM and 3 mM, respectively, were able to cause a significant increase in the measurement (Figure 110A and Figure 110C).

Results with increasing concentrations of glucose, equivalent to the CD concentrations used, showed no significant differences in the FRAP readings (Figure 111), suggesting that the glucidic nature of CDs was not responsible for the variations observed with some of the CDs in the method.

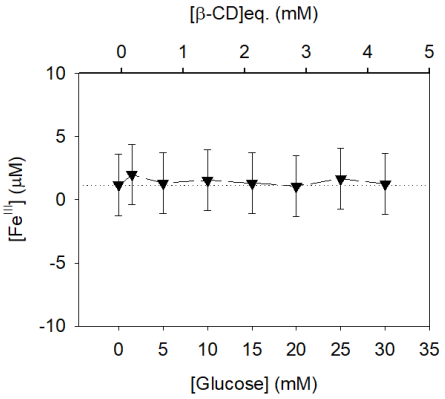

Figure 111. Effect of increasing concentrations of glucose on the FRAP method, after 2 hours

In contrast, the absorption spectra of the Fe-TPTZ complex in the presence of increasing concentrations of β-CD showed significant variations in the signal with respect to the basal spectrum (Figure 112). Concentrations of β-CD below 1 mM decreased the absorbance at 600 nm by 22 – 29 %, while the use of concentrations equal to or above 1 mM increased the absorbance by 11 – 30 % at the selected wavelength.

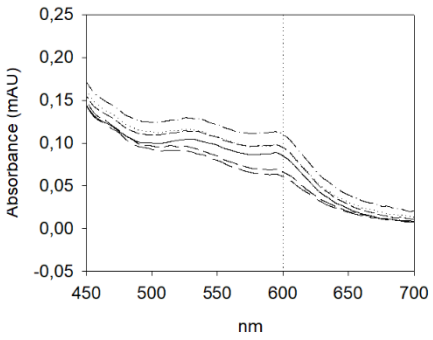

Figure 112. Absorbance spectra of the Fe-TPTZ complex with increasing concentrations of β-CD (0; 0.25; 0.5; 1; 1.5; 2 mM), after 2 hours. The dotted vertical line represents the λ_{max} of Fe^{II}-TPTZ (600 nm)

The molecular docking results also supported the possible interaction between β-CD and the Fe-TPTZ complex, as one of its distal rings entered the CD cavity (Figure 113B). Furthermore, the score value obtained in this conformation was more negative than that obtained in the inclusion complex with oxyresveratrol (Figure 113A), indicating the Fe-TPTZ complex has a higher binding strength with β-CD than oxyresveratrol. Therefore, these results suggest that CDs could also interfere with the FRAP method by interaction with the antioxidant and with the tripyridyl triazine complex during the assay.

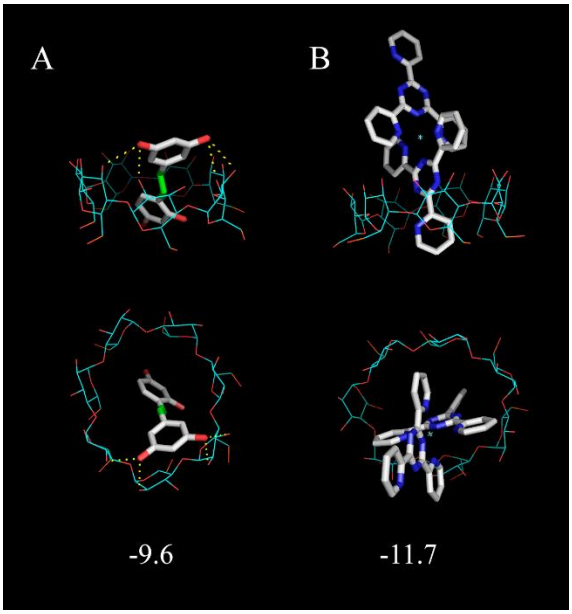

Figure 113. 3D molecular docking and scores of β-CD complexes with A) oxyresveratrol and B) Fe-TPTZ complex. Hydrogen bonds are displayed as yellow dotted lines

5.1.1.2.5. Overall discussion on the influence of CDs on different antioxidant methods

In general, the results of the effect of CDs on the four methods of antioxidant activity determination showed that, above a certain concentration, most of the CDs studied are able to change the measurement, leading to variations in the antioxidant activity values, in the presence and absence of the antioxidant oxyresveratrol.

This variation depends on the concentration and type of CD, and varies according to the method used. In the ORAC method, β-CD, γ-CD and HP-β-CD were the CDs that caused the greatest deviation in the measurements from concentrations of 0.5 – 3 mM. In the ABTS method, the greatest variation was obtained with β-CD, γ-CD and HP-β-CD from 0.3 – 0.6 mM in the absence of oxyresveratrol, and β-CD, γ-CD and M-β-CD from 0.4 – 1 mM in the presence of oxyresveratrol. In the DPPH method, higher concentrations of CD were needed to observe a deviation in the measurement, e.g. β-CD and γ-CD from 4.4 and 10 mM, respectively, gave an apparent increase in activity, while α-CD from 3 – 5 mM, a decrease even below the control without CDs. Finally, the FRAP method required concentrations from 0.25 – 1 mM of β-CD or α-CD, in the presence of oxyresveratrol, to show a positive deviation, but from 2 – 3 mM of α-CD or γ-CD, in the absence of oxyresveratrol.

Since some concentrations of CD gave a different effect depending on the presence of the antioxidant, subtraction of the measurement without antioxidant from the measurement with antioxidant does not seem to guarantee a reliable antioxidant activity value for most methods. Although in the DPPH method the variations with and without oxyresveratrol were very similar, this could not be assumed for other antioxidants.

According to UV-Vis spectra and molecular docking results, this effect is probably due to the ability of the CDs to encapsulate the reagents involved in the redox reactions,

leading to absorbance or fluorescence variations in the spectra of these reagents, which can be misinterpreted as an increase or decrease in antioxidant activity. In contrast, the glucidic nature of the CDs does not seem to be the cause of the interference observed in the methods.

Therefore, when CDs are not present, antioxidants can interact freely with the reagents involved in the redox reaction. In the case of the ORAC method, the following chemical equilibrium would be met:

$$\begin{matrix} FH \\ F^{\cdot} \end{matrix} \leftrightarrows \begin{matrix} R^{\bullet} \\ RH \end{matrix} \leftrightarrows \begin{matrix} AH \\ A^{\bullet} \end{matrix} \tag{33}$$

where FH is the fluorescent probe, R• the free radical and AH the antioxidant.

However, when CDs are present, new chemical species interact, leading to new equilibria and changes in kinetics. For example, in the ORAC method, CDs could encapsulate the antioxidant (oxyresveratrol) (Equation 34), the fluorescent probe (fluorescein) (Equation 35) or the peroxyl radical generator (AAPH) (Equation 36) leading to the following equilibria:

$$\begin{matrix} FH \\ F^{\cdot} \end{matrix} \leftrightarrows \begin{matrix} R^{\bullet} \\ RH \end{matrix} \leftrightarrows \begin{matrix} AH \\ A^{\bullet} \end{matrix} \begin{matrix} +CD \\ +CD \end{matrix} \rightleftarrows \begin{matrix} \boldsymbol{AH-CD} \\ \boldsymbol{A^{\bullet}-CD} \end{matrix} \leftrightarrows \begin{matrix} R^{\bullet} \\ RH \end{matrix} \leftrightarrows \begin{matrix} FH \\ F^{\bullet} \end{matrix} \tag{34}$$

$$\begin{matrix} AH \\ A^{\bullet} \end{matrix} \leftrightarrows \begin{matrix} R^{\bullet} \\ RH \end{matrix} \leftrightarrows \begin{matrix} FH \\ F^{\bullet} \end{matrix} \begin{matrix} +CD \\ +CD \end{matrix} \rightleftarrows \begin{matrix} \boldsymbol{FH-CD} \\ \boldsymbol{F^{\bullet}-CD} \end{matrix} \leftrightarrows \begin{matrix} R^{\bullet} \\ RH \end{matrix} \leftrightarrows \begin{matrix} AH \\ A^{\bullet} \end{matrix} \tag{35}$$

$$\begin{matrix} FH \ / \ AH \\ F^{\bullet} \ / \ A^{\bullet} \end{matrix} \leftrightarrows \begin{matrix} R^{\bullet} \\ RH \end{matrix} \begin{matrix} +CD \\ +CD \end{matrix} \rightleftarrows \begin{matrix} \boldsymbol{R^{\bullet}-CD} \\ \boldsymbol{RH-CD} \end{matrix} \leftrightarrows \begin{matrix} FH \ / \ AH \\ F^{\bullet} \ / \ A^{\bullet} \end{matrix} \tag{36}$$

This multiplies the possible reactions that may occur during the assay, generating products with different kinetics that could result in different signals in the spectrophotometer or spectrofluorometer, as demonstrated.

All the CDs studied gave variations in the measurement with at least some of the methods studied. Although there were methods in which some CDs did not show a significant deviation, as well as CD concentrations below which the measurements were not altered, it should be considered that encapsulation with CDs consists of a chemical equilibrium in which time determines the concentration of free and complexed substrate. Therefore, these results may vary if different incubation times than those used in these studies are applied. In addition, the use of different concentrations of antioxidant and/or reagents, as well as other types of antioxidants that have a different affinity for the CD cavity, could also affect the results, and interference in the methods with any of the CDs cannot be discarded.

For example, previous studies of antioxidant activity of HP-β-CD complexes with resveratrol by the DPPH method showed different results when using different concentrations of antioxidant and free radical. While in the research performed by Lucas-Abellán *et al*. (2011), no differences were observed when increasing the concentration of HP-β-CD in the presence of 5 or 15 μM resveratrol and 93 μM $DPPH^{\bullet}$, in the work by Lu *et al*. (2009), a notable increase in activity was obtained when using the same concentrations of HP-β-CD, but in the presence of a higher concentration of the same antioxidant (25 μM) and lower concentration of the free radical (60 μM). Likewise, previous studies have also shown that the use of antioxidants with different structures can give completely different results in the effect with each of the CDs, as is the case with tyrosol and caffeic acid (García-Padial et al., 2013). While the former showed an increase in antioxidant activity by the ORAC method when increasing the concentration of various CDs, the latter showed no variation in activity due to the presence of these agents in the medium.

5.1.2. Cytotoxicity of stilbene analogues of resveratrol

The antiproliferative activity of resveratrol on colorectal cancer cell lines has been extensively investigated (Honari et al., 2019; Rauf et al., 2018; Vernousfaderani et al., 2021). However, the effect of other stilbene analogues is not as well studied, with limited comparative studies with various stilbenes to establish structure-activity relationships in this family of bioactive compounds (González-Sarrías et al., 2022; Paul et al., 2010). For this reason, the cytotoxic activity of resveratrol and eight of its hydroxylated and/or methoxylated analogues: oxyresveratrol, piceatannol, gnetol, pinostilbene, pterostilbene, isorhapontigenin, rhapontigenin and trimethoxystilbene, was analysed.

Results with different concentrations of these stilbenes revealed that, at 25 μM, only pterostilbene, trimethoxystilbene and piceatannol are able to inhibit cell proliferation in the Caco-2 line significantly compared to the solvent control (Figure 114). Upon doubling the concentration, stilbene pinostilbene, isorhapontigenin, rhapontigenin and resveratrol also gave cytotoxic activity against tumour cells, while oxyresveratrol and gnetol required a concentration of 100 μM to show any effect (Figure 114).

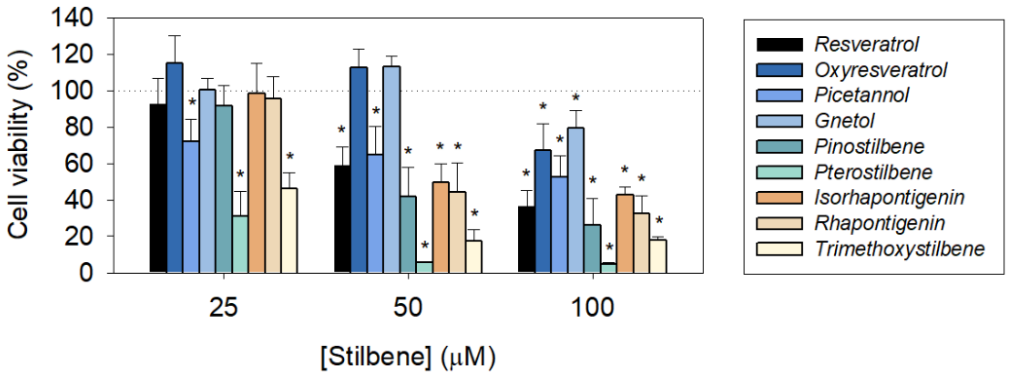

*Figure 114. Viability of Caco-2 cells after 48 h incubation with various stilbenes, determined with neutral red and calculated with the solvent control (DMSO = 0.1 % (v/v)). * Significance p-value < 0.05*

The hydroxyl and methoxy groups of the stilbenes had a clear influence on the cytotoxic activity in Caco-2 cells. In particular, cell viability correlates positively with the number of hydroxyl groups (50 µM: R^2 = 0.718), and negatively with the number of methoxy groups (50 µM: R^2 = 0.655) (Figure 115). Thus, stilbenes such as trimethoxystilbene or pterostilbene, which have more methoxy radicals and less hydroxyl radicals, inhibited colorectal cancer cell proliferation the most. Meanwhile, oxyresveratrol and gnetol, with less methoxy and more hydroxyl radicals, showed the least effect (Figure 115). Fulda *et al*. (2010) also concluded in their review that the substitution of hydroxyl for methoxy groups in resveratrol enhanced its cytotoxic activity.

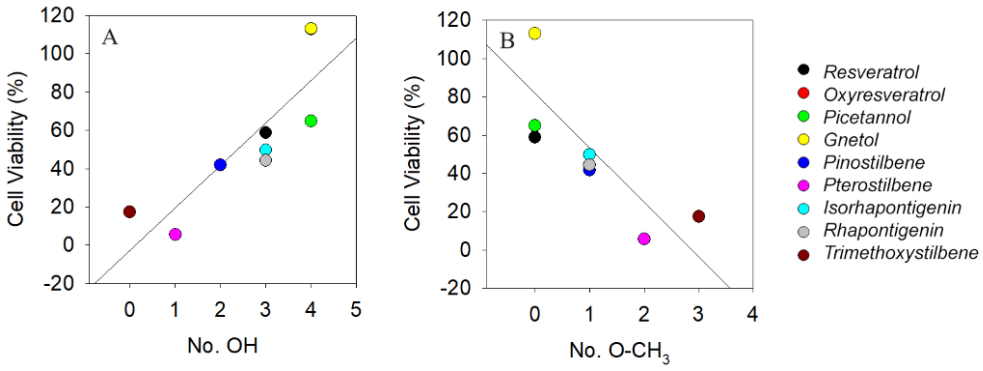

Figure 115. Correlation between cytotoxicity in Caco-2 (48 h, neutral red) and the number of A) hydroxyl and B) methoxy groups in various stilbenes at 50 µM

However, piceatannol with the same number of hydroxyl groups as oxyresveratrol and gnetol showed higher cytotoxic activity than these stilbenes. In fact, 50 µM piceatannol gave similar activity to that of resveratrol, which has a lower number of hydroxyl groups (Figure 114). This could be due to the ability of the hydroxyl groups of piceatannol in the *ortho* position to form a more stable semiquinone (Rossi et al., 2008). Therefore, it is not only the number and type of functional groups that influence the cytotoxic activity of stilbenes in colon cancer, but the position of these groups may also play a key role. Although in the case of the isomeric stilbenes, isorhapontigenin and

rhapontigenin, the difference in the position of their methoxy group does not seem to have such an impact on their cytotoxic activity, probably due to the impossibility of forming the semiquinone that enhances the activity of piceatannol (Figure 115).

In order to compare the results with previous literature, IC50 values for most of the stilbenes tested were estimated from the above data (Table 25). Although piceatannol was one of the few stilbenes to exhibited activity at 25 μM (Figure 114), its IC50 was among the highest because it did not generate large changes in activity with increasing concentration, unlike other stilbenes such as resveratrol or pinostilbene.

Table 25. Comparison of the IC50 (μM) of various stilbenes in Caco-2 cells obtained in this thesis and by other authors with different techniques and/or incubation times

	This Thesis	(Nutakul et al., 2011)	(González-Sarrías et al., 2022)	(González-Sarrías et al., 2022)	(Paul et al., 2010)
	48 h	**48 h**	**48 h**	**72 h**	**72 h**
	Neutral red	**MTT**	**MTT**	**MTT**	**[^{3}H]Thymidine**
Resveratrol	76.20 ± 10.8	65	50.4 ± 3.4	18.8 ± 1.6	24.35 ± 0.2
Oxirresveratrol	> 100	-	74.7 ± 11.5	55.4 ± 2.5	-
Piceatanol	> 95	-	55.4 ± 10.8	42.0 ± 9.8	-
Gnetol	> 100	-	-	-	-
Pinoestilbeno	62.53 ± 13.4	-	-	-	19.21 ± 2.9
Pteroestilbeno	22.65 ± 6.9	15	67.6 ± 12.3	43.0 ± 11.6	14.46 ± 1.2
Isorapontigenina	78.95 ± 10.5	-	-	-	-
Rapontigenina	67.95 ± 12.7	-	-	-	-
Trimetoxiestilbeno	27.73 ± 7.4	-	-	-	11.95 ± 2.9

These results correlate with those obtained by Paul *et al*. (2010), in which they determined the IC50 of methoxylated resveratrol analogues after 72 hours, observing the following order of activity in the colon cancer lines Caco-2 and HT-29: trimethoxystilbene ≥ pterostilbene > pinostilbene > resveratrol. In the results of this thesis, higher IC50 values were achieved, probably due to the shorter incubation time, and the differences between the IC50 of trimethoxystilbene and pterostilbene were not significant, as well as those of pinostilbene and resveratrol (Table 25). In a more recent study, González-Sarrías *et al*. (2022) analysed the IC50 of some hydroxylated and methoxylated resveratrol analogues at 48 and 72 hours, obtaining a different order

depending on the cell line. In Caco-2 this order was: resveratrol ≥ piceatannol ≥ pterostilbene ≥ oxyresveratrol, while in HT-29 it was: pterostilbene ≥ resveratrol ≥ piceatannol > oxyresveratrol. The order of activity obtained in this thesis with the Caco-2 cell line is more similar to that obtained by these authors with the HT-29 cell line. Although in our results and those obtained by Paul *et al*. (2010), pterostilbene showed greater cytotoxic activity than resveratrol, González-Sarrías *et al*. (2022) observed the opposite. It is possible that the use of different techniques to determine cell viability is the reason for this discrepancy.

5.1.3. Anti-obesity activity of hydrophobic resveratrol derivatives

The effects of hydrophobic resveratrol derivatives and resveratrol on obesity were studied in the 3T3-L1 cell line. For adipogenesis assays, treatments were applied to immature pre-adipocytes, while for lipolysis assays, they were applied to mature adipocytes.

5.1.3.1. Effect on adipogenesis and lipid accumulation

Adipogenesis is the process by which pre-adipocytes differentiate into mature adipocytes with the capacity to accumulate lipids, and is of vital importance in obesity. Since the synthesised derivatives are intended to be delivered to adipocytes, where hydrolysed stilbene has been shown to have a beneficial effect by inhibiting adipogenesis and lipogenesis (Aguirre et al., 2014; Scapagnini et al., 2014), it was also analysed whether the esterified derivatives have some activity before being hydrolysed.

After 3 days from the start of differentiation, the control cells began to change from a typical fibroblast morphology to a more spherical one, with small lipid droplets inside, which could be easily detected by their greater brightness. After 10 days, the cells

were already differentiated into mature adipocytes, exhibiting a larger and more spherical morphology that contained large lipid droplets inside (Figure 116).

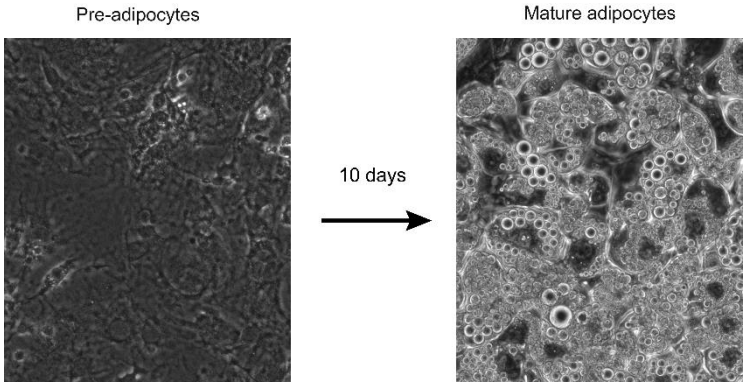

Figure 116. Morphological changes during differentiation of 3T3-L1 cells (untreated) at day 0 (pre-adipocytes) and day 10 (mature adipocytes with lipid droplets). Monochromatic images at 20x magnification and variable exposure

At the end of the assay (day 10), lipid accumulation in the cells was quantified by ORO staining followed by UV-Vis spectrophotometry (Figure 117A). The results revealed that the hydrophobic resveratrol derivatives not only no longer had the ability of resveratrol to inhibit adipogenesis, but were able to cause an increase in lipid accumulation from 50 – 100 µM, with little difference between the three derivatives tested, nor between the highest concentrations of 100 and 150 µM (Figure 117A). Meanwhile, resveratrol significantly inhibited adipogenesis from 50 µM, with most cells showing little differentiation and mild lipid accumulation under the microscope (Figure 117), in agreement with previous studies (Aguirre et al., 2014).

Since ORO staining is a destructive method and lipid droplets in 3T3-L1 cells were easily visualised by microscopy, the possibility of quantifying lipid accumulation in these cells without staining was explored. For this purpose, monochromatic images of the cells were taken in representative fields, prior to ORO staining. The exposure was fixed so that lipids from cells with a high level of adipogenesis could be visualised in white

(Figure 117B). Image processing enabled to quantify the lipids inside the cells, obtaining similar results to those obtained with ORO staining, but with more pronounced differences in the resveratrol treatments (Figure 117). This system of lipid quantification in 3T3-L1 cells without the need for staining made it possible to analyse the evolution of adipogenesis in the same well at several differentiation times (Figure 118).

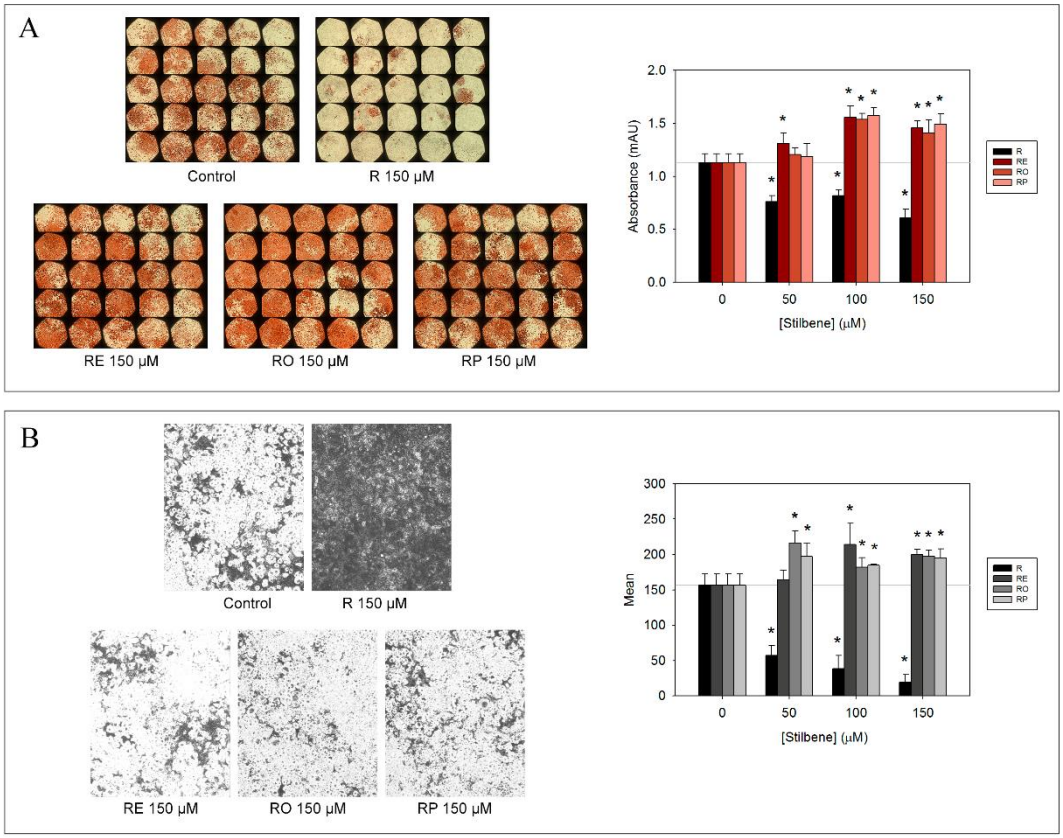

*Figure 117. Lipid quantification in 3T3-L1 cells, control (DMSO 0.5 % (v/v/v)) and treated with resveratrol and its hydrophobic derivatives, after 10 days of differentiation. A) Determination by ORO staining. Colour images of 5x5 contiguous fields at 5x magnification and exposure = 0.5. B) Determination without staining, by microscopy and image analysis. Monochrome images of 5x5 contiguous fields at 20x magnification and exposure = 2.0. * Significance p-value < 0.05*

The evolution of adipogenesis in control and treated cells proceeded at a moderate rate during the first three days after the onset of differentiation. However, it accelerated markedly from day three, and decelerated from day seven onwards, in a variable manner depending on the treatment (Figure 118). The different concentrations of resveratrol used

significantly inhibited adipogenesis from day 3, resulting in a lipid accumulation that was 3 to 8 times lower than that of the control at day 10. Meanwhile, the hydrophobic resveratrol derivatives were able to increase or maintain a lipid level similar to the control, depending on the concentration used (Figure 118). In general, the lower concentration of 50 µM hydrophobic derivatives had almost no effect on lipid accumulation on the different days, with the exception of resveratrol oleate and palmitate at day 10. In cells treated with resveratrol or resveratrol stearate, the highest lipid accumulation values were reached at day 10, regardless of concentration. However, in cells treated with 100 – 150 µM resveratrol oleate or 100 µM resveratrol palmitate there was no significant difference in lipid accumulation between days 7 and 10 (Figure 118).

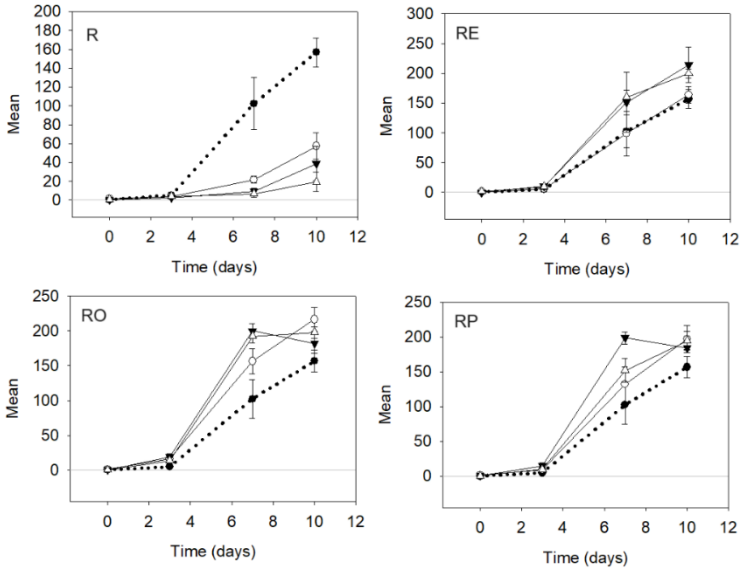

Figure 118. Evolution of lipid accumulation in 3T3-L1 cells during adipogenesis after administration of (●, dotted line) 0 µM (DMSO 0.5 % (v/v)), (○) 50 µM, (▼) 100 µM and (△) 150 µM resveratrol or its hydrophobic derivatives, determined by microscopy and image analysis

Overall, these results show that esterification of resveratrol with fatty acids negatively affects its ability to inhibit adipogenesis, being able to activate this process depending on the concentration and type of derivative used. It is possible that the incubation time selected for the treatment of pre-adipocytes was not long enough for the

hydrolysis of hydrophobic stilbene derivatives, and since these derivatives have a lipid structure, they could activate pathways that promote adipogenesis and lipogenesis just like the fatty acids used in the derivatization (Malodobra-Mazur et al., 2019; Yanting et al., 2018).

5.1.3.2. Gene expression during adipogenesis

Apart from studying lipid accumulation in 3T3-L1 cells during adipogenesis, it was investigated the expression of obesity-related genes, to find out which processes might be involved in the results observed when cells were treated with hydrophobic resveratrol derivatives. The following target genes were studied (Table 26):

Table 26. Obesity-related target genes in 3T3-L1 cells

Gene	Encoded protein	Metabolic process
fasn	Fatty acid synthase	Lipogenesis
slc2a4	GLUT4	Glucose transport control
mfn2	Mitofusin 2	Mitochondrial fusion
adipoq	Adiponectin	Lipid metabolism and insulin sensitivity
sirt3	Sirtuin 3	Energy homeostasis
ucp1	Thermogenin	Thermogenesis
lep	Leptin	Appetite regulation

Control cells showed a large increase in *adipoq*, *lep* and *slc2a4* gene expression, a moderate increase in *ucp1*, *fasn* and *sirt3* genes, and a very slight increase in *mfn2*, during adipogenesis, especially from day 3 onwards (Figure 119). In general, the highest level of expression was reached on day 10 after cell differentiation started. However, the *mfn2* and *fasn* genes gave the highest level of expression on day 7, showing little difference with the level observed on day 10 (Figure 119).

Cells treated with resveratrol showed underexpression of all the genes studied with respect to the control. The *fasn*, *mfn2*, *sirt3* and *ucp1* genes in these cells showed expression levels similar to or even lower than those observed on day 0, i.e. when all the cells were in the pre-adipocyte state (Figure 119). As resveratrol-treated cells have less

differentiation and less lipid accumulation, it is reasonable that they maintain similar expression levels to those observed at day 0, giving less variation in genes that promote adipogenesis and are overexpressed in the control. For example, underexpression of *fasn*, which encodes the enzyme fatty acid synthase involved in the synthesis of fatty acids that form part of the triacylglycerides that accumulate in adipose tissue, could explain the lower lipid accumulation in 3T3-L1 cells treated with resveratrol. Other authors also observed lower levels of *fasn* expression in these cells in the presence of resveratrol (Aguirre et al., 2014).

On the other hand, cells treated with the hydrophobic resveratrol derivatives showed, in general, higher or similar expression levels of the analysed genes than the control on the different days after the initiation of cell differentiation (Figure 119).

The three derivatives gave a clear overexpression of *slc2a4* compared to the control from day 3 (Figure 119). The *slc2a4* gene encodes the membrane protein GLUT4 or glucose transporter type 4, which facilitates glucose transport in an insulin-dependent manner (Govers, 2014). In type 2 diabetes there is reduced expression of this gene and its protein in adipocytes (Maianu et al., 2001), and it has been shown that reduced GLUT4 in adipocytes can indirectly lead to insulin resistance in muscle and liver (Abel et al., 2001; Yang et al., 2005). Therefore, the increase in *slc2a4* expression caused by hydrophobic resveratrol derivatives could be of interest in obesity and hyperglycaemia in type 2 diabetes, because it could prompt glucose uptake from the bloodstream by improving insulin sensitivity.

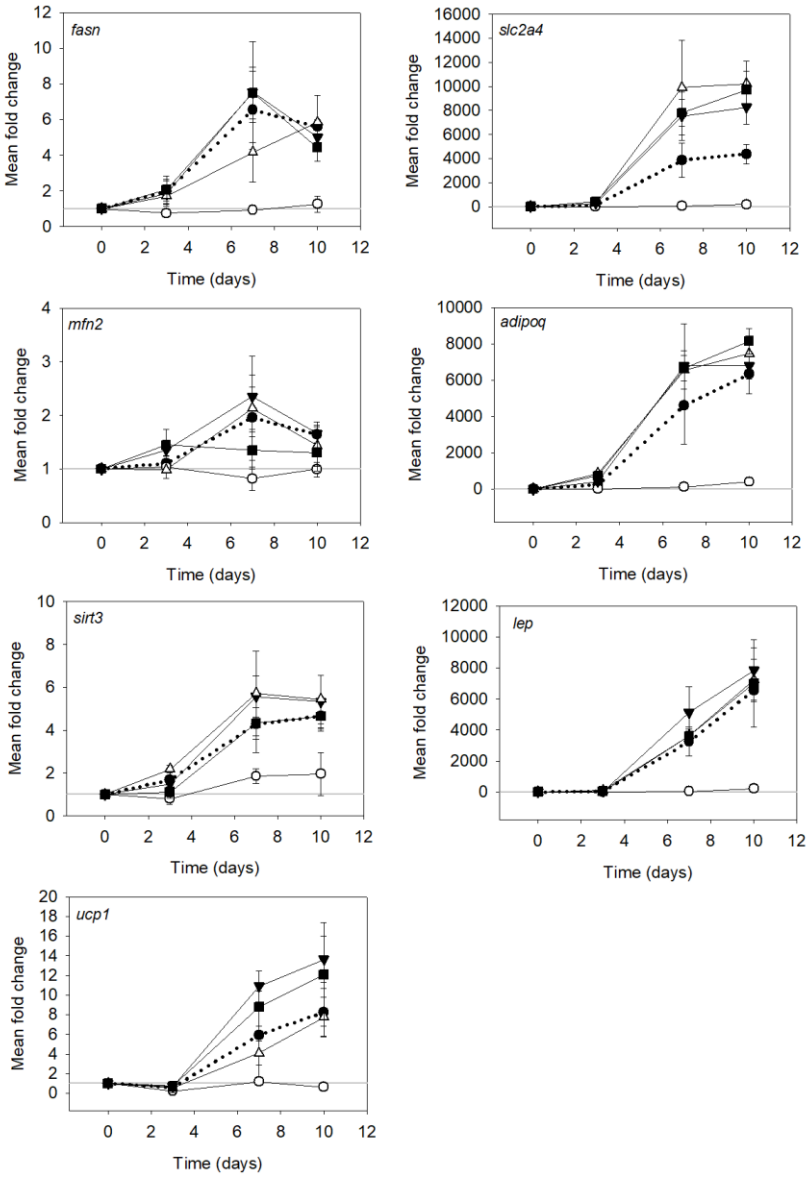

Figure 119. Normalised mRNA levels of obesity-related genes during adipogenesis in 3T3-L1 cells, control (dotted line, ●) (DMSO 0.5 % (v/v/v)), and treated (solid lines) with 150 µM of (○) resveratrol, (▼) resveratrol stearate, (△) resveratrol oleate or (■) resveratrol palmitate, determination by the $2^{-\Delta\Delta Ct}$ comparative quantification method

In cells treated with resveratrol stearate, overexpression of other genes such as *ucp1* on days 7 and 10 of differentiation and *lep* on day 7 was also observed, while resveratrol oleate and resveratrol palmitate kept levels of these genes close to control, with no significant differences (Figure 119). The *ucp1* gene encodes the uncoupling protein 1 or thermogenin, which is responsible for dissipating the proton gradient of the mitochondrial membrane to produce heat instead of synthesising ATP (Chouchani et al.,

2019). Thus, if increased expression also occurs at the post-transcriptional level, resveratrol stearate could help release stored energy in adipocytes as heat, which is relevant to obesity. Furthermore, the *lep* gene, also known as *ob* gene, produces the hormone leptin, which is responsible for regulating appetite. In mice, a homozygous recessive mutation of this gene has been shown to cause animals to be able to ingest much more food than normal mice, making them more prone to obesity (Friedman, 2014). Under normal conditions, leptin is released as a negative feedback signal to the hypothalamus to inhibit appetite when levels of stored fat in adipocytes increase, as well as triggering other processes such as increase in energy expenditure, reduction of lipogenesis and increase in lipolysis in adipose tissue (Münzberg and Morrison, 2015). Therefore, overexpression of *lep* following resveratrol stearate treatment could lead to activation of these relevant processes in obesity control.

The expression levels of *fasn*, *mfn2* and *sirt3* from day 3 in cells treated with the hydrophobic resveratrol derivatives showed no significant differences from the control (Figure 119). However, within derivatives, it highlights the lower expression of *fasn* at day 7 in cells treated with resveratrol oleate compared to cells treated with resveratrol stearate or palmitate, as well as the lower expression of *mfn2* in cells treated with resveratrol palmitate compared to those treated with resveratrol stearate (Figure 119). As described above, the *fasn* gene encodes fatty acid synthase which is involved in lipogenesis, so its lower expression would help to slow down this process, something sought in obesity control (Berndt et al., 2007). Since hydrophobic resveratrol derivatives showed similar or higher lipid accumulation than the control, it would be expected that *fasn* expression levels would be similar or slightly higher than the control. The *mfn2* gene encodes the protein mitofusin 2, a GTPase involved in the control of mitochondrial fusion (Chandhok et al., 2018) and other processes, because a specific deletion of *mfn2* in

adipose tissue has been shown to lead to problems in thermogenesis, lipid mobilisation and β-oxidation of fatty acids (Scheideler and Herzig, 2017). On the other hand, the *sirt3* gene encodes the protein sirtuin 3, an NAD^+-dependent deacetylase found in mitochondria that maintains cellular energy homeostasis by deacetylating a number of proteins that activate catabolic processes and inhibit anabolic processes. Alterations in the pathways controlled by sirtiun 3 lead to various metabolic disorders (Nogueiras et al., 2012). Therefore, the maintenance of expression levels without significant variations after the treatment with hydrophobic resveratrol derivatives could indicate a correct function of these pathways and, therefore, of energy homeostasis.

When the pre-adipocytes had only been differentiated for 3 days, treatment with the derivatives caused a slight overexpression of *adipoq* compared to the control. However, from that day onwards, as the adipocytes became more mature, these differences in expression were no longer significant (Figure 119). The *adipoq* gene encodes the adipose tissue hormone adiponectin, which regulates several processes of lipid metabolism, including improving insulin sensitivity, increasing β-oxidation in skeletal muscle and suppressing lipid accumulation in the liver. In fact, mice with genetically or diet-induced obesity exhibited low levels of *adipoq* (Wang and Scherer, 2016). Therefore, hydrophobic derivatives could generate some improvement in these metabolic processes at day 3 of differentiation because of the slight overexpression of *adipoq*.

5.1.3.3. Effect on lipolysis in mature adipocytes

Lipolysis is another process of special interest in obesity because triacylglycerides accumulated in mature adipose tissue are hydrolysed. Previous studies (Lasa et al., 2012) have shown that resveratrol was able to activate lipolysis via the adipose triglyceride lipase (ATGL), so the effect of hydrophobic derivatives of resveratrol was also

investigated. These studies were carried out in the presence and absence of CL316,243, a β3-adrenergic agonist that induces lipolysis (Morton et al., 2016).

After 24 hours of incubation with mature adipocytes, the results showed that only resveratrol, in the absence or presence of 1 nM CL316.243, was able to activate lipolysis by increasing the concentration of glycerol released into the medium by 52 % and 27 %, respectively (Figure 120). None of the resveratrol derivatives evaluated showed significant differences with respect to the control, nor were significant differences with any of the treatments when using 10 nM CL316,243 (Figure 120). Therefore, structural modification of resveratrol with fatty acids seems to affect its ability to induce lipolysis in mature 3T3-L1 adipocytes.

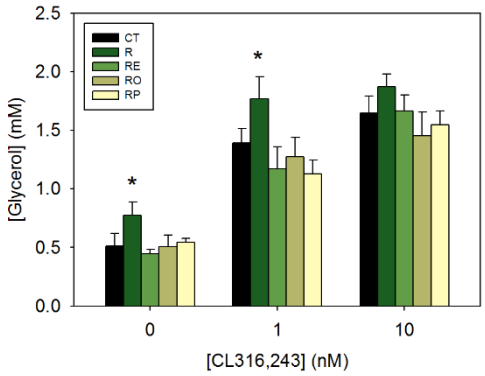

*Figure 120. Lipolysis in mature 3T3-L1 adipocytes after administration of 150 µM resveratrol and its hydrophobic derivatives in the presence and absence of CL316,243, for 24 hours. (CT) Control with DMSO 0.5 % (v/v) * Significance p-value < 0.05*

5.2. *In vivo* biological activity

5.2.1. *C. elegans* animal model

C. elegans is a small nematode widely used to study the effects of bioactive compounds on aging and different diseases or alterations, due to its versatility and high homology of genes involved in human diseases (Ha et al., 2022). In this PhD thesis, this

animal model has been tested with hydrophobic stilbene derivatives and their original stilbenes, in the presence of HBCD-Pols, as previous studies had shown that this type of CD-polymers were safe for nematodes, unlike HP-β-CD (Matencio et al., 2020c). The effect of these compounds on lifespan and lipid accumulation in the wild-type N2 strain, and the effect on oxidative stress in the transgenic strain TJ375 (*hsp-16.2p*::GFP) were investigated.

5.2.1.1. Survival assays

Survival assays in the *C. elegans* animal model provide information on whether a compound can cause toxicity after administration or whether, on the contrary, it is capable of extending the lifespan of individuals. The effect of hydrophobic derivatives of resveratrol and oxyresveratrol, as well as the original stilbenes, was evaluated in the presence of HBCD-Pols, using a Lifespan Machine that automatically monitors each nematode throughout its life.

The results showed that neither the complexes with the hydrophobic derivatives, nor the complexes with the original stilbenes, had any negative effect on the lifespan of the nematodes (Figure 121A – B), with the treatments and the controls giving very close survival rates of 12 – 12.7 days (Figure 121C).

These results suggested that the administration of the hydrophobic stilbene derivatives complexed into HBCD-Pols, at the tested doses, may not cause toxicity in individuals, as well as their original stilbenes. In a previous study (Chen et al., 2013), similar results were also obtained using free resveratrol concentrations of 50 – 200 μM. Furthermore, these authors observed that, although resveratrol was not able to prolong the half-life of nematodes under normal conditions, under stressful conditions by the presence of juglone or high glucose concentration, there was an increase in the lifespan

of *C. elegans* of up to 53.1 % (50 µM) and up to 16 % (200 µM), respectively. In a later study (Lee et al., 2016) that used higher concentrations of free resveratrol and free oxyresveratrol (100 – 1000 µM), it was observed that both stilbenes were able to increase the lifespan of *C. elegans* due to the overexpression of SIR-2.1.

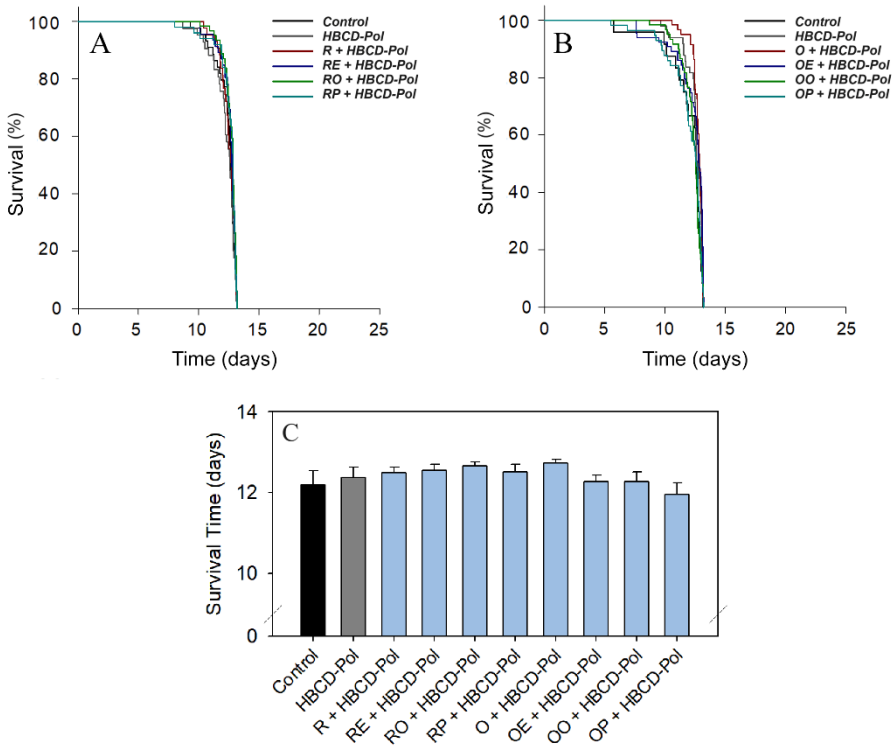

Figure 121. Survival curves of C. elegans N2 treated with 50 µM hydrophobic derivatives of A) resveratrol and B) oxyresveratrol, or their original stilbenes, and 200 ppm HBCD-Pols. C) Average lifespan of C. elegans N2 with the same treatments (90 ≤ n ≤ 130)

5.2.1.2. Oxidative stress assays

The effect of hydrophobic stilbene derivatives on oxidative stress was evaluated in *C. elegans* TJ375. This strain has the *hsp-16.2* gene coupled to GFP, such that under oxidative stress the pharynx of the worms emits fluorescence and any treatment that reduces this stress will result in a reduction of fluorescence.

After subjecting nematodes treated with hydrophobic resveratrol derivatives or resveratrol, in the presence of HBCD-Pols, to oxidative stress by naphthoquinone juglone,

a similar level of fluorescent emission could be observed in all treatments, with no significant differences compared to controls (Figure 122).

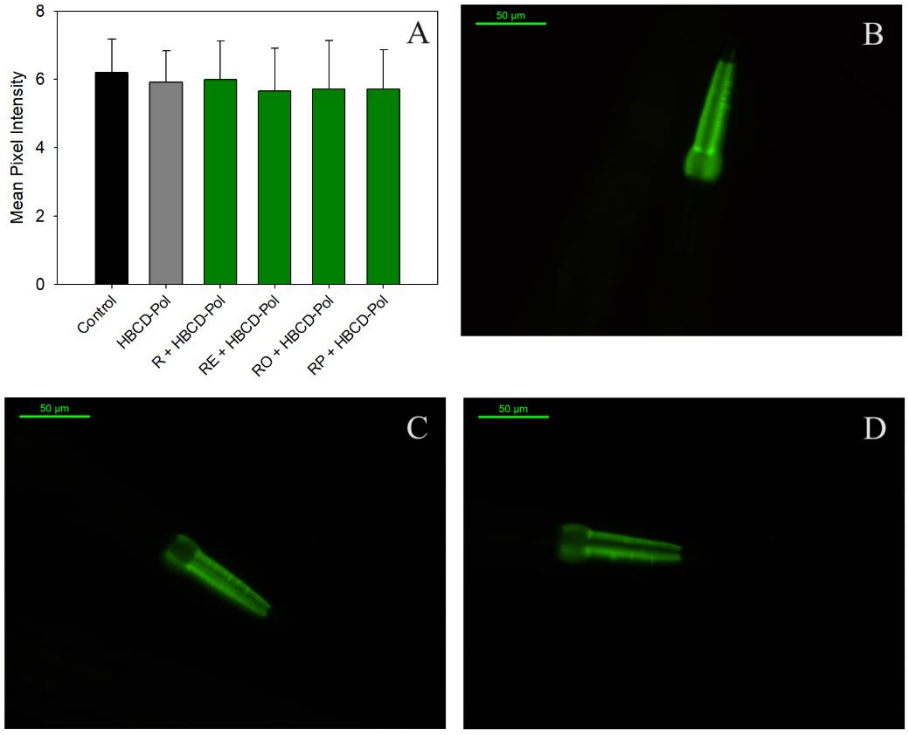

Figure 122. A) Expression of hsp-16.2-GFP in C. elegans TJ375 treated with 50 µM hydrophobic resveratrol derivatives or resveratrol, and 200 ppm HBCD-Pols, subjected to oxidative stress by 20 µM naphthoquinone juglone ($30 \leq n \leq 40$). B) C. elegans control with 0.33 % (v/v) DMSO. C) C. elegans treated with resveratrol + HBCD-Pol. D) C. elegans treated with resveratrol stearate + HBCD-Pol. Magnification 40x

Therefore, the use of hydrophobic resveratrol derivatives or resveratrol at a concentration of 50 µM, together with 200 ppm HBCD-Pol, seems to have no protective effect against oxidative stress in *C. elegans* under the conditions tested. However, previous studies using the same TJ375 strain, but administering resveratrol in the absence of HBCD-Pols, showed an antioxidant effect with resveratrol concentrations of 50 – 200 µM (Chen et al., 2013). This suggests that the interaction of stilbenes with HBCD-Pols may be preventing stilbenes from freely exerting their antioxidant capacity against oxidative stress generated by naphthoquinone juglone treatment.

5.2.1.3. Lipid accumulation assays

Finally, the wild-type strain N2 was selected to analyse lipid accumulation by ORO staining after treatment of the nematodes with the hydrophobic derivatives of resveratrol and oxyresveratrol, as well as resveratrol and oxyresveratrol, in the presence of the HBCD-Pols.

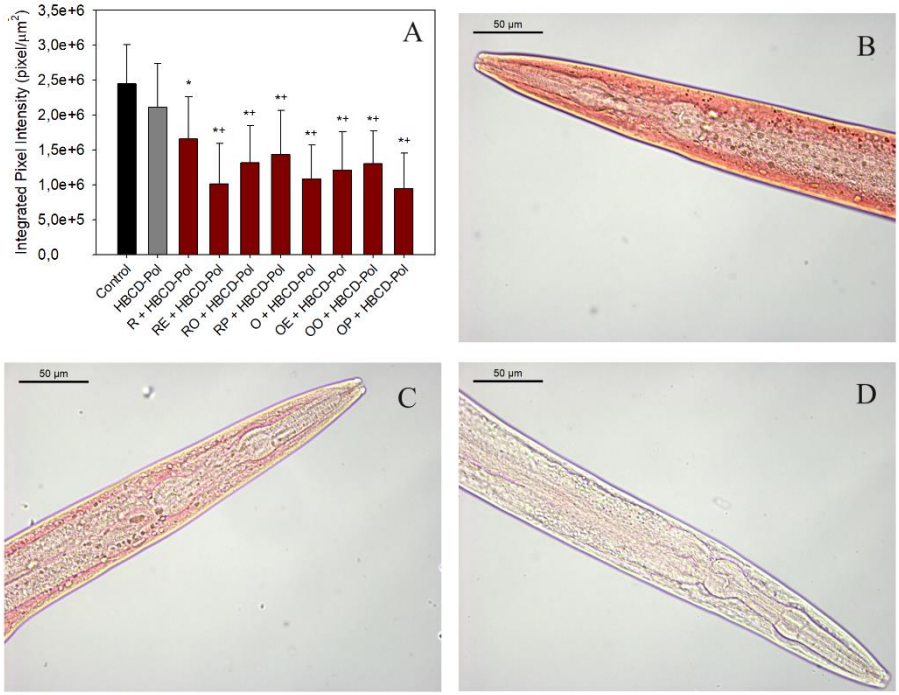

Figure 123. A) Quantification of lipids by ORO staining in C. elegans N2 treated with 50 µM of hydrophobic stilbene derivatives or their original stilbenes, and 200 ppm of HBCD-Pols ($30 \leq n \leq 40$). B) C. elegans control with 0.33 % (v/v) DMSO. C) C. elegans treated with resveratrol + HBCD-Pol. D) C. elegans treated with resveratrol stearate + HBCD-Pol. Magnification 40x. Significance p-value < 0.05 compared to control (*) with DMSO 0.33 % (v/v) or ($^+$) with HBCD-Pol

After ORO staining of the nematodes, a decrease in lipid accumulation could be observed with all treatments, with no significant differences between the two controls (DMSO and HBCD-Pols) (Figure 123). Within treatments, the resveratrol complex showed the highest amount of lipids in the nematodes despite a 32 % decrease compared to the control. Moreover, these were the only results that were not significant compared to the HBCD-Pol control (Figure 123). By contrast, complexes with hydrophobic

resveratrol derivatives decreased lipid accumulation by 41 – 59 %, with resveratrol stearate showing significant differences compared to resveratrol. Meanwhile, oxyresveratrol treatment decreased lipid accumulation in *C. elegans* by 56 %, which was similar to the 47 – 61 % obtained with hydrophobic oxyresveratrol derivatives (Figure 123).

Previous studies by other authors, that tested free resveratrol in the same *C. elegans* strain, observed no significant differences in lipid accumulation with a concentration of 50 μM. However, the addition of twice the concentration or higher significantly decreased triacylglycerides, quantified by Nile red staining or a commercial kit (Aranaz et al., 2020; Shen et al., 2017; Yue et al., 2019). This may suggest that the presence of HBCD-Pols promotes the inhibition of lipid accumulation in *C. elegans* by the stilbenes tested.

Although *in vitro* cultures of 3T3-L1 pre-adipocytes showed that resveratrol alone was able to decrease lipid accumulation in the cells, while its hydrophobic derivatives showed similar or slightly higher levels than the control, the results obtained *in vivo* in the *C. elegans* animal model reveal that the hydrophobic derivatives are able to decrease lipid accumulation in whole organisms, even more than the original stilbenes in the case of resveratrol stearate. Since pharmacokinetic assays in mice showed that resveratrol stearate, despite undergoing some degree of hydrolysis, improved the seum lipid profile more than resveratrol, and gene expression analysis in 3T3-L1 cells also revealed overexpression of some genes involved in lipid and glucose transport, it is possible that the beneficial effects of hydrophobic stilbene derivatives on obesity are due to their interaction with lipid transport into adipocytes, rather than their intrinsic activity in adipose tissue prior to hydrolysis, which may explain the differences between *in cellulo* and *in vivo* assays.

5.2.2. *M. musculus* animal model for melanoma

Following *in vivo* experiments in *C. elegans*, trials were performed in C57BL6/J mice induced with B16-F10 melanoma to study the effect of intratumoral administration of 50 mg/kg resveratrol stearate, free or encapsulated in HP-β-CD (1:5), compared to its parent stilbene, resveratrol, at the same dose. After treatment of the individuals, anti-cancer activity was assessed by monitoring tumour size and weight, determination of tumour microvessel density (TMD), histopathological examination of tumours and other tissues, and analysis of biological markers in blood.

5.2.2.1. Inhibition of tumour growth

From day 16 after melanoma induction in mice, an increase in tumour size could be observed, which varied according to treatment (Figure 124A). PBS (Control) or HP-β-CD (CD) control tumours reached the largest size, quadrupling tumour volume by day 22, with almost no difference between them.

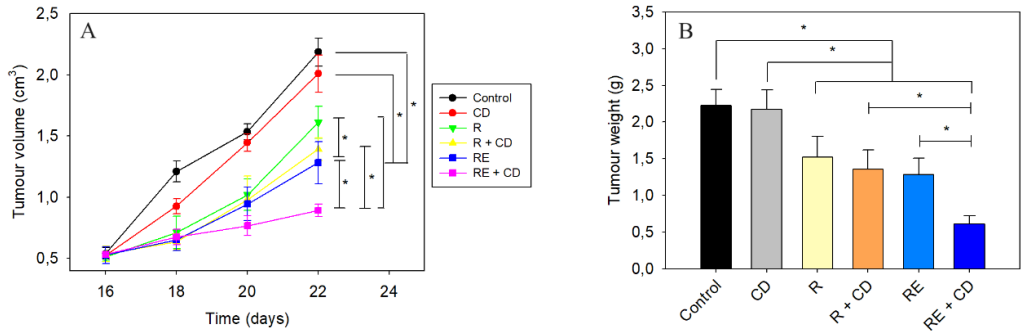

*Figure 124. A) Evolution of tumour size after induction (day 0) and B) final tumour weight of C57BL6/J mice with B16-F10 melanoma treated intratumorally with 50 mg/kg resveratrol (R) or resveratrol stearate (RE), in free form or encapsulated in HP-β-CD 1:5 (+ CD) (n=6) * Significance p-value < 0.05*

In contrast, stilbene treatments resulted in less variation in tumour size. For example, resveratrol stearate, free or encapsulated, gave a 41 – 59 % smaller tumour volume than the control at day 22, while resveratrol, free or encapsulated, gave a 26 – 36

% smaller tumour volume (Figure 124A). In addition, this reduction in tumour size was also reflected in a reduction in tumour weight of up to 42 – 72 % with resveratrol stearate, free or encapsulated, and 32 – 39 % with resveratrol, free or encapsulated (Figure 124B). Overall, intratumoral administration of resveratrol stearate with HP-β-CD was the most effective treatment for delaying melanoma growth in mice (Figure 124). The results obtained with free resveratrol correlate with previous studies by other authors with the same B16-F10 tumour cells (Davoodvandi et al., 2020).

5.2.2.2. Angiogenesis in tumours

Next, TMD was determined by immunohistochemical staining of the CD31 antibody (Moussa et al., 2009), in order to assess blood vessel formation in tumours after treatment with resveratrol stearate or resveratrol, free or encapsulated in HP-β-CD. Previous studies have linked resveratrol's anticancer activity to its ability to inhibit angiogenesis (Davoodvandi et al., 2020).

Immunohistochemical staining images of tumour sections showed clear differences in CD31 expression between treatments, that resulted in different percentages of TMD (Figure 125). While free resveratrol reduced this value by 25 % compared to the control, and encapsulated in HP-β-CD by up to 43 %, resveratrol stearate achieved greater inhibition of angiogenesis giving a 52 % and 75 % lower TMD than the control, in free and encapsulated form, respectively (Figure 125). The differences between the control with PBS (Control) and HP-β-CD (CD) were not significant. The reduced blood vessel formation in tumours treated with resveratrol stearate, especially in its complexed form, correlates with the smaller size and weight of the tumours observed above. Furthermore, the results obtained with free resveratrol correlate with previous findings of other authors (Davoodvandi et al., 2020).

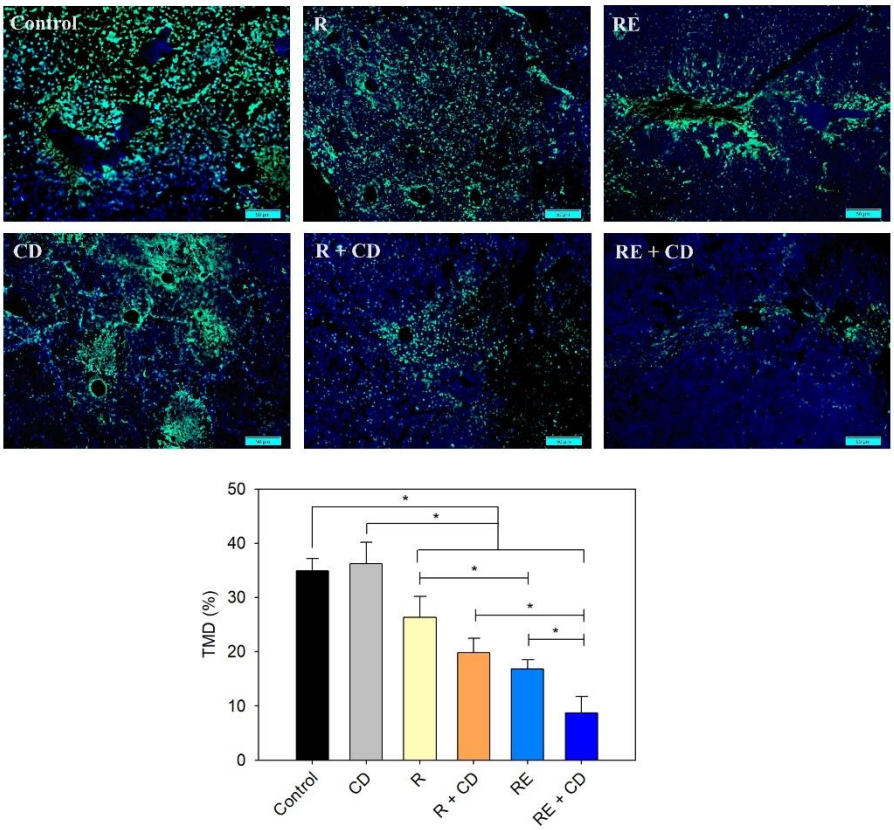

*Figure 125. Immunohistochemical staining of CD31 antibody in tumour tissue sections (top) and quantification of tumour microvessel density (TMD) (bottom) in C57BL6/J mice with B16-F10 melanoma treated intratumorally with 50 mg/kg resveratrol (R) or resveratrol stearate (RE), in free form or encapsulated in HP-β-CD 1:5 (+ CD). (n=6) * Significance p-value < 0.05*

5.2.2.3. Histopathological examination

After sacrifice of the animals treated with the stilbenes, free and encapsulated, a histopathological study of the tumours and adjacent tissues was performed to determine the degree of necrosis, mitosis and angiogenesis, as well as a histopathological study of the liver and kidneys to evaluate possible damage to these tissues.

5.2.2.3.1. Histopathological examination of tumours

Images of representative haematoxylin-eosin stained sections of tumour tissues recovered from control mice showed that the melanomas were expanded aggressively accompanied by a rich blood supply (hypervascularisation) inside, being surrounded by capillaries and larger blood vessels (Figure 126 Control). In this group, anaplastic cells

with pale nucleus and prominent round nucleoli were prominent. The cells often formed a tumour nest with an active growth centre marked by a good blood supply, organised cords of cancer cells, invading vessels and dermis or muscle. In addition, numerous mitotic cells and haemorrhages could be observed (Table 27). Tumour sections from mice that received HP-β-CD showed a similar tumour growth pattern to the control, with no improvement in melanoma features (Figure 126 CD).

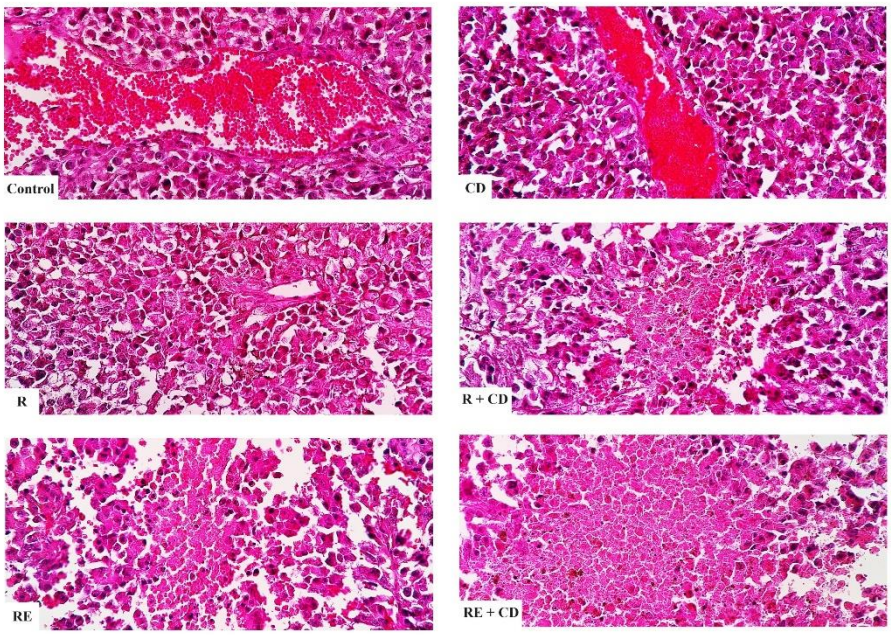

Figure 126. Haematoxylin-eosin staining of B16-F10 tumour sections from C57BL6/J mice treated intratumorally with 50 mg/kg resveratrol (R) or resveratrol stearate (RE), in free form or encapsulated in HP-β-CD 1:5 (+ CD) (n=6). Magnification 400x

In contrast, tumour sections from resveratrol-treated mice showed a less organised tumour structure, exhibiting aggregated nests and a solid growth pattern with detached nest construction and broken cords (Figure 126 R). The cytoplasms were enlarged and the nuclei become spindle shape. In these tumours, fewer mitotic cells could be observed compared to the control (Table 27).

*Table 27. Histopathological evaluation of B16-F10 tumours from C57BL6/J mice treated intratumorally with 50 mg/kg resveratrol (R) or resveratrol stearate (RE), in free form or encapsulated in HP-β-CD 1:5 (+ CD) (n=6). Results mean ± SEM. *, **, *** Significance p-value < 0.05, < 0.01 and < 0.001 compared to Control group, respectively. Necrosis grade I: absent to mild, grade II: moderate and grade III: severe*

	Control	**CD**	**R**	**R + CD**	**RE**	**RE + CD**
Vessel number per field	5.10 ± 0.53	4.87 ± 0.32	3.95 ± 0.26 *	2.45 ± 0.15 **	3.67 ± 0.21 **	1.29 ± 0.31 ***
Mitotic cell number per field	4.95 ± 0.25	4.67 ± 0.16	3.84 ± 0.12 *	2.36 ± 0.09 **	2.45 ± 0.11 **	1.15 ± 0.09 ***
Necrosis grade	I	I	I	II	II	III

Meanwhile, the samples of mice treated with free resveratrol stearate showed necrotic cells (Figure 126 RE), in addition to reduced mitosis and angiogenesis in tumours compared to control and resveratrol treatment (Table 27). The administration of encapsulated resveratrol produced a similar result, showing a progressive increase in necrotic cells and reduced vascular supply in melanoma sections (Figure 126 R + CD). This inhibition of tumour growth could be due to the significant increase in necrosis. Finally, treatment with encapsulated resveratrol stearate was the most effective of all, achieving a higher degree of necrosis, with significant differences compared to free resveratrol stearate and encapsulated resveratrol (Figure 126 RE + CD).

5.2.2.3.2. Histopathological examination of liver

In liver sections of control mice, severe congestion of the central vein along with disorganised sinusoids could be observed. Extensive areas of severe hepatocellular degeneration and necrosis were spotted randomly distributed throughout the parenchyma, as well as a moderate increase in inflammatory cell infiltration (Figure 127 Control). Similarly, sections from the HP-β-CD group showed similar pathological changes to the control, with severely congested central veins and moderately dilated and congested sinusoids (Figure 127 CD). In addition, extensive areas of severe hepatocellular degeneration and necrosis, as well as evidence of mild inflammatory cell infiltration, could be seen in the livers of these mice (Table 28).

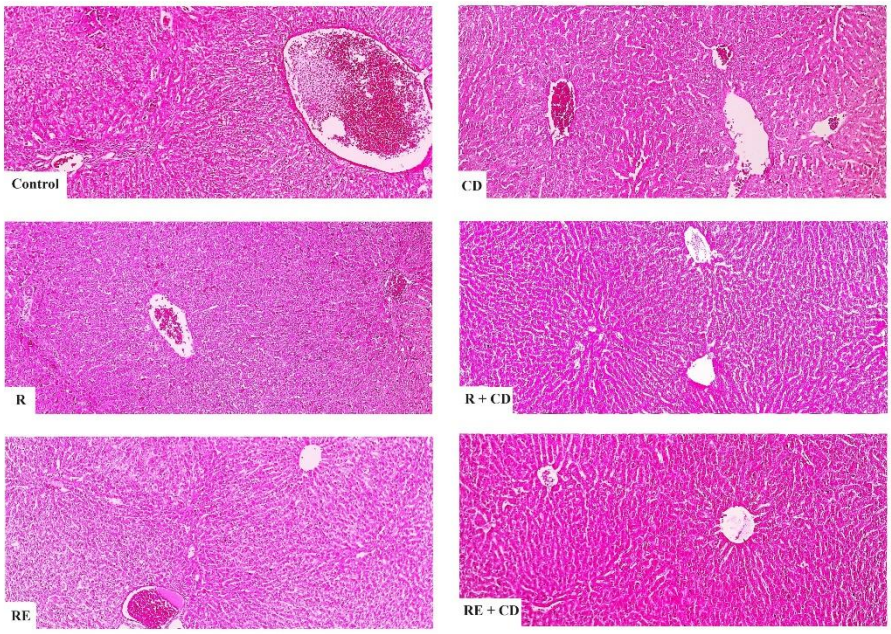

Figure 127. Haematoxylin-eosin staining of liver sections from C57BL6/J mice with B16-F10 melanoma treated intratumorally with 50 mg/kg resveratrol (R) or resveratrol stearate (RE), in free form or encapsulated in HP-β-CD 1:5 (+ CD). (n=6). Magnification 400x

In the liver tissues from animals treated with free resveratrol, moderate central vein congestion and hepatocellular degeneration was observed, along with mild infiltration of inflammatory cell and dilation of sinusoids (Figure 127 R). Meanwhile, tissues from mice treated with free resveratrol stearate showed a moderate hydropic degeneration of hepatocytes in centrilobular regions, mild congestion of central vein and sinusoidal dilatation, as well as lymphocyte infiltration (Figure 127 RE).

Table 28. Histopathological damage in livers of C57BL6/J mice with B16-F10 melanoma treated intratumorally with 50 mg/kg resveratrol (R) or resveratrol stearate (RE), in free form or encapsulated in HP-β-CD 1:5 (+ CD). (n=6). (-) absence, (+) slight, (++) mild, (+++) moderate, (++++) severe

	Control	**CD**	**R**	**R + CD**	**RE**	**RE + CD**
Vacuolar degeneration	++++	++++	+++	++	+++	+
Central vein congestion	++++	+++	+++	++	++	+
Disorganized sinusoid	++++	++++	++	++	++	+
Infiltration of lymphocyte	+++	++	++	++	++	-

The encapsulated stilbene treatments showed a significant improvement in liver histopathological examination (Table 28). The group treated with encapsulated resveratrol showed mild centrilobular degeneration, congestion of the central veins, sinusoidal dilatation and lymphocyte infiltration in the liver tissue (Figure 127 R + CD), while the group treated with encapsulated resveratrol stearate showed only a slight cytoplasmic vacuolisation, central vein congestion and sinusoidal dilatation, with no evidence of inflammatory cell infiltration in the liver of these individuals (Figure 127 RE + CD).

5.2.2.3.3. Histopathological examination of kidneys

Renal tissues from the control group of mice showed severe degeneration and necrosis of tubular epithelial cells, with severe interstitial congestion, oedema and widespread haemorrhages (Figure 128 Control). In addition, severe glomerular collapse and shrinkage, along with hyperemia and luminal hyaline casts were observed in these individuals (Table 29). In mice treated with HP-β-CD, there was no significant improvement in the pathological changes of the renal tissues, showing similar pathologic changes to the control (Figure 128 CD).

However, moderate swelling of tubular epithelial cells, oedema and interstitial congestion were observed in the renal tissues of mice treated with free resveratrol, with the formation of a mild luminal hyaline cast and glomerular hyperemia being evident (Figure 128 R). Meanwhile, treatment with free resveratrol stearate resulted in moderate degeneration of tubular epithelial cells, in addition to mild glomerular and interstitial damages (Figure 128 RE).

Finally, the administration of the encapsulated stilbenes improved the histopathological changes in the mice kidneys (Table 29). The group of mice treated with encapsulated resveratrol showed fewer tubulo-interstitial and glomerular injuries

compared to the groups treated with resveratrol alone or HP-β-CD alone (Figure 128 R + CD). Meanwhile, the group treated with encapsulated resveratrol stearate revealed slight tubular vacuolisation, glomerular hyperaemia and interstitial oedema, with no evidence of luminal hyaline casts in the renal tissues of these mice (Figure 128 RE + CD).

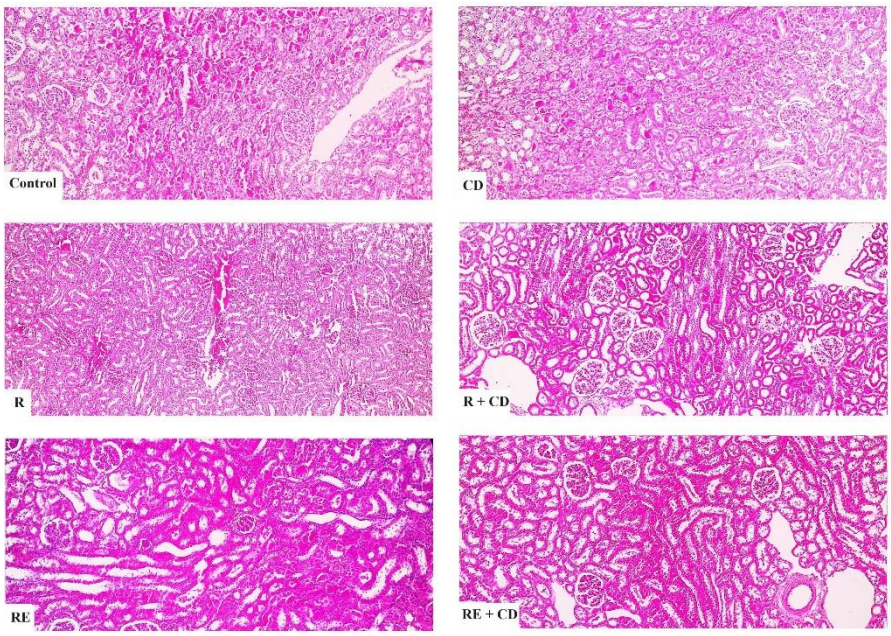

Figure 128. Haematoxylin-eosin staining of kidney sections from C57BL6/J mice with B16-F10 melanoma treated intratumorally with 50 mg/kg resveratrol (R) or resveratrol stearate (RE), in free form or encapsulated in HP-β-CD 1:5 (+ CD). (n=6). Magnification 400x

Table 29. Histopathological damage in kidneys of C57BL6/J mice with B16-F10 melanoma treated intratumorally with 50 mg/kg resveratrol (R) or resveratrol stearate (RE), in free form or encapsulated in HP-β-CD 1:5 (+ CD). (n=6). (-) absence, (+) slight, (++) mild, (+++) moderate, (++++) severe

	Control	**CD**	**R**	**R + CD**	**RE**	**RE + CD**
Tubular epithelial cells swelling	++++	++++	+++	++	+++	+
Interstitial congestion, oedema and haemorrhage	++++	++++	+++	++	++	+
Luminal hyaline cast formation	+++	++	++	+	++	-
Glomerular hyperemia	++++	+++	++	++	++	+

In none of the tissues analysed (tumours, liver and kidneys) metastasis was observed. However, molecular studies would be necessary to specifically determine whether the treatments prevent melanoma metastasis.

5.2.2.4. Serum biomarker analysis

At the end of the trial, blood samples from mice treated intratumourally with 50 mg/kg resveratrol stearate and resveratrol, free and encapsulated in HP-β-CD (1:5), were analysed quantitatively for biomarkers of liver damage, renal function, oxidative stress and inflammation, as was done in the pharmacokinetic studies on BALB/c mice described in Section 4.2.2. In addition, blood samples from healthy mice were analysed to compare the results obtained with the different treatments.

5.2.2.4.1. Hepatic-renal profile

No increase in the concentration of liver damage and kidney function markers was observed, suggesting that the treatments did not cause toxicity in the mice. In fact, the opposite was observed, with a downward trend in the levels of these biomarkers with the treatments (Figure 129). Both stilbenes, free or encapsulated, caused a significant decrease in AST and ALT markers compared to controls, with the latter enzyme also showing significant differences between the administration of the stilbenes in complexed form or free form (Figure 129). The levels of both markers in mice treated with encapsulated resveratrol stearate showed no significant differences compared to levels in healthy mice. Moreover, mice treated with free resveratrol stearate also showed no significant difference in ALT levels compared to healthy individuals. This suggests that resveratrol stearate administration ameliorates possible tumour-induced liver damage.

On the other hand, only resveratrol stearate, with or without HP-β-CD, was able to cause a significant decrease in the concentration of the renal markers BUN and CR, reaching similar values to those of mice without melanoma (Figure 129). For both renal markers, the differences between free resveratrol stearate and free resveratrol treatment were significant.

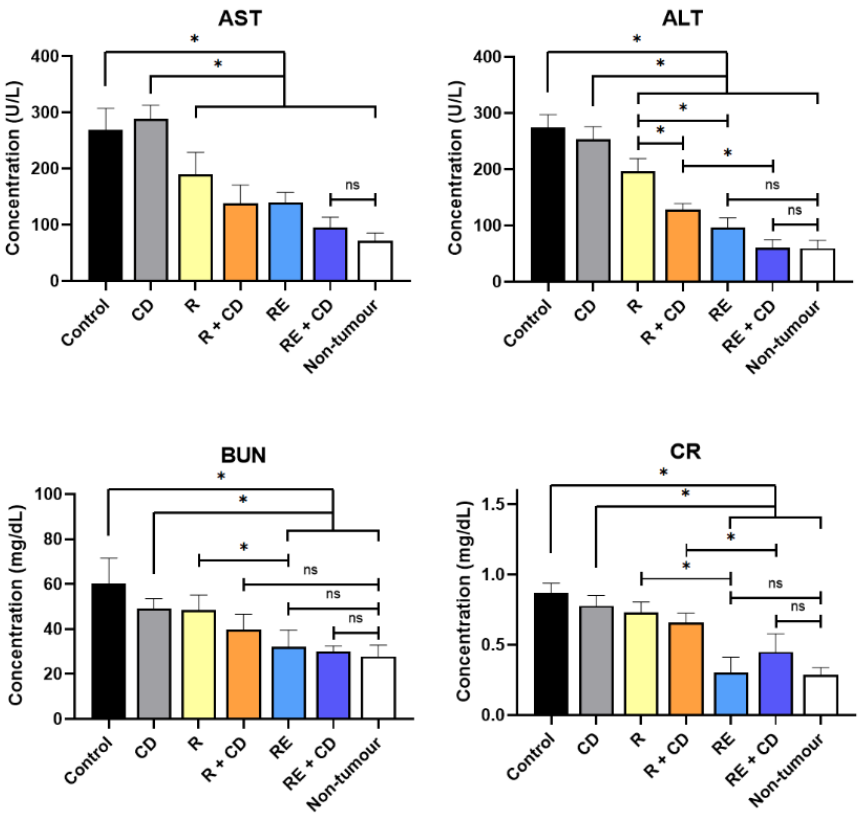

*Figure 129. Quantification of markers of liver damage and kidney function in plasma of healthy (non-tumour) and B16-F10 melanoma C57BL6/J mice after intratumoral administration of 50 mg/kg resveratrol (R) or resveratrol stearate (RE), in free form or encapsulated in HP-β-CD 1:5 (+ CD). (n=6) * Significance p-value < 0.05. (ns) Not significant*

5.2.2.4.2. Oxidative profile

Overall, all treatments used resulted in an improvement in antioxidant markers in the mice by decreasing MDA levels and increasing levels of TAS and the endogenous antioxidant enzymes SOD and GPx (Figure 130).

Encapsulated resveratrol stearate gave the best results, with significant differences compared to free resveratrol stearate in all biomarkers except MDA, and compared to encapsulated resveratrol in all biomarkers except TAS (Figure 130). The treatment with encapsulated resveratrol stearate showed higher endogenous antioxidant enzyme production and total antioxidant status than healthy individuals, as was observed in Section 4.2.2.3. after oral administration in BALB/c mice without melanoma. In addition,

MDA levels after treatment with resveratrol stearate, free or encapsulated, were reduced to a concentration similar to that of healthy mice. For this marker, an improvement was also observed with the use of free CD, giving a MDA concentration similar to that of free resveratrol stearate (Figure 130). Overall, the improvement in antioxidant biomarkers after treatment with stilbenes, especially, encapsulated resveratrol stearate, might contribute to the neutralisation of ROS and/or RNS associated with cancer promotion (Cecerska-Heryć et al., 2021).

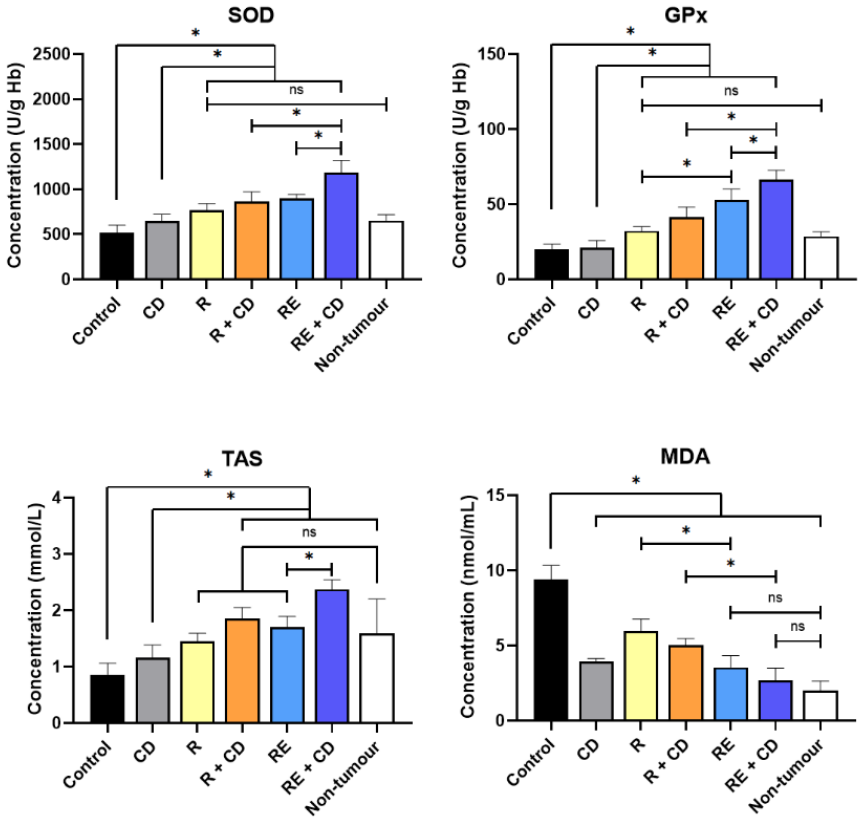

*Figure 130. Quantification of oxidative stress markers in plasma of healthy (non-tumour) and B16-F10 melanoma C57BL6/J mice after intratumoral administration of 50 mg/kg resveratrol (R) or resveratrol stearate (RE), in free form or encapsulated in HP-β-CD 1:5 (+ CD). (n=6) * Significance p-value < 0.05. (ns) Not significant*

5.2.2.4.3. Inflammatory profile

The inflammatory markers content was also modified after the treatment with the hydrophobic stilbene derivative and resveratrol, in free or complexed form. The

concentration of TNF-α, IL-6 and COX-2 decreased significantly with all treatments tested, coming close to the levels of mice without melanoma (Figure 131).

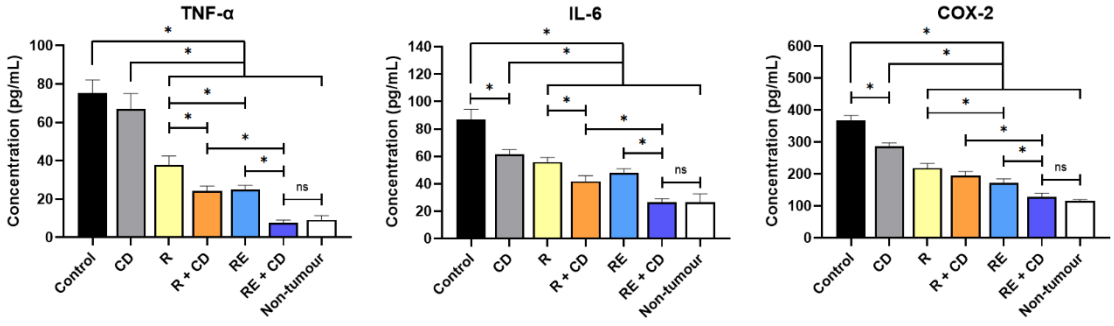

*Figure 131. Quantification of inflammation markers in plasma of healthy (non-tumour) and B16-F10 melanoma C57BL6/J mice after intratumoral administration of 50 mg/kg resveratrol (R) or resveratrol stearate (RE), in free form or encapsulated in HP-β-CD 1:5 (+ CD). (n=6) * Significance p-value < 0.05. (ns) Not significant*

In general, the administration of the encapsulated stilbenes achieved significantly lower values of these biomarkers compared to the administration in free form (Figure 131). Furthermore, encapsulated resveratrol stearate was more effective than encapsulated resveratrol, reaching inflammation levels similar to those in healthy individuals. In free form, resveratrol stearate showed significant differences from free resveratrol in the concentration of TNF-α and COX-2. In addition, the use of CD alone had a beneficial effect on IL-6 and COX-2 levels, achieving similar or slightly higher levels than resveratrol treatment (Figure 131).

Previous studies on resveratrol also showed a decrease in the levels of pro-inflammatory markers associated with an increase in antioxidant markers, justifying the therapeutic potential of resveratrol in cancer and metabolic diseases such as obesity (Koushki et al., 2018; Omraninava et al., 2021; Tung et al., 2015). The hydrophobic resveratrol derivative tested has shown a greater ability to improve these biomarkers, especially when administered with CDs, so its benefits in the prevention and control of cancer and metabolic diseases could be greater than those of resveratrol.

5.3. Conclusions on the *in vitro* and *in vivo* bioactivity of hydrophobic stilbene derivatives and natural stilbenes

The evaluation of the antioxidant capacity of hydrophobic derivatives of resveratrol, oxyresveratrol and pterostilbene by ORAC, ABTS, DPPH and FRAP methods has shown that esterification of stilbenes with fatty acids results in a decrease of their antioxidant activity *in vitro*, associated with the removal of free hydroxyl groups in the molecule. Despite slight variations between methods, oxyresveratrol oleate was the derivative with the highest capacity to neutralise free radicals and reduce ferric complexes, while pterostilbene derivatives were the least reactive, especially pterostilbene stearate. Since in Section 4.2.2.3. it was demonstrated *in vivo* that the derivatives may trigger a higher antioxidant response in whole organisms compared to the original stilbene, this lower *in vitro* reactivity against free radicals and metal complexes could indicate a higher resistance to being oxidised. Therefore, hydrophobic stilbene derivatives are suggested to better preserve the molecule in the presence of oxidising agents in aqueous formulations, which could be an advantage for the development and storage of products fortified with hydrophobic stilbene derivatives as stilbene precursors.

In addition, an alteration of the measurement of antioxidant activity by these methods was detected in the presence of CDs, with or without antioxidant. This deviation varied according to the method, as well as the concentration and type of CD, and it was not possible to obtain a reliable antioxidant activity value in most methods by subtracting the measurement without antioxidant from the measurement with antioxidant. Spectral and bioinformatic assays showed that this interference could be due to the encapsulation of the reagents involved in the redox reactions, in addition to the antioxidant itself. The encapsulation of these reagents leads to variations in absorbance or fluorescence, which

could be misinterpreted as a higher or lower antioxidant activity in the presence of CDs. Since the interaction with CDs is non-covalent and non-specific, interference cannot be discarded when using a different ratio of reagents in the method, substrates with different affinity or different incubation times.

Evaluation of the cytotoxic activity of stilbene analogues of resveratrol in the Caco-2 colorectal cancer cell line enabled structure-activity relationships to be established, identifying those stilbenes with higher activity than resveratrol. Cell viability showed a positive correlation with the number of hydroxyl groups in the stilbene molecule and a negative correlation with the number of methoxy groups. Thus, methoxylated analogues, such as pterostilbene or trimethoxystilbene, achieved greater inhibition of cell proliferation than resveratrol, in contrast to hydroxylated analogues, such as oxyresveratrol or gnetol.

Bioactivity studies *in vitro* in 3T3-L1 cells and *in vivo* in *C. elegans* showed that the derivatisation of resveratrol with fatty acids affected its activity against obesity. In cell culture, it was found that while resveratrol inhibited adipogenesis and activated lipolysis in mature adipocytes, hydrophobic derivatives had no effect on lipolysis and even caused a slight increase in lipid accumulation during cell differentiation, depending on the concentration. Despite this, some hydrophobic resveratrol derivatives showed overexpression of genes related to insulin sensitisation, fat mobilisation and thermogenesis during adipogenesis. If this transcriptional effect is also reflected at the post-transcriptional level, these results may suggest that hydrophobic stilbene derivatives could contribute to glucose uptake and lipodistribution, which may be of interest in diseases such as type 2 diabetes and obesity.

In contrast, in the *C. elegans* animal model, a significant reduction in lipid accumulation was observed after the treatment with the hydrophobic stilbene derivatives

encapsulated in HBCD-Pols, that in the case of resveratrol stearate was even more pronounced than the original stilbene. Since treatment of 3T3-L1 pre-adipocytes with resveratrol stearate showed overexpression of genes related to lipid and glucose transport and, in Section 4.2.2.1., it was observed that resveratrol stearate in mice gave better levels of serum lipid transport biomarkers than resveratrol, it is possible that the beneficial effects of hydrophobic stilbene derivatives on obesity are more related to the way they interact with lipid transport into adipocytes than to their inherent activity within adipose tissue in their non-hydrolysed form. This could explain the differences between the results obtained in cell cultures and preclinical assays in *C. elegans* and *M. musculus*. Besides, the treatment of *C. elegans* with the hydrophobic stilbene derivatives in the presence of the HBCD-Pols did not cause toxicity to the nematodes, maintaining similar survival rates to the control. Furthermore, these treatments had no effect on oxidative stress in the transgenic strain TJ375, probably due to complexation with the HBCD-Pols.

Finally, intratumoral administration of resveratrol stearate, free or encapsulated in HP-β-CD, has demonstrated activity against melanoma in C57BL6/J mice. In fact, a significant decrease in tumour growth associated with a greater inhibition of angiogenesis was observed compared to control or resveratrol-treated individuals, either free or complexed. Encapsulated resveratrol stearate treatment showed the smallest tumours with the least vascularisation, the highest degree of necrosis and the lowest number of mitotic cells, as well as the lowest level of histopathological liver and kidney damage. In addition, these mice exhibited reduced levels of serum biomarkers of inflammation and hepatic-renal damage, approaching concentrations similar to those of mice without melanoma, as well as increased levels of antioxidant markers, which were even higher than in healthy individuals.

Overall, these results show that hydrophobic stilbene derivatives could be of great interest, on their own or as stilbene precursors, for their beneficial activity against obesity and cancer, without having observed hepatic-renal damage or half-life alterations in animal models, when administered alone or together with monomeric or polymeric CDs. Furthermore, these hydrophobic stilbene derivatives could preserve their active form better than the original stilbenes, being less reactive in an aqueous matrix containing oxidising agents and capable of activating endogenous antioxidant activity in whole organisms.

6. PRACTICAL APPLICATION OF HYDROPHOBIC STILBENE DERIVATIVES FOR THE FOOD INDUSTRY

After analysing the bioactivity and absorption of hydrophobic stilbene derivatives, food models of milk and juice enriched with one of these bioactive compounds, resveratrol palmitate, were developed in order to analyse their possible application in the food industry. Soy lecithin, in the presence or absence of γ-CD, was also added to these fortified food models to support the stability of the aqueous formulation. Both compounds are authorised by the EFSA as food additives classified as E-322 and E-458, respectively. Although computational studies showed that, among the CDs currently accepted as food additives, β-CD was the best to encapsulate resveratrol palmitate (Section 3.3.1.), experimentally, it was found that the combination of γ-CD with soy lecithin was able to better solubilise resveratrol palmitate at a lower concentration of CD, something of interest in order not to excessively raise the glycaemic index of the final product. Once the fortified food models were developed, the resistance to heat treatment of the resveratrol palmitate dissolved in the different matrices was evaluated, the industrial quality parameters were monitored and the amount of resveratrol palmitate in the models stored under different light and temperature conditions was periodically quantified.

6.1. Thermostability in fortified food models

Fortified food models were subjected to 121°C for 15 minutes in order to evaluate the impact of a heat treatment on the amount of total resveratrol palmitate and the proportion of its isomers. In the milk models, at near neutral pH, resveratrol palmitate showed no significant difference after treatment, keeping the ratio of its isomers stable, regardless of the presence of CDs (Figure 132A). However, in the juice models, at acidic pH, the presence of γ-CD helped to protect the hydrophobic resveratrol derivative better

and preserve the ratio of its isomers, while its absence resulted in a 12 % decrease in total resveratrol palmitate, with its major isomer RP i2 being the most affected (Figure 132B). Despite the slight decrease in its free form, resveratrol palmitate showed good stability against the heat treatment applied, suggesting that it could effectively resist UHT sterilisation processes in milk or pasteurisation in juices.

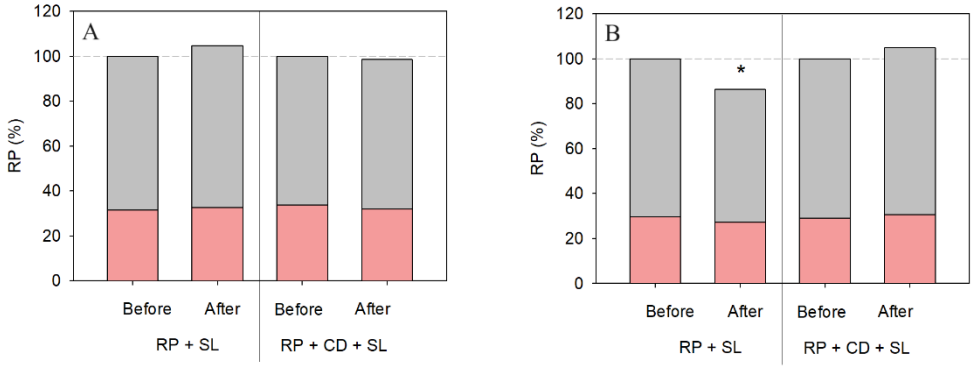

*Figure 132. Relative quantification of total resveratrol palmitate and its isomers RP i1 (pink) and RP i2 (grey), in food models of A) milk and B) juice, fortified with resveratrol palmitate (RP) and soy lecithin (SL), in the absence or presence of γ-CD (CD), before and after being heat treated at 121°C for 15 min, determined by HPLC-UV/Vis. * Significance p-value < 0.05*

6.2. Monitoring of quality parameters in fortified food models

After heat treatment, the models were stored under different light (protected or unprotected) and temperature (ambient or refrigerated) conditions, simulating commercial conditions of these foods. The weekly pH measurements showed no significant differences with respect to the measurements at the initial time, nor with the corresponding controls (Figure 133). Furthermore, no variations in the pH of the models were observed between the different storage conditions. After ten weeks, very similar values of pH to the initial ones were obtained: 6.52 – 6.63 in the milk models and 3.75 – 3.84 in the juice models (Figure 133). Therefore, fortification with resveratrol palmitate, soy lecithin and/or γ-CD, at the selected concentrations, does not seem to alter the pH of the medium, maintaining the values preestablished for these products.

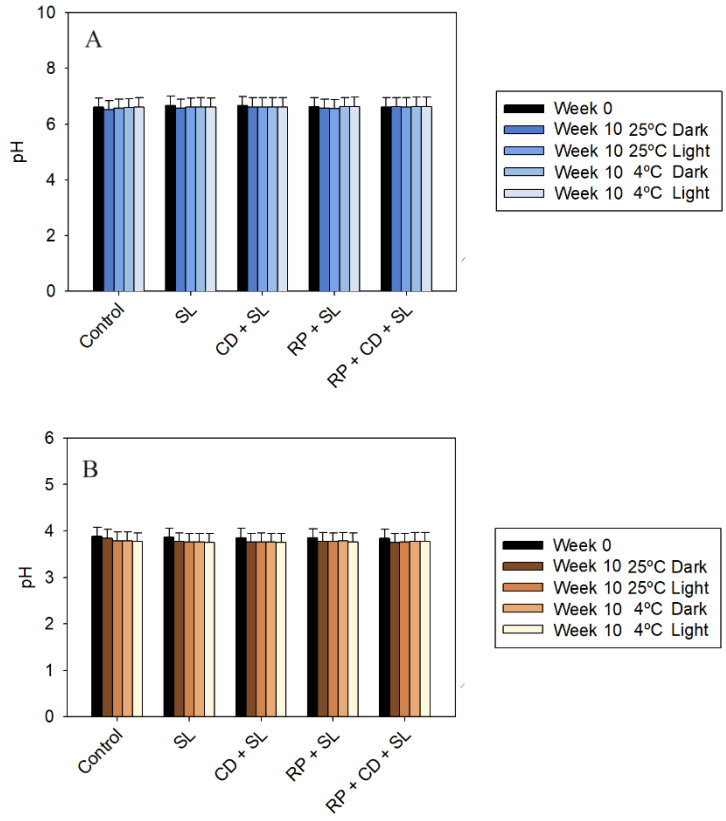

Figure 133. Evolution of pH in food models of A) milk and B) juice, fortified with resveratrol palmitate (RP) and soy lecithin (SL), in the absence or presence of γ-CD (CD), at time 0 and after 10 weeks of storage under different light and temperature conditions

Soluble solids showed slight non-significant variations between the different weeks and storage conditions, and a significant increase in those models containing γ-CD (Figure 134). In the milk models enriched with the inclusion complexes, the increase in Brix was 14 – 17 %, while in the juice models enriched with the inclusion complexes, it reached 19 – 30 % (Figure 134). Because CDs are oligosaccharides, they can cause this effect in foods, which should be considered in the adjustment of soluble solids during manufacturing to avoid increasing the glycaemic index of the final product. Previous studies with food models fortified with free or β-CD-encapsulated oxyresveratrol have also observed an increase in soluble solids after the use of CDs (Matencio et al., 2020d).

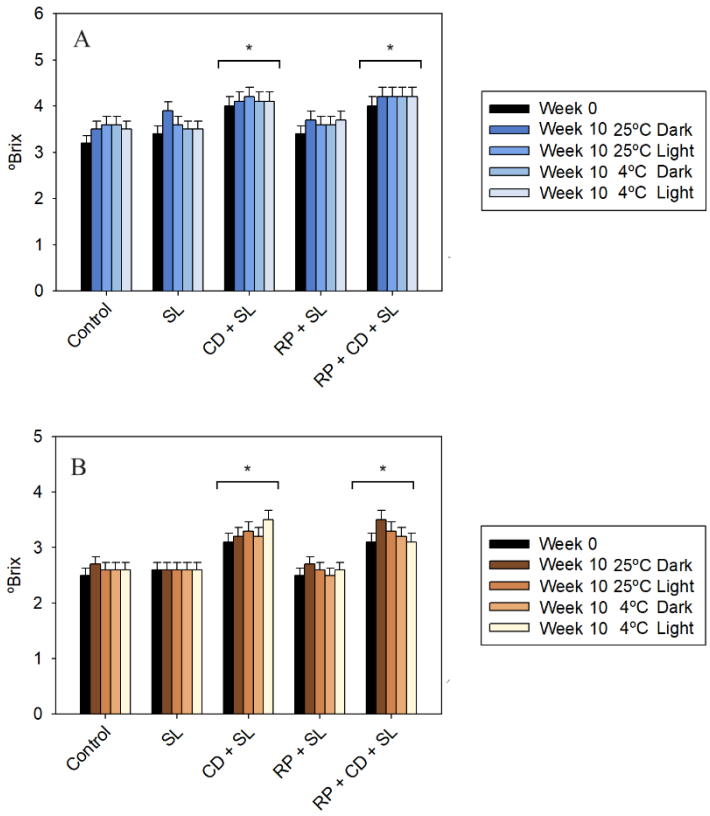

*Figure 134. Evolution of soluble solids in food models of A) milk and B) juice, fortified with resveratrol palmitate (RP) and soy lecithin (SL), in the absence or presence of γ-CD (CD), at time 0 and after 10 weeks of storage under different light and temperature conditions. * Significance p-value < 0.05*

6.3. Stability of the hydrophobic stilbene derivative in the food matrix during storage

The remaining amount of resveratrol palmitate decreased progressively over the weeks according to the storage conditions of the food model (Figure 135). Regardless of the type of food model and the presence of CDs, storage at room temperature and without light protection degraded the bioactive compound the most, maintaining less than 28 % of the initial amount in the tenth week (Figure 135). Storage under refrigeration and without light protection also showed a considerable loss of resveratrol palmitate, although less than at room temperature, maintaining 41 – 54 % of the initial amount at the end of the experiment (Figure 135). On the other hand, the storage of the food models protected

from light exposure, both at room temperature and under refrigeration, proved to be more effective in preserving the bioactive compound. This condition was able to maintain 58 – 70 % of the initial resveratrol palmitate, with little difference between storage temperatures (Figure 135).

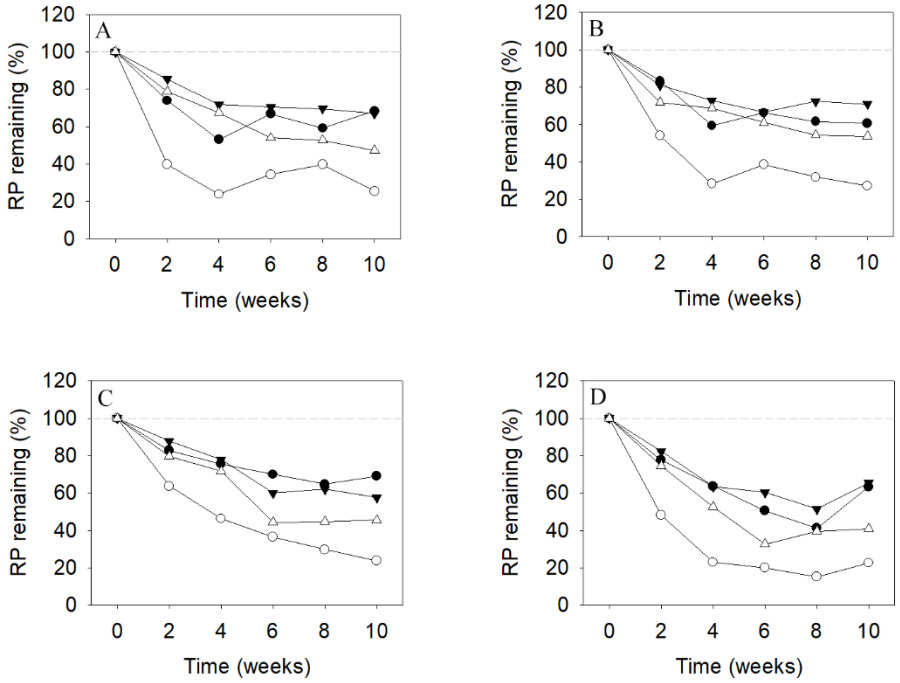

Figure 135. Relative quantification of resveratrol palmitate in food models of (A and B) milk and (C and D) juice, in (A and C) absence or (B and D) presence of γ-CD, stored at room temperature (circles) or refrigerated (triangles) in the dark (black) or unprotected from light (white), determined by UV-Vis spectrophotometry

The effect of molecular encapsulation varied according to the type of food model and storage conditions. In milk models stored at room temperature, the presence of CDs helped to prevent the rapid degradation of resveratrol palmitate during the first four weeks, while in refrigerated milk models little difference was observed (Figure 135). However, in the juice models, the presence of CDs accelerated the loss of resveratrol palmitate during the first six weeks, especially when stored at room temperature (Figure 135).

Overall, resveratrol palmitate showed greater stability in the milk food models compared to the juice models, where greater degradation over time was evident (Figure 135). This finding suggests that hydrophobic stilbene derivatives may be more suitable for the fortification of near-neutral pH foods than for acidic pH foods.

Regarding the resveratrol palmitate isomers, a fairly stable ratio was observed in most of the food models, except for those stored at room temperature without protection from light, whether milk or juice (Figure 136). In these conditions, a more selective degradation of the major isomer of resveratrol palmitate (RP i2) compared to the minor isomer (RP i1) was observed, resulting in a significant variation in the ratio of its isomers. Specifically, it went from 32:68 (RP i1 : RP i2) to almost 50:50 in the milk models, and 58:42 and 46:54 in the juice models without and with CD, respectively (Figure 136).

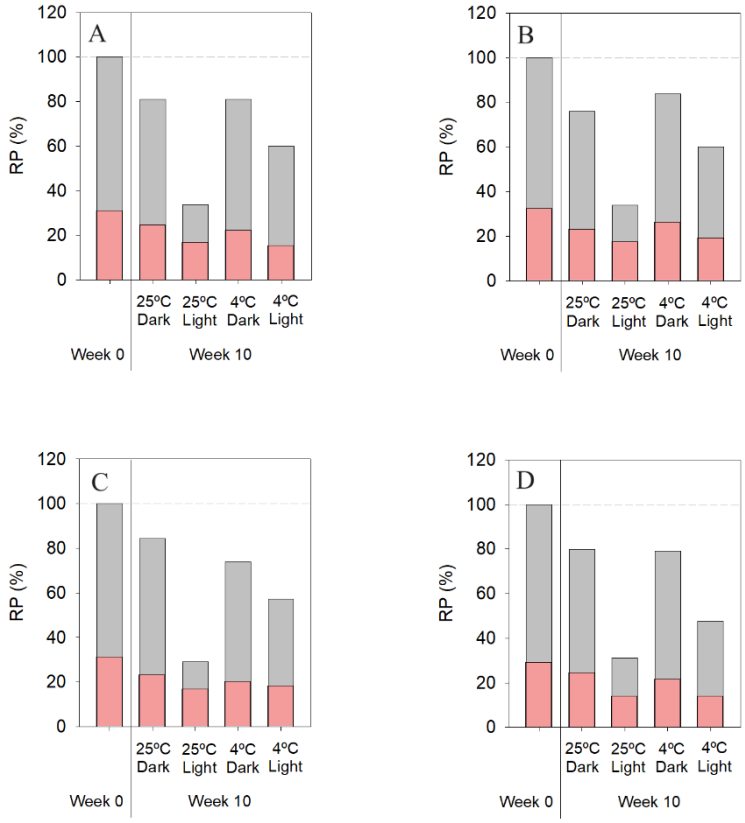

Figure 136. Variation in the ratio of resveratrol palmitate isomers, RP i1 (pink) and RP i2 (grey), in food models of (A and B) milk and (C and D) juice, fortified in (A and C) absence or (B and D) presence of γ-CD, at time 0 and after 10 weeks of storage under different light and temperature conditions, determined by HPLC-UV/Vis

These results suggest that light protection is a crucial factor in the preservation of the hydrophobic stilbene derivative in the food matrix, even more than temperature or the use of encapsulating agents. Therefore, it would be advisable to use opaque packaging for the storage of functional foods enriched in hydrophobic derivatives of stilbenes.

Furthermore, it appears that the major isomer of resveratrol palmitate is the most susceptible to degradation by exposure to light. These findings, together with those previously obtained in pancreatic lipase assays on resveratrol stearate (Section 4.1.1.), may indicate that the majority isomer of the hydrophobic resveratrol derivatives (i2) is, in general, more prone to degradation than the minority isomer (i1).

6.4. Conclusions on the use of hydrophobic derivatives of stilbenes as bioactive ingredients in functional foods

The development of food models fortified with one of the hydrophobic stilbene derivatives has provided valuable information on the optimal food types, additives and storage conditions for the manufacture and marketing of functional foods containing this bioactive compound. The hydrophobic stilbene derivative showed higher stability in milk models with near neutral pH, while higher degradation during heat treatment and storage was observed in juice models with acidic pH. While no significant variations in pH were observed in fortified models, CD supplementation increased soluble solids and had a variable effect on the preservation of the hydrophobic stilbene derivative depending on the food model. In milk models, the presence of CDs retarded the degradation of the bioactive compound during the first weeks, while in juice models, although it improved the stability against heat treatment, it accelerated the degradation during storage. In addition, the major isomer of resveratrol palmitate was found to be the most susceptible

to degradation in food models stored without light protection and at room temperature. In general, light protection in the fortified models during storage was found to be even more critical for preserving the bioactive ingredient than temperature. Therefore, the use of opaque packaging to preserve functional foods fortified with hydrophobic stilbene derivatives would be recommended. This condition allows their storage without the need for refrigeration, providing a practical and effective alternative for marketing and consumption.

CHAPTER V

CONCLUSIONS

CHAPTER V. CONCLUSIONS

The results obtained in this thesis allow the following conclusions to be drawn:

1. A tyrosinase-catalysed method to obtain piceatannol from resveratrol was optimised, achieving up to 56 % stilbene conversion in the presence of the antioxidant ascorbic acid. In addition, phylogenetic analyses revealed that STS proteins may also be present in kingdoms other than plants, such as fungi and bacteria, having evolved from CHS independently within each genus. Recombinant protein expression of a potential STS from an extremophilic microorganism was optimised for future biotechnological applications in stilbene synthesis.

2. The resveratrol analogues gnetol, isorhapontigenin, rhapontigenin and pinostilbene were characterised and encapsulated in CDs in order to improve their solubility and stability in aqueous solution. Some structure-activity relationships were established by comparison with other stilbenes. All inclusion complexes showed 1:1 stoichiometry and higher affinity for HP-β-CD by physicochemical and bioinformatic assays. Encapsulation constants were dependent on pH and temperature of the medium.

3. Hydrophobic stilbene derivatives intended for use as stilbene precursors were synthesised by chemical and enzymatic esterification, yielding up to 78 % and 56 %, respectively, with high specificity for monoester. The derivatisation changed the physicochemical properties of the stilbenes, decreasing their absorptivity but increasing their fluorescence in some cases. These derivatives formed 1:1 complexes with HP-β-CD in the presence of 85 % methanol.

4. The synthesised stilbene derivatives were susceptible to pancreatic lipase activity; however, this hydrolysis could be inhibited by the use of free caffeoylquinic acids. Encapsulation of caffeoylquinic acids improved solubility and protection against enzymatic oxidation, but also supressed their inhibitory effect on pancreatic lipase. CDs promoted selective pancreatic lipase activity on some isomers of hydrophobic stilbene derivatives, probably due to the disaggregation of the micellar conformation in isomers with higher affinity for CD.

5. In cells, the hydrophobic stilbene derivatives seemed to be less susceptible to sulphation and glucuronidation than their original stilbenes. In addition, resveratrol derivatives improved the apparent permeability across intestinal cells. Meanwhile, in mice, CDs seemed to increase the relative oral bioavailability of resveratrol stearate, though mostly hydrolysed. Besides, resveratrol stearate improved serum lipid, hepatic-renal, inflammatory and oxidative biomarkers, especially in the complexed form.

6. Hydrophobic stilbene derivatives were less reactive to free radicals and metal complexes *in vitro* than their original stilbenes, suggesting better preservation of stilbene in the presence of oxidising agents. CDs demonstrated to interfere with some of the most common antioxidant methods due to encapsulation of the reagents involved in the reaction, leading to misinterpretation of readings. Structure-activity relationships were established for the cytotoxicity of natural resveratrol analogues, highlighting the presence of methoxy groups in the molecule.

7. Hydrophobic stilbene derivatives decreased lipid accumulation in *C. elegans*, but not in adipocyte cultures. However, these derivatives enhanced the

expression of some obesity-related genes *in vitro* and serum lipid biomarkers *in vivo*, suggesting a beneficial effect on lipid transport beyond their intrinsic activity in adipose tissue. Even so, the hydrolysed form of the derivatives inhibited adipogenesis and activated lipolysis in adipocytes. Stilbene derivatives showed no toxicity in animal models and decreased tumour growth and angiogenesis in mice with melanoma, especially when administered with CDs. Mice treated with encapsulated resveratrol stearate improved serum hepatic-renal, inflammatory and oxidative biomarkers, reaching levels similar to those of healthy individuals.

8. Functional food models were developed with a free and complexed hydrophobic stilbene derivative as a novel bioactive ingredient. The derivative was more stable in milk models than juice models, which showed slight degradation during heat treatment and storage. Quality parameters remained stable over time, despite a slight increase in soluble solids after CD supplementation. Light protection during storage was even more critical for the preservation of the bioactive ingredient than temperature, encouraging opaque packaging for future industrial applications of these bioactive compounds.

REFERENCES

REFERENCES

Abbas, A.M., 2016. Cardioprotective effect of resveratrol analogue isorhapontigenin versus omega-3 fatty acids in isoproterenol-induced myocardial infarction in rats. J. Physiol. Biochem. 72, 469–484. https://doi.org/10.1007/s13105-016-0494-4

Abel, E.D., Peroni, O., Kim, J.K., Kim, Y.-B., Boss, O., Hadro, E., Minnemann, T., Shulman, G.I., Kahn, B.B., 2001. Adipose-selective targeting of the GLUT4 gene impairs insulin action in muscle and liver. Nature 409, 729–733. https://doi.org/10.1038/35055575

Agrawal, N., Jaiswal, M., 2022. Bioavailability enhancement of curcumin via esterification processes: A review. Eur. J. Med. Chem. Rep. 6, 100081. https://doi.org/10.1016/j.ejmcr.2022.100081

Aguirre, L., Fernández-Quintela, A., Arias, N., Portillo, M.P., 2014. Resveratrol: Anti-Obesity Mechanisms of Action. Molecules 19, 18632–18655. https://doi.org/10.3390/molecules191118632

Ai, R., Zhuang, X.-X., Anisimov, A., Lu, J.-H., Fang, E.F., 2022. A synergized machine learning plus cross-species wet-lab validation approach identifies neuronal mitophagy inducers inhibiting Alzheimer disease. Autophagy 18, 939–941. https://doi.org/10.1080/15548627.2022.2031382

Akinwumi, B.C., Bordun, K.-A.M., Anderson, H.D., 2018. Biological Activities of Stilbenoids. Int. J. Mol. Sci. 19, 792. https://doi.org/10.3390/ijms19030792

Albert, S., Horbach, R., Deising, H.B., Siewert, B., Csuk, R., 2011. Synthesis and antimicrobial activity of (E) stilbene derivatives. Bioorg. Med. Chem. 19, 5155–5166. https://doi.org/10.1016/j.bmc.2011.07.015

Alvarez-Illera, P., García-Casas, P., Arias-del-Val, J., Fonteriz, R.I., Alvarez, J., Montero, M., 2017. Pharynx mitochondrial [Ca 2+] dynamics in live C. elegans worms

during aging. Oncotarget 8, 55889–55900. https://doi.org/10.18632/oncotarget.18600

Álvarez-Parrilla, E., Palos, R., Rosa, L.A. de la, Frontana-Uribe, B.A., González-Aguilar, G.A., Machi, L., Ayala-Zavala, J.F., 2010. Formation of Two 1:1 Chlorogenic Acid: β-cyclodextrin Complexes at pH 5: Spectroscopic, Thermodynamic and Voltammetric study. J. Mex. Chem. Soc. 54, 103–110.

Alvarez-Parrilla, E., Rosa, L.A.D.L., Torres-Rivas, F., Rodrigo-Garcia, J., González-Aguilar, G.A., 2005. Complexation of Apple Antioxidants: Chlorogenic Acid, Quercetin and Rutin by β-Cyclodextrin (β-CD). J. Incl. Phenom. Macrocycl. Chem. 53, 121–129. https://doi.org/10.1007/s10847-005-1620-z

Aranaz, P., Navarro-Herrera, D., Zabala, M., Romo-Hualde, A., López-Yoldi, M., Vizmanos, J.L., Milagro, F.I., González-Navarro, C.J., 2020. Phenolic Compounds Reduce the Fat Content in Caenorhabditis elegans by Affecting Lipogenesis, Lipolysis, and Different Stress Responses. Pharmaceuticals 13, 355. https://doi.org/10.3390/ph13110355

Aree, T., Jongrungruangchok, S., 2018. β-Cyclodextrin encapsulation elevates antioxidant capacity of tea: A closing chapter on non-epicatechins, atomistic insights from X-ray analysis, DFT calculation and DPPH assay. Carbohydr. Polym. 194, 24–33. https://doi.org/10.1016/j.carbpol.2018.04.016

Arthur, J.R., Boyne, R., 1985. Superoxide dismutase and glutathione peroxidase activities in neutrophils from selenium deficient and copper deficient cattle. Life Sci. 36, 1569–1575. https://doi.org/10.1016/0024-3205(85)90381-9

Asensi, M., Medina, I., Ortega, A., Carretero, J., Baño, M.C., Obrador, E., Estrela, J.M., 2002. Inhibition of cancer growth by resveratrol is related to its low

bioavailability. Free Radic. Biol. Med. 33, 387–398. https://doi.org/10.1016/S0891-5849(02)00911-5

Astray, G., Gonzalez-Barreiro, C., Mejuto, J.C., Rial-Otero, R., Simal-Gándara, J., 2009. A review on the use of cyclodextrins in foods. Food Hydrocoll. 23, 1631–1640. https://doi.org/10.1016/j.foodhyd.2009.01.001

Ávila-Gálvez, M.Á., Giménez-Bastida, J.A., Espín, J.C., González-Sarrías, A., 2020. Dietary Phenolics against Breast Cancer. A Critical Evidence-Based Review and Future Perspectives. Int. J. Mol. Sci. 21, 5718. https://doi.org/10.3390/ijms21165718

Ávila-González, R., Pérez-Gilabert, M., García-Carmona, F., 2005. Lipase-catalyzed preparation of *S*-propranolol in presence of hydroxypropyl β-cyclodextrins. J. Biosci. Bioeng. 100, 423–428. https://doi.org/10.1263/jbb.100.423

Babazadeh, A., Ghanbarzadeh, B., Hamishehkar, H., 2016. Novel nanostructured lipid carriers as a promising food grade delivery system for rutin. J. Funct. Foods 26, 167–175. https://doi.org/10.1016/j.jff.2016.07.017

Baile, C.A., Yang, J.-Y., Rayalam, S., Hartzell, D.L., Lai, C.-Y., Andersen, C., Della-Fera, M.A., 2011. Effect of resveratrol on fat mobilization. Ann. N. Y. Acad. Sci. 1215, 40–47. https://doi.org/10.1111/j.1749-6632.2010.05845.x

Bangalore, D.V., McGlynn, W., Scott, D.D., 2005. Effect of β-Cyclodextrin in Improving the Correlation between Lycopene Concentration and ORAC Values. J. Agric. Food Chem. 53, 1878–1883. https://doi.org/10.1021/jf048258m

Barua, C.C., Haloi, P., Barua, I.C., 2015. Gnetum gnemon Linn. : A Comprehensive Review on its Biological, Pharmacological and Pharmacognostical Potentials. Int. J. Pharmacogn. Phytochem. Res. 7, 531–539.

Basini, G., Tringali, C., Baioni, L., Bussolati, S., Spatafora, C., Grasselli, F., 2010. Biological effects on granulosa cells of hydroxylated and methylated resveratrol analogues. Mol. Nutr. Food Res. 54, S236–S243. https://doi.org/10.1002/mnfr.200900320

Beekwilder, J., Wolswinkel, R., Jonker, H., Hall, R., de Vos, C.H.R., Bovy, A., 2006. Production of Resveratrol in Recombinant Microorganisms. Appl. Environ. Microbiol. 72, 5670–5672. https://doi.org/10.1128/AEM.00609-06

Benesi, H.A., Hildebrand, J.H., 1949. A Spectrophotometric Investigation of the Interaction of Iodine with Aromatic Hydrocarbons. J. Am. Chem. Soc. 71, 2703–2707. https://doi.org/10.1021/ja01176a030

Berndt, J., Kovacs, P., Ruschke, K., Klöting, N., Fasshauer, M., Schön, M.R., Körner, A., Stumvoll, M., Blüher, M., 2007. Fatty acid synthase gene expression in human adipose tissue: association with obesity and type 2 diabetes. Diabetologia 50, 1472–1480. https://doi.org/10.1007/s00125-007-0689-x

Bethune, S.J., Schultheiss, N., Henck, J.-O., 2011. Improving the Poor Aqueous Solubility of Nutraceutical Compound Pterostilbene through Cocrystal Formation. Cryst. Growth Des. 11, 2817–2823. https://doi.org/10.1021/cg1016092

Bhatt, P., Fnu, G., Bhatia, D., Shahid, A., Sutariya, V., 2020. Nanodelivery of Resveratrol-Loaded PLGA Nanoparticles for Age-Related Macular Degeneration. AAPS PharmSciTech 21, 291. https://doi.org/10.1208/s12249-020-01836-4

Biasutto, L., Marotta, E., De Marchi, U., Zoratti, M., Paradisi, C., 2007. Ester-Based Precursors to Increase the Bioavailability of Quercetin. J. Med. Chem. 50, 241–253. https://doi.org/10.1021/jm060912x

Billaud, C., Regaudie, E., Fayad, N., Richard-Forget, F., Nicolas, J., 1995. Effect of Cyclodextrins on Polyphenol Oxidation Catalyzed by Apple Polyphenol Oxidase,

in: Enzymatic Browning and Its Prevention, ACS Symposium Series. American Chemical Society, pp. 295–312. https://doi.org/10.1021/bk-1995-0600.ch023

Borato, D.C.K., Parabocz, G.C., Ribas, J.T., Netto, H.P., Erdmann, F.C., Wiecheteck, L.D., Manente, F.A., Mello, L.R. de A., Belló, C., Santos, F.A. dos, Borba, L.M., Vellosa, J.C.R., 2016. Biomarkers in Obesity: Serum Myeloperoxidase and Traditional Cardiac Risk Parameters. Exp. Clin. Endocrinol. Diabetes 124, 49–54. https://doi.org/10.1055/s-0035-1565093

Brandt, B.W., Heringa, J., 2009. webPRC: the Profile Comparer for alignment-based searching of public domain databases. Nucleic Acids Res. 37, W48–W52. https://doi.org/10.1093/nar/gkp279

Bu, L., Gan, L.-C., Guo, X.-Q., Chen, F.-Z., Song, Q., Qi-Zhao, Gou, X.-J., Hou, S.-X., Yao, Q., 2013. *Trans*-resveratrol loaded chitosan nanoparticles modified with biotin and avidin to target hepatic carcinoma. Int. J. Pharm., Special section on Drug disposition: from cradle to cane 452, 355–362. https://doi.org/10.1016/j.ijpharm.2013.05.007

Cahyana, A.H., Ardiansah, B., 2016. Antioxidative and cytotoxic effects of prenylated stilbene derivative-rich Melinjo (Gnetum gnemon L.) fruit rind. AIP Conf. Proc. 1729, 020057. https://doi.org/10.1063/1.4946960

Cai, C., Liu, M., Yan, H., Zhao, Y., Shi, Y., Guo, Q., Pei, W., Han, J., Wang, Z., 2019. A combined calorimetric, spectroscopic and molecular dynamic simulation study on the inclusion complexation of (E)-piceatannol with hydroxypropyl-β-cyclodextrin in various alcohol + water cosolvents. J. Chem. Thermodyn. 132, 341–351. https://doi.org/10.1016/j.jct.2019.01.009

Cai, W.X., Zheng, L.W., Ma, L., Huang, H.Z., Yu, R.Q., Zwahlen, R.A., 2016. Tumorigenicity and Validity of Fluorescence Labelled Mesenchymal and

Epithelial Human Oral Cancer Cell Lines in Nude Mice. BioMed Res. Int. 2016, e4897986. https://doi.org/10.1155/2016/4897986

Cai, Z., Kastell, A., Speiser, C., Smetanska, I., 2013. Enhanced Resveratrol Production in Vitis vinifera Cell Suspension Cultures by Heavy Metals Without Loss of Cell Viability. Appl. Biochem. Biotechnol. 171, 330–340. https://doi.org/10.1007/s12010-013-0354-4

Carando, S., Teissedre, P.L., Waffo-Téguo, P., Cabanis, J.C., Deffieux, G., Mérillon, J.M., 1999. High-performance liquid chromatography coupled with fluorescence detection for the determination of *trans*-astringin in wine. J. Chromatogr. A 849, 617–620. https://doi.org/10.1016/S0021-9673(99)00595-6

Cardile, V., Chillemi, R., Lombardo, L., Sciuto, S., Spatafora, C., Tringali, C., 2007. Antiproliferative Activity of Methylated Analogues of E- and Z-Resveratrol. Z. Für Naturforschung C 62, 189–195. https://doi.org/10.1515/znc-2007-3-406

Carpéné, C., Pejenaute, H., Del Moral, R., Boulet, N., Hijona, E., Andrade, F., Villanueva-Millán, M.J., Aguirre, L., Arbones-Mainar, J.M., 2018. The Dietary Antioxidant Piceatannol Inhibits Adipogenesis of Human Adipose Mesenchymal Stem Cells and Limits Glucose Transport and Lipogenic Activities in Adipocytes. Int. J. Mol. Sci. 19, 2081. https://doi.org/10.3390/ijms19072081

Cassidy, A., Hanley, B., Lamuela-Raventos, R.M., 2000. Isoflavones, lignans and stilbenes – origins, metabolism and potential importance to human health. J. Sci. Food Agric. 80, 1044–1062. https://doi.org/10.1002/(SICI)1097-0010(20000515)80:7<1044::AID-JSFA586>3.0.CO;2-N

Catania, A., Barrajón-Catalán, E., Nicolosi, S., Cicirata, F., Micol, V., 2013. Immunoliposome encapsulation increases cytotoxic activity and selectivity of curcumin and resveratrol against HER2 overexpressing human breast cancer cells.

Breast Cancer Res. Treat. 141, 55–65. https://doi.org/10.1007/s10549-013-2667-y

Cecerska-Heryć, E., Surowska, O., Heryć, R., Serwin, N., Napiontek-Balińska, S., Dołęgowska, B., 2021. Are antioxidant enzymes essential markers in the diagnosis and monitoring of cancer patients – A review. Clin. Biochem. 93, 1–8. https://doi.org/10.1016/j.clinbiochem.2021.03.008

Chandhok, G., Lazarou, M., Neumann, B., 2018. Structure, function, and regulation of mitofusin-2 in health and disease. Biol. Rev. 93, 933–949. https://doi.org/10.1111/brv.12378

Chao, J., Li, H., Cheng, K.-W., Yu, M.-S., Chang, R.C.-C., Wang, M., 2010. Protective effects of pinostilbene, a resveratrol methylated derivative, against 6-hydroxydopamine-induced neurotoxicity in SH-SY5Y cells. J. Nutr. Biochem. 21, 482–489. https://doi.org/10.1016/j.jnutbio.2009.02.004

Charman, W.N., Porter, C.J.H., 1996. Lipophilic prodrugs designed for intestinal lymphatic transport. Adv. Drug Deliv. Rev., Low Molecular Weight Pro Drugs 19, 149–169. https://doi.org/10.1016/0169-409X(95)00105-G

Chen, M.-K., Liu, Y.-T., Lin, J.-T., Lin, C.-C., Chuang, Y.-C., Lo, Y.-S., Hsi, Y.-T., Hsieh, M.-J., 2019. Pinosylvin reduced migration and invasion of oral cancer carcinoma by regulating matrix metalloproteinase-2 expression and extracellular signal-regulated kinase pathway. Biomed. Pharmacother. 117, 109160. https://doi.org/10.1016/j.biopha.2019.109160

Chen, W., Rezaizadehnajafi, L., Wink, M., 2013. Influence of resveratrol on oxidative stress resistance and life span in Caenorhabditis elegans. J. Pharm. Pharmacol. 65, 682–688. https://doi.org/10.1111/jphp.12023

Cheng, K., Song, Z., Chen, Y., Li, S., Zhang, Y., Zhang, H., Zhang, L., Wang, C., Wang, T., 2019. Resveratrol Protects Against Renal Damage via Attenuation of Inflammation and Oxidative Stress in High-Fat-Diet-Induced Obese Mice. Inflammation 42, 937–945. https://doi.org/10.1007/s10753-018-0948-7

Chiba, K., Kawakami, K., Tohyama, K., 1998. Simultaneous evaluation of cell viability by neutral red, MTT and crystal violet staining assays of the same cells. Toxicol. In Vitro 12, 251–258. https://doi.org/10.1016/S0887-2333(97)00107-0

Chong, J., Poutaraud, A., Hugueney, P., 2009. Metabolism and roles of stilbenes in plants. Plant Sci. 177, 143–155. https://doi.org/10.1016/j.plantsci.2009.05.012

Chouchani, E.T., Kazak, L., Spiegelman, B.M., 2019. New Advances in Adaptive Thermogenesis: UCP1 and Beyond. Cell Metab. 29, 27–37. https://doi.org/10.1016/j.cmet.2018.11.002

Chu, X.Y., Yang, S.Z., Zhu, M.Q., Zhang, D.Y., Shi, X.C., Xia, B., Yuan, Y., Liu, M., Wu, J.W., 2020. Isorhapontigenin Improves Diabetes in Mice via Regulating the Activity and Stability of PPARγ in Adipocytes. J. Agric. Food Chem. https://doi.org/10.1021/acs.jafc.0c00515

Chung, Y.C., Hyun, C.-G., 2021. Inhibitory Effects of Pinostilbene on Adipogenesis in 3T3-L1 Adipocytes: A Study of Possible Mechanisms. Int. J. Mol. Sci. 22, 13446. https://doi.org/10.3390/ijms222413446

Coimbra, M., Isacchi, B., van Bloois, L., Torano, J.S., Ket, A., Wu, X., Broere, F., Metselaar, J.M., Rijcken, C.J.F., Storm, G., Bilia, R., Schiffelers, R.M., 2011. Improving solubility and chemical stability of natural compounds for medicinal use by incorporation into liposomes. Int. J. Pharm., 8th European Workshop on Particulate Systems (EWPS) 416, 433–442. https://doi.org/10.1016/j.ijpharm.2011.01.056

Coker, J.A., 2016. Extremophiles and biotechnology: current uses and prospects. F1000Research 5, F1000 Faculty Rev-396. https://doi.org/10.12688/f1000research.7432.1

Colica, C., Milanović, M., Milić, N., Aiello, V., De Lorenzo, A., Abenavoli, L., 2018. A Systematic Review on Natural Antioxidant Properties of Resveratrol. Nat. Prod. Commun. 13, 1934578X1801300923. https://doi.org/10.1177/1934578X1801300923

Costa, P., Medronho, B., Gonçalves, S., Romano, A., 2015. Cyclodextrins enhance the antioxidant activity of essential oils from three Lamiaceae species. Ind. Crops Prod. 70, 341–346. https://doi.org/10.1016/j.indcrop.2015.03.065

Crauste, C., Vigor, C., Brabet, P., Picq, M., Lagarde, M., Hamel, C., Durand, T., Vercauteren, J., 2014. Synthesis and Evaluation of Polyunsaturated Fatty Acid–Phenol Conjugates as Anti-Carbonyl-Stress Lipophenols. Eur. J. Org. Chem. 2014, 4548–4561. https://doi.org/10.1002/ejoc.201402282

Daane, L.L., Harjono, I., Barns, S.M., Launen, L.A., Palleron, N.J., Häggblom, M.M., 2002. PAH-degradation by Paenibacillus spp. and description of Paenibacillus naphthalenovorans sp. nov., a naphthalene-degrading bacterium from the rhizosphere of salt marsh plants. Int. J. Syst. Evol. Microbiol. 52, 131–139. https://doi.org/10.1099/00207713-52-1-131

Dai, M., Yuan, D., Lei, Y., Li, J., Ren, Y., Zhang, Y., Cang, H., Gao, W., Tang, Y., 2022. Expression, purification and structural characterization of resveratrol synthase from *Polygonum cuspidatum*. Protein Expr. Purif. 191, 106024. https://doi.org/10.1016/j.pep.2021.106024

Dai, Y., Li, N., Zhao, Q., Xie, S., 2015. Bioremediation using Novosphingobium strain DY4 for 2,4-dichlorophenoxyacetic acid-contaminated soil and impact on

microbial community structure. Biodegradation 26, 161–170. https://doi.org/10.1007/s10532-015-9724-7

Dai, Y., Lim, J.X., Yeo, S.C.M., Xiang, X., Tan, K.S., Fu, J.H., Huang, L., Lin, H.-S., 2020. Biotransformation of Piceatannol, a Dietary Resveratrol Derivative: Promises to Human Health. Mol. Nutr. Food Res. 64, 1900905. https://doi.org/10.1002/mnfr.201900905

Dai, Y., Yeo, S.C.M., Barnes, P.J., Donnelly, L.E., Loo, L.C., Lin, H.-S., 2018. Pre-clinical Pharmacokinetic and Metabolomic Analyses of Isorhapontigenin, a Dietary Resveratrol Derivative. Front. Pharmacol. 9, 753. https://doi.org/10.3389/fphar.2018.00753

D'Aria, F., Pagano, B., Giancola, C., 2021. Thermodynamic properties of hydroxypropyl-β-cyclodextrin/guest interaction: a survey of recent studies. J. Therm. Anal. Calorim. 147, 1–9. https://doi.org/10.1007/s10973-021-10958-1

Davoodvandi, A., Darvish, M., Borran, S., Nejati, M., Mazaheri, S., Reza Tamtaji, O., Hamblin, M.R., Masoudian, N., Mirzaei, H., 2020. The therapeutic potential of resveratrol in a mouse model of melanoma lung metastasis. Int. Immunopharmacol. 88, 106905. https://doi.org/10.1016/j.intimp.2020.106905

de Vries, K., Strydom, M., Steenkamp, V., 2021. A Brief Updated Review of Advances to Enhance Resveratrol's Bioavailability. Molecules 26, 4367. https://doi.org/10.3390/molecules26144367

Del Valle, E.M.M., 2004. Cyclodextrins and their uses: a review. Process Biochem. 39, 1033–1046. https://doi.org/10.1016/S0032-9592(03)00258-9

Dereeper, A., Guignon, V., Blanc, G., Audic, S., Buffet, S., Chevenet, F., Dufayard, J.-F., Guindon, S., Lefort, V., Lescot, M., Claverie, J.-M., Gascuel, O., 2008.

Phylogeny.fr: robust phylogenetic analysis for the non-specialist. Nucleic Acids Res. 36, W465–W469. https://doi.org/10.1093/nar/gkn180

Detoni, C.B., Souto, G.D., da Silva, A.L.M., Pohlmann, A.R., Guterres, S.S., 2012. Photostability and Skin Penetration of Different E-Resveratrol-Loaded Supramolecular Structures. Photochem. Photobiol. 88, 913–921. https://doi.org/10.1111/j.1751-1097.2012.01147.x

Dhakar, N.K., Matencio, A., Caldera, F., Argenziano, M., Cavalli, R., Dianzani, C., Zanetti, M., López-Nicolás, J.M., Trotta, F., 2019. Comparative Evaluation of Solubility, Cytotoxicity and Photostability Studies of Resveratrol and Oxyresveratrol Loaded Nanosponges. Pharmaceutics 11, 545. https://doi.org/10.3390/pharmaceutics11100545

Dhanapal, J., Balaraman Ravindrran, M., 2018. Chitosan/poly (lactic acid)-coated piceatannol nanoparticles exert an in vitro apoptosis activity on liver, lung and breast cancer cell lines. Artif. Cells Nanomedicine Biotechnol. 46, 274–282. https://doi.org/10.1080/21691401.2017.1422130

Dillard, C.J., German, J.B., 2000. Phytochemicals: nutraceuticals and human health. J. Sci. Food Agric. 80, 1744–1756. https://doi.org/10.1002/1097-0010(20000915)80:12<1744::AID-JSFA725>3.0.CO;2-W

Duan, J., Yue, W., E, J., Malhotra, J., Lu, S., Gu, J., Xu, F., Tan, X.-L., 2016. In vitro comparative studies of resveratrol and triacetylresveratrol on cell proliferation, apoptosis, and STAT3 and NFκB signaling in pancreatic cancer cells. Sci. Rep. 6, 31672. https://doi.org/10.1038/srep31672

Duarte, A., Martinho, A., Luís, Â., Figueiras, A., Oleastro, M., Domingues, F.C., Silva, F., 2015. Resveratrol encapsulation with methyl-β-cyclodextrin for antibacterial

and antioxidant delivery applications. LWT - Food Sci. Technol. 63, 1254–1260. https://doi.org/10.1016/j.lwt.2015.04.004

Dubrovina, A.S., Kiselev, K.V., 2017. Regulation of stilbene biosynthesis in plants. Planta. https://doi.org/10.1007/s00425-017-2730-8

Dvorakova, M., Landa, P., 2017. Anti-inflammatory activity of natural stilbenoids: A review. Pharmacol. Res. 124, 126–145. https://doi.org/10.1016/j.phrs.2017.08.002

Džeba, I., Pedzinski, T., Mihaljević, B., 2015. Photophysical and photochemical properties of resveratrol. J. Photochem. Photobiol. Chem. 299, 118–124. https://doi.org/10.1016/j.jphotochem.2014.11.019

Ebada, S.S., Edrada, R.A., Lin, W., Proksch, P., 2008. Methods for isolation, purification and structural elucidation of bioactive secondary metabolites from marine invertebrates. Nat. Protoc. 3, 1820–1831. https://doi.org/10.1038/nprot.2008.182

Edgar, R.C., 2004. MUSCLE: multiple sequence alignment with high accuracy and high throughput. Nucleic Acids Res. 32, 1792–1797. https://doi.org/10.1093/nar/gkh340

EFSA, 2016. Safety of synthetic trans-resveratrol as a novel food pursuant to Regulation (EC) No 258/97. EFSA J. 14, 4368. https://doi.org/10.2903/j.efsa.2016.4368

EFSA, 2010. Scientific Opinion on the substantiation of health claims related to various food(s)/food constituent(s) and protection of cells from premature aging, antioxidant activity, antioxidant content and antioxidant properties, and protection of DNA, proteins and lipids from oxidative damage pursuant to Article 13(1) of Regulation (EC) No 1924/2006. EFSA J. 8, 1489. https://doi.org/10.2903/j.efsa.2010.1489

EFSA, 2006. Regulation (EC) No 1924/2006 of the European Parliament and of the Council of 20 December 2006 on nutrition and health claims made on foods, OJ L.

El Khawand, T., Courtois, A., Valls, J., Richard, T., Krisa, S., 2018. A review of dietary stilbenes: sources and bioavailability. Phytochem. Rev. 17, 1007–1029. https://doi.org/10.1007/s11101-018-9578-9

El-Gebali, S., Mistry, J., Bateman, A., Eddy, S.R., Luciani, A., Potter, S.C., Qureshi, M., Richardson, L.J., Salazar, G.A., Smart, A., Sonnhammer, E.L.L., Hirsh, L., Paladin, L., Piovesan, D., Tosatto, S.C.E., Finn, R.D., 2019. The Pfam protein families database in 2019. Nucleic Acids Res. 47, D427–D432. https://doi.org/10.1093/nar/gky995

Ellermann, C., Wolfes, J., Kochhäuser, S., Dechering, D.G., Reinke, F., Wasmer, K., Eckardt, L., Frommeyer, G., 2017. Divergent antiarrhythmic effects of resveratrol and piceatannol in a whole-heart model of long QT syndrome. Int. J. Cardiol. 243, 233–238. https://doi.org/10.1016/j.ijcard.2017.06.005

Fan, Y., 2019. Cardioprotective Effect of Rhapontigenin in Isoproterenol-Induced Myocardial Infarction in a Rat Model. Pharmacology 103, 291–302. https://doi.org/10.1159/000496800

Fang, Y., Cao, Z., Hou, Q., Ma, C., Yao, C., Li, J., Wu, X.-R., Huang, C., 2013. Cyclin D1 Downregulation Contributes to Anticancer Effect of Isorhapontigenin on Human Bladder Cancer Cells. Mol. Cancer Ther. 12, 1492–1503. https://doi.org/10.1158/1535-7163.MCT-12-0922

Fang, Y., Yu, Y., Hou, Q., Zheng, X., Zhang, M., Zhang, D., Li, J., Wu, X.-R., Huang, C., 2012. The Chinese Herb Isolate Isorhapontigenin Induces Apoptosis in Human

Cancer Cells by Down-regulating Overexpression of Antiapoptotic Protein XIAP *. J. Biol. Chem. 287, 35234–35243. https://doi.org/10.1074/jbc.M112.389494

Fernández-Marín, M.I., Guerrero, R.F., García-Parrilla, M.C., Puertas, B., Richard, T., Rodriguez-Werner, M.A., Winterhalter, P., Monti, J.-P., Cantos-Villar, E., 2012. Isorhapontigenin: A novel bioactive stilbene from wine grapes. Food Chem. 135, 1353–1359. https://doi.org/10.1016/j.foodchem.2012.05.086

Fernández-Quintela, A., Milton-Laskibar, I., González, M., Portillo, M.P., 2017. Antiobesity effects of resveratrol: which tissues are involved? Ann. N. Y. Acad. Sci. 1403, 118–131. https://doi.org/10.1111/nyas.13413

Ferreira, F. da R., Valentim, I.B., Ramones, E.L.C., Trevisan, M.T.S., Olea-Azar, C., Perez-Cruz, F., de Abreu, F.C., Goulart, M.O.F., 2013. Antioxidant activity of the mangiferin inclusion complex with β-cyclodextrin. LWT - Food Sci. Technol. 51, 129–134. https://doi.org/10.1016/j.lwt.2012.09.032

Folch-Cano, C., Jullian, C., Speisky, H., Olea-Azar, C., 2010. Antioxidant activity of inclusion complexes of tea catechins with β-cyclodextrins by ORAC assays. Food Res. Int. 43, 2039–2044. https://doi.org/10.1016/j.foodres.2010.06.006

Francioso, A., Mastromarino, P., Masci, A., d'Erme, M., Mosca, L., 2014. Chemistry, Stability and Bioavailability of Resveratrol. Med. Chem. 10, 237–245.

Franco, J.G., Lisboa, P.C., Lima, N.S., Amaral, T.A.S., Peixoto-Silva, N., Resende, A.C., Oliveira, E., Passos, M.C.F., Moura, E.G., 2013. Resveratrol attenuates oxidative stress and prevents steatosis and hypertension in obese rats programmed by early weaning. J. Nutr. Biochem. 24, 960–966. https://doi.org/10.1016/j.jnutbio.2012.06.019

Friedman, J., 2014. 20 YEARS OF LEPTIN: Leptin at 20: an overview. J. Endocrinol. 223, T1–T8. https://doi.org/10.1530/JOE-14-0405

Fu, J., Shrivastava, A., Shrivastava, S.K., Srivastava, R.K., Shankar, S., 2019. Triacetyl resveratrol upregulates miRNA-200 and suppresses the Shh pathway in pancreatic cancer: A potential therapeutic agent. Int. J. Oncol. 54, 1306–1316. https://doi.org/10.3892/ijo.2019.4700

Fujiwara, S., 2002. Extremophiles: Developments of their special functions and potential resources. J. Biosci. Bioeng. 94, 518–525. https://doi.org/10.1016/S1389-1723(02)80189-X

Fukuhara, K., Nakanishi, I., Matsuoka, A., Matsumura, T., Honda, S., Hayashi, M., Ozawa, T., Miyata, N., Saito, S., Ikota, N., Okuda, H., 2008. Effect of Methyl Substitution on the Antioxidative Property and Genotoxicity of Resveratrol. Chem. Res. Toxicol. 21, 282–287. https://doi.org/10.1021/tx7003008

Fulda, S., 2010. Resveratrol and derivatives for the prevention and treatment of cancer. Drug Discov. Today 15, 757–765. https://doi.org/10.1016/j.drudis.2010.07.005

Furuya, T., Sai, M., Kino, K., 2018. Efficient monooxygenase-catalyzed piceatannol production: Application of cyclodextrins for reducing product inhibition. J. Biosci. Bioeng. 126, 478–481. https://doi.org/10.1016/j.jbiosc.2018.04.016

Gabaldón, J.A., Núñez Delicado, E., Mercader Ros, M.T., Lucas Abellán, C., Fortea Gorbe, M.I., 2010. Effect of HP-b-cyclodextrins complexation on the antioxidant activity of flavonols. Food Chem. 118.

Gaglio, S.C., Donini, M., Denbaes, P.E., Dusi, S., Perduca, M., 2021. Oxyresveratrol Inhibits R848-Induced Pro-Inflammatory Mediators Release by Human Dendritic Cells Even When Embedded in PLGA Nanoparticles. Molecules 26, 2106. https://doi.org/10.3390/molecules26082106

García-Casas, P., Arias-del-Val, J., Alvarez-Illera, P., Wojnicz, A., de los Ríos, C., Fonteriz, R.I., Montero, M., Alvarez, J., 2019. The Neuroprotector

Benzothiazepine CGP37157 Extends Lifespan in C. elegans Worms. Front. Aging Neurosci. 10. https://doi.org/10.3389/fnagi.2018.00440

García-Padial, M., Martínez-Ohárriz, M.C., Navarro-Blasco, I., Zornoza, A., 2013. The Role of Cyclodextrins in ORAC-Fluorescence Assays. Antioxidant Capacity of Tyrosol and Caffeic Acid with Hydroxypropyl-β-Cyclodextrin. J. Agric. Food Chem. 61, 12260–12264. https://doi.org/10.1021/jf403265b

Gigliotti, C.L., Minelli, R., Cavalli, R., Occhipinti, S., Barrera, G., Pizzimenti, S., Cappellano, G., Boggio, E., Conti, L., Fantozzi, R., Giovarelli, M., Trotta, F., Dianzani, U., Dianzani, C., 2016. In Vitro and In Vivo Therapeutic Evaluation of Camptothecin-Encapsulated β-Cyclodextrin Nanosponges in Prostate Cancer. J. Biomed. Nanotechnol. 12, 114–127. https://doi.org/10.1166/jbn.2016.2144

Giorcelli, A., Sparvoli, F., Mattivi, F., Tava, A., Balestrazzi, A., Vrhovsek, U., Calligari, P., Bollini, R., Confalonieri, M., 2004. Expression of the Stilbene Synthase (StSy) Gene from Grapevine in Transgenic White Poplar Results in High Accumulation of the Antioxidant Resveratrol Glucosides. Transgenic Res. 13, 203–214. https://doi.org/10.1023/B:TRAG.0000034658.64990.7f

Giovinazzo, G., D'Amico, L., Paradiso, A., Bollini, R., Sparvoli, F., DeGara, L., 2005. Antioxidant metabolite profiles in tomato fruit constitutively expressing the grapevine stilbene synthase gene. Plant Biotechnol. J. 3, 57–69. https://doi.org/10.1111/j.1467-7652.2004.00099.x

Gómez-Zorita, S., Fernández-Quintela, A., Lasa, A., Aguirre, L., Rimando, A.M., Portillo, M.P., 2014. Pterostilbene, a dimethyl ether derivative of resveratrol, reduces fat accumulation in rats fed an obesogenic diet. J. Agric. Food Chem. 62, 8371–8378. https://doi.org/10.1021/jf501318b

González-Sarrías, A., Espín-Aguilar, J.C., Romero-Reyes, S., Puigcerver, J., Alajarín, M., Berná, J., Selma, M.V., Espín, J.C., 2022. Main Determinants Affecting the Antiproliferative Activity of Stilbenes and Their Gut Microbiota Metabolites in Colon Cancer Cells: A Structure–Activity Relationship Study. Int. J. Mol. Sci. 23, 15102. https://doi.org/10.3390/ijms232315102

González-Sarrías, A., Tomé-Carneiro, J., Bellesia, A., Tomás-Barberán, F.A., Espín, J.C., 2015. The ellagic acid-derived gut microbiota metabolite, urolithin A, potentiates the anticancer effects of 5-fluorouracil chemotherapy on human colon cancer cells. Food Funct. 6, 1460–1469. https://doi.org/10.1039/C5FO00120J

Govers, R., 2014. Molecular mechanisms of GLUT4 regulation in adipocytes. Diabetes Metab. 40, 400–410. https://doi.org/10.1016/j.diabet.2014.01.005

Grayer, R.J., Chase, M.W., Simmonds, M.S.J., 1999. A comparison between chemical and molecular characters for the determination of phylogenetic relationships among plant families: An appreciation of Hegnauer's "Chemotaxonomie der Pflanzen." Biochem. Syst. Ecol. 27, 369–393. https://doi.org/10.1016/S0305-1978(98)00096-9

Gu, X.Y., Dou, P.C., 2016. Isolation and Characterization of Altererythrobacter sp. DT for Biotreatment of and Sulfur Production from Thiosulfate-Bearing Industrial Wastewater. Water. Air. Soil Pollut. 228, 28. https://doi.org/10.1007/s11270-016-3215-2

Gulcin, İ., 2020. Antioxidants and antioxidant methods: an updated overview. Arch. Toxicol. 1–65. https://doi.org/10.1007/s00204-020-02689-3

Ha, N.M., Tran, S.H., Shim, Y.-H., Kang, K., 2022. Caenorhabditis elegans as a powerful tool in natural product bioactivity research. Appl. Biol. Chem. 65, 18. https://doi.org/10.1186/s13765-022-00685-y

Hain, R., Grimmig, B., 2000. Modification of Plant Secondary Metabolism by Genetic Engineering, in: Verpoorte, R., Alfermann, A.W. (Eds.), Metabolic Engineering of Plant Secondary Metabolism. Springer Netherlands, Dordrecht, pp. 217–231. https://doi.org/10.1007/978-94-015-9423-3_11

Han, S., Mei, L., Quach, T., Porter, C., Trevaskis, N., 2021. Lipophilic Conjugates of Drugs: A Tool to Improve Drug Pharmacokinetic and Therapeutic Profiles. Pharm. Res. 38, 1497–1518. https://doi.org/10.1007/s11095-021-03093-x

Han, S.K., Lee, D., Lee, H., Kim, D., Son, H.G., Yang, J.-S., Lee, S.-J.V., Kim, S., 2016. OASIS 2: online application for survival analysis 2 with features for the analysis of maximal lifespan and healthspan in aging research. Oncotarget 7, 56147–56152. https://doi.org/10.18632/oncotarget.11269

Hansen, J., Bross, P., 2010. A Cellular Viability Assay to Monitor Drug Toxicity, in: Bross, P., Gregersen, N. (Eds.), Protein Misfolding and Cellular Stress in Disease and Aging: Concepts and Protocols. Humana Press, Totowa, NJ, pp. 303–311. https://doi.org/10.1007/978-1-60761-756-3_21

Hanwell, M.D., Curtis, D.E., Lonie, D.C., Vandermeersch, T., Zurek, E., Hutchison, G.R., 2012. Avogadro: an advanced semantic chemical editor, visualization, and analysis platform. J. Cheminformatics 4, 17. https://doi.org/10.1186/1758-2946-4-17

Hao, X., Sun, X., Zhu, H., Xie, L., Wang, X., Jiang, N., Fu, P., Sang, M., 2021. Hydroxypropyl-β-Cyclodextrin-Complexed Resveratrol Enhanced Antitumor Activity in a Cervical Cancer Model: In Vivo Analysis. Front. Pharmacol. 12. https://doi.org/10.3389/fphar.2021.573909

He, J., Zheng, Z.-P., Zhu, Q., Guo, F., Chen, J., 2017. Encapsulation Mechanism of Oxyresveratrol by β-Cyclodextrin and Hydroxypropyl-β-Cyclodextrin and

Computational Analysis. Molecules 22, 1801. https://doi.org/10.3390/molecules22111801

Henikoff, S., Henikoff, J.G., 1994. Position-based sequence weights. J. Mol. Biol. 243, 574–578. https://doi.org/10.1016/0022-2836(94)90032-9

Henry, C., Vitrac, X., Decendit, A., Ennamany, R., Krisa, S., Mérillon, J.-M., 2005. Cellular Uptake and Efflux of trans-Piceid and Its Aglycone trans-Resveratrol on the Apical Membrane of Human Intestinal Caco-2 Cells. J. Agric. Food Chem. 53, 798–803. https://doi.org/10.1021/jf048909e

Herrera, D.P., Chánique, A.M., Martínez-Márquez, A., Bru-Martínez, R., Kourist, R., Parra, L.P., Schüller, A., 2021. Rational Design of Resveratrol O-methyltransferase for the Production of Pinostilbene. Int. J. Mol. Sci. 22, 4345. https://doi.org/10.3390/ijms22094345

Honari, M., Shafabakhsh, R., Reiter, R.J., Mirzaei, H., Asemi, Z., 2019. Resveratrol is a promising agent for colorectal cancer prevention and treatment: focus on molecular mechanisms. Cancer Cell Int. 19, 180. https://doi.org/10.1186/s12935-019-0906-y

Hosseini, S.M., Bahramnejad, B., Douleti Baneh, H., Emamifar, A., Goodwin, P.H., 2017. Hairy root culture optimization and resveratrol production from Vitis vinifera subsp. sylvesteris. World J. Microbiol. Biotechnol. 33, 67. https://doi.org/10.1007/s11274-017-2235-4

Hou, T.J., Zhang, W., Xia, K., Qiao, X.B., Xu, X.J., 2004. ADME Evaluation in Drug Discovery. 5. Correlation of Caco-2 Permeation with Simple Molecular Properties. J. Chem. Inf. Comput. Sci. 44, 1585–1600. https://doi.org/10.1021/ci049884m

Howells, L.M., Berry, D.P., Elliott, P.J., Jacobson, E.W., Hoffmann, E., Hegarty, B., Brown, K., Steward, W.P., Gescher, A.J., 2011. Phase I randomised double-blind pilot study of micronized resveratrol (SRT501) in patients with hepatic metastases - safety, pharmacokinetics and pharmacodynamics. Cancer Prev. Res. Phila. Pa 4, 1419–1425. https://doi.org/10.1158/1940-6207.CAPR-11-0148

Hu, D.-D., Zhang, R.-L., Zou, Y., Zhong, H., Zhang, E.-S., Luo, X., Wang, Y., Jiang, Y.-Y., 2017. The Structure-Activity Relationship of Pterostilbene Against Candida albicans Biofilms. Molecules 22, 360. https://doi.org/10.3390/molecules22030360

Hu, X.-P., Yin, F.-W., Zhou, D.-Y., Xie, H.-K., Zhu, B.-W., Ma, X.-C., Tian, X.-G., Wang, C., Shahidi, F., 2019. Stability of resveratrol esters with caprylic acid during simulated in vitro gastrointestinal digestion. Food Chem. 276, 675–679. https://doi.org/10.1016/j.foodchem.2018.10.062

Huang, D., Ou, B., Hampsch-Woodill, M., Flanagan, J.A., Deemer, E.K., 2002. Development and Validation of Oxygen Radical Absorbance Capacity Assay for Lipophilic Antioxidants Using Randomly Methylated β-Cyclodextrin as the Solubility Enhancer. J. Agric. Food Chem. 50, 1815–1821. https://doi.org/10.1021/jf0113732

Hubatsch, I., Ragnarsson, E.G.E., Artursson, P., 2007. Determination of drug permeability and prediction of drug absorption in Caco-2 monolayers. Nat. Protoc. 2, 2111–2119. https://doi.org/10.1038/nprot.2007.303

Hui, Y., Li, X., Chen, X., 2011. Assessment for the light-induced cis-trans isomerization of rhapontigenin and its glucoside rhaponticin by capillary electrophoresis and spectrometric methods. J. Chromatogr. A 1218, 5858–5866. https://doi.org/10.1016/j.chroma.2011.06.100

Ito, S., Fujiki, Y., Matsui, N., Ojika, M., Wakamatsu, K., 2019. Tyrosinase-catalyzed oxidation of resveratrol produces a highly reactive ortho-quinone: Implications for melanocyte toxicity. Pigment Cell Melanoma Res. 32, 766–776. https://doi.org/10.1111/pcmr.12808

Izumikawa, M., Shipley, P.R., Hopke, J.N., O′Hare, T., Xiang, L., Noel, J.P., Moore, B.S., 2003. Expression and characterization of the type III polyketide synthase 1,3,6,8-tetrahydroxynaphthalene synthase from Streptomyces coelicolor A3(2). J. Ind. Microbiol. Biotechnol. 30, 510–515. https://doi.org/10.1007/s10295-003-0075-8

Jamshidzadeh, A., Baghban, M., Azarpira, N., Bardbori, A.M., Niknahad, H., 2008. Effects of tomato extract on oxidative stress induced toxicity in different organs of rats. Food Chem. Toxicol. 46, 3612–3615. https://doi.org/10.1016/j.fct.2008.09.006

Jarosova, V., Vesely, O., Doskocil, I., Tomisova, K., Marsik, P., Jaimes, J.D., Smejkal, K., Kloucek, P., Havlik, J., 2020. Metabolism of cis- and trans-Resveratrol and Dihydroresveratrol in an Intestinal Epithelial Model. Nutrients 12, 595. https://doi.org/10.3390/nu12030595

Jarosova, V., Vesely, O., Marsik, P., Jaimes, J.D., Smejkal, K., Kloucek, P., Havlik, J., 2019. Metabolism of Stilbenoids by Human Faecal Microbiota. Molecules 24, 1155. https://doi.org/10.3390/molecules24061155

Jeandet, P., Delaunois, B., Conreux, A., Donnez, D., Nuzzo, V., Cordelier, S., Clément, C., Courot, E., 2010. Biosynthesis, metabolism, molecular engineering, and biological functions of stilbene phytoalexins in plants. BioFactors 36, 331–341. https://doi.org/10.1002/biof.108

Jeandet, P., Sobarzo-Sánchez, E., Uddin, Md.S., Bru, R., Clément, C., Jacquard, C., Nabavi, S.F., Khayatkashani, M., Batiha, G.E.-S., Khan, H., Morkunas, I., Trotta,

F., Matencio, A., Nabavi, S.M., 2021. Resveratrol and cyclodextrins, an easy alliance: Applications in nanomedicine, green chemistry and biotechnology. Biotechnol. Adv. 107844. https://doi.org/10.1016/j.biotechadv.2021.107844

Jeong, Y.J., An, C.H., Woo, S.G., Jeong, H.J., Kim, Y.-M., Park, S.-J., Yoon, B.D., Kim, C.Y., 2014. Production of pinostilbene compounds by the expression of resveratrol O-methyltransferase genes in Escherichia coli. Enzyme Microb. Technol. 54, 8–14. https://doi.org/10.1016/j.enzmictec.2013.09.005

Jinadatta, P., Rajshekarappa, S., Sundera Raja Rao, K., Pasura Subbaiah, S.G., Shastri, S., 2019. In silico, in vitro: antioxidant and antihepatotoxic activity of gnetol from Gnetum ula Brongn. BioImpacts BI 9, 239–249. https://doi.org/10.15171/bi.2019.29

Jo, S.-P., Kim, J.-K., Lim, Y.-H., 2014. Antihyperlipidemic Effects of Rhapontin and Rhapontigenin from Rheum undulatum in Rats Fed a High-Cholesterol Diet. Planta Med. 80, 1067–1071. https://doi.org/10.1055/s-0034-1382999

Jo, Y.-J., Cho, H.-S., Chun, J.-Y., 2021. Antioxidant activity of β-cyclodextrin inclusion complexes containing trans-cinnamaldehyde by DPPH, ABTS and FRAP. Food Sci. Biotechnol. 30, 807–814. https://doi.org/10.1007/s10068-021-00914-y

Jullian, C., Orosteguis, T., Pérez-Cruz, F., Sánchez, P., Mendizabal, F., Olea-Azar, C., 2008. Complexation of morin with three kinds of cyclodextrin: A thermodynamic and reactivity study. Spectrochim. Acta. A. Mol. Biomol. Spectrosc. 71, 269–275. https://doi.org/10.1016/j.saa.2007.12.020

Jung, D.-B., Lee, Hyo-Jeong, Jeong, S.-J., Lee, Hyo-Jung, Lee, E.-O., Kim, Y.C., Ahn, K.S., Chen, C.-Y., Kim, S.-H., 2011. Rhapontigenin inhibited hypoxia inducible factor 1 alpha accumulation and angiogenesis in hypoxic PC-3 prostate cancer cells. Biol. Pharm. Bull. 34, 850–855. https://doi.org/10.1248/bpb.34.850

Jung, K.-H., Lee, J.H., Park, J.W., Quach, C.H.T., Moon, S.-H., Cho, Y.S., Lee, K.-H., 2015. Resveratrol-loaded polymeric nanoparticles suppress glucose metabolism and tumor growth in vitro and in vivo. Int. J. Pharm. 478, 251–257. https://doi.org/10.1016/j.ijpharm.2014.11.049

Kaldas, M.I., Walle, U.K., Walle, T., 2003. Resveratrol transport and metabolism by human intestinal Caco-2 cells. J. Pharm. Pharmacol. 55, 307–312. https://doi.org/10.1211/002235702612

Kallscheuer, N., Vogt, M., Stenzel, A., Gätgens, J., Bott, M., Marienhagen, J., 2016. Construction of a *Corynebacterium glutamicum* platform strain for the production of stilbenes and (2*S*)-flavanones. Metab. Eng. 38, 47–55. https://doi.org/10.1016/j.ymben.2016.06.003

Katsuyama, Y., Funa, N., Miyahisa, I., Horinouchi, S., 2007. Synthesis of Unnatural Flavonoids and Stilbenes by Exploiting the Plant Biosynthetic Pathway in *Escherichia coli*. Chem. Biol. 14, 613–621. https://doi.org/10.1016/j.chembiol.2007.05.004

Kershaw, J., Kim, K.-H., 2017. The Therapeutic Potential of Piceatannol, a Natural Stilbene, in Metabolic Diseases: A Review. J. Med. Food 20, 427–438. https://doi.org/10.1089/jmf.2017.3916

Kfoury, M., Geagea, C., Ruellan, S., Greige-Gerges, H., Fourmentin, S., 2019. Effect of cyclodextrin and cosolvent on the solubility and antioxidant activity of caffeic acid. Food Chem. 278, 163–169. https://doi.org/10.1016/j.foodchem.2018.11.055

Kim, H., Seo, K.-H., Yokoyama, W., 2020. Chemistry of pterostilbene and its metabolic effects. J. Agric. Food Chem. https://doi.org/10.1021/acs.jafc.0c00070

Kim, S.M., Kim, S.Z., 2018. Biological Activities of Resveratrol against Cancer. J Phys Chem Biophys 8. https://doi.org/10.4172/2161-0398.1000267

Koushki, M., Dashatan, N.A., Meshkani, R., 2018. Effect of Resveratrol Supplementation on Inflammatory Markers: A Systematic Review and Meta-analysis of Randomized Controlled Trials. Clin. Ther. 40, 1180-1192.e5. https://doi.org/10.1016/j.clinthera.2018.05.015

Krabicová, I., Appleton, S.L., Tannous, M., Hoti, G., Caldera, F., Rubin Pedrazzo, A., Cecone, C., Cavalli, R., Trotta, F., 2020. History of Cyclodextrin Nanosponges. Polymers 12, 1122. https://doi.org/10.3390/polym12051122

Kruger, N.J., 2009. The Bradford Method For Protein Quantitation, in: Walker, J.M. (Ed.), The Protein Protocols Handbook. Humana Press, Totowa, NJ, pp. 17–24. https://doi.org/10.1007/978-1-59745-198-7_4

Kurkov, S.V., Loftsson, T., 2013. Cyclodextrins. Int. J. Pharm., Poorly Soluble Drugs 453, 167–180. https://doi.org/10.1016/j.ijpharm.2012.06.055

Lasa, A., Schweiger, M., Kotzbeck, P., Churruca, I., Simón, E., Zechner, R., Portillo, M. del P., 2012. Resveratrol regulates lipolysis via adipose triglyceride lipase. J. Nutr. Biochem. 23, 379–384. https://doi.org/10.1016/j.jnutbio.2010.12.014

Latva-Mäenpää, H., Wufu, R., Mulat, D., Sarjala, T., Saranpää, P., Wähälä, K., 2021. Stability and Photoisomerization of Stilbenes Isolated from the Bark of Norway Spruce Roots. Molecules 26, 1036. https://doi.org/10.3390/molecules26041036

Laura, R., Franceschetti, M., Ferri, M., Tassoni, A., Bagni, N., 2007. Resveratrol production in Vitis viniferacell suspensions treated with several elicitors. Caryologia 60, 169–171. https://doi.org/10.1080/00087114.2007.10589568

Lee, H.J., Kang, M.-G., Cha, H.Y., Kim, Y.M., Lim, Y., Yang, S.J., 2019. Effects of Piceatannol and Resveratrol on Sirtuins and Hepatic Inflammation in High-Fat Diet-Fed Mice. J. Med. Food 22, 833–840. https://doi.org/10.1089/jmf.2018.4261

Lee, J., Kwon, G., Park, J., Kim, J.-K., Lim, Y.-H., 2016. Brief Communication: SIR-2.1-dependent lifespan extension of Caenorhabditis elegans by oxyresveratrol and resveratrol. Exp. Biol. Med. 241, 1757–1763. https://doi.org/10.1177/1535370216650054

Lee, L.-H., Azman, A.-S., Zainal, N., Eng, S.-K., Fang, C.-M., Hong, K., Chan, K.-G., 2014. Novosphingobium malaysiense sp. nov. isolated from mangrove sediment. Int. J. Syst. Evol. Microbiol. 64, 1194–1201. https://doi.org/10.1099/ijs.0.059014-0

Lee, N., Kim, E.J., Kim, B.-G., 2012. Regioselective Hydroxylation of trans-Resveratrol via Inhibition of Tyrosinase from Streptomyces avermitilis MA4680. ACS Chem. Biol. 7, 1687–1692. https://doi.org/10.1021/cb300222b

Lee, S.-C., Lee, K.-E., Kim, J.-J., Lim, S.-H., 2005. The Effect of Cholesterol in the Liposome Bilayer on the Stabilization of Incorporated Retinol. J. Liposome Res. 15, 157–166. https://doi.org/10.1080/08982100500364131

Lee, S.H., Liu, Q., Hwang, B.Y., Lee, M.K., 2013. Inhibitory Effects of Stilbene Derivatives from Parthenocissus Tricuspidata on Adipocyte Differentiation and Pancreatic Lipase. Nat. Prod. Commun. 8, 1934578X1300801026. https://doi.org/10.1177/1934578X1300801026

Leláková, V., Šmejkal, K., Jakubczyk, K., Veselý, O., Landa, P., Václavík, J., Bobáľ, P., Pížová, H., Temml, V., Steinacher, T., Schuster, D., Granica, S., Hanáková, Z., Hošek, J., 2019. Parallel *in vitro* and *in silico* investigations into anti-inflammatory effects of non-prenylated stilbenoids. Food Chem. 285, 431–440. https://doi.org/10.1016/j.foodchem.2019.01.128

Lepak, A., Gutmann, A., Kulmer, S.T., Nidetzky, B., 2015. Creating a Water-Soluble Resveratrol-Based Antioxidant by Site-Selective Enzymatic Glucosylation. ChemBioChem 16, 1870–1874. https://doi.org/10.1002/cbic.201500284

Li, B., Huang, J., Yi, Y., Liu, S., Liu, R., Xiao, Z., Li, C., 2022. Effects of Rhapontigenin as a Novel Quorum-Sensing Inhibitor on Exoenzymes and Biofilm Formation of Pectobacterium carotovorum subsp. carotovorum and Its Application in Vegetables. Molecules 27, 8878. https://doi.org/10.3390/molecules27248878

Li, G., Zhu, Y., Zhang, Y., Lang, J., Chen, Y., Ling, W., 2013. Estimated Daily Flavonoid and Stilbene Intake from Fruits, Vegetables, and Nuts and Associations with Lipid Profiles in Chinese Adults. J. Acad. Nutr. Diet. 113, 786–794. https://doi.org/10.1016/j.jand.2013.01.018

Li, H., Chang, S.-L., Chang, T.-R., You, Y., Wang, X.-D., Wang, L.-W., Yuan, X.-F., Tan, M.-H., Wang, P.-D., Xu, P.-W., Gao, W.-B., Zhao, Q.-S., Zhao, B., 2021. Inclusion complexes of cannabidiol with β-cyclodextrin and its derivative: Physicochemical properties, water solubility, and antioxidant activity. J. Mol. Liq. 334, 116070. https://doi.org/10.1016/j.molliq.2021.116070

Li, Y., Shin, Y.G., Yu, C., Kosmeder, J.W., Hirschelman, W.H., Pezzuto, J.M., van Breemen, R.B., 2003. Increasing the Throughput and Productivity of Caco-2 Cell Permeability Assays Using Liquid Chromatography-Mass Spectrometry: Application to Resveratrol Absorption and Metabolism. Comb. Chem. High Throughput Screen. 6, 757–767. https://doi.org/10.2174/138620703771826865

Li, Y.-Q., Li, Z.-L., Zhao, W.-J., Wen, R.-X., Meng, Q.-W., Zeng, Y., 2006. Synthesis of stilbene derivatives with inhibition of SARS coronavirus replication. Eur. J. Med. Chem. 41, 1084–1089. https://doi.org/10.1016/j.ejmech.2006.03.024

Likhitwitayawuid, K., 2021. Oxyresveratrol: Sources, Productions, Biological Activities, Pharmacokinetics, and Delivery Systems. Molecules 26, 4212. https://doi.org/10.3390/molecules26144212

Likhitwitayawuid, K., Sornsute, A., Sritularak, B., Ploypradith, P., 2006. Chemical transformations of oxyresveratrol (trans-2,4,3′,5′-tetrahydroxystilbene) into a potent tyrosinase inhibitor and a strong cytotoxic agent. Bioorg. Med. Chem. Lett. 16, 5650–5653. https://doi.org/10.1016/j.bmcl.2006.08.018

Lim, C.G., Fowler, Z.L., Hueller, T., Schaffer, S., Koffas, M.A.G., 2011. High-Yield Resveratrol Production in Engineered Escherichia coli. Appl. Environ. Microbiol. 77, 3451–3460. https://doi.org/10.1128/AEM.02186-10

Lim, Y.R.I., Preshaw, P.M., Lim, L.P., Ong, M.M.A., Lin, H.-S., Tan, K.S., 2020. Pterostilbene complexed with cyclodextrin exerts antimicrobial and anti-inflammatory effects. Sci. Rep. 10, 9072. https://doi.org/10.1038/s41598-020-66031-8

Lin, W.-S., Leland, J.V., Ho, C.-T., Pan, M.-H., 2020. Occurrence, Bioavailability, Anti-inflammatory, and Anticancer Effects of Pterostilbene. J. Agric. Food Chem. 68, 12788–12799. https://doi.org/10.1021/acs.jafc.9b07860

Lipinski, C.A., Lombardo, F., Dominy, B.W., Feeney, P.J., 1997. Experimental and computational approaches to estimate solubility and permeability in drug discovery and development settings. Adv. Drug Deliv. Rev., In Vitro Models for Selection of Development Candidates 23, 3–25. https://doi.org/10.1016/S0169-409X(96)00423-1

Liu, R.H., 2003. Health benefits of fruit and vegetables are from additive and synergistic combinations of phytochemicals23. Am. J. Clin. Nutr. 78, 517S-520S. https://doi.org/10.1093/ajcn/78.3.517S

Liu, Z., Xue, L., Jia, Y., Lou, B., Yang, J., 2019. Solvation effect and binding of rhaponticin with iron: a spectroscopic and DFT/TDDFT study. RSC Adv. 9, 11281–11288. https://doi.org/10.1039/C8RA10153A

Livak, K.J., Schmittgen, T.D., 2001. Analysis of Relative Gene Expression Data Using Real-Time Quantitative PCR and the 2−ΔΔCT Method. Methods 25, 402–408. https://doi.org/10.1006/meth.2001.1262

López-Nicolás, J.M., Bru, R., Sánchez-Ferrer, A., García-Carmona, F., 1995. Use of 'soluble lipids' for biochemical processes: linoleic acid-cyclodextrin inclusion complexes in aqueous solutions. Biochem. J. 308, 151–154. https://doi.org/10.1042/bj3080151

López-Nicolás, J.M., García-Carmona, F., 2010. Effect of hydroxypropyl-β-cyclodextrin on the aggregation of (E)-resveratrol in different protonation states of the guest molecule. Food Chem. 118, 648–655. https://doi.org/10.1016/j.foodchem.2009.05.039

López-Nicolás, J.M., García-Carmona, F., 2008a. Aggregation State and pKa Values of (E)-Resveratrol As Determined by Fluorescence Spectroscopy and UV−Visible Absorption. J. Agric. Food Chem. 56, 7600–7605. https://doi.org/10.1021/jf800843e

López-Nicolás, J.M., García-Carmona, F., 2008b. Rapid, simple and sensitive determination of the apparent formation constants of trans-resveratrol complexes with natural cyclodextrins in aqueous medium using HPLC. Food Chem. 109, 868–875. https://doi.org/10.1016/j.foodchem.2008.01.022

López-Nicolás, J.M., Núñez-Delicado, E., Pérez-López, A.J., Barrachina, Á.C., Cuadra-Crespo, P., 2006. Determination of stoichiometric coefficients and apparent formation constants for β-cyclodextrin complexes of trans-resveratrol using

reversed-phase liquid chromatography. J. Chromatogr. A 1135, 158–165. https://doi.org/10.1016/j.chroma.2006.09.013

López-Nicolás, J.M., Rodríguez-Bonilla, P., García-Carmona, F., 2014. Cyclodextrins and antioxidants. Crit. Rev. Food Sci. Nutr. 54, 251–276. https://doi.org/10.1080/10408398.2011.582544

López-Nicolás, J.M., Rodríguez-Bonilla, P., García-Carmona, F., 2009a. Complexation of Pinosylvin, an Analogue of Resveratrol with High Antifungal and Antimicrobial Activity, by Different Types of Cyclodextrins. J. Agric. Food Chem. 57, 10175–10180. https://doi.org/10.1021/jf902519d

López-Nicolás, J.M., Rodríguez-Bonilla, P., Méndez-Cazorla, L., García-Carmona, F., 2009b. Physicochemical Study of the Complexation of Pterostilbene by Natural and Modified Cyclodextrins. J. Agric. Food Chem. 57, 5294–5300. https://doi.org/10.1021/jf900285e

Lu, X.-Y., Hu, S., Jin, Y., Qiu, L.-Y., 2012. Application of liposome encapsulation technique to improve anti-carcinoma effect of resveratrol. Drug Dev. Ind. Pharm. 38, 314–322. https://doi.org/10.3109/03639045.2011.602410

Lu, Y., Wang, A., Shi, P., Zhang, H., 2017. A Theoretical Study on the Antioxidant Activity of Piceatannol and Isorhapontigenin Scavenging Nitric Oxide and Nitrogen Dioxide Radicals. PLOS ONE 12, e0169773. https://doi.org/10.1371/journal.pone.0169773

Lu, Y., Wang, A., Shi, P., Zhang, H., Li, Z., 2015. Quantum Chemical Study on the Antioxidation Mechanism of Piceatannol and Isorhapontigenin toward Hydroxyl and Hydroperoxyl Radicals. PLOS ONE 10, e0133259. https://doi.org/10.1371/journal.pone.0133259

Lu, Z., Cheng, B., Hu, Y., Zhang, Y., Zou, G., 2009. Complexation of resveratrol with cyclodextrins: Solubility and antioxidant activity. Food Chem. 113, 17–20. https://doi.org/10.1016/j.foodchem.2008.04.042

Lucas-Abellán, C., Fortea, I., López-Nicolás, J.M., Núñez-Delicado, E., 2007. Cyclodextrins as resveratrol carrier system. Food Chem. 104, 39–44. https://doi.org/10.1016/j.foodchem.2006.10.068

Lucas-Abellán, C., Mercader-Ros, M.T., Zafrilla, M.P., Fortea, M.I., Gabaldón, J.A., Núñez-Delicado, E., 2008. ORAC-Fluorescein Assay To Determine the Oxygen Radical Absorbance Capacity of Resveratrol Complexed in Cyclodextrins. J. Agric. Food Chem. 56, 2254–2259. https://doi.org/10.1021/jf0731088

Lucas-Abellán, C., Mercader-Ros, M.T., Zafrilla, M.P., Gabaldón, J.A., Núñez-Delicado, E., 2011. Comparative study of different methods to measure antioxidant activity of resveratrol in the presence of cyclodextrins. Food Chem. Toxicol. 49, 1255–1260. https://doi.org/10.1016/j.fct.2011.03.004

Luo, G., Shi, Z., Wang, H., Wang, G., 2012. Skermanella stibiiresistens sp. nov., a highly antimony-resistant bacterium isolated from coal-mining soil, and emended description of the genus Skermanella. Int. J. Syst. Evol. Microbiol. 62, 1271–1276. https://doi.org/10.1099/ijs.0.033746-0

Luo, Y., Tian, Z., Hua, X., Huang, M., Xu, J., Li, J., Huang, H., Cohen, M., Huang, C., 2020. Isorhapontigenin (ISO) inhibits stem cell-like properties and invasion of bladder cancer cell by attenuating CD44 expression. Cell. Mol. Life Sci. 77, 351–363. https://doi.org/10.1007/s00018-019-03185-3

Ma, Y., Tu, C., Liu, W., Xiao, Y., Wu, H., 2019. Isorhapontigenin Suppresses Interleukin-1β-Induced Inflammation and Cartilage Matrix Damage in Rat Chondrocytes. Inflammation 42, 2278–2285. https://doi.org/10.1007/s10753-019-01092-0

Maafi, M., Al-Qarni, M.A., 2018. Φ-order spectrophotokinetic characterisation and quantification of trans-cis oxyresveratrol reactivity, photodegradation and actinometry. Spectrochim. Acta. A. Mol. Biomol. Spectrosc. 188, 64–71. https://doi.org/10.1016/j.saa.2017.06.067

Maianu, L., Keller, S.R., Garvey, W.T., 2001. Adipocytes Exhibit Abnormal Subcellular Distribution and Translocation of Vesicles Containing Glucose Transporter 4 and Insulin-Regulated Aminopeptidase in Type 2 Diabetes Mellitus: Implications Regarding Defects in Vesicle Trafficking. J. Clin. Endocrinol. Metab. 86, 5450–5456. https://doi.org/10.1210/jcem.86.11.8053

Maier-Salamon, A., Hagenauer, B., Wirth, M., Gabor, F., Szekeres, T., Jäger, W., 2006. Increased Transport of Resveratrol Across Monolayers of the Human Intestinal Caco-2 Cells is Mediated by Inhibition and Saturation of Metabolites. Pharm. Res. 23, 2107–2115. https://doi.org/10.1007/s11095-006-9060-z

Malodobra-Mazur, M., Cierzniak, A., Dobosz, T., 2019. Oleic acid influences the adipogenesis of 3T3-L1 cells via DNA Methylation and may predispose to obesity and obesity-related disorders. Lipids Health Dis. 18, 230. https://doi.org/10.1186/s12944-019-1173-6

Matencio, A., Caldera, F., Cecone, C., López-Nicolás, J.M., Trotta, F., 2020a. Cyclic Oligosaccharides as Active Drugs, an Updated Review. Pharmaceuticals 13, 281. https://doi.org/10.3390/ph13100281

Matencio, A., Dhakar, N.K., Bessone, F., Musso, G., Cavalli, R., Dianzani, C., García-Carmona, F., López-Nicolás, J.M., Trotta, F., 2020b. Study of oxyresveratrol complexes with insoluble cyclodextrin based nanosponges: Developing a novel way to obtain their complexation constants and application in an anticancer study. Carbohydr. Polym. 231, 115763. https://doi.org/10.1016/j.carbpol.2019.115763

Matencio, A., García-Carmona, F., López-Nicolás, J.M., 2017a. The inclusion complex of oxyresveratrol in modified cyclodextrins: A thermodynamic, structural, physicochemical, fluorescent and computational study. Food Chem. 232, 177–184. https://doi.org/10.1016/j.foodchem.2017.04.027

Matencio, A., García-Carmona, F., López-Nicolás, J.M., 2016. Encapsulation of piceatannol, a naturally occurring hydroxylated analogue of resveratrol, by natural and modified cyclodextrins. Food Funct. 7, 2367–2373. https://doi.org/10.1039/C6FO00557H

Matencio, A., Guerrero-Rubio, M.A., Caldera, F., Cecone, C., Trotta, F., García-Carmona, F., López-Nicolás, J.M., 2020c. Lifespan extension in *Caenorhabditis elegans* by oxyresveratrol supplementation in hyper-branched cyclodextrin-based nanosponges. Int. J. Pharm. 589, 119862. https://doi.org/10.1016/j.ijpharm.2020.119862

Matencio, A., Hernández-García, S., García-Carmona, F., Manuel López-Nicolás, J., 2017b. An integral study of cyclodextrins as solubility enhancers of α-methylstilbene, a resveratrol analogue. Food Funct. 8, 270–277. https://doi.org/10.1039/C6FO01677D

Matencio, A., Hoti, G., Monfared, Y.K., Rezayat, A., Pedrazzo, A.R., Caldera, F., Trotta, F., 2021. Cyclodextrin Monomers and Polymers for Drug Activity Enhancement. Polymers 13, 1684. https://doi.org/10.3390/polym13111684

Matencio, A., Navarro-Orcajada, S., Conesa, I., Muñoz-Sánchez, I., Laveda-Cano, L., Cano-Yelo, D., García-Carmona, F., López-Nicolás, J.M., 2020d. Evaluation of juice and milk “food models” fortified with oxyresveratrol and β-Cyclodextrin. Food Hydrocoll. 98, 105250. https://doi.org/10.1016/j.foodhyd.2019.105250

Matencio, A., Navarro-Orcajada, S., García-Carmona, F., López-Nicolás, J.M., 2018. Ellagic acid–borax fluorescence interaction: application for novel cyclodextrin-borax nanosensors for analyzing ellagic acid in food samples. Food Funct. 9, 3683–3687. https://doi.org/10.1039/C8FO00906F

Matencio, A., Navarro-Orcajada, S., González-Ramón, A., García-Carmona, F., López-Nicolás, J.M., 2020e. Recent advances in the treatment of niemann pick disease type c: a mini-review. Int. J. Pharm. 119440. https://doi.org/10.1016/j.ijpharm.2020.119440

Matsui, Y., Mochida, K., 1979. Binding Forces Contributing to the Association of Cyclodextrin with Alcohol in an Aqueous Solution. Bull. Chem. Soc. Jpn. 52, 2808–2814. https://doi.org/10.1246/bcsj.52.2808

Mattio, L., Catinella, G., Iriti, M., Vallone, L., 2021. Inhibitory activity of stilbenes against filamentous fungi. Ital. J. Food Saf. 10, 8461. https://doi.org/10.4081/ijfs.2021.8461

Mehlem, A., Hagberg, C.E., Muhl, L., Eriksson, U., Falkevall, A., 2013. Imaging of neutral lipids by oil red O for analyzing the metabolic status in health and disease. Nat. Protoc. 8, 1149–1154. https://doi.org/10.1038/nprot.2013.055

Messiad, H., Amira-Guebailia, H., Houache, O., 2013. Reversed phase High Performance Liquid Chromatography used for the physicochemical and thermodynamic characterization of piceatannol/β-cyclodextrin complex. J. Chromatogr. B 926, 21–27. https://doi.org/10.1016/j.jchromb.2013.02.024

Mika, A., Sledzinski, T., 2017. Alterations of specific lipid groups in serum of obese humans: a review. Obes. Rev. 18, 247–272. https://doi.org/10.1111/obr.12475

Mikstacka, R., Przybylska, D., Rimando, A.M., Baer-Dubowska, W., 2007. Inhibition of human recombinant cytochromes P450 CYP1A1 and CYP1B1 by trans-

resveratrol methyl ethers. Mol. Nutr. Food Res. 51, 517–524. https://doi.org/10.1002/mnfr.200600135

Miller, N.J., Rice-Evans, C., Davies, M.J., Gopinathan, V., Milner, A., 1993. A novel method for measuring antioxidant capacity and its application to monitoring the antioxidant status in premature neonates. Clin. Sci. Lond. Engl. 84, 407–412. https://doi.org/10.1042/cs0840407

Mohseni, R.M., Hurtubise, R.J., 1990. Retention characteristics of several compound classes in reversed-phase liquid chromatography with β-cyclodextrin as a mobile phase modifier. J. Chromatogr. A 499, 395–410. https://doi.org/10.1016/S0021-9673(00)96987-5

Monfared, Y.K., Mahmoudian, M., Hoti, G., Bisericaru, D.M., Caldera, F., Cavalli, R., Zakeri-Milani, P., Matencio, A., Trotta, F., 2022. Hyper-Branched Cyclodextrin-Based Polymers as Anticoagulant Agents: In Vitro and In Vivo Studies. Bioengineering 9, 765. https://doi.org/10.3390/bioengineering9120765

Morales, M., Barcelo, A., Pedreño, M., 2000. Plant stilbenes: Recent advances in their chemistry and biology. Adv Plant Physiol 3, 39–70.

Moran, B.W., Anderson, F.P., Devery, A., Cloonan, S., Butler, W.E., Varughese, S., Draper, S.M., Kenny, P.T.M., 2009. Synthesis, structural characterisation and biological evaluation of fluorinated analogues of resveratrol. Bioorg. Med. Chem. 17, 4510–4522. https://doi.org/10.1016/j.bmc.2009.05.007

Morton, N.M., Beltram, J., Carter, R.N., Michailidou, Z., Gorjanc, G., McFadden, C., Barrios-Llerena, M.E., Rodriguez-Cuenca, S., Gibbins, M.T.G., Aird, R.E., Moreno-Navarrete, J.M., Munger, S.C., Svenson, K.L., Gastaldello, A., Ramage, L., Naredo, G., Zeyda, M., Wang, Z.V., Howie, A.F., Saari, A., Sipilä, P., Stulnig, T.M., Gudnason, V., Kenyon, C.J., Seckl, J.R., Walker, B.R., Webster, S.P.,

Dunbar, D.R., Churchill, G.A., Vidal-Puig, A., Fernandez-Real, J.M., Emilsson, V., Horvat, S., 2016. Genetic identification of thiosulfate sulfurtransferase as an adipocyte-expressed antidiabetic target in mice selected for leanness. Nat. Med. 22, 771–779. https://doi.org/10.1038/nm.4115

Moussa, R., Sevastre, B., Taulescu, M., Bolfă, P., Gal, A., Marcus, I., Rus, V., Tăbăran, F., Nagy, A., Catoi, C., 2009. Expression of the Vascular Marker CD31 in Dog Cutaneous Melanoma. Bull. Univ. Agric. Sci. Vet. Med. Cluj-Napoca Vet. Med.

Msaddak, A., Rejili, M., Durán, D., Rey, L., Imperial, J., Palacios, J.M., Ruiz-Argüeso, T., Mars, M., 2017. Members of Microvirga and Bradyrhizobium genera are native endosymbiotic bacteria nodulating Lupinus luteus in Northern Tunisian soils. FEMS Microbiol. Ecol. 93, fix068. https://doi.org/10.1093/femsec/fix068

Münzberg, H., Morrison, C.D., 2015. Structure, production and signaling of leptin. Metab. - Clin. Exp. 64, 13–23. https://doi.org/10.1016/j.metabol.2014.09.010

Murias, M., Handler, N., Erker, T., Pleban, K., Ecker, G., Saiko, P., Szekeres, T., Jäger, W., 2004. Resveratrol analogues as selective cyclooxygenase-2 inhibitors: synthesis and structure–activity relationship. Bioorg. Med. Chem. 12, 5571–5578. https://doi.org/10.1016/j.bmc.2004.08.008

Murias, M., Jäger, W., Handler, N., Erker, T., Horvath, Z., Szekeres, T., Nohl, H., Gille, L., 2005. Antioxidant, prooxidant and cytotoxic activity of hydroxylated resveratrol analogues: structure–activity relationship. Biochem. Pharmacol. 69, 903–912. https://doi.org/10.1016/j.bcp.2004.12.001

Narita, Y., Iwai, K., Fukunaga, T., Nakagiri, O., 2012. Inhibitory activity of chlorogenic acids in decaffeinated green coffee beans against porcine pancreas lipase and effect of a decaffeinated green coffee bean extract on an emulsion of olive oil. Biosci. Biotechnol. Biochem. 76, 2329–2331. https://doi.org/10.1271/bbb.120518

Nguyen, A.V., Martinez, M., Stamos, M.J., Moyer, M.P., Planutis, K., Hope, C., Holcombe, R.F., 2009. Results of a phase I pilot clinical trial examining the effect of plant-derived resveratrol and grape powder on Wnt pathway target gene expression in colonic mucosa and colon cancer. Cancer Manag. Res. 1, 25–37.

Nicolosi, G., Spatafora, C., Tringali, C., 2002. Chemo-enzymatic preparation of resveratrol derivatives. J. Mol. Catal. B Enzym. 16, 223–229. https://doi.org/10.1016/S1381-1177(01)00066-2

Nogueiras, R., Habegger, K.M., Chaudhary, N., Finan, B., Banks, A.S., Dietrich, M.O., Horvath, T.L., Sinclair, D.A., Pfluger, P.T., Tschöp, M.H., 2012. Sirtuin 1 and Sirtuin 3: Physiological Modulators of Metabolism. Physiol. Rev. 92, 1479–1514. https://doi.org/10.1152/physrev.00022.2011

Nutakul, W., Sobers, H.S., Qiu, P., Dong, P., Decker, E.A., McClements, D.J., Xiao, H., 2011. Inhibitory Effects of Resveratrol and Pterostilbene on Human Colon Cancer Cells: A Side-by-Side Comparison. J. Agric. Food Chem. 59, 10964–10970. https://doi.org/10.1021/jf202846b

Oh, W.Y., Chiou, Y.-S., Pan, M.-H., Shahidi, F., 2019. Lipophilised resveratrol affects the generation of reactive nitrogen species in murine macrophages and cell viability of human cancer cell lines. J. Food Bioact. 7. https://doi.org/10.31665/JFB.2019.7201

Oh, W.Y., Gao, Y., Shahidi, F., 2021. Stilbenoids: chemistry, occurrence, bioavailability and health effects—a review. J. Food Bioact. 13. https://doi.org/10.31665/JFB.2020.13256

Oh, W.Y., Shahidi, F., 2018. Antioxidant activity of resveratrol ester derivatives in food and biological model systems. Food Chem. 261, 267–273. https://doi.org/10.1016/j.foodchem.2018.03.085

Oh, W.Y., Shahidi, F., 2017. Lipophilization of Resveratrol and Effects on Antioxidant Activities. J. Agric. Food Chem. 65, 8617–8625. https://doi.org/10.1021/acs.jafc.7b03129

Omidian, M., Abdolahi, M., Daneshzad, E., Sedighiyan, M., Aghasi, M., Abdollahi, H., Omidian, P., Dabiri, S., Mahmoudi, M., 2020. The Effects of Resveratrol on Oxidative Stress Markers: A Systematic Review and Meta-Analysis of Randomized Clinical Trials. Endocr. Metab. Immune Disord. - Drug TargetsFormerly Curr. Drug Targets - Immune Endocr. Metab. Disord. 20, 718–727. https://doi.org/10.2174/1871530319666191116112950

Omraninava, M., Razi, B., Aslani, S., Imani, D., Jamialahmadi, T., Sahebkar, A., 2021. Effect of resveratrol on inflammatory cytokines: A meta-analysis of randomized controlled trials. Eur. J. Pharmacol. 908, 174380. https://doi.org/10.1016/j.ejphar.2021.174380

Orgován, G., Gonda, I., Noszál, B., 2017. Biorelevant physicochemical profiling of (E)- and (Z)-resveratrol determined from isomeric mixtures. J. Pharm. Biomed. Anal. 138, 322–329. https://doi.org/10.1016/j.jpba.2016.09.019

Otręba, M., Kośmider, L., Stojko, J., Rzepecka-Stojko, A., 2020. Cardioprotective Activity of Selected Polyphenols Based on Epithelial and Aortic Cell Lines. A Review. Molecules 25, 5343. https://doi.org/10.3390/molecules25225343

Paglia, D.E., Valentine, W.N., 1967. Studies on the quantitative and qualitative characterization of erythrocyte glutathione peroxidase. J. Lab. Clin. Med. 70, 158–169. https://doi.org/10.5555/uri:pii:0022214367900765

Paller, C., Rudek, M., Zhou, X., Wagner, W., Hudson, T., Anders, N., Hammers, H., Dowling, D., King, S., Antonarakis, E., Drake, C., Eisenberger, M., Denmeade, S., Rosner, G., Carducci, M., 2015. A Phase I Study of Muscadine Grape Skin

Extract in Men with Biochemically Recurrent Prostate Cancer: Safety, Tolerability, and Dose Determination. The Prostate 75, 1518–1525. https://doi.org/10.1002/pros.23024

Palm, K., Luthman, K., Unge, A.-L., Strandlund, G., Artursson, P., 1996. Correlation of Drug Absorption with Molecular Surface Properties. J. Pharm. Sci. 85, 32–39. https://doi.org/10.1021/js950285r

Palm, K., Luthman, K., Ungell, A.-L., Strandlund, G., Beigi, F., Lundahl, P., Artursson, P., 1998. Evaluation of Dynamic Polar Molecular Surface Area as Predictor of Drug Absorption: Comparison with Other Computational and Experimental Predictors. J. Med. Chem. 41, 5382–5392. https://doi.org/10.1021/jm980313t

Pany, S., Majhi, A., Das, J., 2012. PKC Activation by Resveratrol Derivatives with Unsaturated Aliphatic Chain. PLOS ONE 7, e52888. https://doi.org/10.1371/journal.pone.0052888

Papuc, C., Goran, G.V., Predescu, C.N., Nicorescu, V., Stefan, G., 2017. Plant Polyphenols as Antioxidant and Antibacterial Agents for Shelf-Life Extension of Meat and Meat Products: Classification, Structures, Sources, and Action Mechanisms. Compr. Rev. Food Sci. Food Saf. 16, 1243–1268. https://doi.org/10.1111/1541-4337.12298

Park, D.-S., Jeong, W.-J., Lee, K.H., Oh, H.-W., Kim, B.-C., Bae, K.S., Park, H.-Y., 2009. Paenibacillus pectinilyticus sp. nov., isolated from the gut of Diestrammena apicalis. Int. J. Syst. Evol. Microbiol. 59, 1342–1347. https://doi.org/10.1099/ijs.0.002261-0

Park, J., Park, J.H., Suh, H.J., Lee, I.C., Koh, J., Boo, Y.C., 2014. Effects of resveratrol, oxyresveratrol, and their acetylated derivatives on cellular melanogenesis. Arch. Dermatol. Res. 306, 475–487. https://doi.org/10.1007/s00403-014-1440-3

Passaro, C., Borriello, F., Vastolo, V., Somma, S.D., Scamardella, E., Gigantino, V., Franco, R., Marone, G., Portella, G., 2015. The oncolytic virus dl 922-947 reduces IL-8/CXCL8 and MCP-1/CCL2 expression and impairs angiogenesis and macrophage infiltration in anaplastic thyroid carcinoma. Oncotarget 7, 1500–1515. https://doi.org/10.18632/oncotarget.6430

Patel, K.R., Brown, V.A., Jones, D.J., Britton, R.G., Hemingway, D., Miller, A.S., West, K.P., Booth, T.D., Perloff, M., Crowell, J.A., Brenner, D.E., Steward, W.P., Gescher, A.J., Brown, K., 2010. Clinical Pharmacology of Resveratrol and its Metabolites in Colorectal Cancer Patients. Cancer Res. 70, 7392–7399. https://doi.org/10.1158/0008-5472.CAN-10-2027

Paul, S., Mizuno, C.S., Lee, H.J., Zheng, X., Chajkowisk, S., Rimoldi, J.M., Conney, A., Suh, N., Rimando, A.M., 2010. In vitro and in vivo studies on stilbene analogs as potential treatment agents for colon cancer. Eur. J. Med. Chem. 45, 3702–3708. https://doi.org/10.1016/j.ejmech.2010.05.019

Pecyna, P., Wargula, J., Murias, M., Kucinska, M., 2020. More Than Resveratrol: New Insights into Stilbene-Based Compounds. Biomolecules 10, 1111. https://doi.org/10.3390/biom10081111

Peng, H., Shahidi, F., 2022. The Effects of Acyl Chain Length on Antioxidant Efficacy of Mono- and Multi-Acylated Resveratrol: A Comparative Assessment. Molecules 27, 1001. https://doi.org/10.3390/molecules27031001

Pokorski, M., Marczak, M., Dymecka, A., Suchocki, P., 2003. Ascorbyl palmitate as a carrier of ascorbate into neural tissues. J. Biomed. Sci. 10, 193–198. https://doi.org/10.1007/BF02256054

Pollastri, M.P., 2010. Overview on the Rule of Five. Curr. Protoc. Pharmacol. 49, 9.12.1-9.12.8. https://doi.org/10.1002/0471141755.ph0912s49

Prior, R.L., Hoang, H., Gu, L., Wu, X., Bacchiocca, M., Howard, L., Hampsch-Woodill, M., Huang, D., Ou, B., Jacob, R., 2003. Assays for Hydrophilic and Lipophilic Antioxidant Capacity (oxygen radical absorbance capacity (ORACFL)) of Plasma and Other Biological and Food Samples. J. Agric. Food Chem. 51, 3273–3279. https://doi.org/10.1021/jf0262256

Rao, V., 2012. Phytochemicals - A Global Perspective of Their Role in Nutrition and Health. InTech. https://doi.org/10.5772/1387

Rastogi, H., Jana, S., 2016. Evaluation of physicochemical properties and intestinal permeability of six dietary polyphenols in human intestinal colon adenocarcinoma Caco-2 cells. Eur. J. Drug Metab. Pharmacokinet. 41, 33–43. https://doi.org/10.1007/s13318-014-0234-5

Rauf, A., Imran, M., Butt, M.S., Nadeem, M., Peters, D.G., Mubarak, M.S., 2018. Resveratrol as an anti-cancer agent: A review. Crit. Rev. Food Sci. Nutr. 58, 1428–1447. https://doi.org/10.1080/10408398.2016.1263597

Ravishankar, D., Albadawi, D.A.I., Chaggar, V., Patra, P.H., Williams, H.F., Salamah, M., Vaiyapuri, R., Dash, P.R., Patel, K., Watson, K.A., Vaiyapuri, S., 2019. Isorhapontigenin, a resveratrol analogue selectively inhibits ADP-stimulated platelet activation. Eur. J. Pharmacol. 862, 172627. https://doi.org/10.1016/j.ejphar.2019.172627

Regev-Shoshani, G., Shoseyov, O., Bilkis, I., Kerem, Z., 2003. Glycosylation of resveratrol protects it from enzymic oxidation. Biochem. J. 374, 157–163. https://doi.org/10.1042/bj20030141

Repetto, G., del Peso, A., Zurita, J.L., 2008. Neutral red uptake assay for the estimation of cell viability/cytotoxicity. Nat. Protoc. 3, 1125–1131. https://doi.org/10.1038/nprot.2008.75

Rhayem, Y., Thérond, P., Camont, L., Couturier, M., Beaudeux, J.-L., Legrand, A., Jore, D., Gardés-Albert, M., Bonnefont-Rousselot, D., 2008. Chain-breaking activity of resveratrol and piceatannol in a linoleate micellar model. Chem. Phys. Lipids 155, 48–56. https://doi.org/10.1016/j.chemphyslip.2008.06.001

Rivière, C., Pawlus, A.D., Mérillon, J.-M., 2012. Natural stilbenoids: distribution in the plant kingdom and chemotaxonomic interest in Vitaceae. Nat. Prod. Rep. 29, 1317–1333. https://doi.org/10.1039/C2NP20049J

Rodríguez-Bonilla, P., Gandía-Herrero, F., Matencio, A., García-Carmona, F., López-Nicolás, J.M., 2017. Comparative Study of the Antioxidant Capacity of Four Stilbenes Using ORAC, ABTS+, and FRAP Techniques. Food Anal. Methods 10, 2994–3000. https://doi.org/10.1007/s12161-017-0871-9

Rodríguez-Bonilla, P., López-Nicolás, J.M., García-Carmona, F., 2010. Use of reversed phase high pressure liquid cromatography for the physicochemical and thermodynamic characterization of oxyresveratrol/β-cyclodextrin complexes. J. Chromatogr. B 878, 1569–1575. https://doi.org/10.1016/j.jchromb.2010.04.016

Rodriguez-Casado, A., 2016. The Health Potential of Fruits and Vegetables Phytochemicals: Notable Examples. Crit. Rev. Food Sci. Nutr. 56, 1097–1107. https://doi.org/10.1080/10408398.2012.755149

Rodríguez-Díaz, M., Lebbe, L., Rodelas, B., Heyrman, J., De Vos, P., Logan, N.A., 2005. Paenibacillus wynnii sp. nov., a novel species harbouring the nifH gene, isolated from Alexander Island, Antarctica. Int. J. Syst. Evol. Microbiol. 55, 2093–2099. https://doi.org/10.1099/ijs.0.63395-0

Ros, J.R., Rodríguez-López, J.N., García-Cánovas, F., 1993. Effect of l-ascorbic acid on the monophenolase activity of tyrosinase. Biochem. J. 295, 309–312. https://doi.org/10.1042/bj2950309

Rossi, M., Caruso, F., Opazo, C., Salciccioli, J., 2008. Crystal and Molecular Structure of Piceatannol; Scavenging Features of Resveratrol and Piceatannol on Hydroxyl and Peroxyl Radicals and Docking with Transthyretin. J. Agric. Food Chem. 56, 10557–10566. https://doi.org/10.1021/jf801923j

Ruan, B.F., Huang, X.F., Ding, H., Xu, C., Ge, H.M., Zhu, H.L., Tan, R.-X., 2006. Synthesis and Cytotoxic Evaluation of a Series of Resveratrol Derivatives. Chem. Biodivers. 3, 975–981. https://doi.org/10.1002/cbdv.200690106

Rubiolo, J.A., Mithieux, G., Vega, F.V., 2008. Resveratrol protects primary rat hepatocytes against oxidative stress damage:: Activation of the Nrf2 transcription factor and augmented activities of antioxidant enzymes. Eur. J. Pharmacol. 591, 66–72. https://doi.org/10.1016/j.ejphar.2008.06.067

Sák, M., Dokupilová, I., Kaňuková, Š., Mrkvová, M., Mihálik, D., Hauptvogel, P., Kraic, J., 2021. Biotic and Abiotic Elicitors of Stilbenes Production in Vitis vinifera L. Cell Culture. Plants 10, 490. https://doi.org/10.3390/plants10030490

Sánchez-Fidalgo, S., Cárdeno, A., Villegas, I., Talero, E., de la Lastra, C.A., 2010. Dietary supplementation of resveratrol attenuates chronic colonic inflammation in mice. Eur. J. Pharmacol. 633, 78–84. https://doi.org/10.1016/j.ejphar.2010.01.025

Sarabia-Vallejo, Á., Caja, M. del M., Olives, A.I., Martín, M.A., Menéndez, J.C., 2023. Cyclodextrin Inclusion Complexes for Improved Drug Bioavailability and Activity: Synthetic and Analytical Aspects. Pharmaceutics 15, 2345. https://doi.org/10.3390/pharmaceutics15092345

Savic, I.M., Jocic, E., Nikolic, V.D., Popsavin, M.M., Rakic, S.J., Savic-Gajic, I.M., 2019. The effect of complexation with cyclodextrins on the antioxidant and antimicrobial activity of ellagic acid. Pharm. Dev. Technol. 24, 410–418. https://doi.org/10.1080/10837450.2018.1502318

Scapagnini, G., Davinelli, S., Kaneko, T., Koverech, G., Koverech, A., Calabrese, E.J., Calabrese, V., 2014. Dose response biology of resveratrol in obesity. J. Cell Commun. Signal. 8, 385–391. https://doi.org/10.1007/s12079-014-0257-3

Scheideler, M., Herzig, S., 2017. Let's burn whatever you have: mitofusin 2 metabolically re-wires brown adipose tissue. EMBO Rep. 18, 1039–1040. https://doi.org/10.15252/embr.201744341

Schindelin, J., Arganda-Carreras, I., Frise, E., Kaynig, V., Longair, M., Pietzsch, T., Preibisch, S., Rueden, C., Saalfeld, S., Schmid, B., Tinevez, J.-Y., White, D.J., Hartenstein, V., Eliceiri, K., Tomancak, P., Cardona, A., 2012. Fiji: an open-source platform for biological-image analysis. Nat. Methods 9, 676–682. https://doi.org/10.1038/nmeth.2019

Seyed, M.A., Jantan, I., Bukhari, S.N.A., Vijayaraghavan, K., 2016. A Comprehensive Review on the Chemotherapeutic Potential of Piceatannol for Cancer Treatment, with Mechanistic Insights. J. Agric. Food Chem. 64, 725–737. https://doi.org/10.1021/acs.jafc.5b05993

Shen, P., Yue, Y., Kim, K.-H., Park, Y., 2017. Piceatannol Reduces Fat Accumulation in Caenorhabditis elegans. J. Med. Food 20, 887–894. https://doi.org/10.1089/jmf.2016.0179

Shen, T., Xie, C.-F., Wang, X.-N., Lou, H.-X., 2013. Stilbenoids, in: Ramawat, K.G., Mérillon, J.-M. (Eds.), Natural Products: Phytochemistry, Botany and Metabolism of Alkaloids, Phenolics and Terpenes. Springer, Berlin, Heidelberg, pp. 1901–1949. https://doi.org/10.1007/978-3-642-22144-6_63

Shi, G., Hua, M., Xu, Q., Ren, T., 2017. Resveratrol improves treatment outcome and laboratory parameters in patients with Takayasu arteritis: A randomized double-

blind and placebo-controlled trial. Immunobiology 222, 164–168. https://doi.org/10.1016/j.imbio.2016.10.008

Shi, Y., Zhao, X., Wang, C., Wang, Y., Zhang, S., Li, P., Feng, X., Jin, B., Yuan, M., Cui, S., Sun, Y., Zhang, B., Sun, S., Jin, X., Wang, H., Zhao, G., 2020. Ultrafast Nonadiabatic Photoisomerization Dynamics Mechanism for the UV Photoprotection of Stilbenoids in Grape Skin. Chem. – Asian J. 15, 1478–1483. https://doi.org/10.1002/asia.202000219

Shimoda, K., Kubota, N., Uesugi, D., Fujitaka, Y., Doi, S., Hamada, H., Kuboki, A., Kiriake, Y., Iwaki, T., Saikawa, T., Ozaki, S., 2019. Synthesis of Glycosides of Resveratrol, Pinostilbene, and Piceatannol by Bioconversion with Phytolacca americana. Nat. Prod. Commun. 14, 1934578X19868396. https://doi.org/10.1177/1934578X19868396

Shin, W.S., Han, S.H., Jo, K.W., Cho, Y., Kim, K.-T., 2023. Pinostilbene inhibits full-length and splice variant of androgen receptor in prostate cancer. Sci. Rep. 13, 16663. https://doi.org/10.1038/s41598-023-43561-5

Shomura, Y., Torayama, I., Suh, D.-Y., Xiang, T., Kita, A., Sankawa, U., Miki, K., 2005. Crystal structure of stilbene synthase from Arachis hypogaea. Proteins Struct. Funct. Bioinforma. 60, 803–806. https://doi.org/10.1002/prot.20584

Shrestha, A., Pandey, R.P., Pokhrel, A.R., Dhakal, D., Chu, L.L., Sohng, J.K., 2018. Modular pathway engineering for resveratrol and piceatannol production in engineered Escherichia coli. Appl. Microbiol. Biotechnol. 102, 9691–9706. https://doi.org/10.1007/s00253-018-9323-8

Sikorski, J., Tindall, B.J., Lowry, S., Lucas, S., Nolan, M., Copeland, A., Glavina Del Rio, T., Tice, H., Cheng, J.-F., Han, C., Pitluck, S., Liolios, K., Ivanova, N., Mavromatis, K., Mikhailova, N., Pati, A., Goodwin, L., Chen, A., Palaniappan,

K., Land, M., Hauser, L., Chang, Y.-J., Jeffries, C.D., Rohde, M., Göker, M., Woyke, T., Bristow, J., Eisen, J.A., Markowitz, V., Hugenholtz, P., Kyrpides, N.C., Klenk, H.-P., Lapidus, A., 2010. Complete genome sequence of Meiothermus silvanus type strain (VI-R2T). Stand. Genomic Sci. 3, 37–46. https://doi.org/10.4056/sigs.1042812

Silva, C.G., Monteiro, J., Marques, R.R.N., Silva, A.M.T., Martínez, C., Canle L., M., Faria, J.L., 2013. Photochemical and photocatalytic degradation of trans-resveratrol. Photochem. Photobiol. Sci. 12, 638–644. https://doi.org/10.1039/c2pp25239b

Singh, D., Mendonsa, R., Koli, M., Subramanian, M., Nayak, S.K., 2019. Antibacterial activity of resveratrol structural analogues: A mechanistic evaluation of the structure-activity relationship. Toxicol. Appl. Pharmacol. 367, 23–32. https://doi.org/10.1016/j.taap.2019.01.025

Sintuyanon, N., Phoolcharoen, W., Pavasant, P., Sooampon, S., 2017. Resveratrol Demonstrated Higher Antiproliferative and Antiangiogenic Efficacy Compared with Oxyresveratrol on Head and Neck Squamous Cell Carcinoma Cell Lines. Nat. Prod. Commun. 12, 1934578X1701201134. https://doi.org/10.1177/1934578X1701201134

Song, J., Seo, Y., Park, H., 2018. Pinosylvin enhances leukemia cell death via down-regulation of AMPKα expression. Phytother. Res. 32, 2097–2104. https://doi.org/10.1002/ptr.6156

Souza, S.M., Araújo, M.F., Silva, A.A., Moreira, M.R.A., Zoccal, K.F., Tefé Silva, C., 2021. Histopathological Analysis of Arctium Lappa Extract in the Treatment of Cutaneous Melanoma in C57BL/6 Mice. Biomed. J. Sci. Tech. Res. 34, 26936–26941.

Srinivasan, B., Kolli, A.R., Esch, M.B., Abaci, H.E., Shuler, M.L., Hickman, J.J., 2015. TEER Measurement Techniques for In Vitro Barrier Model Systems. J. Lab. Autom. 20, 107–126. https://doi.org/10.1177/2211068214561025

Stiernagle, T., 2006. Maintenance of C. elegans.

Stojanović, S., Brede, O., 2002. Elementary reactions of the antioxidant action of trans-stilbene derivatives: resveratrol, pinosylvin and 4-hydroxystilbene. Phys. Chem. Chem. Phys. 4, 757–764. https://doi.org/10.1039/B109063C

Su, D., Cheng, Y., Liu, M., Liu, D., Cui, H., Zhang, B., Zhou, S., Yang, T., Mei, Q., 2013. Comparision of Piceid and Resveratrol in Antioxidation and Antiproliferation Activities In Vitro. PLOS ONE 8, e54505. https://doi.org/10.1371/journal.pone.0054505

Subedi, L., Teli, M.K., Lee, J.H., Gaire, B.P., Kim, M., Kim, S.Y., 2019. A Stilbenoid Isorhapontigenin as a Potential Anti-Cancer Agent against Breast Cancer through Inhibiting Sphingosine Kinases/Tubulin Stabilization. Cancers 11, 1947. https://doi.org/10.3390/cancers11121947

Sueishi, Y., Ishikawa, M., Hori, M., Inazumi, N., 2013. Cyclodextrin Inclusion Interferes with Trolox Oxygen Radical Scavenging Capacity Measurement. Z. Für Phys. Chem. 227, 49–56. https://doi.org/10.1524/zpch.2012.0233

Suh, D.Y., Fukuma, K., Kagami, J., Yamazaki, Y., Shibuya, M., Ebizuka, Y., Sankawa, U., 2000. Identification of amino acid residues important in the cyclization reactions of chalcone and stilbene synthases. Biochem. J. 350, 229–235. https://doi.org/10.1042/bj3500229

Suh, D.-Y., Kagami, J., Fukuma, K., Sankawa, U., 2000. Evidence for Catalytic Cysteine–Histidine Dyad in Chalcone Synthase. Biochem. Biophys. Res. Commun. 275, 725–730. https://doi.org/10.1006/bbrc.2000.3368

Sun, X., Cui, X., 2020. Isorhapontigenin alleviates cerebral ischemia/reperfusion injuries in rats and modulated the PI3K/Akt signaling pathway. Naunyn. Schmiedebergs Arch. Pharmacol. 393, 1753–1760. https://doi.org/10.1007/s00210-019-01794-0

Sun, Y., Wu, X., Cai, X., Song, M., Zheng, J., Pan, C., Qiu, P., Zhang, L., Zhou, S., Tang, Z., Xiao, H., 2016. Identification of pinostilbene as a major colonic metabolite of pterostilbene and its inhibitory effects on colon cancer cells. Mol. Nutr. Food Res. 60, 1924–1932. https://doi.org/10.1002/mnfr.201500989

Suzuki, Y., Muangnoi, C., Thaweesest, W., Teerawonganan, P., Ratnatilaka Na Bhuket, P., Titapiwatanakun, V., Yoshimura-Fujii, M., Sritularak, B., Likhitwitayawuid, K., Rojsitthisak, P., Fukami, T., 2019. Exploring Novel Cocrystalline Forms of Oxyresveratrol to Enhance Aqueous Solubility and Permeability across a Cell Monolayer. Biol. Pharm. Bull. 42, 1004–1012. https://doi.org/10.1248/bpb.b19-00048

Szczepańska, P., Rychlicka, M., Groborz, S., Kruszyńska, A., Ledesma-Amaro, R., Rapak, A., Gliszczyńska, A., Lazar, Z., 2023. Studies on the Anticancer and Antioxidant Activities of Resveratrol and Long-Chain Fatty Acid Esters. Int. J. Mol. Sci. 24, 7167. https://doi.org/10.3390/ijms24087167

Szekeres, T., Fritzer-Szekeres, M., Saiko, P., Jäger, W., 2010. Resveratrol and Resveratrol Analogues—Structure—Activity Relationship. Pharm. Res. 27, 1042–1048. https://doi.org/10.1007/s11095-010-0090-1

Tain, Y.-L., Jheng, L.-C., Chang, S.K.C., Chen, Y.-W., Huang, L.-T., Liao, J.-X., Hou, C.-Y., 2020. Synthesis and Characterization of Novel Resveratrol Butyrate Esters That Have the Ability to Prevent Fat Accumulation in a Liver Cell Culture Model. Molecules 25, 4199. https://doi.org/10.3390/molecules25184199

Tang, F., Xie, Y., Cao, H., Yang, H., Chen, X., Xiao, J., 2017. Fetal bovine serum influences the stability and bioactivity of resveratrol analogues: A polyphenol-protein interaction approach. Food Chem. 219, 321–328. https://doi.org/10.1016/j.foodchem.2016.09.154

Tanyildizi, M.S., Özer, D., Elibol, M., 2005. Optimization of α-amylase production by *Bacillus* sp. using response surface methodology. Process Biochem. 40, 2291–2296. https://doi.org/10.1016/j.procbio.2004.06.018

Teng, R.-W., Bui, T.-K.-A., McManus, D., Armstrong, D., Mau, S.-L., Bacic, A., 2005. Regioselective acylation of several polyhydroxylated natural compounds by Candida antarctica lipase B. Biocatal. Biotransformation 23, 109–116. https://doi.org/10.1080/10242200500132508

Teplova, V.V., Isakova, E.P., Klein, O.I., Dergachova, D.I., Gessler, N.N., Deryabina, Y.I., 2018. Natural Polyphenols: Biological Activity, Pharmacological Potential, Means of Metabolic Engineering (Review). Appl. Biochem. Microbiol. 54, 221–237. https://doi.org/10.1134/S0003683818030146

Tetko, I.V., Tanchuk, V.Y., 2002. Application of associative neural networks for prediction of lipophilicity in ALOGPS 2.1 program. J. Chem. Inf. Comput. Sci. 42, 1136–1145.

Thapa, S.B., Pandey, R.P., Park, Y.I., Sohng, J.K., 2019. Biotechnological Advances in Resveratrol Production and its Chemical Diversity. Molecules 24, 2571. https://doi.org/10.3390/molecules24142571

Thaweesest, W., Buranasudja, V., Phumsuay, R., Muangnoi, C., Vajragupta, O., Sritularak, B., Rashatasakhon, P., Rojsitthisak, P., 2022. Anti-Inflammatory Activity of Oxyresveratrol Tetraacetate, an Ester Prodrug of Oxyresveratrol, on

Lipopolysaccharide-Stimulated RAW264.7 Macrophage Cells. Molecules 27, 3922. https://doi.org/10.3390/molecules27123922

The UniProt Consortium, 2023. UniProt: the Universal Protein Knowledgebase in 2023. Nucleic Acids Res. 51, D523–D531. https://doi.org/10.1093/nar/gkac1052

Tian, B., Liu, J., 2020. Resveratrol: a review of plant sources, synthesis, stability, modification and food application. J. Sci. Food Agric. 100, 1392–1404. https://doi.org/10.1002/jsfa.10152

Tillement, J.-P., Tremblay, D., 2007. 5.02 - Clinical Pharmacokinetic Criteria for Drug Research, in: Taylor, J.B., Triggle, D.J. (Eds.), Comprehensive Medicinal Chemistry II. Elsevier, Oxford, pp. 11–30. https://doi.org/10.1016/B0-08-045044-X/00117-6

Tome-Carneiro, J., Larrosa, M., Gonzalez-Sarrias, A., A. Tomas-Barberan, F., Teresa Garcia-Conesa, M., Carlos Espin, J., 2013. Resveratrol and Clinical Trials: The Crossroad from In Vitro Studies to Human Evidence. Curr. Pharm. Des. 19, 6064–6093.

Torres, P., Poveda, A., Jimenez-Barbero, J., Ballesteros, A., Plou, F.J., 2010. Regioselective Lipase-Catalyzed Synthesis of 3-O-Acyl Derivatives of Resveratrol and Study of Their Antioxidant Properties. J. Agric. Food Chem. 58, 807–813. https://doi.org/10.1021/jf903210q

Torres, P., Poveda, A., Jimenez-Barbero, J., Parra, J.L., Comelles, F., Ballesteros, A.O., Plou, F.J., 2011. Enzymatic Synthesis of α-Glucosides of Resveratrol with Surfactant Activity. Adv. Synth. Catal. 353, 1077–1086. https://doi.org/10.1002/adsc.201000968

Toscano Underwood, C.D., Pearce, R.B., 1991. Astringin and isorhapontin distribution in Sitka spruce trees. Phytochemistry 30, 2183–2189. https://doi.org/10.1016/0031-9422(91)83610-W

Trela, B.C., Waterhouse, A.L., 1996. Resveratrol: Isomeric Molar Absorptivities and Stability. J. Agric. Food Chem. 44, 1253–1257. https://doi.org/10.1021/jf9504576

Tropf, S., Lanz, T., Rensing, S.A., Schröder, J., Schröder, G., 1994. Evidence that stilbene synthases have developed from chalcone synthases several times in the course of evolution. J. Mol. Evol. 38, 610–618. https://doi.org/10.1007/BF00175881

Trott, O., Olson, A.J., 2010. AutoDock Vina: improving the speed and accuracy of docking with a new scoring function, efficient optimization and multithreading. J. Comput. Chem. 31, 455–461. https://doi.org/10.1002/jcc.21334

Tung, B.T., Rodríguez-Bies, E., Talero, E., Gamero-Estévez, E., Motilva, V., Navas, P., López-Lluch, G., 2015. Anti-inflammatory effect of resveratrol in old mice liver. Exp. Gerontol. 64, 1–7. https://doi.org/10.1016/j.exger.2015.02.004

Turfus, S.C., Delgoda, R., Picking, D., Gurley, B.J., 2017. Chapter 25 - Pharmacokinetics, in: Badal, S., Delgoda, Rupika (Eds.), Pharmacognosy. Academic Press, Boston, pp. 495–512. https://doi.org/10.1016/B978-0-12-802104-0.00025-1

Tyukavkina, N.A., Gromova, A.S., Lutskii, V.I., Voronov, V.K., 1972. Hydroxystilbenes from the bark of Pinus sibirica. Chem. Nat. Compd. 8, 570–572. https://doi.org/10.1007/BF00564298

Uesugi, D., Hamada, H., Shimoda, K., Kubota, N., Ozaki, S., Nagatani, N., 2017. Synthesis, oxygen radical absorbance capacity, and tyrosinase inhibitory activity of glycosides of resveratrol, pterostilbene, and pinostilbene. Biosci. Biotechnol. Biochem. 81, 226–230. https://doi.org/10.1080/09168451.2016.1240606

Varoni, E.M., Lo Faro, A.F., Sharifi-Rad, J., Iriti, M., 2016. Anticancer Molecular Mechanisms of Resveratrol. Front. Nutr. 3. https://doi.org/10.3389/fnut.2016.00008

Vernousfaderani, E.K., Akhtari, N., Rezaei, S., Rezaee, Y., Shiranirad, S., Mashhadi, M., Hashemi, A., Khankandi, H.P., Behzad, S., 2021. Resveratrol and Colorectal Cancer: A Molecular Approach to Clinical Researches. Curr. Top. Med. Chem. 21, 2634–2646. https://doi.org/10.2174/1568026621666211105093658

Vitrac, X., Monti, J.-P., Vercauteren, J., Deffieux, G., Mérillon, J.-M., 2002. Direct liquid chromatographic analysis of resveratrol derivatives and flavanonols in wines with absorbance and fluorescence detection. Anal. Chim. Acta 458, 103–110. https://doi.org/10.1016/S0003-2670(01)01498-2

Volkova, T.V., Drozd, K.V., Surov, A.O., 2021. Effect of polymers and cyclodextrins on solubility, permeability and distribution of enzalutamide and apalutamide antiandrogens. J. Mol. Liq. 322, 114937. https://doi.org/10.1016/j.molliq.2020.114937

Walle, T., 2011. Bioavailability of resveratrol. Ann. N. Y. Acad. Sci. 1215, 9–15. https://doi.org/10.1111/j.1749-6632.2010.05842.x

Walle, T., Hsieh, F., DeLegge, M.H., Oatis, J.E., Walle, U.K., 2004. High Absorption but Very Low Bioavailability of Oral Resveratrol in Humans. Drug Metab. Dispos. 32, 1377–1382. https://doi.org/10.1124/dmd.104.000885

Wang, D., Zhang, Y., Zhang, C., Gao, L., Li, J., 2019. Piceatannol pretreatment alleviates acute cardiac injury via regulating PI3K-Akt-eNOS signaling in H9c2 cells. Biomed. Pharmacother. 109, 886–891. https://doi.org/10.1016/j.biopha.2018.10.120

Wang, H., Zhang, X., Yu, B., Peng, X., Liu, Y., Wang, A., Zhao, D., Pang, D., OuYang, H., Tang, X., 2019. Cyclodextrin Ameliorates the Progression of Atherosclerosis via Increasing High-Density Lipoprotein Cholesterol Plasma Levels and Anti-inflammatory Effects in Rabbits. J. Cardiovasc. Pharmacol. 73, 334. https://doi.org/10.1097/FJC.0000000000000660

Wang, M., Jin, Y., Ho, C.-T., 1999. Evaluation of Resveratrol Derivatives as Potential Antioxidants and Identification of a Reaction Product of Resveratrol and 2,2-Diphenyl-1-picryhydrazyl Radical. J. Agric. Food Chem. 47, 3974–3977. https://doi.org/10.1021/jf990382w

Wang, Z.V., Scherer, P.E., 2016. Adiponectin, the past two decades. J. Mol. Cell Biol. 8, 93–100. https://doi.org/10.1093/jmcb/mjw011

White, D.C., Sutton, S.D., Ringelberg, D.B., 1996. The genus *Sphingomonas*: physiology and ecology. Curr. Opin. Biotechnol. 7, 301–306. https://doi.org/10.1016/S0958-1669(96)80034-6

Willenberg, I., Meschede, A.K., Gueler, F., Jang, M.-S., Shushakova, N., Schebb, N.H., 2015. Food Polyphenols Fail to Cause a Biologically Relevant Reduction of COX-2 Activity. PLOS ONE 10, e0139147. https://doi.org/10.1371/journal.pone.0139147

Wong, T., Narayanan, S., Brown, D.P., Chen, Z.-S., 2020. Synthesis and Cytotoxicity Studies of Stilbene Long-Chain Fatty Acid Conjugates. J. Nat. Prod. https://doi.org/10.1021/acs.jnatprod.0c00027

Wongwat, T., Srihaphon, K., Pitaksutheepong, C., Boonyo, W., Pitaksuteepong, T., 2020. Suppression of inflammatory mediators and matrix metalloproteinase (MMP)-13 by *Morus alba* stem extract and oxyresveratrol in RAW 264.7 cells and C28/I2

human chondrocytes. J. Tradit. Complement. Med. 10, 132–140. https://doi.org/10.1016/j.jtcme.2019.03.006

Xia, N., Daiber, A., Förstermann, U., Li, H., 2017. Antioxidant effects of resveratrol in the cardiovascular system. Br. J. Pharmacol. 174, 1633–1646. https://doi.org/10.1111/bph.13492

Xia, N., Daiber, A., Habermeier, A., Closs, E.I., Thum, T., Spanier, G., Lu, Q., Oelze, M., Torzewski, M., Lackner, K.J., Münzel, T., Förstermann, U., Li, H., 2010. Resveratrol Reverses Endothelial Nitric-Oxide Synthase Uncoupling in Apolipoprotein E Knockout Mice. J. Pharmacol. Exp. Ther. 335, 149–154. https://doi.org/10.1124/jpet.110.168724

Xiao, K., Zhang, H.-J., Xuan, L.-J., Zhang, J., Xu, Y.-M., Bai, D.-L., 2008. Stilbenoids: Chemistry and bioactivities, in: Atta-ur-Rahman (Ed.), Studies in Natural Products Chemistry, Bioactive Natural Products (Part N). Elsevier, pp. 453–646. https://doi.org/10.1016/S1572-5995(08)80032-4

Xue, Z., Zhao, K., Sun, Z., Wu, C., Yu, B., Kong, D., Xu, B., 2021. Isorhapontigenin ameliorates cerebral ischemia/reperfusion injury via modulating Kinase Cε/Nrf2/HO-1 signaling pathway. Brain Behav. 11, e02143. https://doi.org/10.1002/brb3.2143

Yan, S., Cheng, Y., Li, L., Zhong, C., Chen, C., Gao, X., 2023. Lipid-based formulations: A promising approach for poorly soluble drug delivery via the intestinal lymphatic system. J. Drug Deliv. Sci. Technol. 87, 104770. https://doi.org/10.1016/j.jddst.2023.104770

Yang, J.S., Tongson, J., Kim, K.-H., Park, Y., 2020. Piceatannol attenuates fat accumulation and oxidative stress in steatosis-induced HepG2 cells. Curr. Res. Food Sci. https://doi.org/10.1016/j.crfs.2020.03.008

Yang, Q., Graham, T.E., Mody, N., Preitner, F., Peroni, O.D., Zabolotny, J.M., Kotani, K., Quadro, L., Kahn, B.B., 2005. Serum retinol binding protein 4 contributes to insulin resistance in obesity and type 2 diabetes. Nature 436, 356–362. https://doi.org/10.1038/nature03711

Yanting, C., Yang, Q.Y., Ma, G.L., Du, M., Harrison, J.H., Block, E., 2018. Dose- and type-dependent effects of long-chain fatty acids on adipogenesis and lipogenesis of bovine adipocytes. J. Dairy Sci. 101, 1601–1615. https://doi.org/10.3168/jds.2017-13312

Yoshioka, T., Kawada, K., Shimada, T., Mori, M., 1979. Lipid peroxidation in maternal and cord blood and protective mechanism against activated-oxygen toxicity in the blood. Am. J. Obstet. Gynecol. 135, 372–376. https://doi.org/10.1016/0002-9378(79)90708-7

Yue, Y., Shen, P., Chang, A.L., Qi, W., Kim, K.-H., Kim, D., Park, Y., 2019. trans-Trismethoxy resveratrol decreased fat accumulation dependent on fat-6 and fat-7 in Caenorhabditis elegans. Food Funct. https://doi.org/10.1039/C9FO00778D

Zakova, T., Rondevaldova, J., Bernardos, A., Landa, P., Kokoska, L., 2018. The relationship between structure and in vitro antistaphylococcal effect of plant-derived stilbenes. Acta Microbiol. Immunol. Hung. 65, 467–476. https://doi.org/10.1556/030.65.2018.040

Zhang, N., Hua, X., Tu, H., Li, J., Zhang, Z., Max, C., 2021. Isorhapontigenin (ISO) inhibits EMT through FOXO3A/METTL14/VIMENTIN pathway in bladder cancer cells. Cancer Lett. 520, 400–408. https://doi.org/10.1016/j.canlet.2021.07.041

Zhang, R., Kang, K.A., Piao, M.J., Lee, K.H., Jang, H.S., Park, M.J., Kim, B.J., Kim, J.S., Kim, Y.S., Ryu, S.Y., Hyun, J.W., 2007. Rhapontigenin from Rheum undulatum

Protects Against Oxidative-Stress-Induced Cell Damage Through Antioxidant Activity. J. Toxicol. Environ. Health A 70, 1155–1166. https://doi.org/10.1080/15287390701252766

Zhang, Y., Li, Y., Sun, C., Chen, Xiang, Han, L., Wang, T., Liu, J., Chen, Xijing, Zhao, D., 2021. Effect of Pterostilbene, a Natural Derivative of Resveratrol, in the Treatment of Colorectal Cancer through Top1/Tdp1-Mediated DNA Repair Pathway. Cancers 13, 4002. https://doi.org/10.3390/cancers13164002

Zhong, Y., Ma, C.-M., Shahidi, F., 2012. Antioxidant and antiviral activities of lipophilic epigallocatechin gallate (EGCG) derivatives. J. Funct. Foods 4, 87–93. https://doi.org/10.1016/j.jff.2011.08.003

Zhu, C., Zhu, Q., Wu, Z., Yin, Y., Kang, D., Lu, S., Liu, P., 2018. Isorhapontigenin induced cell growth inhibition and apoptosis by targeting EGFR-related pathways in prostate cancer. J. Cell. Physiol. 233, 1104–1119. https://doi.org/10.1002/jcp.25968

Zhu, W., Qin, W., Zhang, K., Rottinghaus, G.E., Chen, Y.-C., Kliethermes, B., Sauter, E.R., 2012. Trans-Resveratrol Alters Mammary Promoter Hypermethylation in Women at Increased Risk for Breast Cancer. Nutr. Cancer 64, 393–400. https://doi.org/10.1080/01635581.2012.654926

Zielińska, A., Carreiró, F., Oliveira, A.M., Neves, A., Pires, B., Venkatesh, D.N., Durazzo, A., Lucarini, M., Eder, P., Silva, A.M., Santini, A., Souto, E.B., 2020. Polymeric Nanoparticles: Production, Characterization, Toxicology and Ecotoxicology. Molecules 25, 3731. https://doi.org/10.3390/molecules25163731

Zupančič, Š., Lavrič, Z., Kristl, J., 2015. Stability and solubility of trans-resveratrol are strongly influenced by pH and temperature. Eur. J. Pharm. Biopharm. 93, 196–204. https://doi.org/10.1016/j.ejpb.2015.04.002

Żyżelewicz, D., Oracz, J., Kaczmarska, M., Budryn, G., Grzelczyk, J., 2018. Preparation and characterization of inclusion complex of (+)-catechin with β-cyclodextrin. Food Res. Int. 113, 263–268. https://doi.org/10.1016/j.foodres.2018.07.018

APPENDICES

APPENDICES

APPENDIX 1. Multiple alignment of plant STS sequences obtained with MUSCLE

Residue conservation is depicted below the sequences using the symbols: (*) if they are identical, (:) if there have been conservative substitutions, (.) if there have been semi-conservative substitutions, and ( ) if there is no match.

```
Psilotum_nudum                  MVSGEANGTSYQVRRGQSA-DGPATVLAIGTANPPNVFEQNSYPDFYFNVTNNTHKDELK
Picea_glauca                    -MSAGMTVDLETFRKTQRA-DGPASILAIGTANPPNAVYQSTYPDYYFRITSGEQNTDFK
Picea_jezoensis                 -MSAGMTVELETFRKTQRA-DGPASILAIGTANPPNAVHQSTYPDYYFRITSGEQNTDLK
Picea_sitchensis                -MSAGMTVDLETFRKTQRA-DGPASILAIGTANPPNAVYQSTYPDYYFRITSGEQNTDLK
Rheum_tataricum                 -------MAPEESRHAETAVNRAATVLAIGTANPPNCYYQADFPDFYFRATNSDHLTHLK
Polygonum_cuspidatum            -----MAASTEEMMKAQTA----ATVLAIGTANPPNCYYQADFPDFYFRATNSDHLTHLK
Vitis_vinifera_STS4             ------MASVEEIRNAQRA-KGPATVLAIGTATPDNCLYQSDFADYYFRVTKSEHMTELK
Vitis_labrusca                  ------MASVEEFRNAQRA-KGPATILAIGTATPDHCIYQSDYADYYFRVTKSEHMTELK
Vitis_vinifera_STS6             ------MASVEEFRNAQRA-KGPATILAIGTATPDHCVYQSDYADYYFRVTKSEHMTELK
Vitis_vinifera_STS1             ------MASVEEFRNAQRA-KGPATILAIGTATPDHCVYQSDYADYYFRVTKSEHMTELK
Parthenocissus_henryana         ------MASVEEFRNAQRA-KGPATILAIGTATPDQCVYQSDYADYYFRVTKSEHMTELK
Parthenocissus_quinquefolia     ------MASVEEFRNAQRA-KGPATILAIGTATPDNCVYQSDYADFYFRVTKSEHMTELK
Cissus_rhombifolia              ------MASVEEFRNAQRA-KGPATILAIGTATPDQCVYQSDYADYYFRVTKSEHMTELK
Vitis_vinifera_STS5             ------MASVEEIRNAQRA-KGPATILAIGTATPDHCVYQSDYADYYFKVTKSEHMTELK
Vitis_vinifera_STS3             ------MASVEEIRNAQRA-KGPATILAIGTATPDHCVYQSDYADYYFRVTKSEHMTELK
Vitis_vinifera_STS2             ------MASVEEIRNAQRA-KGPATILAIGTATPDHCVYQSDYADYYFRVTKSEHMTALK
Phanera_variegata               ------MVSVNEIRKVQRA-EGPATVLAIGTANPPNCIEQSTYADYYFKITKSEHKTELK
Arachis_hypogaea_STS3           ------MVSVSGIRKVQRA-EGPATVLAIGTANPPNCIDQSTYADYYFRVTNSEHMTDLK
AArachis_hypogaea_STS1          ------MVSVSGIRKVQRA-EGPATVLAIGTANPPNCVDQSTYADYYFRVTNGEHMTDLK
                                             . : *    *::******.* :   *  :.*:**. *.. :   :*

Psilotum_nudum                  AKFQRMCNRSGIRKRYLSFTEETLKANPSMGIYW-EPSLDVRQDILAVEVPKLAKQASLN
Picea_glauca                    DKFKRICEKSAIKKRYMYLTEEILKENPNMCAFMEVPSLDARQAMLLGEVPRLDKEAADK
Picea_jezoensis                 DKFKRICEKTAIKKRYMYLTEEILKKNPNMCAFMEVPSLDVRQAMLLVEVPRLGKEAADK
Picea_sitchensis                DKFKRICEKTAIKKRYMYLTEEILKENPNMCAFMEVPSLDARQAMLLVEVPRLGKEAADK
Rheum_tataricum                 QKFKRICEKSMIEKRYLHLTEEILKENPNIASFE-APSLDVRHNIQVKEVVLLGKEAALK
Polygonum_cuspidatum            HKFKRICEKSMIEKRYLQLTEDILKENPNIGAYE-APSLDVRHEIQVKGVAQLGKEAALK
Vitis_vinifera_STS4             KKFNRICDKSMIKKRYIHLTEEMLEEHPNIGAYM-APSLNIRQEIITAEVPKLGKEAALK
Vitis_labrusca                  KKFNRICEKSMIKKRYIHLTEEMLEEHPNIGAYM-APSLNIRQEIITAEVPRLGKEAALK
Vitis_vinifera_STS6             KKFNRICDKSMIKKRYIHLTEEMLEEHPNIGAYM-APSLNIRQEIITAEVPRLGRDAALK
Vitis_vinifera_STS1             KKFNRICDKSMIKKRYIHLTEEMLEEHPNIGAYM-APSLNIRQEIITAEVPRLGRDAALK
Parthenocissus_henryana         KKFNRICEKSMIKKRYIHLTEKMLEEHPNIGAYM-APSLNIRQEIITAEVPKLGKEAALK
Parthenocissus_quinquefolia     KKFNRICEKSMIKKRYSHLTEEMLEEHPNIGAYM-APSLNIRQEIITAEVPKLGKEAALK
Cissus_rhombifolia              KKFNRICEKSMIKKRYSHLTEEMLEEHPNIGAYM-APSLNIRQEIITAEVPKLGKEAALK
Vitis_vinifera_STS5             KKFNRICDKSMIKKRYIHLTEEMLEEHPNIGAYM-APSLNIRQEIITAEVPKLGKEAALK
Vitis_vinifera_STS3             KKFNRICDKSMIKKRYIHLTEEMLEEHPNIGAYM-APSLNIRQEIITVEVPKLGKEAALK
Vitis_vinifera_STS2             KKFNRICDKSMIKKRYIHLTEEMLEEHPNIGAYM-APSLNIRQEIITAEVPKLGKEAALK
Phanera_variegata               EKFKRMCERTLIKNRHMHLTEEILKENPSICEYK-APSLDAREDMIIREVPKVGKEAATK
Arachis_hypogaea_STS3           KKFQRICERTQIKNRHMYLTEEILKENPNMCAYK-APSLDAREDMMIREVPRVGKEAATK
AArachis_hypogaea_STS1          KKFQRICERTQIKNRHMYLTEEILKENPNMCAYK-APSLDAREDMMIREVPRVGKEAATK
                                 **:*:*:.: * :*:  :**. *: :*.:  :   ***: *  :    *  : .:*: :
```

```
Psilotum_nudum                  AIKEWGQPISNITHLVFCTTGPVS-PGADAALMQMLGLNPSVKRVLLYMQGCFAGGTVLR
Picea_glauca                    ALQEWGQPKSKITHLIFCSTTTADIPGADCEVAKLLGLHPSVKRVGVFQHGCFAGGTVLR
Picea_jezoensis                 ALQEWGQPKSKITHLIFCSTTTADIPGADCELAKLLGLHPSVKRVGVFQHGCFAGGTVLR
Picea_sitchensis                ALQEWGQPKSKITHLIFCSTTTADIPGADCELAKLLGLHPSVKRVGVFQHGCFAGGTVLR
Rheum_tataricum                 AINEWGQPKSKITRLIVCCIAGVDMPGADYQLTKLLGLQLSVKRFMFYHLGCYAGGTVLR
Polygonum_cuspidatum            AMQEWGQPKSKITHLIVCCIAGVDMPGADYQLTKLLDLNSSVKRFMFYHLGCYAGGTVLR
Vitis_vinifera_STS4             ALKEWGQPKSKITHLVFCTTSGVEMPGADYKLANLLGLEPSVRRVMLYHQGCYAGGTVLR
Vitis_labrusca                  ALKEWGQPKSKITHLVFCTTSGVEMPGADYKLANLLGLETSVRRVMLYHQGCYAGGTVLR
Vitis_vinifera_STS6             ALKEWGQPKSKITHLVFCTTSGVEMPGADYKLANLLGLETSVRRVMLYHQGCYAGGTVLR
Vitis_vinifera_STS1             ALKEWGQPKSKITHLVFCTTSGVEMPGADYKLANLLGLETSVRRVMLYHQGCYAGGTVLR
Parthenocissus_henryana         ALKEWGQPKSKITHLVFCTTSGVEMPGADYKLANLLGLETSVRRVMLYHQGCYAGGTVLR
Parthenocissus_quinquefolia     ALKEWGQPKSKITHLVFCTTSGVEMPGADYKLANLLGLETSVRRVMLYHQGCYAGGTVLR
Cissus_rhombifolia              ALKEWGQPKSKITHLVFCTTSGVEMPGADYKLANLLGLETSVRRVMLYHQGCYAGGTVLR
Vitis_vinifera_STS5             ALKEWGQPKSKITHLVFCTTSGVEMPGADYKLANLLGLETSVRRVMLYHQGCYAGGTVLR
Vitis_vinifera_STS3             ALKEWGQPKSKITHLVFCTTSGVEMPGADYKLANLLGLETSVRRVMLYHQGCYAGGTVLR
Vitis_vinifera_STS2             ALKEWGQPKSKITHLVFCTTSGVEMPGADYKLANLLGLEPSVRRVMLYHQGCYAGGTVLR
Phanera_variegata               AIKEWGQPMSKITHLIFCTTSGVGLPGVDYQLIVLLGLDPYVKRYMMYQQGCFAGGTVLR
Arachis_hypogaea_STS3           AIKEWGQPMSKITHLIFCTTSGVALPGVDYELIVLLGLDPCVKRYMMYHQGCFAGGTVLR
AArachis_hypogaea_STS1          AIKEWGQPMSKITHLIFCTTSGVALPGVDYELIVLLGLDPSVKRYMMYHQGCFAGGTVLR
                                *::***** *:**.*:.*    .  **.*  :  :*.*   *.*  .:  **:*******

Psilotum_nudum                  HAKDLAENNKGARVLVVCSESTAVTFRGPHENHLDNLVGQALFADGAAALIVGSDPIPNV
Picea_glauca                    LAKDVAENNRGARVLVVCSEITAVTFRGPSDTHLDSLVGQALFGDGAAALIVGADPIPQV
Picea_jezoensis                 LAKDVAENNRGARVLVVCSEITAVTFRGPSDTHLDSLVGQALFGDGAAALIVGADPIPQV
Picea_sitchensis                LAKDVAENNRGARVLVVCSEITAVTFRGPSDTHLDSLVGQALFGDGAAALIVGADPIPQV
Rheum_tataricum                 LAKDIAENNKEARVLIVRSEMTPICFRGPSETHIDSMVGQAIFGDGAAAVIVGANPDLSI
Polygonum_cuspidatum            LAKDIAENNKGARVLIVCSEMTPICFRGPSETHIDSMVGQAIFGDGAAAVIVGANPDLTV
Vitis_vinifera_STS4             TAKDLAENNAGARVLVVCSEITVVTFRGPSEDALDSLVGQALFGDGSAAVIVGSDPDISI
Vitis_labrusca                  AAKDLAENNAGARVLVVCSEITVVTFRGPSEDALDSLVGQALFGDGSSAVIVGSDPDVSI
Vitis_vinifera_STS6             TAKDLAENNAGARVLVVCSEITVVTFRGPSEDALDSLVGQALFGDGSSAVIVGSDPDVSI
Vitis_vinifera_STS1             TAKDLAENNAGARVLVVCSEITVVTFRGPSEDALDSLVGQALFGDGSSAVIVGSDPDVSI
Parthenocissus_henryana         TAKDLAENNAGARVLVVCSEITVVTFRGPSETALDSLVGQALFGDGSAAVIVGSDPDISI
Parthenocissus_quinquefolia     TAKDLAENNAGARVLVVCSVITVVTFRGPSETALDSLVGQALFGDGSAAVIVGSDPDILI
Cissus_rhombifolia              TAKDLAENNAGARVLVVCSEITVVTFRGPSETALDSLVGQALFGDGSAAVIVGSDPDILI
Vitis_vinifera_STS5             TAKDLAENNAGARVLVVCSEITVVTFRGPSEDALDSLVGQALFGDGSAAVIVGSDPNVSI
Vitis_vinifera_STS3             TAKDLAENNAGARVLVVCSEITVVTFRGPSEDALDSLVGQALFGDGSAAVIVGSDPDVSI
Vitis_vinifera_STS2             TAKDLAENNAGARVLVVCSEITVVTFRGPSEDALDSLVGQALFGDGSAAVIVGSDPDISI
Phanera_variegata               LAKDLAENNKDARVLIVCSENTAVTFRGPSDTDLDSLVGQALFADGAAAIIIGSDPIPEV
Arachis_hypogaea_STS3           LAKDLAENNKDARVLIVCSENTAVTFRGPSETDMDSLVGQALFADGAAAIIIGSDPVPEV
AArachis_hypogaea_STS1          LAKDLAENNKDARVLIVCSENTAVTFRGPNETDMDSLVGQALFADGAAAIIIGSDPVPEV
                                 ***:****  ****:* *  * : **** :  :*.:****:*.**::*:*:*::*   :

Psilotum_nudum                  EKAWFEISLAESYLIPDSSPAIAGHLKEVGLEFHLTRDVSPVISKNILKILQDAFDGTGI
Picea_glauca                    EKPSFQIAWTTQTILPDSDGAISGKVREVGLTFHLKGAVPDLISTNIENSLVEAFHQFKI
Picea_jezoensis                 EKPSFQIAWTAQTILPDSDDAISGKVREVGLTFHLKGAVPDLISTNIENSLVEAFRQFKI
Picea_sitchensis                EKPSFQIAWTAQTILPDSDGAISGKVREVGLTFHLKGAVPDLISTNIENSLVEAFRQFKI
Rheum_tataricum                 ERPIFELISTSQTIIPESDGAIEGHLLEVGLSFQLYQTVPSLISNCIETCLSKAFTPLNI
Polygonum_cuspidatum            EKPIFELISTAQTIIPESDGAIEGHLLEVGLSFQLYQNVPALVSNNIETCLSEAFTPLNI
Vitis_vinifera_STS4             ERPLFQLVSAAQTFIPNSAGAIAGNLREVGLTFHLWPNVPTLISENIENCLTKAFDPIGI
Vitis_labrusca                  ERPLFQLVSAAQTFIPNSAGAIAGNLREVGLTFHLWPNVPTLISENIEKCLTQAFDPLGI
Vitis_vinifera_STS6             ERPLFQLVSAAQTFIPNSAGAIAGNLREVGLTFHLWPNVPTLISENIEKCLTQAFDPLGI
Vitis_vinifera_STS1             ERPLFQLVSAAQTFIPNSAGAIAGNLREVGLTFHLWPNVPTLISENIEKCLTQAFDPLGI
Parthenocissus_henryana         EQPLFQLVSAAQTFIPNSAGAIAGNLREVGLTFHLWPNVPTLISENIEKCLTQAFDPLGI
Parthenocissus_quinquefolia     ERPLFQLVSAAQTFIPNSAGAIAGNLREVGLTFHLWPNVPTLISENVEKCLTQAFDPLGI
Cissus_rhombifolia              ERPLFQLVSAAQTFIPNSAGAIAGNLREVGLTFHLWPNVPTLISENIEKCLTQAFDPLGI
Vitis_vinifera_STS5             ERPLFQLVSAAQTFIPNSAGAIAGNLREVGLTFHLWPNVPTLISENIEKCLSQAFDPLGI
Vitis_vinifera_STS3             ERPLFQLVSAAQTFIPNSAGAIAGNLREVGLTFHLWPNVPTLISENVEKCLTQAFDPLGI
Vitis_vinifera_STS2             ERPLFQLVSAAQTFIPNSAGAIAGNLREVGLTFHLWPNVPTLISENIEKCLTQAFDPLGI
Phanera_variegata               EKPLFEMVSTDQKILPGSQGATGGLLREVGLTFYLNKSVPDMISQNIKEALVKAFNPLGI
Arachis_hypogaea_STS3           EKPIFELVSTDQKLVPGSHGAIGGLLREVGLTFYLNKSVPDIISQNINDALNKAFDPLGI
AArachis_hypogaea_STS1          ENPIFEIVSTDQQLVPNSHGAIGGLLREVGLTFYLNKSVPDIISQNINGALSKAFDPLGI
                                *.. *::  : . ::* *  *  * : **** * *   *. ::*  :   * .**    *
```

```
Psilotum_nudum                SDWNDVFIIAHPGGPAILDVIEEKLKLVPEKLQASRHVLSEFGNMSSATVHFILDHMRKS
Picea_glauca                  SDWNQLFWIAHPGGRAILDRVEAKLNLDPGKLRATRHVLSEYGNMSSACVHFILDEMRKT
Picea_jezoensis               SDWNQLFWIAHPGGRAILDRVEAKLNLDPGKLRATRHVLSEYGNMSSACVHFILDEMRKT
Picea_sitchensis              SDWNQLFWIAHPGGRAILDRVEARLNLDPGKLRATRHVLSEYGNMSSACVHFILDEMRKT
Rheum_tataricum               SDWNSLFWIAHPGGRAILDDIEATVGLKKEKLKATRQVLNDYGNMSSACVFFIMDEMRKK
Polygonum_cuspidatum          SNWNSLFWIAHPGGPAILDHVEATVGLNKEKLKATRQVLNDYGNMSSACVFFIMDEMRKK
Vitis_vinifera_STS4           SDWNSLFWIAHPGGPAILDAVEAKVGLDKQKLKATRHILSEYGNMSSACVLFILDEMRKK
Vitis_labrusca                SDWNSLFWIAHPGGPAILDAVEAKLNLEKKKLEATRHVLSEYGNMSSACVLFILDEMRKR
Vitis_vinifera_STS6           SDWNSLFWIAHPGGPAILDAVEAKLNLEKKKLEATRHVLSEYGNMSSACVLFILDEMRKK
Vitis_vinifera_STS1           SDWNSLFWIAHPGGPAILDAVEAKLNLEKKKLEATRHVLSEYGNMSSACVLFILDEMRKK
Parthenocissus_henryana       SDWNSLFWIAHPGGPAILDAVEAKLNLDKKKLEATRHVLSEYGNMSSACVLFILDEMRKK
Parthenocissus_quinquefolia   SDWNSLFWIAHPGGPAILDAVEAKLSLDKQKLEATRHVLSEYGNMSSACVLFILDEMRKK
Cissus_rhombifolia            SDWNSLFWIAHPGGPAILDAVEAKLSLDKQKLEATRHVLSEYGNMSSACVLFILDEMRKK
Vitis_vinifera_STS5           SNWNSLFWIAHPGGPAILDAVEAKLNLEKKKLEATRHVLSEYGNMSSACVLFILDEMRKK
Vitis_vinifera_STS3           SDWNSLFWIAHPGGPAILDAVEAKLNLDKKKLEATRHVLSEYGNMSSACVLFILDEMRKK
Vitis_vinifera_STS2           SDWNSLFWIAHPGGPAILDAVEAKLNLDKKKLEATRHVLSEYGNMSSACVLFILDEMRKK
Phanera_variegata             SDYNSIFWIAHPGGRAILDQVEHKLGLKPEKMKATRHVLSKYGNMSSACVLFIMDEMRRR
Arachis_hypogaea_STS3         SDYNSIFWIAHPGGRAILDQVEQKVNLKPEKMKATRDVLSNYGNMSSACVFFIMDLMRKR
AArachis_hypogaea_STS1        SDYNSIFWIAHLGGRAILDQVEQKVNLKPEKMKATRDVLSNYGNMSSACVFFIMDLMRKK
                              *::*.:* *** ** **** :*  : *   *: *:* :*..:****** * **:* **.


Psilotum_nudum                SVEKGCATTGEGYQLGILLGLGPGMTVESIVLKSVPIASLLSS
Picea_glauca                  SRENGYSTTGEGLDMGVLFGFGPGLTVETVVLKSVLLP-----
Picea_jezoensis               SRENGYSTTGEGLEMGVLFGFGPGLTVETVVLKSVLLP-----
Picea_sitchensis              SRENGYSTTGEGLEMGVLFGFGPGLTVETVVLKSVLLP-----
Rheum_tataricum               SLANGQVTTGEGLKWGVLFGFGPGVTVETVVLSSVPLIT----
Polygonum_cuspidatum          SLENGHATTGEGLQWGVLFGFGPGITVETVVLRSVPII-----
Vitis_vinifera_STS4           SLKEGKTTTGEGLDWGVLFGFGPGLTIETVVLHSVGTDSN---
Vitis_labrusca                SLKGENATTGEGLDWGVLFGFGPGLTIETVVLHSIPTVTN---
Vitis_vinifera_STS6           SLKGENATTGEGLDWGVLFGFGPGLTIETVVLHSIPTVTN---
Vitis_vinifera_STS1           SLKGEKATTGEGLDWGVLFGFGPGLTIETVVLHSVPTVTN---
Parthenocissus_henryana       SLKGEKATTGEGLDWGVLFGFGSGLTIETVVLHSIPMVTN---
Parthenocissus_quinquefolia   SLKGEKATTGEGLDRGVLFGFGPGLTIETVVLHSIPMVTN---
Cissus_rhombifolia            SLKGEKATTGEGLDWGVLFGFGPGLTIETVVLHSIPMVTN---
Vitis_vinifera_STS5           SLKGEKATTGEGLDWGVLFGFGPGLTIETVVLHSVPMVTN---
Vitis_vinifera_STS3           SHKGEKATTGEGLDWGVLFGFGPGLTIETVVLHSIPMVTN---
Vitis_vinifera_STS2           SLKGERATTGEGLDWGVLFGFGPGLTIETVVLHSIPMVTN---
Phanera_variegata             SAEDKLSTTGEGLDWGVLFGFGPGLTVETVVLRSVAV------
Arachis_hypogaea_STS3         SLEEGLKTTGEGLDWGVLFGFGPGLTIETVVLRSVAI------
AArachis_hypogaea_STS1        SLETGLKTTGEGLDWGVLFGFGPGLTIETVVLRSMAI------
                              *      ***** . *:*:*:*.*:*:*::** *:
```

APPENDIX 2. Positional model of the HMM generated from plant STS with HMMER

Residue conservation at a position is represented by the total height of the column and the height of the amino acid letters. The total height of the column is directly proportional to the degree of conservation at that position, while the height of a letter is directly proportional to the frequency of that amino acid in that position. When there is a variety of residues at a single position, their corresponding letters are stacked from highest to lowest frequency of occurrence.

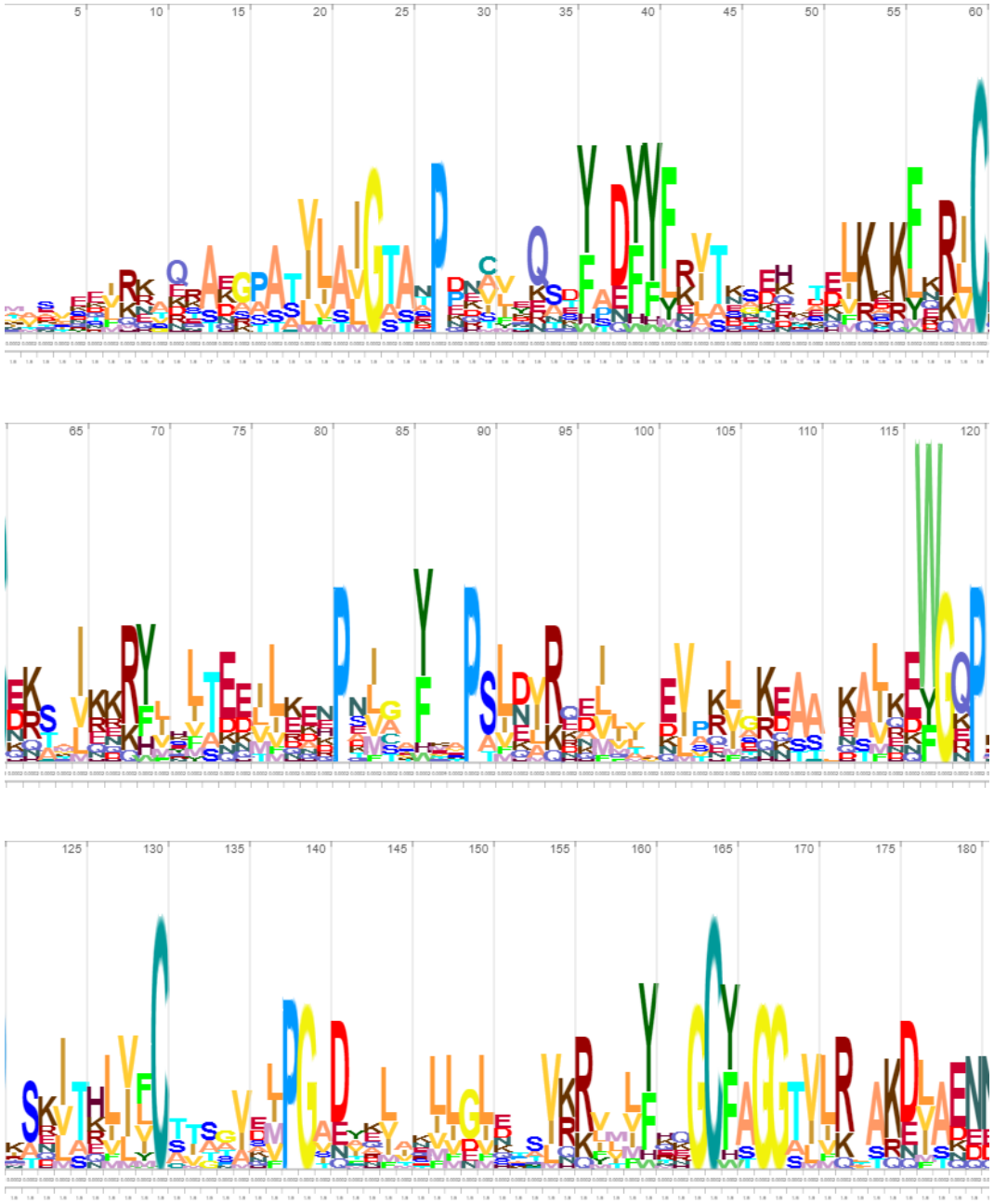

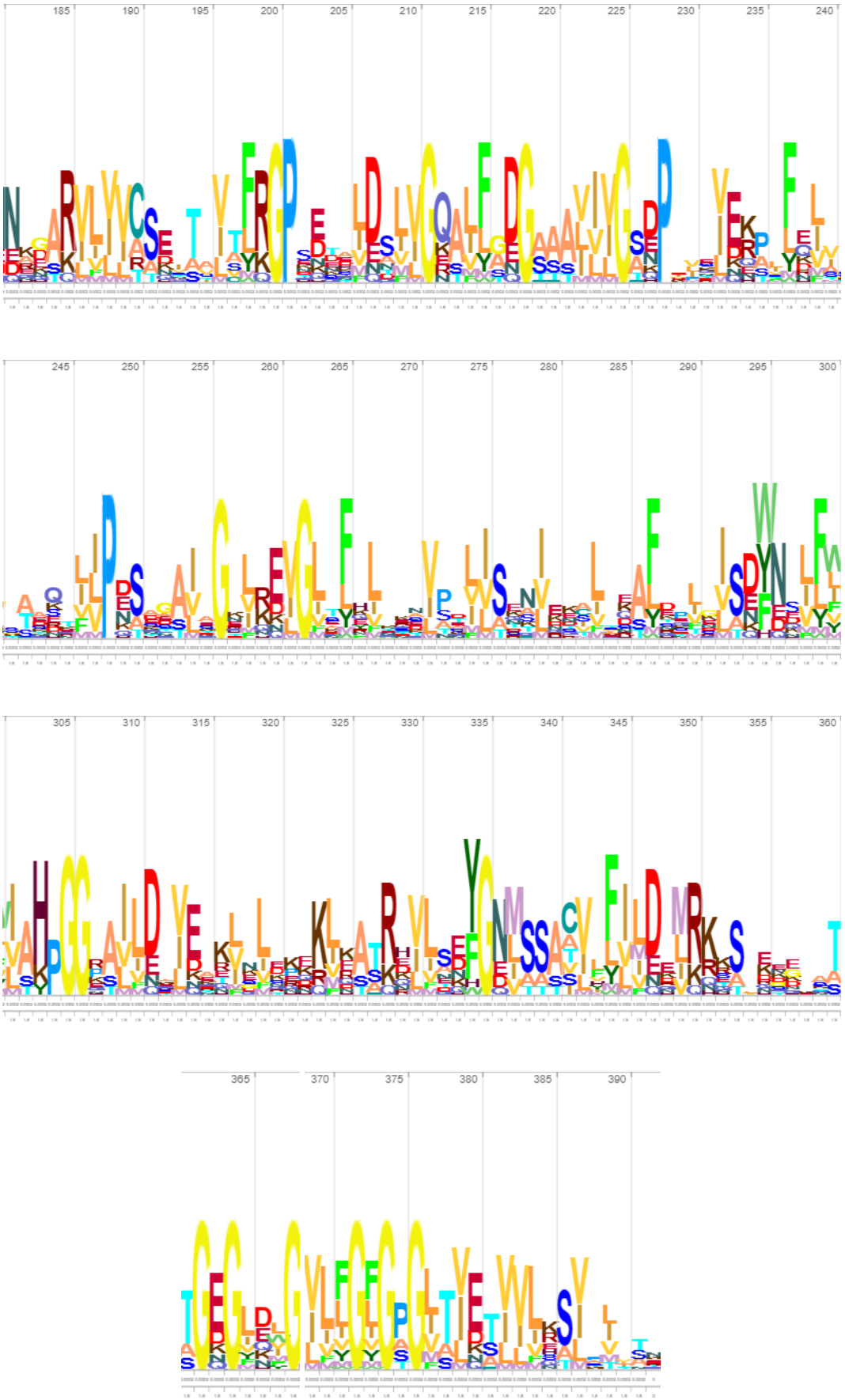
185 190 195 200 205 210 215 220 225 230 235 240
245 250 255 260 265 270 275 280 285 290 295 300
305 310 315 320 325 330 335 340 345 350 355 360
365 370 375 380 385 390

APPENDIX 3. Multiple alignment of plant, fungi, and bacterial STS sequences obtained with MUSCLE

Residue conservation is depicted below the sequences using the symbols: (*) if they are identical, (:) if there have been conservative substitutions, (.) if there have been semi-conservative substitutions, and ( ) if there is no match. Arrows indicate the positions of the amino acids associated with the active centre of the enzyme.

```
Fusarium_langsethiae_STS3          -----------MAAPSAFGELGLSIIGLGTEYPPHSLDYTCLNILGERFYPETPSMQK--
Fusarium_oxysporum_STS3            -----------MSAPSTFGELGLSIIGISAEYPPHSLDYTCLNTLSDRFYPDTPSMQK--
Gibberella_fujikuroi_STS2          -----------MSAPGTFGELGLSIIGIGAEYPPYSLDYTCLNTLSDKFYPDTPSMQK--
Psilotum_nudum                     MVSGEANGTSYQVRRGQSADGPATVLAIGTANPPNVFEQNSYPDFYFNVTNNTHKDELKA
Picea_glauca                       -MSAGMTVDLETFRKTQRADGPASILAIGTANPPNAVYQSTYPDYYFRITSGEQNTDFKD
Picea                              -MSAGMTVELETFRKTQRADGPASILAIGTANPPNAVHQSTYPDYYFRITSGEQNTDLKD
Picea_sitchensis                   -MSAGMTVDLETFRKTQRADGPASILAIGTANPPNAVYQSTYPDYYFRITSGEQNTDLKD
Phanera_variegata                  ------MVSVNEIRKVQRAEGPATVLAIGTANPPNCIEQSTYADYYFKITKSEHKTELKE
Arachis_hypogaea_STS3              ------MVSVSGIRKVQRAEGPATVLAIGTANPPNCIDQSTYADYYFRVTNSEHMTDLKK
Arachis_hypogaea_STS1              ------MVSVSGIRKVQRAEGPATVLAIGTANPPNCVDQSTYADYYFRVTNGEHMTDLKK
Vitis_labrusca                     ------MASVEEFRNAQRAKGPATILAIGTATPDHCIYQSDYADYYFRVTKSEHMTELKK
Vitis_vinifera_STS1                ------MASVEEFRNAQRAKGPATILAIGTATPDHCVYQSDYADYYFRVTKSEHMTELKK
Vitis_vinifera_STS2                ------MASVEEIRNAQRAKGPATILAIGTATPDHCVYQSDYADYYFRVTKSEHMTALKK
Parthenocissus_henryana            ------MASVEEFRNAQRAKGPATILAIGTATPDQCVYQSDYADYYFRVTKSEHMTELKK
Parthenocissus_quinquefolia        ------MASVEEFRNAQRAKGPATILAIGTATPDNCVYQSDYADFYFRVTKSEHMTELKK
Cissus_rhombifolia                 ------MASVEEFRNAQRAKGPATILAIGTATPDQCVYQSDYADYYFRVTKSEHMTELKK
Rheum_tataricum                    ------MAPEESRHAETAVNRAATVLAIGTANPPNCYYQADFPDFYFRATNSDHLTHLKQ
Polygonum_cuspidatum               --------MAASTEEMMKAQTAATVLAIGTANPPNCYYQADFPDFYFRATNSDHLTHLKH
Rhodococcus_sp                     -------------------MTTAYINSISTAVPEHDVHD-DFVAYADSTFTLRRKQLL--
Rhodococcus_sp.                    -------------------MTTAYINAISTAVPEHDVHD-DFVAYADSTFTLRRKQLL--
Mesorhizobium_sp.                  -------------------MSANAYINRIATAVPEHEVHQ-FYLRYAASMLCSDRRKL---
Mesorhizobium_sp.                  -------------------MSANAYINRIATAIPEHEVHQ-FYLRFAASMLAANRRRI---
Erythrobacter_marinus              -------------MSSKKQPIVPRINAIVTAVPECDVHA-RYTDWAEQQLPGRKAAV---
Altererythrobacter_sp.             ---------------MVSGQPVPRINAIACALPASECDA-TYNAWALRQLEGRREVTL--
Erythrobacter_sp.                  --------------------MTARINAIATAVPDCDFEQ-DYRHWAMRQLEGRREAKL--
Sphingomonas_sp.                   --------------MPATAAVTAHVNAIGTAAPPHDIHD-AFIAWAQSRVAGDEARL---
Sphingomonas_endophytica           -------------------MTVTPHLHAIGTATPPYDIHA-TFVDWALPRLAEREARL---
Skermanella_stibiiresistens        -------------------MTAAYINAIGTAVPTHDVHD-KFVSYAPKLLTDERLRKL--
Microvirga_sp.                     ----------------MELVTGAYINRIGTAVPEHDVHQ-TFIGFVDRFLPERKEKLL--
Microvirga_ossetica                -------------------MTGAYINRIGTAVPQNDVHQ-TFIGFVDQFLSERKDKLL--
Novosphingobium_malaysiense        -----------------MTSTIARINRIGTANPPFEVHD-AFVRFVTSELPDEKTRNL--
Novosphingobium_barchaimii         ----------MTGYPARHAPATAHINAIGTALPPHEIHA-AYHGLVDHMLPDPRKRAI--
Paenibacillus_wynnii               -------------MTQLNRNTGAAILGIGTSLPIHSIAQSDVAELIASSLQDSPDLAR--
Paenibacillus_pectinilyticus       ---------------MKQDNRVIAILGIGTAVPEFHLDQADTSQRLTEALRDTPNSAR--
Bacillus_sp.                       ---------------MTKANSNIAILGIGTAVPPYLIDQADTARRLVNALSDKPDSAR--
Paenibacillus_naphthalenovorans    ---------------MEDISPIVSILGIGTAVPAFRMDQADVSQRLAEALREQPHSAR--
                                                                 :  :    *
```

```
Fusarium_langsethiae_STS3          -VLTINRYTGIDSRSSIGT---------PDHPAVNKKD----APSIAELHSIFQSDGVPL
Fusarium_oxysporum_STS3            -VLGINRYTGIDTRSSIGT---------PDHPAVNKKD----APSIAELHTLFLSDGVPL
Gibberella_fujikuroi_STS2          -VLGINRYTGIDTRSSIGT---------PDHPAVNKKD----APSIAELHSLFLSDGVPL
Psilotum_nudum                     KFQRMCNRSGIRKRYLSFTEETLKAN--PSMGIYW-------EPSLDVRQDILAVEVPKL
Picea_glauca                       KFKRICEKSAIKKRYMYLTEEILKEN--PNMCAFME------VPSLDARQAMLLGEVPRL
Picea                              KFKRICEKTAIKKRYMYLTEEILKKN--PNMCAFME------VPSLDVRQAMLLVEVPRL
Picea_sitchensis                   KFKRICEKTAIKKRYMYLTEEILKEN--PNMCAFME------VPSLDARQAMLLVEVPRL
Phanera_variegata                  KFKRMCERTLIKNRHMHLTEEILKEN--PSICEYK-------APSLDAREDMIIREVPKV
Arachis_hypogaea_STS3              KFQRICERTQIKNRHMYLTEEILKEN--PNMCAYK-------APSLDAREDMMIREVPRV
Arachis_hypogaea_STS1              KFQRICERTQIKNRHMYLTEEILKEN--PNMCAYK-------APSLDAREDMMIREVPRV
Vitis_labrusca                     KFNRICEKSMIKKRYIHLTEEMLEEH--PNIGAYM-------APSLNIRQEIITAEVPRL
Vitis_vinifera_STS1                KFNRICDKSMIKKRYIHLTEEMLEEH--PNIGAYM-------APSLNIRQEIITAEVPRL
Vitis_vinifera_STS2                KFNRICDKSMIKKRYIHLTEEMLEEH--PNIGAYM-------APSLNIRQEIITAEVPKL
Parthenocissus_henryana            KFNRICEKSMIKKRYIHLTEKMLEEH--PNIGAYM-------APSLNIRQEIITAEVPKL
Parthenocissus_quinquefolia        KFNRICEKSMIKKRYSHLTEEMLEEH--PNIGAYM-------APSLNIRQEIITAEVPKL
Cissus_rhombifolia                 KFNRICEKSMIKKRYSHLTEEMLEEH--PNIGAYM-------APSLNIRQEIITAEVPKL
Rheum_tataricum                    KFKRICEKSMIEKRYLHLTEEILKEN--PNIASFE-------APSLDVRHNIQVKEVVLL
Polygonum_cuspidatum               KFKRICEKSMIEKRYLQLTEDILKEN--PNIGAYE-------APSLDVRHEIQVKGVAQL
Rhodococcus_sp                     -FRRMADRAQISHRYSAF----------PSIASFYGDDPN--AVDTQARMQEFERTAPGL
Rhodococcus_sp.                    -FRRMADRAQISHRWSAF----------PSIASFYGDDPN--AVDTQARMQEFERTAPGL
Mesorhizobium_sp.                  -FERMAGLAGIDHRFSCFAPALDPEGPSVDLGGIFKRGA---FPGTAARMAMFAEAAPTL
Mesorhizobium_sp.                  -FERMAGLAGIESRYSCFAPAIDPEGAYVDRAGTFVRGA---FPGTAARMAMFCEAAPVL
Erythrobacter_marinus              -FRRMEARGGIDHRFSVLSGTDAA----MDFGSFYMSGS---PPGTAQRMQRYAEAAPDL
Altererythrobacter_sp.             -LERMLQRSGIGRRFTVLSSAETY----QAEGSFYDTAD---APGTLARMEIYSREAPKL
Erythrobacter_sp.                  -YARMAERSGIEHRWSVLDEEDAKL---DEGAGFYAAE----PPSTAERMAIYAKEAPEL
Sphingomonas_sp.                   -FARMARRSGIGHRWSVLPPTREGLSP-VSPGGFYAGA----MPGTAARMGLYADAAPTL
Sphingomonas_endophytica           -FERMATRAGIAHRWSVLPAP-------VADGGFYAPAP---HPGTGERMAVYAREAPAL
Skermanella_stibiiresistens        -FRRMAERCQIEHRYSFFEPDPDPEV--LDQGGFFKRGA---FPDTATRMKFYETHALDL
Microvirga_sp.                     -FRRMVQRSGIEHRYSTLAPSENLDIA-ADQEGFFQPGQ---FAGTAARMDRFETHAVDL
Microvirga_ossetica                -FRRMVQRSGIEHRYSTLTPSENLELA-ADREGFFQPGQ---FVGTGTRMERFETHAIDL
Novosphingobium_malaysiense        -FARMAARSGIAQRYSFLEPVTLGDGTVTDTDSFYGTGS---WPSTAARMQRYERDAPRL
Novosphingobium_barchaimii         -YDRMAKRSAIDRRYSFIRSGDAMDDGYEHADSFYAPGA---YPGTSSRMRQYEKWAPEL
Paenibacillus_wynnii               FAKRIFKSCGVETRYTCDDSYLGS----AETCRYLPSGDQSVIPTTEERMKKYQQEALPL
Paenibacillus_pectinilyticus       WAKKIFKQCGVESRYTCEPNLLES----AEHCRYFSQTNQT-APSTSDRMATYKRESIPL
Bacillus_sp.                       WGRRIFKQCGVESRYTCEPNLLAE----AAECRYLPSATPELAPSTSERMGIYKRESVPL
Paenibacillus_naphthalenovorans    WAKRIFRQCGVETRYTCEPNLLEP----ASGCRYFSSASIEGVPTTAERMATYKKESVPL
                                       :    : *                                          :

Fusarium_langsethiae_STS3          AIRAARKAIDEAKIDTRFITHIVATTCTDSANPGFDHFVAKGLGITHGVEKVLLHGVGCS
Fusarium_oxysporum_STS3            AIRAARKAIDEAKIDTRFITHIVATTCTDSANPGFDHFVAKGLGITHGVEKVLLHGVGCS
Gibberella_fujikuroi_STS2          AIRAARKAIDEAKIDTRFITHIVATTCTDSANPGFDHFVAKGLGISHGVEKVLLHGVGCS
Psilotum_nudum                     AKQASLNAIKEWGQPISNITHLVFCTT-GPVSPGADAALMQMLGLNPSVKRVLLYMQGCF
Picea_glauca                       DKEAADKALQEWGQPKSKITHLIFCSTTTADIPGADCEVAKLLGLHPSVKRVGVFQHGCF
Picea                              GKEAADKALQEWGQPKSKITHLIFCSTTTADIPGADCELAKLLGLHPSVKRVGVFQHGCF
Picea_sitchensis                   GKEAADKALQEWGQPKSKITHLIFCSTTTADIPGADCELAKLLGLHPSVKRVGVFQHGCF
Phanera_variegata                  GKEAATKAIKEWGQPMSKITHLIFCTTSGVGLPGVDYQLIVLLGLDPYVKRYMMYQQGCF
Arachis_hypogaea_STS3              GKEAATKAIKEWGQPMSKITHLIFCTTSGVALPGVDYELIVLLGLDPCVKRYMMYHQGCF
Arachis_hypogaea_STS1              GKEAATKAIKEWGQPMSKITHLIFCTTSGVALPGVDYELIVLLGLDPSVKRYMMYHQGCF
Vitis_labrusca                     GRDAALKALKEWGQPKSKITHLVFCTTSGVEMPGADYKLANLLGLETSVRRVMLYHQGCY
Vitis_vinifera_STS1                GRDAALKALKEWGQPKSKITHLVFCTTSGVEMPGADYKLANLLGLETSVRRVMLYHQGCY
Vitis_vinifera_STS2                GKEAALKALKEWGQPKSKITHLVFCTTSGVEMPGADYKLANLLGLEPSVRRVMLYHQGCY
Parthenocissus_henryana            GKEAALKALKEWGQPKSKITHLVFCTTSGVEMPGADYKLANLLGLETSVRRVMLYHQGCY
Parthenocissus_quinquefolia        GKEAALKALKEWGQPKSKITHLVFCTTSGVEMPGADYKLANLLGLETSVRRVMLYHQGCY
Cissus_rhombifolia                 GKEAALKALKEWGQPKSKITHLVFCTTSGVEMPGADYKLANLLGLETSVRRVMLYHQGCY
Rheum_tataricum                    GKEAALKAINEWGQPKSKITRLIVCCIAGVDMPGADYQLTKLLGLQLSVKRFMFYHLGCY
Polygonum_cuspidatum               GKEAALKAMQEWGQPKSKITHLIVCCIAGVDMPGADYQLTKLLDLNSSVKRFMFYHLGCY
Rhodococcus_sp                     AVRAVDGL--GLGDTAADITHLIVLTCTGFYTPGIDFEIMKQCGVPTSAERTQVGFMGCF
Rhodococcus_sp.                    AVRAVDGL--GLGDAAADITHLIVLTCTGFYTPGIDFEIMKQCGVPTTAERTQVGFMGCF
Mesorhizobium_sp.                  AQKGVDGL--HLGNEASRITHLIVTTCTGFSAPGIDLDLVQRCGLADGVERTMIGFMGCY
Mesorhizobium_sp.                  AKKGVDGL--QLGDEASRITHLIVTTCTGFSAPGIDLDLVLSCGLSDRVERTMIGFMGCY
Erythrobacter_marinus              ALKAIAGL-----PSTDGVTHLVIASCTGFMAPGLDQVIARRLGLATNVERVSIGFMGCY
Altererythrobacter_sp.             ALEAIAEL-----GDLGRVTHLVVASCTGFMAPGLDQVIARRLGLDPTVERVVVGFMGCY
Erythrobacter_sp.                  ALPAIGKL-----GELGTITHIVVASCTGFVAPGIDQIIARRLGLAGSVERVLVGFMGCY
Sphingomonas_sp.                   SLAAVAAL--GERTDLNGISHLVVASCTGFVAPGLDQIVAQRLGLPGSVERLLVGFMGCY
Sphingomonas_endophytica           ALAAIEAL--AAQTSLDGITHLVVASCTGFIAPGLDQIVARRLGLDTRVERVAIGFMGCY
Skermanella_stibiiresistens        AVTSLEAA--GIARHRGGITHLIVTSCTGFYAPGLDLQLARHFELDQSVERTIIGFMGCY
Microvirga_sp.                     AERAVEAL--DLGEELSSLTHLVVASCTGFTAPGLDQQLMERLGLNPSIERTLVGFMGCA
Microvirga_ossetica                AEEAIEAL--DLGESLTSVTHMVVASCTGFTAPGLDQQIMERLNLNPSLERTMVGFMGCA
Novosphingobium_malaysiense        ALDAIAAL--DKDIDKAGITHLVVASCTGFMAPGLDQAIVAGAGLDPGVERTVVGFMGCY
Novosphingobium_barchaimii         ALDAIGQL--DGDIADQGITHVIVASCTGFVAPGLDQILIKRTGIDPSAERTLVGFMGCY
Paenibacillus_wynnii               GLQAAEKALRNAGQSSGDITHLITVSCTGQYLPGLDVMLIRKLGMSPRVNRLPLIFQGCA
Paenibacillus_pectinilyticus       ALDAAKKALADAKADVSDITHVITVSCTGQFLPGLDAVLTQQLGLAPDVNRIPFNFLGCA
Bacillus_sp.                       GLHAARKALADGDVEPAAITHLITVSCTGQFLPGMDAAIVQQLGLAPTITRIPLNFLGCA
Paenibacillus_naphthalenovorans    GLEAARKALSDSGMTASGITHLITVSCTGQFLPGMDAALVQQLGLASTVNRLPLQFLGCA
                                      .            ::.::        ** *  :    :    . .  **
```

```
Fusarium_langsethiae_STS3          GGLAALRTSANLALGHKARGLPARVLCVALEVSTTLVR--SE--LDSINELQQTRIGACL
Fusarium_oxysporum_STS3            GGLATLRTGANLALGHKARGLPARVLCVALEVSTTMVR--SE--LDSINELQQTRIGACL
Gibberella_fujikuroi_STS2          GGLATLRTGANLALGHKARGLPARVLCVALEVSTTMVR--SE--LDSINELQQTRIGACL
Psilotum_nudum                     AGGTVLRHAKDLAENNKG----ARVLVVCSESTAVTFRGPHENHLDNL-------VGQAL
Picea_glauca                       AGGTVLRLAKDVAENNRG----ARVLVVCSEITAVTFRGPSDTHLDSL-------VGQAL
Picea                              AGGTVLRLAKDVAENNRG----ARVLVVCSEITAVTFRGPSDTHLDSL-------VGQAL
Picea_sitchensis                   AGGTVLRLAKDVAENNRG----ARVLVVCSEITAVTFRGPSDTHLDSL-------VGQAL
Phanera_variegata                  AGGTVLRLAKDLAENNKD----ARVLIVCSENTAVTFRGPSDTDLDSL-------VGQAL
Arachis_hypogaea_STS3              AGGTVLRLAKDLAENNKD----ARVLIVCSENTAVTFRGPSETDMDSL-------VGQAL
Arachis_hypogaea_STS1              AGGTVLRLAKDLAENNKD----ARVLIVCSENTAVTFRGPNETDMDSL-------VGQAL
Vitis_labrusca                     AGGTVLRAAKDLAENNAG----ARVLVVCSEITVVTFRGPSEDALDSL-------VGQAL
Vitis_vinifera_STS1                AGGTVLRTAKDLAENNAG----ARVLVVCSEITVVTFRGPSEDALDSL-------VGQAL
Vitis_vinifera_STS2                AGGTVLRTAKDLAENNAG----ARVLVVCSEITVVTFRGPSEDALDSL-------VGQAL
Parthenocissus_henryana            AGGTVLRTAKDLAENNAG----ARVLVVCSEITVVTFRGPSETALDSL-------VGQAL
Parthenocissus_quinquefolia        AGGTVLRTAKDLAENNAG----ARVLVVCSVITVVTFRGPSETALDSL-------VGQAL
Cissus_rhombifolia                 AGGTVLRTAKDLAENNAG----ARVLVVCSEITVVTFRGPSETALDSL-------VGQAL
Rheum_tataricum                    AGGTVLRLAKDIAENNKE----ARVLIVRSEMTPICFRGPSETHIDSM-------VGQAI
Polygonum_cuspidatum               AGGTVLRLAKDIAENNKG----ARVLIVCSEMTPICFRGPSETHIDSM-------VGQAI
Rhodococcus_sp                     AGINGLKLAHHIVRSEPS----ARVLVVSVELCSLHMQKTDD--LETM-------LSFLV
Rhodococcus_sp.                    AGINGLKLAHHIVRSEPA----AKVLVVSVELCSLHMQQTDD--LETM-------LSFLV
Mesorhizobium_sp.                  AAVNGLKLARHIVRSDPG----ARVLLVNIEICTLHIRETTE--LEKL-------LCFCL
Mesorhizobium_sp.                  AAINGLKLARHIVRSDPQ----SRVLLVNIELCTLHLNETTE--LEKL-------LSFCL
Erythrobacter_marinus              AGVTLLRTAAHIVRSQPS----ARVLAVSVELCTLHLQETDD--LESL-------LAMGQ
Altererythrobacter_sp.             AGVTALRTAGHIVRSEPS----ARVLVISVELCTLHLQPTDK--LERL-------LAMAQ
Erythrobacter_sp.                  AAVTALRTARHIVRSEPG----ARVLVVTVELSSLHHQDHDE--IEPL-------LAGAQ
Sphingomonas_sp.                   AAVAALRTARHLVRSEPA----ARVLVICCELSTLHLQDTVA--LEPL-------LAMLQ
Sphingomonas_endophytica           AAITALRTARHIVRSEPD----ARVLVVTVELSTLHLQEDRA--LEPL-------LAMLQ
Skermanella_stibiiresistens        AAMNALKAARHIVRSEPA----SKVAIVNLELCTLHLQETAN--IEEV-------LSFLI
Microvirga_sp.                     AAVNALKLAHHIVRSEPA----AKVLVVNLELCTLHLQETSD--LEVI-------LGALL
Microvirga_ossetica                AAVNALKVAHHIVRSEPA----ARVLVVNLELCTLHLQETSN--LEVI-------LSALL
Novosphingobium_malaysiense        AAVNSLRLAHHIVRSEPG----ARVLVVTLELCSIHFQRSQD--LASL-------LAMLL
Novosphingobium_barchaimii         AAVNSLRLAHHIVRSTPE----ARVLVVNVELCTLHLQETQD--LDKL-------LAMLL
Paenibacillus_wynnii               AGLKAIQMARDVVLGAPG----SKVLVVCVELCTLHFQPAKE--REAL-------FAASF
Paenibacillus_pectinilyticus       AGLKAICLSKQIISTNPT----AQVLVVCVELCTLHIQPSSD--REAL-------FGASF
Bacillus_sp.                       AGLKAIGLSRQIVASDNN----AHVLVVCVELCTLHIQPSGD--RESL-------FAASF
Paenibacillus_naphthalenovorans    AGLKAINLSRQIVSGTPS----AKVLIVCVELCTLHFQPSGD--KEAL-------FAASF
                                   ..   :  .  :          :.*  :         .         :       .
```

```
Fusarium_langsethiae_STS3          FSD-CGSAVVLSNGIGEPSEPVYDLLGWDHRTIPDTEADLGFDVHPAGWKVILTPRVPKL
Fusarium_oxysporum_STS3            FSD-CGSAAVLSNGIGEPSEPVYDLLGWDHRTIPDTEDDLGFDVDPVGWKVVLTPRVPKL
Gibberella_fujikuroi_STS2          FSD-CGSAAVLSNGIGEPSEPVYDLLGWDHRTIPDTEDDLGFDVDPVGWKVVLTPRVPKL
Psilotum_nudum                     FADGAAALIVGSDPIPNVEKAWFEISLAESYLIPDSSPAIAGHLKEVGLEFHLTRDVSPV
Picea_glauca                       FGDGAAALIVGADPIPQVEKPSFQIAWTTQTILPDSDGAISGKVREVGLTFHLKGAVPDL
Picea                              FGDGAAALIVGADPIPQVEKPSFQIAWTAQTILPDSDDAISGKVREVGLTFHLKGAVPDL
Picea_sitchensis                   FGDGAAALIVGADPIPQVEKPSFQIAWTAQTILPDSDGAISGKVREVGLTFHLKGAVPDL
Phanera_variegata                  FADGAAAIIIGSDPIPEVEKPLFEMVSTDQKILPGSQGATGGLLREVGLTFYLNKSVPDM
Arachis_hypogaea_STS3              FADGAAAIIIGSDPVPEVEKPIFELVSTDQKLVPGSHGAIGGLLREVGLTFYLNKSVPDI
Arachis_hypogaea_STS1              FADGAAAIIIGSDPVPEVENPIFEIVSTDQQLVPNSHGAIGGLLREVGLTFYLNKSVPDI
Vitis_labrusca                     FGDGSSAVIVGSDPDVSIERPLFQLVSAAQTFIPNSAGAIAGNLREVGLTFHLWPNVPTL
Vitis_vinifera_STS1                FGDGSSAVIVGSDPDVSIERPLFQLVSAAQTFIPNSAGAIAGNLREVGLTFHLWPNVPTL
Vitis_vinifera_STS2                FGDGSAAVIVGSDPDISIERPLFQLVSAAQTFIPNSAGAIAGNLREVGLTFHLWPNVPTL
Parthenocissus_henryana            FGDGSAAVIVGSDPDISIEQPLFQLVSAAQTFIPNSAGAIAGNLREVGLTFHLWPNVPTL
Parthenocissus_quinquefolia        FGDGSAAVIVGSDPDILIERPLFQLVSAAQTFIPNSAGAIAGNLREVGLTFHLWPNVPTL
Cissus_rhombifolia                 FGDGSAAVIVGSDPDILIERPLFQLVSAAQTFIPNSAGAIAGNLREVGLTFHLWPNVPTL
Rheum_tataricum                    FGDGAAAVIVGANPDLSIERPIFELISTSQTIIPESDGAIEGHLLEVGLSFQLYQTVPSL
Polygonum_cuspidatum               FGDGAAAVIVGANPDLTVEKPIFELISTAQTIIPESDGAIEGHLLEVGLSFQLYQNVPAL
Rhodococcus_sp                     FGDGAAAVLVTAEPTG------LAIDSFRALMIEDSRDLITWRIGGMGFDMVLSGKVPGS
Rhodococcus_sp.                    FGDGAAAVLVTAESTG------LAMDSFQALMIEDSRDLITWRIGGMGFDMVLSGKVPGS
Mesorhizobium_sp.                  WGDGCAASIVTAEPPG------IELDSFRCAVANEQRELMTWDIRDQGFDMVLSGKVPAA
Mesorhizobium_sp.                  WGDGCAAALVTAEPPG------IKLDSFHCVVADERRDLMRWDIRDRGFDMVLSGQVPAA
Erythrobacter_marinus              FADGAAAVLVSAQSEG------LGLGEGLSATLEDSEDLITWTVGDTGFAMHLSGAVPGR
Altererythrobacter_sp.             FADGAAAAIVSAEGEG------LALGQGLSLTLEDSHELITWTIGDTGFDMQLSGEVPGR
Erythrobacter_sp.                  FGDGAAAAIVSGEGPG------LELGEGLSATLEDSDGLITWHIGDTGFHMHLSGEVPGR
Sphingomonas_sp.                   FGDGAAAALVTADPAG------FALGAPFAATLPDSDALIRWTITDTGFAMHLSGEVPRR
Sphingomonas_endophytica           FGDGAAAALVCAEPAG------LALDRPFSATLPVSDTLIRWDITDRGFAMHLSGEVPGR
Skermanella_stibiiresistens        FADGCSACVVSAEPDG------VELESFRATVIPGSADQITWHIGRTGFDMRLAGTVPGT
Microvirga_sp.                     FGDGCAASLVTAEPRG------IALKDFRVATIPETQDLITWRIGDAGFQMSLSGEVPQQ
Microvirga_ossetica                FGDGCAASLVSAEPQG------IALKDFRVATIPDTRDLITWRIGDAGFEMSLSGEVPQQ
Novosphingobium_malaysiense        FGDGAAAALVSAEPGG------IALQDFRAAMIPGTEDAITWTIGDQGFDMHLGGEVPAR
Novosphingobium_barchaimii         FSDGASAALVTAEPKG------IALLDFRAASIPGSADLITWHITDQGFLMHLDGHVPAR
Paenibacillus_wynnii               FGDGAAASVIGAPESHN--NHYLSLGSGYSVLLPDSTEEMTWEVGNIGYDLYLSPRIPKL
Paenibacillus_pectinilyticus       FGDGASACLVGVTSDKH--SRVFQLGNDRSILLQDGADDMKWDVGNYGFDLYLSPNIPKL
Bacillus_sp.                       FGDGASACVIGAAKPPY--QPLFELGKERSVLLPDCAEEMVWEVGNHGFDLYLSPHIPKL
Paenibacillus_naphthalenovorans    FGDGASACIVGCAGAGH--KGIFQLGGDYSVLMPESADEMVWEVGNYGFHLYLSPNIPRL
                                   :.* ..:  :             :                  :   *  . *   :.

Fusarium_langsethiae_STS3          TAASISPAFSDLKASLPQLPSDYQNAADFD-WAMHPGGATILSGAENAM-----GITPEH
Fusarium_oxysporum_STS3            TAASIGPAFNDLKASLPQLPPDYQKAADFD-WAMHPGGATILSGAERAM-----DITPEH
Gibberella_fujikuroi_STS2          TAASIGPAFNDLKASLPQLPPDYQKAADFD-WAMHPGGATILSGAERAM-----DITPEH
Psilotum_nudum                     ISKNILKIL--QDAFDGTGISDWND----VFIIAHPGGPAILDVIEEKL-----KLVPEK
Picea_glauca                       ISTNIENSL--VEAFHQFKISDWNQ----LFWIAHPGGRAILDRVEAKL-----NLDPGK
Picea                              ISTNIENSL--VEAFRQFKISDWNQ----LFWIAHPGGRAILDRVEAKL-----NLDPGK
Picea_sitchensis                   ISTNIENSL--VEAFRQFKISDWNQ----LFWIAHPGGRAILDRVEARL-----NLDPGK
Phanera_variegata                  ISQNIKEAL--VKAFNPLGISDYNS----IFWIAHPGGRAILDQVEHKL-----GLKPEK
Arachis_hypogaea_STS3              ISQNINDAL--NKAFDPLGISDYNS----IFWIAHPGGRAILDQVEQKV-----NLKPEK
Arachis_hypogaea_STS1              ISQNINGAL--SKAFDPLGISDYNS----IFWIAHLGGRAILDQVEQKV-----NLKPEK
Vitis_labrusca                     ISENIEKCL--TQAFDPLGISDWNS----LFWIAHPGGPAILDAVEAKL-----NLEKKK
Vitis_vinifera_STS1                ISENIEKCL--TQAFDPLGISDWNS----LFWIAHPGGPAILDAVEAKL-----NLEKKK
Vitis_vinifera_STS2                ISENIEKCL--TQAFDPLGISDWNS----LFWIAHPGGPAILDAVEAKL-----NLDKKK
Parthenocissus_henryana            ISENIEKCL--TQAFDPLGISDWNS----LFWIAHPGGPAILDAVEAKL-----NLDKKK
Parthenocissus_quinquefolia        ISENVEKCL--TQAFDPLGISDWNS----LFWIAHPGGPAILDAVEAKL-----SLDKQK
Cissus_rhombifolia                 ISENIEKCL--TQAFDPLGISDWNS----LFWIAHPGGPAILDAVEAKL-----SLDKQK
Rheum_tataricum                    ISNCIETCL--SKAFTPLNISDWNS----LFWIAHPGGRAILDDIEATV-----GLKKEK
Polygonum_cuspidatum               VSNNIETCL--SEAFTPLNISNWNS----LFWIAHPGGPAILDHVEATV-----GLNKEK
Rhodococcus_sp                     LSRALDETT--MKT----VLDGAET-SSVDLWAVHPGGRSILDAVEGAL-----HLDADA
Rhodococcus_sp.                    LSRALDETT--MKT----VLSGAET-SSIDLWAVHPGGRSILDAVEGAL-----HLDADA
Mesorhizobium_sp.                  VQEALRSNR-------DVILAGRAP-EAIDLWAVHPGGRSILDAVERAF-----DLEPAA
Mesorhizobium_sp.                  IHDALLSNQ-------DAFLGGRPT-EAIDLWAVHPGGRSILDAVERAL-----NLTPAA
Erythrobacter_marinus              LAEALDDPQ--LQA---TIEGDLRP----EAWAIHPGGRSVLDAAERGL-----KLPSEA
Altererythrobacter_sp.             LAEALSDGA--VAN----SVTEGKPVTEIDAWAVHPGGRSIVDAVERGL-----QLPPEK
Erythrobacter_sp.                  IRDALTSPE--VRA---RIAGDELP----EAFAVHAGGRSILDAVESGL-----GLAPTA
Sphingomonas_sp.                   IADALDDEA--FRRTVTGGCGADAI----DGWAVHAGGRSILDAVEQSL-----ALPEDA
Sphingomonas_endophytica           IGAALRDPA--LVA----AITGSRP---VDTWAIHAGGRSILDAVEQAL-----ALAPDA
Skermanella_stibiiresistens        IGQGLPEAL-------PKILRGRDP-RDVELWAVHPGGRSILDAVASVIAGSGGGSSGDP
Microvirga_sp.                     IAKSLRHEA--TRNDDRGILRGQHK-DDFDLWAVHAGGRTILDAVEQGL-----ELAPDA
Microvirga_ossetica                IARALQREA--TRNDDDGILRGQHK-EDFDLWAVHAGGRTILDAVEQGL-----DLDPDA
Novosphingobium_malaysiense        IAAALAADA--RRNDDLGLLRGQAP-DDFALWAVHAGGRTVLDAVEQGY-----DLPVEA
Novosphingobium_barchaimii         IADALGTER--SRNAPDGILRGQAV-ADYDLWAVHAGGRSILDAVERGL-----ELPAEA
Paenibacillus_wynnii               LGTHLETEL--GVL----FGNKKLP----DLWAIHPGGRGIVDSVQDVM-----KLRDEQ
Paenibacillus_pectinilyticus       IGTWIPEQI--EHL----LDGGPRP----ALWAIHPGGKGILDTLEEVY-----DLEPED
Bacillus_sp.                       IGEFIPAEV--ERL-----CGEEEL----ALWAIHPGGKGIIDILQNKF-----ELTDEQ
Paenibacillus_naphthalenovorans    IGRWLPAVS--GHL----TAGENRP----ELWAIHPGGRGIIDAVQDVY-----GLTDEQ
                                      :                          * **  ::.
```

```
Fusarium_langsethiae_STS3          MRASYDTYINHGNSSSATIFSVMNRLRSKDMD-AMAPDG-RVRDYVVGCAFGPGITVEMC
Fusarium_oxysporum_STS3            QRASYDTYINHGNSSSATIFSVMDRLRSKDMD-AMAPDG-RVRDYVVGCAFGPGITVEMC
Gibberella_fujikuroi_STS2          QRASYDTYINHGNSSSATIFSVMDRLRSRDMD-AMAPDG-RVRDYVVGCAFGPGITVEMC
Psilotum_nudum                     LQASRHVLSEFGNMSSATVHFILDHMRKSSVEKGCATTG-EGYQLGILLGLGPGMTVESI
Picea_glauca                       LRATRHVLSEYGNMSSACVHFILDEMRKTSRENGYSTTG-EGLDMGVLFGFGPGLTVETV
Picea                              LRATRHVLSEYGNMSSACVHFILDEMRKTSRENGYSTTG-EGLEMGVLFGFGPGLTVETV
Picea_sitchensis                   LRATRHVLSEYGNMSSACVHFILDEMRKTSRENGYSTTG-EGLEMGVLFGFGPGLTVETV
Phanera_variegata                  MKATRHVLSKYGNMSSACVLFIMDEMRRRSAEDKLSTTG-EGLDWGVLFGFGPGLTVETV
Arachis_hypogaea_STS3              MKATRDVLSNYGNMSSACVFFIMDLMRKRSLEEGLKTTG-EGLDWGVLFGFGPGLTIETV
Arachis_hypogaea_STS1              MKATRDVLSNYGNMSSACVFFIMDLMRKKSLETGLKTTG-EGLDWGVLFGFGPGLTIETV
Vitis_labrusca                     LEATRHVLSEYGNMSSACVLFILDEMRKRSLKGENATTG-EGLDWGVLFGFGPGLTIETV
Vitis_vinifera_STS1                LEATRHVLSEYGNMSSACVLFILDEMRKKSLKGEKATTG-EGLDWGVLFGFGPGLTIETV
Vitis_vinifera_STS2                LEATRHVLSEYGNMSSACVLFILDEMRKKSLKGERATTG-EGLDWGVLFGFGPGLTIETV
Parthenocissus_henryana            LEATRHVLSEYGNMSSACVLFILDEMRKKSLKGEKATTG-EGLDWGVLFGFGSGLTIETV
Parthenocissus_quinquefolia        LEATRHVLSEYGNMSSACVLFILDEMRKKSLKGEKATTG-EGLDRGVLFGFGPGLTIETV
Cissus_rhombifolia                 LEATRHVLSEYGNMSSACVLFILDEMRKKSLKGEKATTG-EGLDWGVLFGFGPGLTIETV
Rheum_tataricum                    LKATRQVLNDYGNMSSACVFFIMDEMRKKSLANGQVTTG-EGLKWGVLFGFGPGVTVETV
Polygonum_cuspidatum               LKATRQVLNDYGNMSSACVFFIMDEMRKKSLENGHATTG-EGLQWGVLFGFGPGITVETV
Rhodococcus_sp                     LTSSRSVLDNYGNMSSATVLFVLADMLER------GDTG-----SGCAMAFGPGLTAETM
Rhodococcus_sp.                    LTSSRRVLENYGNMSSATVLFVLADMLER------GDTG-----SGCAMAFGPGLTAETM
Mesorhizobium_sp.                  LEPSREVLCQYGNMSSPTVMFVMEKMLKQ-------PGG-L---LGCGMSFGPGLTAETM
Mesorhizobium_sp.                  LKPSREVLRRYGNMSSATVMFALQEMLK-------AAPG-L---LGCGMSFGPGLTAETM
Erythrobacter_marinus              LKSSRAVLSECGNMSSATVLFVLQRLMAA------KPEN------GIALAFGPGLAMEGL
Altererythrobacter_sp.             LTASREVLQDCGNMSSATVMFVLKKLMAE------KPRT------GIAIAFGPGLAMEGL
Erythrobacter_sp.                  LDHSRAVLRDFGNMSSSTLMFVLERTLRD------KPRD------GVALAFGPGLAMEGF
Sphingomonas_sp.                   LTASRAVLADHGNMSSATLMFVLERLLA----------G-PPVTNGVALAFGPGLAAEGF
Sphingomonas_endophytica           LDASRAVLRDSGNMSSATLMFVLARILS----------G-PPVDHGVALAFGPGLAAEGL
Skermanella_stibiiresistens        LTDSRAILRDYGNMSSATVMFVLKRMLDR-----FRNTGIGGNSLGCAMAFGPGLTAESM
Microvirga_sp.                     LRWSRGVLRDFGNMSSATLMFVLDRMMQQ------APPD-S---RGFGMAFGPGLVAETF
Microvirga_ossetica                LRWSRGVLRDFGNMSSATLMFVLDRMMQQ------APPA-S---NGFGMAFGPGLVAETF
Novosphingobium_malaysiense        LAPSRSILYDKGNMSSATLMFILARMLAD------GMRG-----AGLALAFGPGMAAESF
Novosphingobium_barchaimii         LAPSRAVLRENGNMSSATLMFVLARMMAG------KTPG-TPPQSGIGMAFGPGLAAESF
Paenibacillus_wynnii               THYSREVLRTAGNLSSVTIMFVLEAMRLD-----MIAQE-SASKEGVAMAFGPGLTAELM
Paenibacillus_pectinilyticus       TRPSRTVLRNYGNMSSATILFVLDETRKE-----LENRE-AGPTSGISLAFGPGLTCEMI
Bacillus_sp.                       TAHSLGVLRDYGNVSSATILFVLDAMRMH-----LQESG-SDAVSGIALAFGPGLTAEMI
Paenibacillus_naphthalenovorans    VDSSRAVLRRYGNLSSATMLFVLDDMRRR-----LQDRR-SGLASGMAVAFGPGLTAEMT
                                      :       ** **  :   :                        .:*.*:. *
                                              ▲                                   ▲

Fusarium_langsethiae_STS3          MMKRNMVHGTSITGLQTPPETPAETESEPSEAGDGD-EWGAENSGSPAERNSTSAYESQD
Fusarium_oxysporum_STS3            MLKRNMSHGAGLPGLQTPPETPAETETEPSEIGDGDGEWGRELSGDPA--------ESPD
Gibberella_fujikuroi_STS2          MLKRNTSYGAGLPGLQTPPETPAETETEPSEIGDGDGEWGRESSGDPA--------ESPD
Psilotum_nudum                     VLKSVPIASLLSS-----------------------------------------------
Picea_glauca                       VLKSVLLP----------------------------------------------------
Picea                              VLKSVLLP----------------------------------------------------
Picea_sitchensis                   VLKSVLLP----------------------------------------------------
Phanera_variegata                  VLRSVAV-----------------------------------------------------
Arachis_hypogaea_STS3              VLRSVAI-----------------------------------------------------
Arachis_hypogaea_STS1              VLRSMAI-----------------------------------------------------
Vitis_labrusca                     VLHSIPTVTN--------------------------------------------------
Vitis_vinifera_STS1                VLHSVPTVTN--------------------------------------------------
Vitis_vinifera_STS2                VLHSIPMVTN--------------------------------------------------
Parthenocissus_henryana            VLHSIPMVTN--------------------------------------------------
Parthenocissus_quinquefolia        VLHSIPMVTN--------------------------------------------------
Cissus_rhombifolia                 VLHSIPMVTN--------------------------------------------------
Rheum_tataricum                    VLSSVPLIT---------------------------------------------------
Polygonum_cuspidatum               VLRSVPII----------------------------------------------------
Rhodococcus_sp                     LFHAS-------------------------------------------------------
Rhodococcus_sp.                    LFHAA-------------------------------------------------------
Mesorhizobium_sp.                  LFRTVS------------------------------------------------------
Mesorhizobium_sp.                  LFRTVS------------------------------------------------------
Erythrobacter_marinus              RFGWETGNA---------------------------------------------------
Altererythrobacter_sp.             RFGWTESDAR--------------------------------------------------
Erythrobacter_sp.                  RFGWSD------------------------------------------------------
Sphingomonas_sp.                   GFRSAS------------------------------------------------------
Sphingomonas_endophytica           SFASAR------------------------------------------------------
Skermanella_stibiiresistens        MFRLAAA-----------------------------------------------------
Microvirga_sp.                     RFDIAG------------------------------------------------------
Microvirga_ossetica                RFTLTG------------------------------------------------------
Novosphingobium_malaysiense        RFAIED------------------------------------------------------
Novosphingobium_barchaimii         RFNLL-------------------------------------------------------
Paenibacillus_wynnii               RFTFVPAYSSSIQEQNHAVL----------------------------------------
Paenibacillus_pectinilyticus       QITYLGVGAKRTAILDEIHV----------------------------------------
Bacillus_sp.                       KIAYVPATIARERGQQQADGAYV--------------------------------------
Paenibacillus_naphthalenovorans    RITYLPSVVGQEQLIGDAR-----------------------------------------
                                    :
```

```
Fusarium_langsethiae_STS3          QYARFVTESLEYLDLD
Fusarium_oxysporum_STS3            QYALFVADSLEHLDLD
Gibberella_fujikuroi_STS2          QYALFVAESLEHLDLD
Psilotum_nudum                     ----------------
Picea_glauca                       ----------------
Picea                              ----------------
Picea_sitchensis                   ----------------
Phanera_variegata                  ----------------
Arachis_hypogaea_STS3              ----------------
Arachis_hypogaea_STS1              ----------------
Vitis_labrusca                     ----------------
Vitis_vinifera_STS1                ----------------
Vitis_vinifera_STS2                ----------------
Parthenocissus_henryana            ----------------
Parthenocissus_quinquefolia        ----------------
Cissus_rhombifolia                 ----------------
Rheum_tataricum                    ----------------
Polygonum_cuspidatum               ----------------
Rhodococcus_sp                     ----------------
Rhodococcus_sp.                    ----------------
Mesorhizobium_sp.                  ----------------
Mesorhizobium_sp.                  ----------------
Erythrobacter_marinus              ----------------
Altererythrobacter_sp.             ----------------
Erythrobacter_sp.                  ----------------
Sphingomonas_sp.                   ----------------
Sphingomonas_endophytica           ----------------
Skermanella_stibiiresistens        ----------------
Microvirga_sp.                     ----------------
Microvirga_ossetica                ----------------
Novosphingobium_malaysiense        ----------------
Novosphingobium_barchaimii         ----------------
Paenibacillus_wynnii               ----------------
Paenibacillus_pectinilyticus       ----------------
Bacillus_sp.                       ----------------
Paenibacillus_naphthalenovorans    ----------------
```